DNA Interstrand Crosslink Repair in *Trypanosoma brucei*

Submitted in partial fulfilment of the requirements of the Degree of Doctor of Philosophy

Ambika Kumar

Supervisor: Dr Shane Wilkinson

School of Biological & Chemical Sciences

Queen Mary University of London

Statement of originality

I, Ambika Kumar, confirm that the research included within this thesis is my own work or that where it has been carried out ins collaboration with, or supported by others, that this is duly acknowledged below, and my contribution indicated. Previously published material is also acknowledged below.

I attest that I have exercised reasonable care to ensure that the work is original, and does not to the best of my knowledge break any UK law, infringe any third party's copyright or other Intellectual Property Right, or contain any confidential material.

I accept that the College has the right to use plagiarism detection software to check the electronic version of the thesis.

I confirm that this thesis has not been previously submitted for the award of a degree by this or any other university.

Signature: 

Date: 24/01/2018

Details of publications:

1. Sullivan, J. et al. Unravelling the role of SNM1 in the DNA repair system of *Trypanosoma brucei*. Mol. Microbiol. 1–39 (2015). doi:10.1111/mmi.12973
2. Meredith, E. L. et al. Distinct activation mechanisms trigger the trypanocidal activity of DNA damaging prodrugs. Mol. Microbiol. (2017). doi:10.1111/mmi.13767
3. Guerrero, S. A. et al. (2017) Functional characterisation of the methionine sulfoxide reductase repertoire in *Trypanosoma brucei*. Free Radic. Biol. Med. 112, 524–533. doi.org/10.1016/j.freeradbiomed.2017.08.023

Acknowledgements

I would like to thank Dr Shane Wilkinson for coming up with the initial ideas for this project as well as his advice and support along the way. I hope all the stress and 'stupid' questions were worth it! I am also very grateful to members of the John Kelly and Sam Alsford laboratories at the London School of Hygiene and Tropical Medicine for their guidance and resources which made it possible for me to carry out this project as well as Dr Emma Louise Meredith for teaching me basic molecular biology and cell culturing techniques. Special thanks to all other research laboratories which have provided antibodies, cell lines and compounds for this project, in particular the McCulloch lab at the University of Glasgow. This gratitude is extended out to Queen Mary University of London for their financial support.

Furthermore, a massive thank you to all members of the 4th floor, both present and past, for their positivity during all the highs and lows of this project and willingness to have tea (and biscuits) at a moment's notice. I'm so glad I decided to do my PhD in such a great department with so many wonderful and talented people (too many to name!). I would also like to appreciate all the love and support from my family, including my parents, brothers and sisters who may not have understood what I was doing but always appreciated how committed I was to this project. Moreover, a huge thank you to everyone at Dongola, GradSoc and Cambridge House for being so understanding and making sure I always had something to laugh about at the end of a long, hard day (despite my constant nagging, unreasonable requests and mood swings). On that note, special thanks to Inva Hoti (soon to be Dr. Hoti) for making me realise exercise and gossiping can help deal with stress just as much as a good laugh!

Finally, I wouldn't have got this far without my amazing, supportive fiancé Abhishek who has always been there for me, regardless of any challenges. I don't know how to thank you for everything you've done for me, but I hope I've made you proud.

Abstract

Genomes are constantly challenged by agents that promote DNA damage, with interstrand crosslinks (ICLs) representing a particularly dangerous lesion. Ongoing work in the Wilkinson laboratory aimed at identifying novel agents that target *Trypanosoma brucei*, the causative agent of African trypanosomiasis, identified several prodrugs that once activated form ICLs in this protozoan parasite. To understand the complexity of ICL repair systems that *T. brucei* employs to resolve such damage, a variety of null mutant lines were generated that lack activities postulated to fix such lesions. Phenotypic screens using various DNA damaging agents revealed that TbMRE11, TbEXO1, TbCSB, TbCHL1, TbFAN1, TbBRCA2 and TbRAD51 all help to resolve ICLs, implicating components of the homologous recombination, nucleotide excision repair and mismatch repair pathways in resolving this form of damage: This approach demonstrated that components of the translesion synthesis pathway (TbREV2 and TbREV3) do not play a significant role in ICL repair. In many organisms, nucleases belonging to the SNM1/PSO2 family play a key and specific role in the repair of ICLs with this property extending to the *T. brucei* homologue, TbSNM1. To assess whether there is a functional linkage between the DNA repair factors noted above and TbSNM1, a series of double null mutants were constructed and the susceptibility of these lines to ICL inducing agents determined. Identification of their epistatic/non-epistatic interactions revealed that *T. brucei* expresses at least two ICL repair systems with one pathway involving the concerted activities of TbSNM1/TbCSB/TbEXO1, that we postulate functions to repair ICLs encountered by the transcriptional machinery, while the other is centred upon TbMRE11/TbFAN1/TbEXO1 that may help resolve lesions which cause stalling of DNA replication forks. By unravelling how *T. brucei* repairs ICLs, specific inhibitors against key components of these pathways could be developed and used in combination with DNA damaging agents to target trypanosomal infections.

Table of Contents

List of figures

List of tables

Abbreviations

AQP	Aquaglyceroporin 2
BER	Base excision repair
BLA	Blasticidin–S-deaminase gene
BSF	Bloodstream form
BSF	Bloodstream form
CATT	Card agglutination test for trypanosomiasis
cDNA	Complementary DNA
CSF	Cerebral spinal fluid
DAPI	4',6-diamidino-2-phenylindole
DFMO	Difluoromethylornithine
DSB	Double strand break (dsDNA break)
dsDNA	Double stranded DNA
dsRNA	Double stranded RNA
EAT	East African trypanosomiasis
EC_{50}	Concentration of drug needed to kill 50% of cells
EP	Epimastigote form
FA	Fanconi anaemia
G418	Neomycin phosphotransferase gene
gDNA	Genomic DNA
GFP	Green fluorescent protein
GG-NER	Global genome-nucleotide excision repair
GOI	Gene of interest
HAT	Human African trypanosomiasis
HN2	Mechlorethamine
HR	Homologous recombination
HU	Hydroxyurea
HYG	Hygromycin phosphotransferase gene
ICL	Interstand Crosslink
K (DNA)	Kinetoplastid (DNA)
LAPT	Low affinity pentamidine transporter
LS-BSF	Long slender bloodstream form trypomastigotes
MGMT	Methylguanine methyltransferase
MMEJ	Microhomology-mediated end joining
MMR	Mismatch repair
MMS	Methyl methanesulfonate
MRN	MRE11-RAD50-NSB1
MSF	Médecins Sans Frontières
MT	Metacyclic trypomastigote
N (DNA)	Nuclear (DNA)
NECT	Nifurtimox eflornithine combinational therapy
NER	Nucleotide excision repair
NGOs	Non-governmental organisations
NHEJ	Non-homologous end joining
NLS	Nuclear localisation signal
NTD	Neglected tropical disease
NTR	Type I nitroreductase
P2	Purine transporter
PAC	Puromycin-N-acetyltransferase gene

PCF	Procyclic form trypomastigotes
PCNA	Proliferating cell nuclear antigen
PCR	Polymerase chain reaction
PHLEO	Bleomycin resistance protein gene
PSO2	Psoralen sensitive 2
RT-qPCR	Reverse transcription-quantitative polymerase chain reaction
SNM1	Sensitive to nitrogen mustard 1
SSB	Single strand break
SS-BSF	Short stumpy bloodstream form trypomastigotes
ssDNA	Single stranded DNA
TC-NER	Transcription coupled-nucleotide excision repair
TLS	Translesion synthesis
UV	Ultraviolet radiation
VSG	Variant surface glycoprotein
WAT	West African trypanosomiasis
WHO	World Health Organisation
WT	Wild type

1. Introduction

1.1 Trypanosomatids

Trypanosomatida represents an order of protozoan parasites belonging to the class Kinetoplastida. Most are monoxenous, primarily affecting insects, although several have evolved strategies to infect secondary hosts that as a grouping can effect a range of organisms including plants, invertebrates or vertebrates (Stevens *et al.*, 2001). Characteristically, trypanosomatid cells in at least one of their life cycle stages have a long slender morphology and possess a single flagellum. Together, these combine to give these parasites a distinctive corkscrew-like motility resulting in the order name: "trypó" and "soma" are Greek for "drill" and "body", respectively. Being eukaryotes, Trypanosomatida contain a number of 'classical' membrane-bound organelles such as the nucleus, mitochondria, endoplasmic reticulum but interestingly also harbour several 'unusual' structures including glycosomes, which represent modified peroxisomes that play a key role in glycolysis, a kinetoplast that contains the mitochondrion genome, and a small invagination of the plasma membrane called the flagellar pocket where the flagellum exits the cytoplasm (Figure 1.1) (Stevens *et al.*, 2001; Barrett *et al.*, 2003; Lopes *et al.*, 2010).

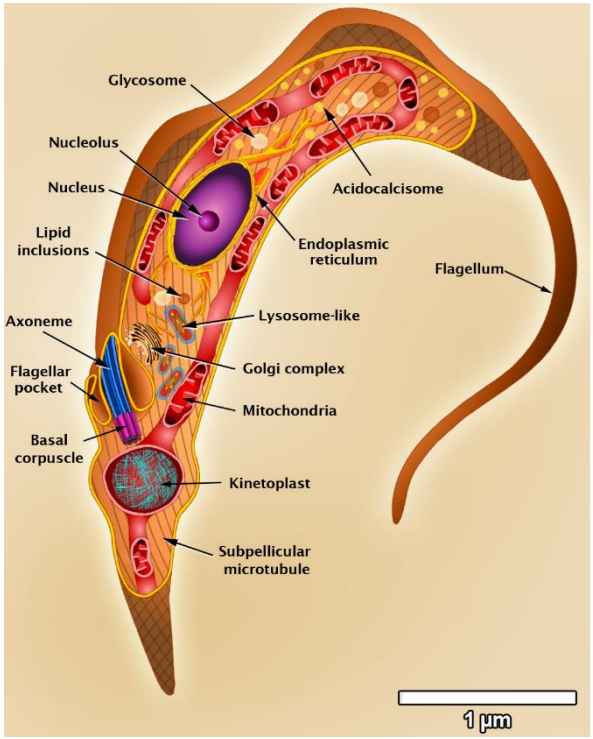

Figure 1.1: Typical structure of trypanosomatid cell.
The image shown is of the trypomastigote form of *Trypanosoma cruzi* and illustrates the organelles found in this parasites life cycle stage (Teixeira *et al.*, 2012).

Trypanosomatids are responsible for a number of insect transmitted diseases that are of medical and veterinary importance. The pathogens *Trypanosoma cruzi*, *Trypanosoma brucei*

and *Leishmania* are of particular note as they cause Chagas disease (also known as American trypanosomiasis), human African trypanosomiasis (HAT; also known as African sleeping sickness) and Leishmaniasis, respectively. Together, over 7 million people are infected by one of these agents resulting in around 55,000 deaths per year ('WHO | World Health Organization', 2018). In addition to their direct effect on human health, these infections have had a major impact on the economic development of poor, rural populations in Latin America, sub-Saharan Africa and south-east Asia. With a series of other viral, bacterial and parasitic diseases, trypanosomatid infections are recognised by the World Health Organisation (WHO) as 'neglected tropical diseases' (NTDs) that often trap individuals and their families in a cycle of poverty and disease (*CDC - Global Health - Neglected Tropical Diseases*, 2018). Breaking this sequence is a major aim of many non-government organizations (NGOs) such as the Drugs of Neglected Diseases initiative, Médecins Sans Frontières and Pan American Health Organization with such agencies playing key roles in the development and implementation of new preventative strategies, novel diagnostic procedures and treatment schedules to combat such deliberating conditions. In relation to human infectious trypanosomatids, these approaches have seen a dramatic fall in HAT and Chagas disease (Simarro *et al.*, 2011). Buoyed by the success of such strategies, Dr Jean Jannin, Coordinator of the Innovative and Intensified Disease Management unit of the WHO Department for Control of Neglected Tropical Diseases, commented that the target is to eliminate HAT as a public-health problem by 2020 by bringing down the incidence of the disease to less than 1 case per 10 000 of the population in at least 90% of the areas where cases exist ('WHO | Trypanosomiasis, human African (sleeping sickness)', 2017).

1.2 Human African trypanosomiasis

The first accounts of HAT are closely linked with the 18th Century slave trade with ship doctors and naval surgeons noting several symptoms associated with the captured people. The first accurate report of the neurological conditions of the disease were identified in 1734 by John Aktins with other characteristic signs such as localised lymphadenopathies subsequently described by the English physician Thomas Winterbottom (Steverding, 2008). It is now recognised that HAT is a problem across the whole of sub-Saharan Africa where two discernible forms of the disease are prevalent with each disorder caused by a different *T. brucei* sub-species. In modern times there have been three major HAT epidemics with the first of these lasting approximately one decade (1896-1906), primarily affecting Uganda, Kenya and the Congo Basin resulting in the death of an estimated 800,000 people (Steverding, 2008). This

resulted in a drive to find a cure for this devastating disease and lead to the development of the organo-arsenical compound tryparsamide and Bayer 205, now known as suramin. During the 1920's through to the late 1940's the second HAT outbreak occurred at a number of sites across sub-Saharan Africa with the above treatments being used to treat infected individuals. This promoted the then colonial powers to implement active measures based on mobile disease surveillance teams to identify and treat infected people, the application of vector/host reservoir control strategies aimed at targeting disease spread and continue the development of new therapies with the latter resulting in discovery of pentamidine and melarsoprol. The most recent epidemic occurred during the last three decades of the 20th Century (1970's to the late 1990's) with highest prevalence in Angola, the Democratic Republic of the Congo, South Sudan and Uganda. The reasons for this outbreak are numerous but are primarily associated with political instability. As such, NGO-mediated intervention and treatment strategies could not be implemented with the estimated number of new cases and deaths hitting a peak in the mid-1990's with an estimated 450,000 new HAT cases and predicted 66,000 deaths in one year alone (Figure 1.2) (Ruiz-Postigo *et al.*, 2012). As political tensions eased, the situation regarding HAT has drastically improved with only 2,804 cases reported in 2015 (Figure 1.2), a figure which grossly underestimates the true extent of the problem, estimated at 20,000 cases ('WHO | Trypanosomiasis, human African (sleeping sickness)', 2017). One major reason for this success has been the employment of the nifurtimox eflornithine combination therapy (NECT), the first co-administered treatment to target this infection. With sustained preventative and therapeutic strategies, the goal for the eradication of HAT as a medical problem from all of its endemic sites by 2030 has been envisaged by the WHO Department of Control of Neglected Tropical Diseases in Geneva (Qian and Zhou, 2016).

1.2.1 Distribution of disease

The distribution of HAT in sub-Saharan Africa is solely determined by the geographical range of its insect vector, the tsetse fly. Approximately 30 different *Glossina* species and sub-species found in riverine, savannah or forest habitats have been recorded to transmit the causative agent through the arthropods haematophagic behaviour. In contrast to some other insect transmitted parasitic diseases (*e.g.* malaria and leishmaniasis), both male and female tsetse flies are able to spread HAT *via* a salivarian route. One area of the insect's life cycle that is amenable to vector control concerns their reproductive strategy. Unlike many other insects, female tsetse flies are viviparous, investing their energy into giving birth to one fully formed larvae at a time. This aspect of the arthropods life cycle allows vector control teams a window

of opportunity to target the fly, thus preventing disease transmission. Other routes for spread of HAT, such as sexual and congenital transmission, modern medical practices (*e.g.* blood transfusions) and lab-based injuries, have been reported for this condition but these are uncommon (Franco, 2014).

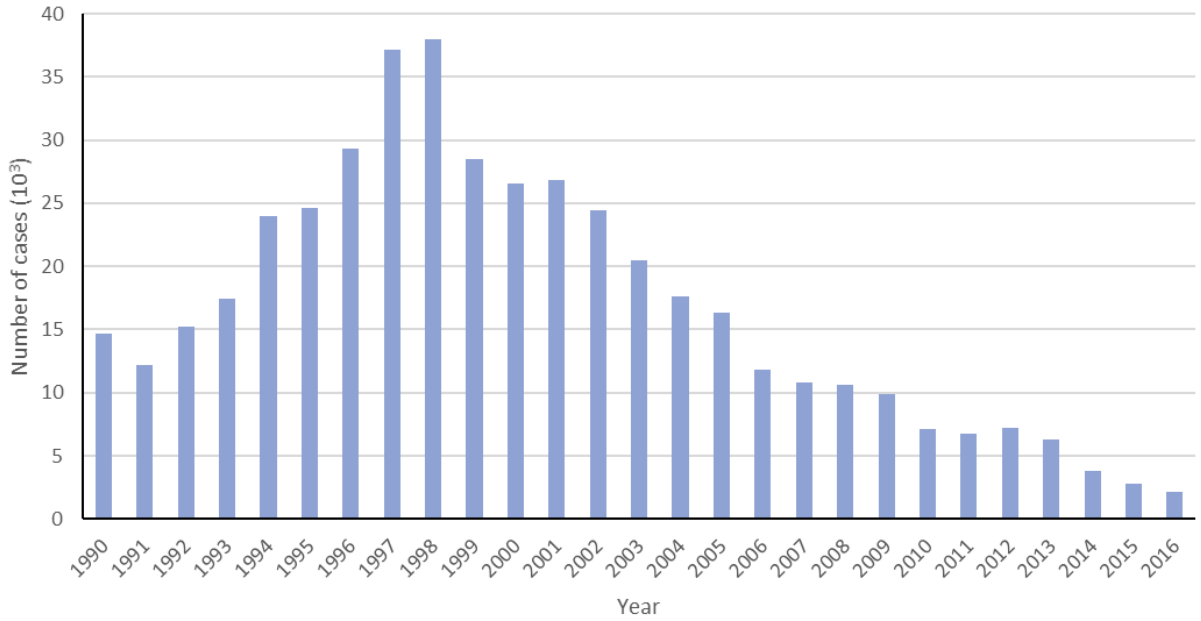

Figure 1.2: Estimated number of human African trypanosomiasis cases.
Total number of estimated new cases of human African trypanosomiasis based on WHO data from 1990–2016 ('WHO | Trypanosomiasis, human African (sleeping sickness)', 2017).

1.3 Causative agent

In relation to location, transmission, epidemiology and disease staging, HAT can be split into two distinct variants, both caused by different sub-species of *T. brucei*. In West and Central Africa, *T. brucei gambiense* is responsible for a chronic infection termed West African trypanosomiasis (WAT) which accounts for 98% of all recorded HAT cases. The parasite is predominantly transmitted anthropomorphically by riverine and forest dwelling tsetse flies with this disease form being commonly associated with rain forest, river or lake habitats (Table 1.1). Within a human host, *T.b. gambiense* parasitaemia is generally low with many individuals being asymptomatic and therefore acting as a reservoir for the disease. In eastern and southern regions of Africa the so-called East African trypanosomiasis (EAT) prevails. Caused by *T. brucei rhodesiense*, the acute form of the disease is associated with dry bush and woodland, and transmitted by savannah dwelling tsetse flies (Table 1.1). Commonly found in animal reservoirs, particularly ungulates, EAT is a zoonosis with high parasitaemia commonly noted in an infected individual. As a result, this form of HAT can kill a patient within a month of being infected (Brun *et al.*, 2010).

	East African trypanosomiasis	West African trypanosomiasis
Causative agent	*T.b rhodesiense*	*T.b gambiense*
Tsetse fly location	Savannah	Riverine
Ecology	Dry bush and woodland	Rain forest, rivers, or lakes
Geographical location	East/Southern Africa	West/Central Africa
Transmission	Zoonotic	Anthropomorphic
Non-human hosts	Wild & domestic animals	Rare
Epidemiology	Sporadic	Endemic with cases of epidemics
Prognosis	Rapid progression to death (weeks to months)	Slow progression (~1 year) leading to death
Parasitaemia	High	Low
Asymptomatic carriers	Rare	Common

Table 1.1: Comparisons between different forms of human African trypanosomiasis
Table adapted from (Stevens *et al.*, 2001)**.**

1.3.1 Parasite life cycle

The two sub-species of *T. brucei* show similar life cycle strategies in their insect and human hosts (Figure 1.3). Transfer of the parasite-infected insect saliva occurs when the tsetse fly takes a blood meal from a mammalian host. Trypanosomes in the metacyclic trypomastigote (MT) form are injected into the victim's blood and/or lymphatic systems where they transform, possibly in response to a temperature shift, into long slender bloodstream form trypomastigotes (LS-BSF). Here, the parasite multiplies by binary fission to colonise the above circulatory systems with fluctuating parasitaemia, and if left untreated, can eventually cross the blood brain barrier to infect the cerebrospinal fluid. The oscillation of *T. brucei* numbers in the bloodstream and lymphatic system occurs in response to antibody-mediated immune insults with this pathogen able to alter its surface coat and hence antigenic profile presented to the host. This process, known as antigenic variation, involves the periodic changing of their variant surface glycoprotein (VSG), which acts as an antigen, with the vast majority of cells in a given wave of parasitaemia expressing the same form of the surface protein. The chronic nature of a HAT infection can be maintained as the parasite is able to call upon more than 1000 encoding genes and pseudogenes (Horn and McCulloch, 2010). At the peak of parasitaemia in a given wave, LS-BSF can express a stumpy induction factor which triggers differentiation of some of these trypanosomes into short stumpy bloodstream form trypomastigotes (SS-BSF) (Seed and Wenck, 2003). This new form of the parasite is pre-adapted for transmission into the insect vector but if not transferred, can be readily cleared from the mammalian host.

When a tsetse fly takes a bloodmeal, both LS-BSF and SS-BSF are taken up into the insect's midgut where the former trypanosome form dies. In response to a drop-in temperature and metabolites (*e.g.* citrate/*cis*-aconitate) present in the flies' digestive tract, the latter trypomastigote then undergoes another round of differentiation leading to procyclic form trypomastigotes (PCF) (Czichos, Nonnengaesser and Overath, 1986). This parasite stage divides by binary fission and colonises this region of the arthropod. The parasite makes its way to the tsetse fly salivary gland, possibly via a mechanism involving conversion of the PCF to an epimastigote form (EP). Here, the EP attaches to epithelial cell lining of this insect organ *via* its flagellum, divides by binary fission and potentially undergoes genetic exchange (the latter step is not an obligatory part of the *T. brucei* life cycle). When the EP density increases to high levels, the cells transform into MT parasites, detaching from the epithelial lining of the salivary gland and entering its lumen ready for transmission into the next mammalian host (Stevens *et al.*, 2001; Matthews, Ellis and Paterou, 2004).

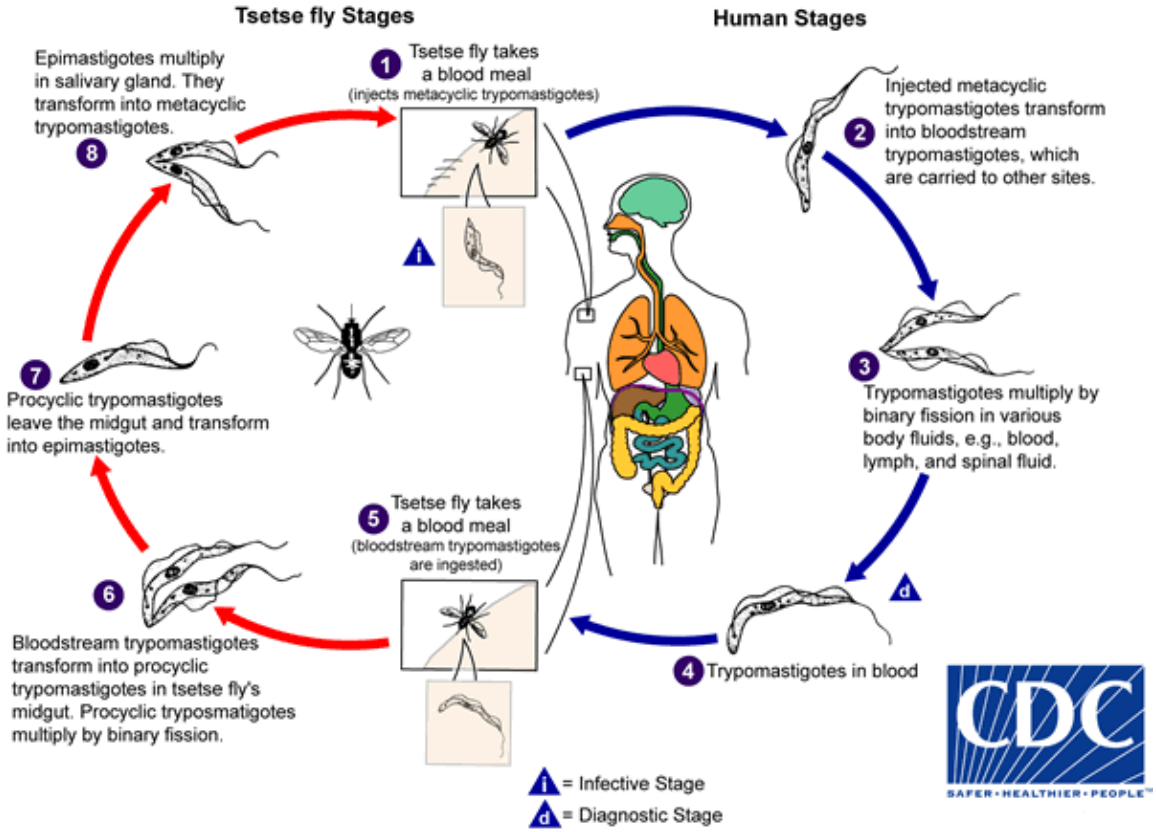

Figure 1.3: *T. brucei* life cycle.
Image sourced from (Center for disease control (CDC) 2015). Available from: http://www.cdc.gov/parasites/sleepingsickness/biology.html.

1.3.2 Staging and pathologies

The interaction of bloodstream form trypomastigotes with the human host causes defined pathological outcomes that can be divided into two distinct stages (Figure 1.4). The early or

haemolymphatic stage of HAT occurs while the parasite is found systemically within the bloodstream and lymphatic system. Towards the peak of parasitaemia, trypanosomes are recognised by host immune mechanisms which stimulates the production of pyrogenic cytokines such as tumour necrosis factor, interleukin-1, interleukin IL-6 and interferons. This results in a characteristic fever which declines following parasite clearance. The process is then repeated with each subsequent wave of parasites such that the patient presents with a so-called relapsing fever with a periodicity of 5 to 7 days. Other signs of HAT can be manifested at this point such as localised lymphadenopathies with 50% of patients infected with *T. b. rhodesiense* also displaying a chancre at the site of the tsetse fly bite. If left untreated, the parasite can penetrate the blood brain barrier resulting in a series of neurological conditions that represent the late or meningoencephalitic stage of HAT. Here, the patient can exhibit anorexia, apathy and lassitude, have severe sleep disturbance patterns (hence the alternative name for HAT, African sleeping sickness) and undergo personality changes. Towards the end of this phase of the disease, patients often start convulsing before becoming comatose and dying (Kennedy, 2013).

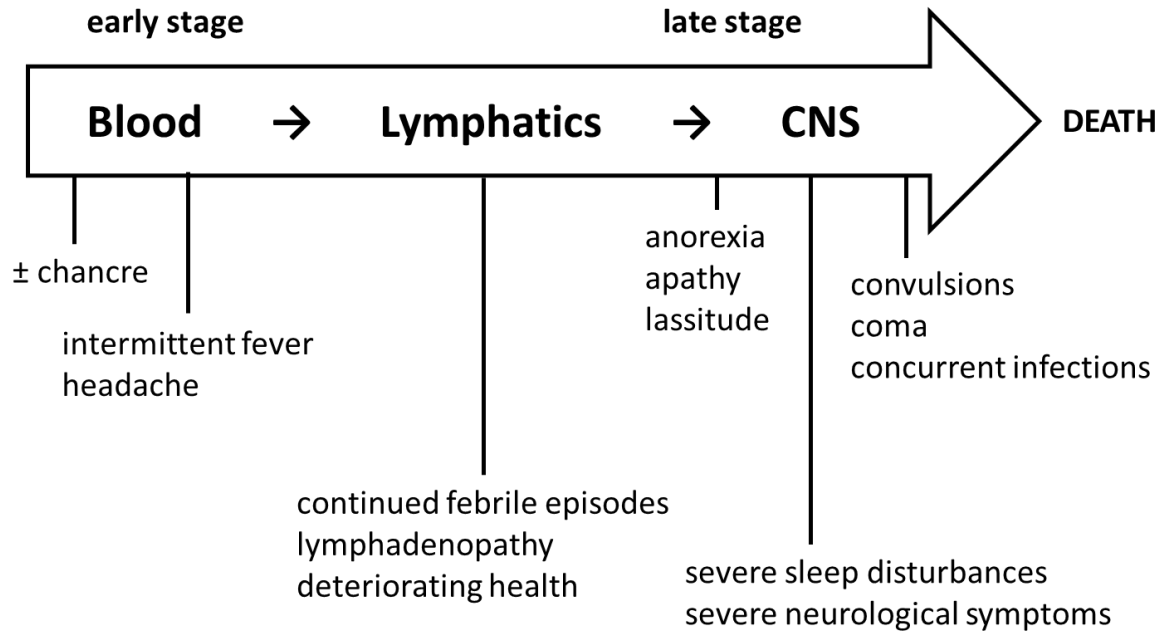

Figure 1.4: Progression of HAT in a human host.
T. brucei rhodesiense and *T. brucei gambiense* progression in a human host. Image adapted from Wiser (2011) ©2010 from Protozoa and Human Disease by Wiser.

1.3.3 Diagnosis

Currently, diagnosis of HAT is based on a combination of direct microscopic screening techniques for the presence of the parasite in blood, lymph and cerebral spinal fluids and/or

indirect serology (Kennedy, 2013). WHO guidelines are only available for WAT which can be applied to patients displaying the aforementioned disease signs and/or populations living in an endemic site. In both cases, undiluted blood samples are collected and analysed using the serology-based Card Agglutination Test for Trypanosomiasis (CATT). If positive, the above analysis is then repeated on a diluted blood sample. If the CATT is negative for either of the above, no further action is required. However, if the individual is positive after screening the diluted sample, the blood is microscopically analysed for the presence of the parasite: For *T.b. gambiense* a parasite enrichment process is often required due to the low parasitaemia associated with such infections. If this proves negative, an additional sample is taken a few days later to account for possible fluctuations in the individual. If either sample is parasite positive, the cerebral spinal fluid of that individual is then checked to determine disease staging. Based on these outcomes, appropriate chemotherapies can then be administered ('WHO | Trypanosomiasis, human African (sleeping sickness)', 2017).

As CATT is specific for *T.b. gambiense*, this element of the diagnostic procedure cannot be applied to EAT. Given the low incidence rate of EAT, it is not financially favourable to develop a diagnostic test for this form of the condition. Here, direct observation of the parasite in bodily fluids is assessed without the need for any form of enrichment step.

1.4 Anti-trypanosomal therapy

Treatment of HAT is comprised of three monotherapies, pentamidine, suramin and melarsoprol, and the combinational therapy NECT. These drugs are used differently according to 1. the disease stage an individual presents with, and 2. the parasite sub-species an individual is infected with.

Pentamidine, an aromatic diamidine (Figure 1.5), administered as daily intramuscular injections over the course of 7-10 days, is the preferred treatment for early stage infections of *T. brucei gambiense*. This drug has restricted usage as its positive charge at physiological pH means it is unable to cross the blood brain barrier to target late stages of HAT. A series of trypanosomal transporters (P2 - purine transporter; AQP - aquaglyceroporin 2; LAPT - low affinity pentamidine transporter) help concentrate the drug in the trypanosomal cell to millimolar concentrations which leads to its cytotoxic effects in the parasite (Bernhard *et al.*, 2007; ORTIZ *et al.*, 2009; Baker *et al.*, 2012; Graf *et al.*, 2013). It is postulated that this drug undergoes a multifactorial attack on the trypanosomes mitochondria by preventing

mitochondrial DNA synthesis and promoting the collapse of the mitochondria membrane potential (Wilkinson and Kelly, 2009; Alsford *et al.*, 2012).

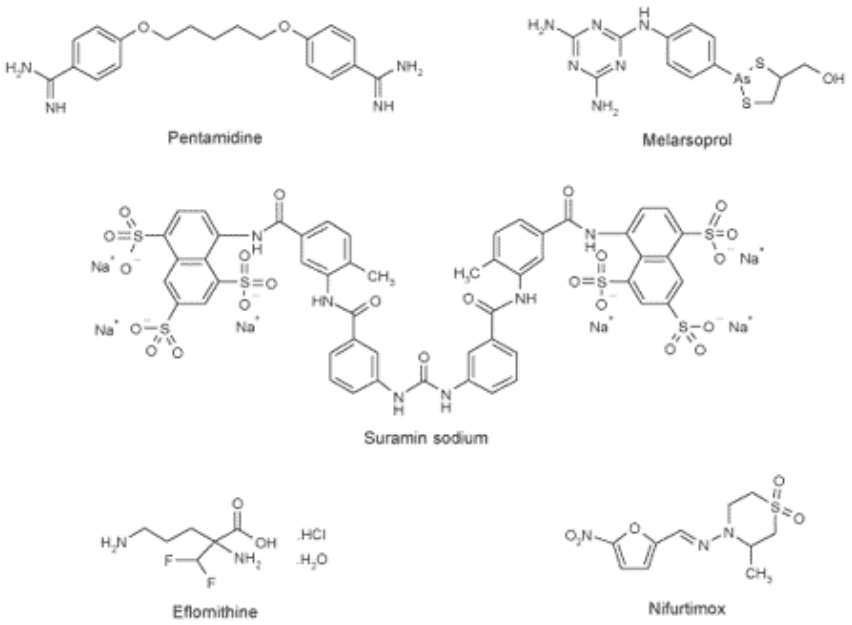

Figure 1.5: Structures of different clinically relevant trypanocidal agents.
Image obtained from (D'Silva, 2007).

Early stage EAT can be treated with the polysulphonated naphthylamine (Figure 1.5) drug suramin that is administrated by weekly intravenous injections over the course of 5-6 weeks. Again, due to charge, this drug does not readily cross the blood brain barrier thus restricting its use. Uptake of suramin occurs through receptor-mediated endocytosis within the flagellar pocket. This process is triggered by binding of the drug to parasite surface proteins such as ISG75 and VSG isoforms with ligand/receptor complexes then transferred through the endocytic pathway to the lysosome (Leung *et al.*, 2011). Through the action of peptidases and proteases, suramin is released and transferred from the vesicular lumen by a major facilitator superfamily transporter. The precise mechanism of suramin is unclear but by virtue of its negative charge, *in vitro* biochemical studies have shown it could block endocytic and glycolytic activities with cell-based phenotypic assays, indicating it may interfere with polyamine synthesis and N-acetylglucosoamine synthesis (Wilkinson and Kelly, 2009; Alsford *et al.*, 2012).

The only drug able to target the late stage of both HAT forms is melarsoprol. This compound is a trivalent, melaminophenyl arsenical prodrug (Figure 1.5) that is administered as a very

painful intravenous injection: the adjuvant used to suspend melarsoprol is polyethylene glycol which causes the collapse of blood vessel epithelial layers that manifests as a burning sensation in the patient. Additionally, this therapy is highly toxic causing death in about 5% of the individuals it is administered too. By uncharacterised mechanisms that may result from host activities, melarsoprol is converted to its druggable form melarsen oxide. This (and melarsoprol) can be internalised by the P2 and AQP transporters where it can readily form complexes with thiol-containing molecules (Bernhard *et al.*, 2007; Baker *et al.*, 2012). The main free thiol in trypanosomes is trypanothione and it has been shown that this can readily conjugate with melarsen oxide, with the resultant complexes inhibiting trypanothione-dependent enzymes (Alsford *et al.*, 2012). Resistance to melarsoprol can be readily achieved in the laboratory through mutation of the P2 transporter and loss or reduction of AQP activity with such lines also displaying cross resistance to pentamidine (Mäser *et al.*, 1999; Graf *et al.*, 2013). Worryingly, these phenotypes have been observed in the field with treatment failures associated with these aforementioned genetic alterations (Bernhard *et al.*, 2007).

Therapeutic switching of both nifurtimox, originally used as an antichagasic treatment, and eflornithine, initially developed as an anticancer agent, has resulted in NECT, the only combinational therapy available against HAT. Previous work revealed that eflornithine was a highly effective anti-HAT agent, earning it the name of the resuscitation or miracle drug. However, it was also extremely expensive, thereby limiting its usage. The use of NECT has drastically reduced the cost of treatment such that it now represents WHOs recommended therapy against late stage WAT. Following intravenous infusion, eflornithine, a variant of ornithine, is taken up by parasite *via* a specific amino acid transporter, AAT6, and then goes on to act as an irreversible inhibitor of ornithine decarboxylase, a key enzyme in polyamine and trypanothione synthesis (Baker, Alsford and Horn, 2011; Schumann Burkard, Jutzi and Roditi, 2011). The orally administered and hydrophobic 5-nitrofuran nifurtimox can readily pass through cell membranes. In the trypanosome, this prodrug enters the parasites single mitochondrion where it undergoes type I nitroreductase (NTR) mediated activation, an enzyme absent from human cells. This reaction goes on to generate a series of nitroso, hydroxylamine and open chain nitrile metabolites with the latter displaying high cytotoxicity. To date, there have been no NECT treatment failures although laboratory-based studies have shown that reduction of AAT6 or NTR activities can result in eflornithine or nifurtimox resistance, respectively (Wilkinson and Kelly, 2009; Alsford *et al.*, 2012).

1.5 DNA damage and repair

DNA is a biological structure that is highly prone to different types of damage. If left unchecked, these can cause alterations to the encoding nucleotide sequence and/or promote chromosome instability. These insults arise from various endogenous sources such as errors in DNA processing and reaction of DNA with metabolic products, or as result of exogenous influences including exposure to chemicals or radiation. As a consequence, cells have evolved a series of distinct and complementary DNA repair pathways that function to fix the variety of lesions that may arise (Sancar *et al.*, 2004; Boiteux and Jinks-Robertson, 2013; Kreuzer, 2013). A healthy cell requires a balance between DNA damage and repair mechanisms with disease or cell death occurring when appropriate DNA repair does not occur (Friedberg, 1995).

1.5.1 General overview

DNA damage can be broadly separated into 1. single base changes, 2. large structural distortions and 3. breakage events, with each type of damage requiring a series of specific repair mechanisms (Figure 1.6).

Single base changes can include nucleotide alkylation, hydrolysis, oxidation, depurination, depyrimidination and deamination events as well as tautomeric shifts which have mutagenic effects on the cellular genome (Waters *et al.*, 2009). These toxic lesions can be neutralized by the direct reversal repair (DRR), base excision repair (BER) or nucleotide excision repair (NER) pathways with the invoked repair mechanism determined by the exact alteration event that has taken place. DNA alkylation events can be readily reversed by the DRR pathway with O^6-alkylguanine DNA alkyltransferase (MGMT) playing a critical role in the transfer of the mutagenic alkyl-group onto its own protein backbone. For other single base changes, the NER and BER operate with the latter pathway playing the major role. BER can be divided into short-patch BER that functions to repair only the affected nucleotide or long-patch BER where a wider region surrounding the damage is fixed. These pathways rely upon the unaltered complementary DNA strand to aid efficient repair (Hakem, 2008).

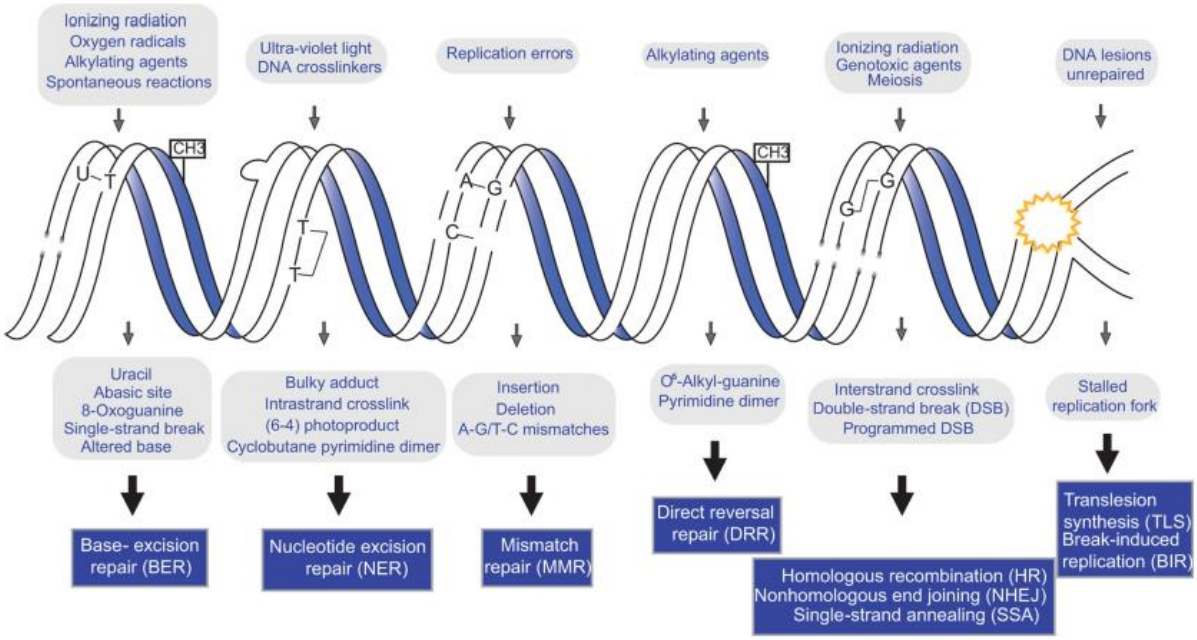

Figure 1.6: DNA damage and repair pathways.
Different types of damage to DNA (both endogenous and exogenous) and the respective cellular repair mechanisms. Image taken from (Genois *et al.*, 2014).

Structural DNA distortions, in particular adduct formation, photodimerism and DNA intercalation events, require more complex repair mechanisms due to the torsional stress created on the nucleic acid backbone (Waters *et al.*, 2009). Photodimerism, most commonly cyclobutane pyrimidine dimers (CPD), is the UV-mediated bonding between up to 4 parallel or neighbouring nucleotides resulting in major helix distortion. DNA intercalation events usually involve the insertion of chemical moieties (*e.g.* ethidium bromide) between nucleotides causing a stretching of the DNA helix. These events are predominantly detected and repaired *via* the NER pathway with additional assistance from the mismatch repair (MMR) pathway. The NER pathway can be divided into transcription-coupled NER (TC-NER) and global-genome NER (GG-NER), with different pathways exploited at different points in the cell cycle.

The most lethal type of DNA damage are breakage events that result in the impediment of both transcription and replication. Exposure to ionizing radiation or cytotoxic agents can result in double strand breaks (DSBs) with potential loss of whole sections of genomic material dependent on 1. the extent of material lost during the damage, 2. the length of the overhanging strand after the breakage event and 3. introduction of errors in the overhanging strands (Jackson, 2002). Due to the lethality of this type of damage, three pathways play a role in repairing such lesions. Substantial damage to both strands of DNA can be repaired by the non-homologous end joining (NHEJ) or homologous recombination (HR) pathways. NHEJ

involves the direct assembly of the 5' and 3' termini of the DNA double helix with the possible loss of 5' and 3' sequences and introduction of base errors. The HR pathway is employed for error-free DSB repair with sequences upstream from the damage used as templates for sister chromatid searches. The translesion synthesis (TLS) pathway can be employed to bypass lesions when repair is unfavourable *e.g.* during transcription/replication.

Single strand breaks are repaired by the single strand annealing (SSA) pathway which involves a simple ligation of the overhanging strand back to the DNA backbone.

In certain situations, DNA crosslinks can form involving reaction of the nucleic acid structure with another, usually nucleophilic chemical entity that contains at least two reactive centres. This can result in 1. intrastrand crosslinks, where the mutagen covalently bonds to bases within the same DNA strand, 2. interstrand crosslinks, where the mutagen covalently bonds to bases within complementary DNA strands or 3. formation of DNA-protein complexes. Any combination of the above 'classical' DNA repair pathways can be invoked as crosslinking can cause single base changes, large structural distortions and/or breakage events (Peter J McHugh, Spanswick and Hartley, 2001).

A comprehensive list of the components of each DNA repair pathway can be found at the Trypanosomatid DNA repair resource; https://sites.google.com/site/trypdnarepair/home.

1.5.2 Trypanosomal DNA repair pathways

Comparative studies relating to how *T. brucei* repairs DNA damage have been performed with many of components of the HR, MMR, BER, TLS, NER and MMEJ pathways identified. A comprehensive list of the components of each DNA repair pathway found at the Trypanosomatid DNA repair resource (reviewed in (Passos-Silva *et al.*, 2010; Genois *et al.*, 2014)). A key finding from such metadata analyses corroborated by experimental observations is that trypanosomes lack a functional NHEJ pathway despite expressing several components of this system (*e.g.* Ku70, Ku80 and ARTEMIS) (Glover, McCulloch and Horn, 2008; Genois *et al.*, 2014).

Functional analysis of the trypanosomal NER pathway indicates that the transcription coupled pathway preferentially operates relative to the global-genome mechanism (Machado *et al.*, 2014). This may reflect that trypanosomatid gene expression is polycistronic with

transcription of the vast majority of genes effectively being 'on' all the while with regulation of each cistron occurring post-transcriptionally. As such there is an absolute requirement in these parasites to have their TC-NER mechanism constantly functioning as a sentinel to identify and repair lesions encountered during transcription. In other organisms, stalled RNA polymerase acts to target CSA and CSB to the site of DNA damage. These enzymes displace the polymerase from the DNA and recruit TFIIH NER factors to promote DNA helix unwinding (*e.g.* XPB, XPD, etc) to create an open bubble structure that is maintained in this state by a preincision complex (*e.g.* RPA, XPA) prior to a dual incision event mediated by the ERCC1-XPF complex and XPG (Lagerwerf *et al.*, 2011; Genois *et al.*, 2014; Iyama *et al.*, 2015). This results in single stranded DNA that is filled in by DNA polymerases using the undamaged, complementary strand as template followed by ligation of the sugar-phosphate backbone. The GG-NER system differs slightly from the TC-NER counterpart primarily in how the damage is detected which involves the damage recognition activities of DDB1/DDB2 or XPC/Rad23b complexes. These then recruit TFIIH NER factors and promote repair as described for TC-NER.

Several components of TC-NER (*e.g.* TbCSB, TbXPB, TbXPBz and TbXPG) and GG-NER (TbXPC) have been identified and characterised in *T. brucei* with their role in the corresponding pathway confirmed. Intriguingly, a number of elements such as CSA, XPA, DDB2 and components of the TFIIH complex are apparently missing (Machado *et al.*, 2014). Based on such differences it is implicit that this parasites TC- and GG-NER pathways are distinct from model eukaryotic organisms, a feature that may be exploitable in terms of chemotherapeutic development.

Cells are able to bypass certain DNA lesions using the TLS pathway with different systems predominating at various points within the cell cycle. During the S-phase, the so-called polymerase switching model operates. Here, stalling of DNA replication complex at a site of DNA damage causes posttranslational modification of proliferating cell nuclear antigen (PCNA) that leads to replacement of the incumbent DNA polymerase within the replication complex with a TLS specific DNA polymerase (Waters *et al.*, 2009). At other times within the cell cycle, the TLS pathway operates through the so-called gap-filling model (Shen *et al.*, 2006; Waters *et al.*, 2009). In this situation, detection of a stalled transcription complex by NER factors can result in recruitment of the TLS specific DNA polymerases (Enoiu, Jiricny and Schärer, 2012). Using ssDNA present in a transcription bubble as template, these protein

complexes guide the addition of nucleotides at the lesion site to generate a dsDNA molecule with DNA ligases then operating to maintain the integrity of the sugar-phosphate backbone. Several TLS specific DNA polymerases can operate in these two models with these differing in their fidelity: TLS DNA polymerases are said to be error-free (high fidelity) or error-prone (low fidelity). In the latter case, the polymerase activity can lead to 'secondary' base mismatch mutations that require downstream repair (*e.g.* by the MMR pathway). To date, little is known about the trypanosomal TLS pathways although these systems are known to operate with at least five TLS polymerases (polymerase nu (PolN), polymerase zeta (PolZ), polymerase theta (PolQ), polymerase eta (PolH) and polymerase kappa (PolK)) implicated in these activities (Machado *et al.*, 2014; Zurita-Leal, 2016). Two trypanosomal TLS polymerases, PPL1 and PPL2, have been implicated with trypanosomal TLS activity (Rudd *et al.*, 2013).

Many trypanosomal components of both HR pathways, single strand annealing and synthesis-dependent strand annealing pathway, have been functionally characterised and linked to one way these parasites undergo antigenic variation (Horn, 2014; Morrison, McCulloch and Hall, 2015). In other organisms, the synthesis-dependent HR pathway relies on detection of a break by the MRE11-RAD50-NBS1 (MRN) complex with DNA resection processing single stranded DNA (ssDNA). This DNA acts as the guide for the strand exchange reaction, carried out by RAD51 and maintained by the activities of BRCA2, PALB2, RAD52 and RAD51 paralogs. This complex carries out the homology search for an intact sister chromatid sequence with RAD51 and RAD54 mediating the cross-over. With strand synthesis complete, the invading strand dissociates from the complex and anneals to the complementary sequence with gaps filled and nicks ligated to complete repair. The single strand annealing pathway operates in a RAD51-independent complex with substantial cleavage of 5' and 3' termini at a DSB followed by single strand annealing and ligation. Several components of the single strand annealing and synthesis-dependent strand annealing pathway have been identified and characterised in *T. brucei* including the initial detection and resection activities of TbMRE11 and TbRAD50, recombinase activity of TbRAD51 and ancillary activities of TbBRCA2 and TbRAD51 paralogues (TbRAD51-1 to TbRAD51-4) (McCulloch and Barry, 1999; Robinson, McCulloch, Conway, Browitt and Barry, 2002; Hartley and McCulloch, 2008; Dobson *et al.*, 2011). This work has shown that not all components of the HR pathway present in this parasite with absence of RAD52 and PALB2 noted in various *in silico* analyses of the *T. brucei* genome (Genois *et al.*, 2014).

Mismatch repair, often referred to as the postreplicative repair pathway, is employed at mismatched base errors with damage recognition carried out by the MutS (MSH2, MSH6 and MSH3) heterodimer and lesions cleaved by the endonuclease activity of MutL (MLH1, MLH3 and PMS1) homodimers. This complex recruits EXO1, a 5'-3' exonuclease, which carries out exonucleolytic degradation of the nucleotide. DNA synthesis is carried out by a DNA polymerase with nicks in both strands sealed by DNA ligases. Almost all components of the MMR machinery are conserved in trypanosomatids: MutS-like genes in the parasite (*e.g.* TbMSH2, TbMSH8 and TbMSH3) have been identified and characterised to play a role in both nuclear and mitochondrial DNA repair (Barnes and McCulloch, 2007), MutL-like genes, primarily PMS1 and MLH1, have also been functionally characterised however no characterisation of an EXO1 homologue has been studied (Szankasi and Smith, 1992; Bell *et al.*, 2004).

1.6 Interstrand crosslinks and their repair

The covalent bonding of two complementary strands of DNA leads to formation of an interstrand crosslink (ICL). This form of DNA damage is highly detrimental to a cell as it can block any process that requires DNA strand separation and can result in stalling of the transcription and/or replication machinery, mismatch errors and loss of genomic material. As few as one ICL in a bacterial cell or 20 in a mammalian cell can result in the death of that cell (Dronkert and Kanaar, 2001). To survive such insults, a series of activities have been co-opted to generate multiple, complementary and overlapping repair systems. These function at different points in the cell cycle with the nature of the mechanisms varying between groups of organisms (P J McHugh, Spanswick and Hartley, 2001; Clauson, Schärer and Niedernhofer, 2013). As such, comparative studies involving humans don't necessarily inform what the situation is in yeast, which in turn do not reflect mechanisms employed by trypanosomes. Therefore, each organism's ICL REPAIRtoire is distinct.

1.6.1 ICLs: definition, formation and significance

ICLs are predominantly but not exclusively formed by exogenous chemicals with many anticancer agents exploiting their detrimental effects. In rare cases, ICLs can be formed endogenously by ionizing radiation, oxidative stress and simple unsaturated aldehydes that are generated during lipid peroxidation and prostaglandin synthesis promoting such lesions (Noll, Mason and Miller, 2006; Clauson, Schärer and Niedernhofer, 2013). These ICL inducing agents have two reactive centres with one of these commonly becoming activated and reacting

with a guanine residue on one DNA strand (Noll, Mason and Miller, 2006). This interaction then promotes activation of the second reactive centre, facilitating binding to a nearby guanine. Many ICL forming chemicals favour interacting with this particular base due to the large electrostatic potential that occurs between two guanine residues resulting in preference of alkylation events at guanine-rich regions of DNA (Noll, Mason and Miller, 2006). The sequences targeted by different ICL promoting compounds vary *e.g.* nitrogen mustards preferentially reacting at 5′-GNC-3′ sites, mitomycin C favouring 5′-CG-3′ sequences, and platinum-based compounds promoting the binding at 5′-GC-3′. An exception to this pattern are the psoralen-based compounds as they show a marginal preference for 5′-TA-3′ and 5′-AT-3′ sequences (Figure 1.7).

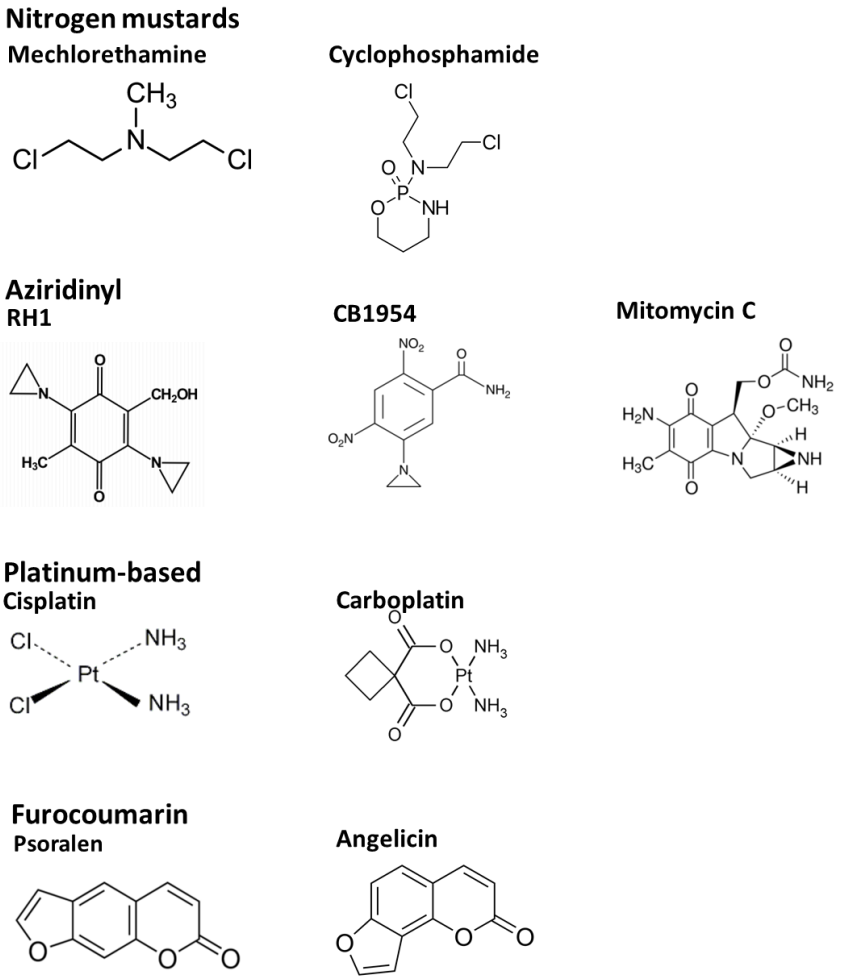

Figure 1.7: Structures of different types of ICL inducing agents.
Structures redrawn on ChemDoodle.

Nitrogen mustards are chemical structures that contain a chloroethylamine grouping in their backbone and function by promoting alkylation events primarily affecting nucleic acid targets.

For those that induce ICLs, *e.g.* mechlorethamine and cyclophosphamide (Figure 1.7), at least two such groupings are present on the structures' backbone, both of which can form highly reactive and nucleophilic centres. In the presence of DNA, particularly where 5′-GNC-3′ sequences are found, the terminal chloride found on one arm of the alkyl reactive centre is displaced to form an aziridinium ion that attacks the N7 position of a guanine resulting in the alkylation of that base. In 1 to 2% of cases the terminal chloride found on the second reactive centre undergoes a similar event leading to ICL formation (Dronkert and Kanaar, 2001). This damage results in structural distortion of the double helix (Rajski and Williams, 1998).

A number of ICL forming compounds contain at least one aziridinyl grouping in their structure with these being embedded within ('trapped') or as a side chain ('free') on the chemicals backbone. In all situations, an activation event is required to promote formation of a reactive centre. For compounds such as CB1954 and RH1 (Figure 1.7) that contain two or more 'free' aziridinyl moieties, the above leads to formation of an aziridinium ion that then promotes ICL formation analogous to that noted for the nitrogen mustards. In chemicals such as the mitomycins, where the azirinidyl is 'trapped', activation causes a redistribution of electrons through the indolequinone ring structure that promotes DNA binding to sites neighbouring the aziridinyl. Initially, a methoxy grouping adjacent to the aziridinyl is eliminated from the chemical backbone leading to formation of a quinone methide. In the presence of DNA, particular where 5′-CG-3′ sequences are found, the methide then functions as a nucleophile to promote formation of firstly a monoadduct at the N2 position of a guanine base on strand of DNA then a bisadduct by reaction with the N2 position of a guanine base on the complementary strand (Meredith *et al.*, 2017).

Other ICL inducing agents of note include the platinum-based and furocoumarin-containing compounds (Figure 1.7). In the case of the former, as represented by cisplatin and carboplatin, moieties in the structure (*e.g.* the chloride ions in cisplatin) are slowly displaced by water to create aquo complex intermediates with the water subsequently supplanted by a purine nucleotide, particularly guanine, at the N7 position. Most damage *via* platinum-based compounds occurs within the same DNA strand (intrastrand crosslink) with a minor component (~10%) being interstrand in nature (Peter J McHugh, Spanswick and Hartley, 2001). In the latter case, 5′-CG-3′ sequences being particularly prone to covalent binding.

Furocoumarin-containing compounds such as psoralen and angelicin promote ICLs by a mechanism distinct from that described above. Analogous to UV-induced pyrimidine dimer formation, these are photoactivated such that their furan and pyrone rings form cyclobutane structures with thymidine residues found on opposite DNA strands leading to the crosslink formation and intercalation at 5'-TA-3′ and 5′-AT-3′ sequences (Friedberg, 1995). As with the platinum-based agents, ICL formation constitutes a minor component of any resultant DNA lesion.

To conserve genome integrity, all cells exploit various combinations of enzymes from the "classical" DNA repair pathways to resolve ICL damage. The precise makeup of these systems is unclear as different mechanisms predominate at different stages in the cell cycle while evolutionary diverse organisms employ distinct mechanisms to accomplish this task (Lehoczký, McHugh and Chovanec, 2007; McVey, 2010; Hashimoto, Anai and Hanada, 2016). Broadly, in a mechanism initiated by stalling of a DNA replication complex, the damaged DNA is processed through "unhooking" of the ICL from the nucleic acid backbone with the concomitant formation of a DSB (Hashimoto, Anai and Hanada, 2016). Using complementary DNA sequences (*e.g.* from a sister chromatid), enzymes from the HR pathway function to fix this break and, in conjunction with components from the TLS pathway, completely remove the "unhooked" ICL from the DNA backbone. In a DNA replication independent mechanism, components of the NER pathway recognise, cleave and "unhook" the ICL from one strand of the DNA backbone (Hashimoto, Anai and Hanada, 2016). This generates a single stranded gap within the nucleic acid molecule with the dsDNA structure restored through TLS activity. Another round of NER and TLS then completely removes the "unhooked" ICL from the DNA. As the above mechanisms involve TLS, which can be error prone, the MMR pathway operates as a sentinel to fix any damage that may arise. Due to the complexity of ICL repair, the focus of this literature review will exclusively centre on the ICL repair systems found in *Escherichia coli*, *Saccharomyces cerevisiae* and mammalian cells.

1.6.2 ICL repair in *E. coli*

Over the last 40 years, a picture of the *E. coli* ICL repair system, often referred to as the Cole Model of ICL repair (Cole, 1971) (Figure 1.8), has been elucidated and shown to involve the coordinated activity of components of the NER and HR pathways. Here, the UvrABC constituents of the bacterial NER pathway function in the 1. DNA damage recognition (UvrA and UvrB), 2. unwinding the DNA strand surrounding the lesion (UvrB), and 3. cleaving the

DNA backbone either side of the ICL (UvrC) (Houten *et al.*, 1986). In certain cases where the torsion strain caused by the crosslinking event creates structural distortions to the DNA double helix, additional helicase activities (e.g. UvrD) can be employed to aid the unwinding process (Noll, Mason and Miller, 2006). The above generates an 'unhooked crosslink' with the ICL remaining covalently attached to one strand of the DNA backbone. Sequences immediately upstream of the initial incision are processed by the exonuclease activity of DNA Polymerase I (Pol I) which in turn recruits RecA from the HR pathway. By virtue of its recombinase activity, RecA then promotes strand invasion from a related DNA sequence, a process aided by the activities of RecB, RecC, and RecD (these act in strand recognition, binding of terminal ends and processing of breaks). The above results in a Holliday junction that can be resolved using the RuvABC complex (Houten *et al.*, 1986). Following recombination, a second round of UvrABC-mediated incision is performed on the other strand, releasing the 'unhooked crosslink' from the DNA backbone to create a gap that is filled by Pol I and DNA ligase activities.

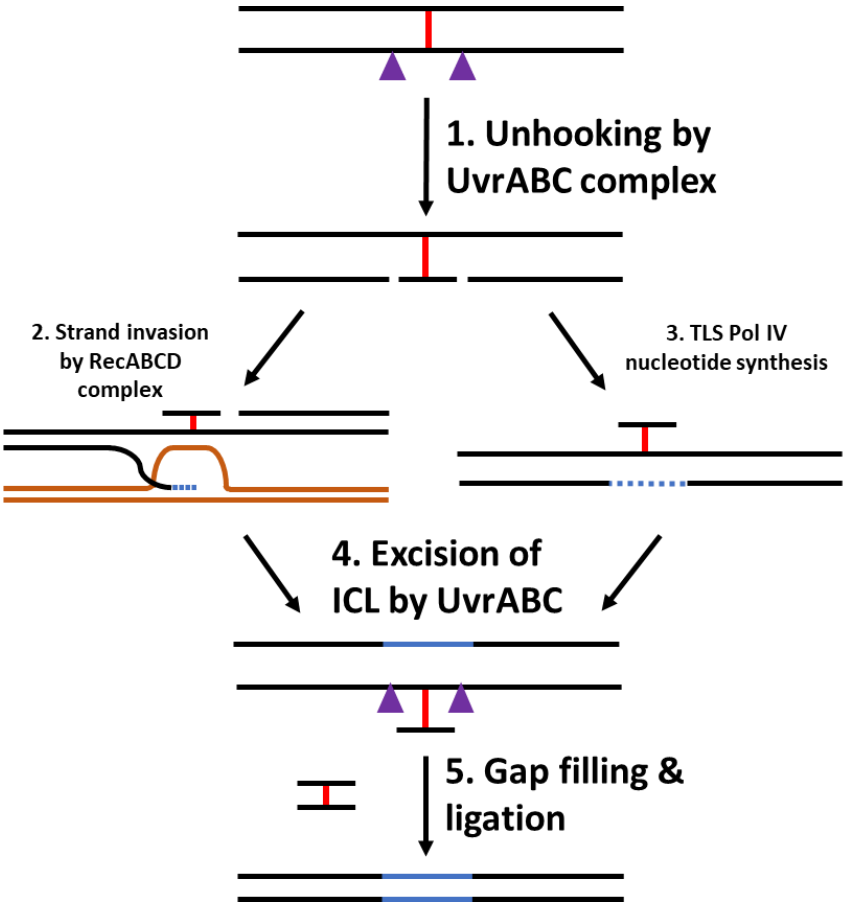

Figure 1.8: ICL repair systems in *E. coli*.
E. coli expresses two distinct ICL repair systems one being HR-dependent and the other being a TLS-dependent mechanism. Crosslinked DNA (DNA and crosslink shown in black and red, respectively) is unhooked from the double helix by the activity of NER factors (purple arrows)

(part 1). The unhooked ICL remains attached to one of the DNA strands while a small formed in the other. This gap can then filled by a HR-mediated strand invasion process (part 2) or a TLS-dependent mechanism (part 3): The homologous template used in the former is shown in brown while the newly synthesised DNA noted in the latter is in blue. The ICL is then completely removed from the DNA structure by a second round of NER (part 4) followed by DNA polymerase and DNA ligase activities (part 5). Parts 1, 2, 4 and 5 constituent the so-called Cole Model for ICL repair. Imaged adapted from (Huang and Li, 2013).

In addition to the above Cole Model, an alternative recombination-independent ICL repair system has been also proposed. In this case, following the initial UvrABC incision, DNA Pol IV catalyses TLS activity past the still attached 'unhooked crosslink' with the integrity of the sugar-phosphate backbone maintained by downstream DNA ligase activity. As above, a second round of UvrABC incision completely removes the crosslink from the genome with Pol I and DNA ligase activities filling in the resultant gaps (Kumari *et al.*, 2008)

1.6.3 *S. cerevisiae* ICL repair systems

Many of the features displayed in the *E. coli* ICL repair system are mirrored in simple eukaryote organisms such as budding yeast, *S. cerevisiae*, although the complexity and overlapping nature of these systems alters throughout the cell cycle (Figure 1.9). Throughout most of this cycle (G0-, G1-, early S- and G2-phase), a NER and TLS pathway similar to the bacterial mechanism predominates, which additionally incorporates novel ICL repair specific activities displayed by the nuclease PSO2 (also known as SNM1) (Part A of Figure 1.9). In this system, stalling of the transcriptional machinery at an ICL promotes ubiquitination of PCNA that then functions to recruit components, including nucleases, of the NER pathway. These proceed to mediate the unhooking of the ICL from one strand of the double helix (Waters *et al.*, 2009). RAD1 (with RAD10) and RAD2 possess endonuclease activities that cleave sequences 5' and 3' around the damaged DNA, respectively, with RAD4/RAD14 postulated to aid in recognition of the adduct and the RAD3/RAD25 helicases acting to unwind the DNA helix (Sarkar *et al.*, 2006). The PSO2 nuclease then processes the 'unhooked crosslink' to remove all the bases up to and across the linkage present within this sequence (Bonatto *et al.*, 2005). The resultant gap is then filled by damage-tolerant TLS polymerases (*e.g.* REV1 and REV3) with the sugar-phosphate backbone reformed by DNA ligases (Ho *et al.*, 2011). As with the *E. coli* systems, a second round of NER coupled with DNA polymerase/ligase activities help to completely remove the ICL from the DNA template.

Cells that encounter ICLs while in the late S-phase utilize a series of factors from the NER, MMR and HR pathways that act in concert help resolve the lesion (Part C of Figure 1.9). In this system, the NER pathway is believed to carry out the initial incision events either side of the ICL. If not repaired by the PSO2-dependent pathway, an approaching replication fork can stall in the immediate vicinity of the lesion resulting in recruitment of MPH1, MUTSα and MGM101. MPH1 causes the replication fork to reverse and allows loading of EXO1 onto the 'unhooked crosslink' (Ward *et al.*, 2012). This nuclease then removes the bases from this sequence up to but not beyond the ICL, with any resulting gap on the other strand filled by damage-tolerant TLS polymerases and DNA ligases. A second round of NER activity begins processing the DNA strand containing the 'unhooked crosslink' with the lesion being completely uncoupled from this backbone with any gap filled *via* DNA polymerase/ligase activities. Before DNA replication can recommence, the nascent leading or lagging (one not

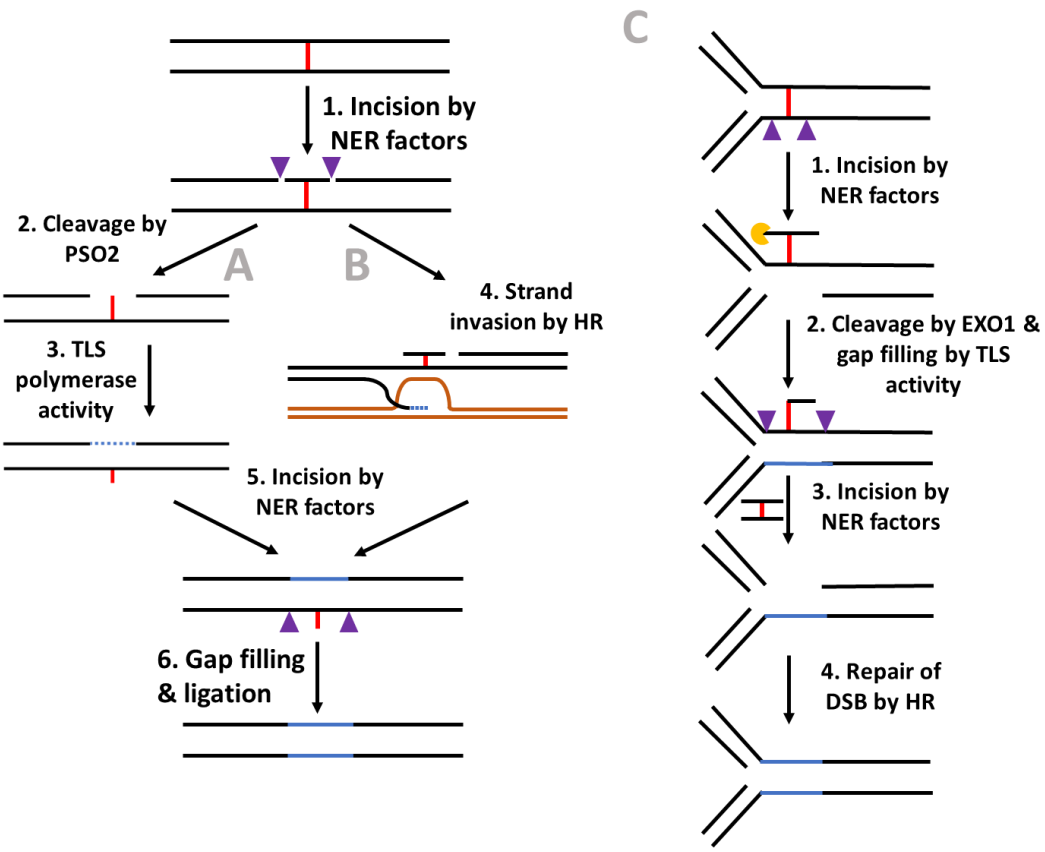

Figure 1.9: ICL repair systems in yeast.
Yeast express at least three distinct ICL repair mechanisms whose activities appear to be cell cycle dependent. Initial incision of the damaged DNA is common to these systems and employs NER factors. For cells in the G0-, G1-, early S- or G2 phase, a PSO2/TLS-dependent mechanism functions (A) while cells in the S-phase employ HR-based activities (B). An alternative G2-phase system that functions independently of PSO2 and involves EXO1 in conjunction with TLS activities has also been reported (C). The final steps of mechanisms A,

B and C is common with the ICL completely removed from the DNA structure by a second round of NER followed by DNA polymerase and DNA ligase activities. Starting DNA and crosslink are shown in back and red, respectively while the purple arrows correspond to the incisions made by NER factors. Newly synthesised DNA as a result of DNA repair is shown in blue, the homologous DNA template used in the HR mechanism is shown in brown while newly synthesised leading and lagging DNA strands associated with replication forks is in green. Image adapted from (Barber *et al.*, 2005)**.**

both) DNA strand undergoes a DSB that is repaired by components of the single strand annealing HR pathway: RAD52 is recruited to the site of DNA damage through interaction with MGM101 with ancillary factors such as CHL1 and SLX4 aiding this event (Kenneth F. Grossmann *et al.*, 2001; Ward *et al.*, 2012; Munari *et al.*, 2013).

In addition to the PSO2-dependent G2-phase ICL repair system, an alternative mechanism may also operate (Part B of Figure 1.9). Incision and processing events possibly involving NER components leads to unhooking of the ICL with sister chromatids then providing a template for MRE11- and RAD51-dependent HR (Kenneth F. Grossmann *et al.*, 2001). It is hypothesised that a second round of NER coupled with DNA polymerase/DNA ligase activities completely removes the ICL from the genome.

1.6.4 Mammalian ICL repair

Two cell-cycle dependent ICL repair systems have been identified in mammalian cells. A transcription-coupled ICL repair system utilises components of the NER and TLS pathways as well as the ICL-specific activity of SNM1 (homolog of PSO2) for removal of crosslinks (Figure 1.10). The second and dominant ICL repair system termed the Fanconi Anaemia (FA) pathway is a replication-coupled mechanism (Sancar *et al.*, 2004). This system is favoured due to a readily available sister chromatid sequence which enables error-free repair (mammalian cells are diploid organisms) (Hashimoto, Anai and Hanada, 2016) (Figure 1.11). This system was initially discovered through genetic profiling of patients with Fanconi Anaemia, a genetic condition associated with bone marrow failure, of which over 20 linkage groups and hence defective genes (termed FA factors) have been described (Moldovan and D'Andrea, 2009; Krishnan, Tay and Ito, 2015).

1.6.4.1 *ICL repair in transcriptionally active cells*

In transcriptionally active cells, an ICL can block progression of the transcription machinery leading to stalling of the RNA polymerase complex. This results in recruitment of factors such as CSB and UHRF1 (a RING finger protein) to the lesion site with these interacting directly or

through a partner(s) with other DNA repair enzymes such as SNM1, XPG and XPF-ERCC1 (Iyama *et al.*, 2015; Hashimoto, Anai and Hanada, 2016). The XPF-ERCC1 and XPG endonucleases make the initial 5' and 3' incisions around the ICL with nucleolytic degradation of the resultant unhooked sequence occurring through SNM1 (PSO2 in yeast) processing (Al-Minawi *et al.*, 2009; Wood, 2011; Zhang and Walter, 2014; Abdullah *et al.*, 2017). The resultant gap on the strand not containing the unhooked ICL is then filled using damage tolerant TLS polymerases such as Pol ζ, Pol η, Pol ι, Pol Θ or Pol κ in conjunction with DNA ligase (Sarkar *et al.*, 2006; Ho *et al.*, 2011; Sharma and Canman, 2012). Once this strand has been repaired the ICL is completely removed by a second round of NER incision, DNA polymerase and DNA ligase activities.

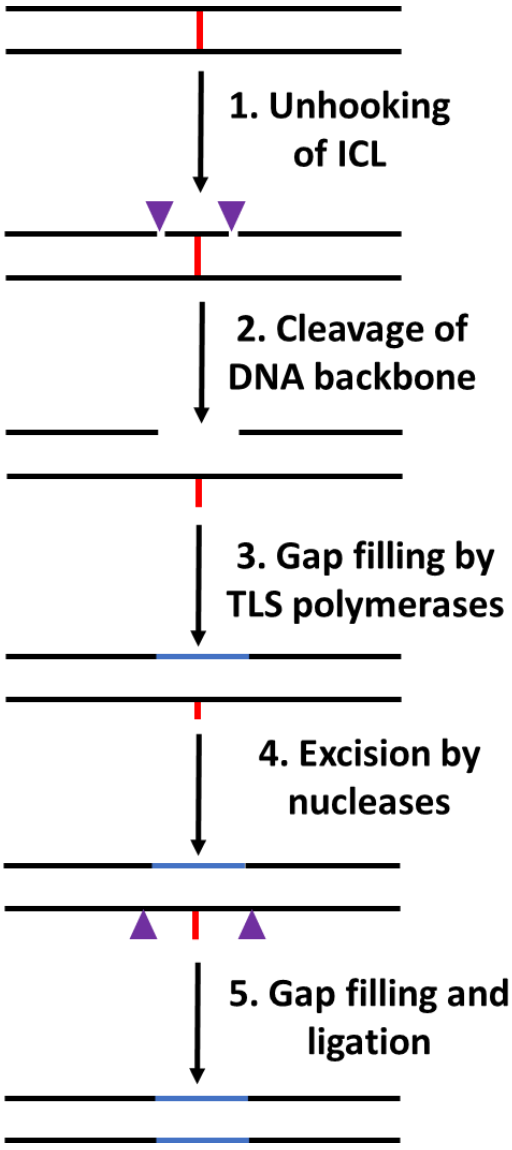

Figure 1.10: ICL repair system in transcriptionally active mammalian cells.
The mechanism outlined here is analogous to that of the Cole Model (see Figure 1.8). Image adapted from (Huang and Li, 2013).

1.6.4.2 *ICL repair in dividing cells*

ICL-induced collapse of replication forks are recognised and repaired in a mechanism that involves: 1. recognition of the damaged DNA and assembly of eight proteins that form the so-called FA core complex, 2. activation of the FANCD2/FANCI heterodimer that functions as a recruitment complex and 3. association of effector factors that operate to resolve the ICL. The activities of all these proteins constitute the FA pathway (Figure 1.11) with the components involved listed in Table 1.2: Note, the factors listed in this table are those that have been directly associated with FA but it is clear that other components are implicated in this repair system but loss of these activities do not result in the genetic condition (or have not yet been identified).

Factor	Function/DNA
FA core complex	
FANCA	Creation of FA core complex in nucleus
FANCB	FA core complex structure dimerization.
FANCC	Adaptor for substrates in FA core complex
FANCE	Adaptor for substrates in FA core complex
FANCF	Anchor FANCM to FA core complex
FANCG (XRCC9)	Creation of FA core complex in nucleus
FANCL	Part of the FA core complex as a E3 ligase to alter ubiquitinated proteins
FANCM (MPH1)	Helicase activity to detect damage and upregulate FANCD2/FANCI for ubiquitination
FA recruitment complex	
FANCD2	Ubiquitinated when DNA damage sensed by FA core complex
FANCI	Ubiquitinated when DNA damage sensed by FA core complex
FA effector proteins	
FANCD1 (BRCA2)	Homologous recombination
FANCJ (CHL1)	Helicase downstream of FANCD2/FANCI ubiquitination
FANCN (PALB2)	Regulates and interacts with FANCD1 after ubiquitination of FANCD2
FANCO (RAD51C)	Homologous recombination
FANCP (SLX4)	Endonuclease to cleave ICL
FANCQ (XPF)	Exonuclease to cleave ICL
FANCR (RAD51)	Homologous recombination
FANCS (BRCA1)	Unloading of replication machinery at stalled replication fork
FANCT (UBE2T)	E2 enzyme for ubiquitin transfer to substrates
FANCU (XRCC2)	Homologous recombination
FANCV (MAD2)	Cell cycle checkpoint protein

Table 1.2: FA Repair factors:
The above table depicts the key proteins involved in the Fanconi Anaemic Repair Pathway including their aliases (in parenthesis) where available (Moldovan and D'Andrea, 2009; Genois *et al.,* 2014).

ICL damage can lead to stalling of a replication fork(s) and alteration of the chromatin structure. Together, this alteration in the DNA configuration is recognised by the FANCM helicase that goes on to recruit other components of the FA core complex (FANCA, -B, -C, -E, -F, -G and -L) to the lesion site, a process aided by various ancillary factors such as FAAP24, MHF1 and MHF2 (Moldovan and D'Andrea, 2009; Tan and Deans, 2017). Within this complex, FANCF acting as a scaffold protein, FANCA and FANCG function to guide the complex to nucleus and to site of DNA damage within the genome while FANCC and FANCE act as adapters for various substrates required for downstream activities: Note that the displacement of the replication fork does not occur during the assembly of the FA core complex but is reversed back along the newly synthesised DNA strands under the guidance of FANCM. The key role of the FA complex is to act as a ubiquitin ligase, an activity mediated by FANCL and FANCT, resulting in the monoubiquitination and activation of lysine residues present on FANCD2 and FANCI (Moldovan and D'Andrea, 2009; Ward *et al.*, 2012).

Activation of the FANCD2/FANCI heterodimeric results in recruitment of FAN1 and FANCP (SLX4) to the site of DNA damage which together with FANCQ (XPF)-ERCC1 and MUS81-EME1 cleaves the DNA backbone at sequences 5' and 3' to the DNA lesion ((Moldovan and D'Andrea, 2009; Siddiqui *et al.*, 2017). This results in the unhooking of the ICL from one of the DNA strands creating a gap within the other strand adjacent to where the newly synthesised DNA strands associated with replication forks is found (Part A of Figure 1.11). TLS polymerases along with DNA ligase fill in the gap and links the parental ICL-containing DNA molecule to one of the newly synthesised DNA strands. The ICL is then completely removed by a second round of NER/DNA polymerase and DNA ligase activity. During the above gap filling, the other newly synthesised DNA strand forms a DSB that is presumably recognised by the MRN complex. This guides components of the HR pathway (*e.g.* FANCD1, FANCR, FANCO, FANCU) to mediate recombination between the broken dsDNA molecule with the newly repaired DNA structure generated from the second round of NER/DNA polymerase and DNA ligase activities. This results in reformation of the Y-sharked forked structure that can serve as a template for recommencement of DNA replication (Wang, 2007).

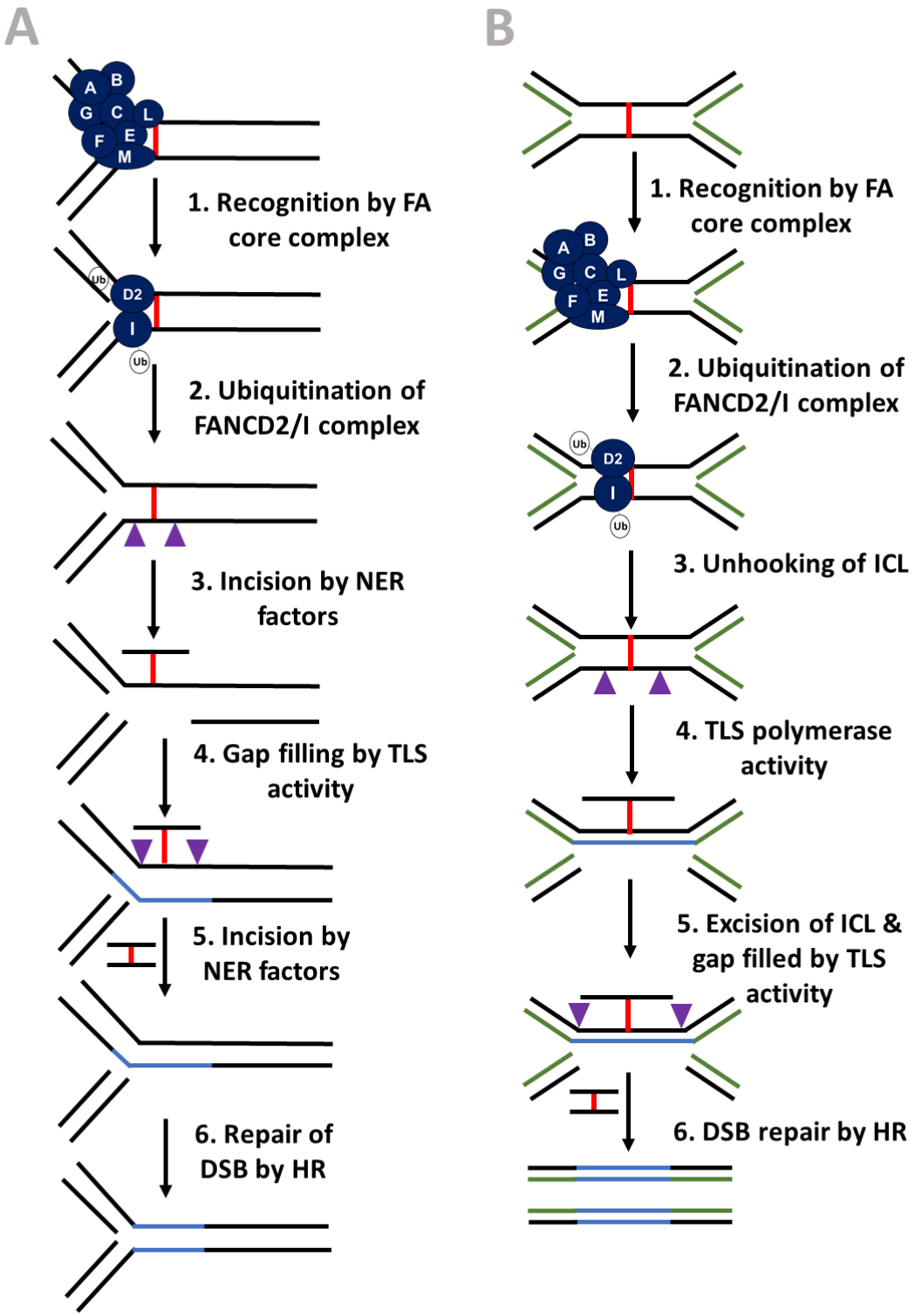

Figure 1.11: ICL repair in dividing mammalian cells.
FA factors (dark blue) recognise crosslinked DNA (red and black) through stalling of a single replication fork (A) or convergence of two replication forks (B) resulting in the recruitment of FA effector proteins. These proteins unhook and process the DNA surrounding the ICL to create a double strand break which is repaired by the HR pathway (blue). Given this pathway is activated by stalling of the replication fork, leading and lagging strands are shown in green. The activity of TLS polymerases fill any remaining gaps in the DNA strand (blue). The ICL is completely removed from DNA by a second round of incision by NER factors. Image adapted from (Huang and Li, 2013; Krishnan, Tay and Ito, 2015).

Due to the bidirectional nature of DNA replication, ICLs can actually cause the stalling of two converging DNA replication forks (I. Chaudhury, Stroik and Sobeck, 2014; Zhang and Walter, 2014). Such X-shaped structures (Part B of Figure 1.11) can be resolved using the mechanism outlined above although in this case two of the other newly synthesised DNA strands both form DSBs. In this situation, the above HR mediated repair systems are activated with the newly repaired DNA strand serving as template. The outcome of this event is formation of two dsDNA molecules and the disassociation of the replication machinery.

1.7 ICL repair in *T. brucei*

To date reports relating to how trypanosomes resolve ICLs are limited although some components of the NER pathways (*e.g.* TbXPC, TbCSB, TbXPG and TbXPBz) may potentially be involved in this process (Machado *et al.*, 2014). Recent work has established that *T. brucei* expresses TbSNM1, a member of the SNM1/PSO2 family of nucleases (Sullivan *et al.*, 2015). This group of enzymes are characterised by the presence of metallo-β-lactamase (MβL; pfam12706) and β-CASP (named after its representative members **C**PSF, **A**rtemis, **S**NM1 and **P**SO2; pfam10996) domains that together function to bind zinc atom(s) that is central to their catalytic activity (Allerston *et al.*, 2015) (Figure 1.12). Most eukaryotic organisms express one SNM1/PSO2 homologue with these playing a key and specific role in ICL repair (Li and Moses, 2003): They do not participate in the resolution of any other form of DNA damage. Mammals are unusual in that they possess three distinct orthologs belonging to this family of nucleases with SNM1A (or DRLCE1A) functioning in solely ICL repair, SNM1B (or Apollo) playing additional roles in the processing DNA hairpin structures and telomeric maintenance, while SNM1C (or Artemis) is involved in generate antibody diversity through VDJ recombination (Dominski, 2007; Hazrati *et al.*, 2008).

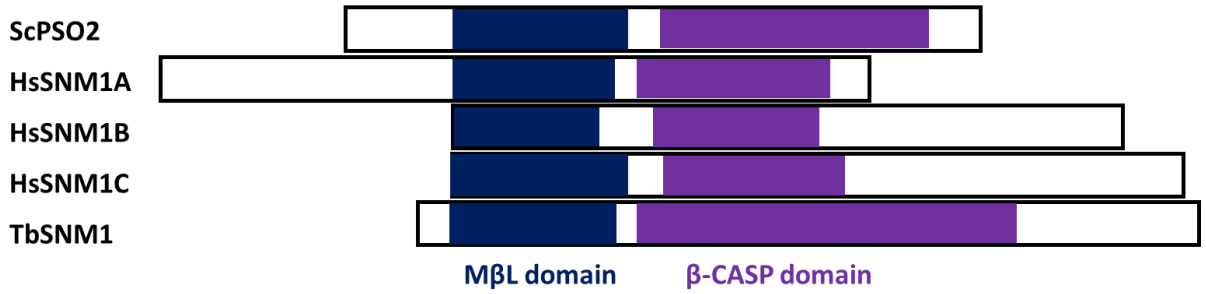

Figure 1.12: Comparison of domain structure in SNM1/PSO2 nucleases.
Schematic diagrams showing the domain alignment of the yeast (ScPSO2), human (HsSNM1A, HsSNM1B and HsSNM1C) and trypanosomal (TbSNM1) SNM1/SPO2 homologues (Sengerová *et al.*, 2012).

For those members of the SNM1/PSO2 family that have been characterised, a 5′-3′ exonuclease and flap endonuclease catalytic activity have been reported dependent upon the substrate present which play a key role in the processing of unhooked ICLs (Li, Hejna and Moses, 2005; Hazrati *et al.*, 2008). Unusually, these enzymes mediate the nucleolytic degradation of such unhooked regions up to and beyond the crosslink with this resulting in them playing a key role in the resolution of such damage. The structure of human SNM1A and B has recently been solved and shown to contain an MβL fold consisting of 11 β-sheets with the β-CASP domain inserted between strands 10 and 11 (Figure 1.13) (Allerston *et al.*, 2015). Several charged residues have been implicated in zinc co-factor coordination although the number of metals ions appears to vary between the two mammalian isoforms; SMM1A binds one zinc ion, facilitated by residues H732, H734, D736, H737, H793, D815, D838, E993, and H994 while SNM1B interacts with two metal ions using these same conserved residues Binding of the nuclease to the template is *via* a wide DNA binding groove located between the two domains with the size of this region governing the ability of the enzyme to read through a crosslink.

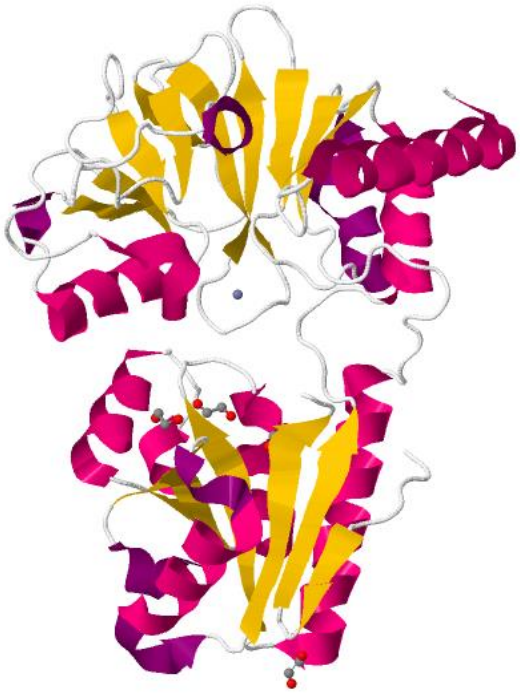

Figure 1.13: Overall structure of SNM1A.
SNM1A, PDB 4B87, is shown as a cartoon representation with α-helices shown in purple and β-sheets in yellow. The zinc ion is centrally depicted as a grey sphere. The β-CASP domain (bottom) is an insert between MBL (top) strands 10 and 11.

1.8 Research Aims

The goal of this project centres upon deciphering the repair systems used by *T. brucei* to resolve ICLs. By analysing these mechanisms, we aim to unravel their importance to the pathogen with the future intention of exploiting these systems in drug development. The specific aims are to:

1. Identify which *T. brucei* DNA repair proteins are involved in resolving ICLs within the parasite.
2. Evaluate for any epistatic or non-epistatic interaction between components of the trypanosomal ICL repair system(s)
3. Assess the relationship between TbSNM1 structure & function by analysing the relative importance of key amino acids postulated to be involved in catalytic activity, nucleic acid substrate specificity and localisation.
4. Inform on the mechanism of action of clinically used and novel trypanocidal prodrugs

2. Material and Methods

2.1 Cell culturing and storage

2.1.1 Maintenance of bacterial strains

The *E. coli* strain XL1-Blue (*rec*A1, *end*A1, *gyr*A96, *thi*-1, *hsd*R17(rK-, mK+), *sup*E44, *rel*A1, *lac*, [F', *proAB*, *lac*IqZΔM15::Tn10(tetr)]) was grown in NZCYM (10 g l^{-1} enzymatic casein digest, 1 g l^{-1} Casamino acids, 5 g l^{-1} yeast extract, 5 g l^{-1} NaCl, 0.98 g l^{-1} MgSO4; Melford Laboratories Ltd) broth or on plates (NZCYM broth supplemented with 15g l^{-1} bacteriological agar no. 1; Oxoid) at 37°C. Recombinant *E. coli* were cultivated in or on this medium supplemented with 100 µg ml^{-1} ampicillin (Sigma-Aldrich).

For long-term storage, bacterial strains were deposited at -80°C in 1 ml aliquots of growth medium containing sterile 20% (w/v) glycerol (Sigma-Aldrich) in 1.2 ml cyrogenic vials (Nunc). To revive such reserves, a small scrapping (~10-50 µl) of the frozen bacterial line was transferred into NZCYM broth (5 ml) and cultured at 37°C.

2.1.2 Maintenance of *Trypanosoma brucei brucei*

The *Trypanosoma brucei brucei* (referred to here as *Trypanosoma brucei/T. brucei*) bloodstream form (BSF) trypomastigotes stocks used in this project are listed in Table 2.1.

Organism	Source
T. brucei Lister 427, antigenic type MITat 1.2, clone 221a	(Doyle JJ, Hirumi H, Hirumi K, Lupton EN, 1980)
T. brucei 221 Tb*snm1*Δ	(Sullivan *et al.*, 2015)
T. brucei 2TAG1	(Alsford *et al.*, 2005)
T. brucei 2TAG1 Tb*snm1*Δ *gfp*-Tb*snm1*	(Sullivan *et al.*, 2015)
T. brucei 2TAG1 *gfp*-Tb*snm1*	(Sullivan *et al.*, 2015)
T. brucei 2T1 pBSF-TbNTR-9e10	(Wilkinson *et al.*, 2008)
T. brucei 2T1 RNAi-TbTAO	Prof J. Kelly, LSHTM
T. brucei SMB	(Wirtz *et al.*, 1999)
T. brucei SMB RNAi-TbSODB	(Wilkinson *et al.*, 2006)
T. brucei 221 $RH1^R$	(Meredith *et al.*, 2017)

Table 2.1: *Trypanosoma brucei* strains used in this project.

T. brucei BSF trypomastigotes were cultured at 37°C under a 5% (v/v) CO_2 atmosphere in HMI-9 (Hirumi H, 1989) (Invitrogen) media supplemented with 3g l^{-1} sodium bicarbonate (Sigma-Aldrich), 0.014% (w/v) β-mercaptoethanol (Sigma-Aldrich) and 10% (w/v) heat-inactivated Foetal Bovine Serum (Pan Biotech) (Hirumi H, 1989). Genetically modified

parasite lines were maintained in this medium containing 2.5 μg ml^{-1} hygromycin, 10 μg ml^{-1} blasticidin, 2 μg ml^{-1} puromycin, 2 μg ml^{-1} G418 or 2 μg ml^{-1} phleomycin. In certain experiments where activation of an inducible promoter was required, 1 μg ml^{-1} tetracycline (Sigma-Aldrich) was added to the growth medium.

For long-term storage, trypanosomal cultures were frozen slowly (2-3 days) to -80°C as a 1 ml aliquot (growth medium containing 20% (w/v) glycerol (Sigma-Aldrich)) in 1.2 ml cyrogenic vials (Nunc) using a Cryo 1°C Mr. Frosty™ Freezing Container (Nalgene) containing isopropanol. Samples were then transferred into liquid N_2. To revive parasite stocks, the entire 1 ml stabilate was quickly thawed, transferred to fresh parasite growth medium (10 ml) and cultured as described above.

2.2 Trypanocidal compounds and DNA damaging agents

A range of anti-parasitic agents and treatments, many of which promote DNA damage, were used in this project. These were purchased from Sigma-Aldrich (methyl methanesulfonate (MMS), hydroxyurea (HU), phleomycin, CB1954), Melford Laboratories Ltd (blasticidin, puromycin, G418, hygromycin) or Cambridge Biosciences (mechlorethamine). Other chemicals were supplied free of charge by Prof. Mike Barrett (University of Glasgow; difluoromethylornithine (DFMO), megazol), Prof. Simon Croft (London School of Hygiene and Tropical Medicine; benznidazole, nifurtimox), Prof. Longqin Hu (Rutgers, The State University of New Jersey, New Jersey, USA; LH34), and Prof. Chris Scofield & Prof. Peter McHugh (University of Oxford; ML302-HCl, ML302-F Na, Si4-33, LBE314, Ceftriaxone). UV irradiation was performed with a Stratalinker UV crosslinker (Stratagene).

2.2.1 Plasmids

The precursor plasmids used in this study to construct the trypanosomal gene deletion/disruption/expression vectors reported here are pKO-TcFHM-HYG, pKO-TcFHM –NEO, pKO-TcFHM –BLA, pKO-TcFHM–PAC (all de Padua *et al.*, 2017), pKO-TbSNM1-BLA, pKO-TbSNM1-PAC and pRPA-GFP-TbSNM1 (all Sullivan *et al.*, 2015) (Appendix 1a).

2.3 Nucleic Acid Extractions

Plasmid DNA was extracted from *E. coli* using the GeneJet™ Plasmid Miniprep kit (ThermoFischer Scientific) according to the manufacturer's on-line protocol (https://tools.thermofisher.com/content/sfs/manuals/MAN0013117_GeneJET_Plasmid_Miniprep_UG.pdf: last accessed 26/12/2017). Purified plasmid DNA was stored at -20°C.

T. brucei genomic DNA (gDNA) was extracted from Phosphate Buffer Saline (PBS: Sigma Aldrich) washed parasites (approximately 5×10^7) using the GeneJet™ Genomic DNA purification kit (ThermoFischer Scientific) according to the manufacturer's on-line 'Cultured Mammalian Cells Genomic DNA Purification Protocol' (https://tools.thermofisher.com/content/sfs/manuals/MAN0012656_Genomic_DNA_Purification_UG.pdf: last accessed 26/12/2017). Purified gDNA was stored at 4°C.

T. brucei total RNA was extracted from PBS washed parasites (approximately 5×10^7) using the RNeasy® Mini kit with the QIAshredder homogenizer and the RNase-free DNase hit add-ons (all Qiagen) according to the manufacturer's 'Purification of Total RNA from Animal Cells using Spin Technology' on-line (http://www.bea.ki.se/documents/EN-RNeasy%20handbook.pdf: last accessed 26/12/2017). All RNA samples were stored at -20°C.

2.4 Nucleic acid manipulation

2.4.1 cDNA synthesis

Complementary DNA (cDNA) was synthesized from purified *T. brucei* total RNA using the qScript™ cDNA Synthesis Kit (Quantabio). Briefly, in a 0.2 ml thin walled micro-centrifuge tube, parasite RNA (10 µl), nuclease-free H_2O (5 µl), 5X qScript Reaction Mix (containing an optimized buffer, magnesium, oligo(dT) and random primers, and dNTPs) (4 µl) and qScript reverse transcriptase (1 µl) were combined to give a 20 µl total volume. The reaction was then placed in a TC-412 thermal cycler (Techne) and subjected to once cycle at 5 minutes at 22°C, 60 minutes at 42°C, 5 minutes at 85°C and then held at 4°C.

2.4.2 DNA amplification

A variety of DNA fragments were amplified from different DNA templates (parasite genomic DNA, parasite cDNA, plasmid DNA *etc*) using oligonucleotide primers synthesised by Sigma Aldrich (see Appendix 1b for primer information) and dNTP stocks purchased from ThermoFisher Scientific. Dependent upon the downstream usage of the DNA fragment, some

reactions were performed using the high-fidelity Vent® DNA polymerase (New England Biolabs) while others were conducted with a low fidelity Taq DNA Polymerase (New England Biolabs) and their respective x10 buffers.

A typical DNA amplification reaction with a final volume of 50 µl was set up and contained 1 x Taq Buffer with KCl-Mg^{2+} free (20 mM Tris HCl, 10 mM $(NH_4)_2SO_4$, 10 mM KCl), 200 µM dNTPs, 1.5 to 5 mM Mg^{2+}, 2.5 % (v/v) DMSO (Sigma Aldrich), ~0.1 ng μl^{-1} template DNA, 50 pmol of each forward/reverse primer and 1 U Vent® or Taq DNA polymerase. Using a peqSTAR thermal cycler (PEQLab Biotechnologie GmbH) or TC-412 thermal cycler (Techne), a standard PCR programme was performed. This consisted of an initial denaturation step at 96 °C for 2 minutes, followed by 30 cycles of 96 °C for 30 seconds (denaturation), 55 °C for 30 seconds (annealing) and 72 °C for 30 seconds (extension). At the end of the 30th cycle, a further extension step of 10 minutes at 72°C was added and the samples were then incubated at 4°C. Dependent upon the template and primer combination used, the denaturation/annealing/extension conditions (temperature and time) were adjusted to optimise each amplification.

In some cases, and using MyTaq™ Red Mix (Bioline), a multiplex PCR method was used to generate several amplicons in a single reaction. A typical DNA amplification with a final volume of 25 µl contained 1x MyTaq™ Red Mix ($MgCl_2$, dNTPs, MyTaq DNA Polymerase and enhancers concentrations optimized by manufacturer), *T. brucei* gDNA (~20 ng) and forward/reverse primers (usually 1 pmol μl^{-1}; see Appendix 1b). Using a peqSTAR thermal cycler (PEQLab Biotechnologie GmbH) or TC-412 thermal cycler (Techne), a standard PCR programme was performed (see above).

2.4.3 Reverse transcription quantitative PCR

Reverse transcription quantitative PCR (RT-qPCR) was performed on *T. brucei* cDNA using PerfeCTa® SYBR® Green FastMix® kit (Quantabio). A typical reaction contained 1x PerfeCTa SYBR Green FastMix ($MgCl_2$, dNTPs, AccuFast Tag DNA polymerase, SYBR Green I dye and stabilizers concentrations optimized by manufacturer), cDNA (100 to 1000 ng) and a pre-optimised concentration of forward/reverse primer (usually 1 pmol μl^{-1}). In some cases, additional $MgCl_2$ was added to the above mix to optimise the reaction. Samples were loaded into the wells of a clear 96 well plate and an adhesive cover (Bio-Rad) used to seal the plate. Using a CFX96 Touch™ Real-Time PCR Detection System (Bio-Rad), an amplification

programme was performed. This consisted of a single initial denaturation step at 95 °C for 2 minutes, followed by 30 cycles of 95 °C for 30 seconds (denaturation), 55 °C for 30 seconds (annealing) and 68 °C for 30 seconds (extension). At completion of the amplification, a melt curve analysis was carried out to ensure target specificity. Fluorescence data collected during the amplification was analysed using CFX96 Touch Software (Bio-Rad). From the resultant sigmoidal curves, cycle threshold (CT) values were obtained and exported into Excel 2007 (Microsoft). Data was analysed by the comparative CT method (Schmittgen TD, 2008) by normalizing the sequence of interest against a standardized control (Tb*tert*) that was examined in parallel (Brenndörfer and Boshart, 2010).

2.4.4 Site directed mutagenesis

The Single Primer Reactions In Parallel-Site Directed Mutagenesis (SPRINP-SDM) approach (Edelheit, Hanukoglu and Hanukoglu, 2009), as outlined in Figure 2.1, was used to introduce specific mutations into Tb*snm1* using the template plasmid pRPa-GFP-Tbsnm1 (Sullivan *et al.*, 2015). A total of fourteen mutations were attempted in order to alter the amino acid of interest to alanine (primers used are shown in Table 2.2). Four of the residues evaluated were hypothesised to play a role in protein localisation (R428, R429, R430 & H431), one in mediating nucleic acid specificity (V518) and nine in catalytic activity/zinc co-factor binding (D40, H78, H80, D82, H83, H159, H178, D221 & H496). These were selected based on the sequence alignment shown in (Sullivan *et al.*, 2015).

A typical 25 µl SPRINP-SDM reaction was set up by combining 1× Q5 reaction buffer containing 2 mM $MgSO_4$ (New England Biolabs), 200 µM dNTPs (New England Biolabs), 5 % (v/v) DMSO (New England Biolabs), 500 ng pRPa-GFP-TbSNM1 template DNA, 10 pmol μl^{-1} primer (either the forward or reverse; Table 2.2) and 0.5 U Q5 high fidelity polymerase (New England Biolabs) in a thin-walled 0.5 ml microcentrifuge tube. The tube contents were consolidated by centrifugation and the sample subject to DNA amplification using a TC-412 thermal cycler (Techne). A standard DNA amplification programme consisted of a single initial denaturation cycle (98 °C for 30 seconds), followed by 30 cycles of 96 °C for 10 seconds (denaturing stage), 50 °C for 30 seconds (annealing stage), 72 °C for 600 seconds (extension stage) before a single, final extension cycle (72 °C for 120 seconds). Samples were then maintained at 4 °C.

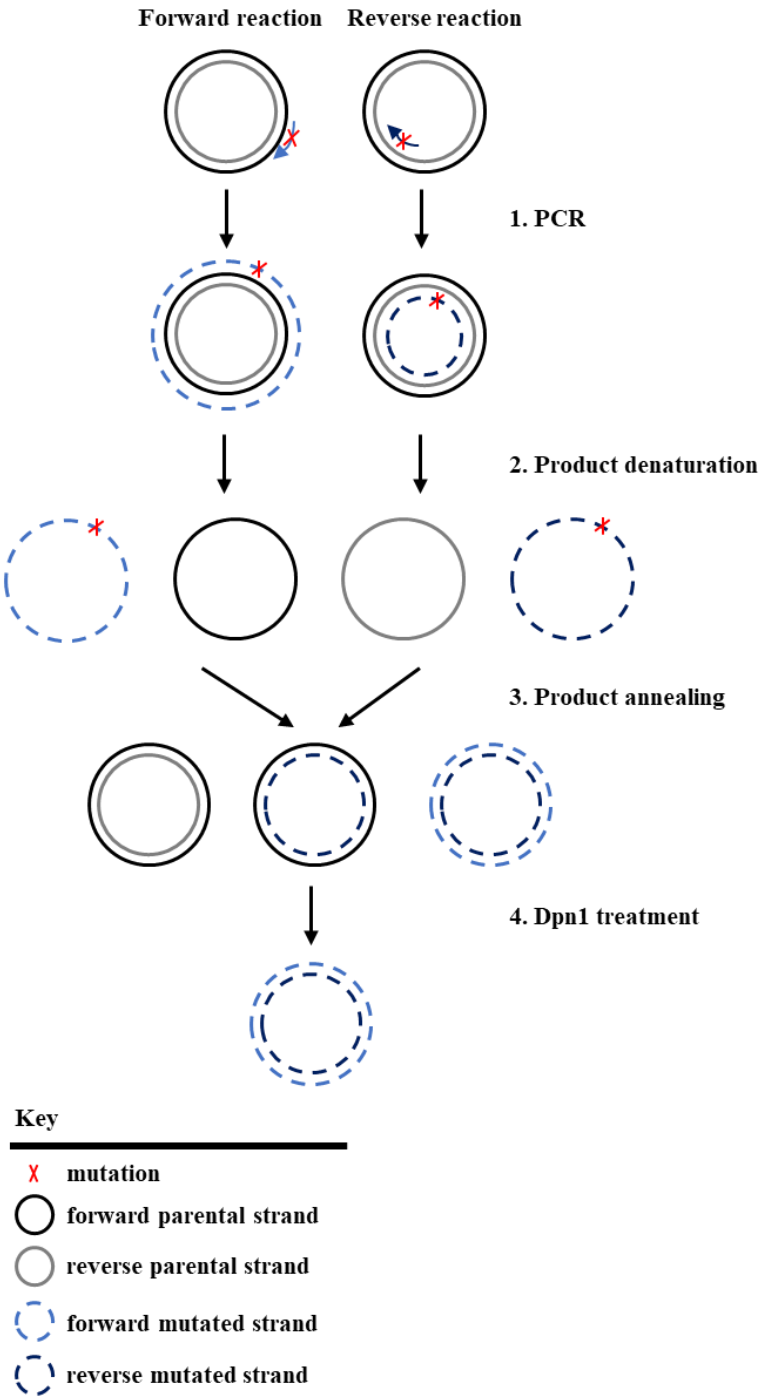

Figure 2.1: Single Primer Reactions In Parallel Site Directed Mutagenesis (SPRINP-SDM).
A forward and reverse reaction, each containing a primer modified with the desire mutation, was carried out separately. Both forward and reverse reactions were combined for annealing. There were three possible combination during annealing: 1. forward parental strand with reverse parental strand, 2. forward PCR product strand annealing to reverse PCR product strand, 3. parental strand with PCR product strand with the second option as the desired combination. DpnI treatment was used to remove methylated parental DNA (methylation not shown).

Residue role /primer name	Primer sequence (5'→3')	Resultant plasmid
Localisation		
Tbsnm1-R428A-F	GGCAGACCAGTGAGAGCAAGGCATGGAGAAGGC	pRPa-GFP-Tbsnm1-R428A
Tbsnm1-R428A-R	GCCTTCTCCATGCCTTGCTCTCACTGGTCTGCC	
Tbsnm1-R429A-F	GGCAGACCAGTGAGAGCAAGGCATGGAGAAGGC	pRPa-GFP-Tbsnm1- R429A
Tbsnm1-R429A-R	GCCTTCTCCATGCCTTGCTCTCACTGGTCTGCC	
Tbsnm1-R430A-F	AGACCAGTGAGAAGAGCACATGGAGAAGGCACC	pRPa-GFP-Tbsnm1- R430A
Tbsnm1-R430A-R	GGTGCCTTCTCCATGTGCTCTTCTCACTGGTCT	
Tbsnm1-H431A-F	CCAGTGAGAAGAAGGGCAGGAGAAGGCACCGCA	pRPa-GFP-Tbsnm1- R431A
Tbsnm1-H431A-R	TGCGGTGCCTTCTCCTGCCCTTCTTCTCACTGG	
Substrate specificity		
Tbsnm1-V518A-F	CTCGTGGTGCCAACGGCATCAAAAGAAGCGTTC	pRPa-GFP-Tbsnm1-V518A
Tbsnm1-V518A-R	GAACGCTTCTTTTGATGCCGTTGGCACCACGAG	
Enzyme activity/co-factor binding		
Tbsnm1-D40A-F	GTTGCTATCCTTGTTGCAGCGTTTGTTCACACA	pRPa-GFP-Tbsnm1-D40A
Tbsnm1-D40A-R	TGTGTGAACAAACGCTGCAACAAGGATAGCAAC	
Tbsnm1-H78A-F	TTGTTTTTTCTCTCGGCATTCCATTCGGATCAT	pRPa-GFP-Tbsnm1-H78A
Tbsnm1-H78A-R	ATGATCCGAATGGAATGCCGAGAGAAAAAACAA	
Tbsnm1-H80A-F	TTTCTCTCGCACTTCGCATCGGATCATTACAGCGG	pRPa-GFP-Tbsnm1-H80A
Tbsnm1-H80A-R	CCGCTGTAATGATCCGATGCGAAGTGCGAGAGAAA	
Tbsnm1-D82A-F	TCGCACTTCCATTCGGCACATTACAGCGGTATT	pRPa-GFP-Tbsnm1-D82A
Tbsnm1-D82A-R	AATACCGCTGTAATGTGCCGAATGGAAGTGCGA	
Tbsnm1-H83A-F	CACTTCCATTCGGATGCATACAGCGGTATTACT	pRPa-GFP-Tbsnm1-H83A
Tbsnm1-H83A-R	AGTAATACCGCTGTATGCATCCGAATGGAAGTG	
Tbsnm1-H159A-F	TTGATACCCGCTAATGCATGTCCTGGTGCAGTT	pRPa-GFP-Tbsnm1-H159A
Tbsnm1-H159A-R	AACTGCACCAGGACATGCATTAGCGGGTATCAA	
Tbsnm1-H178A-F	TTCGGCACGATTCTCGCAACGGGTGATTTTCGC	pRPa-GFP-Tbsnm1-H178A
Tbsnm1-H178A-R	GCGAAAATCACCCGTTGCGAGAATCGTGCCGAA	
Tbsnm1-D221A-F	GATGTGCTCTTCCTTGCAAATACATACTGCCAA	pRPa-GFP-Tbsnm1-D221A
Tbsnm1-D221A-R	TTGGCAGTATGTATTTGCAAGGAAGAGCACATC	
Tbsnm1-H496A-F	ATTCCCTACAGTGAGGCATGTTGCTTTTCCGAA	pRPa-GFP-Tbsnm1-H496A
Tbsnm1-H496A-R	TTCGGAAAAGCAACATGCCTCACTGTAGGGAAT	

Table 2.2: Primers used to create single point mutations in pRPA-GFP-TbSNM1 plasmid. Primers to mutate D40, H78, H80, D82, H83, H159, H178, D221, H496, R428, R429, R430, H431 & V518 residues into alanines in the pRPa-GFP-Tbsnm1 plasmid with resultant plasmids are shown. Highlighted sequences correspond to the mutated residues to alanine residues.

The two DNA amplification reactions (forward and reverse) associated with each mutation were combined and subject to an annealing temperature gradient. Here, the samples were incubated at 95 °C for 300 seconds, before sequentially transferring to 90 °C for 60 seconds, 80 °C for 60 seconds, 70 °C for 30 seconds, 60 °C for 30 seconds, 50 °C for 30 seconds and

40 °C for 30 seconds. The DNA were then digested at overnight 37 ºC with DpnI (New England Biolabs).

2.4.5 Fractionation of DNA by conventional agarose gel electrophoresis

Conventional agarose gel electrophoresis was used to separate DNA molecules between 100 bp to 10 kbp. Dependent on the fragment sizes, the gels used varied in regard to their size and agarose concentrations while the voltage and run times were altered to achieve the desired fractionation result. A standard 0.8-1.2% (w/v) agarose gel was made by dissolving (0.8 to 1.2 g) agarose powder (Bioline) in (100 ml) 1X TAE (40 mM Tris base (Sigma-Aldrich), 40 mM acetic acid (VWR), 1 mM EDTA (Sigma-Aldrich)) containing ethidium bromide (0.1 mg l^{-1}: Sigma-Aldrich) by boiling using a microwave. The molten agarose was allowed to cool to around 60°C, dispensed into a sealed gel tray containing a comb and the agarose allowed to solidify. Once cast, the gel was placed into a gel electrophoresis tank containing 1X TAE supplemented with 0.1 mg l^{-1} ethidium bromide. DNA samples (containing DNA loading dye) and a 1 kb GeneRuler™ (Thermo Fischer Scientific) were loaded onto the gel and the samples fractionated through the gel by applying a constant voltage (70-100 V) across the gel for 40 minutes to 2 hours: in some cases overnight electrophoresis (18 hours) using a 15 V constant voltage were performed. Migration of the samples through the agarose matrix was followed by monitoring the bromophenol blue and xylene cyanol dye fronts present in the samples loading buffer. When the DNA had migrated the desired distance, the agarose gel was visualized on a UV transluminator and documented (Syngene).

2.4.6 Restriction digestion

The restriction enzymes (and the associated 10x restriction buffers) used in this project are listed in Table 2.3 and were sourced from New England Biolabs and/or ThermoFisher Scientific. A typical 20 µl restriction digestion was set up by combining the DNA sample (4 µl) sample, 10x restriction buffer (2 µl), sterile distilled water (13 µl) and restriction enzyme (1 µl: ~10 units) in a 1.5 ml microcentrifuge tube. The tube contents were consolidated by centrifugation and incubated at an appropriate incubation temperature, typically 37 °C, for 1 to 3 hours. The reaction was halted by addition of a $1/10^{th}$ volume (2 µl) of loading dye (10 mM Tris-HCl pH 7.6, 0.03% bromophenol blue, 0.03% xylene cyanol FF, 60% glycerol, 60 mM EDTA) (Fermentas) to the mixture.

Enzyme	Restriction site	NEB Buffer	Enzyme	Restriction site	NEB Buffer
Asc1	GG^CGCGCC	4	HindIII	A^AGCTT	2
ApaI	GGGCC^C	4	Kpn1	GGTAC^C	1
BamHI	G^GATCC	3	Not1	GC^GGCCGC	3
BglI	GCCNNNN^NGGC	3	SacI	GAGCT^C	1
Cla1	AT^CGAT	4	SacII	CCGC^GG	4
EcoRI	G^AATTC	EcoRI	XbaI	T^CTAGA	4
EcoRV	GAT^ATC	3			

Table 2.3: Restriction enzymes, their restriction sites and corresponding buffer used in this study.
The above table details restriction enzymes, the corresponding restriction site and resultant buffer used in the cloning steps of this project. The "^" symbol denotes the DNA cleavage site on the single strand shown.

2.4.7 DNA purification

DNA fragments (~200 bp to 10 kb) were purified in solution or from an agarose gel slice using the GeneJet™ Gel Extraction kit (ThermoFischer Scientific) according to the manufacturer's on-line protocol (https://tools.thermofisher.com/content/sfs/manuals/ MAN0012661_ GeneJET_ Gel_Extraction_UG.pdf: last accessed 26/12/2017). Purified DNA was stored at -20°C.

2.4.8 DNA Ligation

A typical ligation reaction (final volume of 30 µl) was set up by combining purified, digested vector (5 µl) and insert (21 µl) DNAs, 10x ligation buffer (50 mM Tris-HCl, 10 mM $MgCl_2$, 10 mM dithiothreitol, 1 mM ATP, pH 7.5) (3 µl) (New England Biolabs) and T4 DNA ligase (1 µl; 400 units) (New England Biolabs) in a 1.5 ml microcentrifuge tube. The tube contents were consolidated by centrifugation and incubated at room temperature for a minimum of 2 hrs. In parallel, a control ligation was performed where the insert DNA had been replaced with sterile distilled H_2O.

2.4.9 Construction of gene deletion/disruption vectors

A flow diagram illustrating the cloning steps used to generate the gene deletion/disruption vectors used in this project is shown in Figure 2.2. In this process, DNA fragments containing the 5' or 3' untranslated region (UTR)/coding sequence of the gene of interest (Tb*csb*, Tb*mre11*, Tb*exo1*, Tb*rev2*, Tb*rev3*, Tb*fan1*, Tb*chl1*, Tb*hel1*) were amplified from *T. brucei* gDNA and digested with SacI (or SacII where appropriate)/XbaI or ApaI/KpnI, respectively. These fragments were gel purified and sequentially cloned either side of a drug resistance

cassette containing genes that encode for hygromycin B phosphotransferase (*hyg*), neomycin phosphotransferase (*neo*), blasticidin-S deaminase (*bla*) or puromycin N-acetyltransferase (*pac*), plus ancillary sequences needed for the correct processing of the transcript. These above enzymes confer resistance to the selective agents hygromycin B, G418, blasticidin and puromycin, respectively. The primer combinations, band sizes and the resultant gene deletion/interruption vectors are listed in Table 2.4.

2.4.10 DNA Sequencing

The concentration of the template DNA was determined using a NanoDrop™ UV Spectrophotometer (ThermoFisher Scientific). An aliquot of this sample (~1 µg) along with an appropriate primer (20-30 pM) was then commercially sequenced by Eurofins Genomics. The resultant outputs were analysed on Chromas (http://technelysium.com.au/wp/chromas/) and BLAST (https://blast.ncbi. nlm.nih.gov/Blast.cgi).

2.5 Bioinformatics

DNA sequences encoding for or having potential to encode for TbCSB (Tb927.7.4080), TbMRE11 (Tb927.2.4390), TbEXO1 (Tb927.8.3220), TbREV2 (Tb927.7.1090), TbREV3 (Tb927.8.3290), TbCHL1 (Tb927.10.3550), TbHEL1 (Tb927.7.2970) and TbFAN1 (Tb927.10.7540) along with their flanking regions were identified from the TriTryp database (http://tritrypdb.org/tritrypdb/) with homologues identified using a reciprocal best Blast hit analysis. The deduced protein sequences were aligned to the counterparts expressed by other organisms using CLUSTALΩ (http://www.ebi.ac.uk/Tools/msa/clustalo/) and domain structures evaluated using HMMR (http://www.ebi.ac.uk/Tools/hmmer/). To determine potential cellular localisation and possible amino acid targeting motifs, a variety of on-line tools were used including TrypTag (Dean, Sunter and Wheeler, 2017), PSORT II (https://psort.hgc.jp/), NucPred (http://www.sbc.su.se/~maccallr/nucpred/), Nuc-PLoc (http://www.csbio.sjtu.edu.cn/bioinf/) Nuc-PLoc/) and cNLS Mapper (http://nlsmapper.iab.keio.ac.jp/cgi-bin/NLS_Mapper_form.cgi). Phylogenetic relationships of DNA sequences were evaluated using the Phylogeny.fr "One Click" mode tool (http://www.phylogeny.fr/index.cgi) (Dereeper *et al.*, 2008): sequence alignments were performed using MUSCLE (Edgar, 2004), curation using GBLOCKS (Castresana, 2000), phylogeny using PhyML 3.0 (Guindon *et al.*, 2010) and tree rendering using TreeDyn (http://www.treedyn.org/). Molecular modelling was carried out

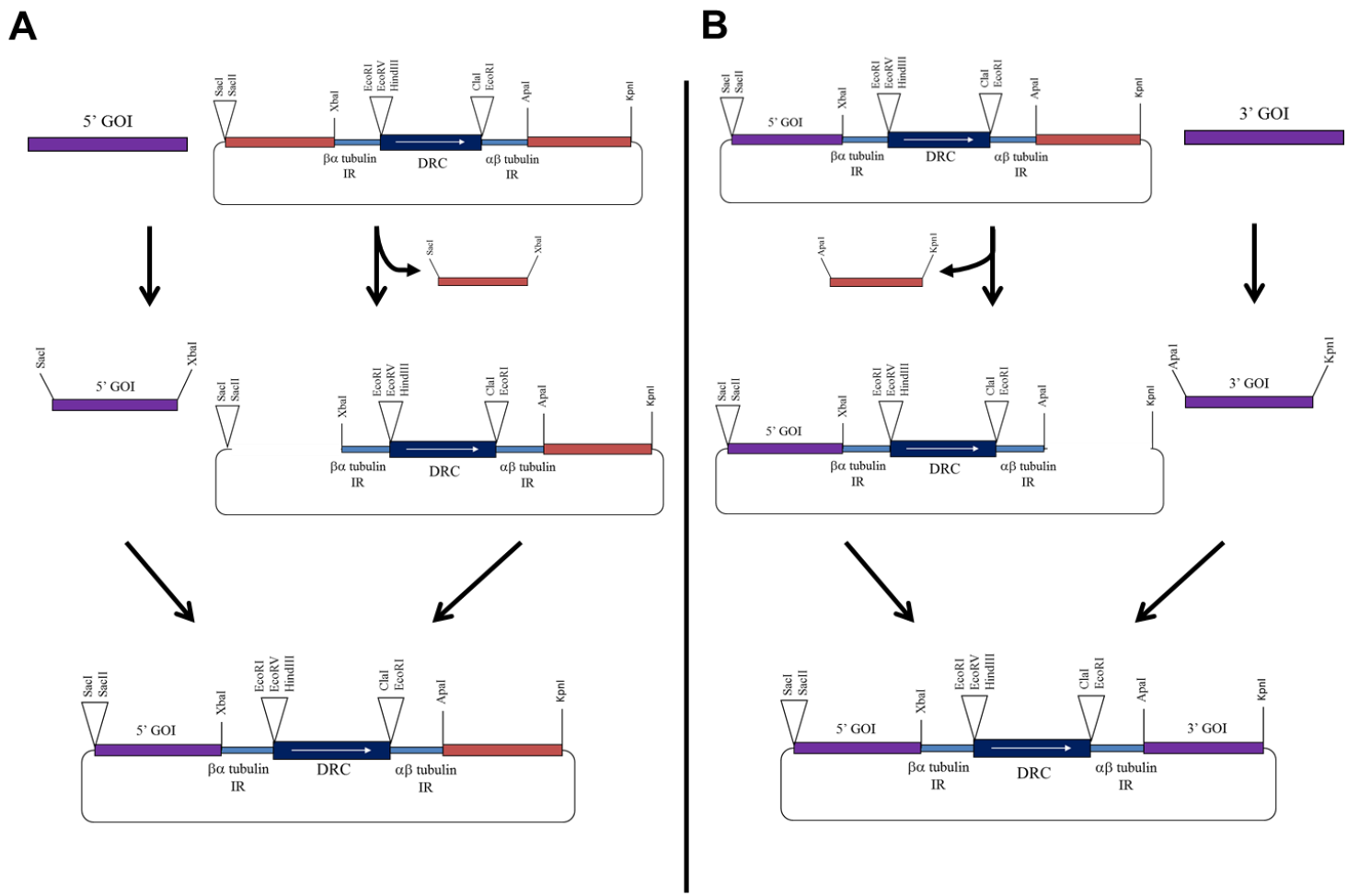

Figure 2.2: Cloning schematic to create disruption vectors.
A. Illustration depicting insertion of a PCR-amplified 5' untranslated region (UTR)/coding sequence of the gene of interest (GOI) into a vector containing a drug resistance cassette (DRC) to facilitate disruption of genes (see Appendix 1a). Both DNA pieces were digested with SacI/XbaI and ligated together. B. Insertion of the 3' GOI/UTR into the previously generated vector. These DNA fragments were digested with ApaI/KpnI, purified and ligated together to create the final disruption/deletion vector.

using Phyre2 (http://www.sbg.bio.ic.ac.uk/phyre2/html/page.cgi?id=index) (Kelley *et al.*, 2015) with data analysed (and *in silico* mutagenesis) carried out on PyMOL (https://pymol.org/2/).

2.6 Bacterial Transformation

Competent *E. coli* were generated using a $CaCl_2$-based technique (M. Mandel, 1970). Briefly, a bacterial stock culture was diluted 1:10 into fresh NZCYM medium (generally 1 ml stock in 10 ml fresh medium) and the new culture grown with aeration at 37°C for two hours: at this point the optical density at 600 nm of the culture was between 0.6-1.0. The cells were harvested by centrifugation (3,555 g for 5 minutes), suspended in an equal volume (generally 10 ml) ice cold 0.1 M CaCl2 and incubated on ice for 10 minutes. The cells were re-harvested by centrifugation (3,555 g for 5 minutes) and the pellet suspended in a $1/10^{th}$ volume (generally 1 ml) of ice cold 0.1 M $CaCl_2$. The DNA to be transformed (generally 30 µl of a ligation reaction or 1 µl purified plasmid DNA) was added to an aliquot (100 µl) of the $CaCl_2$ suspended competent cells, the mixture held on ice for 10-30 minutes, heat shocked at 42 °C for 2 minutes then immediately returned to ice for a further 2 minutes. The transformed bacteria were plated onto NZCYM agar plates containing an appropriate antibiotic for plasmid selection and left to incubate overnight at 37 °C to allow growth of colonies.

2.7 *T. brucei* nucleofection

T. brucei was transformed using the Amaxa® nucleofection system (Lonza) (Burkard, Fragoso and Roditi, 2007). Parasites (5 to 7 $x10^7$ per transfection) in the exponential phase of growth were harvested by centrifugation (1,600 g for 10 minutes at room temperature), residual growth medium removed and the pellet resuspended in 100 µl Human T-cell Nucleofector® solution (Lonza): this solution was made no more than 5 minutes before use by combining 82 µl of reagent A with 18 µl reagent B in the Human T-cell Nucleofector® kit. The cell suspension was immediately transferred to a nucleofection cuvette containing ~10 µg DNA (in 10 µl) to be transformed and parasite electroporation performed using the Amaxa Nucleofector® device set to programme X-001. The cells were transferred into pre-warmed HMI-11 (generally 48 ml) medium and left at 37 °C. After at least 6 hours, selective antibiotics were added to the transformed culture, aliquots (generally 2 ml) transferred into the wells of a 24 well plate and the parasites incubated at 37 °C under a 5 % (v/v) CO_2 atmosphere. In some cases, a 1:10 dilution of the transformed culture were set up prior to addition of the selective antibiotics.

Gene	Nature of integration	5' fragment region	3' fragment region	Vectors generated
Tb*mre11*	gene disruption (34%)	670 bp - 5' region of Tb*mre11* (Tbmre11-KO1/ Tbmre11-KO2)	768 bp - 3' region of Tb*mre11* (Tbmre11-KO3/ Tbmre11-KO4)	pKO-Tbmre11-hyg pKO-Tbmre11-neo pKO-Tbmre11-bla pKO-Tbmre11-pac
Tb*exo1*	gene disruption (50%)	600 bp - 5' region of Tb*exo1* (Tbexo1-KO1/ Tbexo1-KO2)	594 bp - 3' region of Tb*exo1* (Tbexo1-KO3/ Tbexo1-KO4)	pKO-Tbexo1-hyg pKO-Tbexo1-neo pKO-Tbexo1-bla pKO-Tbexo1-pac
Tb*csb*	gene deletion (100%)	425 bp - 5' UTR of Tb*csb* (Tbcsb-KO1/ Tbcsb-KO2)	538 bp - 3' UTR of Tb*csb* (Tbcsb-KO3/ Tbcsb-KO4)	pKO-Tbcsb-hyg pKO-Tbcsb-neo
Tb*rev2*	gene disruption (67%)	806 bp - 5' region of Tb*rev2* (TbREV2-KO1/ TbREV2-KO2)	809 bp - 3' region of Tb*rev2* (TbREV2-KO3/ TbREV2-KO4)	pKO-Tbrev2-hyg pKO-Tbrev2-neo
Tb*rev3*	gene disruption (80%)	344 bp - 5' region of Tb*rev3* (Tbrev3-KO1/ Tbrev3-KO2)	787 bp - 3' region of Tb*rev3* (Tbrev3-KO3/ Tbrev3-KO4)	pKO-Tbrev3-hyg pKO-Tbrev3-neo
Tb*hel1*	gene disruption (60%)	495 bp - 5' UTR of Tb*hel1* (Tbhel1-KO1/ Tbhel1-KO2)	482 bp - 3' region of Tb*hel1* (Tbhel1-KO3/ Tbhel1-KO4)	pKO-Tbhel1-hyg pKO-Tbhel1-neo pKO-Tbhel1-bla pKO-Tbhel1-pac
Tb*chl1*	gene disruption (65%)	557 bp - 5' region of Tb*chl1* (Tbchl1-KO1/ Tbchl1-KO2)	546 bp - 3' region of Tb*chl1* (Tbchl1-KO3/ Tbchl1-KO4)	pKO-Tbchl1-hyg pKO-Tbchl1-pac
Tb*fan1*	gene disruption (72%)	415 bp - 5' region of Tb*fan1* (Tbfan1-KO1/ Tbfan1-KO2)	400 bp - 3' region of Tb*fan1* (Tbfan1-KO3/ Tbfan1-KO4)	pKO-Tbfan1-hyg pKO-Tbfan1-neo

Table 2.4: Schematic for interruption/deletion of all genes analysed in this study.
The above table lays out percentage disruption/deletion of every gene studied in this report, with percentage deletion/disruption of said gene calculated according to percentage of gene removed using this technique. Also shown are the primers (sequences can be found in Appendix 1b) used to amplify 5' and 3' UTRs/GOIs with resulting band sizes for each amplification reaction. This enabled the creation of all vectors listed in the last column.

Drug-resistant *T. brucei* were apparent 5-7 days post-transfection.

Using the above approach, a series of genetically engineered *T. brucei* lines were generated. The lines created were divided into those that were:

1. null for a single DNA repair enzyme (Table 2.5)
2. null for two DNA repair enzymes (Table 2.6)
3. expressing mutated version of Tb*snm*1 in a Tb*snm1*-deficient background (Table 2.7)
4. expressing Tb*ntr* in a Tb*mre11*- or Tb*exo1*-deficient background (Table 2.8)

***T. brucei* line**	**Selectable markers**
221 Tb*mre11*Δ	Hygromycin, G418
221 Tb*csb*Δ	Hygromycin, G418
221 Tb*exo1*Δ	Hygromycin, G418
221 Tb*rev2*Δ	Hygromycin, G418
221 Tb*rev3*Δ	Hygromycin, G418
221 Tb*hel1*Δ	Hygromycin, G418
221 Tb*chl1*Δ	Hygromycin, puromycin
221 Tb*fan1*Δ	Hygromycin, G418

Table 2.5: Parasite lines lacking one DNA repair enzyme.
Each single null parasite line generated in this study with corresponding selectable markers used to maintain the engineered line.

***T. brucei* line**	**Selectable markers**
221 *Tbsnm1*Δ Tb*mre11*Δ	Blasticidin, puromycin, hygromycin, G418
221 *Tbsnm1*Δ Tb*csb*Δ	Blasticidin, puromycin, hygromycin, G418
221 *Tbsnm1*Δ Tb*exo1*Δ	Blasticidin, puromycin, hygromycin, G418
221 *Tbsnm1*Δ Tb*rev2*Δ	Blasticidin, puromycin, hygromycin, G418
221 *Tbsnm1*Δ Tb*rev3*Δ	Blasticidin, puromycin, hygromycin, G418
221 *Tbsnm1*Δ Tb*hel1*Δ	Blasticidin, puromycin, hygromycin, G418
221 *Tbsnm1*Δ Tb*chl1*Δ	Blasticidin, puromycin, hygromycin, G418
221 *Tbsnm1*Δ Tb*fan1*Δ	Blasticidin, puromycin, hygromycin, G418
221 Tb*mre11*Δ Tb*csb*Δ	Blasticidin, puromycin, hygromycin, G418
221 Tb*mre11*Δ Tb*fan1*Δ	Blasticidin, puromycin, hygromycin, G418
221 Tb*mre11*Δ Tb*exo1*Δ	Blasticidin, puromycin, hygromycin, G418
221 Tb*csb*Δ Tb*exo1*Δ	Blasticidin, puromycin, hygromycin, G418

Table 2.6: Parasites lacking two DNA repair enzymes.
Shown in this table are all double null lines generated for this report, including each selectable marker used to maintain the null line.

T. brucei line	Selectable markers
2TAG1 Tb*snm1*Δ gfp-Tbsnm1-D40A	Blasticidin, puromycin, hygromycin
2TAG1 Tb*snm1*Δ gfp-Tbsnm1-H78A	Blasticidin, puromycin, hygromycin
2TAG1 Tb*snm1*Δ gfp-Tbsnm1-H80A	Blasticidin, puromycin, hygromycin
2TAG1 Tb*snm1*Δ gfp-Tbsnm1-D82A	Blasticidin, puromycin, hygromycin
2TAG1 Tb*snm1*Δ gfp-Tbsnm1-H83A	Blasticidin, puromycin, hygromycin
2TAG1 Tb*snm1*Δ gfp-Tbsnm1-H159A	Blasticidin, puromycin, hygromycin
2TAG1 Tb*snm1*Δ gfp-Tbsnm1-H178A	Blasticidin, puromycin, hygromycin
2TAG1 Tb*snm1*Δ gfp-Tbsnm1-D221A	Blasticidin, puromycin, hygromycin
2TAG1 Tb*snm1*Δ gfp-Tbsnm1-R428A	Blasticidin, puromycin, hygromycin
2TAG1 Tb*snm1*Δ gfp-Tbsnm1-R429A	Blasticidin, puromycin, hygromycin
2TAG1 Tb*snm1*Δ gfp-Tbsnm1-R430A	Blasticidin, puromycin, hygromycin
2TAG1 Tb*snm1*Δ gfp-Tbsnm1-R431A	Blasticidin, puromycin, hygromycin
2TAG1 Tb*snm1*Δ gfp-Tbsnm1-V518A	Blasticidin, puromycin, hygromycin
2TAG1 Tb*snm1*Δ gfp-Tbsnm1-H496A	Blasticidin, puromycin, hygromycin

Table 2.7: Parasite lines expressing mutated version of Tb*snm1* in a Tb*snm1*-deficient background.
Conditional cell lines generated for TbSNM1 structure and function assays in this study with lines null for Tb*snm1* and expressing a mutated GFP-tagged TbSNM1. Also shown are the selectable markers used to maintain all cell lines detailed. The parental 2TAG1 (2T1) is phleomycin resistant.

T. brucei line	Selectable markers
2TAG1 Tb*mre11*Δ Tb*ntr*$^{++}$	Blasticidin, puromycin, hygromycin
2TAG1 Tb*exo1*Δ Tb*ntr*$^{++}$	Blasticidin, puromycin, hygromycin

Table 2.8: Tb*ntr* expressing lines generated in this study.
Tb*exo1* and Tb*mre11* were both deleted in a background overexpressing TbNTR with all selectable markers used to maintain said lines shown above. The parental 2TAG1 (2T1) is phleomycin resistant.

2.8 Analysis of recombinant parasites

2.8.1 Cumulative growth assays

T. brucei BSF parasites in the logarithmic phase of growth were seeded at 1×10^4 parasites ml^{-1} in 5 ml HMI-11 medium in a well of a 6-well plate and then incubated at 37 ºC in a 5 % (v/v) CO_2 atmosphere. Each day, the cell density of each culture was measured using a Neubauer haemocytometer. When the number of parasites reached ~1 to x 10^6 ml^{-1}, a new culture seeded at 1×10^4 parasites ml^{-1} was set up. This analysis was carried out over a 8 to 14 day period. Growth curves were generated using GraphPad Prism (GraphPad Software Inc.). All growth assays were performed in triplicate and each count at each time point expressed as a mean ± standard deviation. Mean generation times were calculated using http://www.doubling-time.com/compute.php.

2.8.2 Anti-proliferation assays

All growth inhibition assays were carried out in 96-well plates. *T. brucei* BSF parasites in the logarithmic phase of growth were seeded at 1 x 10^4 cells ml^{-1} in 200 µl HMI-11 medium containing various concentrations of the compound under study. Control assays performed in parallel included culturing cells grown in the absence of drug (100 % growth) and a medium background control. After incubation at 37 °C for 3 days, resazurin (Sigma Aldrich) was added to each well at a final concentration of 12.5 mg l^{-1} (or 2.5 µg resazurin per well). The plates were further incubated for 6-8 hours at 37 °C before measuring the fluorescence of each culture using a Gemini Fluorescent Plate reader (Molecular Devices) at λ_{EX} =530 nM and λ_{EM} =585 nM with a filter cut off at 550 nM. The colour change (and subsequent fluorescence) of resazurin (blue) to resorufin (reddish pink) stems from the reduction of the input dye by viable cells with the change in fluorescence being proportional to the amount of cells present. Therefore, the highest fluorescence values were observed in untreated cultures, whereas the lowest was observed in the absence of cells (*e.g.* background control).

To calculate the fluorescence value at each compound concentration (fl_v), the following calculation was used:

$$fl_v = fl_{raw} - fl_{background} \qquad \text{equation 1}$$

where fl_{raw} is the raw fluorescence value at a given compound concentration and $fl_{background}$ is the average background fluorescence value of the medium control.

The fluorescence value at a given compound concentration (fl_v) was then expressed as a % growth relative to the average fluorescence value for untreated cultures ($fl_{drug=0}$):

$$\% \text{ growth at given [compound]} = fl_v/fl_{drug=0} \times 100 \qquad \text{equation 2}$$

Data expressed as % growth was used to construct dose response curves from which the compound concentration that inhibits cell growth by 50 % (EC_{50}) was extrapolated using the non-linear regression tool on GraphPad Prism (GraphPad Software Inc.). The statistical significance of any differences in parasite susceptibilities was assessed using the Student's *t* test calculator (GraphPad Software Inc.).

2.8.3 Cell imaging

T. brucei BSF parasites in the logarithmic phase of growth and cultured with (or without) 1 µg ml^{-1} tetracycline for 36 hours were pelleted (800 g for 10 minutes), washed twice in PBS before being suspended in 2% (w/v) paraformaldehyde in PBS at a density of ~1 x 10^7 cells ml^{-1}.

Following incubation at room temperature for 20 minutes, an aliquot (20 µl) of the parasite suspension (~1 x 10^5 cells) was air dried onto a single well of a 10-well printed microscope slide (Hendley-Essex). The slides were then incubated in 100 % (v/v) methanol at -20 °C for 30 minutes, washed once in PBS before being allowed to dry. Vectashield Mounting Medium containing 4′,6-diamidino-2-phenylindole (DAPI) (Vectorshield Laboratories) was dispensed across the surface of the slide, a cover slip placed over the wells of that slide and a seal (clear nail varnish) applied around the edge of the coverslip. The seal was allowed to harden overnight at room temperature in the dark and the slides stored at 4 °C until use. Florescence, DAPI and phase images were captured using a Leica DMRA2 upright epi-fluorescent microscope fitted with a digital camera (Hamamatsu Photonics).

For cell cycle arrest assays, *T. brucei* were treated as described above except that the parasites were incubated for varying time periods in different concentrations of mechlorethamine prior to fixation, their immobilization onto a slide and the DAPI/phase images captured. The DAPI and phase images were then merged using ImageJ. To determine whether mechlorethamine treatment affected the trypanosome, parasites at various stages in cell cycle were identified in asynchronous cultures by staining their nuclear (N) and mitochondrial (known as the kinetoplast (K)) genomes with DAPI. The ratio of these two DNA-containing structures within a single cell represents an excellent marker for the trypanosomal cell cycle, with *T. brucei* in the G1/S phase having a 1N1K arrangement, those in G2/M phase possessing a 1N2K ratio while cells displaying a 2N2K profile are in the post-M stage (Woodward and Gull, 1990; T.N. Siegel, D.R. Hekstra, 2008; Glover and Horn, 2012). For each cell line at each mechlorethamine treatment, the DNA staining pattern observed for a minimum of 600 cells was analysed and the number of cells at each cell cycle stage expressed as a % relative to the total parasite count.

2.8.4 Immuno-fluorescence assay

T. brucei BSF parasites in the logarithmic phase of growth and cultured in the presence of 30µm mechlorethamine for varying time periods, were pelleted (800 g for 10 minutes), washed twice in PBS before being suspended in 2% (w/v) paraformaldehyde in PBS at a density of ~1 x 10^7 cells ml^{-1}. Following incubation at room temperature for 20 minutes, an aliquot (20 µl) of the parasite suspension (~1 x 10^5 cells) was air dried onto a single well of a 10-well printed microscope slide (Hendley-Essex). The slides were then washed in PBS for 5 minutes, treated with 0.5 % Triton-X (Sigma) in PBS for 15 minutes followed by an additional wash of the slide

in PBS (5 minutes). Slides were then incubated in blocking solution (50 % [v/v] Fetal Bovine Serum (FBS) in PBS) for 45 minutes followed by incubation in blocking solution (3 % (v/v) FBS in PBS) containing primary antibody (rabbit anti-γH2AX (supplied by Dr R. McCulloch, University of Glasgow (Glover and Horn, 2012) at a 1:250 dilution) for 45 minutes. Slides were then washed twice in PBS for 5 minutes with subsequent incubation of slides in blocking solution (3 % (v/v) FBS in PBS) containing secondary antibody (Goat anti-Mouse IgG (H+L) Alexa Fluor 488 at a dilution of 1:1000) for 45 minutes. Slides were finally washed three times in PBS, 5 minutes per wash. Vectashield Mounting Medium containing 4′,6-diamidino-2-phenylindole (DAPI) (Vectorshield Laboratories) was dispensed across the surface of the slide, a cover slip placed over the wells of that slide and a seal (clear nail varnish) applied around the edge of the coverslip. The seal was allowed to harden overnight at room temperature in the dark and the slides stored at 4 °C until use. Florescence, DAPI and phase images were captured using a Leica SP5 confocal microscope (Leica Microsystems (UK) Ltd. Images were subsequently measured for intensity levels using Fiji (https://fiji.sc/) with additional collation of images on Microsoft Powerpoint.

2.8.5 Parasite extracts

Parasites (5 to 8 x 10^7) in the logarithmic phase of growth were pelleted by centrifugation (1,640 g for 10 minutes), suspended in sterile PBS (1 ml) and transferred to a 1.5 ml microcentrifuge tube. The cells were harvested (16,000 g for 1 minute), the supernatant removed and the parasites lysed in Laemmli buffer (10 % (v/v) glycerol, 2.3 % (w/v) SDS, 5 % (v/v) β-mercaptoethanol, 62 mM Tris.Cl pH 6.8, 0.002 % (w/v) bromophenol blue) at a density of 1 x 10^6 cells μl^{-1}. Aliquots were denatured (96ºC for 5 minutes) prior to separation alongside a PageRuler prestained Protein Ladder (ThermoFischer Scientific) on a 12 % SDS-PAGE in a 1x SDS-PAGE running buffer (25 mM Tris-HCl, 200 mM glycine, 0.1% (w/v) SDS) using a Mini-PROTEAN® II cell system (Bio-Rad) set at a constant voltage 120 V for 90-120 minutes at 4 °C. Gels were either stained for 1 hour in Coomassie Blue solution (0.05 % (w/v) Coomassie brilliant blue, 10 % (v/v) acetic acid, 50 % (v/v) methanol) followed by destaining in boiling distilled water (gels scanned using a Xerox Flatbed Scanner), or transferred to 0.45 µm Protan nitrocellulose membrane (GE Healthcare).

2.8.6 Protein blotting and immunodetection

Protein blotting was carried out using a Trans-Blot Semi-Dry Transfer Cell (Bio-Rad), in accordance with the manufacturer's instructions. A piece of 0.45 μm Protan nitrocellulose membrane (GE Healthcare) and 8 pieces of standard thickness blotting paper (Whatman), all cut to the size of the SDS-PAGE gel, and the SDS-PAGE gel itself were soaked in transfer buffer (25 mM Tris, 192 mM glycine, 0.5 % (w/v) SDS, 20 % (v/v) methanol) for 15 minutes. Four piece of wetted blotting paper were laid on the anode of the transfer cell on to which was placed the nitrocellulose membrane. The SDS-PAGE gel was then sandwiched between the membrane and four additional pieces of wetted filter paper, with the cathode plate placed on top of the wetted filter paper, completing the transfer cell. A constant voltage of 15 volts for 1 hour was then applied to the apparatus and protein transfer confirmed by observing the presence of prestained markers on the membrane.

A near infrared fluorescence system was used for protein detection. Protein containing membranes were washed in blocking solution (5 % (w/v) marvel powdered milk, PBS, 0.1% (v/v) Tween 20) for one hour at room temperature. The membrane was transferred to a 50 ml centrifuge tube and challenged with primary antibody diluted in blocking buffer (20 ml) for 1 hour at room temperature with gentle rotation. Following copious washes (4 x 5 minutes washed) in PBS containing 0.1% (v/v) Tween 20 the membrane was then challenged with the secondary antibody, diluted in blocking buffer, for 1 hour at room temperature with gentle rotation. After four washes in PBS containing 0.1% (v/v) Tween 20 and two in PBS alone, detection of the near infrared fluorescence signal was monitored using an Odyssey® CLx infrared imaging system (LI-COR). Band signal intensity measurements were carried out using the Analysis Tool in Image Studio™ Lite (Li-COR Biosciences).

The primary antibodies used during this project were a rabbit anti-γH2AX (supplied by Dr R. McCulloch, University of Glasgow) at a 1:1,000 dilution and a rabbit anti-enolase (Prof J. Lukes, University of South Bohemia) at a 1:150,000 dilution. The secondary antibodies used were a goat anti-rabbit IRDye™ 800CW antibody (LI-COR) and an goat anti-mouse IRDye™ 680LT antibody (LI-COR), both diluted 1:5,000.

3. Evaluating the extent of the *T. brucei* ICL REPAIRtoire

3.1 Identifying trypanosomal ICL repair proteins

In many model organisms, ICL repair is a complex process. It involves the concerted action of factors from various DNA repair pathways (*e.g.* HR, NER, and FA etc.) that function to resolve this lesion in a cell cycle dependent manner. Work from the McHugh, Moses, Hashimoto, and Symington laboratories (K F Grossmann *et al.*, 2001; Lam, Krogh and Symington, 2008; Iyama *et al.*, 2015; Hashimoto, Anai and Hanada, 2016) has shown that enzymes such as SNM1, MRE11, CSB, EXO1, REV2 and REV3 all play a role in repairing ICLs. This chapter will involve the construction and characterisation of *T. brucei* null mutant lines lacking TbMRE11, TbCSB, TbEXO1, TbREV2 and TbREV3 with the goal of identifying which of these constitute components of the parasites ICL REPAIRtoire.

3.2 Creation and validation of single null lines

3.2.1 Generation of gene disruption vectors

To assess whether a *T. brucei* DNA repair enzyme plays a role in the repair of ICLs, a classical genetic-based approach was taken. This involved the construction of parasite lines that lack a specific activity by deleting or interrupting the encoding gene from the trypanosome genome. This can then be followed up using phenotypic screens to characterise such recombinant cells. To initiate this, a series of DNA constructs were designed to facilitate replacement (for Tb*csb* (Tb927.7.4080)) or disruption (for Tb*mre11 (*Tb927.2.4390), Tb*exo1* (Tb927.8.3220), Tb*rev2* (Tb927.7.1090), Tb*rev3* (Tb927.8.3290)) of each allelic copy of the gene target with an appropriate drug resistance marker. A schematic diagram outlining how such plasmids were made is shown in Figure 2.2. Briefly, DNA fragments containing the 5' or 3' flanking or coding sequences from the gene of interest were amplified from wild type *T. brucei* genomic DNA. These were then digested with restriction enzymes (5' sequences were processed with SacI (or SacII, where appropriate) and XbaI while 3' sequences were treated with ApaI and KpnI) and cloned either side of a DNA cassette containing a gene that encodes for the hygromycin B phosphotransferase (*hyg*), neomycin phosphotransferase (*neo*), blasticidin-S deaminase (*bla*) or puromycin N-acetyltransferase (*pac*) and supplementary sequences (*T. brucei* βα tubulin and αβ tubulin intergenic regions) needed for the correct processing of the transcript. The cloned fragments in the resultant gene interruption plasmids were confirmed using a combination of restriction mapping and DNA sequencing.

3.2.2 Development of null mutant lines

To generate parasite null mutant lines, the gene deletion/disruption plasmids (see Table 2.4) were digested to completion with SacI/KpnI, for vectors containing the *neo*, *hyg*, or *pac* resistance cassettes, or SacII/KpnI, for vectors containing the *bla* resistance cassette. The resultant fragments were purified, heat-treated at 70°C for 30 minutes to minimise contamination and then introduced into wild type *T. brucei* by nucleofection. To remove both allelic copies of the target gene, two rounds of nucleofection were performed to firstly create heterozygous and then null mutant lines. The latter cells were subsequently validated by DNA amplification approaches using genomic DNA or cDNA as template. Below, an example of the above strategy is given detailing how trypanosomes lacking Tb*csb* were made.

The plasmids pKO-Tbcsb-neo and pKO-Tbcsb-hyg, which facilitate deletion of Tb*csb* and are based around the *neo* and *hyg* resistance cassettes, were digested with SacI/KpnI and the resultant DNA fragments purified. The SacI/KpnI-treated pKO-Tbcsb-hyg DNAs were introduced into wild type *T. brucei* with hygromycin resistant putative Tb*csb* heterozygote parasite clones obtained 5 to 7 days post-transformation. These cells were then transformed with SacI/KpnI-treated pKO-Tbcsb-neo DNAs with hygromycin and G418 resistant putative Tb*csb*Δ null mutant trypanosomes selected 5 to 7 days post transformation.

To confirm that integration of the introduced DNA fragment had occurred at the correct genetic loci, DNA amplifcation reactions using gDNA extracted from *T. brucei* wild type and putative Tb*csb*Δ as template were performed. Such PCRs used primer combinations that generate biomarker fragments specific for the intact Tb*csb* gene or the *hyg* and *neo* disrupted alleles (*Tbcsb –hyg* and Tb*csb –neo*, respectively). When using a primer combination designed to detect intact Tb*csb* (Tbcsb-KO1/Tbcsb-q2), DNA amplification generated a band of the expected size (~1.4 kb) from gDNA extracted from wild type parasites with no band(s) observed in DNA isolated from *T. brucei* Tb*csb*Δ cells (Figure 3.1b). In contrast, primer combinations that detect the Tb*csb-hyg* (Tbcsb-KO1/hyg-2) or Tb*csb-neo* (Tbcsb-KO1/neo-1) alleles generated amplicons of the predicted size (~1.7 and ~1.5 kb, respectively) but only from the gDNA purified from *T. brucei* Tb*csb*Δ null mutant line: No band(s) was observed when using *T. brucei* wild type gDNA as template.

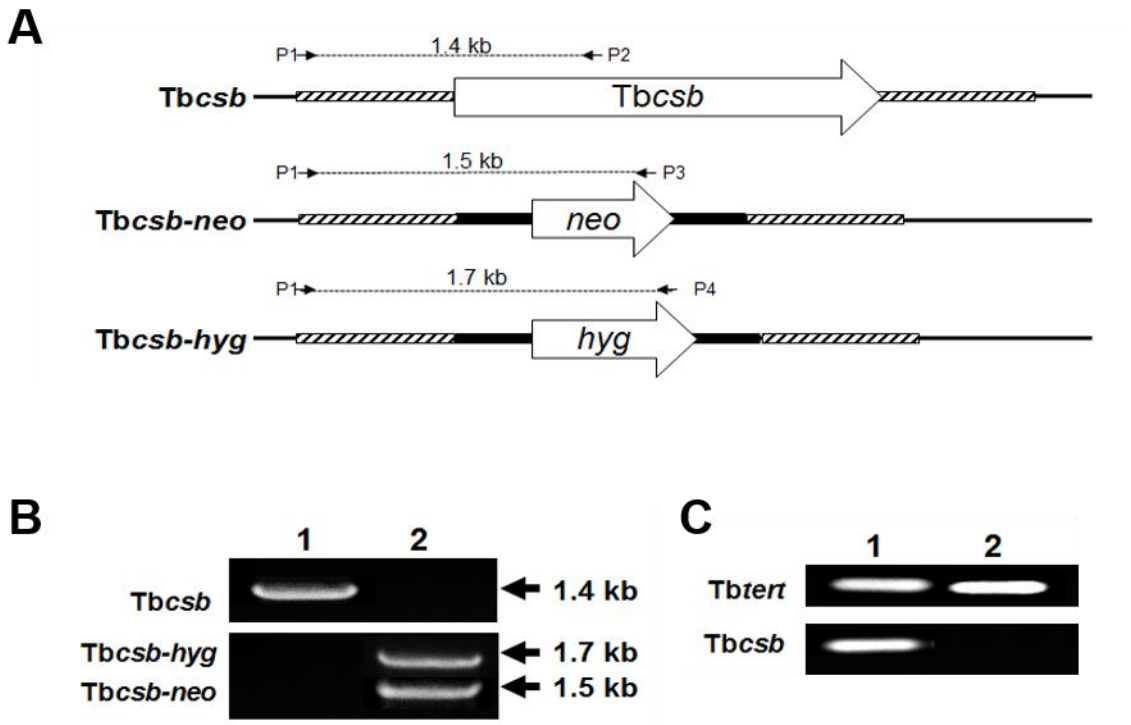

Figure 3.1: Generation of *T. brucei* line lacking TbCSB.
A. Schematic representation of the Tb*csb* allele and the effects of gene disruption using genes encoding for neomycin (*neo*) and hygromycin (*hyg*) resistance. P1 (Tbcsb-KO1), P2 (Tbcsb-q2), P3 (neo-2) and P4 (hyg-2) correspond to the regions where the primers anneal to in the appropriate allele.
B. DNA fragments obtained after amplification on gDNA extracted from *T. brucei* wild type (lane 1) and *T. brucei* Tb*csb*Δ (lane 2) using primer combinations that specifically amplify biomarkers corresponding to the Tb*csb* (Tbcsb-KO1/Tbcsb-q2), Tb*csb-hyg* (Tbcsb-KO1/hyg-2) or Tb*csb-neo* (Tbcsb-KO1/neo-2) alleles.
C. DNA fragments obtained after amplification on cDNA derived from RNA extracted from *T. brucei* wild type (lane 1) or *T. brucei* Tb*csb*Δ (lane 2) using primer combinations that specifically amplify intact Tb*csb* (Tbcsb-q1/Tbcsb-q2). In both cases, the integrity of the cDNA (and hence RNA) was evaluated by amplification of a control fragment, Tb*tert*.

To show that the *T. brucei* Tb*csb*Δ null mutant line was not expressing the interrupted gene, PCRs were performed using a primer combination (Tbcsb-q1/Tbcsb-q2) designed to generate a Tb*csb* specific amplicon against cDNA generated from total RNA (Figure 3.1c). When using wild type cDNA as template, a single band of the expected size (~140 bp) was observed with no band(s) detected in material derived from *T. brucei* Tb*csb*Δ. To confirm that RNA had been extracted from both cell lines and that cDNA had indeed been made, control reactions amplifying Tb*tert* were conducted in parallel. For all tested samples a band of the expected size (~100 bp) was observed showing that the template nucleic acid was suitable for these studies.

Parasites lines null for other *T. brucei* genes (Tb*mre11*, Tb*exo1*, Tb*rev2* or Tb*rev3*) were generated as described above. Validation of the resultant recombinant trypanosomes was performed using similar PCR strategies with this showing that integration of the input DNA fragments had successfully occurred into the appropriate loci in the parasite's genome and confirmed that the Tb*mre11*, Tb*exo1*, Tb*rev2* or Tb*rev3* transcripts were not expressed by the corresponding null mutant. All the confirmatory data relating to the validation of *T. brucei* Tb*mre11*Δ, Tb*exo1*Δ, Tb*rev2*Δ and Tb*rev3*Δ is presented in Appendices 2a-2d.

3.3 Phenotypic analysis of null lines

3.3.1 Growth analysis

To assess whether lack of a given DNA repair activity affected parasite growth, the growth properties of the null mutants generated in Section 3.2 (Tb*csb*Δ Tb*mre11*Δ, Tb*exo1*Δ, Tb*rev2*Δ and Tb*rev3*Δ) was determined and compared against wild type *T. brucei* grown in parallel (Figure 3.2). For all lines tested, three independent cultures containing 1 x 10^4 parasites ml^{-1} were established. Every day over a period of 8 days, the number of cells in each culture was determined using a haemocytometer with the cells in these cultures maintained in the exponential phase of growth: Cultures with a density approaching ~1x10^6 cells ml^{-1} were used to establish a new culture containing 1x10^4 cells ml^{-1}. From the resultant cumulative cell density curves, the Tb*exo1*Δ, Tb*csb*Δ, Tb*rev2*Δ and Tb*rev3*Δ lines all exhibited a profile equivalent to wild type. From this data the growth rate, expressed as the mean generation or doubling time, of wild type cells was calculated to be 6.2 hours as compared to 6.5, 6.4, 6.1 and 6.3 hours displayed by the Tb*exo1*Δ, Tb*csb*Δ, Tb*rev2*Δ, and Tb*rev3*Δ lines, respectively. In contrast, cells lacking TbMRE11 exhibited a slightly longer mean generation time relative to wild type: Tb*mre11*Δ and wild type parasites had a mean generation time of 7.5 and 6.2 hours, respectively. This is in keeping with previous findings from the McCulloch and Cross Laboratories (Robinson, McCulloch, Conway, Browitt and David Barry, 2002; Tan, Leal and Cross, 2002).

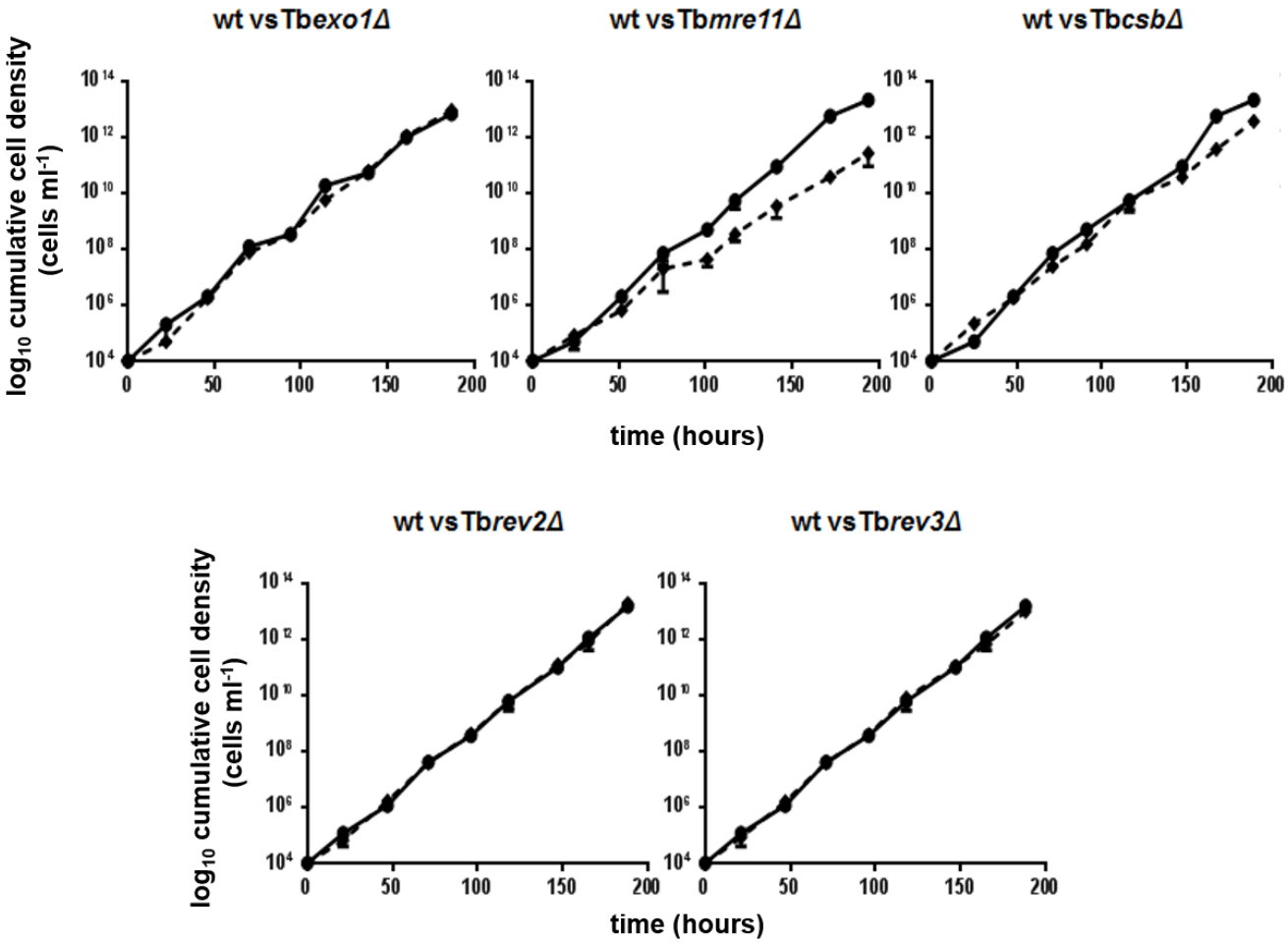

Figure 3.2: Cumulative growth of *T. brucei* null mutants.
The cumulative cell density of *T. brucei* Tb*exo1*Δ, Tb*mre11*Δ, Tb*csb*Δ, Tb*rev2*Δ and Tb*rev3*Δ (dashed line) cultures was followed for 8 days and compared against wild type *T. brucei* (solid line) cultures grown in parallel. Each data point represents the mean cell density ± standard deviation from three independent cultures.

3.3.2 Cell cycle analysis

To further evaluate the above growth characteristics, the cell cycle progression of Tb*mre11*Δ and Tb*csb*Δ was evaluated relative to wild type and Tb*snm1*Δ lines. Asynchronous cultures of bloodstream form parasites in the exponential phase of growth (cultures contained ~5 to 10 x 10^5 trypanosomes ml^{-1}) were fixed, permeabilised and their nuclear (N) and mitochondrial (known as the kinetoplast (K)) genomes stained with DAPI. By determining the ratio of these two DNA-containing structures in a single trypanosome, the stage that each parasite is in within the cell cycle can be determined. *T. brucei* in the G1/S phase of the cell cycle have a 1K1N arrangement, those that possess a 2K1N ratio are said to be in the G2/M phase while trypanosomes displaying a 2K2N profile are in the post M phase (Figure 3.3a) (Woodward and Gull, 1990; T.N. Siegel, D.R. Hekstra, 2008; Glover and Horn, 2012). For wild type *T. brucei*, Tb*snm1*Δ and Tb*csb*Δ, most cells (~75%) in the asynchronous population were in G1/S phase, with ~20% in the G2/M phase and ~5% in the post M phase of the cell cycle (Figure 3.3b). In contrast, fewer Tb*mre11*Δ cells (~55%) were in the G1/S phase, with a concomitant increase (~40%) of cells in the G2/M phase and 5% in the post M phase of the cell cycle. This indicates that the increased mean generation time exhibited by Tb*mre11*Δ cells may be due the stalling of the replication forks. This causes a delay at this point in the cell cycle, an event probably driven by a reduced ability of this null mutant line to repair DNA damage *via* HR pathways (Grossmann, Ward and Moses, 2000; Robinson, McCulloch, Conway, Browitt and Barry, 2002; Tan, Leal and Cross, 2002). This cell cycle checkpoint checks the integrity of DNA before the final commitment of cell division, therefore, preventing cells containing damaged DNA progressing into mitosis. In contrast to our data, other researchers have not observed the above trait in relation to TbMRE11-deficient cells (Robinson, McCulloch, Conway, Browitt and Barry, 2002). Potentially this difference could be accounted for by the different assay systems used.

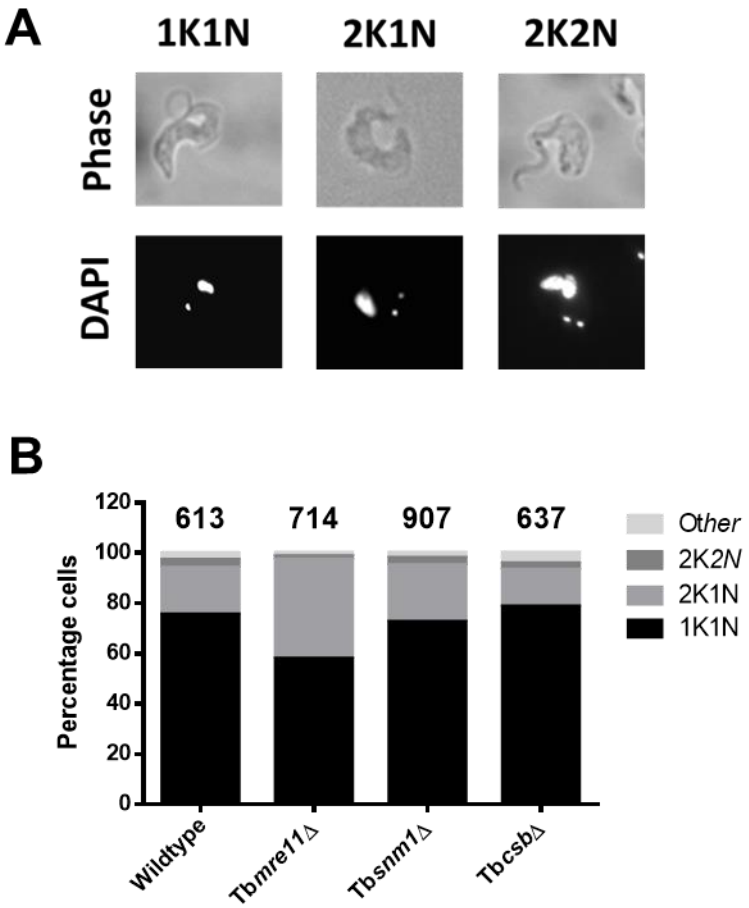

Figure 3.3: Cell cycle analysis of *T. brucei* null mutants.
A. The ratio of DAPI-stain kinetoplast (K) and one nuclear (N) genomes in one trypanosomes represents a frequently used marker for the *T. brucei* cell cycle. Images show cells with a 1K1N, 2K1N and 2K2N arrangement which is indicative of the G1/S, G2/M and post M stages, respectively.
B. The relative number of nuclear and mitochondrial genomes structures from asynchronous cultures of wild type, Tb*mre11*Δ Tb*snm1*Δ *and* Tb*csb*Δ parasites was evaluated. The number of cells analysed per cell line is given above each bar.

3.3.3 Susceptibility of *T. brucei* null mutants towards DNA damaging agents

To evaluate whether lack of a given DNA repair activity affects parasite susceptibility to various types of DNA damaging agent, a series of growth inhibition assays were performed. The treatments used were hydroxyurea (which promotes base oxidation), phleomycin (causes DNA DSBs), methyl methanesulfonate (MMS; alkylation leading to DNA DSBs) and ultraviolet radiation (UV; pyrimidine dimer formation). In many organisms, specific pathways operate to repair the type of DNA damage these treatments induce e.g. the NER pathway functions in the repair of UV induced lesions while HR plays a central role in resolving DNA DSBs. In these inhibition assays, parasites (*T. brucei* wild type, Tb*mre11*Δ, Tb*csb*Δ, Tb*exo1*Δ, Tb*rev2*Δ and Tb*rev3*Δ; Tb*snm1*Δ as analysed in parallel) were grown for 3 days in the presence

of different concentrations of compound (hydroxyurea, phleomycin, MMS) or exposed to a single bolus prior to culturing for 3 days (UV) with the number of cells in each sample then determined using the vital dye resazurin. The resultant data was then plotted to generate dose response curves from which the treatment EC_{50} value was calculated (see Materials and Methods). Figure 3.4 illustrates the type of dose response curves generated using *T. brucei* wild type and Tb*mre11*Δ against the four previously noted treatments with all the calculated EC_{50} values shown in Table 3.1. A bar chart emphasising the fold differences displayed by each treatment against each cell lines is also shown (Figure 3.5).

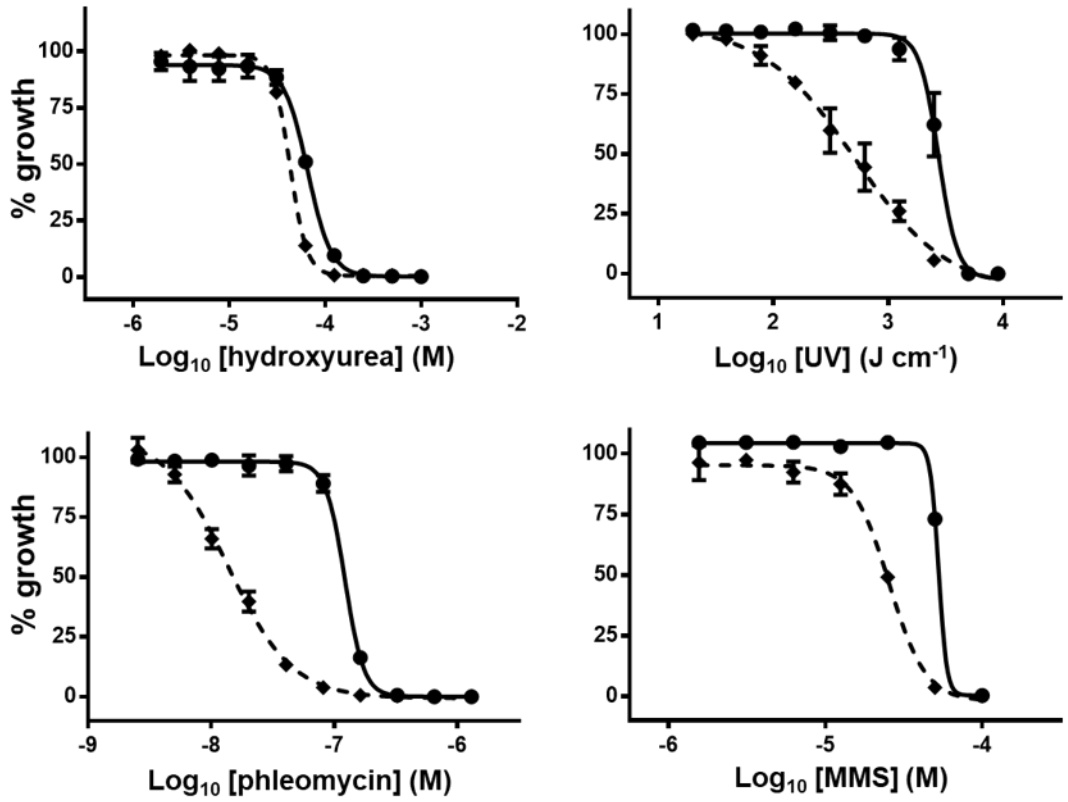

Figure 3.4: Susceptibility of *T. brucei* Tb*mre11* null mutant towards various DNA damaging treatments.
Dose response curves of *T. brucei* wild type (solid line) and Tb*mre11*Δ (dotted line) to hydroxyurea, UV, phleomycin and MMS. All data points are mean values ± standard deviations from experiments performed in quadruplicate.

Treatment	*T. brucei* EC_{50}		Fold difference
	wild type	Tb*snm1Δ*	
Hydroxyurea (μM)	47.56 ± 1.90	38.62 ± 2.71	1.3
Phleomycin (μM)	0.12 ± 0.00	0.12 ± 0.00	1.0
MMS (μM)	33.02 ± 0.28	35.82 ± 0.29	0.9
UV (kJ/cm)	2.58 ± 0.39	2.66 ± 0.18	1.0

Treatment	*T. brucei* EC_{50}		Fold difference
	wild type	Tb*exo1Δ*	
Hydroxyurea (μM)	47.56 ± 1.90	52.59 ± 1.54	0.9
Phleomycin (μM)	0.12 ± 0.00	0.06 ± 0.00*	2.0
MMS (μM)	27.89 ± 0.63	32.46 ± 0.71	0.9
UV (kJ/cm)	3.54 ± 0.20	2.07 ± 0.14	1.7

Treatment	*T. brucei* EC_{50}		Fold difference
	wild type	Tb*mre11Δ*	
Hydroxyurea (μM)	53.37 ± 3.68	43.10 ± 0.84	1.3
Phleomycin (μM)	0.12 ± 0.01	0.01 ± 0.00*	12.0
MMS (μM)	33.02 ± 0.28	12.63 ± 0.47*	2.5
UV (kJ/cm)	2.58 ± 0.39	0.53 ± 0.11*	4.9

Treatment	*T. brucei* EC_{50}		Fold difference
	wild type	Tb*csbΔ*	
Hydroxyurea (μM)	71.88 ± 0.89	69.00 ± 2.67	1.0
Phleomycin (μM)	0.04 ± 0.00	0.04 ± 0.00	1.0
MMS (μM)	27.78 ± 5.17	26.73 ± 8.54	1.0
UV (kJ/cm)	2.12 ± 0.18	0.42 ± 0.14*	5.1

Treatment	*T. brucei* EC_{50}		Fold difference
	wild type	Tb*rev2Δ*	
Hydroxyurea (μM)	67.39 ± 0.65	58.18 ± 0.39	1.2
Phleomycin (μM)	0.06 ± 0.00	0.04 ± 0.00	1.5
MMS (μM)	41.41 ± 3.56	37.82 ± 1.16	1.1
UV (kJ/cm)	3.61 ± 0.29	3.74 ± 0.35	1.0

Treatment	*T. brucei* EC_{50}		Fold difference
	wild type	Tb*rev3Δ*	
Hydroxyurea (μM)	67.39 ± 0.65	50.68 ± 0.83	1.3
Phleomycin (μM)	0.06 ± 0.00	0.05 ± 0.00	1.2
MMS (μM)	41.41 ± 3.56	38.65 ± 1.49	1.1
UV (kJ/cm)	3.46 ± 0.45	5.52 ± 1.08	0.6

Table 3.1: Susceptibility of *T. brucei* null lines to DNA damaging treatments.
Data represents EC_{50} values of *T. brucei* wild type, Tb*snm1*Δ, Tb*exo1*Δ, Tb*mre11Δ*, Tb*csb*Δ, Tb*rev2*Δ and Tb*rev3*Δ against hydroxyurea, phleomycin, MMS and UV. All values are means ± standard deviations from experiments performed in quadruplicate. The ratio of EC_{50} values between wild type and null mutant lines is given as fold difference. *Indicates significant differences in susceptibility ($P < 0.0001$ between wild type and null lines, as assessed by Student's *t* test (GraphPad Software).

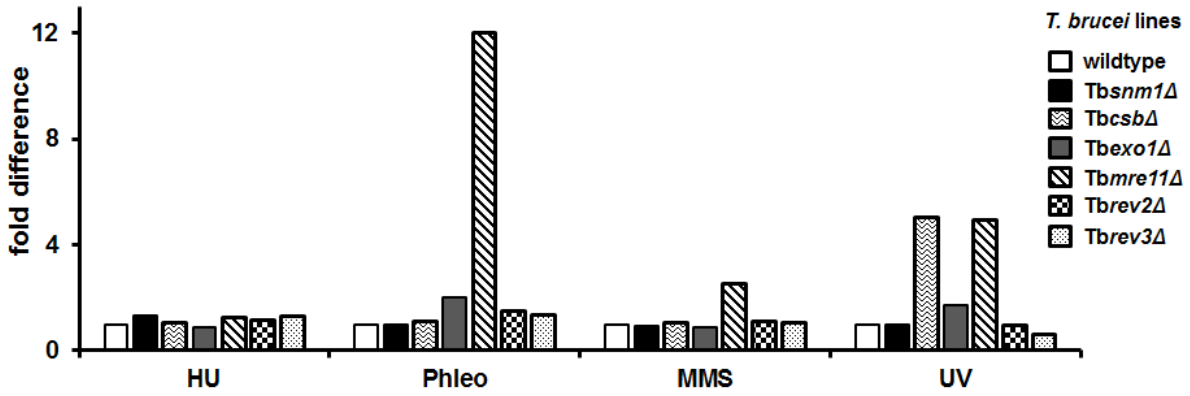

Figure 3.5: Comparison of *T. brucei* null mutant EC_{50} values.
The susceptibility of *T. brucei* wild type and the various null mutant lines against hydroxyurea (HU), phleomycin (Phleo), methyl methanesulfonate (MMS) and ultraviolet radiation (UV), as judged by their EC_{50} values, was compared and expressed as a fold difference.

Based on dose response curves and extrapolated EC_{50} values, trypanosomes lacking TbSNM1, TbREV2 and TbREV3 are as equally sensitive to the tested DNA damaging treatments as wild type indicating that they do not play a front line role in resolving the resultant lesions. For TbSNM1, this confirms previously published data (Sullivan *et al.*, 2015) while the TbREV2 and TbREV3 data indicates that the different DNA polymerases involved in TLS may be able complement for each other: *T. brucei* expresses at least 5 such enzymes (Zurita-Leal, 2016).

In the case of the Tb*csb*Δ line, a wild type response was noted towards hydroxyurea, phleomycin and methyl methanesulfonate. In contrast, cells lacking this helicase were 5-fold more sensitive to UV relative to controls. This data confirmed previous findings that TbCSB is only involved in the parasites NER pathway (Machado *et al.*, 2014).

Interestingly, TbEXO1-deficient cells are only slightly more susceptible (2-fold) to phleomycin than wild type while exhibiting wild type sensitivities towards the other 3 treatments. It had initially been envisaged that this particular mutant should also be more sensitive to other dsDNA generating agents such as MMS but our observations contradict our initial hypothesis. This may be due to how the dsDNA break arises, for example due to base alkylation (MMS) or DNA intercalation (phleomycin), or which trypanosomal repair pathway predominants to fix such lesions. The data presented here indicates that the initial repair of phleomycin induced DNA damage results in base mismatches that are subsequently resolved

using the MMR pathway, of which TbEXO1 is part. This indicates that MMS does not cause such secondary alterations.

For the final null line, Tb*mre11*Δ cells displayed increased sensitivity to 3 out of the 4 treatments relative to wild type. As expected and in keeping with the published literature, TbMRE11 deficient cells were more susceptible to agents that promote dsDNA breaks (phleomycin and MMS) with the HR pathway well known to play a role in repairing this type of damage (Robinson, McCulloch, Conway, Browitt and David Barry, 2002; Tan, Leal and Cross, 2002). Intriguingly, these mutants were also 5-fold more sensitive to UV, not previously documented in relation to trypanosomes. One reason to account for this latter observation may stem from the formation of double-strand DNA breaks caused by the arrest of replication forks at UV-induced damaged sites (Limoli *et al.*, 2002).

3.3.4 Susceptibility of *T. brucei* null mutants towards mechlorethamine

The above growth inhibition assays were extended to investigate the phenotype displayed by *T. brucei* null mutants towards mechlorethamine, an archetypal ICL inducing agent. As noted previously, the resultant cell number data was plotted as dose response curves from which EC_{50} values were extrapolated (Figure 3.6: Table 3.2). Again, the fold differences displayed by each mutant cell line against the ICL inducing compound is emphasised in Figure 3.7.

Previous work has shown that TbSNM1 plays an important role in resolving the damage caused by mechlorethamine with our data confirming this earlier finding (Sullivan *et al.*, 2015): Cells lacking TbSNM1 are >8-fold more susceptible to this compound as compared to controls. A similar alteration in sensitivity was also observed in cells deficient in TbMRE11, TbCSB or TbEXO1. Intriguingly, the difference in EC_{50} values displayed by these 3 mutants relative to wild type was not as great as that noted for Tb*snm1*Δ cells; Tb*mre11*Δ, Tb*csb*Δ and Tb*exo1*Δ cells were 3-, 4- and 2-fold more susceptible to mechlorethamine than wild type. This could suggest the relative importance of each enzyme in the so-called *T. brucei* ICL REPAIRtoire. In contrast, cells lacking TbREV2 or TbREV3 displayed wild type sensitivities towards the ICL inducing agent indicating they play no significant role in resolving this type of damage.

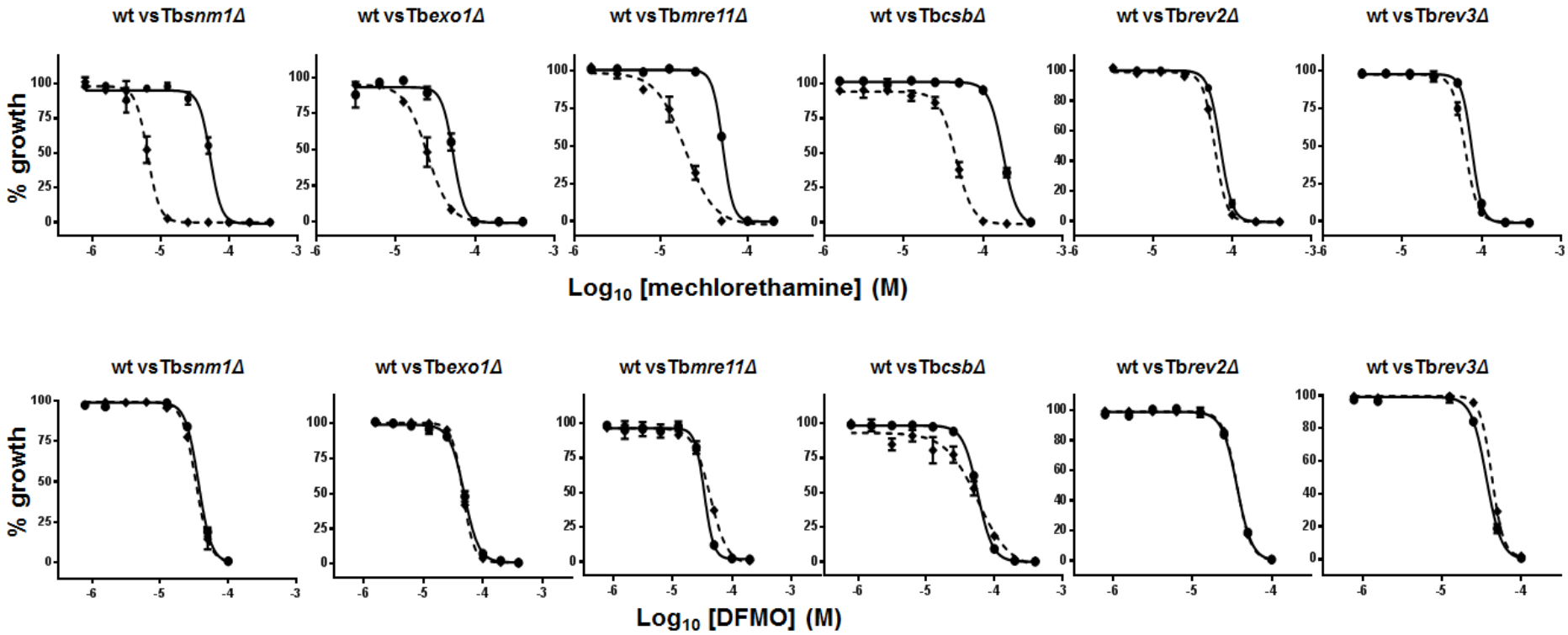

Figure 3.6: Susceptibility of *T. brucei* null mutants towards mechlorethamine and DFMO.
Dose response curves of *T. brucei* wild type (solid line) and the various null mutants (dotted line) towards mechlorethamine and DFMO. All data points are mean values ± standard deviations from experiments performed in quadruplicate.

Treatment	*T. brucei* EC_{50}		Fold difference
	wild type	Tbs*nm1*Δ	
mechlorethamine	50.47 ± 4.39	6.43 ± 0.49*	8.3
DFMO	48.77 ± 2.19	38.61 ± 2.18	1.3

Treatment	*T. brucei* EC_{50}		Fold difference
	wild type	Tb*exo1*Δ	
mechlorethamine	50.47 ± 4.39	24.94 ± 2.87*	2.0
DFMO	48.77 ± 2.19	46.41 ± 0.32	1.1

Treatment	*T. brucei* EC_{50}		Fold difference
	wild type	Tb*mre11*Δ	
mechlorethamine	51.82 ± 0.32	18.76 ± 1.43*	2.7
DFMO	34.57 ± 0.87	42.95 ± 1.50	0.8

Treatment	*T. brucei* EC_{50}		Fold difference
	wild type	Tb*csb*Δ	
mechlorethamine	70.08 ± 2.55	18.68 ± 1.64*	4.2
DFMO	57.14 ± 0.48	57.40 ± 5.44	1.0

Treatment	*T. brucei* EC_{50}		Fold difference
	wild type	Tb*rev2*Δ	
mechlorethamine	70.94 ± 1.25	60.17 ± 0.90	1.2
DFMO	36.75 ± 0.57	31.40 ± 0.54	1.2

Treatment	*T. brucei* EC_{50}		Fold difference
	wild type	Tb*rev3*Δ	
mechlorethamine	61.94 ± 1.90	75.20 ± 2.22	0.8
DFMO	36.75 ± 0.57	42.97 ± 0.64	0.9

Table 3.2: Null mutants towards mechlorethamine and DFMO.

EC_{50} values of *T. brucei* wild type, Tbs*nm1*Δ, Tb*exo1*Δ, Tb*mre11Δ*, Tbc*sb*Δ, Tb*rev2*Δ and Tb*rev3*Δ against mechlorethamine and DFMO. All values are means ± standard deviations from experiments performed in quadruplicate. The ratio of EC_{50} values between wild type and null mutant lines is given as fold difference. *Indicates significant differences in susceptibility ($P < 0.0001$) between wild type and null lines, as assessed by Student's *t* test (GraphPad Software).

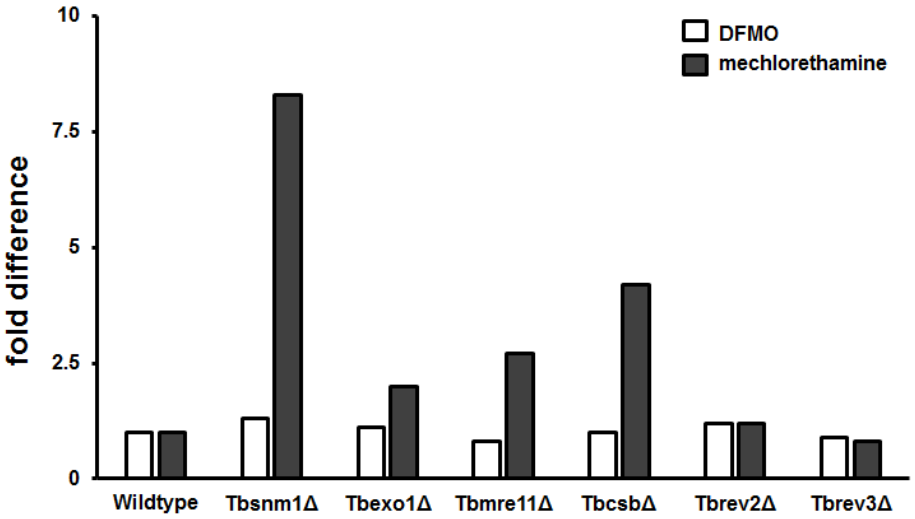

Figure 3.7: Comparison of *T. brucei* null mutant EC_{50} values.
The susceptibility of *T. brucei* wild type and the various null mutant lines against mechlorethamine and DFMO, as judged by their EC_{50} values, was compared and expressed as a fold difference.

To confirm that the above phenotyping was due to the engineered gene deletion/disruption events and not due to off target effects, the susceptibility of all mutants towards the non-DNA damaging trypanocidal agent DFMO was analysed. In all cases the null lines were as equally sensitive to this compound as each other and the wild type, providing evidence that the above susceptibility profiles are specific for each DNA damaging treatment. The above data implicates TbSNM1, TbCSB, TbMRE11 and TbEXO1 in the bloodstream form *T. brucei* ICL repair system and thus constituting a part of this parasites ICL REPAIRtoire.

3.3.5 Production of DNA double strand breaks by mechlorethamine

Previous work on the formation of ICLs has shown that crosslinked DNA can be further processed to form double strand breaks (Li and Moses, 2003). In many cases, nuclear damage (some of which may include DSBs), results in the phosphorylation of histone H2A to form γH2A, with this post-translational modification representing a useful biomarker for detecting DNA damage (Fernandez-Capetillo, Allis and Nussenzweig, 2004). This response is well conserved in eukaryotes and has been shown to take place in *T. brucei* (Glover and Horn, 2012).

To demonstrate whether mechlorethamine promotes nuclear damage which is associated with this phosphorylation event, wild type parasites were treated with mechlorethamine (30, 10 and 3 μM) with samples taken from these cultures at various time points over an 8-hour period. Protein extracts from these cells were generated and probed for γH2A formation by

western blot analysis using antiserum against this modified histone and enolase as a loading control (Figure 3.8). The band intensities of γH2A and enolase for each treatment on each cell line were determined using Image Studio™ Lite (Li-COR Biosciences) with the signals normalised against untreated controls (Figure 3.9).

For all mechlorethamine concentrations tested, a gradual increase in the γH2A signal is observed peaking around 4 hours after initiating treatment. The marker then began to decline over the next 4 hours indicating resolution of the DNA damage. When these studies were extended to the null lines, various outcomes were observed. TbSNM1- and TbEXO1-deficient cells behaved in a similar way to wild type cells. It is tempting to speculate that this nuclear damage is due to ICL-induced DSBs and that these enzymes play no role in processing the such lesions. In Tb*csb*Δ cells, the formation of γH2A was delayed, peaking around 6 hours after initiating treatment and staying at the elevated level for the remainder of the experiment. This indicates that these null cells are unable to effectively recognise and resolve the ICL-induced DSBs: In other organisms, stalling of the transcriptional machinery at such sites leads to post-translational modification of the RNA polymerase which then acts to recruit CSB to the DSB (Batenburg *et al.*, 2015). Intriguingly, when following γH2A in cells lacking TbMRE11, no alteration in signal intensity was observed suggesting this enzyme plays an important role in detecting nuclear damage, which leads to phosphorylation of histone H2A (Lavin, 2008; Zha, Boboila and Alt, 2009; Panier and Durocher, 2013).

To further evaluate mechlorethamine and DSB formation in mutant lines, cells treated for 8 hours in the presence of the ICL inducing agent (30 μM) were analysed using immunofluorescence microscopy to detect γH2A (Figure 3.10). For wild type, Tb*snm1*Δ, Tb*csb*Δ and Tb*exo1*Δ, a signal throughout the whole nucleus was observed showing that nuclear damage formation occurs throughout the whole genome; no discrete foci were observed, even when analysing earlier time points (data not shown). In contrast, and confirming the western blot data, no signal was observed in mechlorethamine treated TbMRE11 null parasites.

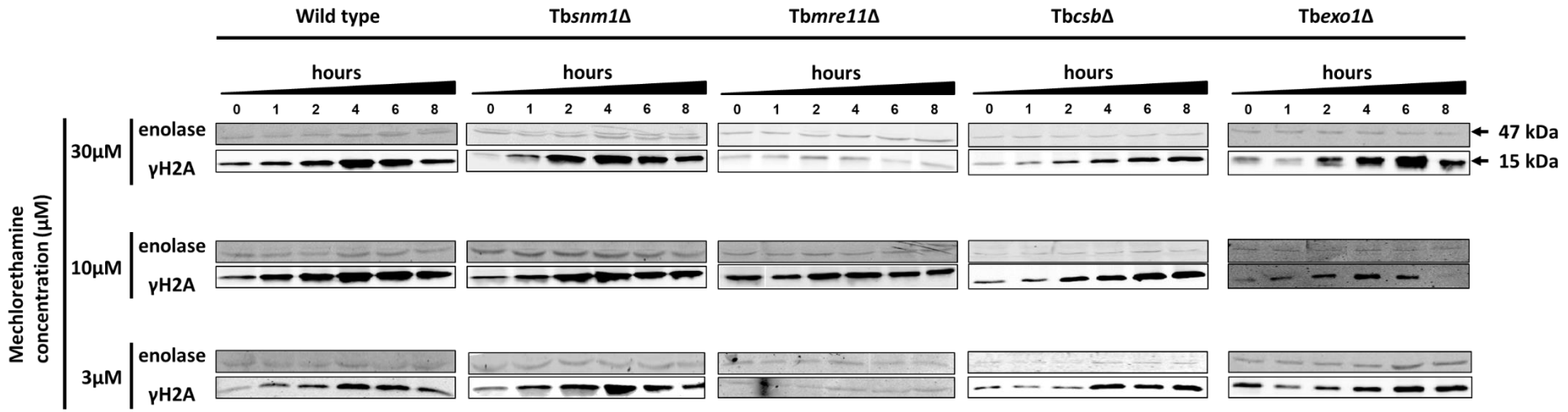

Figure 3.8: γH2A formation in mechlorethamine treated wild type and null lines.
T. brucei wild type, Tb*snm1*Δ, Tb*mre11*Δ, Tb*csb*Δ and Tb*exo1*Δ were treated with 30, 10 or 3μM concentrations of mechlorethamine. Cell lysates were generated at time intervals (0, 1, 2, 4, 6, and 8 hours) and analysed by western blot using anti-*T. brucei* enolase (loading control) and anti-*T. brucei* γH2A antiserum.

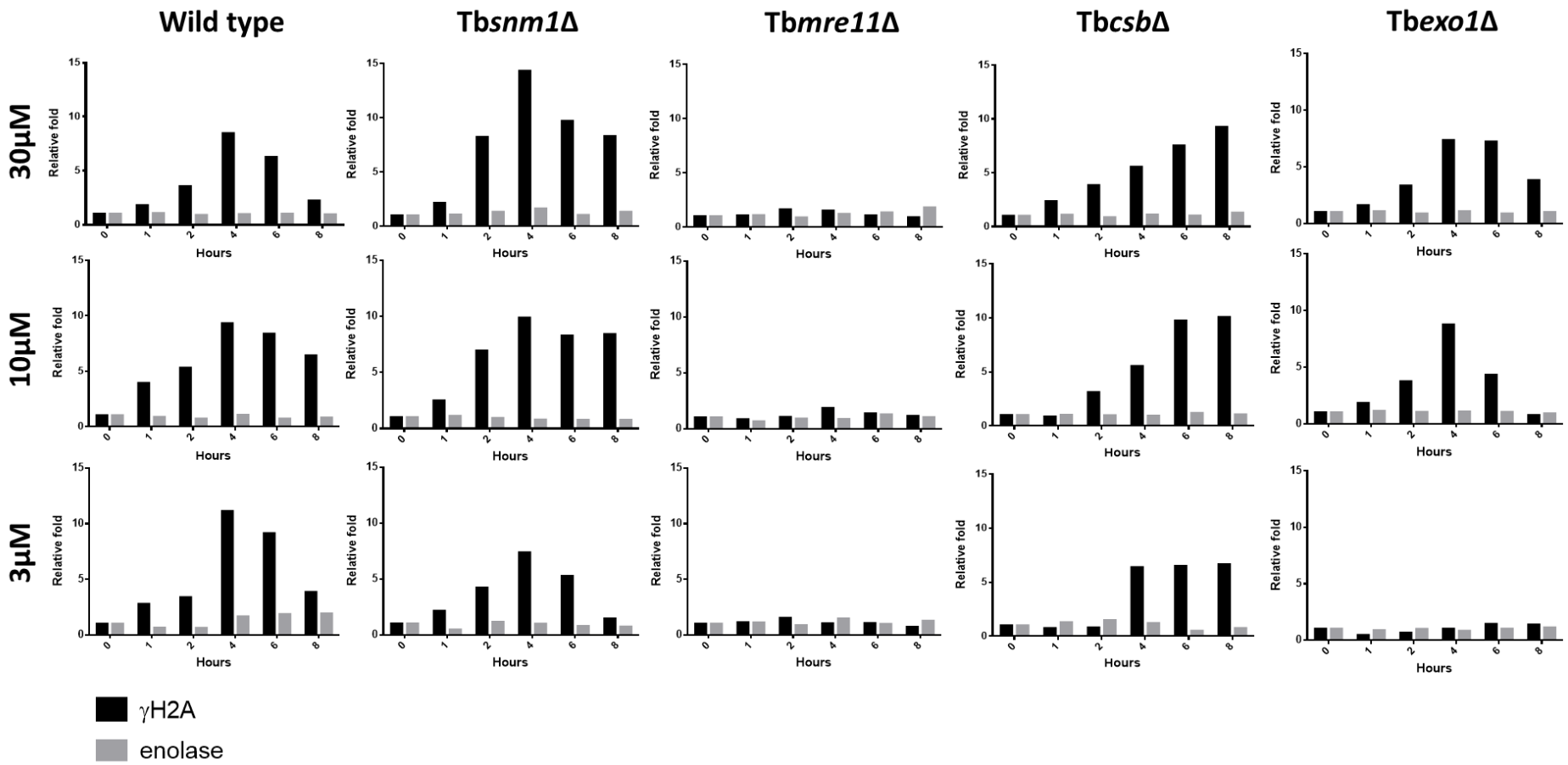

Figure 3.9: Comparison of γH2A signals in mechlorethamine treated *T. brucei* null mutants.
The γH2A and enolase signal intensities obtained from western blot analysis were determined using Image Studio™ Lite (Li-COR Biosciences) with the signals normalised against untreated controls.

.

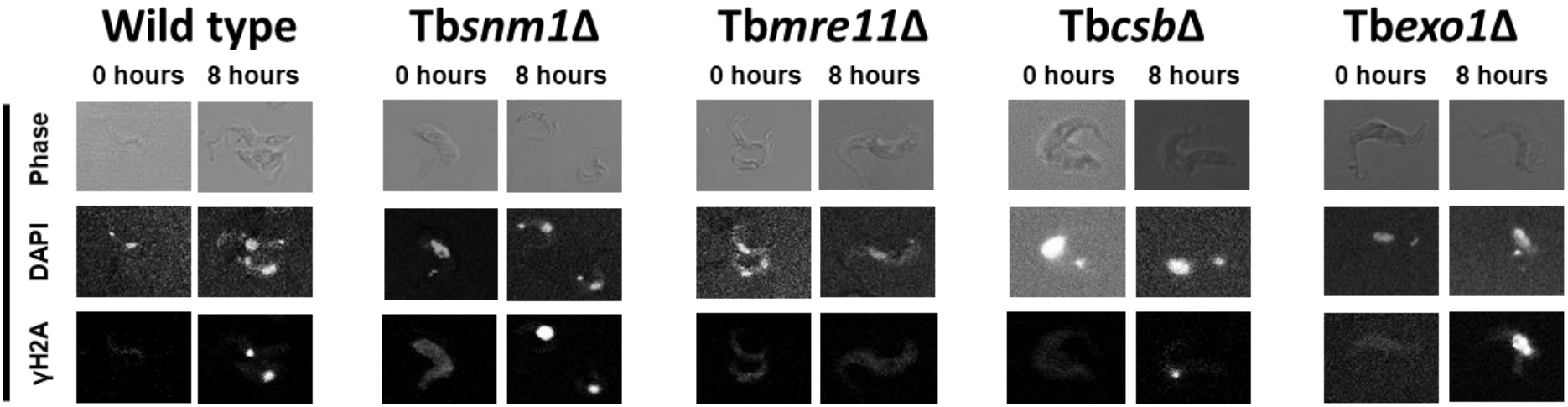

Figure 3.10: Comparison of γH2A formation in mechlorethamine treated *T. brucei* null mutants.
T. brucei wild type, Tb*snm1*Δ, Tb*mre11*Δ, Tb*csb*Δ and Tb*exo1*Δ were treated with 30μM of mechlorethamine for 8 hours and analysed by immunofluorescence assay using anti-*T. brucei* γH2A antisera. Florescence, DAPI and phase images were captured using a Leica SP5 confocal microscope (Leica Microsystems (UK) Ltd.) and were subsequently processed using Fiji.

3.4 Chapter Summary

In this chapter we have:

1. Successfully deleted Tb*csb* and disrupted Tb*exo1*, Tb*mre11*, Tb*rev2* and Tb*rev3* from the *T. brucei* genome to create null mutant lines
2. Demonstrated that, in agreement with the published literature, cells lacking TbMRE11 display a growth defect due to a delay in the progression through the G2/M phase of the cell cycle
3. Shown that cells lacking TbMRE11 are more susceptible to chemical (in agreement with the published literature) and UV-induced dsDNA breaks relative to controls
4. Confirmed that TbCSB deficient cells are more susceptible to UV DNA damage
5. Established that TbMRE11, TbCSB and TbEXO1 represent key components of the *T. brucei* ICL REPAIRtoire
6. Shown that TbREV2 and TbREV3 do not function in ICL repair in the parasite
7. Revealed that mechlorethamine induced ICLs in trypanosomes promote nuclear damage, most likely in the form of dsDNA breaks
8. Revealed that TbMRE11 plays a crucial role in the formation of γH2A at sites of nuclear damage

4. Studying the interplay of ICL repair proteins

The interplay between components of the *S. cerevisiae* / human ICL repair system has been evaluated with studies showing these organisms express multiple, complementary and overlapping mechanisms to mediate repair of this type of DNA damage (Hashimoto, Anai and Hanada, 2016). However, the precise molecular basis of these pathways in a given organism remains unclear. Broadly, these ICL repair mechanisms operate in a cell cycle dependent manner with HR based pathways predominating during the S-phase, while through the remainder of the cell cycle factors from NER, TLS, and MMR prevail (Zhang and Walter, 2014). In yeast, the assignment of a DNA repair activity to a given system was established using a genetics-based approach through the generation of fungal lines lacking two or more activities. The susceptibility of such cells to ICL inducing agents was determined to reveal whether the components under investigation function in an epistatic or non-epistatic manner. Here, we have extended this approach to evaluate the interplay of the trypanosomal ICL repair factors identified previously (TbSNM1;(Sullivan *et al.*, 2015)) and in the earlier chapter (TbMRE11, TbCSB and TbEXO1).

4.1 Evaluating the central role of TbSNM1 in ICL repair

4.1.1 Creation and validation of *T. brucei* null mutant lines

As an initial step to analysing the relationship between components of the trypanosomal ICL repair system, the genes encoding for TbEXO1, TbMRE11 or TbCSB were deleted or disrupted in a Tb*snm1*-deficient *T. brucei* line, thereby creating a series of double null mutant lines (Table 2.6). Although not primarily involved in resolving ICLs, TbREV2 and TbREV3 were also taken forward in this analysis to determine whether their activities in ICL repair become apparent in the absence of TbSNM1: Some yeast ICL factors are only apparent when the activity of another DNA repair protein is missing (Ward *et al.*, 2012). The *hyg*- and *neo*-based gene integration vectors used in the previous chapter were digested to completion with SacI/KpnI, the fragments purified and then heat-treated (70°C for 30 minutes) to minimise contamination. The digested DNAs were sequentially introduced into *T. brucei* Tb*snm1*Δ cells by nucleofection (in this mutant line, Tb*snm1* has been disrupted using gene integration vectors based around *pac* and *bla*; (Sullivan *et al.*, 2015)) to generate heterozygous and subsequent null mutant lines. The recombinant cell lines were then validated by DNA amplification-based approaches using gDNA or cDNA templates. Below, an example of the above strategy is given detailing how Tb*snm1*-deficient trypanosomes also lacking Tb*csb* were made.

Purified SacI/KpnI-digested pKO-Tbcsb-hyg DNA fragments were introduced into *T. brucei* Tb*snm1*Δ cells with hygromycin/blasticidin/puromycin resistant parasite clones (putatively designated as Tb*snm1*Δ Tb*csb*$^{+/-}$) obtained 5 to 7 days post-transformation. These cells were subsequently transformed with purified SacI/KpnI-digested pKO-Tbcsb-neo DNA fragments with selection carried out using blasticidin/puromycin/hygromycin/G418. Clones resistant to the four selective agents (putatively designated as Tb*snm1*Δ Tb*csb*Δ null mutant trypanosomes) were obtained 5 to 7 days post-transformation.

Confirmation that the input DNA fragments had integrated at the correct genetic loci in the trypanosome genome was carried out by PCR (Figure 4.1). Here, gDNA extracted from four *T. brucei* lines (wild type, Tb*snm1*Δ, Tb*csb*Δ and Tb*snm1*Δ Tb*csb*Δ) was probed for the presence or absence of intact Tb*snm1* and Tb*csb*, and their disrupted alleles (*Tbsnm1–bla*; Tb*snm1–pac;* Tb*csb-hyg*; Tb*csb-neo*). When using a primer combination to detect intact Tb*snm1* (Tbsnm1-KO1/Tbsnm1-seq1), an amplicon of ~1.3 kb was detected only in gDNA extracted from *T. brucei* wild type and Tb*csb*Δ (no bands observed using Tb*snm1*Δ and Tb*snm1*Δ Tb*csb*Δ gDNA) (Figure 4.1c). In contrast, when probing for the Tb*snm1-bla* (Tbsnm1-KO1/bla-1) or Tb*snm1-pac* (Tbsnm1-KO1/pac-1) alleles, DNA fragments of the predicted size (~1.1 and ~1.7 kb, respectively) were generated only by gDNA purified from *T. brucei* Tb*snm1*Δ and Tb*snm1*Δ Tb*csb*Δ lines. Analysis of the Tb*csb* loci using primers to detect intact Tb*csb* (Tbcsb-KO1/Tbcsb-q2) amplified a band of the expected size (~1.4 kb) only from gDNA extracted from *T. brucei* wild type and Tb*snm1*Δ (no band noted when using gDNA derived from Tb*csb*Δ and Tb*snm1*Δ Tb*csb*Δ cells). When probed with Tbcsb-KO1/hyg-2 or Tbcsb-KO1/neo-2, primer combinations used to detect for the Tb*csb-hyg* and Tb*csb-neo* alleles respectively, bands of the expected size (~1.7 and ~1.5 kb) were detected only in gDNA derived from Tb*csb*Δ and Tb*snm1*Δ Tb*csb*Δ.

Additional validation of the double null mutant line was performed aimed at assessing whether Tb*snm1* and Tb*csb* were expressed by *T. brucei* Tb*snm1*Δ Tb*csb*Δ cells. DNA amplification reactions were performed on cDNA templates generated from total RNA using primer combinations that detect Tb*snm1* (Tbsnm1-q1/Tbsnm1-q2) or Tb*csb* (Tbcsb-q1/Tbcsb-q2). For RNA extracted from *T. brucei* wild type and Tb*csb*Δ a single, correctly sized (~110 bp) amplicon corresponding to Tb*snm1* was observed with no band(s) detected in material derived from Tb*snm1*Δ and Tb*snm1*Δ Tb*csb*Δ cells (Figure 4.1d). Similarly, a single, correctly sized (~140 bp) amplicon corresponding to Tb*csb* was only observed in reactions using cDNA

derived from *T. brucei* wild type and Tb*snm1*Δ cDNA (and hence RNA) integrity used in these reactions was evaluated by probing the template for Tb*tert* (Tbtert-F/Tbtert-R). In all cases, an amplicon of ~100 bp was noted showing that the template nucleic acid was appropriate for these studies.

Together, the above DNA amplification reactions validate the *T. brucei* Tb*snm1*Δ Tb*csb*Δ double null mutant line, confirming that Tb*csb* had indeed been successfully disrupted in Tb*snm1*Δ parasites leading to the associated loss in gene expression.

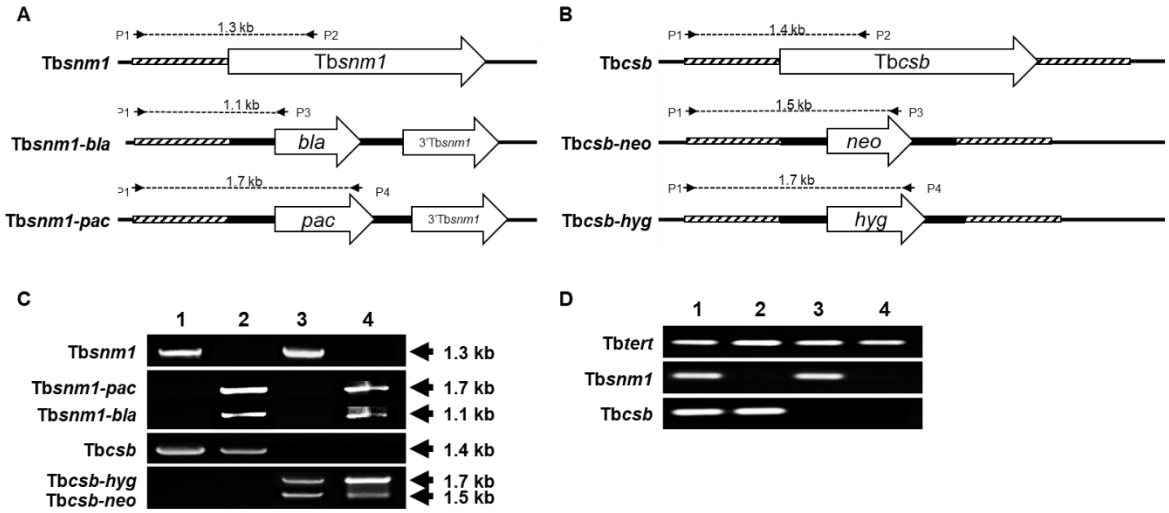

Figure 4.1: Validating the *T. brucei* Tb*snm1*Δ Tb*csb*Δ null mutant line.
A. Diagram illustrating the Tb*snm1* allele and resultant changes upon disruption of this locus using genes encoding for blasticidin (*bla*) and puromycin (*pac*) resistance. P1 (Tbsnm1-KO1), P2 (Tbsnm1-seq1), P3 (bla-1) and P4 (pac-1) correspond to regions where the primers anneal at the specific allele.
B. Schematic representation of the Tb*csb* allele and effects of disrupting this allele with genes encoding for neomycin (*neo*) and hygromycin (*hyg*) resistance. P1 (Tbcsb-KO1), P2 (Tbcsb-q2), P3 (neo-2) and P4 (hyg-2) correspond to regions where the primers anneal at the specific allele.
C. Amplicons corresponding to the Tb*snm1* (Tbsnm1-KO1/Tbsnm1-seq1), Tb*snm1-bla* (Tbsnm1-KO1/bla-1), Tb*snm1-pac* (Tbsnm1-KO1/pac-1), Tb*csb* (Tbcsb-KO1/Tbcsb-q2), Tbcsb-hyg (Tbcsb-KO1/hyg-2) or Tb*csb-neo* (Tbcsb-KO1/neo-2) were generated from template gDNA extracted from *T. brucei* wild type (lane 1), *T. brucei* Tb*snm1*Δ (lane 2), *T. brucei* Tb*csb*Δ (lane 3) and *T. brucei* Tb*snm1*Δ Tb*csb*Δ (lane 4).
D. DNA fragments amplified from cDNA derived from RNA extracted from *T. brucei* wild type (lane 1), Tb*snm1*Δ (lane 2), Tb*csb*Δ (lane 3) and Tb*snm1*Δ Tb*csb*Δ (lane 4) using primer combinations that specifically amplify intact Tb*snm1* (Tbsnm1-q1/Tbsnm1-seq1), Tb*csb* (Tbcsb-q1/Tbcsb-q2) or Tb*tert* (Tbtert-F/Tbtert-R).

Double null mutant parasites lines (Tb*snm1*Δ Tb*mre11*Δ, Tb*snm1*Δ Tb*csb*Δ, Tb*snm1*Δ Tb*rev2*Δ and Tb*snm1*Δ Tb*rev3*Δ) were generated and validated as described above. All the confirmatory data relating to validation is shown in Appendix 3a-3d.

4.1.2 Phenotypic analysis of *T. brucei* double null lines

4.1.2.1 Growth analysis of T. brucei double null lines

To evaluate whether lack of TbSNM1 and TbCSB, TbMRE11, TbEXO1, TbREV2 or TbREV3 affects parasite growth, the growth properties of the double null mutants was determined and compared against wild type *T. brucei* (Figure 4.2). From the resulting cumulative cell density curves, Tb*snm1*Δ Tb*exo1*Δ, Tb*snm1*Δ Tb*csb*Δ, Tb*snm1*Δ Tb*rev2*Δ and Tb*snm1*Δ Tb*rev3*Δ all grew at roughly the same rate as wild type, with mean generation times of 7.0, 6.7, 7.0 and 6.6 hours respectively, in comparison to 6.6 hours for wild type cells. In contrast, Tb*snm1*Δ Tb*mre11*Δ cells exhibited a slightly longer mean generation time relative to wild type (7.8 hours vs 6.6 hours) which is comparable to the growth properties previously noted for Tb*mre11*Δ cells (See Chapter 3; Robinson et al., 2002; Tan, Leal and Cross, 2002).

4.1.2.2 Susceptibility of T. brucei double null lines towards DNA damaging agents

Growth inhibition assays were carried out on the double null mutant lines to determine whether these cells exhibit altered susceptibility to different DNA damaging agents relative to wild type and single null mutant controls. Assays were performed as described previously (see Materials and Methods and Chapter 3) with the data used to create dose response curves from which EC_{50} values were derived. Figure 4.3 illustrates dose response curves generated from *T. brucei* wild type, Tb*snm1*Δ, Tb*mre11*Δ, and Tb*snm1*Δ Tb*mre11*Δ cells against the treatments used with concomitant EC_{50} values given in Table 4.1. A bar chart emphasising the fold differences displayed by each treatment against each cell line is also shown (Figure 4.4).

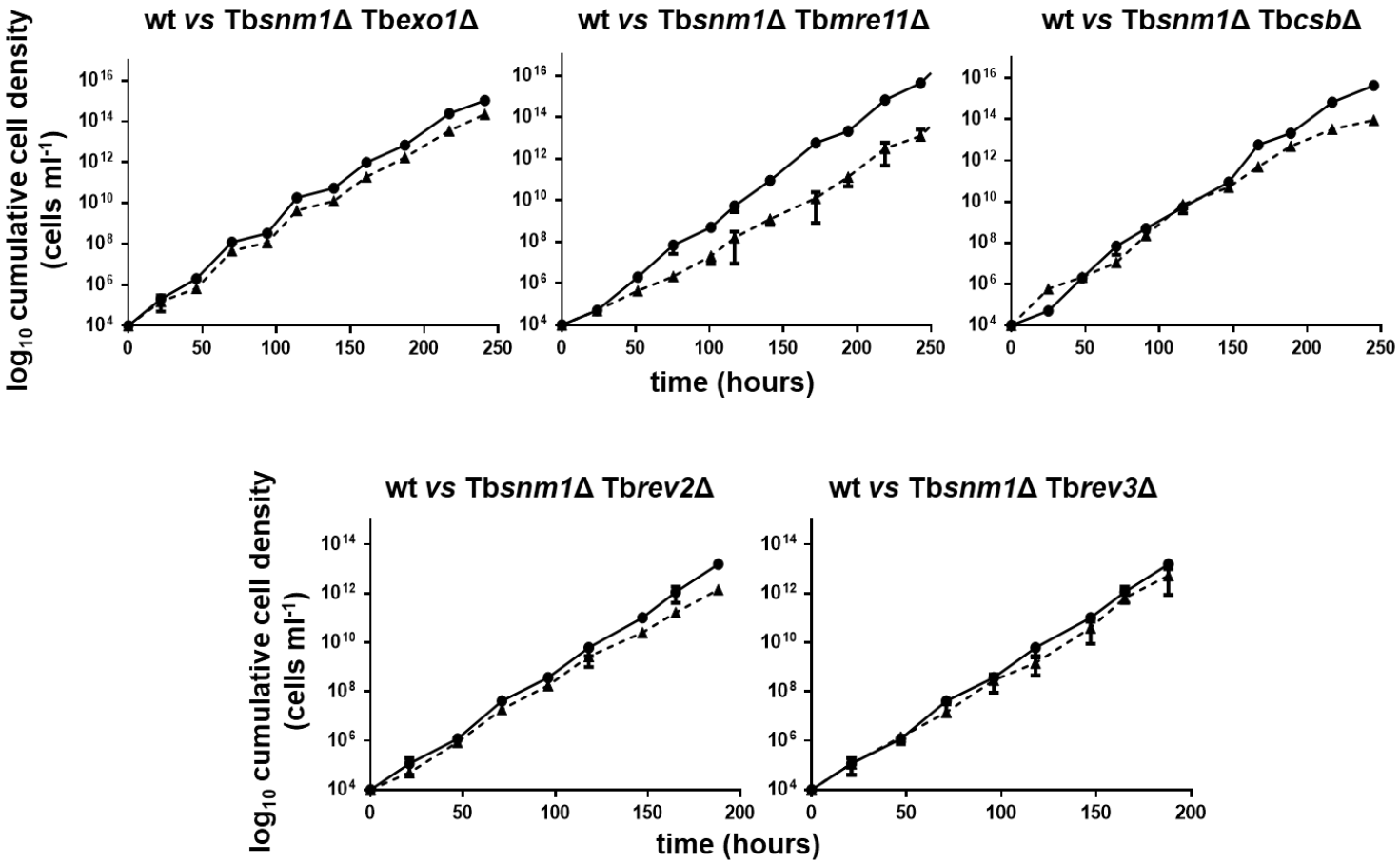

Figure 4.2: Cumulative growth of *T. brucei* double mutant lines.
The cumulative cell density of *T. brucei* Tb*snm1*Δ Tb*exo1*Δ, Tb*snm1*Δ Tb*mre11*Δ, Tb*snm1*Δ Tb*csb*Δ, Tb*snm1*Δ Tb*rev2*Δ, and Tb*snm1*Δ Tb*rev3*Δ (▲) cultures was followed for 8 days and compared against *T. brucei* wild type (●) cells, grown in parallel. Each data point represents the mean cell density ± standard deviation from three independent cultures.

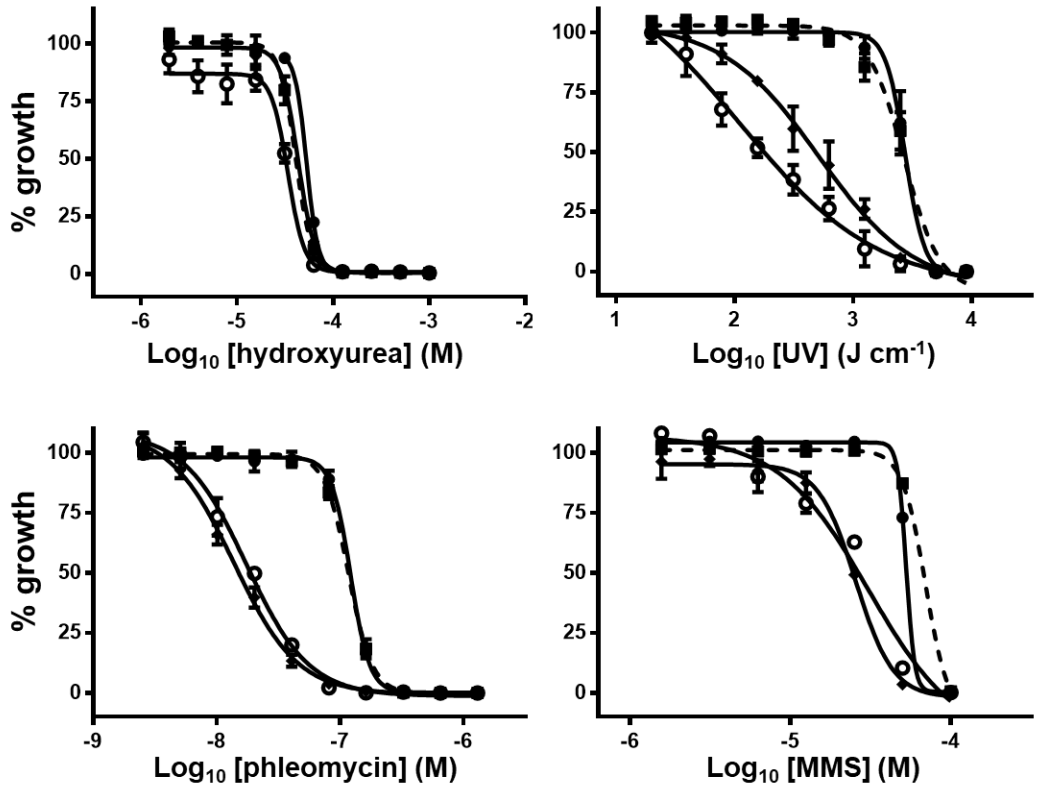

Figure 4.3: Susceptibility of *T. brucei* Tb*snm1*Δ Tb*mre11*Δ null line towards various DNA damaging treatments.
Dose response curves of *T. brucei* wild type (●), Tb*snm1*Δ (■), Tb*mre11*Δ (♦), and Tb*snm1*Δ Tb*mre11*Δ (o) cell lines to hydroxyurea, UV, phleomycin and MMS. All data points are mean values ± standard deviations from experiments performed in quadruplicate.

For most of the DNA damaging treatments tested, the susceptibility displayed by the double null mutant lines was equivalent to the more sensitive phenotype shown by the single null for each gene pairing. For example, all Tb*csb*-deficient cell types are approximately 5-fold more susceptible to UV than wild type or Tb*snm1*Δ lines such that the Tb*snm1*Δ Tb*csb*Δ line have an EC_{50} similar to Tb*csb*Δ parasites. As such, lack of TbSNM1 and TbCSB activities in the same cell does not lead to an increase in susceptibility to UV. The only situation where a combinatorial effect on susceptibility was observed in cells lacking TbSNM1 and TbMRE11. Intriguingly, such double null mutant parasites were more than 20-fold more sensitive to UV-induced lesions relative to *T. brucei* wild type and Tb*snm1*Δ and 4-fold more sensitive relative to Tb*mre11*Δ. This difference may be an experimental artefact possibly due to how the UV dosage was applied or could reflect that TbSNM1 does plays a secondary role in resolving UV-induced damage, a phenotype that is only apparent in cells comprised in the HR pathway.

Treatment	*T. brucei* EC_{50}			
	Wild type	**Tb*snm1Δ***	**Tb*mre11Δ***	**Tb*snm1Δ*Tb*mre11Δ***
Hydroxyurea (μM)	53.37 ± 3.68	40.62 ± 2.26 (1.3)	43.10 ± 0.84 (1.2)	33.77 ± 0.38 (1.6)
Phleomycin (μM)	0.12 ± 0.01	0.12 ± 0.00 (1.0)	0.01 ± 0.00 (12.0)*	0.01 ± 0.00 (12.0)*
MMS (μM)	33.02 ± 0.28	35.82 ± 0.29 (0.9)	12.63 ± 0.47 (2.5)*	15.32 ± 1.32 (2.2)*
UV (kJ/cm)	2.58 ± 0.39	2.66 ± 0.18 (1.0)	0.53 ± 0.11 (4.9)*	0.11 ± 0.09 (23.3)*

Treatment	*T. brucei* EC_{50}			
	Wild type	**Tb*snm1Δ***	**Tb*exo1Δ***	**Tb*snm1Δ* Tb*exo1Δ***
Hydroxyurea (μM)	47.56 ± 1.90	38.62 ± 2.71 (1.2)	52.59 ± 1.54 (0.9)	43.59 ± 1.84 (1.1)
Phleomycin (μM)	0.12 ± 0.00	0.12 ± 0.00 (1.0)	0.063 ± 0.00 (1.9)*	0.05 ± 0.00 (2.2)*
MMS (μM)	27.89 ± 0.63	42.28 ± 2.89 (0.7)	32.46 ± 0.71 (0.9)	40.44 ± 1.32 (0.7)
UV (kJ/cm)	3.54 ± 0.20	3.90 ± 0.32 (0.9)	2.07 ± 0.14 (1.7)	3.15 ± 0.98 (1.1)

Treatment	*T. brucei* EC_{50}			
	Wild type	**Tb*snm1Δ***	**Tb*csbΔ***	**Tb*snm1Δ* Tb*csbΔ***
Hydroxyurea (μM)	71.88 ± 0.89	67.91 ± 1.80 (1.1)	69.00 ± 2.67 (1.0)	69.77 ± 2.38 (1.0)
Phleomycin (μM)	0.04 ± 0.00	0.03 ± 0.00 (1.3)	0.04 ± 0.00 (1.1)	0.04 ± 0.00 (1.1)
MMS (μM)	27.78 ± 5.17	30.94 ± 13.45 (0.9)	26.73 ± 8.54 (1.0)	31.22 ± 10.4 (0.9)
UV (kJ/cm)	2.12 ± 0.18	2.47 ± 1.49 (0.9)	0.42 ± 0.14 (5.1)*	0.47 ± 0.05 (4.5)*

Treatment	*T. brucei* EC_{50}			
	Wild type	**Tb*snm1Δ***	**Tb*rev2Δ***	**Tb*snm1Δ* Tb*rev2Δ***
Hydroxyurea (μM)	67.39 ± 0.65	50.21 ± 1.72 (1.3)	58.18 ± 0.39 (1.2)	52.20 ± 1.94 (1.3)
Phleomycin (μM)	0.062 ± 0.00	0.046 ± 0.00 (1.4)	0.042 ± 0.00 (1.5)	0.046 ± 0.00 (1.4)
MMS (μM)	41.41 ± 3.56	45.76 ± 0.65 (0.9)	37.82 ± 1.16 (1.1)	45.97 ± 0.38 (0.9)
UV (kJ/cm)	3.61 ± 0.29	3.17 ± 0.34 (1.1)	3.74 ± 0.94 (1.0)	3.87 ± 0.35 (0.9)

Treatment	*T. brucei* EC_{50}			
	Wild type	**Tb*snm1Δ***	**Tb*rev3Δ***	**Tb*snm1Δ* Tb*rev3Δ***
Hydroxyurea (μM)	67.39 ± 0.65	50.21 ± 1.72 (1.3)	50.68 ± 0.83 (1.3)	52.20 ± 1.76 (1.3)
Phleomycin (μM)	0.062 ± 0.00	0.046 ± 0.00 (1.4)	0.046 ± 0.00 (1.4)	0.038 ± 0.00 (1.6)
MMS (μM)	41.41 ± 3.56	45.76 ± 0.65 (0.9)	38.65 ± 1.49 (1.0)	33.88 ± 0.70 (1.2)
UV (kJ/cm)	3.46 ± 0.45	3.92 ± 1.56 (0.9)	5.51 ± 1.08 (0.6)	5.55 ± 0.73 (0.6)

Table 4.1: Susceptibility of *T. brucei* double null lines to DNA damaging treatments.
Data represents EC_{50} values of various *T. brucei* lines against hydroxyurea, phleomycin, MMS and UV. All values are means ± standard deviations from experiments performed in quadruplicate. The ratio of EC_{50} values between wild type and single/double null mutant lines is shown as fold difference, in parentheses. *Indicates significant differences in susceptibility ($P < 0.0001$ between wild type and null lines, as assessed by Student's *t* test (GraphPad Software).

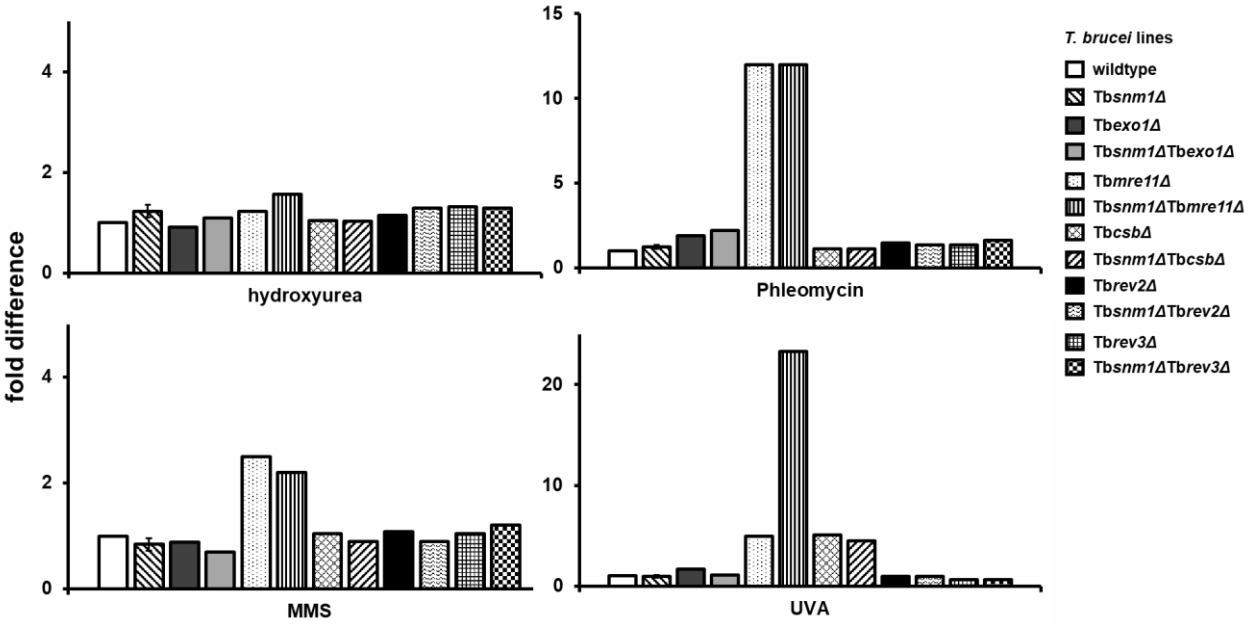

Figure 4.4: Comparison of *T. brucei* null mutant EC_{50} values.
The susceptibility of *T. brucei* various single and double null mutant lines against hydroxyurea (HU), phleomycin (Phleo), methyl methanesulfonate (MMS) and ultraviolet radiation (UV), as judged by their EC_{50} values, was compared and expressed as a fold difference relative to wild type.

4.1.2.3 Susceptibility of T. brucei double null lines towards mechlorethamine

As with the single null mutant lines, a series of phenotypic screens were performed using mechlorethamine as the selective agent. The resultant cell density data was analysed, plotted as dose response curves from which EC_{50} values was determined (Figure 4.5; Table 4.2). Again, the fold differences for each single and double null mutant line against the ICL inducing agent was displayed as a bar chart (Figure 4.6).

The growth profiles and EC_{50} values show a number of interesting features relating to how components of the *T. brucei* ICL repair interact. Firstly, cells lacking TbSNM1 and TbMRE11 display a hypersensitivity phenotype towards mechlorethamine as compared to wild type cells and Tb*snm1* or Tb*mre11* single null mutant lines: Tb*snm1*Δ Tb*mre11*Δ parasites are approximately 40-, 6- and 15-fold more susceptible to this agent relative to *T. brucei* wild type, Tb*snm1*Δ and Tb*mre11*Δ, respectively. This increase in sensitivity shown by the double null trypanosomes is indicative that the DNA repair enzymes TbSNM1 and TbMRE11 function in a non-epistatic fashion and do not operate in the same ICL repair system. Secondly, cells lacking TbSNM1 and TbCSB exhibit a mechlorethamine sensitivity similar to Tb*snm1*Δ parasites with both lines being more susceptible to this compound than wild type and Tb*csb*Δ cells. As the double null cells do not show an additional increase in sensitivity to the ICL-

inducing agent, it is plausible that TbSNM1 and TbCSB are epistatic and as such do operate in the same ICL repair system. This epistatic interaction appears to extend across to TbEXO1 with the Tb*snm1*Δ Tb*exo1*Δ double null cells showing a similar trait as the Tb*snm1*Δ Tb*csb*Δ line. Finally, TbREV2 and TbREV3 do not play a discernible role in trypanosomal ICL repair, even in the absence of TbSNM1, confirming the observations reported in Chapter 3.

Control growth inhibition assays using DFMO revealed that the above susceptibility profiles displayed by each double mutant line were not due to off target effects as all lines showed similar sensitivities to this trypanocidal agent.

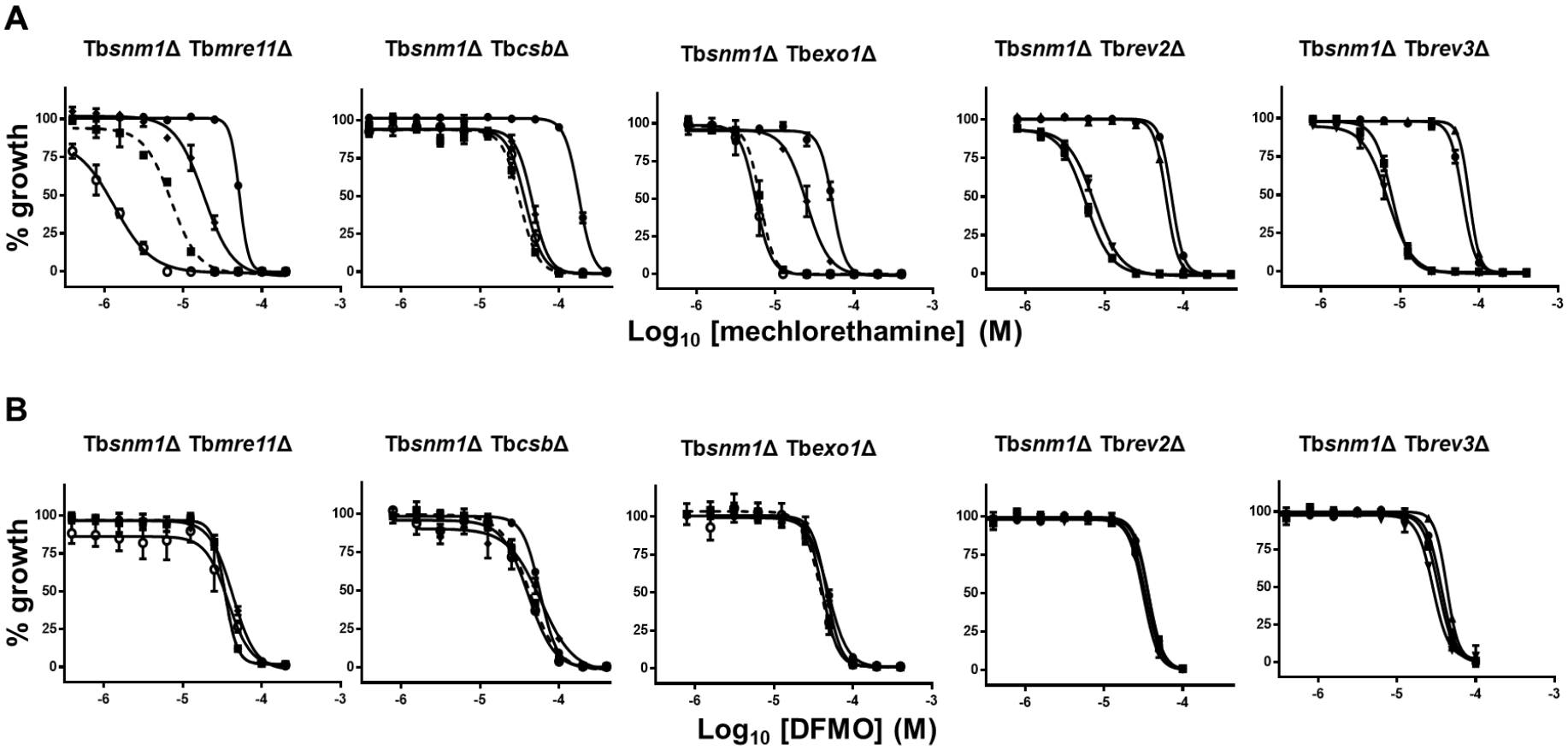

Figure 4.5: Susceptibility of *T. brucei* null mutants towards mechlorethamine and DFMO.
Dose response curves of *T. brucei* wild type (●), Tb*snm1*Δ (■), single null mutant (♦) and double null mutant line (o) towards mechlorethamine (A) and DFMO (B). All data points are mean values ± standard deviations from experiments performed in quadruplicate.

Treatment	*T. brucei* EC_{50}			
	Wild type	**Tb*snm1*Δ**	**Tb*mre11*Δ**	**Tb*snm1*ΔTb*mre11*Δ**
mechlorethamine	51.82 ± 0.32	7.09 ± 0.28 (7.3)*	18.76 ± 1.43 (2.8)*	1.26 ± 0.44 (41.1)*
DFMO	34.57 ± 0.87	34.14 ± 0.37 (1.0)	42.95 ± 1.50 (0.8)	37.18 ± 3.38 (0.9)

Treatment	*T. brucei* EC_{50}			
	Wild type	**Tb*snm1*Δ**	**Tb*csb*Δ**	**Tb*snm1*Δ Tb*csb*Δ**
mechlorethamine	37.10 ± 8.58	1.43 ± 0.25 (26.5)*	3.10 ± 0.33 (12.0)*	1.61 ± 0.06 (23.1)*
DFMO	57.14 ± 0.48	42.65 ± 2.72 (1.3)	57.40 ± 5.44 (1.0)	40.60 ± 1.96 (1.4)

Treatment	*T. brucei* EC_{50}			
	Wild type	**Tb*snm1*Δ**	**Tb*exo1*Δ**	**Tb*snm1*Δ Tb*exo1*Δ**
mechlorethamine	50.47 ± 4.39	6.43 ± 0.49 (7.5)*	24.94 ± 2.87 (2.0)*	5.68 ± 0.56 (8.9)*
DFMO	48.77 ± 2.19	38.61 ± 2.18 (1.3)	46.41 ± 0.32 (1.1)	44.30 ± 2.04 (1.1)

Treatment	*T. brucei* EC_{50}			
	Wild type	**Tb*snm1*Δ**	**Tb*rev2*Δ**	**Tb*snm1*Δ Tb*rev2*Δ**
mechlorethamine	70.94 ± 1.25	5.76 ± 0.41 (12.3)*	60.17 ± 0.90 (1.2)	7.45 ± 0.21 (9.5)*
DFMO	36.75 ± 0.57	34.09 ± 2.60 (1.1)	31.40 ± 0.54 (1.2)	36.46 ± 0.59 (1.0)

Treatment	*T. brucei* EC_{50}			
	Wild type	**Tb*snm1*Δ**	**Tb*rev3*Δ**	**Tb*snm1*Δ Tb*rev3*Δ**
mechlorethamine	61.94 ± 1.90	7.87 ± 0.39 (7.9)*	75.20 ± 2.22 (0.8)	6.99 ± 0.70 (8.9)*
DFMO	36.75 ± 0.57	33.81 ± 2.20 (1.0)	42.97 ± 0.64 (0.9)	29.31 ± 0.40 (0.9)

Table 4.2: Susceptibility of double null mutants towards mechlorethamine and DFMO.

EC_{50} values of *T. brucei* wild type and null lines against mechlorethamine and DFMO (in μM). All values are means ± standard deviations from experiments performed in quadruplicate. The ratio of EC_{50} values between wild type and null mutant lines is given as fold difference in parentheses. *Indicates significant differences in susceptibility ($P < 0.0001$) between wild type and null lines, as assessed by Student's *t* test (GraphPad Software).

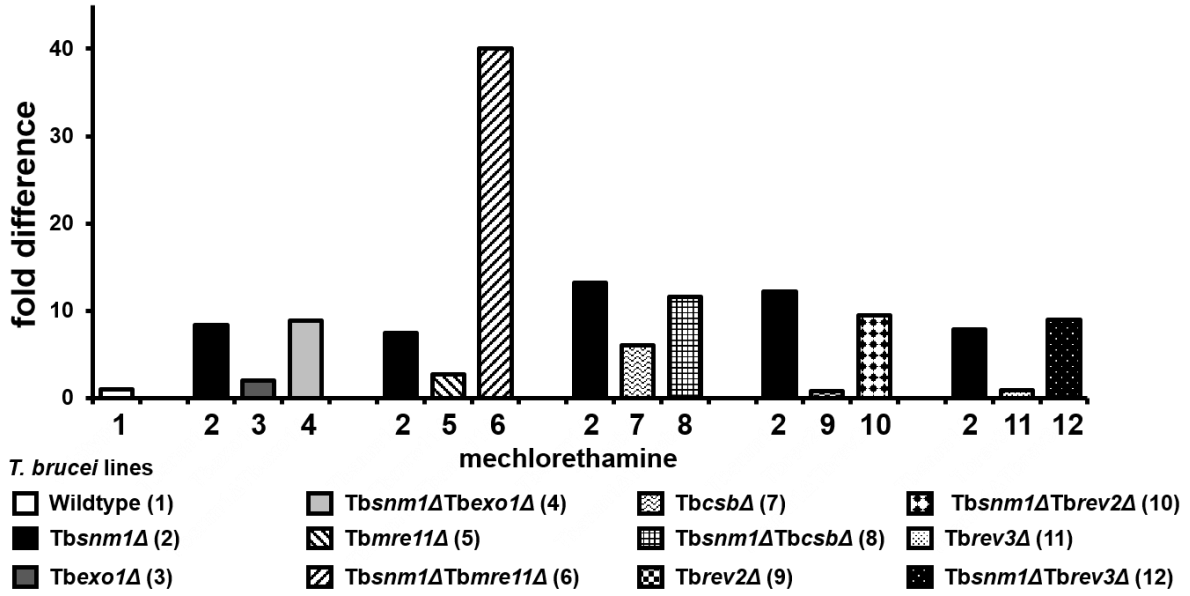

Figure 4.6: Comparison of *T. brucei* double null mutant EC_{50} values.
The susceptibility of *T. brucei* various single and double null mutant lines against mechlorethamine, as judged by their EC_{50} values, was compared and expressed as a fold difference relative to wild type.

4.2 Confirming the interplay of HR, NER, and MMR pathways in ICL repair

Based on our initial findings, we hypothesised that *T. brucei* expresses two distinct ICL repair systems, one involving the activities of TbSNM1/TbCSB/TbEXO1 with the other centred on TbMRE11. To explore this further a series of additional double null lines were generated to investigate the interplay between TbMRE11, TbCSB and TbEXO1.

Using the previously described gene interruption plasmids in conjunction with nucleofection, *T. brucei* lines lacking TbCSB and TbMRE11 (Tb*csb*Δ Tb*mre11*Δ), TbEXO1 and TbMRE11 (Tb*exo1*Δ Tb*mre11*Δ) or TbCSB and TbEXO1 (Tb*csb*Δ Tb*exo1*Δ) activities were made and subsequently validated (see Appendices 3e-3g). The susceptibility of these lines to mechlorethamine was then tested with dose response curves drawn and EC_{50} values determined and compared (Figure 4.7 & Table 4.3). Fold differences are shown in bar chart form in Figure 4.8.

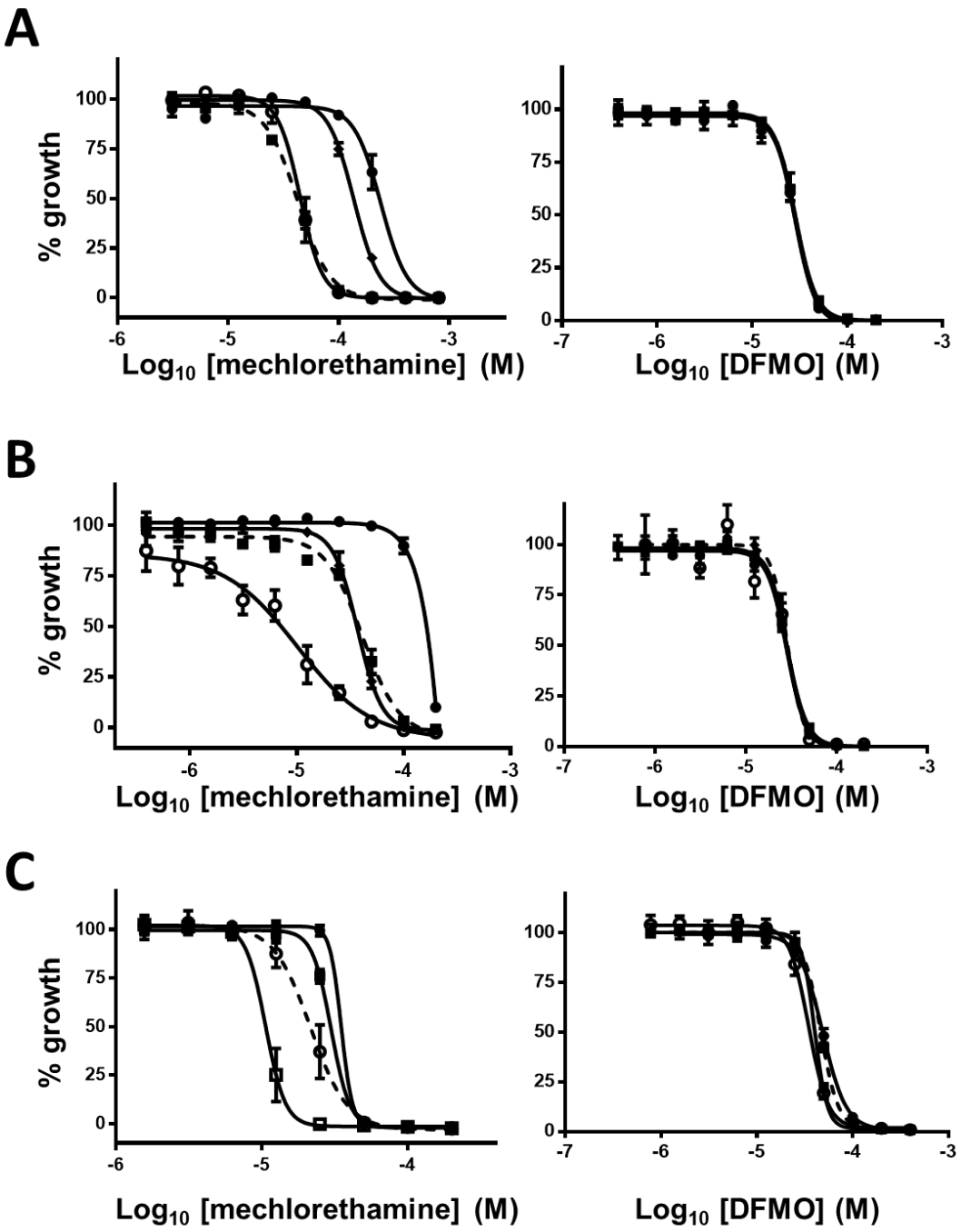

Figure 4.7: Susceptibility of *T. brucei* double null mutants towards mechlorethamine and DFMO.

A. Dose response curves of *T. brucei* wild type (●), Tb*csb*Δ (■), Tb*exo1*Δ (■) and Tb*csb*Δ Tb*exo1*Δ (○) towards mechlorethamine (A) and DFMO.

B. Dose response curves of *T. brucei* wild type (●), Tb*csb*Δ (■), Tb*mre11*Δ (▲) and Tb*csb*Δ Tb*mre11*Δ (○) towards mechlorethamine (A) and DFMO.

C. Dose response curves of *T. brucei* wild type (●), Tb*exo1*Δ (■), Tb*mre11*Δ (○) and Tb*exo1*Δ Tb*mre11*Δ (□) towards mechlorethamine (A) and DFMO.

All data points are mean values ± standard deviations from experiments performed in quadruplicate.

Treatment	*T. brucei* EC_{50} (μM)			
	Wild type	**Tb*csbΔ***	**Tb*exo1Δ***	**Tb*csbΔ* Tb*exo1Δ***
mechlorethamine	204.25 ± 38.44	62.19 ± 3.30 (3.3)*	159.35 ± 3.81 (1.6)*	44.48 ± 5.86 (4.5)*
DFMO	41.85 ± 0.68	48.14 ± 1.00 (1.1)	46.41 ± 0.32 (1.1)	45.70 ± 4.12 (1.1)
	Wild type	**Tb*csbΔ***	**Tb*mre11Δ***	**Tb*csbΔ* Tb*mre11Δ***
mechlorethamine	140.05 ± 5.10	37.08 ± 3.03 (3.8)*	41.40 ± 3.62 (3.4)*	10.30 ± 1.90 (13.6)*
DFMO	41.85 ± 0.68	48.14 ± 1.00 (1.1)	42.95 ± 1.50 (1.0)	45.88 ± 2.16 (1.1)
	Wild type	**Tb*exo1Δ***	**Tb*mre11Δ***	**Tb*exo1Δ*Tb*mre11Δ***
mechlorethamine	223.43 ± 2.83	81.27 ± 1.83 (2.8)*	60.57 ± 3.60 (3.7)*	50.31 ± 5.91 (4.4)*
DFMO	48.77 ± 2.16	46.41 ± 0.32 (0.9)	40.31 ± 1.74 (0.8)	34.92 ± 1.90 (0.7)

Table 4.3: Susceptibility of null mutants towards mechlorethamine and DFMO.
EC_{50} values of *T. brucei* wild type and null lines against mechlorethamine and DFMO. All values are means ± standard deviations from experiments performed in quadruplicate. The ratio of EC_{50} values between wild type and null mutant lines is given as fold difference in parentheses. *Indicates significant differences in susceptibility ($P < 0.0001$) between wild type and null lines, as assessed by Student's *t* test (GraphPad Software).

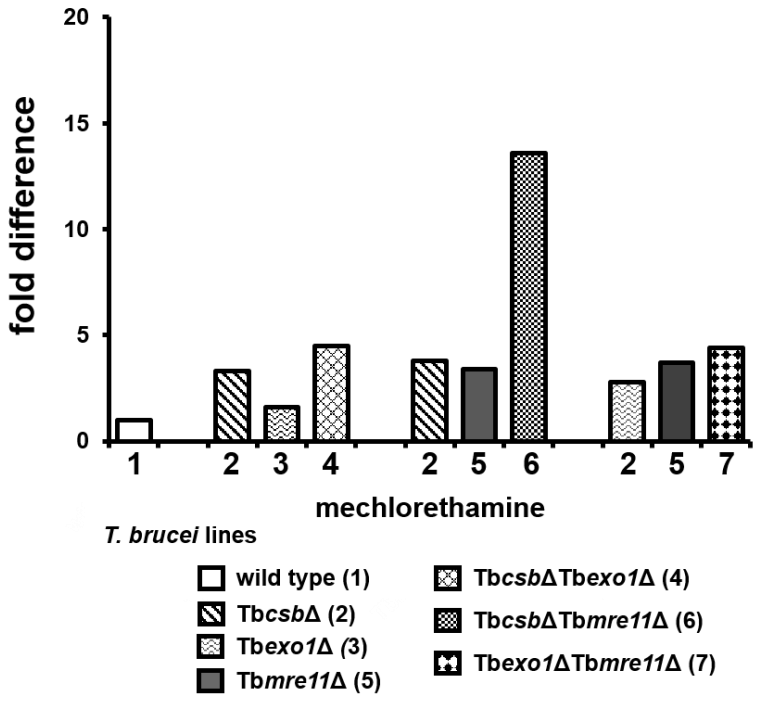

Figure 4.8: Comparison of *T. brucei* double null mutant EC_{50} values.
The susceptibility of *T. brucei* various single and double null mutant lines against mechlorethamine, as judged by their EC_{50} values, was compared and expressed as a fold difference relative to wild type.

As before, observations relating to the mechlorethamine growth inhibition data confirms our initial hypothesis. Cells lacking TbCSB and TbEXO1 reveal that these two DNA repair

enzymes, one involved in TC-NER and the other in MMR, function epistatically in ICL repair: The Tb*csb*Δ Tb*exo1*Δ parasites exhibit a mechlorethamine sensitivity similar to Tb*csb*Δ trypanosomes with both the single and double mutants being more susceptible to the ICL inducing compound than wild type. In contrast and analogous to observations made using the Tb*snm1*Δ Tb*mre11*Δ line, *T. brucei* Tb*csb*Δ Tb*mre11*Δ exhibit hypersensitivity towards mechlorethamine relative to wild type cells and either of the single null mutant lines. This increase in sensitivity is indicative that TbCSB and TbMRE11 function in a non-epistatic fashion and do not operate in the same ICL repair system. Finally, cells lacking TbEXO1 and TbMRE11 exhibit an epistatic relationship with the fold difference in mechlorethamine susceptibility between the Tb*exo1*Δ Tb*mre11*Δ and Tb*mre11*Δ lines being approximately the same (4-fold). This indicates that TbEXO1 can also operate in the MRE11-dependent pathway.

All of the double null mutant data involving TbSNM1, TbCSB, TbEXO1 and TbMRE11 clearly shows that *T. brucei* expresses at least two distinct ICL repair systems with one involving the concerted action of TbSNM1, TbCSB and TbEXO1 with the other using TbMRE11 and TbEXO1. It is tempting to speculate that given TbCSB plays a role in TC-NER, that the former SNM1-dependent pathway functions to resolve ICLs encountered during DNA transcription while the MRE11-dependent system helps remove ICLs encountered during DNA replication.

4.3 Chapter Summary

This chapter has focused on understanding the relationship between various DNA repair proteins that function in different DNA repair pathways to help resolve ICLs. Here, we have shown that:

1. *T. brucei* possesses at least two distinct ICL repair systems
    a. An SNM1-dependent ICL repair system where TbSNM1 co-operates with TC-NER (TbCSB) and MMR (TbEXO1) enzymes to repair the encountered damaged, possibly triggered as a result of RNA polymerase stalling
    b. An SNM1-independent ICL repair systems which utilises components the HR (TbMRE11) and MMR (TbEXO1) pathways to repair the encountered damaged, possibly triggered as a result of DNA polymerase stalling
2. The TbREV2 DNA helicase and TbREV3 DNA polymerase appear to play no role in ICL repair

5. The trypanosomal Fanconi Anaemia System

The Fanconi Anaemia (FA) repair pathway is the major ICL repair system in mammalian cells. This mechanism, first discovered through genetic profiling of patients with the disorder Fanconi Anaemia, involves at least 30 proteins which can be divided into four groupings comprising of 1. The FA core complex, 2. Recruitment factors, 3. Effector proteins and 4. FA-associated proteins (Figure 5.1). It is now recognised that other eukaryotes including fish, plants, insects and fungi all have their own version of the FA pathway, with such organisms often expressing a subset of homologues related to the human FA proteins (Moldovan and D'Andrea, 2009; Jones and Huang, 2012; McHugh, Ward and Chovanec, 2012; Zhang and Walter, 2014).

This chapter focuses on the identification of FA factors present in *T. brucei* and further unravelling of their function in relation to ICL repair. To determine whether the parasite possesses components of this system, human, zebrafish (*D. rerio*), fruit fly (*D. melanogaster*), plant (*A thaliana*) and yeast (*S. cerevisiae*) FA protein sequences (complete or a specific domain) were used to search for trypanosome homologues held on the TriTryp and NCBI databases using a reciprocal Blast analysis. This revealed that *T. brucei* has the potential to express a minimal FA repair pathway, analogous to the situation noted for yeast (Ward *et al.*, 2012). Out of the 31 sequences examined, *T. brucei* has discernible homologues for 9 activities (Figure 5.1). Most of these are direct homologues of FA effector proteins that play or are postulated to function in the parasite's HR pathway (FANCD1 (known as BRCA2; (Hartley and McCulloch, 2008)), FANCJ (referred to as CHL1), FANCO (or RAD51C; (Dobson *et al.*, 2011)), and FANCR (commonly known as RAD51; (Proudfoot and McCulloch, 2005))), NER pathway (FANCQ (or XPF; (Machado *et al.*, 2014))) or as an essential spindle checkpoint protein (FANCV (known as MAD2)). Of the remaining trypanosomal sequences, only one showed homology to a component of the FA core complex (FANCM (also known as MPH1)) and two related to FA-associated proteins (FAN1 and USP1). Interestingly, *T. brucei* appears to have no detectable versions of FANCD2 or FANCI, the two FA recruitment factors proteins.

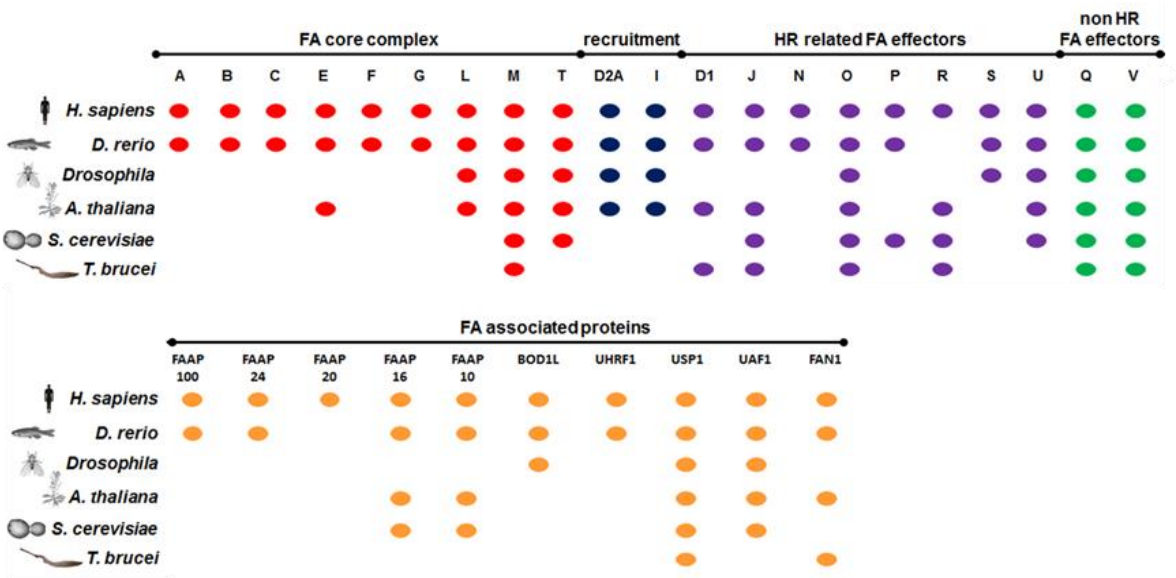

Figure 5.1: Identification of putative components of the trypanosomal FA pathway. Comparison of the FA pathway components expressed by *Danio rerio* (*D. rerio*; fish), *Drosophila melanogaster* (*Drosophila*; insect), *Arabidopsis thaliana* (*A. thaliana*; plant), *Saccharomyces cerevisiae* (*S. cerevisiae*; yeast) and *T. brucei* in relation to the system possessed by humans (*H. sapiens*). Trypanosomal FA factors were identified using a reciprocal Blast analysis against human FA factors. A coloured circle indicates the possibility for the presence of a given factor whereas no circle indicates that that component is most probably absent. In mammalian cells, the FA ICL repair pathway can be subdivided the FA core complex (red), recruitment factors (blue), FA effectors (further split as to whether it involves homologous recombination (HR) (purple) or other pathways (green)) and FA-associated proteins (orange). Figure layout derived from (Zhang *et al.*, 2009; Dong *et al.*, 2015).

5.1 Analysis of the *T. brucei* FANCM homologue

Analysis of the *T. brucei* genome database indicated that this parasite has the potential to express only one component of the FA core complex, namely TbFANCM (Tb927.7.2970; referred from now on as TbHEL1 due to presence of a helicase domain in the protein sequence). The deduced trypanosomal amino acid sequence showed identity to the amino termini of human FANCM (23 %) and DICER (21 %) with this homology centring on the DEAD (PF00270) and Helicase C (PF00271) domains, regions found in members of the helicase superfamily 2 (SF2) RigI group (Figure 5.2). Intriguingly, the equivalent HEL1 sequence was found in other *Trypanosoma* species that are predominantly found in the bloodstream of their mammalian host (*e.g. T. congolense*, *T. evansi*, *T. vivax*), some other trypanosomatids (*e.g. Crithidia fasciculate*, *Leptomonas pyrrhocoris*) but absent from intracellular *Trypanosoma* and *Leishmania* species (*e.g. T. cruzi*, *L. major*, *L. donovani*). Phylogenetic analysis of the trypanosomatid *hel1* genes with their plant, fungus and vertebrate *fancm* counterparts using the Phylogeny.fr algorithm revealed that the parasite sequences are evolutionarily distinct from

homologues expressed in the other organisms, forming their own distinct clade (Figure 5.3). In relation to higher eukaryotic organisms, this difference was unsurprising given that the encoded proteins generally possess additional domains in their backbone (Figure 5.2). For the human FANCM, these extra regions facilitate 1. binding of the helicase to double stranded DNA *via* a FANCM-MHF (PF16783) domain, 2. function to activate downstream cell cycle kinases *via* a mediator of replication checkpoint 1 (MRC1; PF09444) domain and 3. cleave the target substrate through a ERCC4 nuclease (PF02732) domain. Given that equivalent regions are apparently absent from TbHEL1 then the trypanosomal enzyme, if it does function as a DNA helicase, does so by a mechanism distinct from its mammalian counterpart. The yeast FANCM homologue which has been shown to function in ICL repair (Ward *et al.*, 2012) also lacks many of these additional domains but in our phylogenetic analysis the fungal sequences tend to be more closely rooted to the helicases expressed by vertebrates.

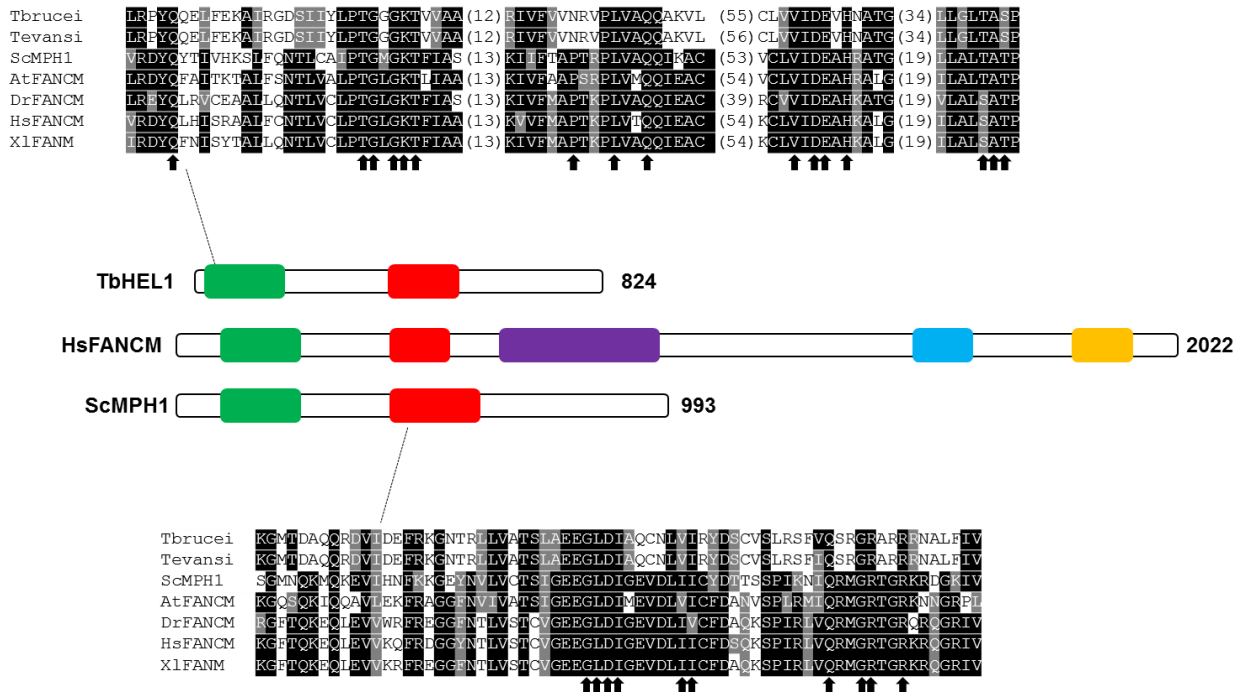

Figure 5.2: Domain and sequence analysis of TbHEL1.
Schematic diagram showing the organization of conserved domains found in *H. sapiens* FANCM (HsFANCM; BC140776), *S. cerevisiae* MPH1 (ScMPH1; KI893982) and TbHEL1 (Tb927.7.2970). The regions highlighted include the DEAD (green; PF00270), Helicase C (red; PF00271), FANCM-MHF (purple; PF16783), MRC1 (light blue; PF09444) and ERCC4 (yellow; PF02732) domains. The DEAD (top alignment) and Helicase C (bottom alignment) domains of TbHEL1 was compared with the equivalent regions from *T. evansi* (TevSTIB805.7.3080), *S. cerevisiae* MPH1, *Arabidopsis thaliana* FANCM (NM_001198212), *Drosophilia melanogaster* FANCM (EF088195), *H. sapiens* FANCM and *Xenopus laevis* (XM_012969053). Conserved residues (in black or grey) are highlighted with arrows marking the conserved amino acids that form the HMM logo**.**

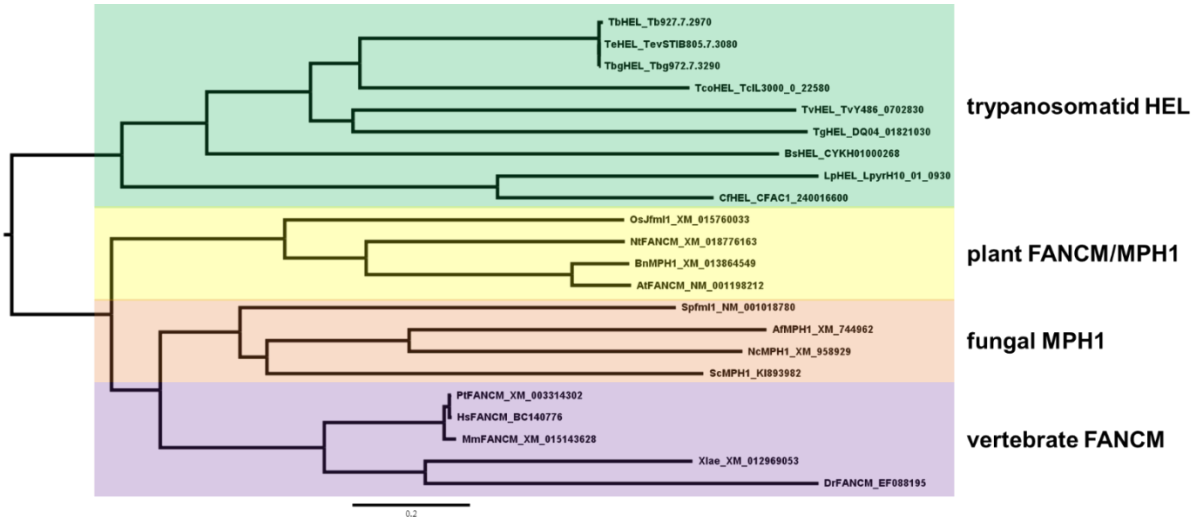

Figure 5.3: Phylogenetic tree analysis of FANCM sequences.
Phylogenetic analysis of the trypanosomatid *hel1* genes (green) forms a different clade to plant (yellow), fungal (pink), and vertebrate genes (purple) homologues. The sequences analysed using the Phylogeny.fr tool were *T. brucei hel1* (Tb*hel1*, Tb927.7.2970), *T.b.gambiense hel1* (Tbg972.7.3290), *T. congolense hel1* (TcIL3000_0_22580), *T. evansi hel1* (TevSTIB805.7.3080), *T. vivax hel1* (TvY486_0702830), *T. grayi hel1* (DQ04_01821030), *C. fasiculata hel1* (CFAC1_240016600), *L. pyrrhocoris hel1* (LpyrH10_01_0930), *B. saltans hel* (CYKH01000268), *H. sapiens fancm* (BC140776), *P. troglodytes fancm* (XM_003314302), *M. mulatta fancm* (XM_015143628), *Drosophilia melanogaster fancm* (EF088195), *S. cerevisiae mph1* (KI893982), *Xenopus fancm* (XM_012969053), *Arabidopsis thaliana fancm* (NM_001198212), *S. pombe fml1* (NM_01018780), *A. fumigatus mph1* (XM_744962), *B. rape mph1* (XM_013864549), *N. crassa mph1* (XM_958929), *O.s. Japonica fml1* (XM_015760033), and *N. tomentosiformis fancm* (XM_018776163).

5.1.1 Construction and validation of null mutant lines

Using the previously described gene deletion approach from Section 3, DNA constructs based around the hygromycin and neomycin resistance cassettes (pKO-Tbhel1-hyg and pKO-Tbhel1-neo DNA) were generated, the DNAs processed by restriction enzyme digestion and fragments purified. These were sequentially transformed into *T. brucei* wild type and Tb*snm1*-deficient cells, creating the Tb*hel1*Δ and Tb*snm1*Δ Tb*hel1*Δ lines. The gene interruption events and resultant loss of gene expression was validated using PCR-based approaches described earlier, with this data presented in Appendix 4a.

5.1.2 Phenotypic analysis of *T. brucei* lines lacking *hel1*

Following confirmation of the *T. brucei* single and double null Tb*hel1* null mutant lines, their growth properties were evaluated in comparison to wild type cells. This demonstrates that the recombinant cell lines grew at an equivalent rate as the controls (data not shown). The susceptibility of Tb*hel1*-deficient cells to various DNA damaging agents was then tested to evaluate whether the encoded enzyme does function in DNA repair. For each treatment, dose

response curves were generated (Figure 5.4), EC_{50} values calculated (Table 5.1) and the fold difference of EC_{50} values between wild type and null lines determined (in parentheses of Table 5.1). Together, this data strongly indicates that TbHEL1 has no role in any DNA repair pathway tested here, including any mechanism used to resolve ICLs.

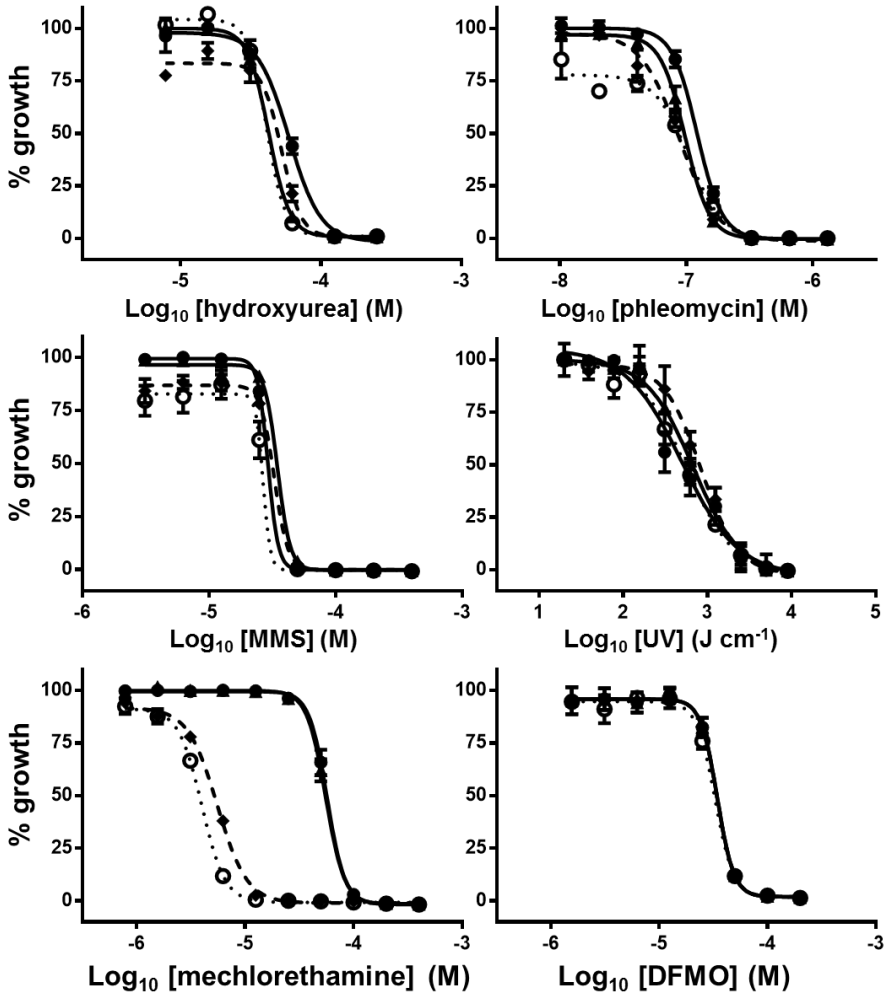

Figure 5.4: Susceptibility of *T. brucei* Tb*hel1*-deficient null lines towards various DNA damaging treatments.
Dose response curves of *T. brucei* wild type (●), Tb*snm1*Δ (■), Tb*hel1*Δ (♦), and Tb*snm1*Δ Tb*hel1*Δ (o) cell lines to hydroxyurea, UV, phleomycin, MMS, mechlorethamine and DFMO. All data points are mean values ± standard deviations from experiments performed in quadruplicate.

Treatment	*T. brucei* EC_{50} (µM)			
	Wild type	**Tb*snm1*Δ**	**Tb*hel1*Δ**	**Tb*snm1*ΔTb*hel1*Δ**
hydroxyurea	57.76 ± 2.20	48.97 ± 2.03 (1.2)	42.46 ± 0.34 (1.4)	41.12 ± 0.98 (1.4)
phleomycin	0.12 ± 0.00	0.08 ± 0.01 (1.5)	0.10 ± 0.00 (1.2)	0.09 ± 0.01 (1.3)
MMS	32.70 ± 0.12	36.35 ± 0.62 (0.9)	38.88 ± 0.53 (0.8)	29.90 ± 1.22 (1.1)
UV (kJ/cm)	0.52 ± 0.15	0.84 ± 0.11 (0.6)	0.76 ± 0.17 (0.7)	0.57 ± 0.03 (0.9)
mechlorethamine	56.85 ± 2.26	5.55 ± 0.07 (10.2)*	55.37 ± 2.08 (1.0)	3.99 ± 0.15 (14.3)*
DFMO	25.74 ± 1.90	34.14 ± 0.37 (0.8)	33.38 ± 0.15 (0.8)	32.73 ± 0.48 (0.8)

Table 5.1: Susceptibility of *T. brucei* Tb*hel1* null lines to DNA damaging treatments.
Data represents EC_{50} values of *T. brucei* wild type, Tb*snm1*Δ, Tb*hel1Δ* and Tb*snm1*Δ Tbh*el1Δ* against hydroxyurea, phleomycin, MMS, UV, mechlorethamine and DFMO. All values are means ± standard deviations from experiments performed in quadruplicate. The ratio of EC_{50} values between wild type and null mutant lines is given as a fold difference, in parentheses. *Indicates significant differences in susceptibility ($P < 0.0001$ between wild type and null lines, as assessed by Student's *t* test (GraphPad Software).

5.1.3 TbHEL1 and its role in RNA interference

Given that TbHEL1 appears to play no role in DNA repair and also has significant identity to the helicase domain of HsDICER, we next evaluated whether it could function in the trypanosomal RNA interference pathway. As with the FANCM alignment, comparison of the trypanosomatid HEL1s with DICERs and DRHs (DICER related helicases) from various other organisms showed that sequence homology was most pronounced in the DEAD (PF00270) and Helicase C (PF00271) domains (Figure 5.5). Again, phylogenetic analysis revealed that the protozoan parasites gene sequences were evolutionarily distinct from their counterparts possessed by other organisms, reflecting the early branching nature of trypanosomatid on the tree of life and potentially indicating that these pathogens have an unconventional DICER activity (Figure 5.6).

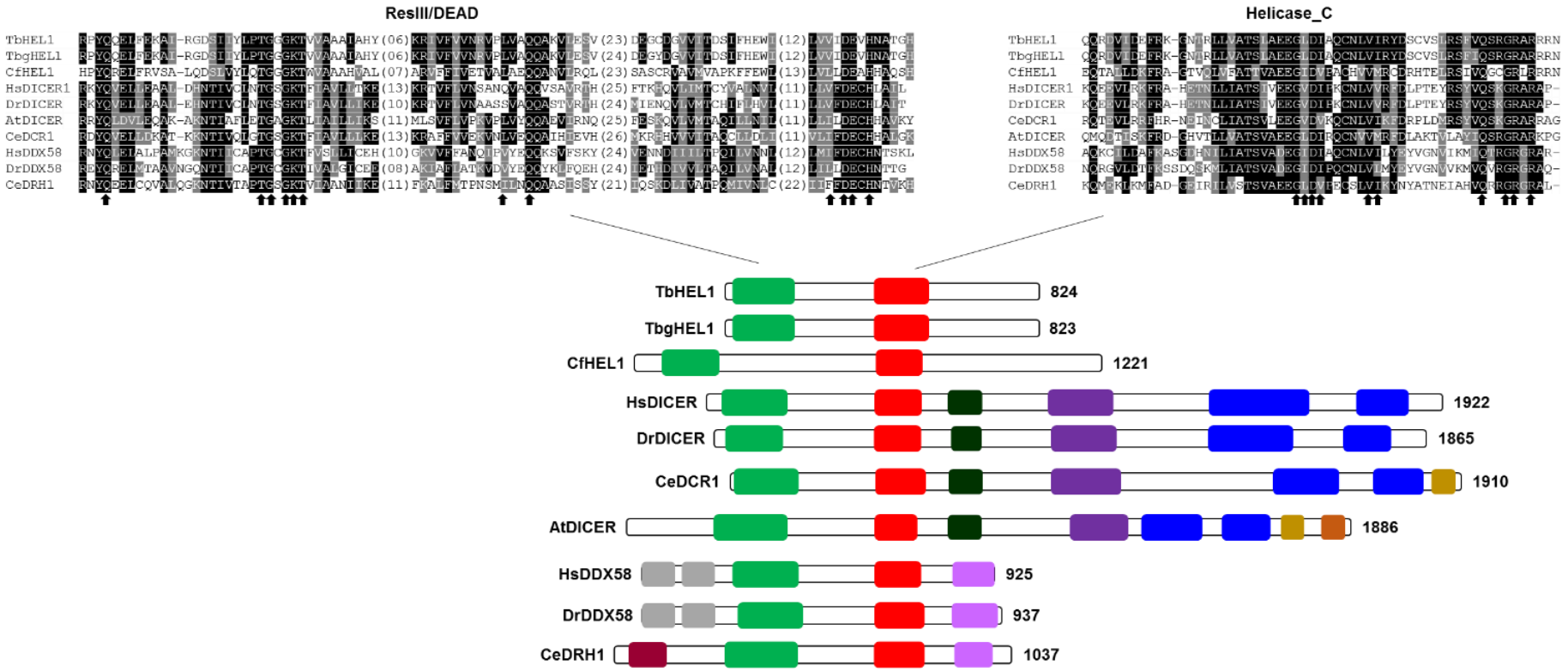

Figure 5.5: Domain and sequence analysis of TbHEL1.
Comparisons between the domain structure of *T. brucei* HEL1 (TbHEL1; Tb927.7.2970), *T.b.gambiense* HEL1 (TbgHEL1; Tbg972.7.3290), *C. fasiculata* HEL1 (CfHEL1; CFAC1_240016600), *H. sapiens* DICER (HsDICER; NM_0012916281), *D. rerio* DICER (DrDICER; NM_001161453), *C. elegans* DCR1 (CeDCR1; NM_068617), *A. thaliana* DICER (AtDICER; JN661702), *H. sapiens* DDX58 (HsDDX58; NM_014314), and *C. elegans* DRH1 (CeDRH1; NM_068617) with further comparisons made on conserved residues (emphasised using arrows). Domains shown include DEAD domain (green; PF00270), Helicase C domain (red; PF00271), RIG-1 domain (light purple; PF11648), Dicer dimerization domain (dark green; PF03368), PAZ domain (dark purple; PF02170), ribonuclease domain (blue; PF00636), CARD_2 (grey; PF16739), Sec34 (burgundy; PF04136), dsrm (yellow; PF00035), and DND1_DSRM (orange; PF14709).

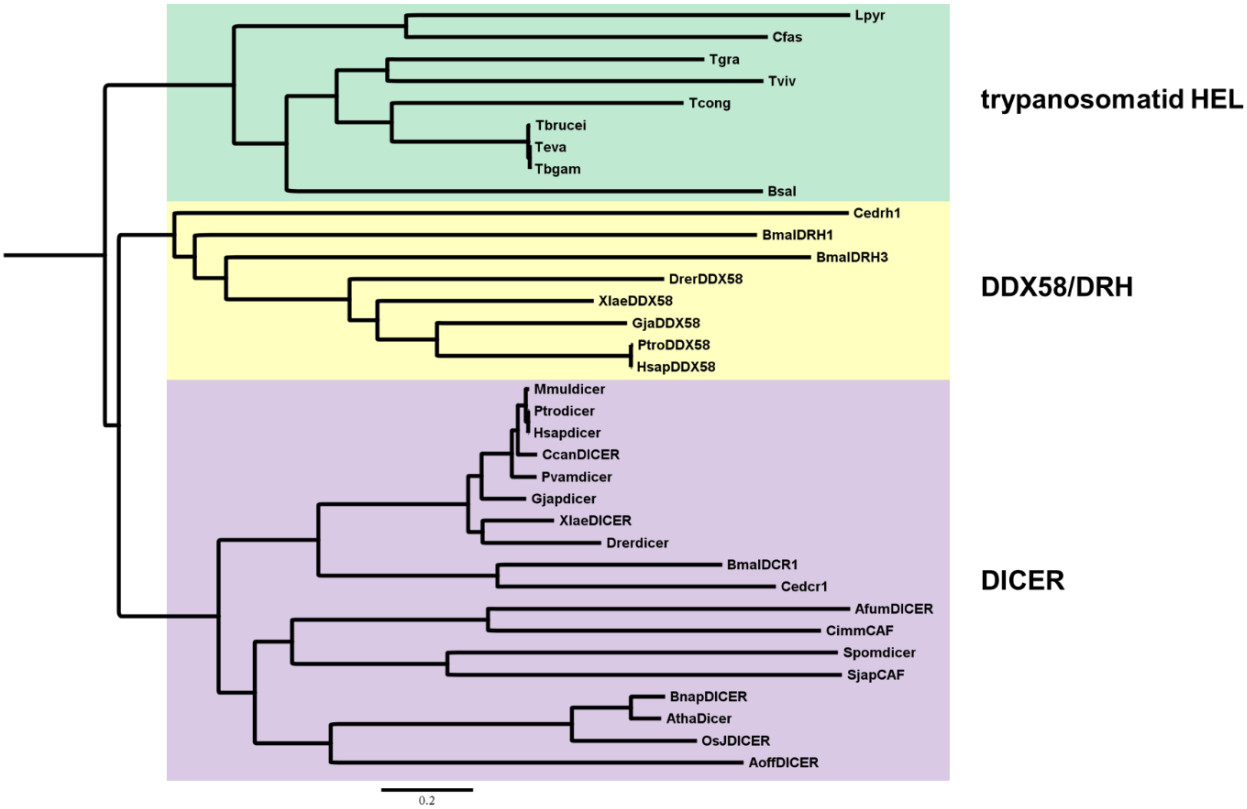

Figure 5.6: Phylogenetic tree analysis of TbHEL1 and DICER sequences.
The phylogenetic tree outlines the trypanosomatid HEL genes (green) in a different clade to that of the plant (yellow) and vertebrate genes (purple) with plant FANCM genes outlined as evolutionarily distinct from that of vertebrate. Gene names and sequence identities are given on the end of each clade: Lpyr (*L. pyrrhocoris*; LpyrH10_01_0930), Cfas (*C. fasciculate*; CFAC1_240016600), Tgra (*T. grayi*; DQ04_01821030), Tviv (*T. vivax*; TvY486_0702830), Tcong (*T. congolense;* TcIL3000_0_22580), Tbrucei (*T. brucei*; Tb927.7.2970), Teva (*T. evansi*; TevSTIB805.7.3080), Tbgam (*T. brucei gambiense*; Tbg972.7.3290), Bsal (*B. saltans*; CYKH01000268), Cedrh1 (*C. elegans* drh1; NM_068617), BmalDRH1 (*B. malayi* DRH1; LN855620)**,** BmalDRH3 (*B. malayi* DRH3; LN856998)**,** DrerDDX58 (*D. rerio* DDX58; NM_001306095)**,** XlaeDDX58 (*X. laevis* DDX58; XM_018257225)**,** GjaDDX58 (*G. japonicus* DDX58; XM_015414538)**,** Ptro (*P. troglodytes* DDX58; XM_001156662), HsapDDX58 (*H. sapiens*; NM_014314), Mmul dicer (*M. mulatta* dicer; NM_001257872), Ptrodicer (*P. troglodytes* dicer; XM_001154369), Hsapdicer (*H. sapiens* dicer; NM_0012916281), CcanDICER (*C. canadensis* DICER1; GFFV01000155)**,** Pvamdicer (*P. vampyrus* dicer; XM_011379597), Gjapdicer (*G. japonicus* dicer; XM_015416341)**,** XlaeDICER (*X. laevis* DICER; XM_018230462), Drerdicer (*D. rerio* dicer; NM_001161453), Bmal (*B. malayi* DCR1; LN857010), Cedcr1 (*C. elegans* dcr-1; NM_066360), AfumDICER (*A. fumigatus*; XM_748378), CimmCAF (*C. immitis* CAF; DS017001), Spomdicer (*S. pombe* dicer; NM_001023205), SjapCAF (*S. japonicus* CAF; XM_002174789), BnapDICER (*B. napus* DICER; XM_013841052), AthaDicer (*A. thaliana* Dicer; JN661702)**,** OsjDICER (*O.s. Japonica* DICER; CM000140) and AoffDICER (*A. officinalis* DICER; XM_020390741).

To see whether Tb*hel1* functions in the *T. brucei* RNAi pathway, gene integration vectors based around puromycin and blasticidin resistance cassettes (pKO-Tbhel1-bla and pKO-Tbhel1-pac) were constructed, processed by restriction enzyme digestion and the resultant

fragments purified. These were then sequentially transformed into *T. brucei* lines that could be induced to undergo RNAi against Tb*tao* or Tb*sodB*. These two lines were used because 1. the targeted activities, namely trypanosomal alternative oxidase or superoxide dismutase isoform b, respectively, are essential for the growth of bloodstream form trypanosomes (Helfert *et al.*, 2001; Wilkinson *et al.*, 2006) and 2. the dsRNA that promotes down regulation of the Tb*tao* or Tb*sodB* transcript are formed by a stem loop or linear RNA molecule, respectively. The resultant null parasites, designated as RNAi Tb*tao* Tb*hel1*Δ and RNAi Tb*sodB* Tb*hel1*Δ, were then subject to PCR validation that confirmed that Tb*hel1* had been successfully interrupted in both lines with an accompanying loss of Tb*hel1* expression (Figure 5.7).

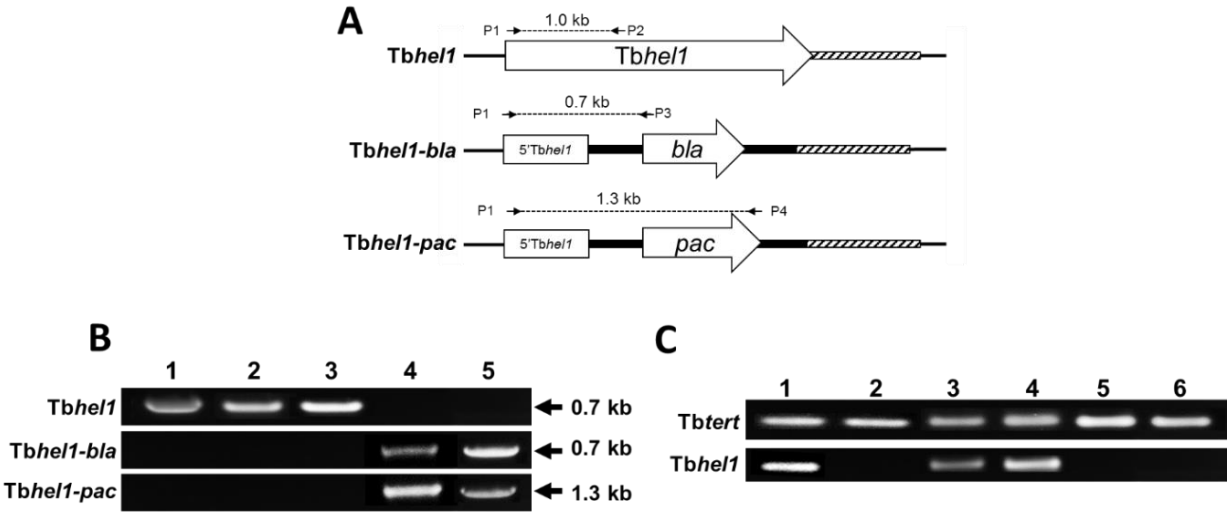

Figure 5.7: Confirming the deletion of Tb*hel1*.
A. Schematic for the representation of the Tb*hel1* allele and effects of disrupting this allele with genes encoding for blasticidin (*bla*) and puromycin (*pac*) resistance. P1 (Tbhel1-KO1), P2 (Tbhel1-q2), P3 (bla-1) and P4 (pac-1) correspond to regions where the primers anneal at the specific allele.
B. DNA fragments obtained after amplification on gDNA extracted from *T. brucei* wild type (lane 1), *T. brucei* RNAi-Tb*tao* (lane 2), *T. brucei* RNAi-Tb*sodb* (lane 3), RNAi-Tb*tao* Tb*hel1*Δ (lane 4), and RNAi-Tb*sodb* Tb*hel1*Δ (lane 5). Extractions from all lines were tested using primer combinations that specifically amplify biomarkers corresponding to the Tb*hel1* (Tbhel1-KO1/Tbhel1-q2), Tb*hel1-pac* (Tbhel1-KO1/pac-1) or Tb*hel1-bla* (Tbhel1-KO1/bla-1) alleles.
C. DNA fragments obtained after amplification on cDNA derived from RNA extracted from *T. brucei* wild type (lane 1), Tb*hel1*Δ (lane 2), RNAi-Tb*tao* (lane 3), RNAi-Tb*sobB* (lane 4), RNAi Tb*tao* Tb*hel1*Δ (lane 5), and RNAi Tb*sodB* Tb*hel1*Δ (lane 6) using primer combinations that specifically amplify intact Tb*hel1* (Tbhel1-q1/Tbhel1-q2) and Tb*tert* (Tbtert-F/Tbtert-R).

Following validation, the growth properties of the various Tb*hel1* null mutants that can undergo RNAi was determined in the presence/absence of the inducer (tetracycline) which promotes down regulation of the targeted transcript. Upon induction of RNAi in RNAi-Tb*tao*

and RNAi-Tb*sobB* cells (i.e. that contain a functional Tb*hel1*), parasite growth was significantly reduced in the former and halted in the latter in agreement with previous reports (Helfert *et al.*, 2001; Wilkinson *et al.*, 2006). In contrast, Tb*hel1*-deficient cells undergoing RNAi targeting these two transcripts continued to grow at an equivalent rate to non-induced controls (Part A and B of Figure 5.8). This suggests that TbHEL1 plays a crucial role in the *T. brucei* RNAi machinery.

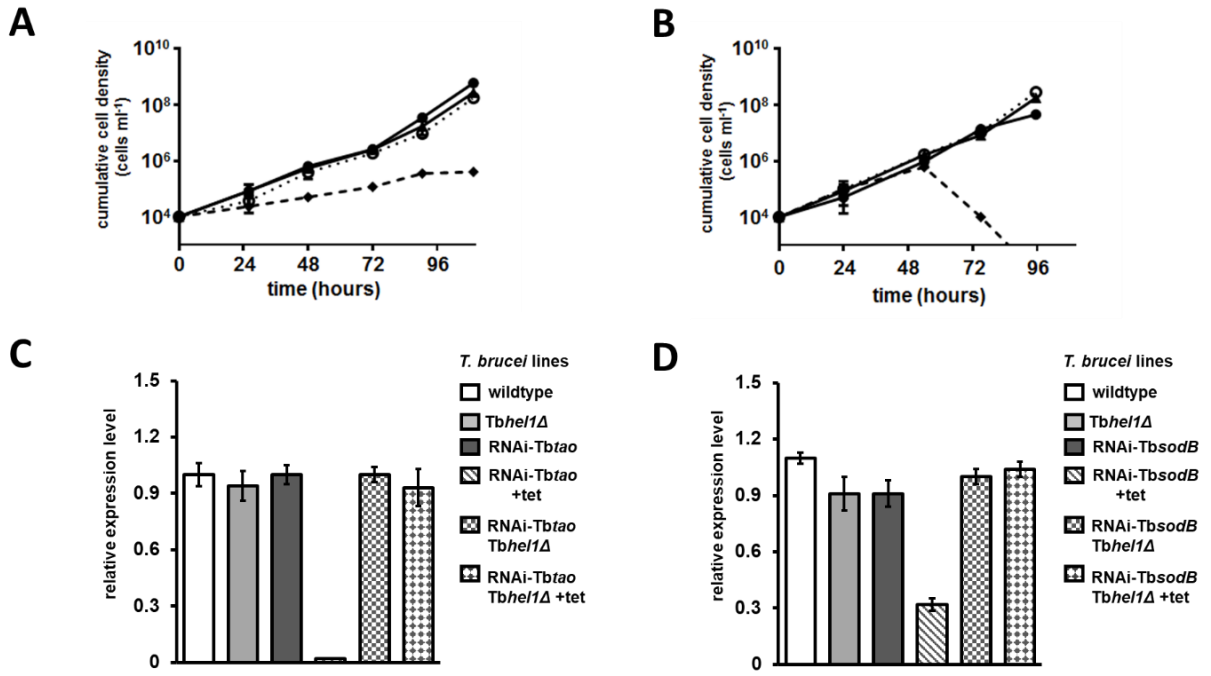

Figure 5.8: Analysing the role of TbHEL1 in RNA interference.
A. Cumulative growth of non-induced RNAi-Tb*tao* (○), induced RNAi Tb*tao* (♦), non-induced RNAi Tb*tao* Tb*hel1*Δ (●) and induced RNAi Tb*tao* Tb*hel1*Δ (▲).
B. Cumulative growth density curves of non-induced RNAi Tb*sodB* (○), induced RNAi Tb*sodB* (■), non-induced RNAi Tb*sodB* Tb*hel1*Δ (●) and induced RNAi Tb*sodB* Tb*hel1*Δ (▲).
C & D. The mRNA levels of *Tb*tao (C) or *Tb*sodB (D) in various induced (+tet) and non-induced parasite lines was evaluated by RT-qPCR and compared against the expression level of a standardized control (Tb*tert*). The average fold difference, as judged by $2^{-(\Delta\Delta C_T)}$ from reactions performed in triplicate standard deviation, plotted as a measure of the relative expression level.

To confirm that down-regulation had been blocked, RT-qPCR to detect the targeted mRNA (Tb*tao*, Tb*sodB*) was performed. In tetracycline treated Tb*hel1*-proficient RNAi-Tb*tao* and RNAi-Tb*sobB* cells, Tb*tao* or Tb*sodB* expression was shown to be ~50-fold and ~3-fold lower than in the non-induced trypanosomes, respectively (Part C and D of Figure 5.8). When Tb*hel1*-deficient parasites undergoing RNAi were analysed, transcript levels were equivalent to that observed in wild type and non-induced controls. This confirms that TbHEL1 does play a key

role in the *T. brucei* RNAi machinery and can interact with both linear and stem loop derived dsRNA templates. The precise interactions of this trypanosomal helicase with other RNAi components was not determined here although it is tempting to speculate that TbHEL1 does interact with TbDCL1 or TbDCL2, atypical DICER enzymes that usually only possess a nuclease domain (Patrick *et al.*, 2009).

5.2 Analysis of the *T. brucei* FANCJ homologue

FANCJ, also known as CHL1 or BRIP1, is one of the many FA effector proteins which are upregulated upon ubiquitination of the FANCD2/I complex to help unwind damaged DNA (Wu and Brosh, 2009; Daee and Myung, 2012; Brosh and Cantor, 2014; Wilson *et al.*, 2017). Searches of the *T. brucei* database identified a putative TbCHL1 homologue (Tb927.10.3550) that shares ~20% identity to counterpart sequences expressed by other organisms with this homology centering on the DEAD (PF00270), DEAD_2 (PF06733) and Helicase C2 (PF00271) domains, regions found in some members of the helicases of the SF2 RAD3 group

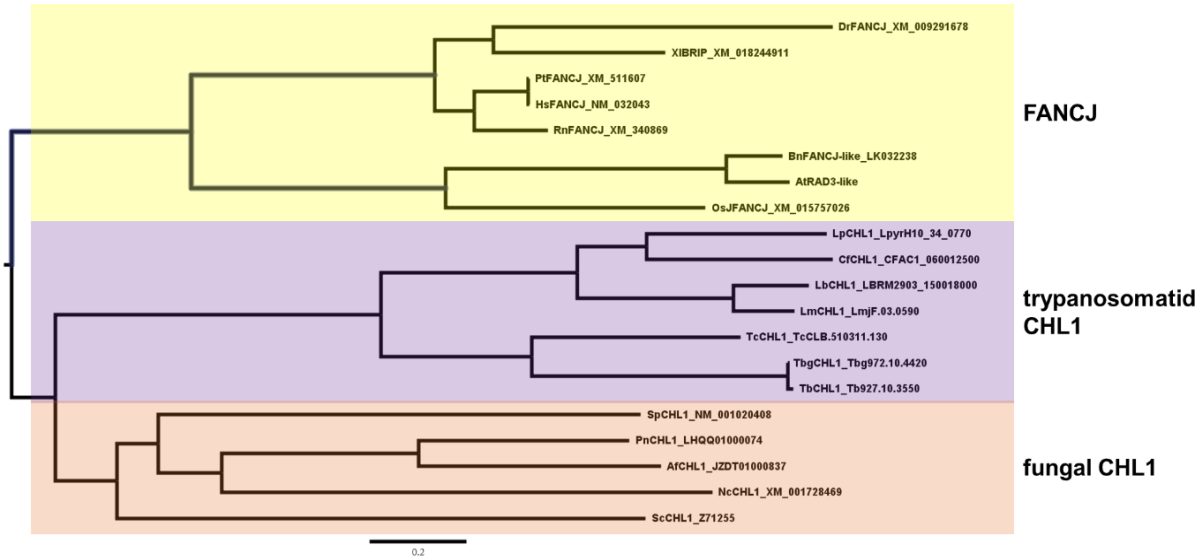

Figure 5.9: Phylogenetic analysis of FANCJ sequences.
A rooted phylogenetic tree of trypanosomatid CHL1 (purple), fungal CHL1 (pink) and vertebrate and plant FANCJ sequences, including humans and Aradopisis (yellow). Gene names and sequence identities are given on the end of each clade. *T. brucei chl1* (Tb927.10.3550), *T.b.gambiense chl1* (Tbg972.10.4420), *T. cruzi chl1* (TcCLB.510311.130), *L. Mexicana chl1* (LmjF.03.0590), *L. panamensis chl1* (LBRM2903_150018000), *C. fasciculate chl1* (CFAC1_060012500), *L. pyrrhocoris chl1* (LpyrH10_34_0770), *H. sapiens fancj* (NM_032043), *R. norvegicus fancj* (XM_340869), *P. troglodytes fancj* (XM_511607), *X. laevis brip* (XM_018244911), *Drosophilia fancj* (XM_009291678), *Aradopsis rad3-like* (AT1G79950), *B. napus fancj-like* (LK032238), *O.s.Japonica fancj* (XM_015757026), *S. cerevisiae chl1* (Z71255), *S. pombe chl1* (NM_001020408), *A. fumigatus chl1* (JZDT01000837), *N. crassa chl1* (XM_001728469), and *P. evpansum chl1* (LHQQ01000074).

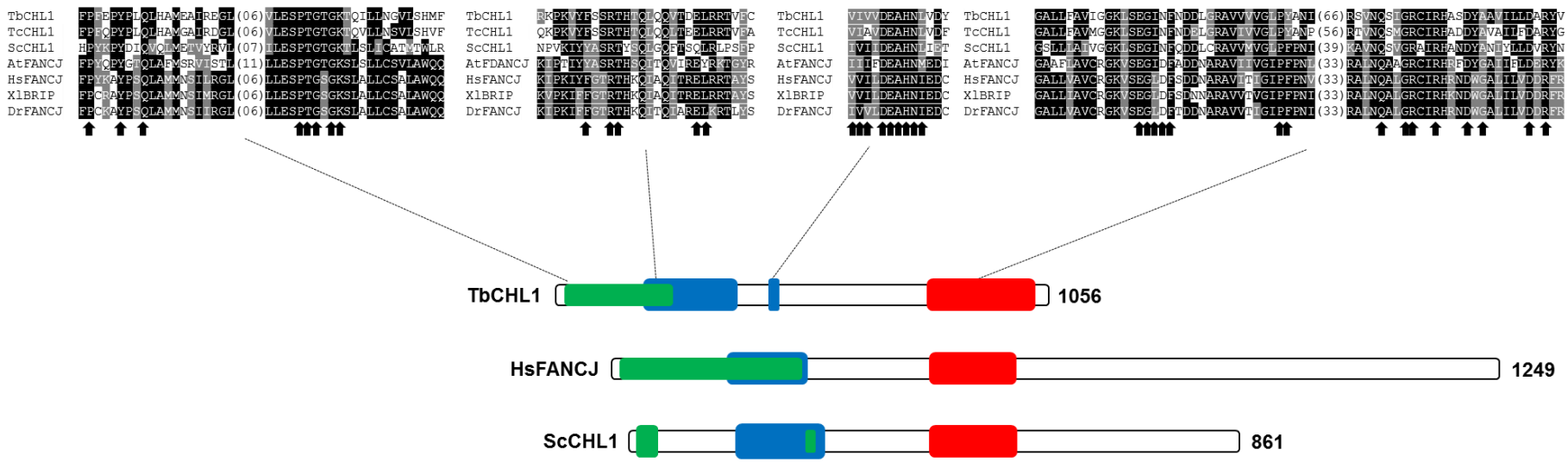

Figure 5.10: Domain and sequence comparisons of TbCHL1.
Schematic diagram showing the organization of conserved domains found *T. brucei* CHL1 (TbCHL1; Tb927.10.3550), *H. sapiens* FANCJ (HsFANCJ; NM_032043) and *S. cerevisiae* CHL1 (ScCHL1; Z71255). The regions highlighted include the DEAD (green; PF00270), DEAD_2 (blue; PF06733) and Helicase C2 domain (red; PF00271) domains. Alignments of the DEAD, DEAD_2 and Helicase C2 domains of the above sequence with *T. cruzi* CHL1 (TcCHL1; TcCLB.510311.130), *Arabidopsis thaliana* FANCJ (AtFANCJ; AT1G79950), *Xenopus laevis* BRIP (XlBRIP; XM_018244911), and *Danio rerio* FANCJ (DrFANCJ; XM_009291678). Conserved residues (in black or grey) are highlighted with arrows marking the conserved amino acids that form the HMM logo.

(Figure 5.10). Phylogenetic analysis of trypanosomal, fungal, vertebrate and plant *fancj*-like sequences revealed that the trypanosomatid *chl1*'s are evolutionarily related to their fungal counterparts that together form a clade distinct from vertebrate and plant homologues (Figure 5.9).

5.2.1 Construction and validation of null mutant lines

Plasmids based around the hygromycin and puromycin resistance cassettes (pKO-Tbchl1-hyg and pKO-Tbchl1-pac DNA) were made and processed by restriction enzyme digestion. The resultant fragments were purified and sequentially transformed into *T. brucei* wild type cells, creating the Tb*chl1*Δ line. These recombinant parasites were then taken and Tb*snm1* deleted using gene integration fragments containing neomycin and blasticidin resistance cassettes. Confirmation of the cell lines at a gDNA and mRNA level is given in Appendix 4b.

5.2.2 Phenotypic analysis of *T. brucei* lines lacking *chl1*

Following confirmation that *T. brucei* single and double null mutant lines lack Tb*chl1*, their growth properties were evaluated relative to wild type cells. This demonstrated that the recombinant cell lines grew at an equivalent rate as the controls (data not shown). The susceptibility of Tb*chl11*-deficient cells to various DNA damaging agents was then tested to evaluate whether the encoded enzyme does function in DNA repair. For each treatment dose response curves were generated (Figure 5.11), EC_{50} values calculated (Table 5.2) and the fold difference of EC_{50} values between wild type and null lines determined (Table 5.2).

Interestingly, no significant change in susceptibility to hydroxyurea, phleomycin, MMS, and UV was observed for Tb*chl1*Δ and Tb*snm1*Δ Tb*chl1*Δ cells as compared against wild type *T. brucei* and Tb*snm1*Δ (Figure 5.11). This indicates that TbCHL1 does not play a major role in the repair of base errors, double strand breaks and the formation of pyrimidine dimers. In contrast, Tb*chl1*Δ cells treated with mechlorethamine were 2-fold more susceptible to the ICL inducing compound indicating that this putative helicase plays a (minor) role in repair of such lesions. When these studies were extended to the Tb*snm1*Δ Tb*chl1*Δ line, the level of sensitive to mechlorethamine of the double null was similar to that of Tb*chl1*Δ cells and not to the Tb*snm1*-deficient line analysed in parallel. This phenotype is rather perplexing as it does not fit in with the "classical" epistatic/non-epistatic interactions observed with other components of the trypanosomal ICL REPAIRtoire. However, it may suggest that TbCHL1 and a

component in the TbSNM1-dependent pathway haves some sort of co-regulatory role, possibly suppressing the activity of other DNA repair factors. In the absence of both TbCHL1 and TbSNM1 these silenced/reduced activities are de-repressed and are able participate in ICL repair. The result observed using this Tb*snm1*Δ Tb*chl1*Δ double null mutant line was observed using multiple clones generated from independent transformations.

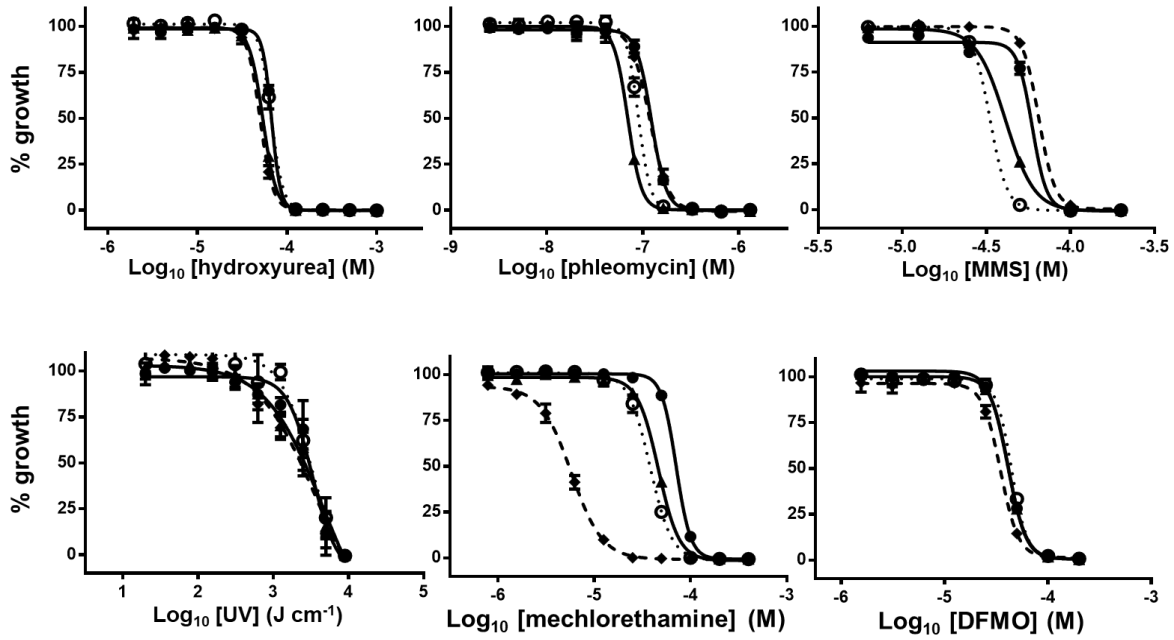

Figure 5.11: Susceptibility of Tb*chl1* null lines towards DNA damaging treatments.
Dose response curves of *T. brucei* wild type (●), Tb*snm1*Δ (■), Tb*chl1*Δ (♦), and Tb*snm1*Δ Tb*chl1*Δ (o) cell lines to hydroxyurea, UV, phleomycin, MMS, mechlorethamine and DFMO. All data points are mean values ± standard deviations from experiments performed in quadruplicate.

Treatment	*T. brucei* EC_{50}			
	Wild type	**Tb*snm1*Δ**	**Tb*chl1*Δ**	**Tb*snm1*Δ Tb*chl1*Δ**
Hydroxyurea	67.39 ± 0.65	50.21 ± 1.72 (1.3)	53.90 ± 0.85 (1.2)	66.67 ± 2.27 (1.0)
Phleomycin	0.04 ± 0.00	0.04 ± 0.00 (1.0)	0.03 ± 0.00 (1.3)	0.06 ± 0.00 (0.7)
MMS	32.70 ± 0.12	36.35 ± 0.62 (0.9)	41.20 ± 0.77 (1.2)	33.56 ± 1.37 (1.0)
UV (kJ/cm)	3.46 ± 0.46	4.58 ± 1.04 (0.8)	4.48 ± 2.18 (0.8)	2.98 ± 0.25 (1.2)
Mechlorethamine	70.94 ± 1.25	5.76 ± 0.41 (12.2)*	46.3 ± 0.75 (1.5)	37.92 ± 1.02 (1.8)
DFMO	41.32 ± 0.81	34.24 ± 0.97 (1.2)	41.30 ± 0.46	44.01 ± 0.76 (0.9)

Table 5.2: Susceptibility of *T. brucei* Tb*chl1* null lines to DNA damaging treatments.
Data represents EC_{50} values of *T. brucei* wild type, Tb*snm1*Δ, Tb*chl1Δ* and Tb*snm1*Δ Tb*chl1*Δ against hydroxyurea, phleomycin, MMS, UV, mechlorethamine and DFMO. All values are means ± standard deviations from experiments performed in quadruplicate. The ratio of EC_{50} values between wild type and null mutant lines is given as fold difference, in parentheses. *Indicates significant differences in susceptibility ($P < 0.0001$ between wild type and null lines, as assessed by Student's *t* test (GraphPad Software)).

5.3 Analysis of the *T. brucei* FAN1 homologue

Following ubiquitination of the FANCD2/FANCI complex, FAN1 (Fanconi-Associated Nuclease 1) is recruited to an ICL site where it functions as a nuclease to cleave the DNA backbone helping to excise the DNA lesion (Takahashi *et al.*, 2015; Jin and Cho, 2017). Searches of *T. brucei* databases identified a single sequence (TbFAN1; Tb927.10.7540) that shares 17 – 20 % identity with FAN1's from a range of different organisms. These enzymes are unique in that they represent the only proteins that contain a VRR-NUC (PF08774) domain found towards the carboxyl terminal (Figure 5.12). This region is centred upon a conserved "PDX_n(D/E)XK" motif that coordinates binding of divalent metal ions (either manganese or magnesium) and is essential for their dual nuclease activities (Fontebasso *et al.*, 2013). Additionally, these enzymes often contain additional domains (*e.g.* TPR_12 (PF13424), HIRAN (PF08797), SAP (PF02037)) that mediate protein:protein interactions with TbFAN1 following this pattern, containing the so-called TPR_2 (Tetratricopeptide repeat 2; PF07719) motifs. As with TbHEL1, phylogenetic analysis of FAN1 sequences indicates that the trypanosomatid homologues forms an outlining group and again is evolutionary distinct from vertebrate, plant, nematode and fungal clades (Figure 5.13). This difference could reflect that for at least *T. brucei*, the factors that recruit FAN1 to the ICL lesion, namely the

FANCD2/FANCI complex, are absent and as such if it does play a role in ICL repair, how it is targeted to the site of DNA damage will be distinct from the reported systems.

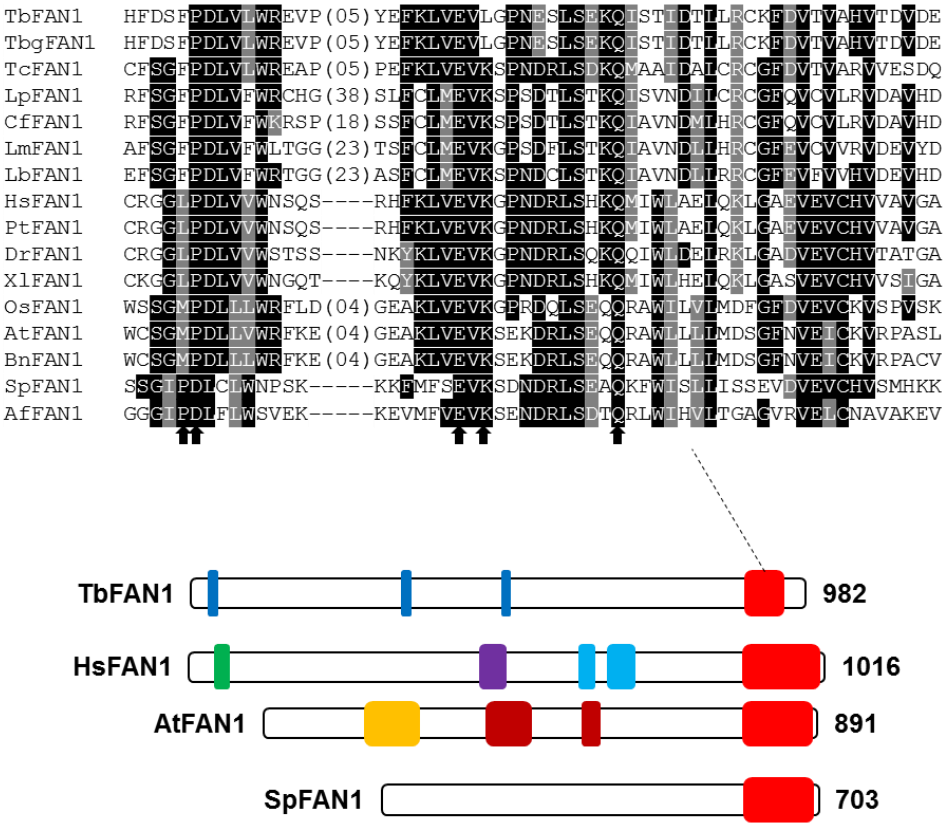

Figure 5.12 Sequence domain analysis of FAN1 sequences.
Schematic diagram showing the domain structure of FAN1 sequences from *Trypanosoma brucei* (TbFAN1; accession number EAN78160), *Homo sapiens* (HsFAN1; NP_055782), *Arabidopsis thaliana* (AtFAN1; Q5XVJ4) and *Schizosaccharomyces pombie* (SpFAN1; Q9Y804). The regions corresponding to VRR_NUC (PF08774), SAP (PF02037), HIRAN (PF08797), TPR_2 (PF07719), TPR_12 (PF13424) and NatB_MDM20 (PF09797) domains are highlighted as red, purple, orange, dark blue, light blue and brown boxes, respectively. An alignment of the VRR_NUC domain of TbFAN1 with other FAN1 proteins is shown. Residues that are common with the TbFAN1 sequence are represented by dots with differences shown. Dashes have been inserted to optimise alignment.

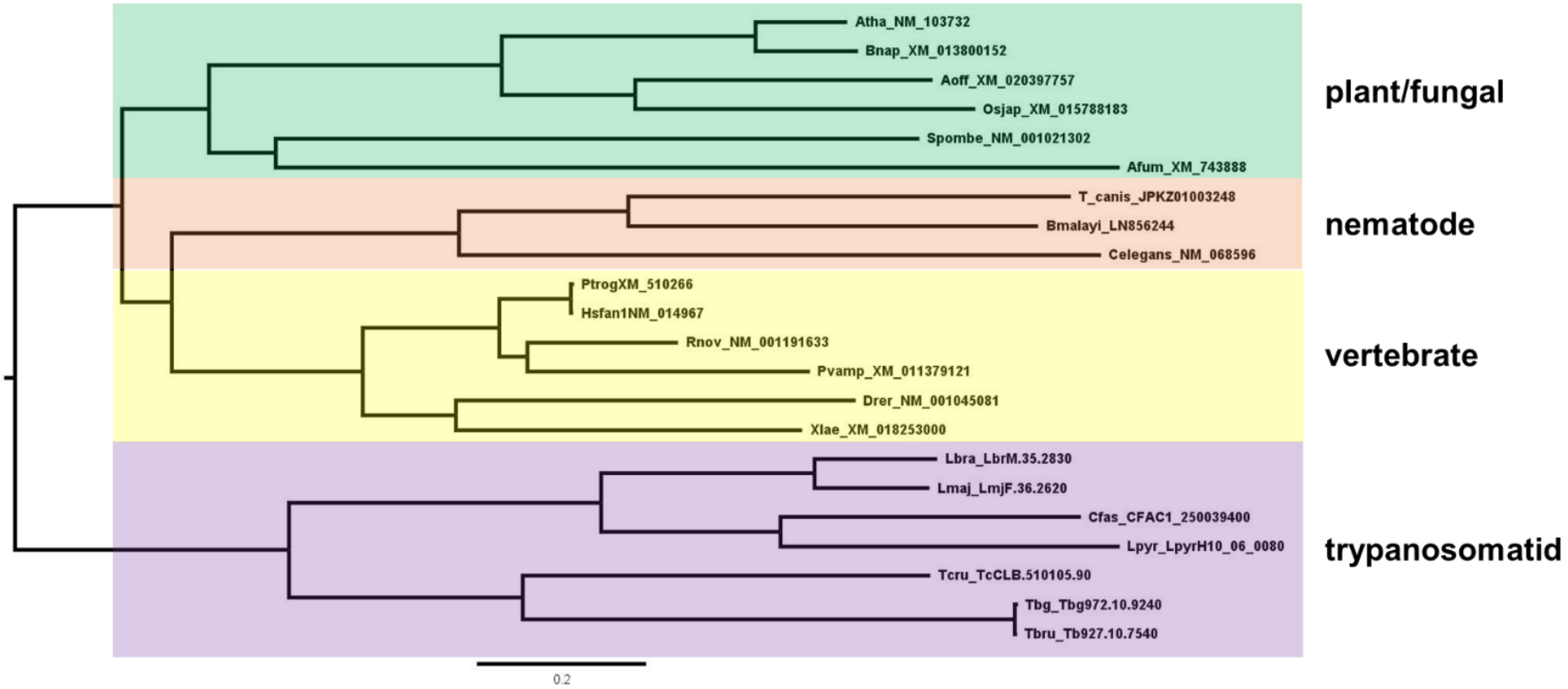

Figure 5.13: Rooted phylogenetic tree analysis of FAN1 sequences.
A rooted phylogenetic tree outlines how trypanosomatid FAN1 (purple) sequences are evolutionarily dissimilar to plant/fungal FAN1 sequences (green), nematode FAN1 sequences (red) and vertebrate FAN1 sequences (yellow). Gene names and sequence identities are given on the end of each clade: *T. brucei fan1* (Tb927.10.7540), *T. cruzi fan1* (TcCLB.510105.90), *L. major fan1* (LmjF.36.2620), *C. fasciculate fan1* (CFAC1_250039400), *L. braziliensis fan1* (LbrM.35.2830), *L. pyrrhocoris fan1* (LpyrH10_06_0080), *T. brucei gambiense fan1* (Tbg972.10.9240), *H. sapiens fan1* (NM_014967), *P. troglodytes fan1* (XM_510266), *A. fumigatus fan1* (XM_743888), *S. pombe fan1* (NM_001021302), *B. napus fan1* (XM_013800152), *O.s. Japonica fan1* (XM_015788183), *A. thaliana fan1* (NM_103732)**,** *X. laevis fan1* (XM_018253000), *D. rerio fan1* (NM_001045081), *C. elegans fan1* (NM_068596), *T. canis fan1* (JPKZ01003248), *B. malayi fan1* (LN856244), *P. vampyrus fan1* (XM_011379121), *R. norvegicus fan1* (NM_001191633) and *A. officinalis fan1* (XM_020397757).

5.3.1 TbFAN1 and ICL Repair

5.3.1.1 Creating and confirming single null mutants

As described elsewhere, Tb*fan1* single null cells were created by the sequential transformation of processed pKO-Tbfan1-hyg and pKO-Tbfan1-neo DNA fragments into *T. brucei* wild type cells. Recombinant parasites were validated using PCR on gDNA or mRNA templates (Appendix 4c).

5.3.1.2 Phenotypic analysis of T. brucei lines lacking fan1

Following confirmation, the growth properties of the *T. brucei* Tb*fan1*Δ was assessed and compared against wild type cells cultivated in parallel. This demonstrate that the null line grew at an equivalent rate as the controls (data not shown). The susceptibility of Tb*fan1*-deficient cells to various DNA damaging agents was then tested to evaluate whether the encoded enzyme does function in DNA repair. For each treatment dose response curves were generated (Figure 5.14), EC_{50} values calculated (Table 5.3) and the fold difference of EC_{50} values between wild type and null lines determined (Table 5.3).

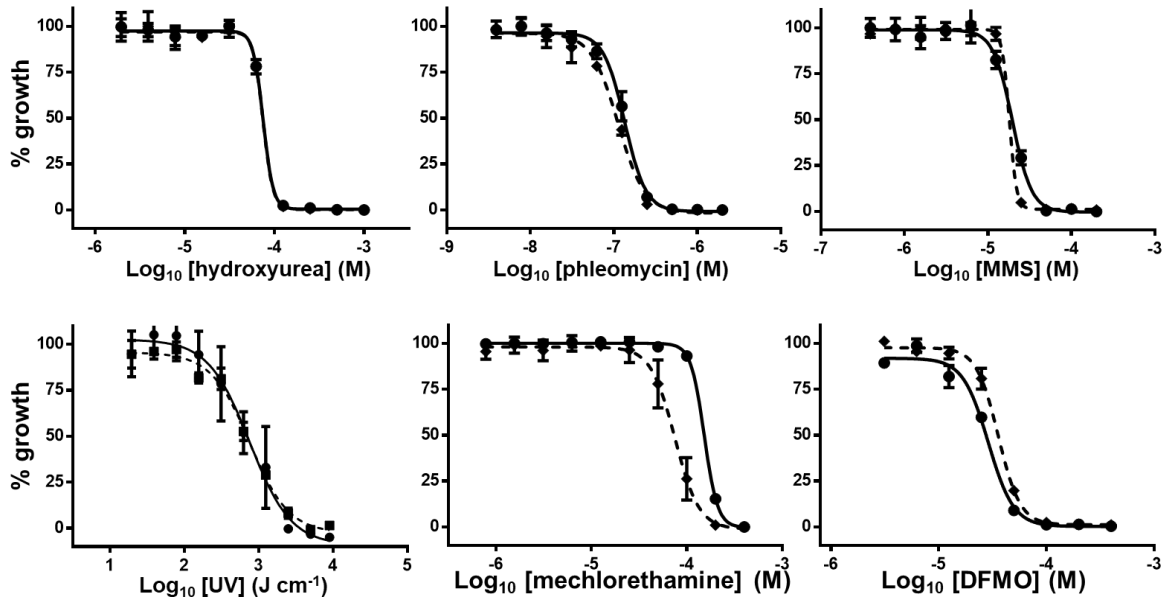

Figure 5.14: Susceptibility of *T. brucei* Tb*fan1* null mutant towards various DNA damaging treatments.

Dose response curves of *T. brucei* wild type (solid line) and Tb*fan1*Δ (dotted line) to hydroxyurea, UV, phleomycin, MMS, mechlorethamine and DFMO. All data points are mean values ± standard deviations from experiments performed in quadruplicate.

Treatment	*T. brucei* EC_{50}	
	Wild type	Tb*fan1Δ*
Hydroxyurea	75.15 ± 1.49	74.57 ± 1.97 (1.0)
Phleomycin	0.14 ± 0.01	0.11 ± 0.01 (1.3)
MMS	39.24 ± 1.64	34.68 ± 1.74 (1.1)
UV (kJ/cm)	0.79 ± 0.11	0.78 ± 0.08 (1.0)
Mechlorethamine	76.28 ± 1.29	37.92 ± 6.03 (2.0)*
DFMO	28.36 ± 0.54	35.64 ± 2.29 (0.8)

Table 5.3: Susceptibility of *T. brucei* Tb*fan1* null line to DNA damaging treatments. Data represents EC_{50} values of *T. brucei* wild type and Tb*fan1*Δ against hydroxyurea, phleomycin, MMS, UV, mechlorethamine and DFMO. All values are means ± standard deviations from experiments performed in quadruplicate. The ratio of EC_{50} values between wild type and null mutant lines is given as fold difference, in parentheses. *Indicates significant differences in susceptibility ($P < 0.0001$ between wild type and null lines, as assessed by Student's *t* test (GraphPad Software).

Analysis of the dose response curve data demonstrates that the Tb*fan1*Δ parasites exhibit a wild type-like response to hydroxyurea, phleomycin, MMS and UV indicating this putative nuclease plays no role in the repair of damage induced by these treatments. When the susceptibility of the null line to mechlorethamine was explored, recombinant cells were slightly (~2-fold) more sensitive to the ICL inducing agent than wild type indicating that this enzyme plays a role in the trypanosomal ICL REPAIRtoire.

5.3.2 Investigating the role of TbFAN1 in the trypanosomal ICL repair system

Our previous data indicates that *T. brucei* possess at least two ICL repair systems with one being dependent on TbSNM1 and the other on TbMRE11. To assess which, if any, of these TbFAN1 operates within, double null mutant lines lacking TbFAN1 and TbSNM1 (Tb*snm1*Δ Tb*fan1*Δ) or TbFAN1 and TbMRE11 (Tb*fan1*Δ Tb*mre11*Δ) were constructed and then validated as described (see Appendix 4d). Culturing of Tb*snm1*Δ Tb*fan1*Δ parasites revealed that they grew at the same rate at wild type and the single null mutant cells (Tb*fan1*Δ and Tb*snm1*Δ) while Tb*fan1*Δ Tb*mre11*Δ trypanosomes exhibited the growth defect displayed by the Tb*mre11*Δ line (data not shown). Further phenotyping of these lines using mechlorethamine as selective agent generated dose response curves (Figure 5.15) and EC_{50} values (Table 5.4) indicting that TbSNM1 and TbFAN1 function non-epistatically while TbMRE11 and TbFAN1 exhibit an epistatic interaction. Cells lacking TbSNM1 and TbFAN1 are hypersensitive to mechlorethamine relative to the single null lines which in turn are more susceptible to the ICL

inducing agent than wild type. In contrast, TbMRE11 and TbFAN1-deficient parasites display the same sensitivity to mechlorethamine as Tb*mre11*Δ.

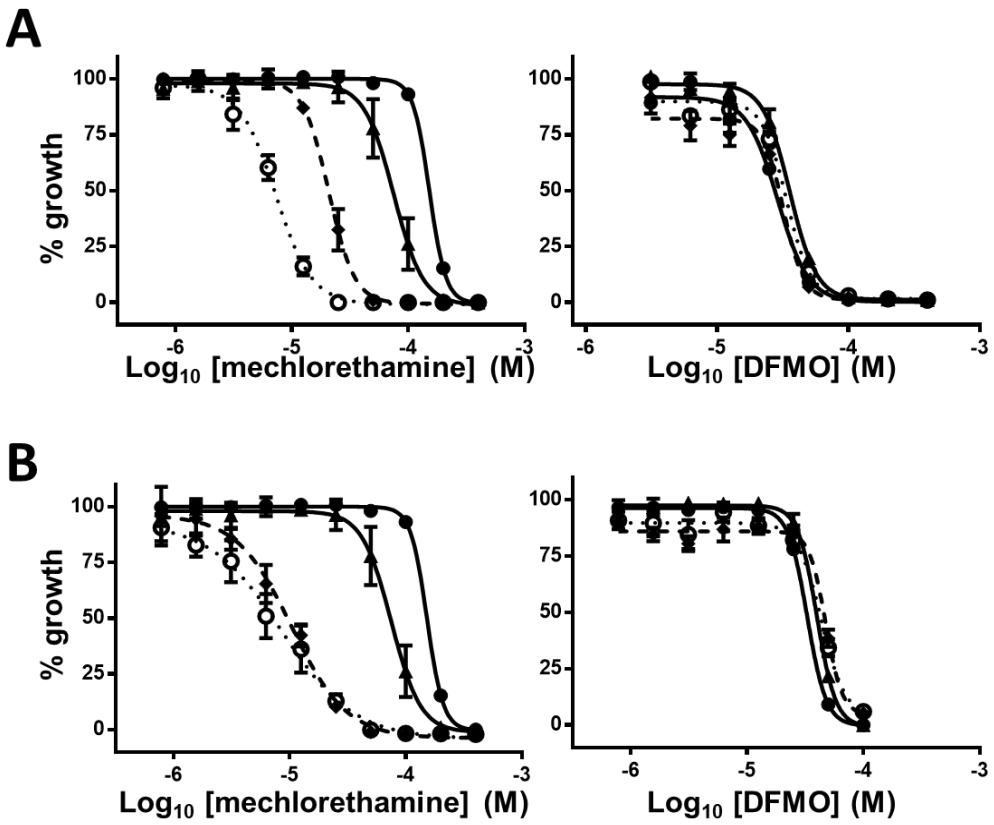

Figure 5.15: Susceptibility screening of *T. brucei* Tb*fan1* double null lines against mechlorethamine and DFMO.

A. Dose response curves of *T. brucei* wild type (●), Tb*snm1*Δ (▲), Tb*fan1*Δ (♦), and Tb*snm1*Δ Tb*fan1*Δ (o) lines to mechlorethamine and DFMO.

B. Dose response curves of *T. brucei* wild type wild type (●), Tb*mre11*Δ (▲), Tb*fan1*Δ (♦), and Tb*mre11*Δ Tb*fan1*Δ (o) to mechlorethamine and DFMO.

All data points are mean values ± standard deviations from experiments performed in quadruplicate.

Treatment	*T. brucei* EC_{50} (μM)			
	Wild type	**Tb*snm1*Δ**	**Tb*fan1*Δ**	**Tb*snm1*Δ Tb*fan1*Δ**
mechlorethamine	76.28 ± 1.29	10.50 ± 0.92 (7.2)*	37.92 ± 6.03 (2.0)*	3.67 ± 0.34 (20.5)*
DFMO	28.36 ± 0.54	31.41 ± 0.61 (1.2)	35.64 ± 2.29 (0.8)	31.20 ± 4.79 (0.9)

Treatment	*T. brucei* EC_{50} (μM)			
	Wild type	**Tb*mre11*Δ**	**Tb*fan1*Δ**	**Tb*mre11*Δ Tb*fan1*Δ**
mechlorethamine	76.28 ± 1.29	10.38 ± 1.05 (7.6)*	37.92 ± 6.03 (2.0)*	9.63 ± 1.67 (7.6)*
DFMO	41.32 ± 0.81	47.35 ± 5.16 (0.9)	39.78 ± 1.61 (1.1)	43.54 ± 3.75 (1.0)

Table 5.4: Susceptibility of *T. brucei* null lines to mechlorethamine and DFMO.
Data represents EC_{50} values of *T. brucei* wild type, Tb*snm1*Δ, Tb*fan1*Δ, Tb*mre11*Δ, Tb*snm1*Δ Tb*fan1*Δ and Tb*fan1*Δ, Tb*mre11*Δ cells treated with mechlorethamine and DFMO. All values are means ± standard deviations from experiments performed in quadruplicate. The ratio of EC_{50} values between wild type and null mutant lines is given as fold difference. *Indicates significant differences in susceptibility ($P < 0.0001$ between wild type and null lines, as assessed by Student's *t* test (GraphPad Software).

5.4 Role of TbFANCD1 and TbFANCR in trypanosomal ICL repair

To evaluate other *T. brucei* FA repair proteins, parasite lines lacking TbFANCD1 (also known as TbBRCA2; (Hartley and McCulloch, 2008) and TbFANCR (also known as TbRAD51; (Dobson *et al.*, 2011) were obtained from Dr Richard McCulloch, University of Glasgow. The susceptibility of these lines towards mechlorethamine was assessed using a modified version of the growth assay reported elsewhere in this thesis: Here the initial cell density used was 10-fold higher (10^5 parasites ml^{-1}) than employed elsewhere due to the slow growth rate of these parasites (Hartley and McCulloch, 2008; Dobson *et al.*, 2011). The resultant dose response curves (Figure 5.16) and EC_{50} values (Table 5.4) indicate that both enzymes function in the *T. brucei* ICL REPAIRtoire. Given that TbBRCA2 and TbRAD51 are known components of the HR pathway, we hypothesise that these function in the TbMRE11-dependent ICL repair system although this may be difficult to confirm given the slow growth rates of all the single null lines.

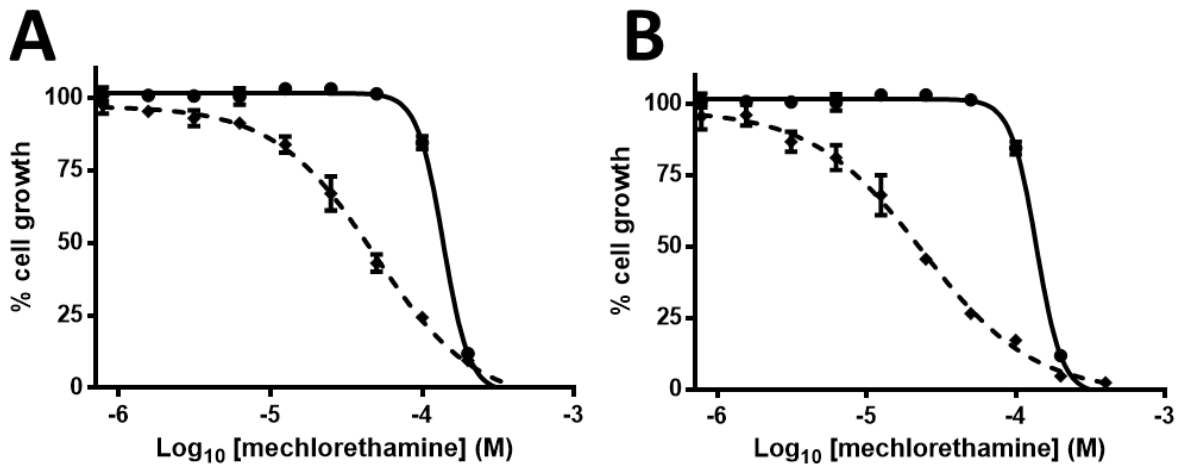

Figure 5.16: Susceptibility screening of Tb*brca2*Δ cells and Tb*rad51*Δ cells against mechlorethamine.
A. Dose response curves of *T. brucei* wild type (●) and Tb*brca2*Δ (♦) cells to mechlorethamine. B. Dose response curves of *T. brucei* wild type (●) and Tb*rad51*Δ (♦) cells to mechlorethamine. All data points are mean values ± standard deviations from experiments performed in quadruplicate.

Treatment	***T. brucei* EC_{50}**		
	wild type	**Tb*rad51Δ***	**Tb*brca2Δ***
Mechlorethamine	138.00 ± 3.0	24.17 ± 1.3 (5.8)	48.47 ± 3.4 (2.9)

Table 5.5: Susceptibility of *T. brucei* null lines to mechlorethamine.
Data represents EC_{50} values of *T. brucei* wild type, Tb*rad51*Δ and Tb*brca2*Δ cells treated with mechlorethamine. All values are means ± standard deviations from experiments performed in quadruplicate. The ratio of EC_{50} values between wild type and null mutant lines is given as fold difference. *Indicates significant differences in susceptibility ($P < 0.0001$ between wild type and null lines, as assessed by Student's *t* test (GraphPad Software).

5.5 Chapter Summary

This chapter has focused on characterising *T. brucei* components the Fanconi Anaemia repair system. This work has shown:

1. *T. brucei* has potential to express a minimal FA pathway, containing 9 putative FA homologues
2. TbHEL1 (initially believed to be a FANCM homologue) plays no role in DNA or ICL repair.
3. TbHEL1 plays a crucial role in the *T. brucei* RNA interference machinery, potentially functioning as the RNA helicase that is absent from the *T. brucei* DICER sequence but present in the counterparts expressed by higher eukaryotes
4. TbCHL1 (a FANCJ homologue) appears to play an ancillary role in the *T. brucei* ICL REPAIRtoire and may have a regulatory function
5. TbFAN1 plays an ancillary role in the *T. brucei* ICL REPAIRtoire and functions in the MRE11-dependent ICL repair system
6. TbBRCA2 (FANCD1) and TbRAD51 (FANCO) play roles in the *T. brucei* ICL REPAIRtoire predicted to be in the MRE11-dependent ICL repair system

6. Structure and function analysis of TbSNM1

6.1 Understanding the role of conserved residues within TbSNM1

Previous work characterising TbSNM1 identified several conserved residues that were hypothesised to play roles in 1. zinc co-factor binding, 2. localisation or 3. nucleic acid specificity (Figure 6.1) (Sullivan *et al.*, 2015). The amino acids involved in metal ion binding (either histidine or aspartic acid) are mostly found in motifs that comprise the MβL domain while the presence of a monopartite 'RRRH' sequence present in the β-CASP domain has potential to target the enzyme to the nucleus. Additionally, a conserved valine residue found towards the carboxyl end of β-CASP could determine the substrate specificity of TbSNM1: SNM1/PSO2 proteins containing this particular residue tend to bind DNA while the presence of histidine results in enzymes interacting with RNA (Callebaut *et al.*, 2002).

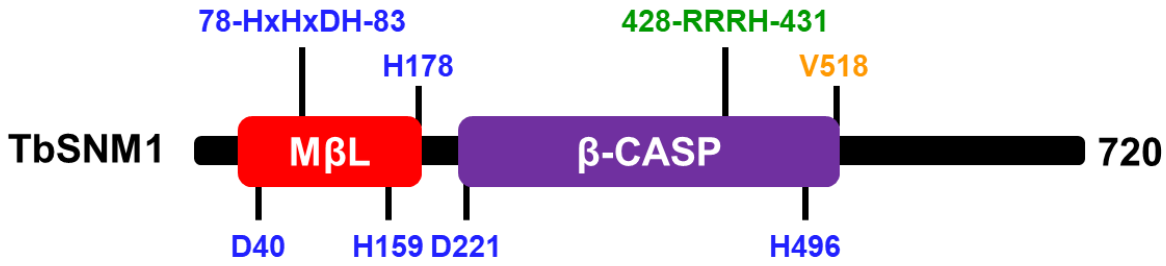

Figure 6.1: Conserved residues of TbSNM1.
TbSNM1 contains two key regions; the metallo-ß-lactamase (MßL; red) and β-CASP (purple) domains. Conserved residues within these domains are emphasised in blue (hypothesised to play a role in zinc cofactor binding), green (theorised to play a role in TbSNM1 nuclear localisation) and orange (TbSNM1 specificity to binding DNA).

Functional analysis of TbSNM1 in BSF *T. brucei* has shown that cells lacking this activity are highly susceptible to ICL inducing agents, a phenotype that can be readily reversed by ectopic expression of an amino terminally GFP tagged version of the enzyme (Sullivan et al., 2015). Using pRPa-GFP-Tbsnm1, the complementation DNA vector used in the above study as template, the SPRINP site-directed mutagenesis technique (Edelheit, Hanukoglu and Hanukoglu, 2009) was used to mutate the residues highlighted in Figure 6.1 to alanine. Following the introduction of the mutated GFP constructs into *T. brucei* Tb*snm1* heterozygotes (heterozygote line referred to as *Tb*snm1$^{+/-}$), the remaining Tb*snm1* allele was interrupted thereby creating the desired null mutant line. Comparison of the susceptibility profiles displayed by these lines against wild type, Tb*snm1*Δ and Tb*snm1*Δ parasites engineered to express GFP tagged Tb*snm1* enabled us to test whether a given residue does play a role in

TbSNM1 1. catalytic activity, 2. localisation and/or 2. substrate specificity. This functional analysis was augmented by *in silico* studies where the TbSNM1 protein sequence was modelled onto the recently described HsSNM1A (PDB:4B87) and HsSNM1B (PDB: 5AHO) structures (Figure 6.2) (Allerston *et al.*, 2015) using Phyre 2 and PyMOL programs. Analysis at the gross level indicated that TbSNM1 contained 12 β-pleated sheets that fold to form the MβL domain with the β-CASP domain inserted between β-sheets 10 and 11, typical of members of the SNM1/PSO2 family. Further predictions indicate that the *T. brucei* enzyme binds one zinc ion similar to HsSNM1A and distinct from HsSNM1B which binds two, with analysis of interactions at specific sites showing the molecular effects of each individual mutation.

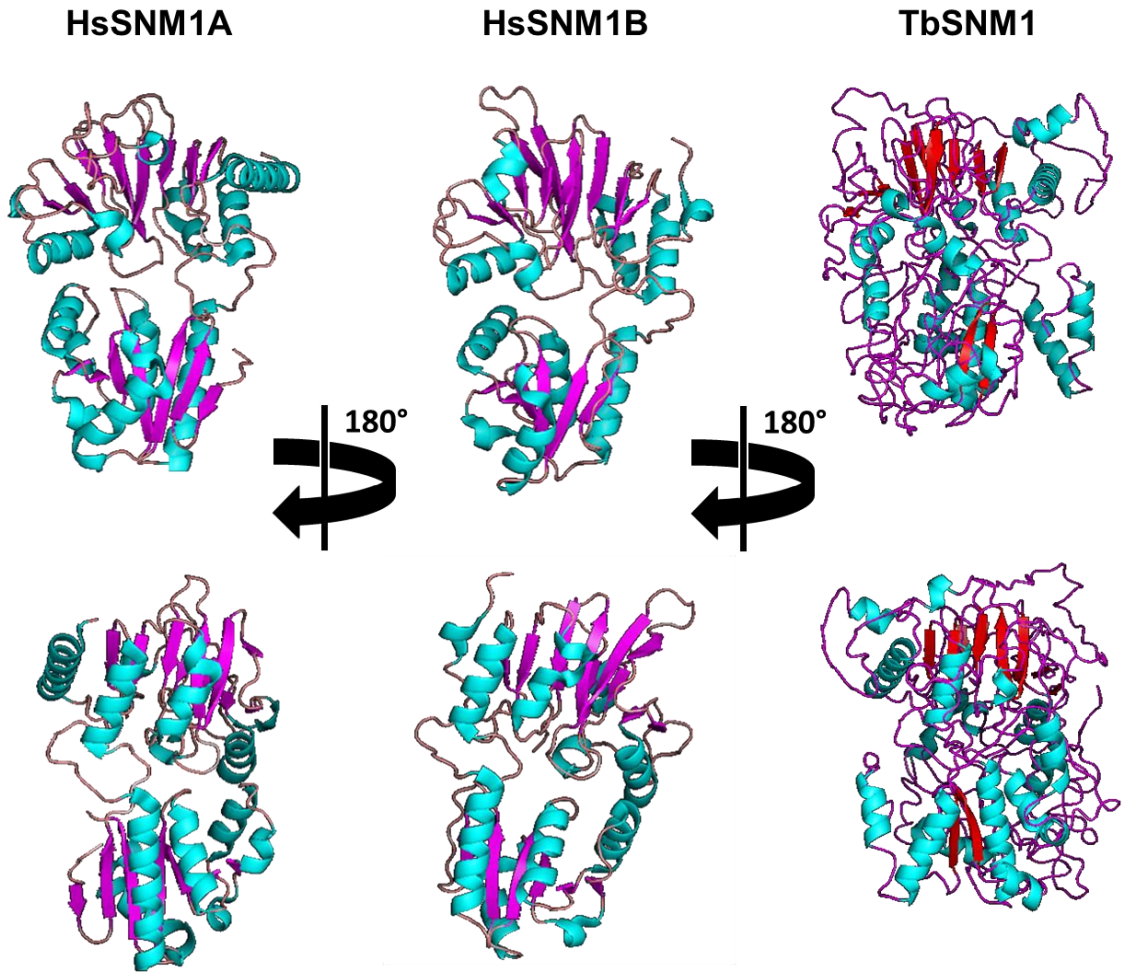

Figure 6.2: Predicted model of TbSNM1.
Molecular model of TbSNM1, as compared against HsSNM1A and HsSNM1B. Created using Phyre 2 and Pymol. The α-helices in TbSNM1 are shown in blue (also blue in HsSNM1A and HsSNM1B) with β-pleated sheets shown in red (purple in HsSNM1A and HsSNM1B).

6.2 Analysis of putative TbSNM1 zinc binding residues

Comparison of the TbSNM1 sequence with other SNM1/PSO2 proteins identified several residues, including D40, H78, H80, D82, H83, H159, H178, D221 and H496 (numbering for TbSNM1), as potentially playing a role in zinc binding. Using the plasmid pRPa-gfp-Tbsnm1 as template, the codons that translate for each of these amino acids were mutated to alanine using the SPRINP approach (Figure 6.3).

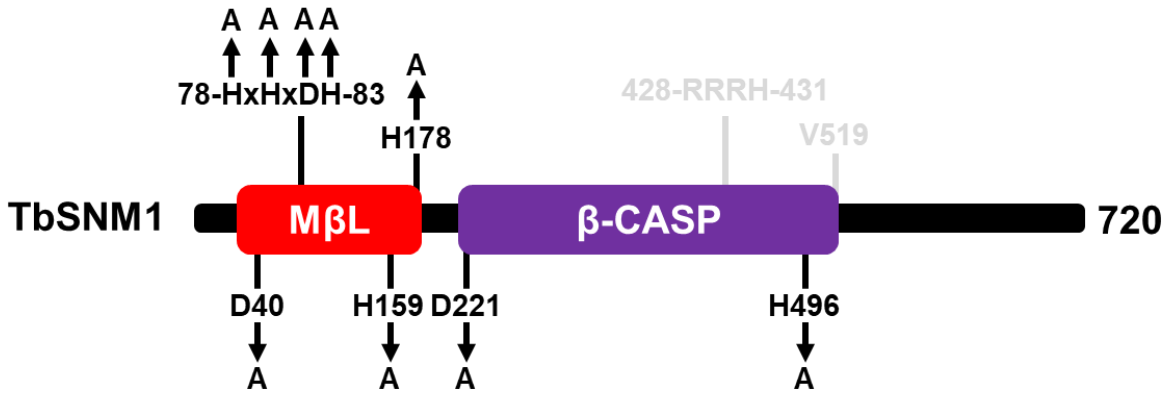

Figure 6.3: Residues in TbSNM1 postulated to bind the metal ion.
Nine conserved residues across both TbSNM1 domains (D40, H78, H80, D82, H83, H159, H178, D221 and H496) are hypothesised to play a role in coordination of the zinc ion. These were independently mutated to alanine residues.

Following confirmation of their sequence, the mutated plasmids were digested with AscI with the purified fragments introduced into a *T. brucei* 2T1 *Tb*snm1$^{+/-}$ line (this line is blasticidin and puromycin resistant). Cultures were placed under selective pressure and hygromycin/blasticidin resistance cultures selected 5 to 7 days post-transformation: integration of RPa-GFP-Tbsnm1 is selected for using hygromycin while blasticidin is used to maintain selection for the Tb*snm1* disruption. Cells were then tested for puromycin sensitivity (2T1, the parental line, is puromycin resistant, a phenotype that should be lost upon integration of the ectopic construct) with susceptible clones then transformed with DNA fragments containing a puromycin resistant cassette that facilitates interruption of the remaining Tb*snm1* allele. As before, cultures were placed under selective pressure and hygromycin/blasticidin/puromycin resistance cultures selected 5 to 7 days post-transformation.

To confirm that Tb*snm1* had been successfully interrupted, that mutated *gfp*-Tb*snm1* DNA fragment had integrated into the *T. brucei* genome and that the recombinant lines expressed the fusion gene, DNA amplification-based validation strategies were performed. To assess for appropriate integration events, PCR on gDNA extracted from wild type and manipulated cell

lines was carried out using primer combinations to amplify biomarkers corresponding to 1. intact Tb*snm1* (Tbsnm1-KO1/Tbsnm1-seq1), 2. the Tb*snm1-bla* and Tb*snm1-pac* disrupted alleles (Tbsnm1-KO1/bla-1 and Tbsnm1-KO1/pac-1, respectively) and 3. the *gfp*-Tb*snm1* allele (GFP/Tbsnm1-seq1) (Figure 6.4). Amplification of intact Tb*snm1* generated a band of 1.1 kb (the size predicted from *in silico* mapping) in templates purified from wild type and Tb*snm1*$^{+/-}$ cells with no band(s) seen in genetic material purified from the other lines tested. In contrast, primer combinations that detect the Tb*snm1-bla* and Tb*snm1-pac* alleles generated amplicons of the predicted size (~1.3 and ~1.7 kb, respectively) but only from the gDNA purified from *T. brucei* Tb*snm1*Δ, *T. brucei* 2T1 Tb*snm1*Δ *gfp*-Tb*snm1* and all the Tb*snm1*Δ lines engineered to express mutated versions of the GFP-TbSNM1 fusion protein. In contrast, no bands were observed in wild type *T. brucei* while only the Tb*snm1-bla* allele was detected in the *Tb*snm1$^{+/-}$ line. Finally, a DNA band of 0.4 kb (the size predicted from *in silico* mapping) that spans the *gfp*-Tb*snm1* fusion was detected only from parasites containing wild type or mutated Tb*snm1* in the ectopic expression vector. These strategies indicate that the appropriate cell lines have been made:

T. brucei 2T1 Tb*snm1*Δ *gfp*-Tb*snm1*-D40A → line now referred to as TbSNM1-D40A

T. brucei 2T1 Tb*snm1*Δ *gfp*-Tb*snm1*-H78A → line now referred to as TbSNM1-H78A

T. brucei 2T1 Tb*snm1*Δ *gfp*-Tb*snm1*-H80A→ line now referred to as TbSNM1-H80A

T. brucei 2T1 Tb*snm1*Δ *gfp*-Tb*snm1*-H82A→ line now referred to as TbSNM1-H82A

T. brucei 2T1 Tb*snm1*Δ *gfp*-Tb*snm1*-D83A→ line now referred to as TbSNM1-D83A

T. brucei 2T1 Tb*snm1*Δ *gfp*-Tb*snm1*-H159A→ line now referred to as TbSNM1-H159A

T. brucei 2T1 Tb*snm1*Δ *gfp*-Tb*snm1*-H178A → line now referred to as TbSNM1-H178A

T. brucei 2T1 Tb*snm1*Δ *gfp*-Tb*snm1*-D221A→ line now referred to as TbSNM1-D221A

T. brucei 2T1 Tb*snm1*Δ *gfp*-Tb*snm1*-H496A → line now referred to as TbSNM1-H496A

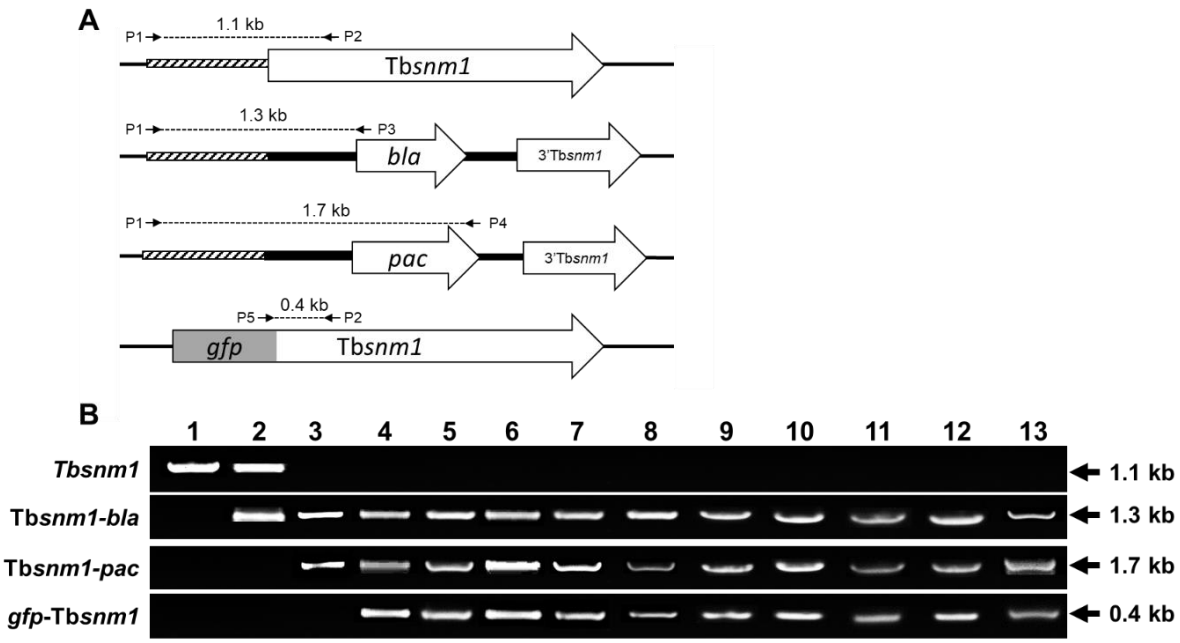

Figure 6.4: Validating engineered *T. brucei* lines.
A. Diagram representing the Tb*snm1* allele and resultant changes upon disruption of this loci using genes encoding for blasticidin (*bla*) and puromycin (*pac*) resistance. In parallel, changes to the landing pad locus after integration of *gfp*-Tb*snm1* was also analysed. P1 (Tbsnm1-KO1), P2 (Tbsnm1-seq1), P3 (bla-1), P4 (pac-1) and P5 (GFP) correspond to regions where the primers anneal at the specific allele.
B. DNA fragments obtained from amplification reactions on genomic DNA extracted from *T. brucei* wild type (lane 1), Tb*snm1*$^{+/-}$ (lane 2), Tb*snm1*Δ (lane 3), Tb*snm1*Δ GFP-Tb*snm1* (lane 4), TbSNM1-D40A (lane 5), TbSNM1-H78A (lane 6), TbSNM1-H80A (lane 7), TbSNM1-D82A (lane 8), TbSNM1-H83A (lane 9), TbSNM1-H159A (lane 10), TbSNM1-H178A (lane 11), TbSNM1-D221A (lane 12), and finally TbSNM1-H496A (lane 13) cells. Primer combinations amplified intact Tb*snm1* (Tbsnm1-KO1/Tbsnm1-seq1), Tb*snm1-bla* (Tbsnm1-KO1/bla-1), Tb*snm1-pac* (Tbsnm1-KO1/pac-1), or *gfp*-Tb*snm1* (GFP/Tbsnm1-seq1) alleles.

To assess whether the above recombinant lines express the GFP-TbSNM1 fusion, DNA amplification reactions were carried out on cDNA (generated from total RNA extracted from tetracycline induced parasites) using primers GFP/Tbsnm1-seq1 (Figure 6.5): ectopic expression of the wild type or mutated GFP-TbSNM1 protein in the 2T1 genetic background is under control of a tetracycline induced T7 promoter system (Alsford *et al.*, 2005). When using material generated from wild type *T. brucei*, Tb*snm1*$^{+/-}$ and Tb*snm1*Δ cells, no band was observed indicating these lines do not express a version of *gfp*-Tbsnm1. In contrast, a band of the expected size (0.4 kb) was noted in all lines engineered to express variants of the fusion protein. The integrity of all cDNA (and hence RNA) samples was confirmed as control reactions amplifying Tb*tert* (primer combinations Tbtert-F/Tbtert-R) carried out in parallel yielded a band of the expected size (~100 bp).

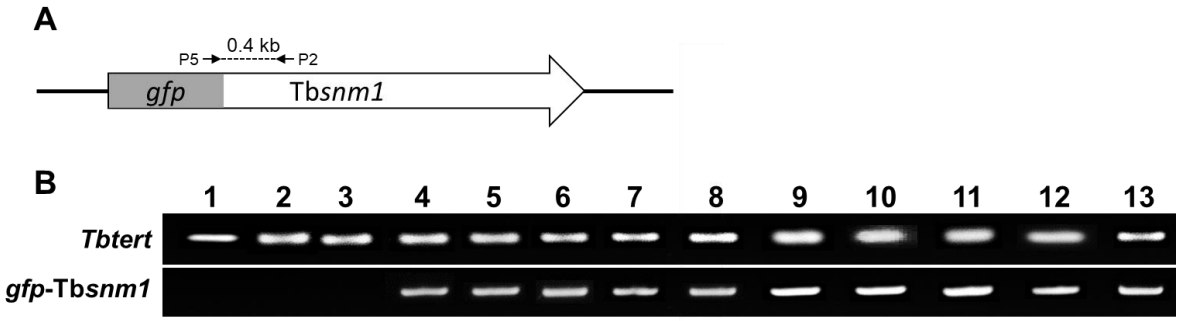

Figure 6.5: Confirming expression of *gfp*-Tb*snm1*.
A. Schematic of integrated *gfp*-Tb*snm1* analysing using primer combination P2 (Tbsnm1-seq1) and P5 (GFP) which amplified a band of 0.4kb across the GFP and TbSNM1 fusion.
B. DNA fragments obtained from amplification on cDNA derived from RNA extracted from *T. brucei* wild type (lane 1), Tb*snm1*$^{+/-}$ (lane 2), Tb*snm1*Δ (lane 3), Tb*snm1*Δ GFP-Tb*snm1* (lane 4), TbSNM1-D40A (lane 5), TbSNM1-H78A (lane 6), TbSNM1-H80A (lane 7), TbSNM1-D82A (lane 8), TbSNM1-H83A (lane 9), TbSNM1-H159A (lane 10), TbSNM1-H178A (lane 11), TbSNM1-D221A (lane 12), and finally TbSNM1-H496A (lane 13) cells using primer combinations that specifically amplify *gfp*-Tb*snm1* (GFP/Tbsnm1-seq1) and Tb*tert* (Tbtert-F/Tbtert-R).

To evaluate whether a given TbSNM1 mutation effects localisation of the enzyme, the DNA of fixed parasites from tetracycline induced and non-induced cultures was stained with DAPI then imaged by epifluorescent microscopy (Figure 6.6). For most (8) TbSNM1 mutants, tetracycline induced expression of the GFP tagged protein within the trypanosome resulted in a pattern that coincided with the larger and more intense of the DAPI signals. As DAPI stains the trypanosomal nuclear and single mitochondrial genomes, with the latter presenting as a small, faint band relative to the former, the observed pattern reveals that most fusion proteins can be translocated to the *T. brucei* nucleus. It is therefore implicit that mutation of most putative zinc binding amino acids does not affect protein localisation and presumably folding. The only exception to this pattern related to the TbSNM1-D221A line where a non-specific GFP signal was noted throughout the cell. This suggests that this particular amino acid may play a key role in TbSNM1 folding with the metal co-factor potentially affecting this process.

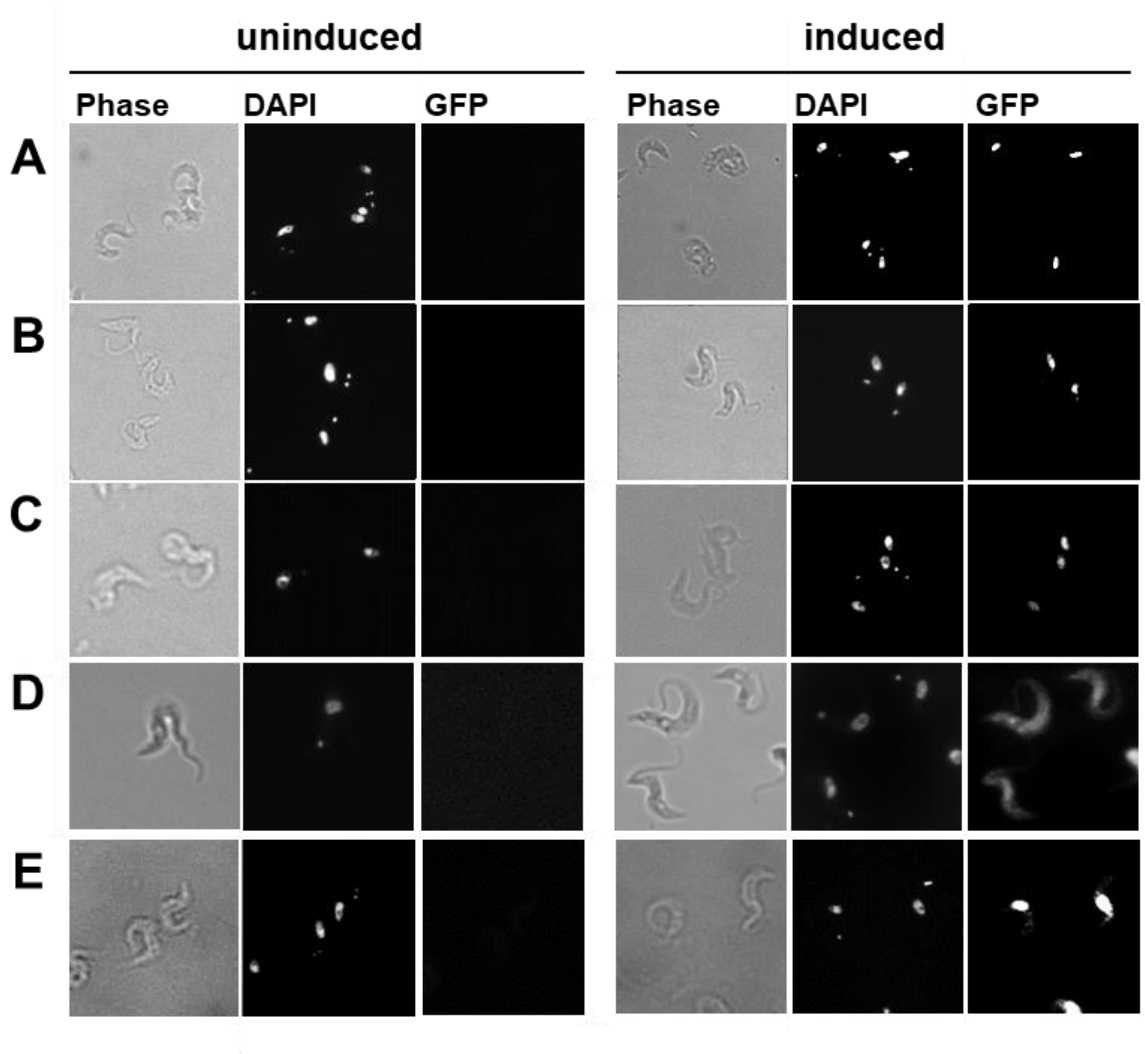

Figure 6.6: Localisation of mutant GFP-TbSNM1 in bloodstream form *T. brucei*.
T. brucei Tb*snm1*Δ cells expressing GFP-TbSNM1 (wild type or mutant) were fixed, stained with DAPI and imaged by epifluorescent microscopy under a x40 objective. Examples of the phase, DAPI and GFP signal images are shown for selected cell lines: Tb*snm1*Δ GFP-Tb*snm1* (A), TbSNM1-D40A (B), TbSNM1-H80A (C), TbSNM1-D221A (D) and TbSNM1-H496A (E). The cells analysed were derived from tetracycline treated (induced) cultures and compared to parasites grown in the absence of this antibiotic (uninduced).

To assess if ectopic expression of a given TbSNM1 mutation could complement for the susceptibility phenotype displayed by Tb*snm1*Δ, the growth of recombinant parasite lines in the presence/absence of tetracycline and mechlorethamine was determined. The data was plotted as dose response curves (Figure 6.7) from which EC_{50} values were determined (Table 6.1). A ratio between uninduced and induced EC_{50} values is shown as a fold differences (Table 6.1).

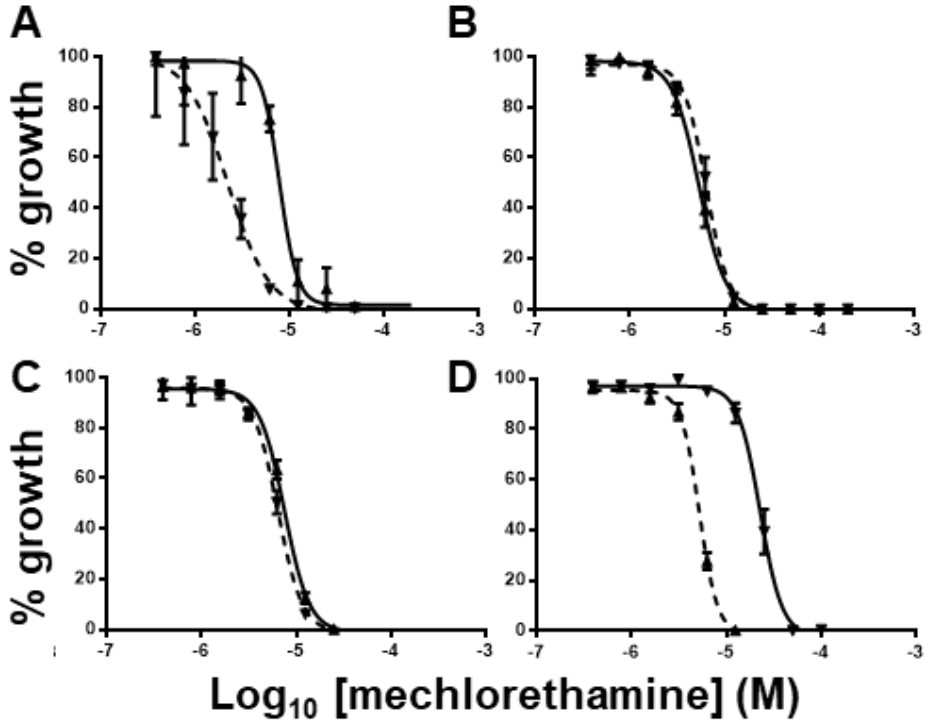

Figure 6.7: Susceptibility of *T. brucei* lines towards mechlorethamine.
Dose response curves of tetracycline induced (▲) and uninduced (▼) *T. brucei* Tb*snm1*Δ *gfp*-Tb*snm1* (A), TbSNM1-D40A (B), TbSNM1-H80A (C) and TbSNM1-H496A (D). All data points are mean values ± standard deviations from experiments performed in quadruplicate.

Cell line	*T. brucei* EC_{50} (μM)		Fold difference	Complements?
	uninduced	induced		
Tb*snm1*Δ *gfp*-Tb*snm1*	4.52 ± 0.41	14.69 ± 1.78	3.3*	Y
TbSNM1-D40A	5.27 ± 0.43	6.45 ± 0.59	1.2	N
TbSNM1-H78A	5.40 ± 0.35	16.67 ± 0.92	3.1*	Y
TbSNM1-H80A	5.52 ± 3.68	5.27 ± 0.79	1.0	N
TbSNM1-D82A	4.50 ± 1.84	4.26 ± 0.80	0.9	N
TbSNM1-H83A	2.00 ± 0.89	10.39 ± 0.37	5.2*	Y
TbSNM1-H159A	4.70 ± 0.25	5.00 ± 0.10	1.1	N
TbSNM1-H178A	1.73 ± 0.58	12.91 ± 0.55	7.5*	Y
TbSNM1-D221A	3.06 ± 0.44	4.48 ± 1.67	1.5	N
TbSNM1-H496A	5.19 ± 0.20	22.81 ± 1.80	4.4*	Y

Table 6.1: Susceptibility of *T. brucei* null lines to mechlorethamine.
Data represents EC_{50} values of induced and uninduced null lines towards mechlorethamine. All values are means ± standard deviations from experiments performed in quadruplicate. The ratio of EC_{50} values between induced and uninduced null lines is given as a fold difference. *Indicates significant differences in susceptibility ($P < 0.0001$ between wild type and null lines, as assessed by Student's *t* test (GraphPad Software).

The above data demonstrates that expression of H78, H83 H178 and H496 mutant forms of TbSNM1 can readily compensate for the mechlorethamine sensitivity phenotype displayed by the TbSNM1 null line with these enzymes behaving similarly to wild type TbSNM1 analysed in parallel. It is therefore implicit that these residues do not play a fundamental role in the activity of this enzyme. In comparison, alteration of D40, H80, D82 and H159 results in impaired TbSNM1 activity such that expression of these mutants in the Tb*snm1*Δ line fails to complement for the susceptibility phenotype. Molecular modelling of TbSNM1 wild type and mutants (Figure 6.8) structures indicates that these four residues all cluster near to the site where the zinc ion is predicted to sit. It is tempting to speculate that conversion of D40, H80, D82 and H159 to alanine affects coordination of the metal ion possibly affecting electron distribution in this region which can manifest itself as a reduction in the DNA cleaving activity. Whether the above amino acids interact directly with the zinc ion itself, function in an ancillary role to help with in this interaction or facilitate binding and/or cleavage of DNA backbone could not be determined due to the lack of an experimentally derived structure.

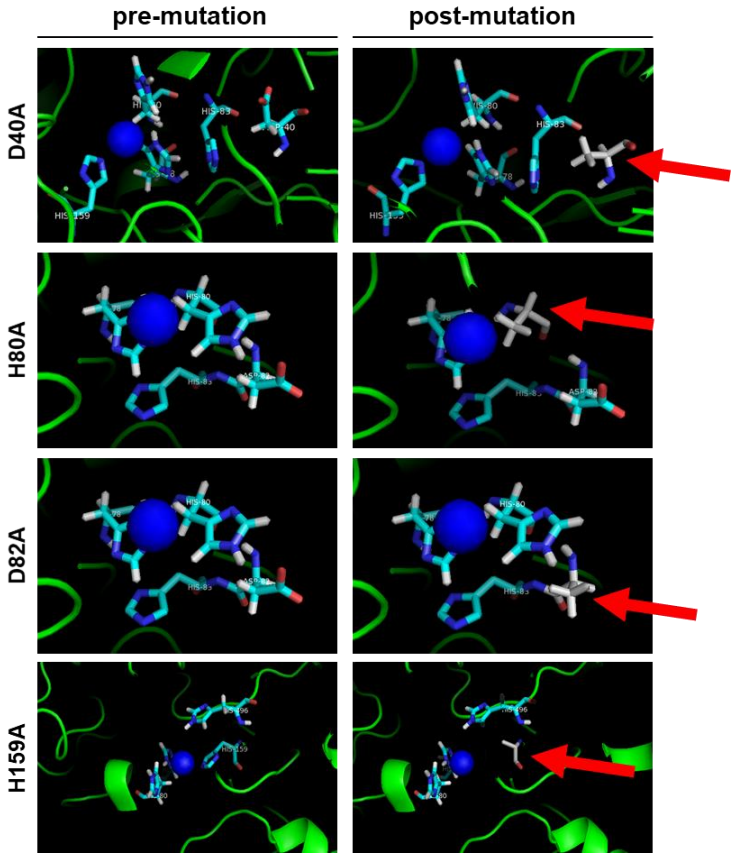

Figure 6.8: Structure of wild type and mutated forms of TbSNM1.
Illustration showing the effect of TbSNM1 D40A, H80A, D82A and H159A mutations (post mutation) in relation to wild type TbSNM1 (pre-mutation). Images were generated using the PyMOL *in silico* mutagenesis tool. The blue sphere corresponds to where the zinc ion is predicted to sit and the red arrows represent the mutation under analysis.

6.3 Evaluating the specificity of TbSNM1 to DNA

TbSNM1 possesses a conserved PTV motif in the carboxyl region of its β-CASP domain with the valine at this site (V518) possibly involved in DNA binding (Callebaut *et al.*, 2002). To test this hypothesis, the codon for this amino acid was mutated to the base triplet for alanine (Figure 6.9) using pRPA-gfp-Tbsnm1 as template. The confirmed 'mutant' plasmid was used to generate the *T. brucei* 2T1 Tb*snm1*Δ *gfp*-Tb*snm1*-V518A (referred to as TbSNM1-V518A) line and subsequently validated as described in section 6.2 (validation shown in Appendix 5).

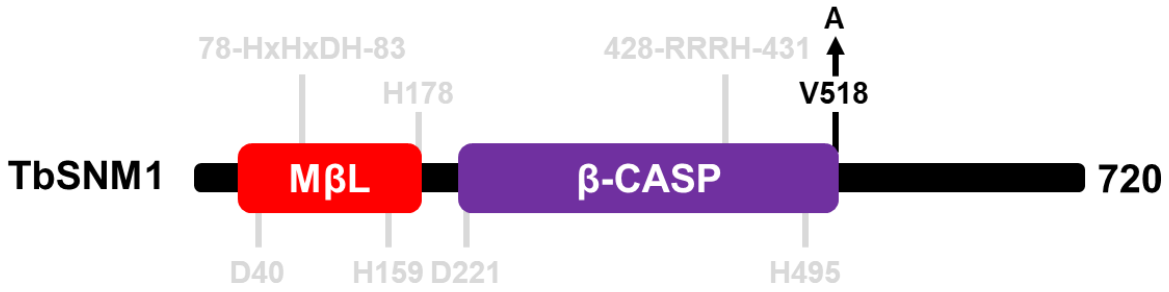

Figure 6.9: Location of V518 residue.
TbSNM1 V518 (located in the β-CASP domain of the protein) was mutated into an alanine due to non-bulky, chemically inert nature of this residue using site directed mutagenesis on the pRPA-*gfp*-Tb*snm1* plasmid.

Characterisation of the above cell line revealed that the mutated TbSNM1 was targeted to the nucleus (Appendix 5) while mechlorethamine susceptibility screens revealed that the modified enzyme could reverse the sensitivity phenotype that stems from lack of TbSNM1 expression from the endogenous loci (Figure 6.10; Table 6.2).

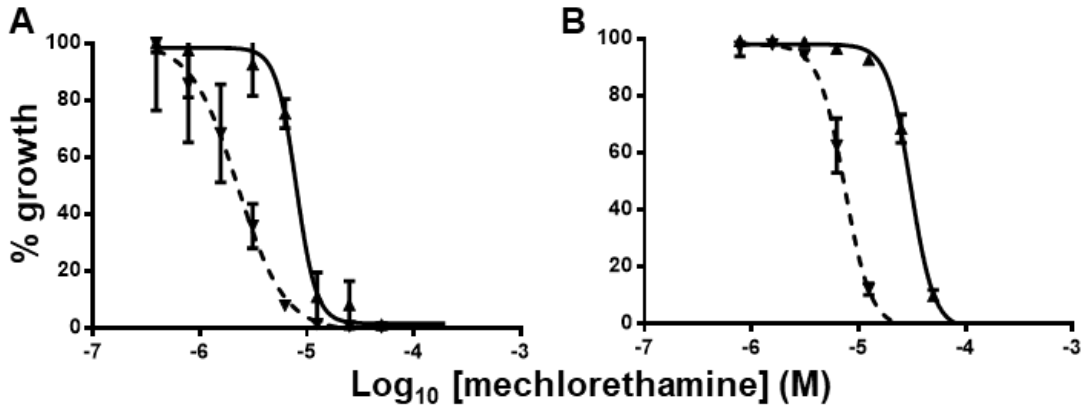

Figure 6.10: Susceptibility of *T. brucei* lines towards mechlorethamine.
Dose response curves of induced (▲) and non-induced (▼) *T. brucei* Tb*snm1*Δ *gfp*-Tb*snm1* (A) and TbSNM1-V518A (B). All data points are mean values ± standard deviations from experiments performed in quadruplicate.

Cell line	*T. brucei* EC_{50}		Fold difference	Complements?
	uninduced	induced		
Tb*snm1*Δ *gfp*-Tb*snm1*	4.52 ± 0.41	14.69 ± 1.78	3.3*	Y
TbSNM1-V518A	3.70 ± 0.34	15.37 ± 0.68	4.2*	Y

Table 6.2: Susceptibility of *T. brucei* lines to mechlorethamine.
Data represents EC_{50} values of induced and uninduced null lines towards mechlorethamine. All values are means ± standard deviations from experiments performed in quadruplicate. The ratio of EC_{50} values between induced and uninduced null lines is given as a fold difference. *Indicates significant differences in susceptibility ($P < 0.0001$ between wild type and null lines, as assessed by Student's t test (GraphPad Software).

Together, this implies that the valine at position 518 in TbSNM1 plays no role in determining substrate specificity. However, molecular modelling (Figure 6.11) at this site shows that because of the relatedness of the valine and alanine structures, the latter amino acid may, at least partially, be still able to promote DNA binding. As such additional experiments to analyse this particular residue could involve mutation of the valine to more diverse amino acids with one potential alteration involving conversion to histidine, the residue that may confer RNA interacting activity (Callebaut *et al.*, 2002).

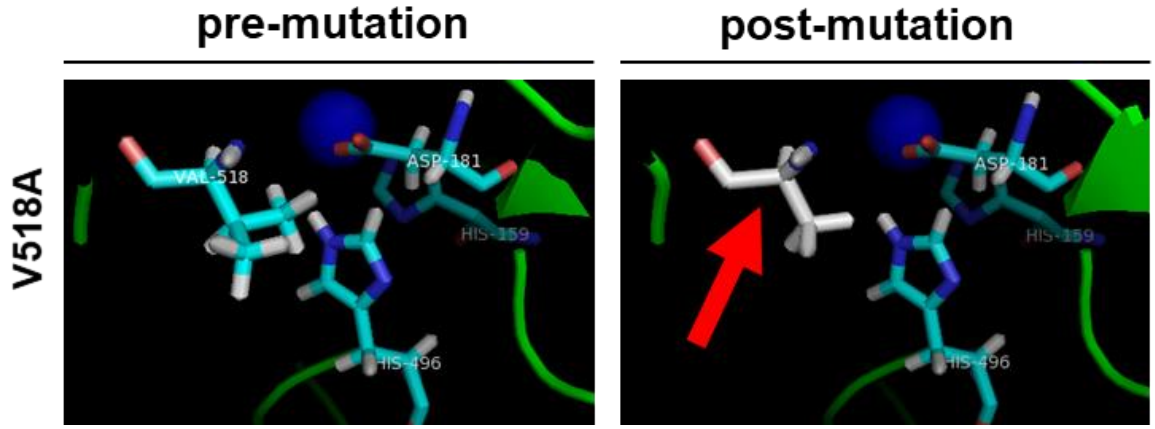

Figure 6.11: Effect of the V518A mutation on TbSNM1.
Structural effects of mutating V518 into an alanine (mutated residue emphasised with red arrow).

6.4 Dissecting the TbSNM1 nuclear localisation signal

In silico analysis of TbSNM1 (NucPred software) predicted that the RRRH motif starting at position 428 could function as a nuclear localisation signal (NLS) (Sullivan *et al.*, 2015). The combination of amino acids at this site (Figure 6.12) forms a classical, monopartite NLS with the basic amino acids in this region guiding the protein to the neutrally-charged nucleus (Lange *et al.*, 2007). This type of signal has been observed to function in trypanosomatids (Marchetti *et al.*, 2000).

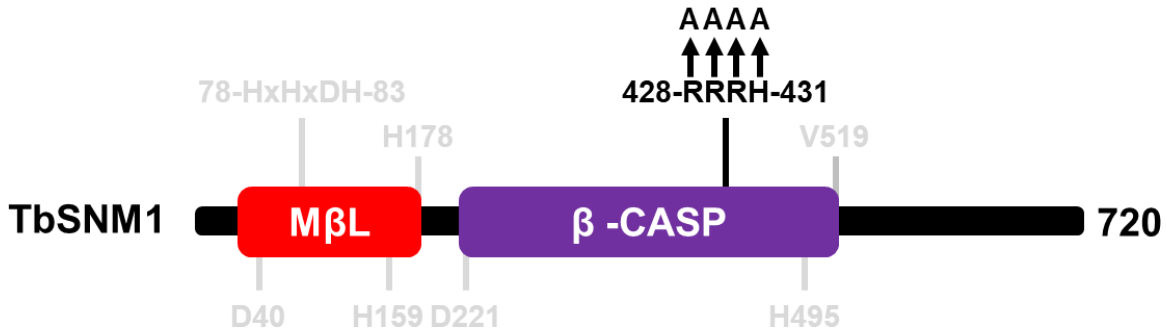

Figure 6.12: Predicted NLS of TbSNM1.
Four key residues (R428, R429, R430, and H431A; located in the β-CASP domain of the protein) were identified *in silico* to function in TbSNM1 localisation to the nucleus. Each residue was mutated to alanine to study this hypothesised function.

Using the approaches described above, variants of pRPA-GFP-Tbsnm1 containing appropriate mutations were generated, used to construct the corresponding recombinant *T. brucei* lines (Tb*snm1*Δ *gfp*-Tb*snm1*-R428A (referred to as TbSNM1-R428A), Tb*snm1*Δ *gfp*-Tb*snm1*-R429A (referred to as TbSNM1-R429A), Tb*snm1*Δ *gfp*-Tb*snm1*-R430A (referred to as TbSNM1-R430A) and Tb*snm1*Δ *gfp*-Tb*snm1*-H431A (referred to as TbSNM1-H431A)) with these parasites then validated using the aforementioned PCR-based strategy (validation shown in Appendix 5).

To assess the effect of each mutation on TbSNM1 localisation, the DNA of trypanosomes grown in the absence or presence of tetracycline was stained, the cells visualized by epifluorescent microscopy and the GFP pattern analysed **(**Figure 6.13). In situations where the outer two amino acids of the RRRH tetrapeptide had been mutated (ARRH or RRRA) a fluorescence signal within the nucleus was observed but only in tetracycline induced cultures. In contrast, alteration of each of the middle amino acids (RARH or RRAH) resulted in a non-nuclear arrangement thus indicating that the arginine residues at position 429 or 430 are both

key for targeting TbSNM1 to this organelle. However, it must also be noted that the pattern observed when expressing the R429 or 430 mutants in *T. brucei* could also reflect that these proteins are incorrectly folded and therefore non-functional.

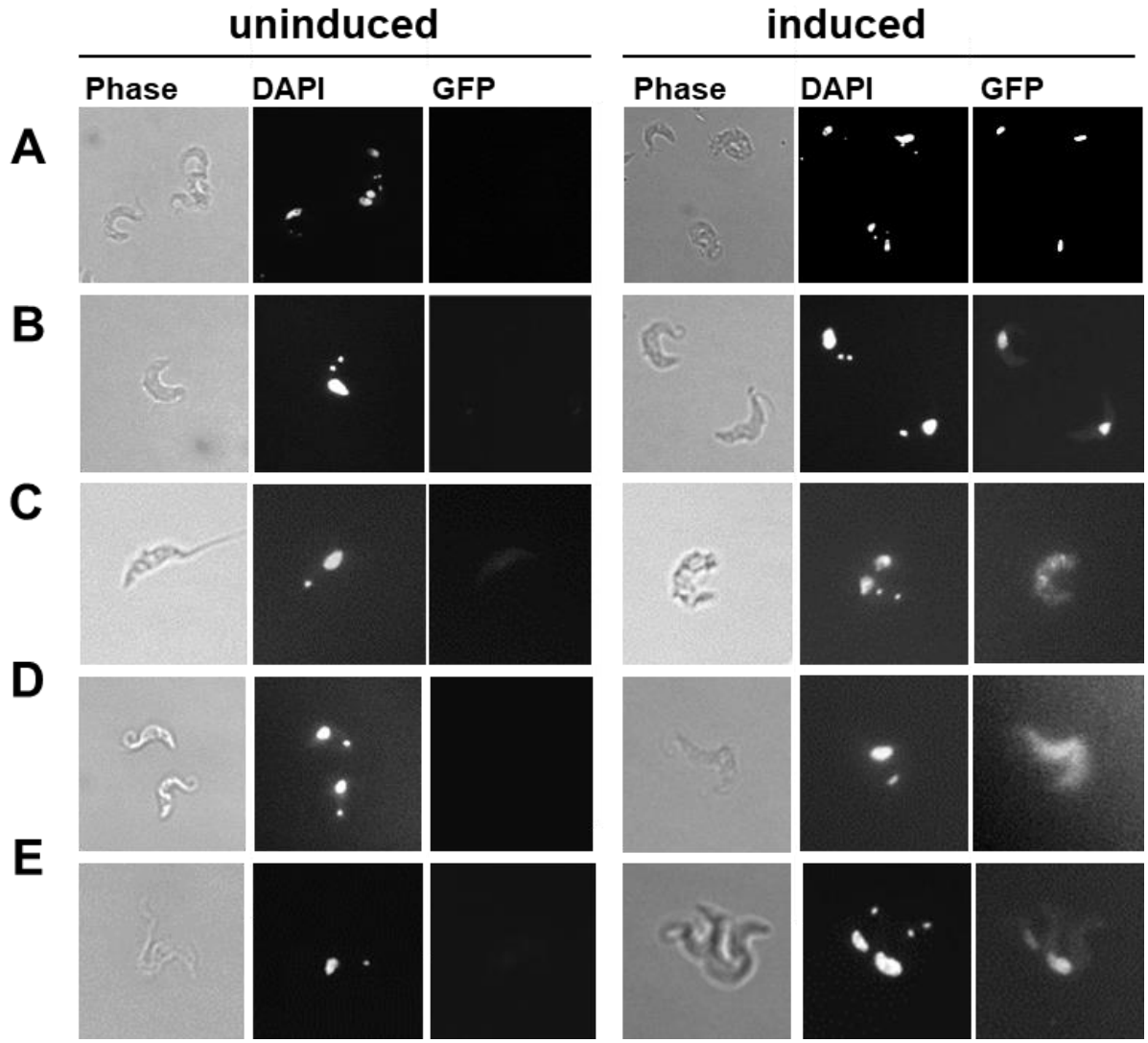

Figure 6.13: Localisation of *T. brucei* mutant GFP-TbSNM1.
Parasites expressing GFP-TbSNM1 (mutant or wild type) were stained with DAPI and examined by epifluorescent microscopy under a x40 objective lens with phase, DAPI and GFP signal images shown: Tb*snm1*Δ GFP-Tb*snm1* (A), TbSNM1-R428A (B), TbSNM1-R429A (C), TbSNM1-R430A (D) and TbSNM1-H431A (E).

To determine whether there was an association between the above localisation patterns and mechlorethamine susceptibility, Tb*snm1*Δ parasites that also express the mutant TbSNM1s cultured in medium containing or lacking tetracycline were treated with the ICL inducing agent and growth inhibition determined. The resulting cell number data was analysed and plotted as dose response curves (Figure 6.14), generating EC_{50} and fold difference values (Table 6.3).

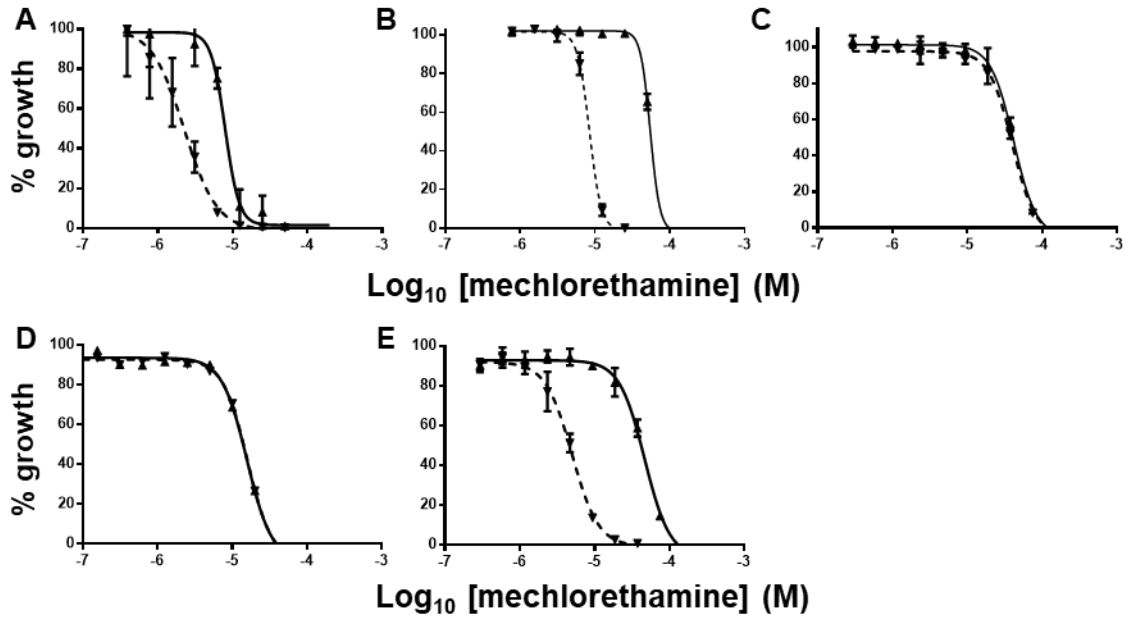

Figure 6.14: Susceptibility of *T. brucei* conditional null lines against mechlorethamine.
Dose response curves of induced (▲) and non-induced (▼) *T. brucei* Tb*snm1*Δ *gfp*-Tbsnm1 (A), TbSNM1-R428A (B), TbSNM1-R429A (C). TbSNM1-R430A (D) and TbSNM1-H431A (E). All data points are mean values ± standard deviations from experiments performed in quadruplicate.

Cell line	*T. brucei* EC50		Fold difference	Complements?
	uninduced	induced		
Tb*snm1*Δ *gfp*-Tb*snm1*	4.52 ± 0.41	14.69 ± 1.78	3.3*	Y
TbSNM1-R428A	8.44 ± 0.47	54.70 ± 1.32	6.5*	Y
TbSNM1-R429A	3.97 ± 0.14	4.14 ± 0.12	1.0	N
TbSNM1-R430A	7.99 ± 0.26	7.81 ± 0.20	1.0	N
TbSNM1-H432A	4.91 ± 0.32	46.63 ± 0.56	9.5*	Y

Table 6.3: Susceptibility of *T. brucei* null lines to mechlorethamine.
Data represents EC_{50} values of induced and uninduced null lines towards mechlorethamine. All values are means ± standard deviations from experiments performed in quadruplicate. The ratio of EC_{50} values between induced and uninduced null lines is given as a fold difference. *Indicates significant differences in susceptibility ($P < 0.0001$ between wild type and null lines, as assessed by Student's *t* test (GraphPad Software).

The above complementation data mirrors the localisation observations. Expression of TbSNM1 mutated in either of the outer two amino acids (R428 and H431) readily complements for the mechlorethamine sensitivity displayed by cells that lack TbSNM1 expressed from an endogenous loci. In contrast, alteration of R429 and 430 residues in TbSNM1 to alanine generates variant proteins that are unable function in the same way.

6.5 Chapter Summary

This chapter has focused on understanding the structure and function of TbSNM1. The amalgamation of alanine scanning, conditional null mutant lines, cellular localisation assays and susceptibility screening demonstrated that:

1. D40, H80, D82, and H159 play a key role in TbSNM1 activity, with comparative studies and *in silico* modelling suggesting they may be involved in zinc co-factor binding
2. R429 and R430, but not R428 and H431, play a crucial role in the localisation of the protein to the nucleus
3. Conversion of the valine at position 518 to alanine has no effect on TbSNM1 localisation and activity

7. DNA damage and trypanocidal compounds

A major challenge in the field of infectious disease biology is the development of new therapies to target a given pathogen. In the case of HAT, the last treatment to be added to the WHO List of Essential Medicines was NECT in 2009. The anti-microbial effects of this therapy uses two partner drugs that have been in clinical use to target trypanosomal infections for more than 30 years. In this chapter we have utilised the cell lines reported earlier in the thesis to assess whether: 1. TbSNM1 can be exploited as a drug target using compounds supplied by Prof Chris Scoffield (University of Oxford), 2. novel prodrugs activated by a trypanosome specific nitroreductase mediate their downstream effects by promoting DNA damage and 3. existing nitroheterocyclic-based therapies cause DNA damage within the parasite.

7.1 Evaluating trypanocidal effects of HaSNM1A inhibitors

ICL inducing agents are extensively used in medicine to treat a range of conditions with compounds including mitomycin C, cisplatin, cyclophosphamide and mechlorethamine being used to target certain forms of cancer (Huang and Li, 2013). It is envisaged that cells compromised in their ICL repair systems should be more susceptible to such therapies. This has led to the identification of several cephalosporin-based SNM1 inhibitors that are believed to interact with this nuclease *via* their MβL fold (Lee *et al.*, 2016): Cephalosporins are β-lactam antibiotics target bacterial cell wall biosynthesis with resistance mediated by β-lactamases, enzymes that contain a MβL domain.

To examine whether these SNM1 inhibitors display activity against BSF *T. brucei*, the growth inhibition of Ceftriaxone (a cephalosporin) and four other compounds (ML302-HCl, ML302-F, LBE314, Si4-33) against the BSF of the parasites was assessed (Figure 7.1; Table 7.1). This revealed that two of the structures (Ceftriaxone and ML302-F) do not have any trypanocidal effects at concentrations up to 100 μM. In contrast, the remaining three compounds displayed moderate, unimpressive, activity against this form of the parasite (EC_{50} values between 15 to 30 μM).

To elucidate whether this growth inhibition targets TbSNM1, the susceptiblity of *T. brucei* lacking or over expressing this activity was determined (Sullivan *et al.*, 2015) (Figure 7.1; Table 7.1). In all cases, the recombinant lines were as sensitive as wild type to each of the three chemicals tested. Therefore, it is implicit that the trypanocidal activity displayed by these

compounds does not involve TbSNM1 inhibition. Analysis of the TriTryp genome database indicates that in addition to TbSNM1, *T. brucei* expresses at least 8 other sequences that contain a β-lactamase like domain with potentially one (or more) of these being inhibited by the compounds tested here.

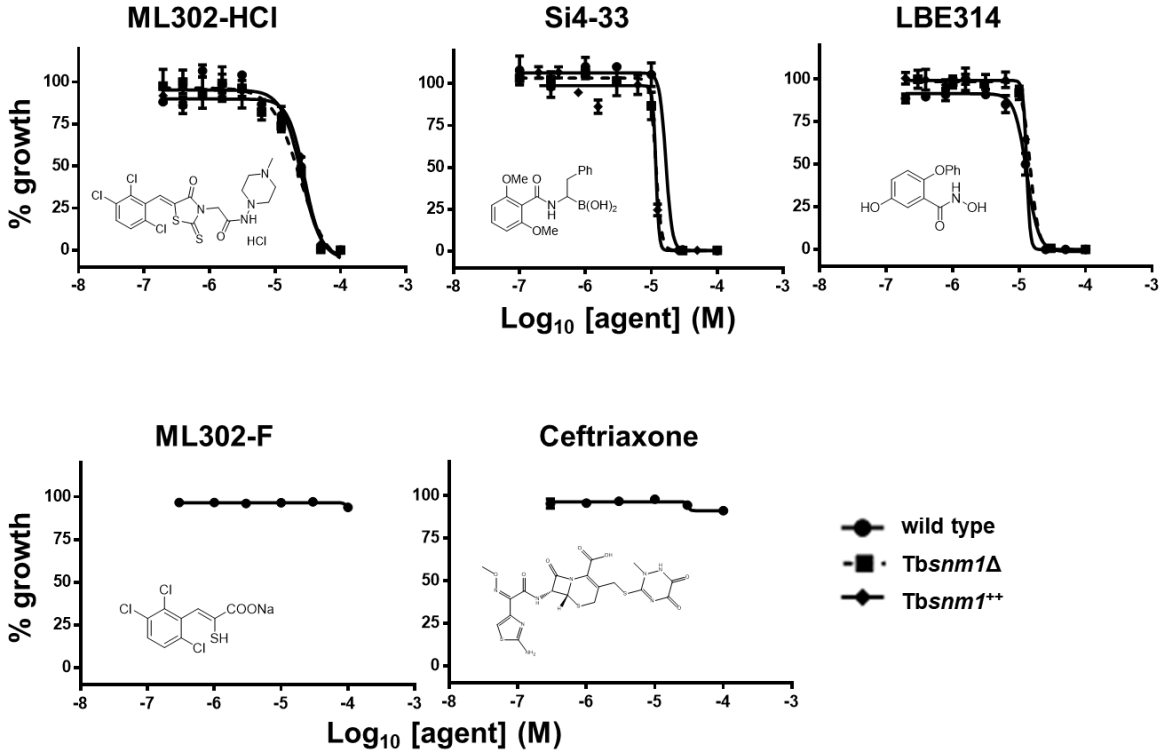

Figure 7.1: Susceptibility screening of *T. brucei* against inhibitors of HaSNM1A.
Dose response curves of wild type *T. brucei* (●), Tb*snm1*Δ (■), and Tb*snm1*$^{++}$ (♦) lines against ML302-HCl, Si4-33, LBE314, ML302-F and ceftriaxone. All data points are mean values ± standard deviations from experiments performed in quadruplicate.

	***T. brucei* EC_{50} (μM)**		
	Wild type	**Tb*snm1*Δ**	**Tb*snm1*$^{++}$**
ML302-HCl	26.57 ± 0.99	24.28 ± 1.75	28.45 ± 0.90
ML302-F Na	>100	-	-
LBE314	13.51 ± 0.25	16.33 ± 1.57	13.02 ± 0.69
Si4-33	15.41 ± 1.33	12.03± 0.80	11.16 ± 0.76
Ceftriaxone	>100	-	-

Table 7.1: Susceptibility of *T. brucei* lines to inhibitors of HaSNM1A.
Data represents EC_{50} values of wild type *T. brucei*, Tb*snm1*Δ and Tb*snm1*$^{++}$ lines towards ML302-HCl, Si4-33, LBE314, ML302-F and ceftriaxone. All values are means ± standard deviations from experiments performed in quadruplicate.

7.2 Unravelling the mode of action of nitro-based prodrugs

Ongoing work in the Wilkinson lab involves determining how nitro-based trypanosomal agents mediate their trypanocidal mode of action (Hall *et al.*, 2010; Bot *et al.*, 2010, Hall, Meredith and Wilkinson, 2012; Meredith *et al.*, 2017). One theme arising from these studies is that the most potent agents with the best selectivity contain chemical motifs that in other organisms promote DNA (specifically ICL) damage. To determine whether this was the case, various trypanocidal nitroaromatic compounds, including benznidazole, nifurtimox, CB1954 and LH34, were screened against a number of single and double null mutant lines engineered to lack different DNA repair proteins (see section 3.2 and 4.1). The data was expressed as dose response curves (example shown in Figure 7.2) from which EC_{50} values were extrapolated (Table 7.2).

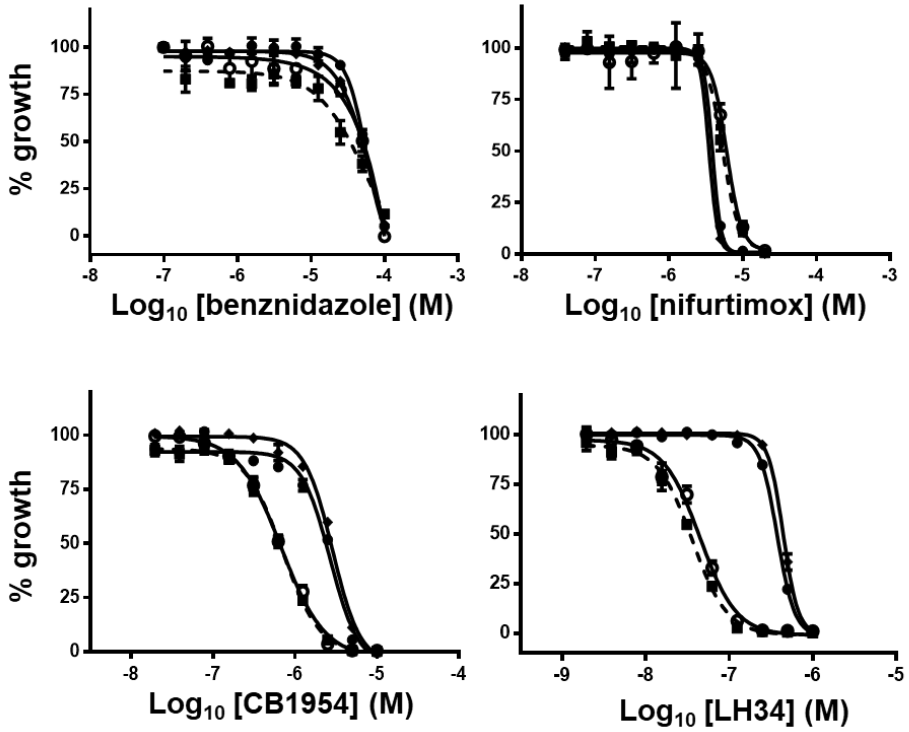

Figure 7.2: Susceptibility of *T. brucei* null lines towards anti-trypanosomal agents.
Dose response curves of *T. brucei* wild type (●), Tb*snm1*Δ (■), Tb*csb*Δ (♦) and Tb*snm1*Δ Tb*csb*Δ (o) to benznidazole, nifurtimox, CB1954 and LH34. All data points are mean values ± standard deviations from experiments performed in quadruplicate.

Treatment	*T. brucei* EC_{50}			
	wild type	**Tb*snm1*Δ**	**Tb*mre11*Δ**	**Tb*snm1*ΔTb*mre11*Δ**
Benznidazole	57.28 ± 4.82	44.84 ± 5.50 (1.3)	22.88 ± 3.50 (2.6)*	24.19 ± 2.76 (2.4)*
Nifurtimox	3.90 ± 0.02	5.31 ± 0.20 (0.8)	2.86 ± 0.05 (1.3)	4.67 ± 0.22 (0.9)
CB1954	3.67 ± 0.24	1.49 ± 0.03 (2.5)*	0.91 ± 0.03 (4.1)*	0.42 ± 0.04 (9.3)*
LH34	197.85 ± 8.92	9.71 ± 0.88 (20)*	33.40 ± 1.01 (6)*	2.55 ± 0.68 (66)*

	wild type	**Tb*snm1*Δ**	**Tb*exo1*Δ**	**Tb*snm1*Δ Tb*exo1*Δ**
Benznidazole	57.28 ± 4.82	45.57 ± 4.70 (1.3)	69.27 ± 11.40 (0.8)	50.29 ± 2.76 (1.1)
Nifurtimox	3.90 ± 0.02	5.31 ± 0.20 (0.8)	3.50 ± 0.05 (1.1)	6.07 ± 0.26 (0.7)
CB1954	2.68 ± 0.04	0.71 ± 0.04 (3.9)*	2.88 ± 0.08 (0.9)	0.68 ± 0.05 (3.9)*
LH34	188.23 ± 8.94	18.07 ± 1.28 (10)*	222.50 ± 13.20 (0.8)	22.25 ± 3.82 (8.5)*

	wild type	**Tb*snm1*Δ**	**Tb*csb*Δ**	**Tb*snm1*Δ Tb*csb*Δ**
Benznidazole	66.24 ± 0.84	76.39 ± 1.01 (0.9)	62.14 ± 2.59 (1.1)	60.19 ± 1.61 (1.1)
Nifurtimox	3.28 ± 0.10	3.15 ± 0.23 (1.0)	3.71 ± 1.84 (0.9)	3.62 ± 0.19 (0.9)
CB1954	3.67 ± 0.24	0.72 ± 0.05 (5.3)*	1.56 ± 0.16 (2.5)*	0.07 ± 0.02 (53)*
LH34	280.45 ± 13.47	15.36 ± 1.41 (18.7)*	91.93 ± 5.91 (3.0)*	11.98 ± 0.78 (23.3)*

Table 7.2: Susceptibility of *T. brucei* double null lines to anti-trypanosomal agents.
Data represents EC_{50} values of various *T. brucei* lines against benznidazole, nifurtimox, CB1954 (all in μM) and LH34 (in nM). All values are means ± standard deviations from experiments performed in quadruplicate. *Indicates significant differences in susceptibility ($P < 0.0001$ between wild type and null lines, as assessed by Student's *t* test (GraphPad Software).

The above data reveals that TbEXO1 plays no role in the trypanocidal mechanism of action of any of the nitroaromatic compounds tested: Cells lacking TbEXO1 display sensitivities to benznidazole, nifurtimox, CB1954 and LH34 similar to that observed with wild type cells while *T. brucei* lacking both TbEXO1 and TbSNM1 exhibit susceptibilities equivalent to those that are deficient only for TbSNM1. This implies that these agents do not promote a form of DNA damage that involves the MMR pathway.

Cells that lack TbCSB, either in a wild type or Tb*snm1*-deficient background, are as equally susceptible to benznidazole and nifurtimox as controls. This indicates that these compounds do

not cause a type of DNA damage that involves resolution using the NER pathway. In contrast, Tb*csb*Δ cells are up to 3-fold more susceptible to CB1954 or LH34 relative to wild type. When examining the sensitivity of cells lacking both TbSNM1 and TbCSB towards these two agents, certain differences were noted. For the LH compound, an epistatic interaction between TbSNM1 and TbCSB was noted with the EC_{50} value for the Tb*snm1*Δ line being similar to that observed using Tb*snm1*Δ Tb*csb*Δ cells. This suggests that this nitrogen mustard containing compound mediates most of its trypanocidal activity through the formation of ICLs. In the case of CB1954, the double null line (Tb*snm1*Δ Tb*csb*Δ) was hypersensitive to this aziridinyl in relation to the Tb*snm1*Δ or Tb*csb*Δ nulls indicating that the two encoded enzymes function non-epistatically to resolve any DNA damage that may ensue. This may reflect that CB1954 can promote various types of lesion within *T. brucei* that require different systems to repair. It is implicit that as TbSNM1 deficient cells are susceptible to CB1954 then one form of DNA damage caused by this agent are ICLs: this enzyme can only function to repair this type of lesion. Other forms of damage that this aziridinyl-based structure could generate include intrastrand crosslinks and monoalkylation products (Nicolini, 1988) that can be resolved using the NER system, a pathway that does not require SNM1 activity.

Cells lacking TbMRE11 (Tb*mre11*Δ and Tb*snm1*Δ Tb*mre11*Δ) are as sensitive to nifurtimox as wild type showing that this nitrofuran does not cause a form of DNA damage that can be repaired by the HR pathway. With benznidazole, parasites deficient in TbMRE11 (Tb*mre11*Δ and Tb*snm1*Δ Tb*mre11*Δ) are ~2-fold more sensitive to this compound than the parental line suggesting that these agents do cause a type of DNA damage that can be repaired *via* the HR pathway. This mechanism of action involving TbMRE11 was shown to extend across to megazol (data not shown), a nitroimidazole that has previously been shown to generate HR repaired lesions (Carvalho *et al.,* 2014). When screening CB1954 and LH34 against the above lines, cells lacking just TbMRE11 were between 4- and 6-fold more susceptible to these agents respectively relative to wild type indicating that the HR pathway does play a role in repairing the damage caused by either compound. This repair activity is non-epistatic with TbSNM1 as cells lacking both enzymes are hypersensitive to the treatments.

7.3 Activation of benznidazole promotes DNA damage

It is now established that activation of benznidazole involves a parasite specific type I nitroreductase (TbNTR) (Wilkinson *et al.,* 2008). To determine whether the DNA damaging activity noted above is linked to this trigger mechanism, parasite lines over expressing TbNTR

while null for TbMRE11 were constructed and validated (Appendix 6b). As a control, a TbEXO1 deficient, TbNTR expressing control line was generated in parallel (Appendix 6a). The susceptibility of the resultant lines towards benznidazole was then tested: The effect of DFMO was also analysed as drug control. The growth inhibition data, expressed as dose response curves (Figure 7.3) and as EC_{50} values (Table 7.3), revealed that cells lacking only TbEXO1 were as equally susceptible to benznidazole as wild type, confirming our previous findings, while cells additionally engineered to over express TbNTR were as sensitive to this nitroimidazole as parasite expressing only elevated levels of the nitroreductase.

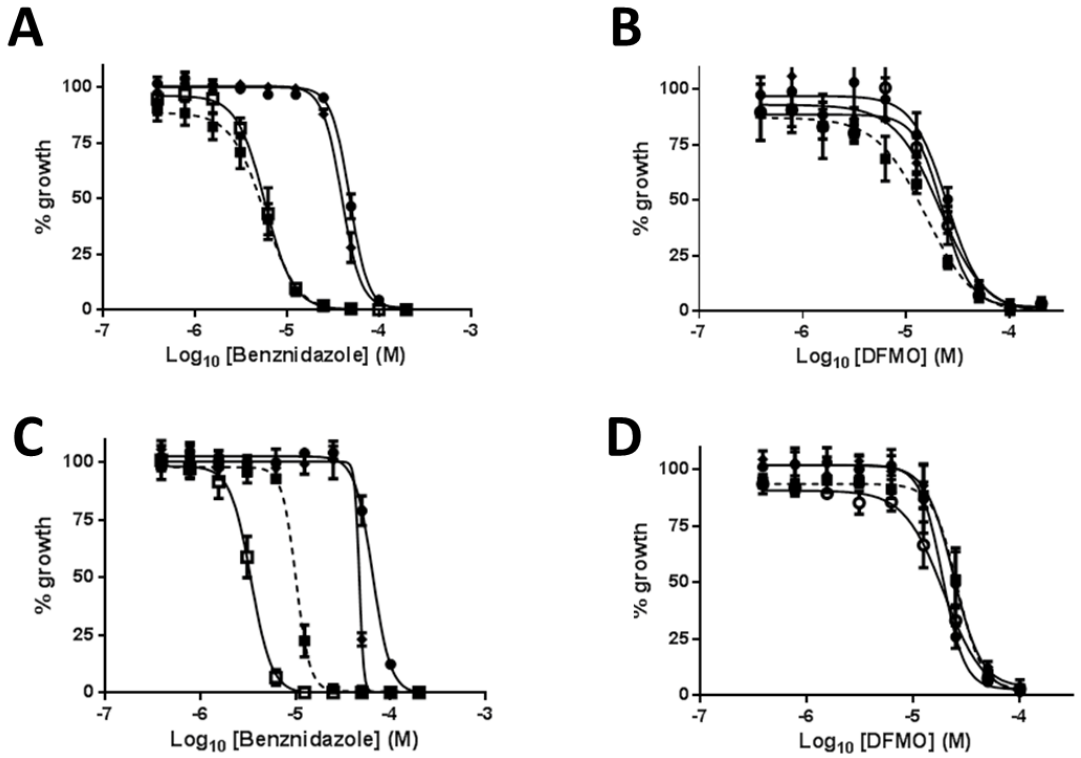

Figure 7.3: Susceptibility of *T. brucei* lines expressing altered levels of TbEXO1, TbMRE11 and/or TbNTR to benznidazole.
Dose response curves of wild type (●), Tb*exo1*Δ (♦), TbNTR over expression (■), and Tb*exo1*Δ TbNTR over expression (○) *T. brucei* to benznidazole (A) or DFMO (B).
Dose response curves of wild type (●), Tb*mre11*Δ (♦), TbNTR overexpression (■), and Tb*mre11*Δ TbNTR overexpressing (○) *T. brucei* to benznidazole (C) or DFMO (D). All data points are mean values ± standard deviations from experiments performed in quadruplicate.

When benznidazole was tested against *T. brucei* cells expressing altered levels of TbNTR and/or TbMRE11, a different outcome was observed. For TbMRE11-deficient cells or parasites expressing elevated levels of just TbNTR, treatment with the nitroimidazole resulted in increased susceptibility when compared against controls, with the TbNTR overexpressing cells being more sensitive than the null line: Tb*mre11*Δ cells and *T. brucei* expressing an ectopic

copy of Tb*ntr* were ~1.6- and ~6.5-fold more sensitive to benznidazole, respectively than wild type. For TbMRE11 null parasites overexpressing TbNTR, this increase in potency was enhanced with these cells showing a 19-fold increase in susceptibility indicating a link between activation of benznidazole by TbNTR and downstream DNA lesion formation.

Treatment	***T. brucei* EC_{50} (μM)**			
	Wild type	**Tb*exo1*Δ**	**TbNTR overexpression**	**Tb*exo1*Δ TbNTR overexpression**
Benznidazole	48.73 ± 2.30	39.67 ± 2.45 (1.3)	5.67 ± 0.66 (8.6)*	5.91 ± 0.79 (8.2)*
DFMO	23.93 ± 1.02	26.42 ± 1.17(0.8)	21.35 ± 1.30 (1.1)	21.57 ± 1.26 (1.1)

Treatment	***T. brucei* EC_{50} (μM)**			
	Wild type	**Tb*mre11*Δ**	**TbNTR overexpression**	**Tb*mre11*Δ TbNTR overexpression**
Benznidazole	65.49 ± 2.90*	42.97 ± 3.53 (1.6)*	10.24 ± 0.73 (6.5)*	3.47 ± 0.28 (22)*
DFMO	18.79 ± 2.08	26.19 ± 3.18 (0.7)	24.19 ± 3.72 (0.7)	19.46 ± 1.98 (1.0)

Table 7.3: Data represents EC_{50} values of genetically engineered lines against benznidazole and DFMO.

All values are means ± standard deviations from experiments performed in quadruplicate. The ratio of EC_{50} values between wild type and null mutant lines is given as fold difference, in parentheses. *Indicates significant differences in susceptibility ($P < 0.0001$ between wild type and null lines, as assessed by Student's *t* test (GraphPad Software).

7.4 Chapter Summary

This chapter has focused on evaluating whether TbSNM1 can be exploited as a drug traget and determining if various trypanocidal agents mediate at least part of the mode of action by promoting DNA damage. We have demonstrated that:

1. Some of the SNM1 inhibitors tested displayed trypanocidal activity but this did not involve targeting TbSNM1.
2. Nifurtimox does not appear to promote DNA damage that is repaired by selected components of the NER, MMR, HR or ICL pathways/systems .
3. The nitrogen mustard LH34 promotes formation of ICLs that are resolved using SNM1-dependent and SNM1-independent repair systems.
4. The azrinidyl agent CB1954 promotes formation of ICLs that are resolved using the SNM1-dependent and SNM1-independent repair systems
5. The azrinidyl agents CB1954 also promotes formation of additional DNA leisons that are repaired by components of the NER pathway
6. Activation of benznidazole results in cytotoxic moities that promote a form of DNA damage that can be resolved using components of the HR pathway.

8. Discussion

The plan for the eradication of HAT by 2030 can only take place by the development of new, active preventative/curative therapies. Work carried out in the Wilkinson laboratory has studied clinically used HAT treatment regimes to identify and study the mode of action of novel trypanocidal agents. These studies have broadened our repository of trypanocidal agents and our understanding of trypanosomal cell and molecular biology (Wilkinson and Kelly, 2009; Meredith *et al.*, 2017). These structure–activity relationship studies have focused on nitrogen- and quinone-containing chemicals which have revealed that many of these compounds promote mutagenic and clastogenic effects in the cell. These prodrugs, activated by a type 1 nitroreductase (TbNTR), are processed in the parasite to form an open aziridine structure which has the ability to form adducts with negatively charged DNA, predominantly at guanine bases, with a repeat of this event resulting in the formation of interstrand crosslinks (Hall, Bot and Wilkinson, 2011; Bot *et al.*, 2013; Meredith *et al.*, 2017).

This is the first study to comparatively analyse how trypanosomes repair crosslinks in DNA, with previous work carried out by the Machado & McCulloch laboratories speculating a role for the TC-NER pathway in trypanosomal intrastrand crosslink repair (Machado *et al.*, 2014). Using an *in vitro* genetics-based approach, a series of null mutant lines were generated to delete/disrupt key components of 'classical' DNA repair pathways. Growth inhibition assays were carried out on these cell lines using various agents which promote DNA damage to assess the relative importance of each DNA repair protein in trypanosomal DNA and ICL repair mechanisms. This enabled us to 1. understand whether the DNA repair protein has a role in removing lesions introduced in the genome, 2. appreciate if the enzyme has a role(s) in removing ICLs and 3. unravel the epistatic/non-epistatic relationship between trypanosomal ICL repair factors to create the first model of trypanosomal ICL repair systems. The same cell lines generated for this project were used to evaluate how clinically relevant and novel trypanocidal agents mediate their cytotoxic activities by analysing the prodrug mode of action, especially in relation to ICL formation.

The construction of null mutant lines was carried out using a traditional plasmid- and homologous recombination-based approach. This project could have exploited the newly-developed CRISPR-Cas9 system created for *T. cruzi* and Leishmania organisms in *T. brucei* (Peng *et al.*, 2014; Beneke *et al.*, 2017) but given the ease of creating genetically engineered

null lines in *T. brucei* and readily available resources to carry this out, the development and exploitation of a CRISPR-Cas9 system in this parasite was not deemed necessary. However, it would be interesting to use this now well-established tool to confirm observations made in this thesis and to expand these studies into analysis of ICL repair systems in other protozoan parasites.

Phenotypic screening was carried out on all null lines after a PCR-based approach was exploited to validate the genetically engineered lines: Confirmation at the protein level using western blotting-based techniques was not deemed necessary as absent RNA expression can be correlated to a lack of protein expression. This susceptibility screening was not extended out to heterozygote null mutants (which would give us an understanding into haploinsufficiency) due to time constraints with multiple, independently-generated clones analysed to confirm observations made. These phenotypic screens used mechlorethamine as the ICL inducing agent of choice to enable valid comparisons to be made against similar studies carried out in fungal lines (Lam, Krogh and Symington, 2008) and because mechlorethamine binds DNA with high affinity to produce stable ICLs (Bauer and Povirk, 1997). The use of other ICL inducing agents (*e.g.* psoralen-based compounds) would have confirmed conclusions made in this thesis but due to time constraints, this was not deemed a priority.

8.1 Trypanosomal ICL repair systems

The afore-mentioned approach has revealed that trypanosomes utilise the activities of TbSNM1, TbMRE11 (HR pathway), TbCSB (NER pathway) and TbEXO1 (MMR pathway) alongside factors of the FA pathway (TbRAD51, TbBRCA2, TbFAN1 and TbCHL1) for repair of ICLs with all data summarised in Table 8.1. Intriguingly, no evidence for a role of TbREV2 and TbREV3 (TLS pathway) was identified. Further studies using double null mutant lines lacking two DNA repair proteins revealed that trypanosomes possess at least two distinct pathways for the repair of ICLs; an SNM1-dependent ICL repair pathway which employs the functions of TbSNM1, TbCSB and TbEXO1 and an SNM1-independent ICL repair pathway, which utilised the functions of TbMRE11, TbFAN1, TbEXO1, and possibly the activities of TbRAD51 and TbBRCA2. Which system predominates in trypanosomes is yet to be answered but it is clear that similar pathways are being exploited by this parasite as seen in *E. coli*, yeast and mammalian cells (Houten *et al.*, 1986; Barber *et al.*, 2005; Hashimoto, Anai and Hanada, 2016).

Alongside this work on dissecting trypanosomal ICL repair systems, studies on how crosslinked DNA is processed to form DSBs were undertaken and demonstrated a clear time-dependent formation of γH2A, a marker for DSBs, in cells treated with the mechlorethamine. It was clear from these results that this ICL inducing agent forms damage in the trypanosome which can be processed to form DSBs, in keeping with previous observations on the processing of crosslinked DNA with the exact mechanism behind this still to be unravelled (Bessho, 2003; Sczepanski *et al.*, 2009). Accumulation of DSBs in mechlorethamine treated cells peaked at 4 hours incubation time which possibly reflects the time taken for the ICL inducing agent to crosslink DNA and produce the DSB. If this is the case, it would be interesting to understand the limiting factor for cleaving ICLs as well as how this relates to the different ICL repair systems. This could be evaluated using PFGE DNA fragmentation studies, the comet assay or the I-SceI meganuclease system (Singh *et al.*, 1988; Lam, Krogh and Symington, 2008; Chiurillo *et al.*, 2016).

8.1.1 SNM1-dependent ICL repair system

Studies on the trypanosomal SNM1-dependent ICL repair system has hypothesised that this mechanism functions by 1. stalling of RNA polymerase for recruitment of TbCSB, which unwinds damaged and neighbouring nucleotides for the recruitment of nucleases, 2. nucleolytic degradation of the unhooked DNA by TbSNM1 up to and past the crosslinked bases, and 3. TbEXO1 nuclease activity on crosslinked DNA as well as processing of base errors introduced into the genome during ICL repair. If this hypothesis is true, the SNM1-dependent ICL repair system operates like that seen in the transcription-coupled ICL repair system identified in mammalian cells as well as the dominant, PSO2-dependent mechanism employed by yeast (K F Grossmann *et al.*, 2001; Enoiu, Jiricny and Schärer, 2012). Given these similarities, the enzymes employed to carry out the initial ICL unhooking event needs to be evaluated to fully understand this pathway (Clauson, Schärer and Niedernhofer, 2013).

8.1.1.1 Nuclease activity of TbSNM1

Studies on the SNM1/PSO2 family of proteins has centered around the key and specific activity of this metallonuclease towards ICLs, as demonstrated in mammalian cells (Munari *et al.*, 2013), yeast (Hazrati *et al.*, 2008), *C. elegans* (Wilson *et al.*, 2017), *A. thaliana* (Johnson, Hellens and Love, 2011) and *O. sativa* (rice) (Kimura *et al.*, 2005). This activity has been extended out to *T. brucei* with parasites lacking TbSNM1 displaying an increased sensitivity

towards ICL-inducing agents, as shown in both this study and published literature (Sullivan *et al.*, 2015). This project has also shown that cells lacking TbSNM1 do not display any growth defects or arrest at any point in the cell cycle, with no growth defects also noted in yeast and *C. elegans* (Li, Hejna and Moses, 2005; Wilson *et al.*, 2017). This is possibly linked to TbSNM1 functioning independently of the homologous recombination-coupled ICL repair system.

Moreover, data represented here has not directly implicated TbSNM1 in the repair of pyrimidine dimers, double strand breaks or base oxidation, in keeping with previously published work (Sullivan *et al.*, 2015). However, work shown in this thesis has indicated that TbSNM1 plays a compensatory role for the repair of UV-induced damage in the absence of TbMRE11, indicating that both proteins have common substrates for this form of damage. This observation has not been noted in any previous reports of SNM1/PSO2 activity other than expression of PSO2 is inducible by UV (Wolter, Siede and Brendel, 1996). Both SNM1 and MRE11 possess endonuclease and exonuclease activity (Paull and Gellert, 1998; Li, Hejna and Moses, 2005) with the exonuclease activity being strand specific, *i.e.* SNM1 cleaves strands 5'-3' and MRE11 cleaves DNA 3'-5'. This suggests that the endonuclease activity of both proteins is required for processing of dimerised DNA at a collapsed replication fork (Paull and Gellert, 1998; Limoli *et al.*, 2002; Li, Hejna and Moses, 2005). It is possible that this endonuclease activity is critical for the creation of DSBs which initiates firing of a new replication origin as well as HR-mediated repair (Jones and Petermann, 2012).

Taking into consideration the wild type-like γH2A formation displayed by cells absent for TbSNM1, it is unlikely that this nuclease has a role in the incision of unhooked ICLs for DSB formation, which has also been observed in yeast where PSO2 nuclease activity does not lead to DSB formation (Dudás *et al.*, 2007). It is most likely that TbSNM1 functions in the cleavage of the DNA backbone, up to and beyond the ICL, revealing the damaged site for further processing (Tiefenbach *et al.*, 2007) and possibly in the processing of the double strand breaks formed from the interstrand cross link (Li and Moses, 2003). It would be interesting to see how this differs in cells treated with UV, given earlier observations.

Gene	Growth properties		Growth inhibition assays					DSB formation
	Growth	**Cell cycle**	**Phleomycin**	**MMS**	**UV**	**Hydroxyurea**	**HN2**	**γH2A**
TbSNM1	WT	WT	WT	WT	WT	WT	↓↓↓↓	WT
TbCSB	WT	WT	WT	WT	↓	WT	↓↓↓	↓
TbMRE11	↓	↑1N2K ↓1K1N WT 2K2N	↓	↓	↓	WT	↓↓	NIL
TbEXO1	WT	ND	↓	WT	WT	WT	↓	WT
TbREV2	WT	ND	WT	WT	WT	WT	WT	ND
TbREV3	WT	ND	WT	WT	WT	WT	WT	ND
TbFAN1	WT	WT	WT	WT	WT	WT	↓	WT
TbHEL1	WT	ND	WT	WT	WT	WT	WT	ND
TbCHL1	WT	WT	WT	WT	WT	WT	↓	WT
TbRAD51	↓↓	WT*	↓*	↓*	WT*	ND*	↓↓*	WT*
TbBRCA2	↓	↓ 1K1N WT 2K2N & 1N2K**	↓**	↓**	ND**	ND**	↓↓**	ND**

Table 8.1: Summary of data presented for all trypanosomal DNA repair factors.
Arrows indicate an increase (↑) or a decrease (↓) in phenotypic response when compared to wild type (WT) cells with multiple arrows shown for larger increases/decreases. ND stands for not determined for when an experiment was not performed. NIL refers to no increase or decrease seen. Corresponding data relating to TbBRCA2 was obtained from (Hartley and McCulloch, 2008) (denoted by *). Data obtained from (McCulloch and Barry, 1999; Proudfoot and McCulloch, 2005) relating to responses of TbRAD51 are denoted by **.

8.1.1.2 Critical role of TbCSB in damage recognition

CSB (Tijsterman *et al.*, 1997; Stevnsner *et al.*, 2008) has repeatedly been shown to play a pivotal role in transcription-associated damage recognition, an activity which has been extended out to trypanosomal transcription-coupled repair (Machado *et al.*, 2014; Wilson *et al.*, 2017). TbCSB is a nuclear protein (Dean, Sunter and Wheeler, 2017) which repairs UV-induced damage with no evidence for a direct role in repair of DSBs or base oxidation events, similar to observations noted by the McCulloch laboratory (Machado *et al.*, 2014). An intriguing observation from these studies was a delayed accumulation of DSBs in Tb*csb*-deficient cells, as seen by a late accumulation of γH2A in mechlorethamine treated null cells. This could be explained by stalling of the transcriptional machinery which causes recruitment of CSB to the site of damage and downstream processing of such damage into double strand breaks for repair *via* the HR pathway. CSB has been associated with regulation of double strand breaks at sites of transcription which indicates that this helicase remains at the site of the lesion during the repair process, possibly for activiation of cell cycle checkpoints (Batenburg *et al.*, 2015). Given that CSB is one of the first factors to be called upon at a stalled RNA polymerase, this key role in transcription-associated recognition of multiple types of damage is plausible (Tijsterman *et al.*, 1997).

The role of TbCSB in repair of crosslinked DNA has been previously studied using cells expressing reduced levels of the helicase coupled with phenotypic screening using the crosslinking agents cisplatin and cyclophosphamide (Machado *et al.*, 2014). This project has extended this initial work by screening of Tb*csb*-deficient cells against the archetypal ICL inducing agent, mechlorethamine which has confirmed the role of TbCSB in ICL repair, specifically *via* the SNM1-dependent ICL repair system. The epistatic interaction between SNM1 and CSB has been extensively studied in mammalian cells (Iyama *et al.*, 2015) with no discernible role for the yeast CSB homolog, RAD26, shown for ICL repair (Lambert *et al.*, 2003; Barber *et al.*, 2005). This work on mammalian cells has revealed that HsCSB stimulates the activity of HsSNM1A to help promote ICL processing in a transcription-associated, replication-independent repair system (Iyama *et al.*, 2015). The process of HsCSB upregulation occurs through halting of the RNA polymerase which leads to a hyperphosphorylation event of the polymerase and immediate upregulation of CSB (Luo *et al.*, 2001; Lagerwerf *et al.*, 2011). HsCSB enhances the substrate specificity of HsSNM1A at the lesion site for processing of the unhooked ICL (carried out by the activities of XPF-ERCC1). It would be convienent to

assume that a similar post-translational modification of trypanosomal RNA polymerases could lead to TbCSB recruitment to site of DNA damage with further studies needed to evaluate this (Deaconescu, 2013). Biochemical *in vitro* assays are also needed to prove that the epistatic interaction of TbCSB and TbSNM1 is extended out to a physical, protein-protein interaction. With this information, the non-epistatic interaction between TbCSB and TbMRE11 was unsurprising as there is no currently evidence for a role of CSB in recombination-coupled ICL repair (Enoiu, Jiricny and Schärer, 2012).

It is important to note that TbCSB has also been linked to promoting TLS polymerase activity to bypass damaged DNA (Machado *et al.*, 2014). If this is the case, TbCSB may play a critical role in this repair mechanism, acting as a regulator for all steps during transcription-associated repair. Whether CSA plays a similar role in ICL repair is yet to be studied (Iyama, Wilson and III, 2016).

8.1.1.3 The combinatorial role of TbEXO1 in trypanosomal ICL repair

This is the first study to look into the role of TbEXO1, an important nuclease of the MMR pathway, in trypanosomal DNA repair with other factors of the MMR previously studied elsewhere (Bell *et al.*, 2004). This project has shown absence of TbEXO1 does not cause any growth defects, cell cycle defects or enhanced sensitivity to agents which promote base oxidation or pyrimidine dimers. Intriguingly, enhanced sensitivity of this null mutant line was seen towards phleomycin but not MMS, despite both agents promoting DSB formation. This may reflect the differences in how DSBs are generated by both agents with the length of the flap overhang (Pizzolato *et al.*, 2015) affecting the efficiency of the 5'-3' exonuclease activity of TbEXO1 (Keijzers, Bohr and Rasmussen, 2015). DSBs formed from stalling of the replication fork (as seen with MMS (Ensminger *et al.*, 2014)) produce large overhangs, with these substrates displaying a reduced processing efficiency towards EXO1. This differs from DSBs formed from phleomycin-induced oxygen free radicals which create DSBs with overhangs of only a few nucleotides. In this latter case, efficiency/binding of EXO1 to the damaged DNA is higher (Keijzers, Bohr and Rasmussen, 2015). Given the MMR pathway repairs single/few damaged bases, this low processing power for EXO1 is understandable and could be extended out to the activity of TbEXO1 in relation to ICL and MMR repair pathways.

EXO1 has been implicated in the fungal replication-coupled, PSO2-independent ICL repair system for the cleavage of unhooked DNA prior to strand annealing (Lam, Krogh and Symington, 2008; Ward *et al.*, 2012; Kato, Kawasoe, Williams, Coates, Roy, Shi, Lorena S. Beese, *et al.*, 2017). It has been shown that EXO1 acts as the alternative 5'-3' exonuclease in the absence of PSO2 (alongside factors of the MMR factors e.g. MutSa) (Ward *et al.*, 2012). This differs from the situation seen in trypanosomes as TbEXO1 functions in both the SNM1-dependent and -independent ICL repair systems, epistatically interacting with TbSNM1, TbCSB and TbMRE11. Trypanosomes may utilise the activity of TbEXO1 in both systems to 1. function as the alternative nuclease in the SNM1-independent ICL repair pathway (as seen in yeast (Ward *et al.*, 2012; Kato, Kawasoe, Williams, Coates, Roy, Shi, Lorena S Beese, *et al.*, 2017)) and 2. repair errors introduced by the error-prone, SNM1-dependent ICL repair system (this mechanism is called 'error-prone' as the activity of TLS polymerases promotes base errors). To further evaluate the latter hypothesis, similar epistatic/non-epistatic studies should be carried out on cells lacking multiple factors of the MMR pathway, with the best candidate for this study being MSH2 given its well-characterised role in ICL repair (Williams *et al.*, 2011; Ward *et al.*, 2012; Kato, Kawasoe, Williams, Coates, Roy, Shi, Lorena S. Beese, *et al.*, 2017).

8.1.1.4 Absent role for TLS factors TbREV2 & TbREV3

The TLS pathway plays a crucial role in ICL repair, filling gaps created by the cleavage activity of nucleases (Ho *et al.*, 2011). Work in yeast has shown us that not all TLS polymerases play a role in ICL repair, where only five out of the fifteen polymerases are shown to function in this system (Kozmin and Jinks-Robertson, 2013). Absence of a growth, DNA or ICL repair phenotype for both TbREV2 and TbREV3, trypanosomal TLS enzymes, was peculiar but given that only two out of five of the TLS polymerases present in *T. brucei* were studied, it is still plausible that the TLS pathway plays a key role in trypanosomal ICL repair. Evidence for this can be seen when analysing the role of the TLS factor polymerase theta (Θ) of the protozoan parasite *Leishmania infantum* which has been shown to play a key role in repair of interstrand crosslinks (Fernández-Orgiler *et al.*, 2016). Furthermore, trypanosomal TLS polymerases could be acting in a compensatory manner, functioning on behalf of another trypanosomal TLS polymerase when one is absent. With this in mind, a different approach may have to be undertaken to understand whether these TLS polymerases function in ICL repair. It is

hypothesised that the TLS pathway functions in both the SNM1-dependent and -independent pathway, given how these ICL repair systems operate in yeast and mammalian cells.

8.1.2 SNM1-independent ICL repair system

It is clear that trypanosomes possess a separate ICL repair system which utilises the activities of components of the homologous recombination and mismatch repair pathways, functioning independently of TbSNM1. It is hypothesised that this pathway involves 1. stalling of the replication fork resulting in the recruitment of nucleases to unhook the ICL, 2. cleavage of crosslinked DNA by the nuclease activity of TbMRE11, TbEXO1 and TbFAN1 (possibly resulting in DSB formation), and 3. error-free repair by the HR pathway utilising the activities of the TbRAD51, TbBRCA2 and TbCHL1 proteins. Trypanosomal FA homologues have been implicated in this system as many of the components identified in the parasites genome have additional roles in the HR pathway, a mechanism which has already been associated with the SNM1-independent ICL repair pathway by the activity of TbMRE11.

8.1.2.1 Concerted actions of TbMRE11 & TbEXO1

Studies carried out here on the role of TbMRE11 in trypanosomes has brought to light many interesting observations. The growth defect and G2/M cell cycle arrest displayed by the Tb*mre11* null lines suggests this nuclease has a role in nuclear DNA replication. Work in mammalian cells has shown that ATM (ATM serine/threonine kinase) and ATR (Ataxia Telangiectasia) acts in the recruitment of MRE11 at the site of a collapsed replication fork (Trenz *et al.*, 2006). This recruitment of MRE11 initiates the restart of the replication fork, thus preventing accumulation of DSBs and chromosomal abnormalities. *T. brucei* possesses homologues for both ATM (Tb927.2.2260) and ATR (Tb927.11.14680), which could make up the replication-coupled, DNA damage signalling network in trypanosomatids, alongside the recognition and repair activities of TbMRE11. This agrees with observations made from assays looking at γH2A formation, an indicator for DSBs, where Tb*mre11* null cells show no phosphorylation event for this histone in mechlorethamine treated cells, indicating a key role for this nuclease in detection of DSBs and warrants further investigation into the regulation and checkpoint signalling of trypanosomal repair systems.

Phenotypic screening of Tb*mre11*-deficient cells revealed a clear role for this nuclease in repair of lesions created by phleomycin, MMS, UV and mechlorethamine. Growth inhibition

data relating to MMS and phleomycin agrees with the McCulloch and Cross laboratories which have shown that cells lacking TbMRE11 are more sensitive to phleomycin and MMS, respectively, implicating this nuclease in the HR pathway (Robinson, McCulloch, Conway, Browitt and Barry, 2002; Tan, Leal and Cross, 2002). Our results have also implicated a role for TbMRE11 in repair of UV-induced lesions with work in mammalian cells relating this observation to stalling of the replication fork at the site of dimerised DNA. This event leads to recruitment of the MRN complex for replication fork restart (Limoli *et al.*, 2002), connecting observations made in both trypanosomal and mammalian cell lines.

The role of TbMRE11 in trypanosomal ICL repair was unsurprising due to the well-documented role of MRE11 in both mammalian and yeast cells, functioning independently of SNM1/PSO2 (Pichierri, Averbeck and Rosselli, 2002; Lam, Krogh and Symington, 2008). The epistatic interaction of TbEXO1 and TbMRE11 has been linked with processing of unhooked ICLs as MRE11 possesses 3'-5' exonuclease activity and EXO1 has 5'-3' exonuclease activity, ideal for cleavage at this site (Barber *et al.*, 2005). Whether this processing leads to DSB formation is yet to be studied. This data could also explain why trypanosomes do not require the activity of TbSNM1 in the MRE11-dependent system: TbEXO1 is able to compensate for the activity of SNM1 (Pizzolato *et al.*, 2015). It is tempting to speculate that this system is coupled with ICLs encountered during replication due to the correlation between factors of the homologous recombination pathway and DNA damage at a DNA replication fork (S-phase of the cell cycle). This also explains the non-epistatic interaction of TbMRE11 and TbCSB; unwinding of the double helix is not required due to the presence of the large replication bubble.

8.1.2.2 Trypanosomal FA factors and the SNM1-independent ICL repair system

This study has identified and characterised trypanosomal homologues of FA factors with these results demonstrating that trypanosomes employ a similar system to yeast where these FA proteins function alongside the classical DNA repair pathways to resolve such lesions (Daee and Myung, 2012; McHugh, Ward and Chovanec, 2012). The early branching nature of the trypanosomatid tree of life has resulted in trypanosomes exploiting components of classical DNA repair pathways for the removal of crosslinks as opposed to evolving a dedicated ICL repair pathway. Many organisms including *A. thaliana* (Molinier, Stamm and Hohn, 2004) and *S. cerevisiae* function in a similar mechanism with these factors predominantly acting in SNM1/PSO2 independent DNA repair pathways. Zebrafish are one of the few organisms, other

than humans, which possess all homologues of the FA core complex with these factors also playing a role in sex determination and genomic stability (Rodríguez-Marí and Postlethwait, 2011).

The FA pathway consists of 1. recognition of the damaged DNA and assembly of eight proteins that form the so-called FA core complex, 2. activation of the FANCD2/FANCI heterodimer that functions as a recruitment complex, and 3. association of effector proteins that operate to resolve the ICL. The absence of all components of the FA core complex (except FANCM) in and homologues of FANCD2 and FANCI suggests that trypanosomes employ a separate mechanism for ICL recognition and factor recruitment, possibly *via* stalling of the replication fork leading to the recruitment of ATM and/or ATR, which when phosphorylated, are able to upregulate DNA repair factors *e.g.* EXO1/MRE11 (Moldovan and D'Andrea, 2009). This also explains the absence of UHRF1 and UAF1, both of which are involved in recruitment/deubiquitination of FANCD2, respectively (Moldovan and D'Andrea, 2009; Liang *et al.*, 2015).

Many FA effector proteins are also putatively absent from the trypanosome genome. FANCP, SLX4, is a key endonuclease which plays a role in the initial incision step for unhooking of the ICL and resolution of the Holliday junction (Cybulski and Howlett, 2011). Its absence in trypanosomes is intriguing given various endonucleases are exploited for cleavage of ICLs in mammalian cells. Studies in this thesis have implicated endonucleases TbSNM1, TbMRE11 and TbFAN1 in ICL repair and given that trypanosomes are simple eukaryotes, these parasites may only require a minimal number of nucleases for ICL processing, possibly explaining the absence of FANCP. Furthermore, absence of FANCN (PALB2), FANCS and FANCU (XRCC2) can be explained by TbBRCA2 and TbRAD51 paralogues carrying out their given roles in the FA pathway (Simhadri *et al.*, 2014; Park *et al.*, 2016). The nuclear localisation of FA effector proteins and RAD51-heterodimer formation for strand exchange, which is associated with the activities of these FA factors, can be carried out by TbBRCA2 and TbRAD51 paralogues, explaining their absence from the trypanosomal genome (Dobson *et al.*, 2011; Genois *et al.*, 2014)

Despite the absence of many FA factors, trypanosomes express some FA effector proteins, primarily belonging to the HR pathway. Studies in this thesis have shown a key role for TbRAD51 (or TbFANCR), TbBRCA2 (or TbFANCD1), TbCHL1 (or TbFANCJ) and

TbFAN1 in trypanosomal ICL repair with TbHEL1 being the only trypanosomal FA factor to display no evidence for a role in ICL repair. The only FA factors yet to be studied include FANCQ, FANCV and USP1.

8.1.2.3 Functions of TbRAD51 and TbBRCA2 in trypanosomal ICL repair

It is unsurprising that TbRAD51 and TbBRCA2 play a role in ICL repair as both proteins have been extensively characterised in fungal and mammalian ICL repair systems (K F Grossmann *et al.*, 2001; Noll, Mason and Miller, 2006; Ward *et al.*, 2012). TbRAD51 and TbBRCA2 possess recombinase/helicase activity, respectively, to search for homologous sequences on sister chromatid DNA for error-free ICL repair. It would be interesting to understand the role of the four RAD51 paralogs identified within the *T. brucei* genome (RAD51-3 (also known as FANCO), RAD51-4, RAD51-5 and RAD51-6) and how they influence this activity and ICL repair (Dobson *et al.*, 2011). It would also be interesting to identify whether a single residue in these proteins aids ICL repair, as seen with mammalian RAD51 (Wang *et al.*, 2015), a feature that may be exploitable in terms of chemotherapeutic development.

It would have been interesting to carry out epistatic/non-epistatic relationship studies between TbMRE11 and these enzymes but due to the growth defects observed by the single null lines and the need for the HR pathway to generate these genetically engineered lines, this was not possible. A new approach is needed to fully understand the interaction of these HR factors with one possible method exploiting tagged-TbMRE11 lines generated in the Wilkinson laboratory for co-immunoprecipitation studies with this approach being an excellent tool for understanding this ICL repair at a protein-protein level by revealing the physically interacting partners of TbMRE11.

8.1.2.4 Nuclease activities of TbFAN1 on crosslinked DNA

Recent work has highlighted the importance of FAN1 in this repair system with many research groups demonstrating its function as comparable to SNM1 with activities carried out by a highly conserved and FAN1-specific VRR-NUC domain (O'Donnell and Durocher, 2010; Jin and Cho, 2017). TbFAN1, a nuclear DNA repair protein (Dean, Sunter and Wheeler, 2017), possesses a similar VRR-NUC domain and "$PDX_n(D/E)XK$" motif which was sufficient evidence to state this protein as true TbFAN1 homologue (Fontebasso *et al.*, 2013). Phenotypic susceptibility screening of TbFAN1-deficient cells revealed no altered sensitivity to hydroxyurea, UV, MMS and phleomycin with a clear increase in susceptibility to

mechlorethamine. It would be interesting to analyse the sensitivity of this null line to mitomycin C, the archetypal DNA damaging agent for characterisation of FA factors (Jin and Cho, 2017).

This clear role for FAN1 in trypanosomes has further developed our understanding on how damaged DNA is processed for the BRCA2-RAD51 complex. Previous work on the role of FAN1 in ICL repair has shown that upon recruitment by FANCD2, this nuclease cleaves around the damaged DNA and acts as a replication fork recovery factor. Mammalian cells absent for FANCD2 cause MRE11-dependent access for FAN1 at a stalled replication fork to degrade damaged DNA strands (Indrajit Chaudhury, Stroik and Sobeck, 2014). Given that no trypanosomal homologue of FANCD2 has been identified and TbFAN1 and TbMRE11 function epistatically, a similar FANCD2-independent incision event may occur in trypanosomes. Upon stalling of the replication fork, it is hypothesised that these nucleases (TbMRE11 and TbFAN1) carry out extensive nucleolytic degradation of the DNA strands to create substrates which RAD51 is able to bind, thus promoting HR repair. Alongside this, they function in creating a new replication origin for fork restart to help promote DNA replication. New replication fork origins are needed to repair DNA without affecting the speed of DNA replication (Stanojcic *et al.*, 2016). As FAN1 homologues incise DNA three or four nucleotides near the ICL, transversing the crosslink, it is predicted that FAN1 can unhook the ICL and incise flapped DNA surrounding the ICL which may explain how ICL-induced DSBs are formed in trypanosomes (Pizzolato *et al.*, 2015).

8.1.2.5 The baffling function of TbCHL1

TbCHL1, a nuclear ATP-dependent helicase (Dean, Sunter and Wheeler, 2017), has been implicated as a trypanosomal ICL repair factor and taken together with information from literature, TbCHL1 is hypothesised to function in the SNM1-independent (Brosh and Cantor, 2014). As seen with TbFAN1-deficient cells, Tb*chl1* null lines display no altered susceptibility to phleomycin, MMS, UV or hydroxyurea with additional work needed to look at susceptibility to mitomycin C to confirm a role in the FA pathway.

Analysis into the role of TbCHL1 in trypanosomal ICL repair has revealed some interesting findings with dose response curves against mechlorethamine demonstrating a regulatory role for TbCHL1 in ICL repair. It is hypothesised that TbCHL1 is acting as a co-regulator for the

activities of ICL repair factors with these factors acting to compensate for the activity of TbSNM1. Absence of both TbSNM1 and TbCHL1 releases these activities, restoring the cells ability to repair ICLs. Typically, FANCJ acts as a unique helicase which unwinds 5'ssDNA forked duplex substrates which contains at least 15 nucleotides (Wu and Brosh, 2009). In yeast cells, FANCJ plays a role in the Pso2-independent ICL repair pathway, functioning alongside the Mph1-Mgm101-MutSα complex for the activation and recruitment of Exo1 to the damage site (Ward *et al.*, 2012). This contrasts observations made in this thesis as a classical, non-epistatic interaction would have been predicted if TbSNM1 and TbCHL1 functioned in independent ICL repair systems, as seen in yeast. Further studies are needed to explore the role of TbCHL1 in detail.

8.1.3 Summary

Our data and the work carried out on yeast and mammalian cells suggests that there is more than one system for the repair of ICLs, dependent on the temporal and spatial nature of ICL detection, with each system differing in relation to enzymes employed to the site of damage (Shen and Li, 2010). Whether the SNM1-independent or -dependent system is the central ICL repair mechanism is yet to be evaluated: ICL repair studies carried out on mammalian cells indicates that the FA, replication-coupled system is the dominant ICL repair mechanism. Given the multigenic nature of transcription in this parasite, we hypothesise the SNM1-dependent ICL repair pathway is the preferred repair system as regulation at a transcriptional level is of great importance in the parasite. It is tempting to speculate the fold differences observed between wild type and null lines reflects the relative importance of the ICL repair protein being tested however it is more likely that the variation observed here reflects the role of that enzyme in repair associated with transcription or replication: an asynchronous culture of trypanosomes contains more transcriptionally active cells than dividing cells. A summary of both trypanosomal ICL repair systems is shown in Figure 8.1.

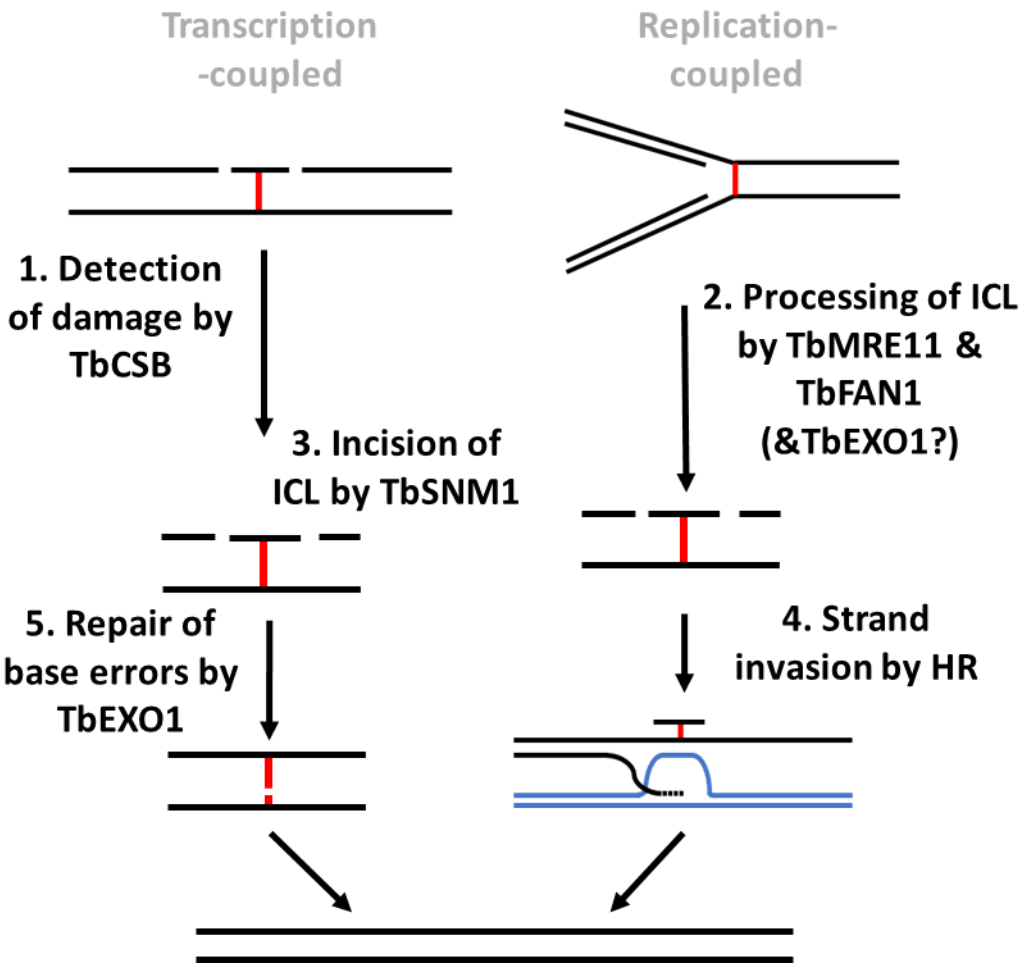

Figure 8.1: Current model for trypanosomal ICL repair.

8.2 TbSNM1 structure and function

Initial *in silico* analyses carried out on TbSNM1 were extended to understand the proteins 1. catalytic activity, 2. substrate specificity and 3. nuclear localisation (Sullivan *et al.*, 2015). This work was carried out by ectopic, inducible expression of either wild type or mutated GFP-tagged TbSNM1 in a genetic background absent for TbSNM1 which has proven to be an excellent tool to developing a clear understanding of which residues play a key role in this enzymes activity. Results from this analysis have demonstrated a role for residues D40, H80, D82 and H159 in TbSNM1 catalytic activity, residues R429 and R430 in protein localisation and a possible structural role for the D221 residue (Table 8.2). Structural consequences of mutating TbSNM1 were analysed *in silico* using a predicted TbSNM1 model created from both human SNM1 proteins as the structural templates. Ideally the residues hypothesised to be responsible for the coordination of the zinc metal ion in TbSNM1 would have been confirmed biochemically (e.g. using isothermal titration calorimetry) but given time constraints and lack of appropriate resources, this was not carried out. This model predicted TbSNM1 to bind one

zinc ion, possibly in an octahedral arrangement, similar to that observed by HaSNM1A, which may indicate that TbSNM1 solely functions in ICL repair, as seen with HaSNM1A (Sengerová *et al.*, 2012).

Putative function	TbSNM1 Mutation	Localisation	Complementation
Co-factor binding	D40A	Nuclear	No
	H78A	Nuclear	Yes
	H80A	Nuclear	No
	D82A	Nuclear	No
	H83A	Nuclear	Yes
	H159A	Nuclear	No
	H178A	Nuclear	Yes
	D221A	Non-specific	No
	H496A	Nuclear	Yes
Localisation	R428A	Nuclear	Yes
	R429A	Non-specific	No
	R430A	Non-specific	No
	H431A	Nuclear	Yes
Substrate specificity	V518A	Nuclear	Yes

Table 8.2: Summary of TbSNM1 mutational analysis.

8.2.1 Key residues in TbSNM1 nuclease activity

Four key residues have been implicated in TbSNM1 nuclease activity with one of these residues being the arginine at position 40. The analogous residue in HsSNM1B, D14, has an important structural role for formation of hydrogen bonds to coordinate H36 (motif 2) and H99 (motif 3) residues, with both of these motifs having a direct role in enzyme catalytic activity (Allerston *et al.*, 2015). Molecular modelling places the D40 residue in close proximity to residues of motif 2 (78-HxHxDH-83), suggesting that this residue may be playing a critical role in the coordination of this motif to the zinc ion as opposed to a direct role in zinc binding.

Furthermore, it was identified that residues H80 and D82 of the 'HxHxDH' motif play an important role in TbSNM1 catalytic activity with both residues in close proximity to the zinc metal ion. Given all residues of this motif in HsSNM1A play a role in coordination of the metal ion, it was predicted that mutation of H78 and H83 would have also displayed a similar phenotype as mutation of H80 and D82 residues (Hazrati *et al.*, 2008). It is likely that the exact activity of these residues can only be revealed by biochemical analysis of the TbSNM1 structure (Sengerová *et al.*, 2012).

Studies on the H159 residue of motif 3 have shown a key role in protein enzyme function. In HaSNM1A, this residue also plays a critical role in enzyme function to coordinate the third bond with the zinc ion, with the other two bonds coordinated by motifs 1 and 2, alongside motif 4 (Allerston *et al.*, 2015). It is hypothesised that the residue H159 also functions in a similar manner as molecular modelling shows a clear interaction of this motif with all other TbSNM1 motifs. The conserved residue of motif 4, H178, did not display any evidence for a role in TbSNM1 catalytic activity, despite this motif playing a clear role in HaSNM1A activity. Furthermore, residue H496 did not show any indication for a role in TbSNM1 nuclease activity with the respective conserved residue in HsSNM1A (H994) also not displaying any evidence for a role in nucleotide hydrolysis. However, the corresponding residue in PSO2 (H611) does show evidence for mediating the catalytic reaction with damaged DNA (Sengerová *et al.*, 2012) which confirms that TbSNM1 functions in a similar manner to HsSNM1A and not HsSNM1B or PSO2. This data demonstrates that conserved residues found in motifs 1, 2 and 3 all play a key role in TbSNM1 nuclease activity which differs from other SNM1 homologs where all 4 motifs have catalytic functions. It is hypothesised that this histidine-rich coordination of the zinc metal ion aids redistribution of electrons around the aromatic imidazole ring of the amino acid to carry out the nucleophilic attack on DNA.

Further to this, it has been hypothesised that the D221 residue of motif 4 plays an important structural role in TbSNM1. Motif 4 in other SNM1 homologs contributes to the bridge between zinc ions and residues (Allerston *et al.*, 2015), playing a critical process in maintaining this structure. This could explain why mutation of D221 into alanine resulted in a loss of TbSNM1 structural integrity; this residue plays a key role in maintaining this structure, potentially aiding the connection between the zinc binding pocket and the rest of the protein. Inhibitors of this residue could prove to be great therapeutic targets against TbSNM1.

8.2.2 Evaluating TbSNM1 substrate specificity

TbSNM1 substrate specificity has been associated with a conserved valine residue at position 518 with mutation of this residue displaying no evidence for altered TbSNM1 activity. This result has also been observed with HsSNM1A when mutation of the equivalent residue to either alanine or histidine maintained the nucleases enzymatic activity (Sengerová *et al.*, 2012). It is plausible that many residues confer substrate specificity in the SNM1 family of proteins. Residues E213 and H254 in HsSNM1A have been hypothesised to aid this DNA specificity

which suggests that a triple mutation of all three residues may alter the enzymes ability to bind DNA efficiently (de Villartay *et al.*, 2009). Although equivalent and conserved residues to E213 and H254 have not been identified in TbSNM1, further work on identifying residues responsible for TbSNM1 DNA binding is important to gain a full understanding of the proteins activity.

8.2.3 Dissecting the TbSNM1 nuclear localisation signal

This study has implicated two key residues, R429 and R430, in TbSNM1 nuclear localisation with no analogous role for R428 and R431 residues seen. With no comparable work carried out in mammalian and yeast homologues of this nuclease, it is hard to determine whether this trait is conserved within other organisms. It is tempting to speculate that residues R428 and R431 in TbSNM1 are required for protein localisation given that all four amino acids interact directly on the model of TbSNM1 and are all exposed on the surface of the protein, an attribute which is vital when targeting proteins to the nucleus. To test this, mutation of multiple residues may be required. Regardless, this data could be exploited for the development of inhibitors against TbSNM1.

8.2.4 Summary

The results observed here merit further investigation into the structural properties of TbSNM1. These same cell lines can be used to carry out pull-down assays to identify if these mutations affect the physical interacting partners of TbSNM1. The plasmids used for this assay can also be used for protein purification and *in vitro* activity assays to develop our knowledge on this structure-function relationship. Studies could also be broadened out to understand how mutation of two residues affects TbSNM1 catalytic activity. It would be interesting to undertake a biochemical analysis of TbSNM1 to analyse the enzymes binding specificity towards single stranded DNA and double stranded DNA. This could reveal how TbSNM1 hydrolyses DNA and whether it acts in a similar manner to HsSNM1A where small activity towards RNA is also seen. Structural, biophysical and fluorometric assays could be used to understand the processing power of TbSNM1 in relation to its efficiency in digesting past the ICL, as seen with HsSNM1A (Sengerová *et al.*, 2012). This high processing power of HsSNM1A has been related to residues K904-K906 with mutations of these residues reducing the processing power of the enzyme but not affecting the enzymes catalytic activity (Allerston *et al.*, 2015). This mutation resulted in a reduced capacity to digest substrate DNA with

premature termination of digestion. These lysine residues are semi-conserved in TbSNM1 with arginine residues present in the trypanosomal sequence, both of which are positively charged amino acids. Given that mutation of these residues does not affect the enzymes nuclease activity, studies carried out in this study cannot be used to evaluate the role of these residues with biochemical studies needed to dissect the function of these conserved arginine residues.

8.3 Cytotoxic effects of trypanocidal compounds

The cytotoxic effects towards DNA of clinically used and novel trypanocidal agents were evaluated to reveal that nifurtimox does not cause the formation of any DNA damage on the parasites genome, benznidazole promotes DNA damage which is repaired by the HR pathway (Campos *et al.*, 2017), LH34 promotes ICL formation and CB1954 promotes both adduct and ICL formation in the parasite. The damage incurred by benznidazole involves prodrug activation which creates electrophilic drug metabolites which can lead to oxidative stress and adduct formation. Nitroreduction of CB1954 can result in the production of 4-hydroxylamine which can be processed to act as an electrophilic intermediate, alkylating cellular nucleophiles such as DNA (Meredith *et al.*, 2017). This nitroreduction event can also result in the formation of 2-nitroso and 2-amine metabolites, both of which are able to alklyate DNA to create monoadducts (Mitchell and Minchin, 2008). Arizidinyl compounds vary in their structure which is reflected in the type of lesions formed on DNA. This could explain why LH34 only displays evidence for promotion of ICLs and no other adducts. This can help broaden our understanding of how arizidinyl-containing compounds function intracellularly, potentially extending the number of compounds which can be used in anti-tumour therapy. Many ICL-inducing agents are exploited to target cancer, with arizidine-containing compounds no exception.

8.4 An unexpected journey

TbHEL1, initially presumed to be a homologue of FANCM, displayed no evidence for a role in DNA repair, despite *in silico* analyses indicating a typical FANCM-like conserved protein domain and sequence structure. Given this, it was clear why trypanosomes are also absent for some ancillary FA factors (*e.g.* FAAP100, FAAP24, FAAP16 and FAAP20) as these proteins aid in FANCM localisation to chromatin and recognition of ICLs. Further studies on this enzyme has indicated a key role in trypanosomal RNA interference, possibly acting as the

missing helicase from DICER (Patrick *et al.*, 2009). It is postulated that TbHEL1 directly interacts with TbDCL1 and TbDCL2 for the cleavage of double stranded RNA (dsRNA) molecules to produce siRNA molecules which are degraded by the RISC complex (Hammond, 2005). TbHEL1 could operate to determine which RNA molecules undergo dicer-mediated cleavage and process hairpin precursor microRNAs. Given that most DICER proteins possess both incision and helicase activities, this arrangement is rather strange but has been noted in other species e.g. *Sporotrichum thermophile* where dicer related helicases operate in a separate system to the DICER enzyme (Kidwell, Chan and Doudna, 2014). Other protozoan parasites are also able to undergo RNA interference but by different mechanisms which indicates that this silencing event in eukaryotes occurred at a very early point in evolution. Gene silencing in *Plasmodium* and *Giardia* species is hypothesised to operate in a classical RNA interference system, as seen in mammalian cells, with other trypanosomal RNA interference mechanisms similar to the above, multifactorial system (Ullu, Tschudi and Chakraborty, 2004). It is plausible that this complex RNA interference pathway requires the aid of additional helicases and ancillary proteins which are yet to be identified and studied in this parasite. It would be interesting to analyse the interaction of dsRNA and TbHEL1, including conserved residues responsible for this interaction and how the length of the dsRNA molecule affects the helicase activity of TbHEL1.

9. Future work

This is the first comprehensive study to look at how trypanosomes repair ICLs with many unanswered questions still remaining. Which other DNA repair factors are employed to remove ICLs? Are there any additional ICL repair systems employed by the parasite? Does *T. brucei* possess additional ICL repair specific factors currently not identified in prokaryotes or eukaryotes? How do these results compare with ICL repair systems in other protozoan parasites e.g. *T. cruzi* or *Leishmania*?

The next step for this project is confirming the dominant ICL repair system, particularly in relation to the different stages of the cell cycle. This could be carried out by stalling null lines at distinct stages of the cell cycle with further evaluation of their response to mechlorethamine (Nair *et al.*, 2014). Evaluating whether these ICL repair systems are coupled to stalling of the transcription/replication machinery can be tested using inhibitors of RNA/DNA polymerases to evaluate how this affects sensitivity of null lines to ICL inducing agents. Furthermore, SMARD can be used to look at replication changes, both rate and direction, in mechlorethamine treated null cells (Calderano *et al.*, 2015) with the hypothesis that any factors involved in replication-coupled ICL repair will display a prolonged rate of replication due to the lack of ICL repair. A similar study can be used to study transcription-coupled ICL repair factors with RT-qPCR carried out on a single polycistron to look at transcriptional changes upon treatment with mechlorethamine.

Identification of other trypanosomal ICL repair factors should focus on understanding how the initial unhooking event occurs in the parasite. A similar genetics-based approach (either using plasmid-based knockouts or the CRISPR-Cas9 system) coupled with susceptibility screening can be used to look at the ICL repair activities of TbXPG (Tb927.9.11760), TbERCC1 (Tb927.7.2060), TbXPF (Tb927.5.3670), TbMUS81 (Tb927.8.6740), TbSLX1 (Tb927.3.1220) with EME1 and SLX4 absent from the trypanosome genome (Genois *et al.*, 2014; Machado *et al.*, 2014). TbXPG has been studied for a role in the TC-NER pathway and is hypothesised to carry out these nuclease activities in the SNM1-dependent repair pathway (Machado *et al.*, 2014). The activity of TbXPF was not assessed in the aforementioned study but given its activity in mammalian cells, it can be hypothesised to function alongside TbERCC1 in the SNM1-dependent repair pathway. The endonuclease activities of both these nucleases in trypanosomes can be tested by incubation of purified proteins with crosslinked,

circular DNA with cleavage activities confirmed by linearization of DNA (Wood, 2011; Klein Douwel *et al.*, 2017). TbMUS81 has been functionally characterised by the McCulloch laboratory in relation to its role in recombination repair (Devlin, 2015) with its role in ICL repair currently unstudied. Given the interacting partner of TbMUS81 is absent, EME1, it is highly unlikely that this complex plays a role in removal of ICL lesions.

Identifying the role of the remaining FA factors identified in the trypanosome genome (FANCO, FANCQ, FANCV and USP1) would complete this analysis into the role of the trypanosomal FA pathway. FANCQ (XPF) is hypothesised to play a nuclease function for the unhooking of damaged DNA. FANCO, RAD51-C, has been studied for its auxiliary role in the HR pathway and may function alongside TbRAD51 and TbBRCA2 for strand invasion (Dobson *et al.*, 2011). FANCV, MAD2, functions as a cell cycle checkpoint protein in spindle assembly during the metaphase-anaphase transition and has been hypothesised to play a role in the SNM1-independent ICL repair pathway for regulation of the cell cycle (Actis *et al.*, 2016). Finally, USP1 functions in the deubiquitination of FANCD2 with several potential homologues of USP1 identified in the parasite genome (Kim and Kim, 2016). With the absence of FANDC2 in the parasite, this hydrolase may function in other regulatory mechanisms *e.g.* the post-translational modification of TbBRCA2 for protein activation (Schoenfeld *et al.*, 2004). Studies identifying new ICL repair factors should also be carried out using a genome wide RNAi screen, RIT-seq (RNAi target sequencing) screen with mechlorethamine as the selective agent of choice (Stortz *et al.*, 2017). This would reveal any novel DNA repair proteins involved in the trypanosomal ICL repair system as well as the ICL damage signalling pathways.

An extension of the above-mentioned biochemical analysis for TbSNM1 will reveal any potential targetable sites for the development of inhibitors of this protein. This can involve carrying out pull down assays on the ectopic expression of an amino terminally GFP tagged version of the enzyme to evaluate the physically interacting partners of TbSNM1, potentially identifying trypanosome-specific ICL repair factors. Further to this, purification of TbSNM1 and crystallisation studies would help advance the structure and function analysis shown in this thesis. This work would confirm the exo- and endonuclease activity of TbSNM1, substrate specificity, and interactions with the zinc co-factor. With components of the trypanosomal ICL repair systems identified, it would be interesting to develop the understanding of their helicase/nuclease activities using *in vitro* enzyme activity assays carried out on purified proteins and plasmid DNA containing crosslinked DNA.

Thesis summary

1. *T. brucei* possesses at least two distinct ICL repair systems
    a. An SNM1-dependent ICL repair system where TbSNM1 co-operates with TC-NER (TbCSB) and MMR (TbEXO1) enzymes to repair the encountered damaged, possibly triggered as a result of RNA polymerase stalling
    b. An SNM1-independent ICL repair systems which utilises components of the HR (TbMRE11 and potentially also TbRAD51 and TbBRCA2), MMR (TbEXO1) and FA (TbFAN1) pathways to repair the encountered damaged, possibly triggered as a result of DNA polymerase stalling
2. TbHEL1 plays a crucial role in the *T. brucei* RNA interference machinery, potentially functioning as the RNA helicase that is absent from the *T. brucei* DICER sequence but present in the counterparts expressed by higher eukaryotes
3. TbCHL1 (a FANCJ homologue) appears to play an ancillary role in the *T. brucei* ICL REPAIRtoire and may have a regulatory function
4. The TbREV2 and TbREV3 TLS enzymes appear to play no role in ICL repair suggesting that other TLS factors may function in trypanosomal ICL repair systems
5. D40, H80, D82, and H159 residues play a key role in TbSNM1 activity, with comparative studies and *in silico* modelling suggesting they may be involved in zinc co-factor binding
6. R429 and R430, but not R428 and H431, residues play a crucial role in the localisation of the protein to the nucleus
7. Activation of benznidazole results in cytotoxic moities that promote a form of DNA damage that can be resolved using components of the HR pathway
8. The nitrogen mustard LH34 promotes formation of ICLs that are resolved using SNM1-dependent and SNM1-independent repair systems
9. The aziridinyl agent CB1954 promotes formation of ICLs that are resolved using the SNM1-dependent and SNM1-independent repair systems and additional DNA leisons that are repaired by components of the NER pathway

Appendix 1: Stocks

Plasmid	Source
pKO-TcFHM-HYG	(de Padua *et al.*, 2017)
pKO-TcFHM -NEO	(de Padua *et al.*, 2017)
pKO-TcFHM -BLA	(de Padua *et al.*, 2017)
pKO-TcFHM -PAC	(de Padua *et al.*, 2017)
pKO-TbSNM1-BLA	(Sullivan *et al.*, 2015)
pKO-TbSNM1-PAC	(Sullivan *et al.*, 2015)
pRPa-GFP-TbSNM1	(Sullivan *et al.*, 2015)

Appendix 1a: Starting plasmids used in this study.

All primers used in this study are listed and were sourced from Sigma Aldrich. All primers were resuspended in 1mL of sterile water, roughly equating to 50-100 pmol μl^{-1}.

Primer Name	Primer Sequence
Tbexo1-KO1	5'-ggg*gagctcccgcgg*ATGGGGATTAAAGGGTTATGG-3'
Tbexo1-KO2	5'-ggg*tctaga*CTCCGTTATTACCGCGTCCAC-3'
Tbexo1-KO3	5'-aaa*gggccc*GCTGACCGTGCCAGCGTGCAA-3'
Tbexo1-KO4	5'-aaa*ggtacc*CTACCGTCGCGTATAAGATAA-3'
Tbmre11-KO1	5'-ggg*gagctcccgcgg*TTCAAGTTCCTTGTGACTTC-3'
Tbmre11-KO2	5'-ggg*tctaga*TTGTTTCGTAAATGCCACACT-3'
Tbmre11-KO3	5'-aaa*gggccc*TGCGAACTGTTGAGTAAATGC-3'
Tbmre11-KO4	5'-aaa*ggtacc*CTAATAGTTATCTGGCATGCC-3'
Tbcsb-KO1	5'-ggg*gagctcccgcgg*TCACTTCTGAAGCCAATGTA-3'
Tbcsb-KO2	5'-ggg*tctaga*CACTTTAACTACGATAATGACGCTAA-3'
Tbcsb-KO3	5'-aaa*gggccc*GAGGGATCGTAAAGTGACCTT -3'
Tbcsb-KO4	5'-aaa*ggtacc*CAATTCTATAGCTAACAGCAG -3'
Tbchl1-KO1	5'-ggg*gagctcccgcgg*CATATCCGTTGCAACTCCAC-3'
Tbchl1-KO2	5'-ggg*tctaga*CAACTGTGTGTGAGTACGACT-3'
Tbchl1-KO3	5'-aaa*gggccc*GAGTACGCCTCATGGATTCGC-3'
Tbchl1-KO4	5'-aaa*ggtacc*TCACTTCCGCCGCTCGATAAA-3'
Tbhel1-KO1	5'- ggg*gagctcccgcgg*CGTCTCCCTTACTTCAGTCA-3'
Tbhel1-KO2	5'-ggg*tctaga*TATACATAGAATATGTCCCCG-3'
Tbhel1-KO3	5'-aaa*gggccc*TTATGTATCCCCTCAGCGAAA-3'
Tbhel1-KO4	5'-aaa*ggtacc*TACAGCATCACCGCCACCGAC-3'
Tbfan1-KO1	5'-aaa*gagctcccgcgg*ATGACAGGTGACGTCTGCCCT -3'
Tbfan1-KO2	5'-aaa*tctaga*GCCGAAAGATCGCCTTACCAT -3'
Tbfan1-KO3	5'-aaa*gggccc*TTTGGACCCTGAGGAGTTTCC -3'
Tbfan1-KO4	5'-aaa*ggtacc*TTATACAGGAGGGTGCGCTCC -3'
Tbrev2-KO1	5'-aaa*gagctcccgcgg*ATGCCACCGAGGAAGAGAAG-3'
Tbrev2–KO2	5'-aaa*tctaga*GTCAAATCCAACGCACGGCAA-3'
Tbrev2-KO3	5'-aaa*gggccc*TTTCAAACGAAACTACCGCCC-3'
Tbrev2-KO4	5'-aaa*ggtacc*TCACGCTTGTTGCGCTTGAAG-3'
Tbrev3-KO1	5'-aaa*gagctcccgcgg*ATGAACTTGTACGTAGTCTC-3'
Tbrev3-KO2	5'-aaa*tctaga*AGTGCCTCCATAGCAACCGAC-3'
Tbrev3-KO3	5'-aaa*gggccc*CATTGTTCCTACGCTCGACAG-3'
Tbrev3-KO4	5'-*aaaggtacc*TCAGCGAGTCGTTACGTAGTC-3'
NEO-2	5'- CTAGAAGAACTCGTCAAGAAG-3'

HYG-2	5’- CTATTCCTTTGCCCTCGGACG-3’
BLA1	5’- CTGGCTAATGTTAAAGGTTTTCAT -3’
PAC1	5’- CGGGCTTGCGGGTCATGCACCA-3’
GFP	5’- GGCATGGACGAGCTGTACAAG -3’
Tbsnm1-KO1	5’-aaa*gagctcccgcgg*GCAGGTGGAGCTGCAGGTAAG -3’
Tbsnm1-seq1	5’-CACCAGATCACCATTGCGGAG -3’
Tbsnm1-q1	5’-AGATGCTAAACAAGAAGAGTC -3’
Tbexo1-q1	5’-TCGGTGCCGGATGTCATTCGG -3’
Tbexo1-q2	5’-CAACGCACGTTTCACCGGGTC -3’
Tbmre11-q1	5’-GGGTTTGACATCATTCAGCCG -3’
Tbmre11-q2	5’-CCGGACGACAGGACGAATACT -3’
Tbcsb-q1	5’-GGTCTAGCAGCGTTAGAAGCT -3’
Tbcsb-q2	5’-CGCTACCCTCTGTCTTCACTT -3’
Tbchl1-q1	5’-TATGTACATGTGGCCGGGAGA-3’
Tbchl1-q2	5’-TTTCTGTTTCCGCGCTGTCTT-3’
Tbhel1-q1	5’-TTTGCTTGTCCGGTGGCTTCT-3’
Tbhel1-q2	5’-TTTGCTTGTCCGGTGGCTTCT-3’
Tbfan1-q1	5’-GTGCCACTTCTTGCTTCTTCC-3’
Tbfan1-q2	5’-ATTCCAACACAATATCAGCGC-3’
Tbrev2-q1	5’-TGGGCGGAAGACAGTTCCAAA-3’
Tbrev2-q2	5’-AAAGGACGCGGTGGAAGAGGA-3’
Tbrev3-q1	5’-CGTCGGCGTTACACAACAATT-3’
Tbrev3-q2	5’-CACTAGGGGGTCCTGTGATGT-3’
Tbtert-F	5’-GAGCGTGTGACTTCCGAAGG-3’
Tbtert-R	5’-AGGAACTGTCACGGAGTTTGC-3’

Appendix 1b: Primer names and sequences used in this study. Lowercase, italicised sequences correspond to integrated restriction sites.

Appendix 2: Validation of single null mutant lines

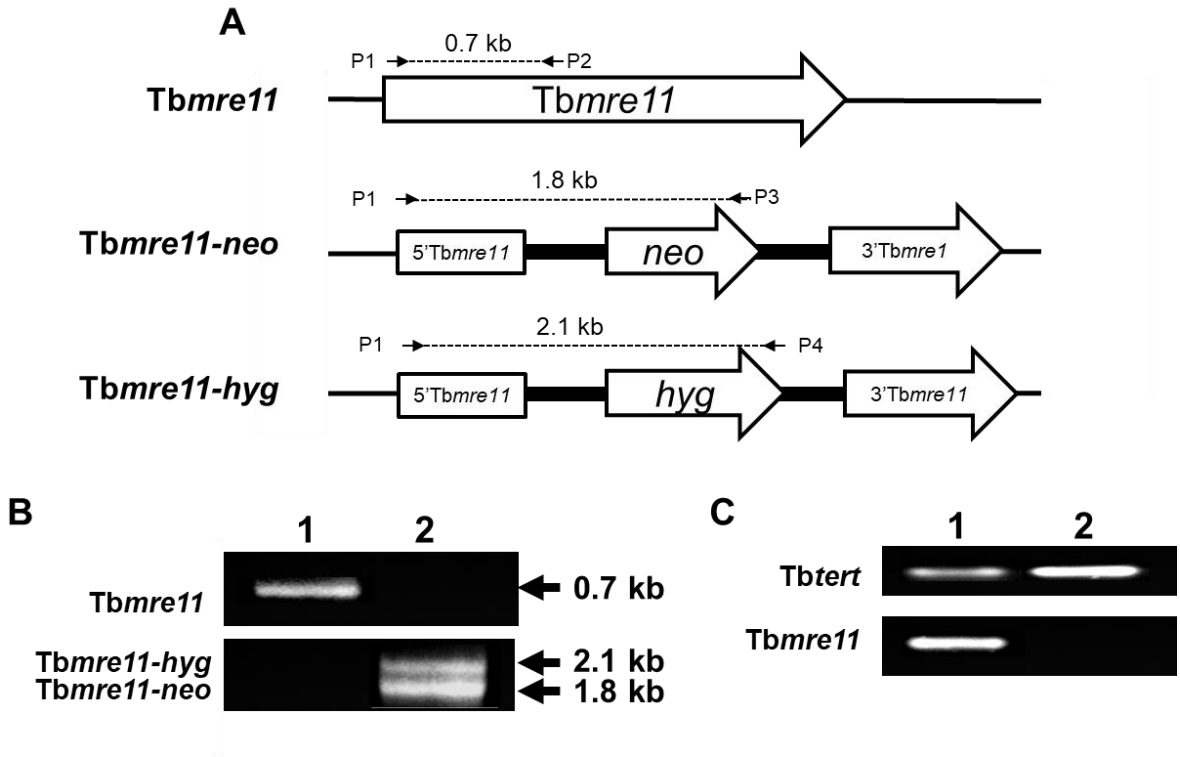

Appendix 2a: Generation of *T. brucei* line lacking TbMRE11.

A. Representation of the Tb*mre11* gene and disrupted alleles using genes encoding for neomycin (*neo*) and hygromycin (*hyg*) resistance. P1 (Tbmre11-KO1), P2 (Tbmre11-q2), P3 (neo-2) and P4 (hyg-2) correspond to the regions where the primers anneal too in the appropriate allele.

B. Amplified products after multiplex PCR on gDNA extracted from *T. brucei* wild type (lane 1) and *T. brucei* Tb*mre11*Δ (lane 2) using primer combinations that specifically amplify alleles corresponding to the Tb*mre11* (Tbmre11-KO1/Tbmre11-q2), Tb*mre11-hyg* (Tbmre11-KO1/hyg-2) or Tb*mre11-neo* (Tbmre11-KO1/neo-2) alleles.

C. Amplified products obtained after PCR on cDNA derived from RNA extracted from *T. brucei* wild type (lane 1) or *T. brucei* Tb*mre11*Δ (lane 2) using primer combinations that specifically amplify intact Tb*mre11* (Tbmre11-q1/Tbmre11-q2). In both cases, the integrity of the cDNA (and hence RNA) was evaluated by amplification of a control fragment, Tb*tert*.

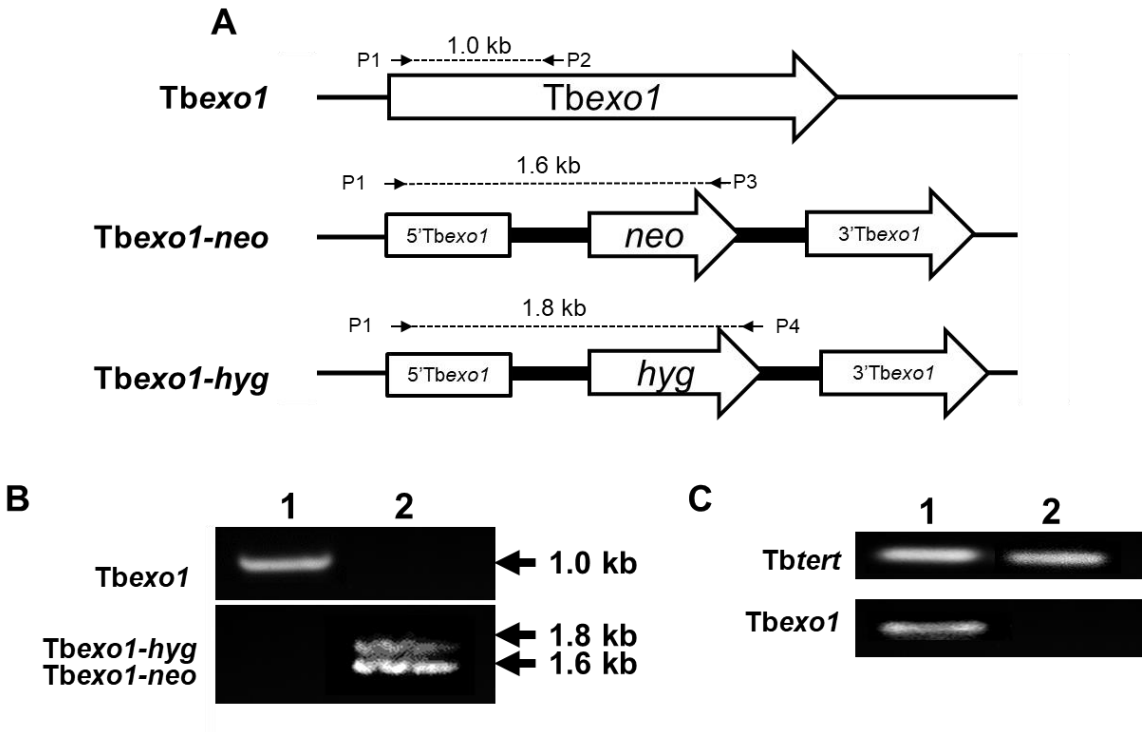

Appendix 2b: Generation of *T. brucei* line lacking TbEXO1.

A. Diagram of the Tb*exo1* gene and disrupted alleles using genes encoding for neomycin (*neo*) and hygromycin (*hyg*) resistance. P1 (Tbexo1-KO1), P2 (Tbexo1-q2), P3 (neo-2) and P4 (hyg-2) correspond to the regions where the primers anneal too in the appropriate allele.

B. DNA products created after amplification reactions carried out on gDNA extracted from *T. brucei* wild type (lane 1) and *T. brucei* Tb*exo1*Δ (lane 2) using primer combinations that specifically amplify alleles corresponding to the Tb*exo1* (Tbexo1-KO1/Tbexo1-q2), Tb*exo1-hyg* (Tbexo1-KO1/hyg-2) or Tb*exo1-neo* (Tbexo1-KO1/neo-2) alleles.

C. DNA products amplified by PCR on cDNA derived from RNA extracted from *T. brucei* wild type (lane 1) or *T. brucei* Tb*exo1*Δ (lane 2) using primer combinations that specifically amplify intact Tb*exo1* (Tbexo1-q1/Tbexo1-q2). In both cases, the integrity of the cDNA (and hence RNA) was evaluated by amplification of a control fragment, Tb*tert*.

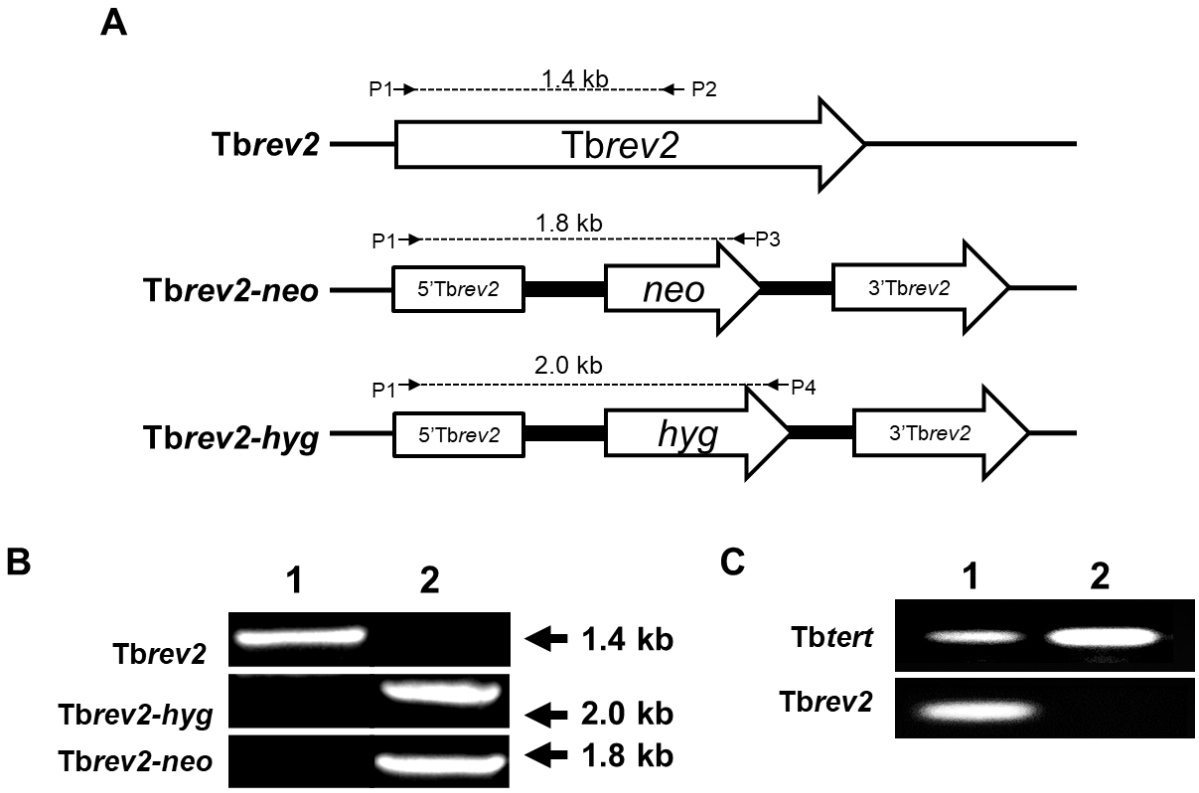

Appendix 2c: Generation of *T. brucei* line lacking TbREV2.

A. Diagram of the Tb*rev2* gene and disrupted alleles using genes encoding for neomycin (*neo*) and hygromycin (*hyg*) resistance. P1 (Tbrev2-KO1), P2 (Tbrev2-q2), P3 (neo-2) and P4 (hyg-2) correspond to the regions where the primers anneal too in the appropriate allele.

B. DNA products created after amplification reactions carried out on gDNA extracted from *T. brucei* wild type (lane 1) and *T. brucei* Tb*rev2*Δ (lane 2) using primer combinations that specifically amplify alleles corresponding to the Tb*rev2* (Tbrev2-KO1/Tbrev2-q2), Tb*rev2-hyg* (Tbrev2-KO1/hyg-2) or Tb*rev2-neo* (Tbrev2-KO1/neo-2) alleles.

C. DNA products amplified by PCR on cDNA derived from RNA extracted from *T. brucei* wild type (lane 1) or *T. brucei* Tb*rev2*Δ (lane 2) using primer combinations that specifically amplify intact Tb*rev2* (Tbrev2-q1/Tbrev2-q2). In both cases, the integrity of the cDNA (and hence RNA) was evaluated by amplification of a control fragment, Tb*tert*.

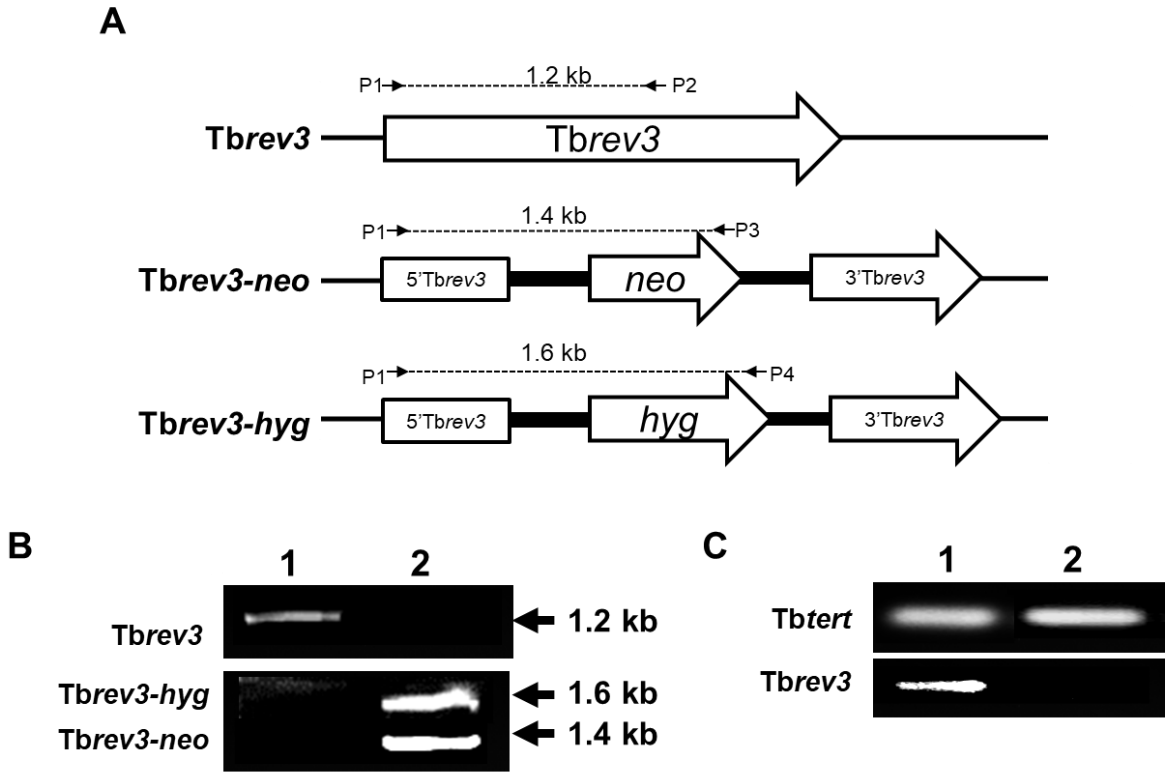

Appendix 2d: Generation of *T. brucei* line lacking TbREV3.

A. Schematic representation of the Tb*rev3* allele and the effects of gene disruption using genes encoding for neomycin (*neo*) and hygromycin (*hyg*) resistance. P1 (Tbrev3-KO1), P2 (Tbrev3-q2), P3 (neo-2) and P4 (hyg-2) correspond to the regions where the primers anneal too in the appropriate allele.

B. DNA fragments obtained after amplification on gDNA extracted from *T. brucei* wild type (lane 1) and *T. brucei* Tb*rev3*Δ (lane 2) using primer combinations that specifically amplify biomarkers corresponding to the Tb*csb* (Tbrev3-KO1/Tbrev3-q2), Tb*rev3-hyg* (Tbrev3-KO1/hyg-2) or Tb*rev3-neo* (Tbrev3-KO1/neo-2) alleles.

C. DNA fragments obtained after amplification on cDNA derived from RNA extracted from *T. brucei* wild type (lane 1) or *T. brucei* Tb*rev3*Δ (lane 2) using primer combinations that specifically amplify intact Tb*rev3* (Tbrev3-q1/Tbrev3-q2). In both cases, the integrity of the cDNA (and hence RNA) was evaluated by amplification of a control fragment, Tb*tert*.

Appendix 3: Validation of double null lines

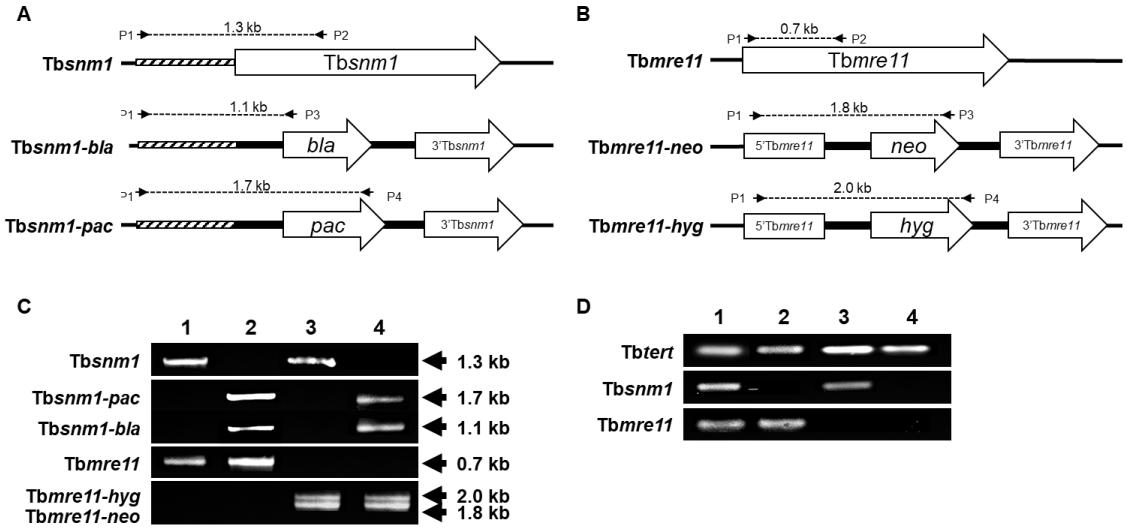

Appendix 3a: Disruption and confirmation of Tb*snm1*Δ Tb*mre11*Δ.

A. Diagram illustrating the Tb*snm1* allele and resultant changes upon disruption of this loci using genes encoding for blasticidin (*bla*) and puromycin (*pac*) resistance. P1 (Tbsnm1-KO1), P2 (Tbsnm1-seq1), P3 (bla-1) and P4 (pac-1) correspond to regions where the primers anneal at the specific allele.

B. Schematic for the representation of the Tb*mre11* allele and effects of disrupting this allele with genes encoding for neomycin (*neo*) and hygromycin (*hyg*) resistance. P1 (Tbmre11-KO1), P2 (Tbmre11-q2), P3 (neo-2) and P4 (hyg-2) correspond to regions where the primers anneal at the specific allele. C. DNA fragments obtained after amplification on gDNA extracted from *T. brucei* wild type (lane 1), *T. brucei* Tb*snm1*Δ (lane 2), *T. brucei* Tb*mre11*Δ (lane 3), and *T. brucei* Tb*snm1*Δ Tb*mre11*Δ (lane 4). Extractions from all 4 lines were tested using primer combinations that specifically amplify biomarkers corresponding to the Tb*snm1* (Tbsnm1-KO1/Tbsnm1-seq1), Tb*snm1-bla* (Tbsnm1-KO1/bla-1) or Tb*snm1-pac* (Tbsnm1-KO1/pac-1), Tb*mre11* (Tbmre11-KO1/Tbmre11-q2), Tb*mre11-hyg* (Tbmre11-KO1/hyg-2) or Tb*mre11-neo* (Tbmre11-KO1/neo-2) alleles.

D. DNA fragments obtained after amplification on cDNA derived from RNA extracted from *T. brucei* wild type (lane 1), Tb*snm1*Δ (lane 2), Tb*mre11*Δ (lane 3) and Tb*snm1*Δ Tb*mre11*Δ (lane 4) using primer combinations that specifically amplify intact Tb*snm1* (Tbsnm1-q1/Tbsnm1-seq1), Tb*mre11* (Tbmre11-q1/Tbmre11-q2) and Tb*tert* (Tbtert-F/Tbtert-R).

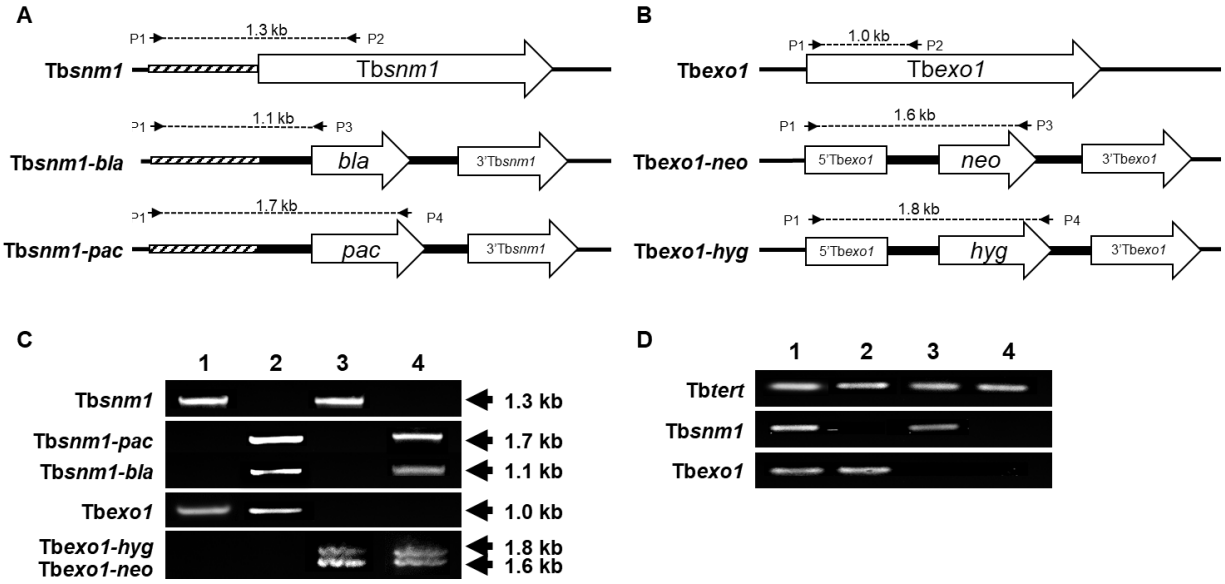

Appendix 3b: Disruption and confirmation of Tb*snm1*Δ Tb*exo1*Δ null line.

A. Diagram illustrating the Tb*snm1* allele and resultant changes upon disruption of this loci using genes encoding for blasticidin (*bla*) and puromycin (*pac*) resistance. P1 (Tbsnm1-KO1), P2 (Tbsnm1-seq1), P3 (bla-1) and P4 (pac-1) correspond to regions where the primers anneal at the specific allele.

B. Schematic for the representation of the Tb*exo1* allele and effects of disrupting this allele with genes encoding for neomycin (*neo*) and hygromycin (*hyg*) resistance. P1 (Tbexo1-KO1), P2 (Tbexo1-q2), P3 (neo-2) and P4 (hyg-2) correspond to regions where the primers anneal at the specific allele.

C. DNA fragments obtained after amplification on gDNA extracted from *T. brucei* wild type (lane 1), *T. brucei* Tb*snm1*Δ (lane 2), *T. brucei* Tb*exo1*Δ (lane 3), and *T. brucei* Tb*snm1*Δ Tbexo1Δ (lane 4). Extractions from all 4 lines were tested using primer combinations that specifically amplify biomarkers corresponding to the Tb*snm1* (Tbsnm1-KO1/Tbsnm1-seq1), Tb*snm1-bla* (Tbsnm1-KO1/bla-1) or Tb*snm1-pac* (Tbsnm1-KO1/pac-1), Tb*exo1* (Tbexo1-KO1/Tbexo1-q2), Tb*exo1-hyg* (Tbexo1-KO1/hyg-2) or Tb*exo1-neo* (Tbexo1-KO1/neo-2) alleles.

D. DNA fragments obtained after amplification on cDNA derived from RNA extracted from *T. brucei* wild type (lane 1), Tb*snm1*Δ (lane 2), Tb*exo1*Δ (lane 3) and Tb*snm1*Δ Tb*exo1*Δ (lane 4) using primer combinations that specifically amplify intact Tb*snm1* (Tbsnm1-q1/Tbsnm1-seq1), Tb*exo1* (Tbexo1-q1/Tbexo1-q2) and Tb*tert* (Tbtert-F/Tbtert-R).

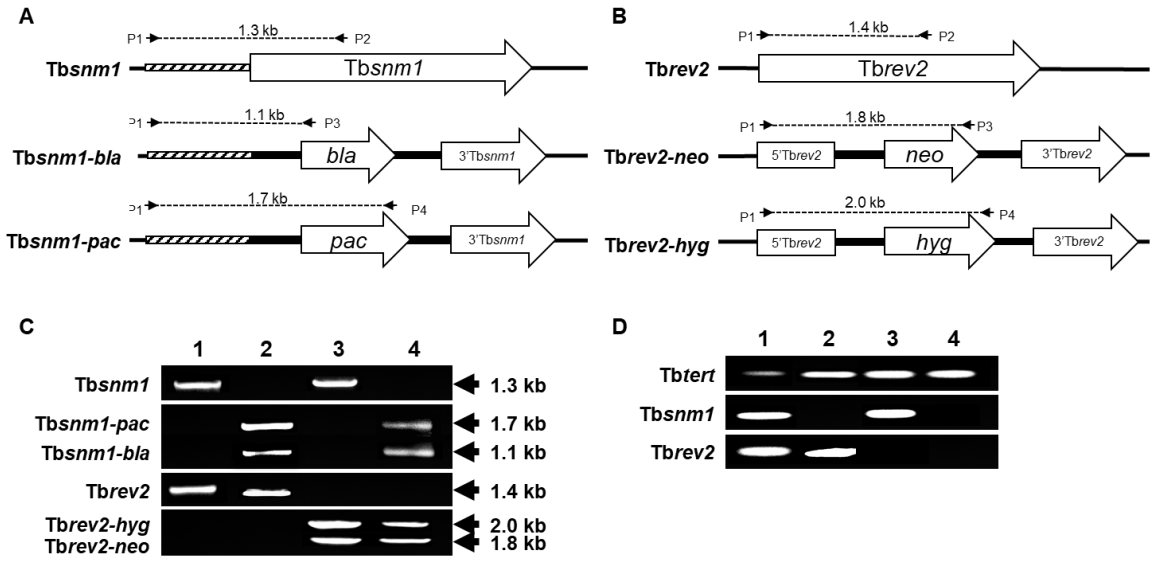

Appendix 3c: Disruption and confirmation of Tb*snm1*Δ Tb*rev2*Δ.

A. Diagram illustrating the Tb*snm1* allele and resultant changes upon disruption of this loci using genes encoding for blasticidin (*bla*) and puromycin (*pac*) resistance. P1 (Tbsnm1-KO1), P2 (Tbsnm1-seq1), P3 (bla-1) and P4 (pac-1) correspond to regions where the primers anneal at the specific allele.

B. Schematic for the representation of the Tb*rev2* allele and effects of disrupting this allele with genes encoding for neomycin (*neo*) and hygromycin (*hyg*) resistance. P1 (Tbrev2-KO1), P2 (Tbrev2-q2), P3 (neo-2) and P4 (hyg-2) correspond to regions where the primers anneal at the specific allele.

C. DNA fragments obtained after amplification on gDNA extracted from *T. brucei* wild type (lane 1), *T. brucei* Tb*snm1*Δ (lane 2), *T. brucei* Tb*rev2*Δ (lane 3), and *T. brucei* Tb*snm1*Δ Tb*rev2*Δ (lane 4). Extractions from all 4 lines were tested using primer combinations that specifically amplify biomarkers corresponding to the Tb*snm1* (Tbsnm1-KO1/Tbsnm1-seq1), Tb*snm1-bla* (Tbsnm1-KO1/bla-1) or Tb*snm1-pac* (Tbsnm1-KO1/pac-1), Tb*rev2* (Tbrev2-KO1/Tbrev2-q2), Tb*rev2-hyg* (Tbrev2-KO1/hyg-2) or Tb*rev2-neo* (Tbrev2-KO1/neo-2) alleles.

D. DNA fragments obtained after amplification on cDNA derived from RNA extracted from *T. brucei* wild type (lane 1), Tb*snm1*Δ (lane 2), Tb*rev2*Δ (lane 3) and Tb*snm1*Δ Tb*rev2*Δ (lane 4) using primer combinations that specifically amplify intact Tb*snm1* (Tbsnm1-q1/Tbsnm1-seq1), Tb*rev2* (Tbrev2-q1/Tbrev2-q2) and Tb*tert* (Tbtert-F/Tbtert-R).

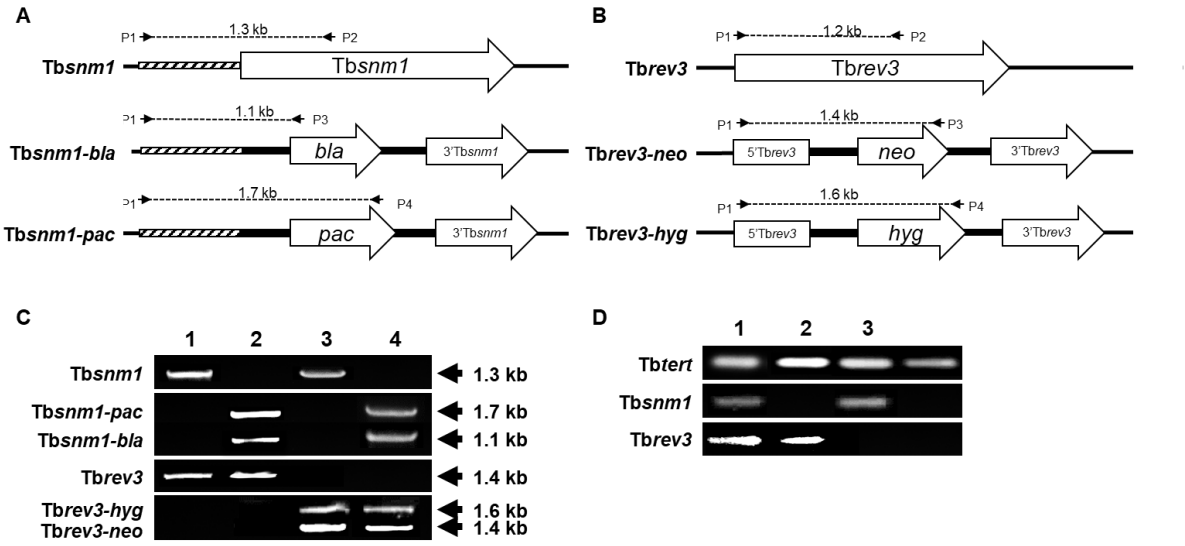

Appendix 3d: Disruption and confirmation of Tb*snm1*Δ Tb*rev3*Δ.

A. Diagram illustrating the Tb*snm1* allele and resultant changes upon disruption of this loci using genes encoding for blasticidin (*bla*) and puromycin (*pac*) resistance. P1 (Tbsnm1-KO1), P2 (Tbsnm1-seq1), P3 (bla-1) and P4 (pac-1) correspond to regions where the primers anneal at the specific allele.

B. Schematic for the representation of the Tb*rev3* allele and effects of disrupting this allele with genes encoding for neomycin (*neo*) and hygromycin (*hyg*) resistance. P1 (Tbrev3-KO1), P2 (Tbrev3-q2), P3 (neo-2) and P4 (hyg-2) correspond to regions where the primers anneal at the specific allele.

C. DNA fragments obtained after amplification on gDNA extracted from *T. brucei* wild type (lane 1), *T. brucei* Tb*snm1*Δ (lane 2), *T. brucei* Tb*rev3*Δ (lane 3), and *T. brucei* Tb*snm1*Δ Tb*rev3*Δ (lane 4). Extractions from all 4 lines were tested using primer combinations that specifically amplify biomarkers corresponding to the Tb*snm1* (Tbsnm1-KO1/Tbsnm1-seq1), Tb*snm1-bla* (Tbsnm1-KO1/bla-1) or Tb*snm1-pac* (Tbsnm1-KO1/pac-1), Tb*rev3* (Tbrev3-KO1/Tbrev3-q2), Tb*rev3-hyg* (Tbrev3-KO1/hyg-2) or Tb*rev3-neo* (Tbrev3-KO1/neo-2) alleles.

D. DNA fragments obtained after amplification on cDNA derived from RNA extracted from *T. brucei* wild type (lane 1), Tb*snm1*Δ (lane 2), Tb*rev3*Δ (lane 3) and Tb*snm1*Δ Tb*rev3*Δ (lane 4) using primer combinations that specifically amplify intact Tb*snm1* (Tbsnm1-q1/Tbsnm1-seq1), Tb*rev3* (Tbrev3-q1/Tbrev3-q2) and Tb*tert* (Tbtert-F/Tbtert-R).

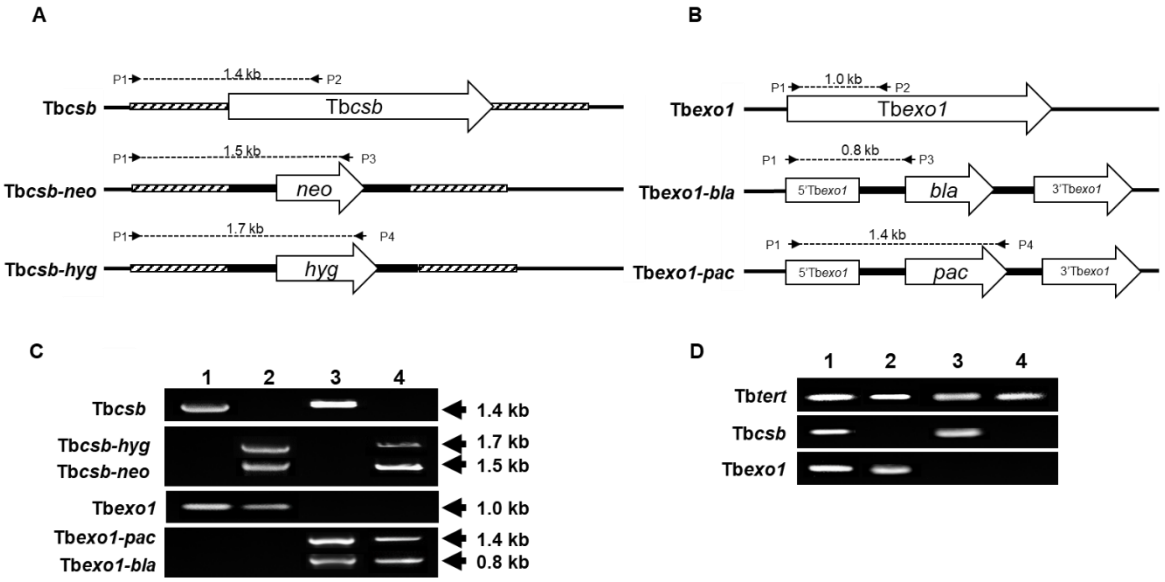

Appendix 3e: Disruption and confirmation of Tb*csb*Δ Tb*exo1*Δ.

A. Schematic for the representation of the Tb*csb* allele and effects of disrupting this allele with genes encoding for neomycin (*neo*) and hygromycin (*hyg*) resistance. P1 (Tbcsb-KO1), P2 (Tbcsb-q2), P3 (neo-2) and P4 (hyg-2) correspond to regions where the primers anneal at the specific allele.

B. Schematic for the representation of the Tb*exo1* allele and effects of disrupting this allele with genes encoding for blastidicin (*bla*) and puromycin (*pac*) resistance. P1 (Tbexo1-KO1), P2 (Tbexo1-q2), P3 (bla-1) and P4 (pac-1) correspond to regions where the primers anneal at the specific allele.

C. DNA fragments obtained after amplification on gDNA extracted from *T. brucei* wild type (lane 1), *T. brucei* Tb*csb*Δ (lane 2), *T. brucei* Tb*exo1*Δ (lane 3), and *T. brucei* Tb*csb*Δ Tb*exo1*Δ (lane 4). Extractions from all 4 lines were tested using primer combinations that specifically amplify biomarkers corresponding to Tb*csb* (Tbcsb-KO1/Tbcsb-q2), Tb*csb-hyg* (Tbcsb-KO1/hyg-2) or Tb*csb-neo* (Tbcsb-KO1/neo-2), Tb*exo1* (Tbexo1-KO1/Tbexo1-q2), Tb*exo1-pac* (Tbexo1-KO1/pac-1) or Tb*exo1-bla* (Tbexo1-KO1/bla-1) alleles.

D. DNA fragments obtained after amplification on cDNA derived from RNA extracted from *T. brucei* wild type (lane 1), Tb*csb*Δ (lane 2), Tb*exo1*Δ (lane 3) and Tb*csb*Δ Tb*exo1*Δ (lane 4) using primer combinations that specifically amplify intact Tb*csb* (Tbcsb-q1/Tbcsb-q2), Tb*exo1* (Tbexo1-q1/Tbexo1-q2) and Tb*tert* (Tbtert-F/Tbtert-R).

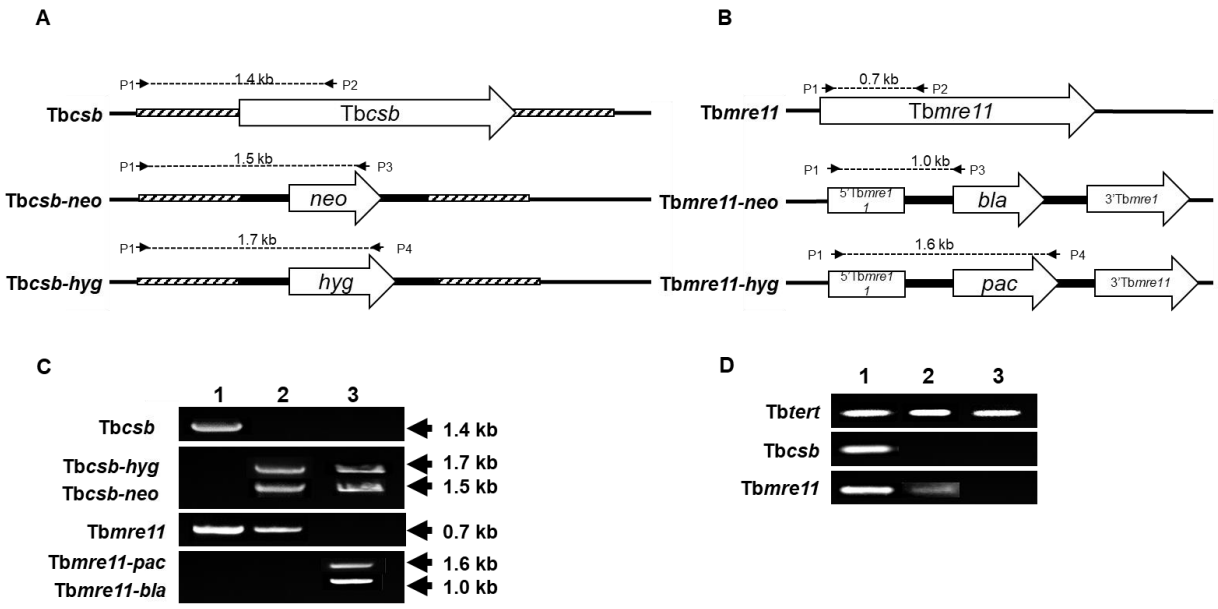

Appendix 3f: Disruption and confirmation of Tb*csb*Δ Tb*mre11*Δ.

A. Schematic for the representation of the Tb*csb* allele and effects of disrupting this allele with genes encoding for neomycin (*neo*) and hygromycin (*hyg*) resistance. P1 (Tbcsb-KO1), P2 (Tbcsb-q2), P3 (neo-2) and P4 (hyg-2) correspond to regions where the primers anneal at the specific allele.

B. Schematic for the representation of the Tb*mre11* allele and effects of disrupting this allele with genes encoding for blasticidin (*bla*) and puromycin (*pac*) resistance. P1 (Tbmre11-KO1), P2 (Tbmre11-q2), P3 (bla-1) and P4 (pac-1) correspond to regions where the primers anneal at the specific allele.

C. DNA fragments obtained after amplification on gDNA extracted from *T. brucei* wild type (lane 1), *T. brucei* Tb*csb*Δ (lane 2) and *T. brucei* Tb*csb*Δ Tb*mre11*Δ (lane 3). Extractions from all 3 lines were tested using primer combinations that specifically amplify biomarkers corresponding to Tb*csb* (Tbcsb-KO1/Tbcsb-q2), Tb*csb-hyg* (Tbcsb-KO1/hyg-2) or Tb*csb-neo* (Tbcsb-KO1/neo-2), Tb*mre11* (Tbmre11-KO1/Tbmre11-q2), Tb*mre11-pac* (Tbmre11-KO1/pac-1) or Tb*mre11-bla* (Tbmre11-KO1/bla-1) alleles.

D. DNA fragments obtained after amplification on cDNA derived from RNA extracted from *T. brucei* wild type (lane 1), Tb*csb*Δ (lane 2) and Tb*csb*Δ Tb*mre11*Δ (lane 3) using primer combinations that specifically amplify intact Tb*csb* (Tbcsb-q1/Tbcsb-q2), Tb*mre11* (Tbmre11-q1/Tbmre11-q2) and Tb*tert* (Tbtert-F/Tbtert-R).

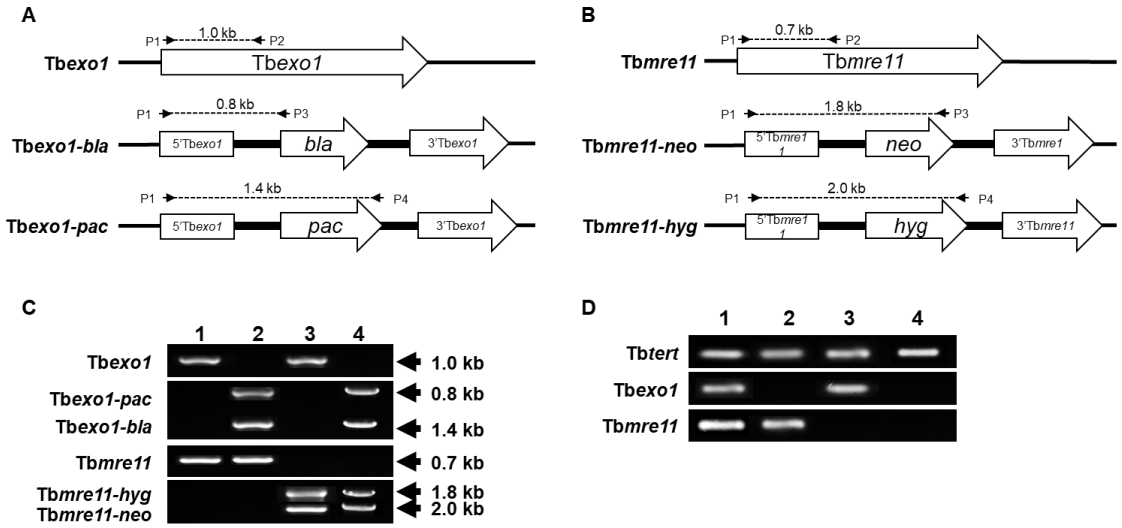

Appendix 3g: Disruption and confirmation of Tb*exo1*Δ Tb*mre11*Δ.

A. Schematic for the representation of the Tb*exo1* allele and effects of disrupting this allele with genes encoding for blastidicin (*bla*) and puromycin (*pac*) resistance. P1 (Tbexo1-KO1), P2 (Tbexo1-q2), P3 (bla-1) and P4 (pac-1) correspond to regions where the primers anneal at the specific allele.

B. Schematic for the representation of the Tb*mre11* allele and effects of disrupting this allele with genes encoding for neomycin (*neo*) and hygromycin (*hyg*) resistance. P1 (Tbmre11-KO1), P2 (Tbmre11-q2), P3 (neo-2) and P4 (hyg-2) correspond to regions where the primers anneal at the specific allele.

C. DNA fragments obtained after amplification on gDNA extracted from *T. brucei* wild type (lane 1), *T. brucei* Tb*exo1*Δ (lane 2), *T. brucei* Tb*mre11*Δ (lane 3) and *T. brucei* Tb*exo1*Δ Tb*mre11*Δ (lane 4). Extractions from all 4 lines were tested using primer combinations that specifically amplify biomarkers corresponding to Tb*exo1* (Tbexo1-KO1/Tbexo1-q2), Tb*exo1-pac* (Tbexo1-KO1/pac-1) or Tb*exo1-bla* (Tbexo1-KO1/bla-1), Tb*mre11* (Tbmre11-KO1/Tbmre11-q2), Tb*mre11-hyg* (Tbmre11-KO1/hyg-2) or Tb*mre11-neo* (Tbmre11-KO1/neo-2) alleles.

D. DNA fragments obtained after amplification on cDNA derived from RNA extracted from *T. brucei* wild type (lane 1), *T. brucei* Tb*exo1*Δ (lane 2), *T. brucei* Tb*mre11*Δ (lane 3) and *T. brucei* Tb*exo1*Δ Tb*mre11*Δ (lane 4) using primer combinations that specifically amplify intact Tb*exo1* (Tbexo1-q1/Tbexo1-q2), Tb*mre11* (Tbmre11-q1/Tbmre11-q2) and Tb*tert* (Tbtert-F/Tbtert-R).

Appendix 4: Validation of lines lacking a trypanosomal FA factor

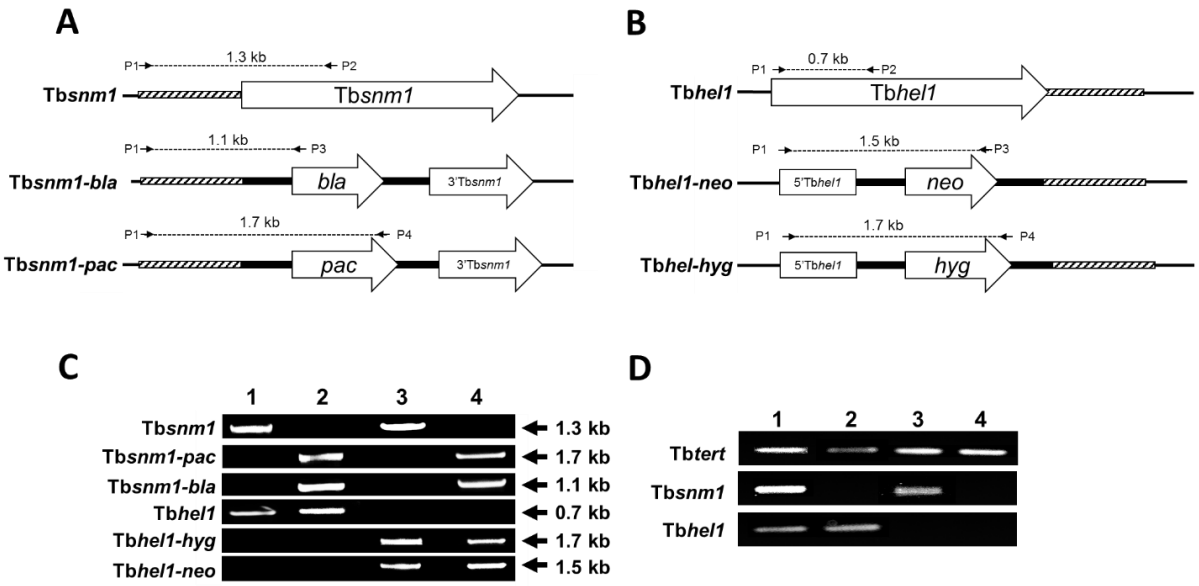

Appendix 4a: Disruption and confirmation of Tb*hel1*Δ and Tb*snm1*Δ Tb*hel1*Δ null line.
A. Diagram illustrating the Tb*snm1* allele and resultant changes upon disruption of this loci using genes encoding for blasticidin (bla) and puromycin (pac) resistance. P1 (Tbsnm1-KO1), P2 (Tbsnm1-seq1), P3 (bla-1) and P4 (pac-1) correspond to regions where the primers anneal at the specific allele.
B. Schematic for the representation of the Tb*hel1* allele and effects of disrupting this allele with genes encoding for neomycin (neo) and hygromycin (hyg) resistance. P1 (Tbhel1-KO1), P2 (Tbhel1-q2), P3 (neo-2) and P4 (hyg-2) correspond to regions where the primers anneal at the specific allele.
C. DNA fragments obtained after amplification on gDNA extracted from *T. brucei* wild type (lane 1), *T. brucei* Tb*snm1*Δ (lane 2), *T. brucei* Tb*hel1*Δ (lane 3), and *T. brucei* Tb*snm1*Δ Tb*hel1*Δ (lane 4). Extractions from all 4 lines were tested using primer combinations that specifically amplify biomarkers corresponding to the Tb*snm1* (Tbsnm1-KO1/Tbsnm1-seq1), Tb*snm1-bla* (Tbsnm1-KO1/bla-1) or Tb*snm1-pac* (Tbsnm1-KO1/pac-1), Tb*hel1* (Tbhel1-KO1/Tbhel1-q2), Tb*hel1-hyg* (Tbhel1-KO1/hyg-2) or Tb*hel1-neo* (Tbhel1-KO1/neo-2) alleles.
D. DNA fragments obtained after amplification on cDNA derived from RNA extracted from *T. brucei* wild type (lane 1), Tb*snm1*Δ (lane 2), Tb*hel1*Δ (lane 3) and Tb*snm1*Δ Tb*hel1*Δ (lane 4) using primer combinations that specifically amplify intact Tb*snm1* (Tbsnm1-q1/Tbsnm1-seq1), Tb*hel1* (Tbhel1-q1/Tbhel1-q2) and Tb*tert* (Tbtert-F/Tbtert-R).

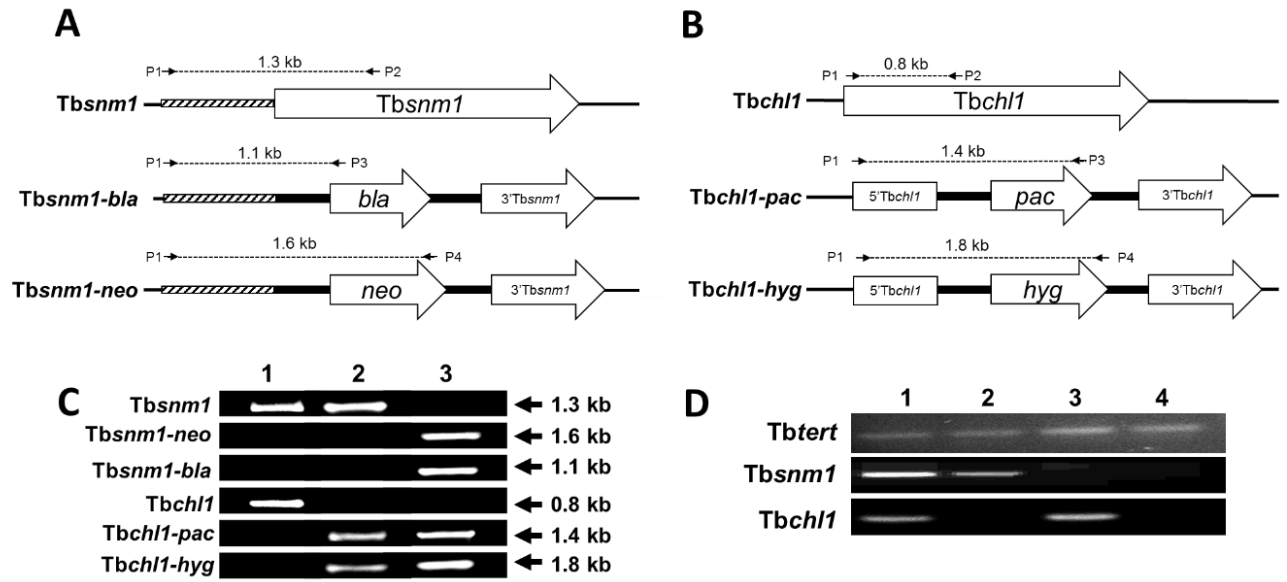

Appendix 4b: Disruption and confirmation of Tb*chl1*-deficient null lines.

A. Diagram illustrating the Tb*snm1* allele and resultant changes upon disruption of this loci using genes encoding for blasticidin (*bla*) and neomycin (*neo*) resistance. P1 (Tbsnm1-KO1), P2 (Tbsnm1-seq1), P3 (bla-1) and P4 (neo-2) correspond to regions where the primers anneal at the specific allele.

B. Schematic for the representation of the Tb*chl1* allele and effects of disrupting this allele with genes encoding for puromycin (*pac*) and hygromycin (*hyg*) resistance. P1 (Tbchl1-KO1), P2 (Tbchl1-q2), P3 (pac-1) and P4 (hyg-2) correspond to regions where the primers anneal at the specific allele.

C. DNA fragments obtained after amplification on gDNA extracted from *T. brucei* wild type (lane 1), *T. brucei* Tb*chl1*Δ (lane 2) and *T. brucei* Tb*snm1*Δ Tb*chl1*Δ (lane 3). Extractions from all 4 lines were tested using primer combinations that specifically amplify biomarkers corresponding to the Tb*snm1* (Tbsnm1-KO1/Tbsnm1-seq1), Tb*snm1-bla* (Tbsnm1-KO1/bla-1) or Tb*snm1-neo* (Tbsnm1-KO1/neo-2), Tb*chl1* (Tbchl1-KO1/Tbchl1-q2), Tb*chl1-hyg* (Tbchl1-KO1/hyg-2) or Tb*chl1-pac* (Tbchl1-KO1/pac-1) alleles.

D. DNA fragments obtained after amplification on cDNA derived from RNA extracted from *T. brucei* wild type (lane 1), Tb*snm1*Δ (lane 2), Tb*chl1*Δ (lane 3) and Tb*snml1*Δ Tb*chl1*Δ (lane 4) using primer combinations that specifically amplify intact Tb*snm1* (Tbsnm1-q1/Tbsnm1-seq1), Tb*chl1* (Tbchl1-q1/Tbchl1-q2) and Tb*tert* (Tbtert-F/Tbtert-R).

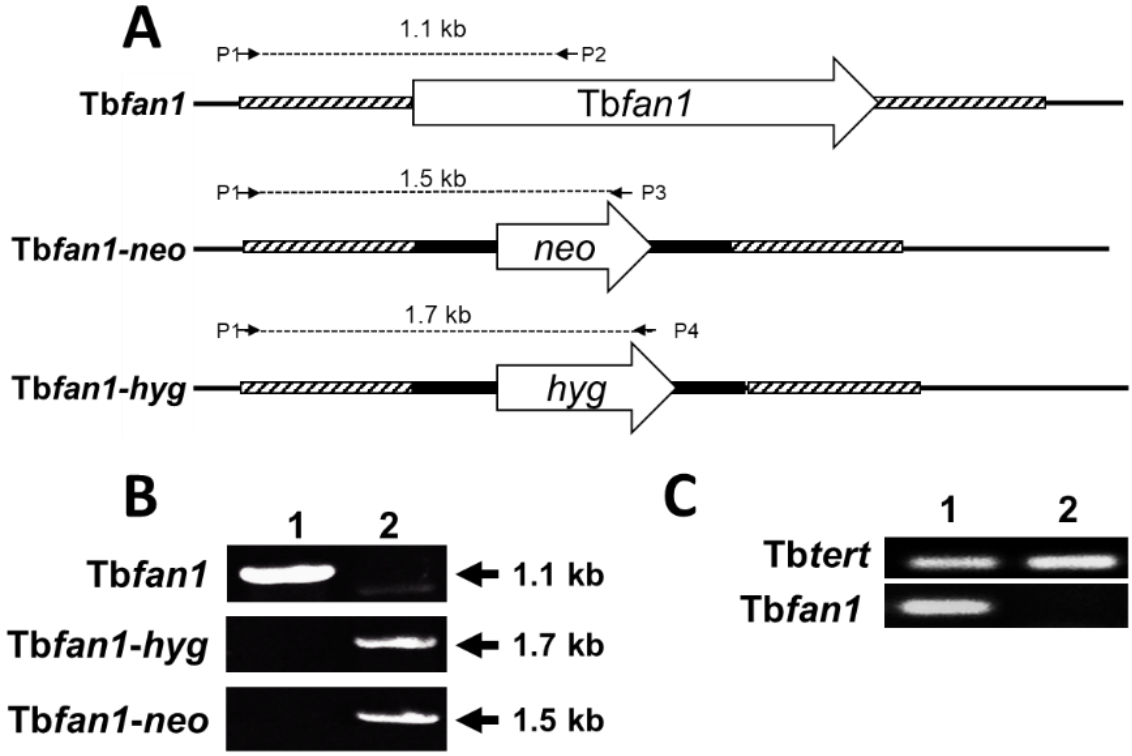

Appendix 4c: Confirmation of Tb*fan1* null line.

A. Schematic representation of the Tb*fan1* allele and the effects of gene disruption using genes encoding for neomycin (*neo*) and hygromycin (*hyg*) resistance. P1 (Tbfan1-KO1), P2 (Tbfan1-q2), P3 (neo-2) and P4 (hyg-2) correspond to the regions where the primers anneal too in the appropriate allele.

B. DNA fragments obtained after amplification on gDNA extracted from *T. brucei* wild type (lane 1) and *T. brucei* Tb*fan1*Δ (lane 2) using primer combinations that specifically amplify biomarkers corresponding to the Tb*fan1* (Tbfan1-KO1/Tbfan1-q2), Tb*fan1-hyg* (Tbfan1-KO1/hyg-2) or Tb*fan1-neo* (Tbfan1-KO1/neo-2) alleles.

C. DNA fragments obtained after amplification on cDNA derived from RNA extracted from *T. brucei* wild type (lane 1) or *T. brucei* Tb*fan1*Δ (lane 2) using primer combinations that specifically amplify intact Tb*fan1* (Tbfan1-q1/Tbfan1-q2). In both cases, the integrity of the cDNA (and hence RNA) was evaluated by amplification of a control fragment, Tb*tert*.

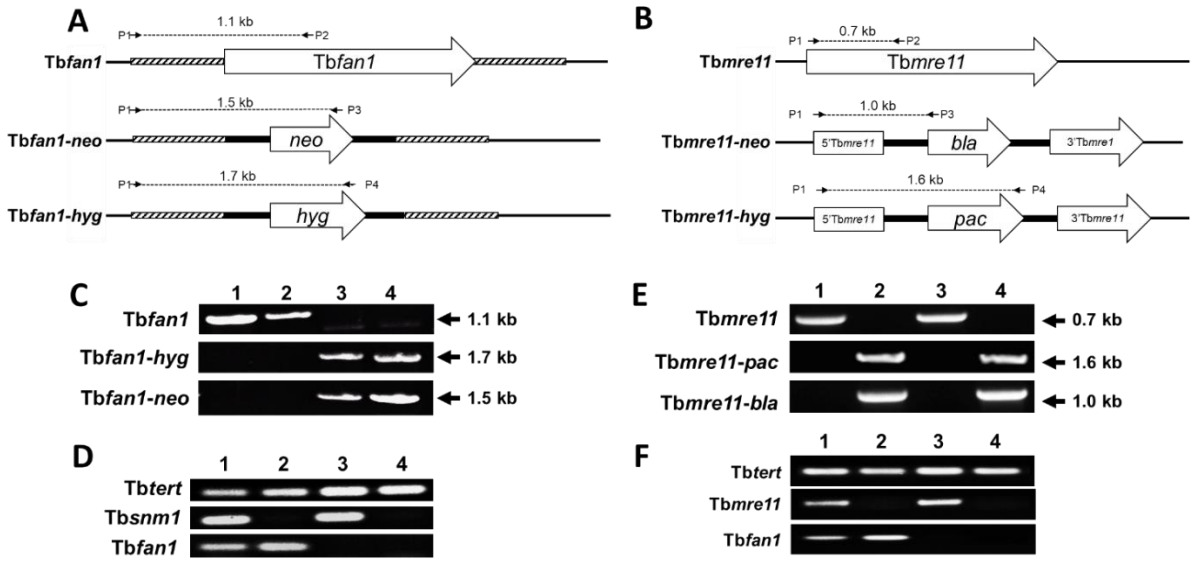

Figure 4d: Validating Tb*fan1* double null lines.

A. Diagram illustrating the Tb*fan1* allele and resultant changes upon disruption of this loci using genes encoding for neomycin (*neo*) and hygromycin (*hyg*) resistance. P1 (Tbfan1-KO1), P2 (Tbfan1-q2), P3 (neo-2) and P4 (hyg-2) correspond to regions where the primers anneal at the specific allele.

B. Schematic for the representation of the Tbmre11 allele and effects of disrupting this allele with genes encoding for blasticidin (bla) and puromycin (pac) resistance. P1 (Tbmre11-KO1), P2 (Tbmre11-q2), P3 (bla-1) and P4 (pac-1) correspond to regions where the primers anneal at the specific allele.

C. DNA fragments obtained after amplification on gDNA extracted from *T. brucei* wild type (lane 1), *T. brucei* Tb*snm1*Δ (lane 2), *T. brucei* Tb*fan1*Δ (lane 3), and *T. brucei* Tb*snm1*Δ Tb*fan1*Δ (lane 4). Extractions from all 4 lines were tested using primer combinations that specifically amplify biomarkers corresponding to Tb*fan1* (Tbfan1-KO1/Tbfan1-q2), Tb*fan1-hyg* (Tbfan1-KO1/hyg-2) or Tb*fan1-neo* (Tbfan1-KO1/neo-2) alleles.

D. DNA fragments obtained after amplification on cDNA derived from RNA extracted from *T. brucei* wild type (lane 1), Tb*snm1*Δ (lane 2), Tb*fan1*Δ (lane 3) and Tb*snm1*Δ Tb*fan1*Δ (lane 4) using primer combinations that specifically amplify intact Tb*snm1* (Tbsnm1-q1/Tbsnm1-seq1), Tb*fan1* (Tbfan1-q1/Tbfan1-q2) and Tb*tert* (Tbtert-F/Tbtert-R).

E. DNA fragments obtained after amplification on gDNA extracted from *T. brucei* wild type (lane 1), Tb*mre11*Δ (lane 2), Tb*fan1*Δ (lane 3) and Tb*mre11*Δ Tb*fan1*Δ (lane 4). Extractions from all 4 lines were tested using primer combinations that specifically amplify biomarkers corresponding to intact Tb*mre11* (Tbmre11-KO1/Tbmre11-q2), Tb*mre11-pac* (Tbmre11-KO1/pac-1) or Tb*mre11-bla* (Tbmre11-KO1/bla-1) alleles.

F. DNA fragments obtained after amplification on cDNA derived from RNA extracted from *T. brucei* wild type (lane 1), Tb*mre11*Δ (lane 2), Tb*fan1*Δ (lane 3) and Tb*mre11*Δ Tb*fan1*Δ (lane 4) using primer combinations that specifically amplify intact Tb*fan1* (Tbfan1-q1/Tbfan1-q2), Tb*mre11* (Tbmre11-q1/Tbmre11-q2) and Tb*tert* (Tbtert-F/Tbtert-R).

Appendix 5: Structure and function studies on TbSNM1

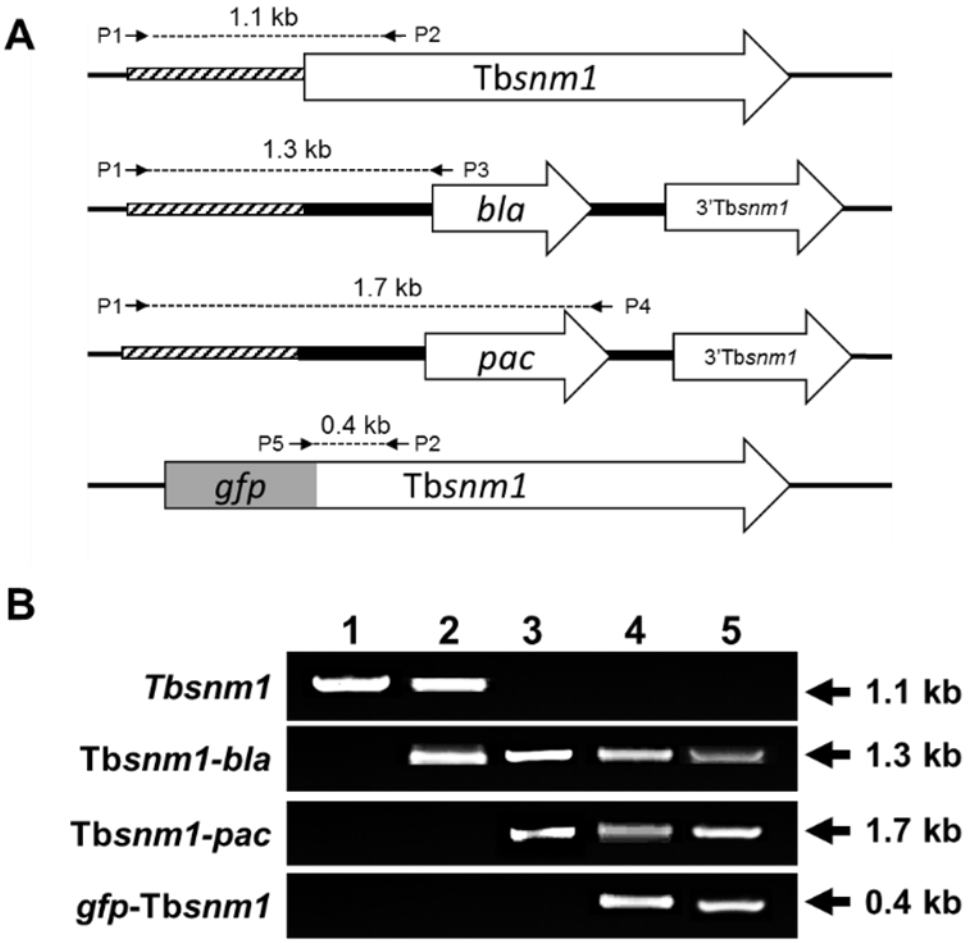

Appendix 4.1: Validating the Tb*snm1*Δ *gfp*-Tb*snm1*-V518A line.
A. Diagram representing the Tb*snm1* allele and resultant changes upon disruption of this loci using genes encoding for blasticidin (*bla*) and puromycin (*pac*) resistance. Alongside this, changes to the landing pad locus after integration of *gfp*-Tb*snm1* was also analysed. P1 (Tbsnm1-KO1), P2 (Tbsnm1-seq1), P3 (bla-1), P4 (pac-1) and P5 (GFP) correspond to regions where the primers anneal at the specific allele.
B. DNA fragments obtained from amplification reactions on genomic DNA extracted from *T. brucei* wild type (lane 1), Tb*snm1*$^{+/-}$ (lane 2), Tb*snm1*Δ (lane 3), Tb*snm1*Δ *gfp*-Tb*snm1* (lane 4), TbSNM1-V518A (lane 5) cells. Primer combinations amplified intact Tb*snm1* (Tbsnm1-KO1/Tbsnm1-seq1), Tb*snm1-bla* (Tbsnm1-KO1/bla-1), Tb*snm1-pac* (Tbsnm1-KO1/pac-1), or *gfp*-Tb*snm1* (GFP/Tbsnm1-seq1) alleles.

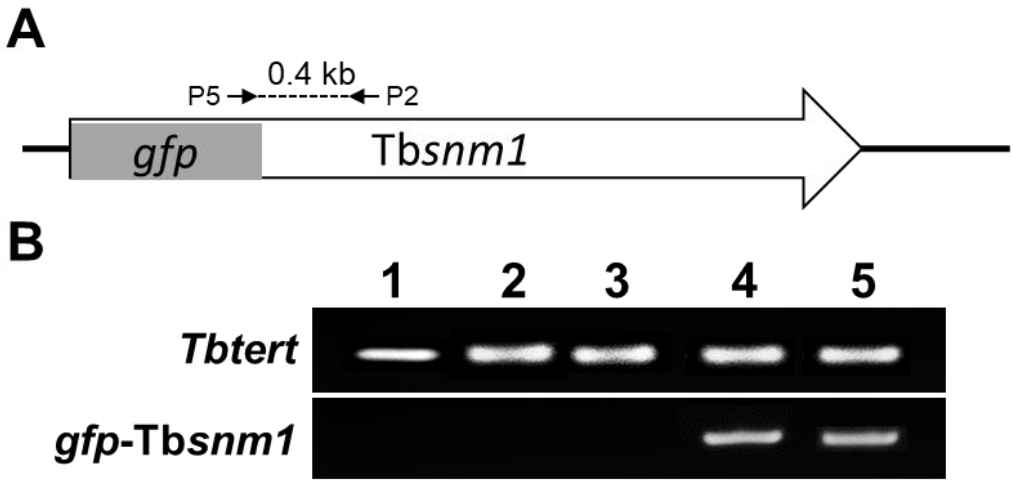

Appendix 4.2: Confirming expression of *gfp*-Tb*snm1*.
A. Schematic of integrated *gfp*-Tb*snm1* analysing using primer combination P2 (Tbsnm1-seq1) and P5 (GFP) which amplified a band of 0.4kb across the GFP and TbSNM1 fusion.
B. DNA fragments obtained after amplification on cDNA derived from RNA extracted from *T. brucei* wild type (lane 1), Tb*snm1*$^{+/-}$ (lane 2), Tb*snm1*Δ (lane 3), Tb*snm1*Δ *gfp*-Tb*snm1* (lane 4), TbSNM1-V518A (lane 5) cells using primer combinations that specifically amplify *gfp*-Tb*snm1* (GFP/Tbsnm1-seq1) and Tb*tert* (Tbtert-F/Tbtert-R).

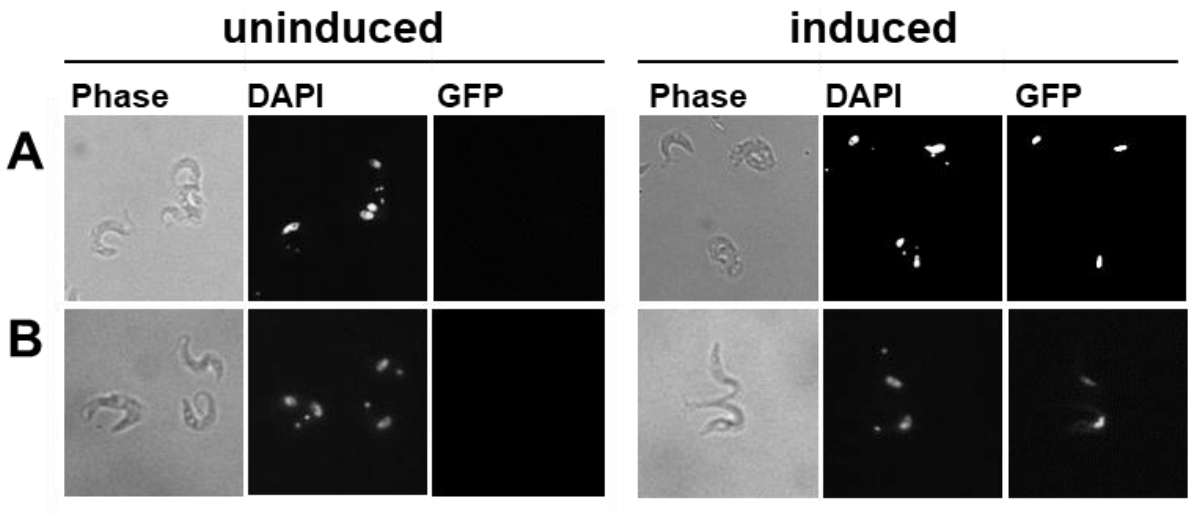

Appendix 4.3: Localisation of mutant GFP-TbSNM1 in bloodstream form *T. brucei*. Parasites expressing GFP-TbSNM1 (mutant or wild type) were stained with DAPI and examined by epifluorescent microscopy under a x40 objective lens with phase, DAPI and GFP signal images shown: Tb*snm1*Δ *gfp*-Tb*snm1* (A) and TbSNM1-V518A (B).

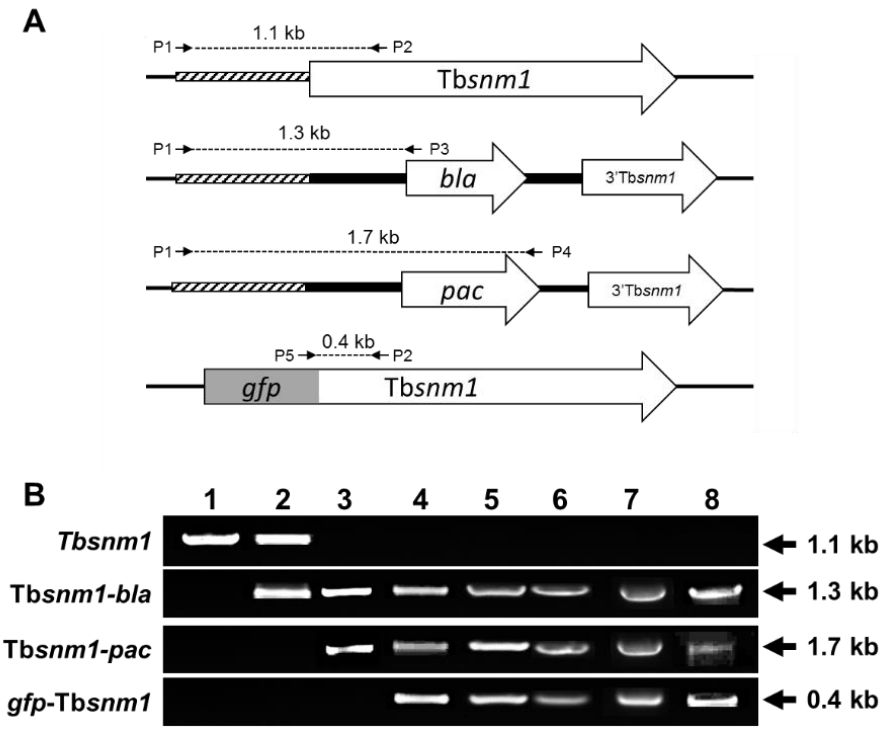

Appendix 4.4: Validating conditional null lines.

A. Diagram representing the Tb*snm1* allele and resultant changes upon disruption of this loci using genes encoding for blasticidin (*bla*) and puromycin (*pac*) resistance. Alongside this, changes to the landing pad locus after integration of *gfp*-Tb*snm1* was also analysed. P1 (Tbsnm1-KO1), P2 (Tbsnm1-seq1), P3 (bla-1), P4 (pac-1) and P5 (GFP) correspond to regions where the primers anneal at the specific allele.

B. DNA fragments obtained from amplification reactions on genomic DNA extracted from *T. brucei* wild type (lane 1), Tb*snm1*$^{+/-}$ (lane 2), Tb*snm1*Δ (lane 3), Tb*snm1*Δ *gfp*-Tb*snm1* (lane 4), TbSNM1-R428A (lane 5), TbSNM1-R429A (lane 6), TbSNM1-R430A (lane 7) and TbSNM1-H431A (lane 8) cells. Primer combinations amplified intact Tb*snm1* (Tbsnm1-KO1/Tbsnm1-seq1), Tb*snm1-bla* (Tbsnm1-KO1/bla-1), Tb*snm1-pac* (Tbsnm1-KO1/pac-1), or *gfp*-Tb*snm1* (GFP/Tbsnm1-seq1) alleles.

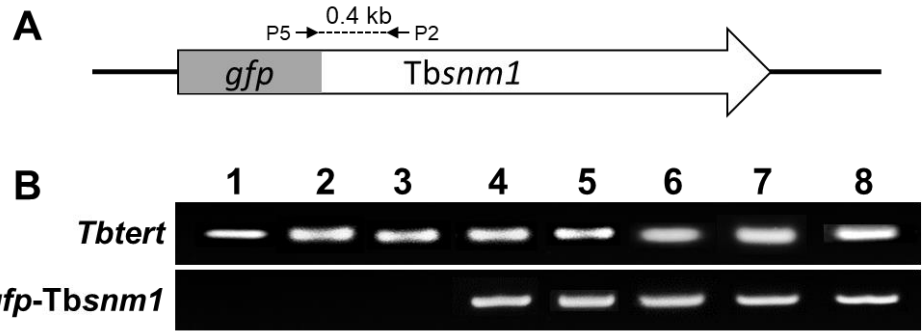

Appendix 4.5: Confirming expression of *gfp*-Tb*snm1*.
A. Schematic of integrated *gfp*-Tb*snm1* analysing using primer combination P2 (Tbsnm1-seq1) and P5 (GFP) which amplified a band of 0.4kb across the GFP and TbSNM1 fusion.
B. DNA fragments obtained after amplification on cDNA derived from RNA extracted from *T. brucei* wild type (lane 1), Tb*snm1*$^{+/-}$ (lane 2), Tb*snm1*Δ (lane 3), Tb*snm1*Δ *gfp*-Tb*snm1* (lane 4), TbSNM1-R428A (lane 5), TbSNM1-R429A (lane 6), TbSNM1-R430A (lane 7) and TbSNM1-H431A (lane 8) cells using primer combinations that specifically amplify gfp-Tbsnm1 (GFP/Tbsnm1-seq1) and Tbtert (Tbtert-F/Tbtert-R).

Appendix 6: Validation of Tb*ntr* expressing lines

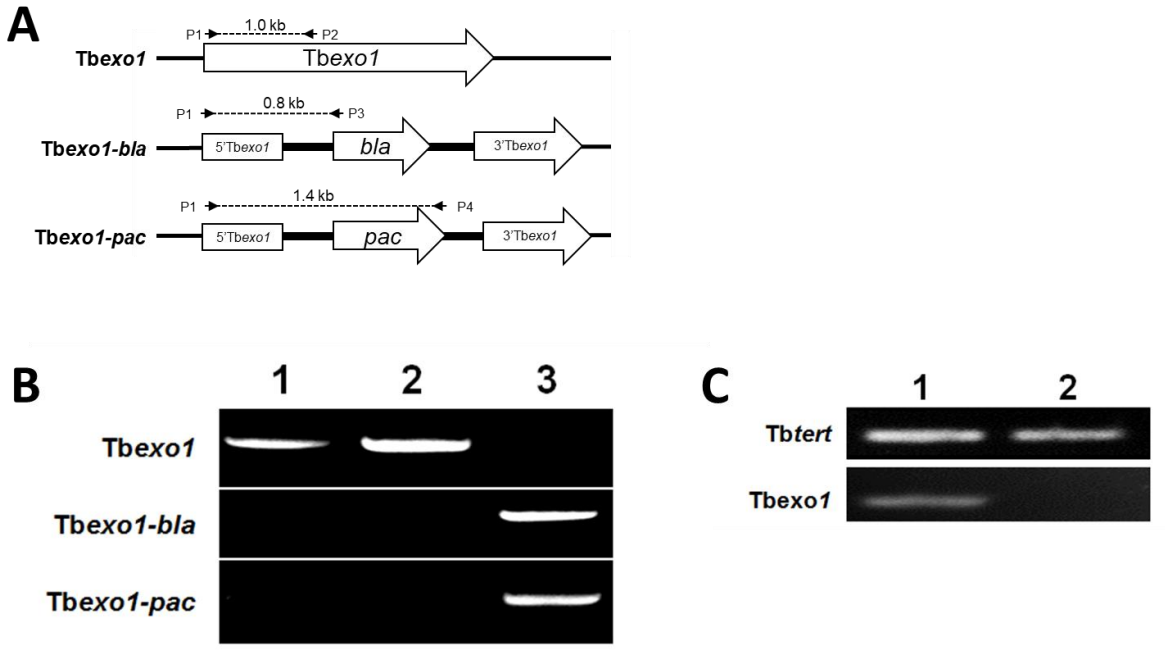

Appendix 5a: Validating the interruption of Tb*exo1* in *T. brucei*.

A. Representative diagram of the Tb*exo1* allele and effects of disrupting this allele with genes encoding for blastidicin (*bla*) and puromycin (*pac*) resistance. P1 (Tbexo1-KO1), P2 (Tbexo1-q2), P3 (bla-1) and P4 (pac-1) correspond to regions where the primers anneal at the specific allele.

B. DNA fragments obtained after amplification on gDNA extracted from *T. brucei* wild type (lane 1), 2T1 BSF-TbNTR 9e10 (lane 2) and 2T1 BSF-TbNTR 9e10 Tb*exo1*Δ (lane 3). Extractions from all 3 lines were tested using primer combinations that specifically amplify biomarkers corresponding to Tb*exo1* (Tbexo1-KO1/Tbexo1-q2), Tb*exo1-pac* (Tbexo1-KO1/pac-1) or Tb*exo1-bla* (Tbexo1-KO1/bla-1) alleles.

C. DNA fragments obtained after amplification on cDNA derived from RNA extracted from *T. brucei* wild type (lane 1) and 2T1 BSF-TbNTR 9e10 Tb*exo1*Δ (lane 2) using primer combinations that specifically amplify intact Tb*exo1* (Tbexo1-q1/Tbexo1-q2) and Tb*tert* (Tbtert-F/Tbtert-R).

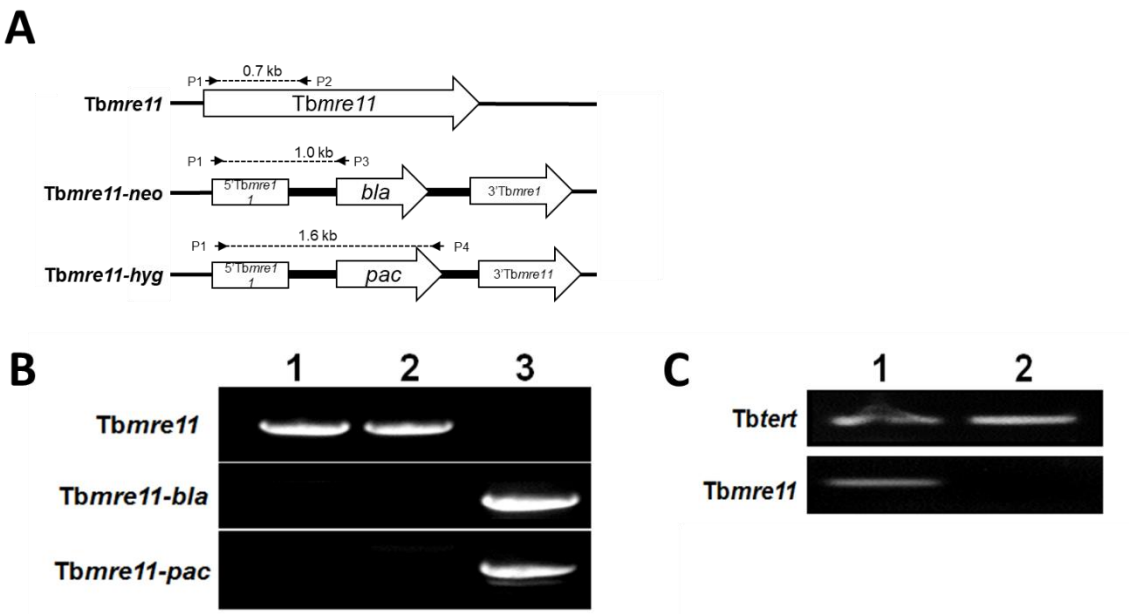

Appendix 5b: Validating the interruption of Tb*mre11* in *T. brucei*.

A. Representative diagram of the Tb*mre11* allele and effects of disrupting this allele with genes encoding for blastidicin (*bla*) and puromycin (*pac*) resistance. P1 (Tbmre11-KO1), P2 (Tbmre11-q2), P3 (bla-1) and P4 (pac-1) correspond to regions where the primers anneal at the specific allele.

B. DNA fragments obtained after amplification on gDNA extracted from *T. brucei* wild type (lane 1), 2T1 BSF-TbNTR 9e10 (lane 2) and 2T1 BSF-TbNTR 9e10 Tb*mre11*Δ (lane 3). Extractions from all 3 lines were tested using primer combinations that specifically amplify biomarkers corresponding to Tb*mre11* (Tbmre11-KO1/Tbmre11-q2), Tb*mre11-pac* (Tbmre11-KO1/pac-1) or Tb*mre11-bla* (Tbmre11-KO1/bla-1) alleles.

C. DNA fragments obtained after amplification on cDNA derived from RNA extracted from *T. brucei* wild type (lane 1) and 2T1 BSF-TbNTR 9e10 Tb*mre11*Δ (lane 2) using primer combinations that specifically amplify intact Tb*mre11* (Tbmre11-q1/Tbmre11-q2) and Tb*tert* (Tbtert-F/Tbtert-R).

Appendix 7: Published papers

Unravelling the role of SNM1 in the DNA repair system of *Trypanosoma brucei*

James A. Sullivan,[1] Jie Lun Tong,[1] Martin Wong,[1] Ambika Kumar,[1] Hajrah Sarkar,[1] Sarah Ali,[1] Ikran Hussein,[1] Iqra Zaman,[1] Emma Louise Meredith,[1] Nuala A. Helsby,[2] Longqin Hu[3] and Shane R. Wilkinson[1]*

[1]*School of Biological & Chemical Sciences*, *Queen Mary University of London*, *Mile End Road, London E1 4NS, UK*.

[2]*Department of Molecular Medicine and Pathology*, *University of Auckland*, *Private Bag 92019, Auckland, New Zealand*.

[3]*Department of Medicinal Chemistry*, *Ernest Mario School of Pharmacy*, *Rutgers*, *The State University of New Jersey*, *Piscataway, NJ 08854, USA*.

Summary

All living cells are subject to agents that promote DNA damage. A particularly lethal lesion are interstrand cross-links (ICL), a property exploited by several anti-cancer chemotherapies. In yeast and humans, an enzyme that plays a key role in repairing such damage are the PSO2/SNM1 nucleases. Here, we report that *Trypanosoma brucei*, the causative agent of African trypanosomiasis, possesses a *bona fide* member of this family (called TbSNM1) with expression of the parasite enzyme able to suppress the sensitivity yeast *pso2* mutants display towards mechlorethamine, an ICL-inducing compound. By disrupting the Tb*snm1* gene, we demonstrate that TbSNM1 activity is non-essential to the medically relevant *T. brucei* life cycle stage. However, trypanosomes lacking this enzyme are more susceptible to bi- and tri-functional DNA alkylating agents with this phenotype readily comple-mented by ectopic expression of Tb*snm1*. Genetically modified variants of the null mutant line were subse-quently used to establish the anti-parasitic mecha-nism of action of nitrobenzylphosphoramide mustard and aziridinyl nitrobenzamide prodrugs, compounds previously shown to possess potent trypanocidal properties while exhibiting limited toxicity to mamma-lian cells. This established that these agents, following activation by a parasite specific type I nitroreductase, produce metabolites that promote formation of ICLs leading to inhibition of trypanosomal growth.

Accepted 16 February, 2015. *For correspondence. E-mail s.r.wilkinson@qmul.ac.uk; Tel. (+44) 20 7882 3057; Fax (+44) 20 882 7732.

Introduction

The socioeconomic development of sub-Saharan Africa has been hindered by a group of medical and veterinary infections collectively known as African trypanosomiasis. The causative agents of many of these diseases are protozoan parasites belonging to the species *Trypano-soma brucei*, organisms that live and multiply extracellu-larly in the bloodstream and tissue fluids of their mammalian hosts. Transmission occurs *via* the blood-feeding habits of the insect vector, the tsetse fly. Over the last 15 years implementation of improved health surveil-lance programmes combined with new treatment regimens has led to a dramatic fall in the estimated number of new cases of the human form of the disease, known as human African trypanosomiasis (HAT) from around 450 000 in 1997 to about 20 000 in 2012 (Barrett, 2006; WHO, 2014). This situation has resulted in World Health Organization aiming to eliminate HAT as a public health problem by 2020. In contrast, animal African trypanosomiasis, particu-larly in domesticated livestock, remains a major problem with these infections killing around 3 million head of cattle each year and causing an annual loss of income estimated to be about US$4.75 billion (UNFAO, 2004).

With no immediate prospect of a vaccine or chemopro-phylaxis and with vector control being problematic, drug treatment represents the only option available to combat HAT. However, the current chemotherapies used are few in number and their use is controversial, as they can be costly, often require medical supervision for administration, some have limited efficacy and may cause adverse side effects, with drug resistance becoming more widespread (Wilkinson and Kelly, 2009; Alsford *et al*., 2013). One way to facilitate the development of new drugs targeting HAT is to better understand the mechanism of action of existing treatments with the properties that underlie parasite selec-tivity incorporated into the development of new trypano-cidal agents. For example, melamine rings have been incorporated into several compounds to exploit the sub-strate specificity displayed by the P2 adenosine trans-

porter, a permease implicated in the uptake of pentamidine and melarsoprol (Stewart *et al*., 2004; Baliani *et al*., 2005; Chollet *et al*., 2009; Klee *et al*., 2010; Capes *et al*., 2012; Giordani *et al*., 2014). Similarly, a parasite nitroreductase (NTR), an enzyme responsible for the activation of nifurti-mox (Wilkinson *et al*., 2008; Hall *et al*., 2011), has been used to screen nitroaromatic libraries for anti-*T. brucei* properties (Bot *et al*., 2010; 2013; Hall *et al*., 2010; 2012; Hu *et al*., 2011; Papadopoulou *et al*., 2011; 2012; 2013). In the latter case, several NTR-activated chemicals contain-ing nitrogen mustard or aziridine functional groups that promote DNA damage *via* formation of cross-linkages have been identified as having significant anti-parasitic activities and low mammalian cell toxicity (Bot *et al*., 2010; Hall *et al*., 2010; Hu *et al*., 2011).

Genomes are constantly challenged by endogenous and exogenous agents that promote DNA damage, with interstrand cross-links (ICLs) representing a particularly dangerous lesion (O'Connor and Kohn, 1990). Formed when the two complementary strands within the DNA double helix become covalently linked, ICLs block essen-tial cellular process that require DNA strand separation including DNA replication and transcription, leading to chromosomal breakage, rearrangements, or cell death (Dronkert and Kanaar, 2001; McHugh *et al*., 2001; Deans and West, 2011; Sengerova *et al*., 2011). Estimates indi-cate that a single ICL can kill a unicellular microbe with as few as 20 being fatal to a mammalian cell (Magana-Schwencke *et al*., 1982; Lawley and Phillips, 1996). In order to preserve the integrity and functionality of DNA, eukaryotic cells have evolved a series of complementary and overlapping pathways to repair ICLs, although the precise mechanisms involved in these systems are not fully understood (Deans and West, 2011). In *Saccharomy-ces cerevisiae*, many of the major DNA repair pathways [nucleotide excision repair (NER), mismatch repair, post-replication repair/translesion synthesis and homologous recombination] have been implicated in fixing ICL damage, although only a few proteins specifically involved in ICL lesion repair have been identified (Barber *et al*., 2005; Lehoczky *et al*., 2007; Daee *et al*., 2012; Ward *et al*., 2012). Of these, Pso2p (also known as Snm1) is of great interest as cells lacking this activity are specifically and highly susceptible to ICL-forming agents including pso-ralen, cisplatin and mechlorethamine but not to any other forms of DNA damage (Henriques and Moustacchi, 1980; Ruhland *et al*., 1981a,b). The precise role played by Pso2p in this repair system remains unknown, although biochemi-cal studies have shown that it displays a 5′ exonuclease activity (Li *et al*., 2005). This coupled with the observation that *pso2* cells exposed to ICL-inducing compounds tend to accumulate DNA double stranded breaks indicates that Pso2p does not function in the initial incision event, which in yeast is primarily controlled by NER, but may be involved in the processing of DNA ends created during the genera-tion of ICL-associated DNA double stranded breaks (Li and Moses, 2003; Barber *et al*., 2005; Dudas *et al*., 2007). Intriguingly, Pso2p also displays a structure-specific DNA hairpin opening endonuclease activity providing evidence that it may have other functions outside ICL repair (Tiefenbach and Junop, 2012).

Here, we report that *T. brucei* expresses a Pso2/Snm1 homologue that can readily complement for the suscepti-bility phenotype exhibited by *pso2* yeast cells towards an ICL forming agent. Deletion of the gene, designated Tb*snm1*, from the parasite genome revealed that although the encoded enzyme is not essential for viability and growth of bloodstream form (BSF) trypanosomes, cells lacking this activity were more susceptible to bifunctional nitrogen mustard- and aziridine-based ICL-inducing agents. Using recombinant *T. brucei* expressing altered levels of Tb*snm1*, we establish that the trypanocidal mechanism of several potent nitroaromatic-based agents that contain ICL-promoting grouping are dependent on an initial activation catalysed by a parasite specific type I NTR that generates metabolites that then promote DNA damage.

Results

Identifying trypanocidal chemical tools for studying DNA repair

Previous screening studies have identified nitroaromatic-based azirindyl/nitrogen mustard compounds to be effec-tive trypanocidal agents (Bot *et al*., 2010; Hall *et al*., 2010; Hu *et al*., 2011). The antimicrobial activity of these involves a parasite specific activation step catalysed by a type I NTR that leads to metabolites postulated to promote DNA damage. To determine if the above compounds do function *via* this pathway, a range of anti-cancer compounds known to mediate their cytotoxicity by promoting DNA cross-linkages were screened for trypanocidal activity against BSF *T. brucei*. The structures tested included non-nitroaromatic-based aziridines and nitrogen mustards, nitrosoureas, platinum complexes, an alkyl sulfonate and non-classical DNA cross-linking agents.

Out of the non-nitroaromatic anti-cancer compounds assessed, 17 had no effect on parasite growth at concen-trations of up to 30 μM, including busulfan, the only alkyl sulfonate analysed here, and all five non-classical DNA cross-linking agents (Table 1). These were not analysed further. For the remaining compounds, the concentration that inhibits parasite growth by 50% (IC_{50}'s) was deter-mined (Table 1). For all the remaining classes of DNA cross-linking agents, two or more compounds displayed trypanocidal activities with IC_{50} values ranging from 13 nM for mitomycin C, the most potent agent identified here, to approximately 35 μM for mechlorethamine and ThioTEPA.

Table 1. Susceptibility of *T. brucei* lines to DNA damaging agents.

	T. brucei IC_{50}	
Compound	**Wild type**	**Tb*snm1*$^{-/-}$**
Nitrogen mustards		
Chlorambucil, cyclophosphamide, uramustine, trofosfamide, ifosfamide, bendamustine	>30.000	nd
Mechlorethamine	34.240± 1.270	8.210 ±1.180
Melphalan	8.660± 0.660	3.960 ±0.320
Estramustine	9.370± 1.150	nd
Prednimustine	13.870± 1.330	nd
LH7	10.870± 0.240	0.580 ±0.050
LH17	4.160± 0.130	0.380 ±0.040
LH32	0.245± 0.079	0.021 ±0.004
LH33	0.215± 0.008	0.015 ±0.000
LH34	0.067± 0.006	0.006 ±0.001
LH37	0.097± 0.009	0.005 ±0.000
Aziridines		
ThioTEPA	37.830± 1.730	13.880 ±0.970
Triethylenemelamine	1.130± 0.150	0.300 ±0.020
Mitomycin C	0.013± 0.001	0.010 ±0.001
CB1954	3.900± 0.420	0.690 ±0.050
NH1	0.120± 0.004	0.044 ±0.013
Nitrosoureas		
Carmustine, nimustine, NSC270516	>30.000	nd
Lomustine	16.650± 0.440	17.310 ±0.210
Streptozotocin	21.800± 5.020	nd
Semustine	4.760± 0.050	3.780 ±0.070
Alkyl sulfonate		
Busulfan	>30.000	nd
Non-classical DNA cross-linking agents		
Altretamine, pipobroman, dacarbazine, temozolomide, mitobronitol	>30.000	nd
Platinum-based		
Oxaliplatin, nedaplatin	>30.000	nd
Cisplatin	2.280± 0.130	3.400 ±0.280
Carboplatin	5.030± 0.040	nd
Other agents		
Hydroxyurea	105.970± 10.190	88.200 ±7.300
H_2O_2	43.710± 5.950	50.06 ±7.520
UV irradiation	214.000± 13.000	196.000 ±30.000
MMS	16.125± 1.379	14.020 ±1.343
DMFO	24.150± 3.940	24.240 ±6.710
Nifurtimox	2.850± 0.020	2.250 ±0.090
Benznidazole	46.140± 1.440	37.680 ±1.630

Tb*snm1*$^{-/-}$

The cell lines analysed were *T. brucei* (wild type) and *T. brucei* null mutants (Tb*snm1*$^{-/-}$). IC_{50} values are given in μM except for UV irradiation, which is in J m^{-1}. LH7, LH17, LH32-34, LH37, CB1954 and NH1 represent structures previously identified as trypanocidal agents (Bot *et al*., 2010; Hall *et al*., 2010; Hu *et al*., 2011). nd is not determined.

Identification of the DNA repair enzyme TbSNM1

In other eukaryotes, the SNM1/PSO2 family of nucleases play an important role in repairing damage caused by DNA cross-linking agents (Cattell *et al*., 2010). Analysis of the *T. b. brucei* genome database (Aslett *et al*., 2010) identified a single hypothetical gene (designated as Tb*snm1*) of 2163 bp located on chromosome 4 with potential to encode for a 79.5 kDa enzyme (TbSNM1; Gene ID: Tb927.4.1480) related to this family of enzymes. Full-length TbSNM1 is 42% identical to the *T. cruzi* homo-logue (GenBank accession no. XP_816034) and has 27–32% identity to the leishmanial enzymes LmSNM1 (XP_001686430) and LdSNM1 (XP_003864463). When compared with yeast, plant and mammalian counterparts sequence identity ranged from 15% to 24%. Based on sequence, TbSNM1 can be divided into two regions (Fig. 1). The amino terminal section (residues 36–182) constitutes a non-canonical metallo-ß-lactamase (MBL; pfam12706) domain containing four motifs (motifs 1–4), including a characteristic HxHxDH signature (motif 2), that in other SNM1/PSO2 proteins cooperate to mediate zinc cofactor binding. The second section represents a β-CASP (named after its representative members **C**PSF, **A**rtemis, **S**NM1 and **P**SO2; pfam10996) region (residues 213–519) that contains within it a stretch of 31 amino acids comprising a DRMBL (DNA repair metallo-ß-lactamase; pfam07522) domain (residues 488–519). The β-CASP region contains a fifth zinc binding motif (motif 5) but as with other SNM1/PSO2 sequences the precise location of this has yet to be defined: *in silico* analysis of TbSNM1 indicates that D220 or H497 (motifs 5′ and 5″ respectively) may fulfil this role with H497 being the most likely of the two candidate residues (Callebaut *et al*., 2002). The β-CASP domain of TbSNM1 also contains a diagnostic valine residue (position 519) that indicates that the parasite enzyme is involved in DNA processing: DNA processing MBLs contain a valine residue at the equiva-lent site, whereas RNA processing MBLs contain a histi-dine (Callebaut *et al*., 2002).

To investigate whether the *T. brucei* enzyme is a SNM1/PSO2 homologue, Tb*snm1* minus its ATG initiation codon was amplified and cloned into a version of the yeast expression vector pYCYlac111 that contains a DNA sequence encoding for the FLAG-tag epitope. The result-ant plasmid was transformed into the *S. cerevisiae* wild type and *pso2* strains and expression of recombinant TbSNM1 confirmed by western blot analysis (Fig. 2A). The susceptibility of the fungal lines to mechlorethamine, a DNA cross-linking agent, was then determined and from the resultant dose-response curves the IC_{50} value for each strain calculated (Fig. 2B and C). Yeast lacking *pso2* were clearly more susceptible to the nitrogen mustard than wild type with the null mutant displaying an IC_{50} value approxi-mately 40% that of the control strain. When Tb*snm1* was expressed in wild type yeast a slight (1.4-fold) resistance was noted. This phenotype was also observed in the *pso2* strain expressing Tb*snm1* correlating with an increase in the IC_{50} value from 1.3 μM in cells lacking Pso2p to 5.7 μM in *pso2* yeast expressing FLAG-TbSNM1. These data

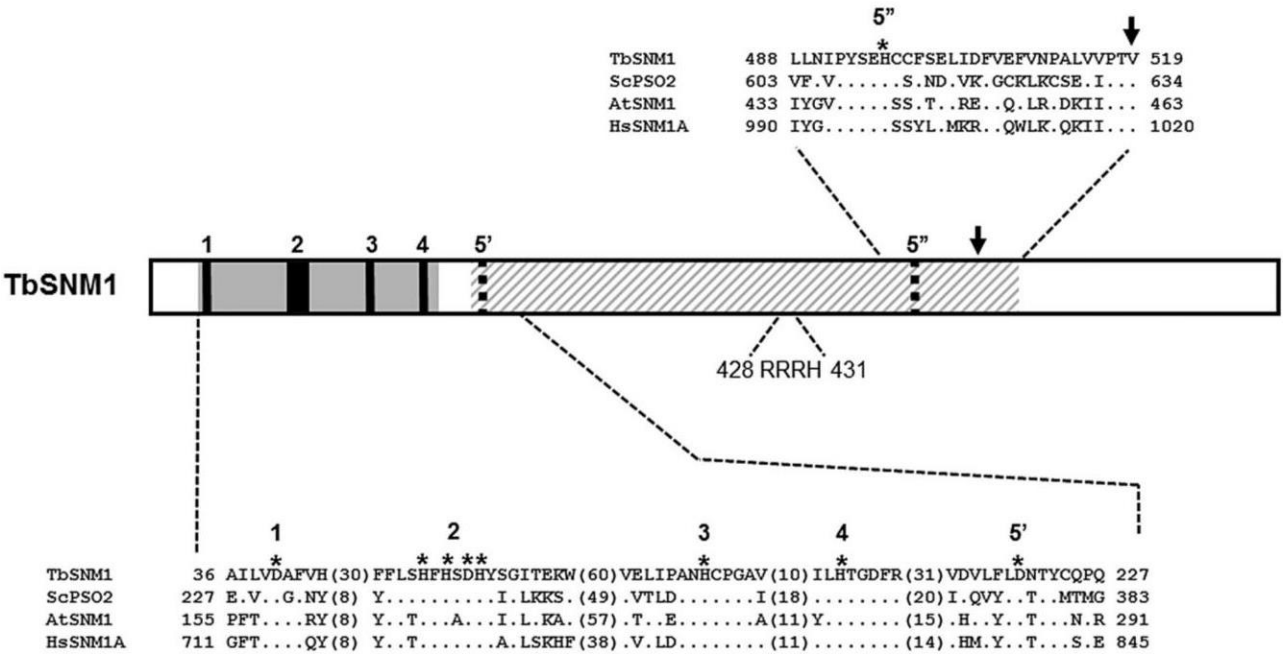

Fig. 1. Sequence analysis of TbSNM1. The sequence corresponding to the metallo-ß-lactamase (MBL; grey box) and β-CASP (hatched box) domains of TbSNM1 was aligned with other members of the SNM1A/PSO2 family of nucleases. The residues that are common with the TbSNM1 sequence are represented by dots. Sequence differences when compared with TbSNM1 are shown. In the alignments, amino acids marked with an asterisks (solid line in TbSNM1 schematic) correspond to motif 1–4, regions postulated to co-ordinate the metal (zinc) cofactor binding. The two possible residues that may represent motif 5 (5′ or 5″; dotted line in TbSNM1 schematic) are also shown. The down arrow highlights the amino acid that distinguishes DNA from RNA processing metallo-β-lactamases, whereas the RRRH sequence corresponds to a putative nuclear 'pattern 4' targeting signal. The sequences aligned are: *T. brucei* TbSNM1 (GenBank AAZ10739), *Saccharomyces cerevisiae* ScPSO2 (NP_013857), *Arabidopsis thaliana* AtSNM1 (NP_189302) and *Homo sapiens* HsSNM1A (NP_001258745).

clearly show that TbSNM1 can complement for the *pso2* mutation and that the trypanosomal enzyme is a *bona fide* SNM1/PSO2 homologue.

TbSNM1 is targeted to the T. brucei *nucleus*

When analysed using the PSORTII and WoLFPSORT algorithms, TbSNM1 was predicted to be targeted to the nucleus *via* a 'four pattern' RRRH (residues 428–431) nuclear localisation signal. To confirm this, the full-length Tb*snm1* gene minus its ATG initiation codon was amplified and ligated in-frame and downstream of the gene encoding for the enhanced green fluorescence protein (GFP) in a trypanosomal vector that facilitated tetracycline inducible gene expression (Alsford *et al*., 2005). The resultant construct was used to transform BSF *T. brucei*, and parasite clones were selected.

To induce expression of the tagged protein, cells were incubated in the presence of tetracycline for 48 hours. Recombinant parasites were examined by Western blot-ting using a monoclonal antibody against GFP (Fig. 3A), with extracts derived from these cells containing a band of the expected size (~ 105 kDa), or were fixed and examined by confocal microscopy (Fig. 3B). For parasites expressing GFP-TbSNM1, GFP fluorescence was restricted to a large single spot, a pattern reported for trypanosomal proteins localised to nucleus (Fig. 3B). To confirm this, cells were co-stained with the DNA dye, DAPI. When the images were compared, the pattern of localisation indicated that GFP-TbSNM1 was located in the larger of two compartments (the nucleus) where DAPI is found with the smaller, faint spot corresponding to the kinetoplast, the genome found in the parasites' single mitochondrion.

Functional analysis of TbSNM1 in T. brucei

To assess whether TbSNM1 was essential to BSF *T. brucei*, an RNAi-based approach was initially employed. A DNA fragment corresponding to an internal region of Tb*snm1* was cloned into p2T7^{Ti} (Wilkinson *et al*., 2003) and the construct transformed into BSF *T. brucei*. In the absence of tetracycline, recombinant clones were found to grow at approximately the same rate as the parental cells. Addition of tetracycline to parasites harbouring the RNAi construct did not affect the growth rate suggesting that TbSNM1 is not essential to BSF *T. brucei*. To confirm this,

DNA fragments corresponding to the 5′ flank of Tb*snm1* and the 3′ region of the Tb*snm1* gene were cloned either side of a cassette containing blasticidin or puromycin resistance markers. The integration constructs were trans-

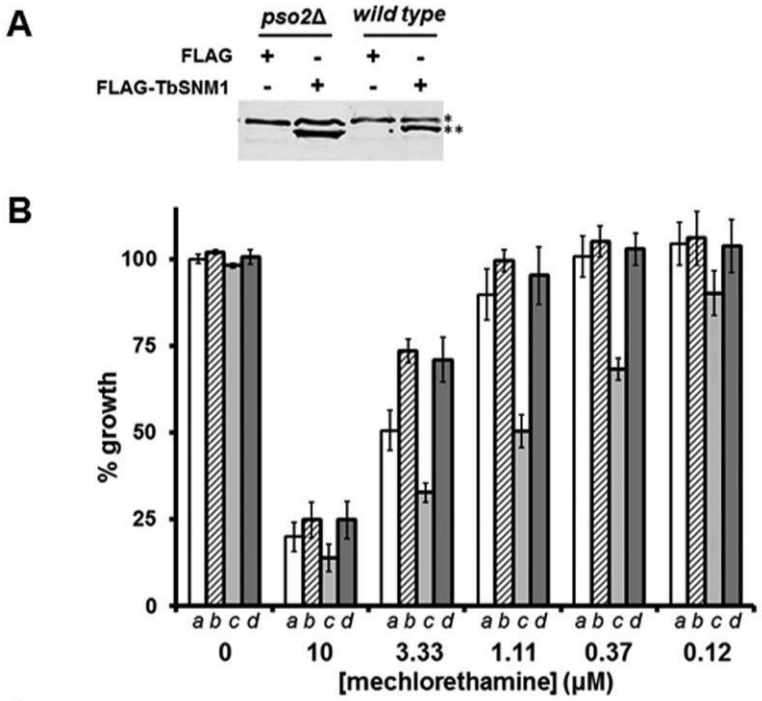

C

	Yeast IC_{50} (μM)			
	wild type + FLAG	wild type + FLAG-TbSNM1	*pso2*Δ + FLAG	*pso2*Δ + FLAG-TbSNM1
mechlorethamine	3.6 ± 0.4	5.1 ± 0.5 (1.4)	1.3 ± 0.6 (0.4)	5.7 ± 0.7 (1.6)

Fig. 2. Complementation of the yeast *pso2* mutation.
A. Western blot analysis was carried out using a monoclonal antibody to the FLAG-tag epitope on cell extracts made from *S. cerevisiae* BY4742 (wild type) and *pso2* strains expressing the FLAG epitope (control) or FLAG-TbSNM1. A band of ~ 80 kDa (indicated by **) was observed in lysates derived from cell expressing the recombinant trypanosomal protein. A cross-reactive epitope (*) and Ponceau S staining of the membrane (not shown) were used as loading controls.
B and C. The susceptibility of wild type (*a* and *b*) and *pso2* (*c* and *d*) yeast strains expressing FLAG (*a* and *c*) or FLAG-TbSNM1 (*b* and *d*) to different concentrations of mechlorethamine. All data are mean values ± standard deviations from experiments performed in triplicate. In C, the values given in parenthesis represent the fold difference in IC_{50} values (in μM) relative to wild-type controls.

formed into BSF *T. brucei* with heterozygote (Tb*snm1*$^{+/-}$) and then null mutant (Tb*snm1*$^{-/-}$) lines selected. Southern hybridisation was used to confirm each integration event demonstrating that both copies of the *Tbsnm1* gene could readily be deleted from the parasite genome (Fig. 4A and B), whereas quantitative RT-PCR data analysed using the comparative C_T method showed that a full-length Tb*snm1* mRNA was not expressed (data not shown) (Schmittgen and Livak, 2008). Reduction or lack of TbSNM1 had no effect on trypanosome growth (data not shown). Therefore, TbSNM1 is non-essential to BSF *T. brucei* under normal culture conditions confirming the RNAi observations.

To evaluate whether deletion of both copies of Tb*snm1* from the *T. brucei* genome altered sensitivity to chemicals that promote DNA cross-linkage, null mutant cells were grown in the presence of these agents, and the IC_{50} values for each compound were determined (Table 1).

Cells lacking TbSNM1 were more susceptible to a range of nitrogen mustard and aziridinyl compounds, including several of the trypanocidal nitroaromatic structures previously identified (Bot *et al*., 2010; Hall *et al*., 2010; Hu *et al*., 2011). Intriguingly, Tb*snm1*$^{-/-}$ cells exhibited a larger difference in their sensitivities to the nitrogen mus-tards screened than that observed when using the aziridi-nyl compounds. When these growth assays were extended to look at other DNA damaging agents including mitomycin C, semustine, cisplatin, methyl methanesul-phonate (MMS), H_2O_2, hydroxyurea and UV light, and to the clinically used trypanocidal drugs nifurtimox, benzni-dazole or *difluoromethylornithine* (DFMO), no difference in IC_{50} was observed.

In order to demonstrate conclusively that the altered susceptibility phenotypes were specifically due to lack of TbSNM1, a complementation strategy was used. In

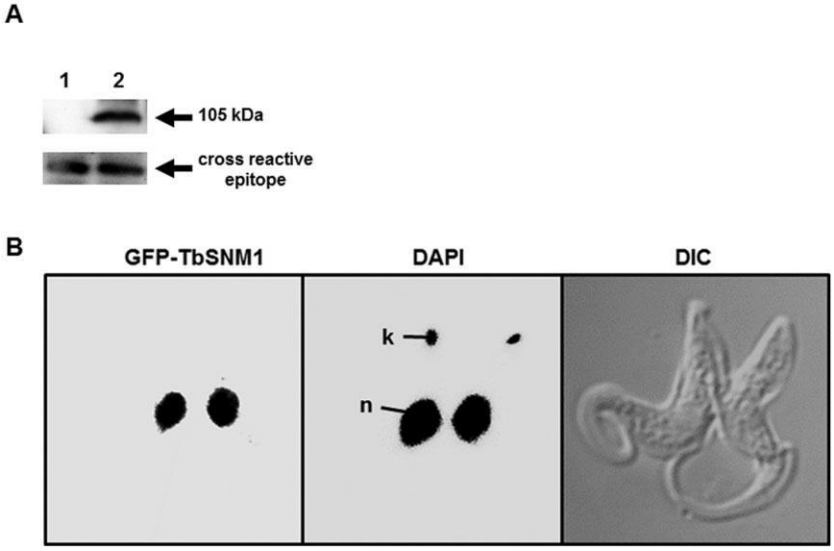

Fig. 3. Localisation of TbSNM1 in bloodstream form *T.brucei*.
A. Expression of GFP-TbSNM1 was examined by probing a blot containing cell lysates from *T. brucei* wild type (lane 1) and GFP-TbSNM1 expressing cells (lane 2) using an anti-GFP antibody (upper panel). Protein from 1.5×10^7 cells was loaded in each track and a cross-reactive epitope (lower panel) and by Coomassie staining (not shown) were used as loading controls.
B. Parasites expressing GFP-TbSNM1 were co-stained with DAPI (DNA) and the cells examined by confocal microscopy. The TbSNM1 signal is coincidental with the nucleus (n; large DAPI spot); the smaller DAPI spot corresponds to the kinetoplast (k), the trypanosome mitochondrial genome.

these experiments, Tb*snm1*$^{-/-}$ cells were transformed with a vector that facilitates constitutive expression of an ectopic copy of Tb*snm1* integrated into one of the parasite's tubulin arrays: wild-type cells also expressing this vector were also generated. The IC_{50} of these parasites towards selected nitrogen mustard and aziridinyl compounds was determined and compared with values obtained using wild type and Tb*snm1* null mutant lines (Fig. 5A). When the susceptibility of the complemented line to the nitrobenzyl-containing nitrogen mustard (LH34) and aziridinyl (NH1) compounds was tested, the resultant dose response curves (and associated IC_{50} values) were distinct from the Tb*snm1*$^{-/-}$ cells, which displayed increased sensitivity to both agents, and equivalent to the plots observed using Tb*snm1* expressing parasites (wild type and wild-type cells engineered to express elevated levels of TbSNM1) (Fig. 5A). When the screens were extended to investigate the complemented line's susceptibility to non-nitroaromatic nitrogen mustard (mechlorethamine) and aziridinyl (triethylenemelamine) compounds, a resistance phenotype was noted, with the dose response curves (and associated IC_{50} values) in the complemented line mirroring that obtained for wild-type parasites expressing elevated levels of TbSNM1 (Fig. 5A): trypanosomes (wild type and Tb*snm1* null mutants) expressing an ectopic copy of Tb*snm1* were up

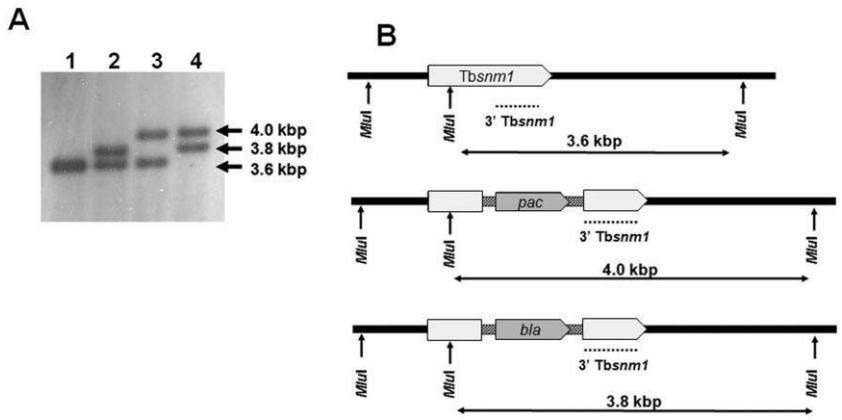

Fig. 4. Disruption of Tb*snm1* in *T. brucei*.
A. Diagram of the Tb*snm1* alleles and the effects of gene disruption. A 5′ Tb*snm1* flanking sequence and a 3′ Tb*snm1* coding region were amplified and cloned sequentially either side of a puromycin (*pac*) or blasticidin (*bla*) cassette (plus *T. brucei* tubulin intergenic elements required for processing of mRNA (hashed boxes). The dotted lines correspond to the probe used to check integration. The position of the predicted *Mlu*I sites plus the band sizes (in kbp) obtained after hybridisation are shown.
B. Southern blot analysis of *Mlu*I digested genomic DNA from *T. brucei* (lane 1), Tb*snm1*$^{+/-}$ *bla* and Tb*snm1*$^{+/-}$ *pac* heterozygous clones (lanes 2 and 3 respectively) and a Tb*snm1*$^{-/-}$ null mutant line (lane 4). Blots were hybridised with labelled 3′ region of sequences. Sizes given are in kbp.

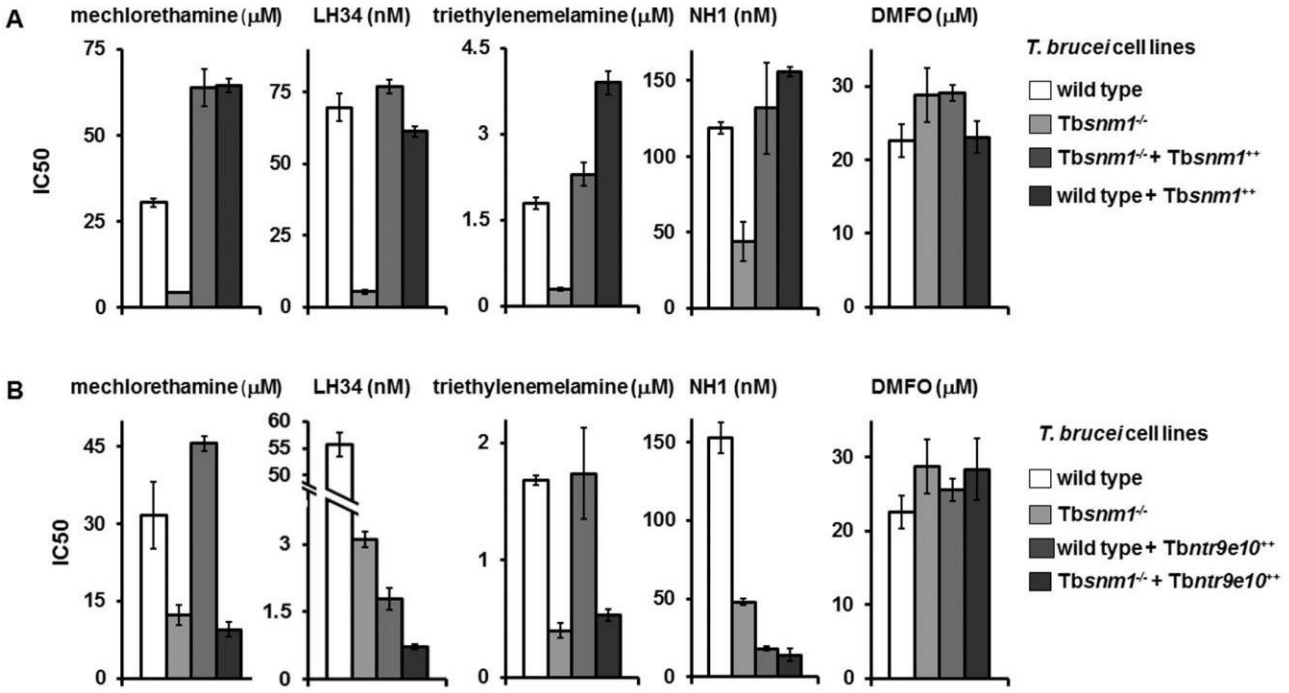

Fig. 5. Susceptibility of *T. brucei* lines expressing altered levels of TbSNM1 to DNA damaging agents.
A. Growth inhibitory effects (expressed as IC_{50} values in μM or nM) of the *T. brucei* wild type, Tb*snm1*$^{-/-}$ null mutant, Tb*snm1*$^{-/-}$ expressing an ectopic copy of Tb*snm1* (Tb*snm1*$^{-/-}$+ Tb*smn1*$^{++}$) and *T. brucei* expressing elevated levels of Tb*snm1* (wild type + Tb*smn1*$^{++}$) lines towards DNA damaging agents. Integration of the Tb*snm1* expression vector into a single tubulin array was confirmed by Southern hybridisation and expression evaluated through qPCR (data not shown).
B. Growth inhibitory effects (expressed as IC_{50} values in μM or nM) of *T. brucei* wild type, Tb*snm1*$^{-/-}$ null mutant, *T. brucei* expressing an ectopic copy of Tb*ntr* (wild type + Tb*ntr9e10*$^{++}$ and Tb*snm1*$^{-/-}$ expressing elevated levels of Tb*ntr* (Tb*snm1*$^{-/-}$ + Tb*ntr9e10*$^{++}$) towards DNA damaging agents. Expression of Tb*ntr* was evaluated through qPCR (data not shown). Data in panels A and B are mean values ± standard deviations from experiments performed in quadruplicate.

to 2.1-fold more resistant to mechlorethamine and triethylenemelamine than wild type.

The above complementation studies indicate that parasites (wild type or Tb*snm1*$^{-/-}$) ectopically expressing Tb*snm1* are resistant to non-nitroaromatic DNA cross-linking agents but not to the nitroaromatic-containing compounds. One reason for this could reflect that the latter structures function as prodrugs and must undergo an NTR catalysed activation step before mediating their trypanocidal DNA damaging activities.

Linking prodrug activation with DNA damage

To identify any link between the DNA damaging and the NTR-activating pathways, both copies of the Tb*snm1* gene were deleted from *T. brucei* cells, expressing an ectopic copy of Tb*ntr* and the susceptibilities of these recombinant cells towards selected nitrogen mustard and aziridinyl compounds determined (Fig. 5B). When treated with mechlorethamine or triethylenemelamine, both Tb*snm1* expressing cell lines (wild type and trypano-somes expressing elevated levels of Tb*ntr*) displayed similar dose response curves and therefore had similar IC_{50}s to either agent (Fig. 5B). When these studies were expanded to investigate the susceptibility of parasites lacking TbSNM1, the Tb*snm1*$^{-/-}$ null mutant line and Tb*snm1*$^{-/-}$ cells expressing the ectopic copy of Tb*ntr* displayed equivalent IC_{50} values, with both being more sensitive to mechlorethamine and triethylenemelamine than wild type (Fig. 5B). Importantly, no difference in IC_{50} was observed using either of the lines lacking Tb*snm1* indicating that Tb*ntr* plays no role in metabolising either mechlorethamine or triethylenemelamine.

When the nitrobenzyl-containing DNA cross-linking agents LH34 and NH1 were tested against the parasite lines expressing altered levels of Tb*snm1* and/or Tb*ntr*, a different outcome was observed (Fig. 5B). For Tb*snm1*$^{-/-}$ parasites or wild-type cells expressing an ectopic copy of Tb*ntr*, treatment with either damaging agents resulted in increased susceptibility when compared against controls, with Tb*ntr* overexpressing trypanosomes being more sen-sitive to LH34 and NH1 than the null mutant lines: Tb*snm1*$^{-/-}$ cells and *T. brucei* overexpressing Tb*ntr* were 18.0- and 24.0-fold more susceptible to LH34, respec-tively, with a 2.7- and 31.1-fold increase in sensitivity noted towards NH1. For Tb*snm1*$^{-/-}$ null parasites express-

ing an ectopic copy of Tb*ntr*, this increase in potency was magnified further with these cells showing a 80.0- and 38.7-fold increase in susceptibility towards LH34 and NH1, respectively, when as compared against wild type.

Discussion

Currently, very little is known about the mechanisms *T. brucei* employs to repair ICL damage even though this parasite is exposed to such deleterious insults throughout its cell and life cycles. In other unicellular eukaryotes such as budding and fission yeast, the processing of ICLs occurs through the concerted activities of several major DNA repair pathways with one enzyme, Pso2p, playing a central and specific role in fixing such lesions. Although non-essential for yeast viability, the importance of Pso2p is only apparent in its absence on exposure to ICL-inducing, bifunctional alkylating agents but not to monofunctional alkylating agents, ionising radiation or ultraviolet light (Henriques and Moustacchi, 1980; Ruhland *et al*., 1981a,b). Here, we report the characterisation of TbSNM1, a trypanosomal Pso2p homologue, and demonstrate that this enzyme plays a key role in processing ICL lesions when generated by bifunctional nitrogen mustard and aziridinyl compounds including several nitroaromatic-based agents previously shown to have potent anti-trypanosomal properties with low toxicity to mammalian cells (Bot *et al*., 2010; Hall *et al*., 2010; Hu *et al*., 2011).

In terms of its sequence, TbSNM1 displays the main characteristics found in other PSO2/SNM1 proteins, pos-sessing adjacent MBL and β-CASP domains that together form the enzyme's zinc-binding central catalytic core (Cattell *et al*., 2010). To confirm the *in silico* identification, a complementation approach was undertaken. This involved ectopically expressing the trypanosomal enzyme in a yeast *pso2* line and then evaluating the susceptibility of the resultant cells to mechlorethamine, a bifunctional alkylat-ing agent routinely used as an ICL-inducing agent. In this genetic background, the parasite protein was able to revert the susceptibility phenotype displayed by the *pso2* line resulting in an additional slight (approximately twofold) resistance towards this nitrogen mustard. This confirmed that the trypanosomal enzyme is a genuine Pso2p homo-logue and that it plays a role in the processing of ICL lesions. Furthermore, as TbSNM1 can complement for the *pso2* mutation then the parasite enzyme may interact with the same partner proteins as its yeast counterpart. For example, Pso2p contains an ubiquitin binding zinc finger (UBZ) C2HC motif upstream of its catalytic core (Yang *et al*., 2010). By analogy with hSNM1A, the only human PSO2/SNM1 homologue able to complement the yeast *pso2* mutation (Hazrati *et al*., 2008), this signature sequence is able to facilitate binding to monoubiquinated PCNA leading to recruitment of this repair enzyme to ICL-stalled replication forks (Yang *et al*., 2010). Interest-ingly, *in silico* searches failed to identify any known UBZ C2HC domain or any other type of ubiquitin interaction motifs (UIMs) in the parasite protein sequence. Therefore, if formation of PSO2/SNM1-containing DNA repair com-plexes at the site of ICL damage does involve PCNA ubiquitylation, then the molecular mechanisms underlying TbSNM1 recruitment to such lesions occurs through an as yet uncharacterised UIM or *via* interactions involving a conserved adapter protein. Recently, it has been shown that the β-CASP domain of Pso2p can be phosphorylated leading to the suggestion that this event may play a role in modulating the enzyme's exo- or endo-nucleolytic activity (Munari *et al*., 2014). Whether TbSNM1 undergoes a similar post-translational modification, and how this effects its nuclease activity has yet to be established.

The endogenous function of TbSNM1 is non-essential to replicating *T. brucei*: both copies of *Tbsnm1* could be deleted from the genome of BSF trypomastigote parasites. However, the importance of this enzyme to the trypano-some only became evident following exposure to ICL-inducing compounds: null mutant cells were more susceptible to bi- and tri-functional alkylating agents as compared with controls, whereas these recombinant cells display an equivalent sensitivity to wild type when exposed to MMS, UV irradiation and H_2O_2, treatments normally repaired by homologous recombination, nucleotide exci-sion repair or base excise repair pathways. This trait was solely due to loss of TbSNM1 activity as expression of an ectopic copy of Tb*snm1* in the null mutant genetic back-ground restored the recombinant parasites IC_{50} near to wild-type levels. Intriguingly, the range of compounds that elicits the change in susceptibility in the Tb*snm1*$^{-/-}$ trypa-nosomes although similar to that noted for the yeast *pso2* line does have some notable differences (Henriques and Moustacchi, 1980; Ruhland *et al*., 1981a,b). For example, yeast *pso2* mutants are reported to be more susceptible to cisplatin and mitomycin C, whereas *T. brucei* lacking TbSNM1 displays sensitivities similar to that exhibited by wild-type parasites. This may be because that although both compounds can function as ICL-inducing agents they can also mediate their cytotoxic activities *via* other mecha-nisms including promoting formation of intrastrand cross-links, activating signal transduction pathways, stimulating redox cycling, acting as enzyme inhibitors or alkylating other biological molecules (Sharma and Tomasz, 1994; Pagano *et al*., 2003; Siddik, 2003; Rabik and Dolan, 2007; Paz *et al*., 2012). One (or a combination) of these alterna-tive modes of action (or possibly another unidentified mechanism) may account for cisplatin's and mitomycin C's trypanocidal properties, therefore negating the require-ment for a TbSNM1-dependent ICL repair pathway.

Previous trypanocidal screening programmes have identified nitrobenzylphosphoramide mustards and aziridi-

nyl nitrobenzamides as having potent anti-parasitic activity (Bot *et al*., 2010; Hall *et al*., 2010; Hu *et al*., 2011). These agents function as prodrugs and must be activated before they can mediate their cytotoxic effects, a reaction cata-lysed a NADH-dependent type I NTR. This reduction causes the conversion of a conserved electron withdraw-ing nitro-group present on the compound's benzyl ring to an electron donating hydroxylamine derivative (Bot *et al*., 2010; Hall *et al*., 2010; Hu *et al*., 2011). This action effec-tively acts as an electronic switch that is believed to turn on the alkylating ability of the nitrogen mustard or aziridinyl moiety causing ICL-mediated DNA damage. Using Tb*snm1* null mutant parasites engineered to express elevated levels of TbNTR, we have now demonstrated a link between prodrug activation and ICL formation. Here we observed that wild-type parasites exhibited the highest IC_{50} values towards LH34 (a nitrobenzylphosphoramide mustard) and NH1 (an aziridinyl nitrobenzamide), whereas trypanosomes lacking TbSNM1 and cells overexpress-ing TbNTR had intermediate sensitivities. Interestingly, Tb*snm1* null mutants that also express elevated levels of TbNTR were the most prone to both compounds. This implies that following uptake, LH34 and NH1 are trans-ported into mitochondrion where they undergo TbNTR-mediated reduction to form the bioactive products. These observations suggest that in parasites where the NTR activity is overexpressed, this conversion occurs at a faster rate than in wild-type cells resulting in increased sensitivity to the compound. A portion of the resulting metabolites are then able to access the nucleus where they induce ICL formation. In the absence of TbSNM1, mutant cells are less able to repair this type of DNA damage, resulting in an increased susceptibility to the ICL-inducing agent. In parasites where both TbSNM1 and TbNTR levels have been altered, this susceptibility phenotype is exacerbated. Intriguingly, the difference in sensitivities between Tb*snm1*$^{-/-}$ cells expressing elevated TbNTR levels from those over expressing TbNTR alone was greater for LH34 than for NH1. This may be attributable to properties of the substrate/TbNTR-generated metabolites, possibly reflect-ing differences in cell and/or organelle uptake [TbNTR is a mitochondrial protein (Wilkinson *et al*., 2008)] or how the substrates interact with, or how the metabolites are released from, TbNTR [*in vitro* nitrobenzyl phosphoramide nitrogen mustard-based compounds interact with TbNTR more readily than the aziridinyl nitrobenzamide (Hall *et al*., 2012)]. Additionally, as this study only considers ICL for-mation and repair in the nuclear genome, it is plausible that LH34 and NH1 reduction products may also affect the mitochondrial genome with the NH1 metabolites preferen-tially affecting this DNA containing region and not the nucleus.

We have now demonstrated that *T. brucei* expresses a *bona fide* homologue of the PSO2/SNM1 nuclease family. The trypanosomal enzyme displays characteristics of its yeast counterpart and is able to repair the DNA damage caused by bi- and tri-functional alkylating agents. By exploiting parasites lacking this enzyme we were able to demonstrate that following TbNTR-mediated activation nitrobenzylphosphoramide mustard and aziridinyl nitrobenzamide agents, compounds previ-ously shown to have potent trypanocidal properties with little/no cytotoxicity in mammalian cells, generate metabolites that promote ICL formation. Although not essential to survival of the medically relevant form of *T. brucei*, in the future TbSNM1 could be targeted through the use of inhibitors to improve the potency of other drugs that do cause parasite death through forma-tion of the extremely lethal ICL.

Experimental procedures

Cell culturing

Bloodstream form *Trypanosoma brucei brucei* [MITat 427 strain; clone 221a and a derivative (2T1) engineered to express elevated levels of TbNTR-myc] was maintained in HMI-9 (Invitrogen) medium supplemented with 3 g l^{-1} sodium bicarbonate, 0.014% (v/v) β-mercaptoethanol and 10% (v/v) foetal calf serum (Hirumi and Hirumi, 1989; Wilkinson *et al*., 2008) at 37°C under a 5% (v/v) CO_2 atmosphere. The 2T1 cells were grown in the presence of 1 μg ml^{-1} phleomycin and 2 μg ml^{-1} puromycin. Transformed *T. brucei* cells were grown in the presence of 2.5 μg ml^{-1} hygromycin, 10 μg ml^{-1} blasti-cidin and/or 2 μg ml^{-1} puromycin.

Saccharomyces cerevisiae strains BY4742 (*MATα his3- 1 leu2- 0 lys2- 0 ura3- 0*) and a *pso2* derivative obtained from the Open Biosystems (Thermo Scientific) knock-out col-lection were maintained in yeast extract-peptone broth containing 2% (w/v) glucose. Transformed cells were grown in Synthetic Complete Dropout medium lacking leucine (Sigma).

Chemicals

The DNA damaging agents were obtained from Drug Synthe-sis and Chemistry Branch, Developmental Therapeutics Program, Division of Cancer Treatment and Diagnosis, National Cancer Institute except CB1954, H_2O_2, MMS and hydroxyurea (all Sigma-Aldrich), NH1 (Helsby *et al*., 2004) and LH7, LH17, LH32-34 and LH37 (Hu *et al*., 2003; 2011; Li *et al*., 2003). Nifurtimox and benznidazole were obtained from Simon Croft (London School of Hygiene and Tropical Medicine) and DFMO from Mike Barrett (University of Glasgow).

Plasmids

The vectors used to delete Tb*snm1* from the *T. brucei* genome were generated as follows. Primers were designed to amplify 897 or 909 bp fragments from the 5′ Tb*snm1* untranslated region and 3′ region of the Tb*snm1* gene respectively. These

were cloned sequentially either side of a puromycin- (*pac*) or blasticidin- (*bla*) containing resistance cassette. The constructs were linearised (SacI/KpnI for the *pac* vector or SacII/KpnI for the *bla* vector) then introduced into BSF *T. brucei* using the Human T-cell Nucleofector® kit and an Amaxa® Nucleofector™ (Lonza AG) set to program X-001. Integration of the DNA constructs into the *T. brucei* genome results in deletion of 60% of the Tb*snm1* open reading frame (amino acids 1 to 425) including all of the non-canonical MBL domain. As this region is essential for Pso2p/SNM1 function (Li and Moses, 2003), removal of the MBL encoding DNA sequence from the trypanosomal genome would generate parasites lacking TbSNM1 activity, effectively producing Tb*snm1* null mutant cells.

The Tb*snm1* trypanosomal expression vector was generated as follows: a 2166 bp DNA sequence corresponding to full-length Tb*snm1* was amplified from *T. brucei* genomic DNA using the primers *cctgcagg*ATGGCAGGTGGA GCTGCAGGT and *gcgcgcc*TTATTCTGAGTC ACTACTCAG (lower-case italics correspond to restriction sites incorporated into the primers to facilitate cloning), digested with SdaI/SgsI and ligated into the corresponding sites of vector pTubEX-LmSpSyn (Taylor *et al*., 2008), replacing Lm*spsyn*. The NotI/XhoI digested construct was introduced into *T. brucei* wild type and *Tbsnm1*$^{-/-}$ cells using nucleofection and recombinant clones selected.

For the localisation construct, a 2166 bp DNA sequence corresponding to full-length Tb*snm1* was amplified from *T. brucei* genomic DNA using the primers *tctaga*GCAGGTGGAGCTGC AGGTAAG and *gagatct*TTATTCTGAGTCACT ACTCAG (lower-case italics correspond to restriction sites incorporated into the primers to facilitate cloning), the fragment digested with XbaI/BglII and ligated into the XbaI/BamHI sites of vector pRPa$^{GFP\text{-}AT2}$ (Alsford *et al*., 2005) to replace the Tb*at2* coding sequence. The cloning was carried out such that the gene coding for the GFP was inserted in-frame at the 5′ end of the *Tbsnm1*-derived DNA fragment. The AscI-digested construct was introduced into *T. brucei* 2T1 parasites.

To construct the yeast complementation vector Tb*snm1* was amplified from the trypanosomal localisation plasmid using the primers *tctaga*GCAGGTGGAGCTGCAGGTAA G and *aagctt*TTATTCTGAGTCACTACTCAG (lower-case italics correspond to restriction sites incorporated into the primers to facilitate cloning). The resultant fragment was digested with XbaI/HindIII and ligated into the corresponding sites of a pYCYlac111 derivative containing a DNA sequence encoding for the FLAG-tag epitope (Novoselova *et al*., 2013). The plasmid was transformed into yeast strains BY4742 and *pso2* . In this system recombinant TbSNM1 is tagged at its amino-terminus with a FLAG-tag epitope detectable with the anti-FLAG monoclonal antibody (Sigma).

Localisation

BSF trypanosomes expressing GFP-TbSNM1 were washed twice in phosphate-buffered saline (PBS), fixed in 2% (w/v) paraformaldehyde/PBS and washed again in PBS. Aliquots of the cell suspension (10^5 cells) were then air dried onto micro-scope slides. Parasite DNA was stained using Vectashield Mounting Medium containing 4′,6-diamidino-2-phenylindole (DAPI) (Vectorshield Laboratories), and slides were viewed using a Leica SP5 confocal microscope (Leica Microsystems (UK) Ltd).

Antiproliferative assays

All assays were performed in a 96-well plate format. *T. brucei* BSF parasites were seeded at 1×10^4 ml^{-1} in 200 µl growth medium containing different concentrations of compound. For UV irradiation, parasites were exposed to doses up to 900 J m^{-2} using a Stratalinker® UV crosslinker (Stratagene). After incubation at 37°C for 3 days, 2.5 µg resazurin (20 µl of 0.125 µg ml^{-1} stock in phosphate buffered saline) was added to each well, and the plates were incubated for a further 6–8 hours (Jones *et al*., 2010). Cell densities were determined by monitoring the fluorescence of each culture using a Gemini Fluorescent Plate Reader (Molecular Devices (UK) Ltd, Wok-ingham, UK) at an excitation wavelength of 530 nm, emission wavelength of 585 nm and a filter cutoff at 550 nm. The drug/treatment concentration that inhibits cell growth by 50% (IC_{50}) was established using the non-linear regression tool on GraphPad Prism (GraphPad Software).

Yeast complementation assay

All assays were performed in a 96-well plate format. The cell density of overnight yeast cultures were equalised according to absorbance at 405 nm in medium containing different concentrations of mechlorethamine. The growth of each strain was then followed by monitoring the change in absorbance at 405 nm using an Absorbance Microplate Reader (BioTek Instruments Ltd). The % growth for each mechlorethamine-treated culture after 18 hours relative to untreated samples was determined.

Acknowledgements

Emma Louise Meredith is a recipient of a BBSRC Doctorial Training Studentship. We would like to thank Martin Taylor (London School of Hygiene and Tropical Medicine) for valuable discussions and comments on the manuscript.

References

Alsford, S., Kawahara, T., Glover, L., and Horn, D. (2005) Tagging a *T. brucei* RRNA locus improves stable transfec-tion efficiency and circumvents inducible expression posi-tion effects. *Mol Biochem Parasitol* **144:** 142–148.

Alsford, S., Kelly, J.M., Baker, N., and Horn, D. (2013) Genetic dissection of drug resistance in trypanosomes. *Parasitology* **140:** 1478–1491.

Aslett, M., Aurrecoechea, C., Berriman, M., Brestelli, J., Brunk, B.P., Carrington, M., *et al*. (2010) TriTrypDB: a functional genomic resource for the Trypanosomatidae. *Nucleic Acids Res* **38:** D457–D462.

Baliani, A., Bueno, G.J., Stewart, M.L., Yardley, V., Brun, R., Barrett, M.P., and Gilbert, I.H. (2005) Design and synthesis of a series of melamine-based nitroheterocycles with activ-

ity against Trypanosomatid parasites. *J Med Chem* **48:** 5570–5579.

Barber, L.J., Ward, T.A., Hartley, J.A., and McHugh, P.J. (2005) DNA interstrand cross-link repair in the *Saccharomyces cerevisiae* cell cycle: overlapping roles for PSO2 (SNM1) with MutS factors and EXO1 during S phase. *Mol Cell Biol* **25:** 2297–2309.

Barrett, M.P. (2006) The rise and fall of sleeping sickness. *Lancet* **367:** 1377–1378.

Bot, C., Hall, B.S., Bashir, N., Taylor, M.C., Helsby, N.A., and Wilkinson, S.R. (2010) Trypanocidal activity of aziridinyl nitrobenzamide prodrugs. *Antimicrob Agents Chemother* **54:** 4246–4252.

Bot, C., Hall, B.S., Alvarez, G., Di Maio, R., Gonzalez, M., Cerecetto, H., and Wilkinson, S.R. (2013) Evaluating 5-nitrofurans as trypanocidal agents. *Antimicrob Agents Chemother* **57:** 1638–1647.

Callebaut, I., Moshous, D., Mornon, J.P., and de Villartay, J.P. (2002) Metallo-beta-lactamase fold within nucleic acids processing enzymes: the beta-CASP family. *Nucleic Acids Res* **30:** 3592–3601.

Capes, A., Patterson, S., Wyllie, S., Hallyburton, I., Collie, I.T., McCarroll, A.J., *et al*. (2012) Quinol derivatives as potential trypanocidal agents. *Bioorg Med Chem* **20:** 1607–1615.

Cattell, E., Sengerova, B., and McHugh, P.J. (2010) The SNM1/Pso2 family of ICL repair nucleases: from yeast to man. *Environ Mol Mutagen* **51:** 635–645.

Chollet, C., Baliani, A., Wong, P.E., Barrett, M.P., and Gilbert, I.H. (2009) Targeted delivery of compounds to *Trypano-soma brucei* using the melamine motif. *Bioorg Med Chem* **17:** 2512–2523.

Daee, D.L., Ferrari, E., Longerich, S., Zheng, X.F., Xue, X., Branzei, D., *et al*. (2012) Rad5-dependent DNA repair functions of the *Saccharomyces cerevisiae* FANCM protein homolog Mph1. *J Biol Chem* **287:** 26563–26575.

Deans, A.J., and West, S.C. (2011) DNA interstrand crosslink repair and cancer. *Nat Rev Cancer* **11:** 467–480.

Dronkert, M.L., and Kanaar, R. (2001) Repair of DNA inter-strand cross-links. *Mutat Res* **486:** 217–247.

Dudas, A., Vlasakova, D., Dudasova, Z., Gabcova, D., Brozmanova, J., and Chovanec, M. (2007) Further characterization of the role of Pso2 in the repair of DNA inter-strand cross-link-associated double-strand breaks in *Saccharomyces cerevisiae*. *Neoplasma* **54:** 189–194.

Giordani, F., Buschini, A., Baliani, A., Kaiser, M., Brun, R., Barrett, M.P., *et al*. (2014) Characterisation of a melamino nitroheterocycle as a potential lead for the treatment of human African trypanosomiasis. *Antimicrob Agents Chem-other* **58:** 5747–5757.

Hall, B.S., Wu, X., Hu, L., and Wilkinson, S.R. (2010) Exploiting the drug-activating properties of a novel trypanosomal nitroreductase. *Antimicrob Agents Chemother* **54:** 1193–1199.

Hall, B.S., Bot, C., and Wilkinson, S.R. (2011) Nifurtimox activation by trypanosomal type I nitroreductases gener-ates cytotoxic nitrile metabolites. *J Biol Chem* **286:** 13088– 13095.

Hall, B.S., Meredith, E.L., and Wilkinson, S.R. (2012) Target-ing the substrate preference of a type I nitroreductase to develop antitrypanosomal quinone-based prodrugs. *Anti-microb Agents Chemother* **56:** 5821–5830.

Hazrati, A., Ramis-Castelltort, M., Sarkar, S., Barber, L.J., Schofield, C.J., Hartley, J.A., and McHugh, P.J. (2008) Human SNM1A suppresses the DNA repair defects of yeast pso2 mutants. *DNA Repair (Amst)* **7:** 230–238.

Helsby, N.A., Atwell, G.J., Yang, S., Palmer, B.D., Anderson, R.F., Pullen, S.M., *et al*. (2004) Aziridinyldinitrobenza-mides: synthesis and structure-activity relationships for activation by *E. coli* nitroreductase. *J Med Chem* **47:** 3295– 3307.

Henriques, J.A., and Moustacchi, E. (1980) Isolation and characterization of pso mutants sensitive to photo-addition of psoralen derivatives in *Saccharomyces cerevisiae*. *Genetics* **95:** 273–288.

Hirumi, H., and Hirumi, K. (1989) Continuous cultivation of *Trypanosoma brucei* blood stream forms in a medium containing a low concentration of serum protein without feeder cell layers. *J Parasitol* **75:** 985–989.

Hu, L., Yu, C., Jiang, Y., Han, J., Li, Z., Browne, P., *et al*. (2003) Nitroaryl phosphoramides as novel prodrugs for *E. coli* nitroreductase activation in enzyme prodrug therapy. *J Med Chem* **46:** 4818–4821.

Hu, L.Q., Wu, X.H., Han, J.Y., Chen, L., Vass, S.O., Browne, P., *et al*. (2011) Synthesis and structure-activity relation-ships of nitrobenzyl phosphoramide mustards as nitroreductase-activated prodrugs. *Bioorg Med Chem Lett* **21:** 3986–3991.

Jones, D.C., Hallyburton, I., Stojanovski, L., Read, K.D., Frearson, J.A., and Fairlamb, A.H. (2010) Identification of a κ-opioid agonist as a potent and selective lead for drug development against human African trypanosomiasis. *Biochem Pharmacol* **80:** 1478–1486.

Klee, N., Wong, P.E., Baragana, B., Mazouni, F.E., Phillips, M.A., Barrett, M.P., and Gilbert, I.H. (2010) Selective deliv-ery of 2-hydroxy APA to *Trypanosoma brucei* using the melamine motif. *Bioorg Med Chem Lett* **20:** 4364–4366.

Lawley, P.D., and Phillips, D.H. (1996) DNA adducts from chemotherapeutic agents. *Mutat Res* **355:** 13–40.

Lehoczky, P., McHugh, P.J., and Chovanec, M. (2007) DNA interstrand cross-link repair in *Saccharomyces cerevisiae*. *FEMS Microbiol Rev* **31:** 109–133.

Li, X., and Moses, R.E. (2003) The beta-lactamase motif in Snm1 is required for repair of DNA double-strand breaks caused by interstrand crosslinks in *S. cerevisiae*. *DNA Repair (Amst)* **2:** 121–129.

Li, X., Hejna, J., and Moses, R.E. (2005) The yeast Snm1 protein is a DNA 5′-exonuclease. *DNA Repair (Amst)* **4:** 163–170.

Li, Z., Han, J., Jiang, Y., Browne, P., Knox, R.J., and Hu, L. (2003) Nitrobenzocyclophosphamides as potential prod-rugs for bioreductive activation: synthesis, stability, enzy-matic reduction, and antiproliferative activity in cell culture. *Bioorg Med Chem* **11:** 4171–4178.

McHugh, P.J., Spanswick, V.J., and Hartley, J.A. (2001) Repair of DNA interstrand crosslinks: molecular mecha-nisms and clinical relevance. *Lancet Oncol* **2:** 483–490.

Magana-Schwencke, N., Henriques, J.A., Chanet, R., and Moustacchi, E. (1982) The fate of 8-methoxypsoralen pho-toinduced crosslinks in nuclear and mitochondrial yeast DNA: comparison of wild-type and repair-deficient strains. *Proc Natl Acad Sci USA* **79:** 1722–1726.

Munari, F.M., Revers, L.F., Cardone, J.M., Immich, B.F.,

Moura, D.J., Guecheva, T.N., *et al*. (2014) Sak1 kinase interacts with Pso2 nuclease in response to DNA damage induced by interstrand crosslink-inducing agents in *Saccharomyces cerevisiae*. *J Photochem Photobiol B* **130:** 241–253.

Novoselova, T.V., Rose, R.S., Marks, H.M., and Sullivan, J.A. (2013) SUMOylation regulates the homologous to E6-AP carboxyl terminus (HECT) ubiquitin ligase Rsp5p. *J Biol Chem* **288:** 10308–10317.

O'Connor, P.M., and Kohn, K.W. (1990) Comparative pharmacokinetics of DNA lesion formation and removal follow-ing treatment of L1210 cells with nitrogen mustards. *Cancer Commun* **2:** 387–394.

Pagano, G., Manini, P., and Bagchi, D. (2003) Oxidative stress-related mechanisms are associated with xenobiotics exerting excess toxicity to Fanconi anemia cells. *Environ Health Perspect* **111:** 1699–1703.

Papadopoulou, M.V., Trunz, B.B., Bloomer, W.D., McKenzie, C., Wilkinson, S.R., Prasittichai, C., *et al*. (2011) Novel 3-nitro-1H-1,2,4-triazole-based aliphatic and aromatic amines as anti-chagasic agents. *J Med Chem* **54:** 8214–8223.

Papadopoulou, M.V., Bloomer, W.D., Rosenzweig, H.S., Chatelain, E., Kaiser, M., Wilkinson, S.R., *et al*. (2012) Novel 3-nitro-1H-1,2,4-triazole-based amides and sulfonamides as potential antitrypanosomal agents. *J Med Chem* **55:** 5554–5565.

Papadopoulou, M.V., Bloomer, W.D., Rosenzweig, H.S., Ashworth, R., Wilkinson, S.R., Kaiser, M., *et al*. (2013) Novel 3-nitro-1H-1,2,4-triazole-based compounds as potential anti-Chagasic drugs: in vivo studies. *Future Med Chem* **5:** 1763–1776.

Paz, M.M., Zhang, X., Lu, J., and Holmgren, A. (2012) A new mechanism of action for the anticancer drug mitomycin C: mechanism-based inhibition of thioredoxin reductase. *Chem Res Toxicol* **25:** 1502–1511.

Rabik, C.A., and Dolan, M.E. (2007) Molecular mechanisms of resistance and toxicity associated with platinating agents. *Cancer Treat Rev* **33:** 9–23.

Ruhland, A., Kircher, M., Wilborn, F., and Brendel, M. (1981a) A yeast mutant specifically sensitive to bifunctional alkylation. *Mutat Res* **91:** 457–462.

Ruhland, A., Haase, E., Siede, W., and Brendel, M. (1981b) Isolation of yeast mutants sensitive to the bifunctional alkylating agent nitrogen mustard. *Mol Gen Genet* **181:** 346–351.

Schmittgen, T.D., and Livak, K.J. (2008) Analyzing real-time PCR data by the comparative C(T) method. *Nat Protoc* **3:** 1101–1108.

Sengerova, B., Wang, A.T., and McHugh, P.J. (2011) Orches-trating the nucleases involved in DNA interstrand cross-link (ICL) repair. *Cell Cycle* **10:** 3999–4008.

Sharma, M., and Tomasz, M. (1994) Conjugation of glutathione and other thiols with bioreductively activated mitomycin C. Effect of thiols on the reductive activation rate. *Chem Res Toxicol* **7:** 390–400.

Siddik, Z.H. (2003) Cisplatin: mode of cytotoxic action and molecular basis of resistance. *Oncogene* **22:** 7265– 7279.

Stewart, M.L., Bueno, G.J., Baliani, A., Klenke, B., Brun, R., Brock, J.M., *et al*. (2004) Trypanocidal activity of melamine-based nitroheterocycles. *Antimicrob Agents Chemother* **48:** 1733–1738.

Taylor, M.C., Kaur, H., Blessington, B., Kelly, J.M., and Wilkinson, S.R. (2008) Validation of spermidine synthase as a drug target in African trypanosomes. *Biochem J* **409:** 563–569.

Tiefenbach, T., and Junop, M. (2012) Pso2 (SNM1) is a DNA structure-specific endonuclease. *Nucleic Acids Res* **40:** 2131–2139.

UNFAO (2004) *Programme against African trypanosomosis – the disease*. URL http://www.fao.org/ag/againfo/programmes/en/paat/disease.html

Ward, T.A., Dudasova, Z., Sarkar, S., Bhide, M.R., Vlasakova, D., Chovanec, M., and McHugh, P.J. (2012) Components of a Fanconi-like pathway control Pso2-independent DNA interstrand crosslink repair in yeast. *PLoS Genet* **8:** e1002884.

WHO (2014) Human African trypanosomiasis (sleeping sickness). *Factsheet* **259:**. URL http://www.who.int/mediacentre/factsheets/fs259/en/

Wilkinson, S.R., and Kelly, J.M. (2009) Trypanocidal drugs: mechanisms, resistance and new targets. *Expert Rev Mol Med* **11:** e31.

Wilkinson, S.R., Horn, D., Prathalingam, S.R., and Kelly, J.M. (2003) RNA interference identifies two hydroperoxide metabolizing enzymes that are essential to the bloodstream form of the African trypanosome. *J Biol Chem* **278:** 31640–31646.

Wilkinson, S.R., Taylor, M.C., Horn, D., Kelly, J.M., and Cheeseman, I. (2008) A mechanism for cross-resistance to nifurtimox and benznidazole in trypanosomes. *Proc Natl Acad Sci USA* **105:** 5022–5027.

Yang, K., Moldovan, G.L., and D'Andrea, A.D. (2010) RAD18-dependent recruitment of SNM1A to DNA repair complexes by a ubiquitin-binding zinc finger. *J Biol Chem* **285:** 19085– 19091.

Molecular Microbiology (2017) 106(2), 207–222 doi:10.1111/mmi.13767 First published online 31 August 2017

Distinct activation mechanisms trigger the trypanocidal activity of DNA damaging prodrugs

Emma Louise Meredith,[1†] Ambika Kumar,[1†] Aya Konno,[1] Joanna Szular,[1] Sam Alsford,[2] Karin Seifert,[2] David Horn [3] and Shane R. Wilkinson [1*]

[1]School of Biological and Chemical Sciences, Queen Mary University of London, Mile End Road, London, E1 4NS, UK.

[2]Department of Infectious and Tropical Diseases, London School of Hygiene and Tropical Medicine, Keppel Street, London, UK.

[3]The Wellcome Trust Centre for Anti-Infectives Research, School of Life Sciences, University of Dundee, Dundee, UK.

Summary

Quinone-based compounds have been exploited to treat infectious diseases and cancer, with such chemicals often functioning as inhibitors of key met-abolic pathways or as prodrugs. Here, we screened an aziridinyl 1,4-benzoquinone (ABQ) library against the causative agents of trypanosomiasis, and cutane-ous leishmaniasis, identifying several potent struc-tures that exhibited EC_{50} values of <100 nM. However, these compounds also displayed signifi-cant toxicity towards mammalian cells indicating that they are not suitable therapies for systemic infec-tions. Using anti-T. brucei ABQs as chemical probes, we demonstrated that these exhibit different trypano-cidal modes of action. Many functioned as type I nitroreductase (TbNTR) or cytochrome P450 reduc-tase (TbCPR) dependent prodrugs that, following activation, generate metabolites which promote DNA damage, specifically interstrand crosslinks (ICLs). Trypanosomes lacking TbSNM1, a nuclease that spe-cifically repairs ICLs, are hypersensitive to most ABQ prodrugs, a phenotype exacerbated in cells also engineered to express elevated levels of TbNTR or TbCPR. In contrast, ABQs that contain substituent groups on the biologically active aziridine do not function as TbNTR or TbCPR-activated prodrugs and do not promote DNA damage. By unravelling how ABQs mediate their activities, features that facilitate the desired anti-parasitic growth inhibitory effects could be incorporated into new, safer compounds targeting these neglected tropical diseases.

Accepted 4 August, 2017. *For correspondence. E-mail s.r.wilkinson@ qmul.ac.uk; Tel. 144 (0)20 7882 3057; Fax 144 20 882 7732. †These authors contributed equally to this work.

Introduction

The protozoan parasites Trypanosoma brucei, T. cruzi and various Leishmania species are the etiological agents of human African trypanosomiasis (HAT), Cha-gas disease and Leishmaniasis, respectively. Spread by the hematophagous habits of insect vectors, these pathogens cause more than 55,000 deaths per year and are prevalent in many regions of the world least able to deal with the associated economic burden (http://www.dndi.org/diseases-projects/). Implementation of new sur-veillance and treatment programmes in conjunction with improved housing and vector control strategies has resulted in a dramatic reduction in disease prevalence. For example, the number of new cases of HAT has fallen from an estimated peak of 450,000 in 1997 to below 20,000 in 2014 while Chagas disease has been eliminated from Chile, Uruguay and several regions of Argentina and Brazil (Barrett, 2006; Schofield et al., 2006; WHO, 2014). The success of such strategies has led to the World Health Organization (WHO) aiming to eliminate HAT as a public health problem by 2020 (WHO, 2013).

Currently, drugs represent the only viable option to combat trypanosomal and leishmanial infections although their use is problematic. They often require supervision for administration, can be costly, have lim-ited efficacy and may cause significant toxicity. Addition-ally, drug resistance is beginning to further limit the efficacy of the available chemotherapeutic arsenal, with antimonials no longer recommended as a first line treat-ment for leishmaniasis on the Indian sub-continent (Wilkinson and Kelly, 2009; Barrett and Croft, 2012; Alsford et al., 2013; Perry et al., 2015). In the case of HAT and Chagas disease, the front line treatments involve nitroheterocyclic-based prodrugs with nifurtimox

or benznidazole monotherapies used to target T. cruzi while nifurtimox, in combination with difluoromethylornithine (DFMO), is used against a form of HAT prevalent throughout West and Central Africa (Priotto et al., 2009; Yun et al., 2010; Wilkinson et al., 2011). To mediate their trypanocidal effects, nifurtimox and benznidazole undergo an activation reaction catalysed by an FMN-containing, mitochondrial type I nitroreductase (NTR), generating cytotoxic reduction products (Wilkinson et al., 2008; Hall et al., 2011; Hall and Wilkinson, 2012). For nifurtimox, this results in the production of an unsatu-rated open chain nitrile while benznidazole is processed to glyoxal via a series of highly reactive intermediates. As type I NTRs are expressed by some unicellular eukar-yotes (including trypanosomes and Leishmania) but not by metazoan organisms, the bioreductive activity of this enzyme has been exploited to develop a series of novel antiparasitic nitroaromatic- and benzoquinone-based pro-drugs (Wilkinson et al., 2011; Patterson and Wyllie, 2014). Several of these display significant potency against T. brucei in vitro while exhibiting little or no toxicity towards cultured mammalian cells.

Quinones represent a class of organic compounds that contain two carbonyl groups attached to a six mem-bered carbocyclic backbone. They are ubiquitous in nature, functioning in various oxidoreductase cascades, with some natural and synthetic variants being of phar-macological interest. In the latter case, many quinone-based agents often function as prodrugs and must undergo activation before they can mediate their cyto-toxic effects, reactions catalysed by quinone oxidoreduc-tases (McKeown et al., 2007; Siegel et al., 2012). Based on oxygen-sensitivity, such enzymes can be divided into two groups. Oxygen-sensitive quinone oxidoreductases, such as NADH cytochrome b5 reductase and cyto-chrome P450 reductase (CPR), can mediate the $1e^-$ reduction of one of the quinone's carbonyl oxygens to form an unstable semiquinone radical that, under hypoxic conditions, can be further reduced to the hydro-quinone derivative (Powis, 1989; O'Brien, 1991). How-ever, in the presence of oxygen, the semiquinone radical can undergo futile cycling, generating superoxide anions and regeneration of the parent compound. In contrast, oxygen-insensitive quinone oxidoreductases, such as NAD(P)H quinone oxidoreductase 1 (NQO1), cat-alyse the simultaneous $1e^-$ reduction of both the qui-none's carbonyl oxygens to form the hydroquinone directly (Ernster et al., 1962; Iyanagi and Yamazaki, 1970; Siegel et al., 2012). Dependent on structural context, this conversion can result in stable pharmacologically active products, as is the case for the benzoquinone ansamycin antibiotics, or unstable metabolites that undergo further rearrangement before exerting their toxic effects, as seen with the antitumor agents mitomycin A and b-lapachone (Siegel et al., 2012).

Due to their favorable redox and electrochemical properties, compounds containing a quinone pharmacophore represent attractive scaffolds for antimicrobial drug development (Pinto and de Castro, 2009; Beena and Rawat, 2013). Screening against trypanosomes has resulted in the identification of various natural and synthetic lead structures postulated to function as prodrugs promoting oxidative stress within the parasite or through formation of toxic bioreductive products (Henderson et al., 1988; Kubata et al., 2002; Hoet et al., 2004; Pinto and de Castro, 2009; Ramos et al., 2009; Garavaglia et al., 2010; Hall et al., 2012). Using recombinant T. brucei that lack TbSNM1, a DNA repair enzyme that specifically fixes interstrand crosslinks (ICLs) (Sullivan et al., 2015), while expressing elevated levels of oxygen-sensitive (TbCPR) or –insensitive (TbNTR) quinone oxidoreductases, we demonstrate that many aziridinyl 1,4-benzoquinones (ABQs) possess significant potency towards trypanosomatid parasites, with different struc-tures undergoing distinct activation mechanisms to gen-erate metabolites that subsequently promote DNA damage within the parasite nucleus.

Results

Antiparasitic activity of aziridinyl benzoquinones

Compounds containing an ABQ core display potent anti-cancer properties particularly against cells where NADPH quinone oxidoreductase 1 (NQO1) expression is upregulated (Lin et al., 1972; Lusthof et al., 1989; Dehn et al., 2004). Recently, the antiparasitic activities of such compounds towards Plasmodium falciparum and T. brucei has been investigated with several poten-tial lead structures identified (Grellier et al., 2010; Hall et al., 2012). Here, we have expanded on these initial trypanosomal screens to evaluate the growth inhibitory properties of a larger ABQ library against T. brucei, T. cruzi and L. major (Table 1). Out of the 34 compounds tested, 20, 14 and 16 had no effect on T. brucei, T. cruzi and L. major growth, respectively, at concentrations of up to 10 mM. These were not analysed further. For the remaining compounds, RH1 exhibited potencies, expressed as the compound concentration that inhibits cell growth by 50% (EC_{50}), of <100 nM towards blood-stream form T. brucei, with a further five (DZQ, ABQ3, ABQ6, TZQ and ABQ22) exhibiting moderate potency towards this parasite (EC_{50} values of 100–500 nM). Against T. cruzi epimastigotes, DZQ, TZQ and RH1 were highly active, yielding EC_{50} values <10 nM, with others displaying high (EC_{50} values between 10 and

Table 1. Potency of aziridinyl benzoquinones.

	T. brucei[a]		T. cruzi		L. major		THP-1[b]
Compound	EC_{50} (nM)	SI	EC_{50} (nM)	SI	EC_{50} (nM)	SI	EC_{50} (nM)
Nifurtimox	2700 6 100	>37	2600 6 400	>38	6280 6 40	>16	>100000
ABQ7, 9–12, 16–19, 28, 31, 32, 34	>10000	–	>10000		>10000		–
DZQ	272 6 1	1	5 6 1	36	60 6 1	3	181 6 5
MeDZQ	698 6 57	1	55 6 2	16	560 6 139	2	885 6 23
ABQ3[c]	400 6 30	–	6200 6 1160	–	199 6 4	–	–
ABQ4	1180 6 160	–	106 6 25	–	663 6 6	–	–
RH1	19 6 1	<5	3 6 1	<33	68 6 1	<1<100	
ABQ6	283 6 41	2	205 6 53	5	664 6 2	2	1067 6 159
ABQ8	670 6 30	4	1300 6 108	2	1870 6 184	2	29516 770
ABQ13	>10000	–	5550 6 240	–	>10000	–	–
ABQ14	>10000	–	445 6 30	–	2270 6 17	–	–
ABQ15	>10000	–	3310 6 200	–	>10000	–	–
AZQ	8233 6 272	–	6000 6 283	–	>10000	–	–
TZQ	179 6 1	<1	3 6 1	<33	9 6 1	<11	<100
ABQ22	148 6 1	1	55 6 2	3	218 6 20	1	138 6 25
ABQ23	2300 6 60	<1	2180 6 670	<1	348 6 166	1	<400
ABQ24	1470 6 120	<1	37 6 1	<11	473 6 123	<1<400	
ABQ25	>10000	–	–	–	80 6 6	–	–
ABQ26	>10000	–	8638 6 736	–	2360 6 230	–	–
ABQ27	>10000	–	620 6 180	–	210 6 10	–	–
ABQ29	–	–	975 6 25	–	175 6 5	–	–
ABQ30	7400 6 190	<1	980 6 25	4	174 6 10	22	3750 6 320
ABQ33	>10000	–	>10000	–	8157 6 80	–	–

Data represent the EC_{50} values of various ABQs towards bloodstream form T. brucei, T. cruzi epimastigotes, L. major promastigotes and differentiated THP-1 cells. All values are means 6 standard deviation of four (parasites) or three (mammalian cells) independent experiments.
a. Activity of DZQ, MeDZQ, RH1, TZQ and ABQ's 6–9, 14, 15, 20, 22 against T. brucei was previously reported (Hall et al., 2012).
b. Differentiated THP-1 EC_{50} value towards nifurtimox taken from (Voak et al., 2013). The Selectivity Index (SI) of certain compounds (fold difference in EC_{50} values of the THP-1 line relative to parasite) is noted.
c. ABQ3 was unstable with its potency diminishing following repeated freeze/thawing.

100 nM; MeDZQ, ABQ22 and ABQ24) or moderate (EC_{50} values between 100 and 500 nM; ABQ4, ABQ6 and ABQ14) growth inhibitory effects. When tested against L. major promastigotes, TZQ exhibited an EC_{50} of <10 nM, with three other compounds (DZQ, RH1 and ABQ25) exhibiting high potency and eight others yielding moderate potency. Of all the ABQs analysed, RH1 was the most potent agent tested against all three parasites, yielding EC_{50} values of 19 6 1, 3 6 1 and 68 6 1 nM against T. brucei, T. cruzi and L. major, respectively.

Cytotoxicity against mammalian cells

To evaluate whether those ABQs that displayed activity against the three trypanosomatid parasites exhibited toxicity to mammalian cells, their inhibitory properties against differentiated THP-1 cells was determined (Table 1). For all structures tested, an in vitro toxicity was observed (EC_{50} values <10 mM), with two compounds, including RH1, being extremely toxic and yielding EC_{50} values of <100 nM. Comparison of the mammalian toxicity and antiparasitic EC_{50} data allowed a crude measure of each agent's selectivity (the Selectivity Index or SI) toward the pathogen. In many cases, the ABQs displayed a higher potency against THP-1 cells relative to the parasite, resulting in a SI value <1. Of those that did display preferential activity against the parasite, the observed selective toxicity of most was equivalent to that seen with nifurtimox, an agent whose use in humans is problematic. The toxicity of these compounds towards cultured mammalian cells precluded any attempt to establish the potency of these structures against the intracellular amastigote forms of T. cruzi and L. major.

As THP-1 cells are an immortal human monocyte line and ABQs have potent activity against cancerous cells (Tan et al., 1984; Lee et al., 1986; Moore et al., 1997), a series of screens using a selected quinone series on non-cancerous mouse peritoneal macrophages were performed. For DZQ, RH1, TZQ and ABQ22, substantial toxicity towards this line was observed with the compounds generating EC_{50} values of 255, <100, <100 and 120 nM, respectively. This clearly demonstrates that ABQs are toxic to primary cells, thus supporting our THP-1 findings. In light of the mammalian toxicity issues, our focus on ABQs switched from exploring them as potential treatments for infectious diseases to

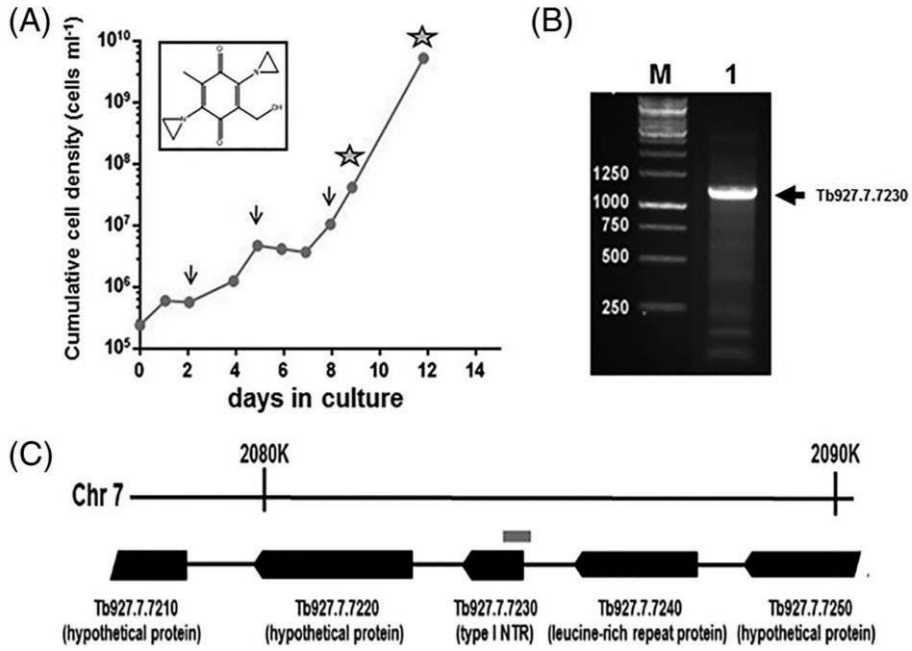

Fig. 1. Screening for RH1 resistant determinants using a genome-scale T. brucei RNAi library.

A. The bloodstream form T. brucei RNAi library (Alsford et al., 2012) was co-treated with RH1 (30 nM) and tetracycline (1 mg ml^{21}), the latter to induce RNAi, with the cumulative cell growth of the culture followed. The arrows correspond to culture dilution and addition of fresh RH1 (30 nM) and tetracycline (1 mg ml^{21}). Genomic DNA (as indicated by stars) was extracted from parasites at days 9 and 12. Insert shows structure of RH1.

B. Amplification of the RNAi target from the RH1 screen using genomic DNA extracted on day 9 of selection and the LIB2f (TAGCCCCTCGAGGGCCAGT) and LIB2r (GGAATTCGATATCAAGCTTGGC) primers (lane 1) produced a major fragment mapping to the type I nitroreductase (Tbntr) locus (gene id Tb927.7.7230 on the TriTrypDB; http://tritrypdb.org/tritrypdb/). M indicates a size marker in bp.

C. Genetic map (black boxes represent protein-coding sequences) of the Tbntr locus, indicating the location of the major RNAi target fragment (grey box) recovered from the library following RH1-selection.

using them as tools to dissect trypanosomal pro-drug activation pathways and the structure-activity relation-ships among this class of compound.

Different trypanosomal mechanisms activate aziridinyl benzoquinone prodrugs

The application of genome-scale RNAi screens has helped elucidate the trypanocidal mechanism of action of a number of agents and identify how the affected path-ways may impinge on drug resistance (Alsford et al., 2012; 2013). As an initial step to understanding how ABQs mediate their antiparasitic activities, a loss-of-function screen was conducted on bloodstream form T. brucei, using RH1 as the selective agent (Fig. 1A). Treat-ment of the parasite RNAi library with this compound resulted in reduced T. brucei growth over the first week followed by the outgrowth of an RH1-resistant population. Genomic DNA was extracted from the RH1-selected cells and RNAi targets were amplified, from which a single 1.1 kbp fragment was identified as the major amplicon (Fig. 1B). Sequence analysis and comparison against the reference genome database revealed that this RH1-resistance-associated fragment mapped to a region encompassing the 5^0 untranslated region and 5^0 coding sequence of the open reading frame (Gene ID: Tb927.7.7230 on TriTrypDB - http://tritrypdb.org/tritrypdb/) for the type I nitroreductase, TbNTR (Fig. 1C). This was not unexpected given that this protein had been previ-ously associated with the activation of trypanocidal nitroheterocyclic-based prodrugs, nifurtimox and benzni-dazole (Wilkinson et al., 2008; Baker et al., 2011; Hall et al., 2011; Hall and Wilkinson, 2012) and postulated to function as a NADH dependent quinone oxidoreductase (Wilkinson et al., 2008; Alsford et al., 2012; Hall et al., 2012).

To conclusively show that TbNTR is the key activator of ABQs, we evaluated the susceptibility of a T. brucei Tbntr heterozygote line to RH1. These recombinant cells displayed an EC_{50} approximately 2.5-fold greater than that observed using wild type parasites (Fig. 2A) confirming that reduction of TbNTR expression through loss of one of the alleles encoding for this oxidoreduc-tase is sufficient to generate resistance to RH1. As reduction of TbNTR activity leads to RH1 resistance, gain of function via over expression of the oxidoreduc-tase should have the converse effect, generating cells that are more susceptible to the ABQ. To determine if

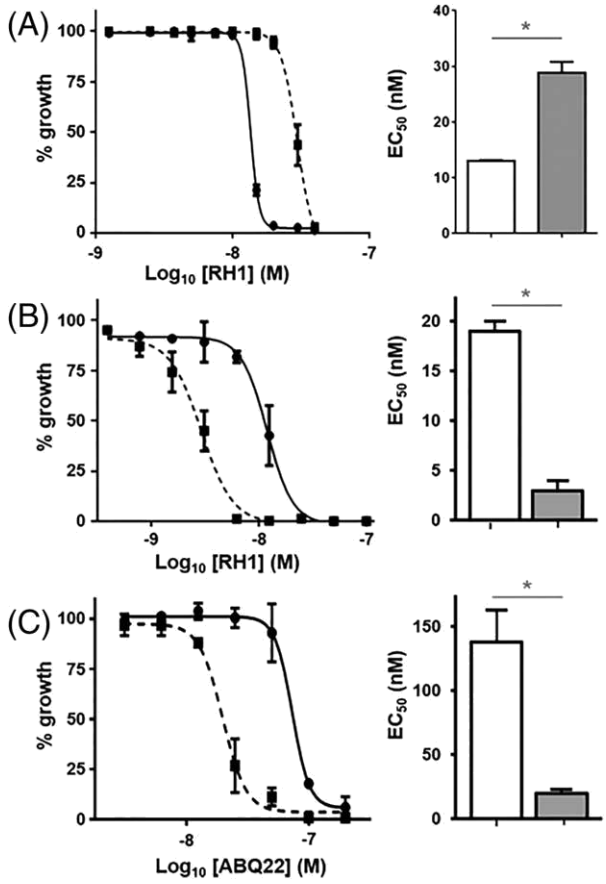

Fig. 2. Susceptibility of T. brucei expressing altered levels of activator to RH1 or ABQ22.

A. Dose response curve of wild type (solid line) and Tbntr heterozygous (dotted line) T. brucei to RH1. The extrapolated EC_{50} values (in nM) of wild type (white bar) and Tbntr heterozygous (grey bar) T. brucei to RH1 are shown.

B. Dose response curve of wild type (solid line) and TbNTR overexpressing (dotted line) T. brucei to RH1. The EC_{50} values (in nM) of wild type (white bar) and TbNTR overexpressing (grey bar) T. brucei to RH1 are shown.

C. Dose response curve of wild type (solid line) and TbCPR2 overexpressing (dotted line) T. brucei to ABQ22. The extrapolated EC_{50} values (in nM) of wild type (white bar) and TbCPR2 overexpressing (grey bar) T. brucei to RH1 are shown.

All data are means for experiments performed in quadruplicate 6 standard deviation. The asterisk indicates significant differences in susceptibility ($P < 0.01$) between wild type and genetically modified cells to RH1, as assessed by Student's t test (GraphPad Software).

this was the case, the quinone-sensitivity of a T. brucei line engineered to express elevated levels of the enzyme was evaluated. In agreement with previous findings, parasites over expressing TbNTR were hyper-sensitive (approximately fourfold) to RH1 as compared to controls (Fig. 2B).

To determine whether TbNTR plays a role in activat-ing other ABQs, the susceptibility of TbNTR over expressing parasites towards a selected group of com-pounds, was tested (Table 2). Out of the additional

Table 2. Growth inhibitory effect of ABQs towards T. brucei expressing elevated levels of potential activators.

	EC_{50} (nM)		
Compound[a]	Control	Tbntr[11]	Tbcpr2[11]
DFMO	27500 6 108	30720 6 1330 (1.12)	33250 6 5123 (1.21)
Nifurtimox	2980 6 30	315 6 15 (0.11*)	–
DZQ	318 6 38	90 6 3(0.28*)	–
MeDZQ	740 6 18	115 6 3(0.16*)	–
RH1	19 6 1	3 6 1(0.16*)	20 6 3 (1.05)
TZQ	225 6 26	60 6 9(0.27*)	284 6 13 (1.26)
ABQ22	138 6 25	148 6 9(1.07)	20 6 3 (0.14**)
ABQ23	2935 6 420	3315 6 540 (1.13)	3556 6 96 (1.21)
ABQ24	1470 6 120	2090 6 160 (1.42)	1698 6 23 (1.16)
ABQ30	7400 6 190	8670 6 1670 (1.12)	–

Data represent the EC_{50} values of parasites expressing wild type (control), elevated levels of TbNTR (Tbntr[11]) or TbCPR2 (Tbcpr2[11]). All values are means 6 standard deviation of four inde-pendent experiments. The fold difference in EC_{50} values of the over expressing lines relative to control is given in parentheses. Para-sites over expressing TbCPR3 behaved similarly to those express-ing elevated levels of TbCPR2.

a. Trypanocidal activity of DZQ MeDZQ, RH1, ABQ6, TZQ and ABQ22 towards T. brucei cells over expressing Tbntr was previ-ously reported (Hall et al., 2012).

*The difference in susceptibility of wild type and Tbntr[11] lines to nifurtimox, DZQ, MeDZQ, RH1 and TZQ was statistically significant ($P < 0.01$), as assessed by Student's t test.

**The difference in susceptibility of wild type and Tbcpr[11] lines to ABQ22 was statistically significant ($P < 0.01$), as assessed by Stu-dent's t test.

compounds screened, three (DZQ, MeDZQ and TZQ) showed the same hypersensitivity profile as RH1, with TbNTR over expressing T. brucei being up to 3.5-fold more susceptible to the aziridinyl agents than controls. In contrast, ABQ22–24 and 30 did not follow this pat-tern, with the TbNTR over expressers exhibiting an EC_{50} equivalent to that observed against control cells.

Dependent on backbone configuration, the carbonyl oxygen atoms in a quinone can undergo 1 or $2e^-$ reduc-tion, with the former reaction carried out by a range of ubiquitous flavoproteins, including CPR, while the latter is catalysed by enzymes, such as NQO1 and type I NTRs. To determine whether the trypanocidal activity displayed by selected ABQs can undergo activation via a $1e^-$ reduction mechanism, the susceptibility of T. bru-cei lines engineered to express ectopic copies of the TbCPR2 or 3 (Hall et al., 2011) to RH1, TZQ and ABQ22–24 was evaluated (Table 2). With RH1, TZQ, ABQ23 and ABQ24, the TbCPR over expressing lines exhibited EC_{50} values similar to those observed using control cells, indicating that the $1e^-$ reduction pathway plays no significant role in their activation. When the T. brucei line expressing elevated levels of TbCPR2 or 3 was tested against ABQ22, the recombinant lines were hypersensitive to this tetra-aziridinyl agent relative to controls (Fig. 2C).

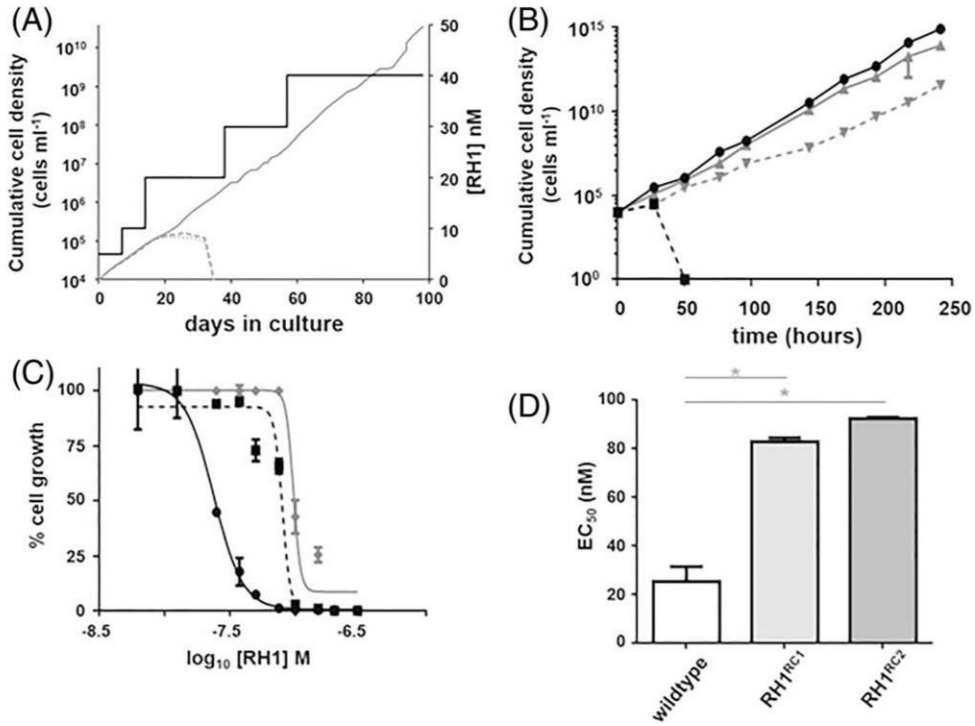

Fig. 3. RH1 resistance selection in T. brucei.
A. Selection of RH1 resistant T. brucei was performed by the stepwise increase of the ABQ (black line). The cumulative cell density of three independent cultures (grey lines) were monitored throughout the selection with only one of these ($RH1^R$) generating an outgrowth in medium containing >20 nM RH1. Clones from the $RH1^R$ culture were then generated following limiting dilution.
B. Cumulative cell density of wild type T. brucei (black lines) and a clone ($RH1^{RC1}$) derived from $RH1^R$ (grey lines) grown in medium lacking (solid lines) or containing 40 nM RH1 (dashed lines). Data points are averages 6 standard deviation from experiments performed in quadruplicate. A second $RH1^R$ derived clone ($RH1^{RC2}$) analysed in parallel displayed similar growth properties (data not shown).
C. Dose response curves of wild type T. brucei (black solid line), $RH1^{RC1}$ (black dashed line) and $RH1^{RC2}$ (grey solid line) to RH1. All data points are averages from experiments performed in quadruplicate 6 standard deviation.
D. Susceptibility of T. brucei to RH1 as judged by the EC_{50} values (in nM). The asterisk indicates significant differences in susceptibility ($P < 0.001$) between wild type and genetically modified cells to RH1, as assessed by Student's t test (GraphPad Software).

Based on the above data, the trypanocidal activity of ABQs can be divided into compounds such as RH1 and TZQ that function as TbNTR-dependent (oxygen-insensitive quinone oxidoreductase) prodrugs, structures including ABQ22 that function as TbCPR-dependent (oxygen-sensitive quinone oxidoreductase) prodrugs and agents such as ABQ23 and 24 that are not activated by either of these two mechanisms: ABQ23 and 24 may still function as prodrugs undergoing activation by an alternative mechanism(s) to that explored here.

Trypanosomes selected for resistance toward RH1 have reduced NTR expression

A further approach to determine how ABQs mediate their trypanocidal activity involved the selection of T. brucei lines resistant to RH1. Wild type bloodstream form parasites were grown in the presence of RH1 over a 100 day period, starting with a compound concentra-tion that inhibits T. brucei growth by 10% (5 nM) and progressively increasing this to twice the EC_{50} (40 nM) (Fig. 3A). The cumulative cell density of selected cul-tures was followed throughout the experiment. Of the three replica cultures analysed, two stopped growing when the selective pressure was increased to 20 nM. In contrast, cells in the third culture remained viable in 40 nM RH1 and parasites in this population were cloned by limiting dilution (designated as $RH1^{RC}$). We then evaluated the growth properties of two $RH1^{RC}$ lines ($RH1^{RC1}$ and $RH1^{RC2}$) (Fig. 3B). In the absence of RH1, the doubling time of the two clones was comparable to the parental line (doubling time of 7.5 hours). When grown in medium containing RH1 (40 nM), the doubling time of the resistant clones increased 1.5-fold (dou-bling time of 10.5 hours); by comparison, no growth of wild type T. brucei was detected after 24 hrs. Next, we determined the susceptibility of the $RH1^{RC}$ lines towards RH1 with this showing that both lines were 3.5-fold less sensitive to the ABQ than wild type (Fig. 3C and D); wild type, $RH1^{RC1}$ and $RH1^{RC2}$ exhibited EC_{50} val-ues of 25 6 6, 83 6 2 and 92 6 1 nM against RH1,

Table 3. Susceptibility of RH1 resistant T. brucei to trypanocidal agents.

Compound	EC_{50} values (nM) Wild type	$RH1^{RC1}$	ratio
Aziridines			
Triethylenemelamine	2400 6 86	2774 664	1.1
ThioTEPA	39423 6 796	56298 61960	1.4
RH1[a]	25 6 6	83 62*	3.3
ABQ22	197 6 31	232 627	1.2
CB1954[a]	2161 6 125	13086 6972*	6.5
Nitrogen mustards			
Mechlorethamine	32063 6 1021	27203 61288	0.8
Melphalan	8740 6 200	10430 6230	1.2
LH17[a]	5438 6 444	17998 61106*	3.6
Nitrosoureas			
Lomustine	16650 6 443	15463 6665	0.9
Semustine	15025 6 3457	17100 63619	1.1
Other agents			
DFMO	16763 6 2691	22177 6383	1.3
Nifurtimox[a]	2700 6 100	7050 6311*	2.6
Megazol[a]	166 6 1	454 64*	2.7

Data represent the growth-inhibitory effect as judged by their EC_{50} values of various agents on BSF T. brucei wild type and $RH1^{RC1}$ cells. All values are means 6 standard deviation from independent experiments preformed in quadruplicate. The ratio represents the fold difference in EC_{50} value between the $RH1^{RC1}$ and wild type lines to a given compound.

a. Identifies TbNTR-activated prodrugs.

*Indicates significant differences in susceptibility ($P < 0.001$) between wild type and $RH1^{RC1}$ lines, as assessed by Student's t test (GraphPad Software).

respectively. This resistance phenotype was not lost following 100 generations in medium lacking RH1. Indeed, the resistant lines were still 4.5-fold less sensitive to the ABQ than controls; wild type, $RH1^{RC1}$ and $RH1^{RC2}$ exhibited EC_{50} values of 19 6 1, 86 6 3 and 91 6 11 nM against RH1, respectively. When the above susceptibility studies were extended to TbNTR-activated prodrugs, cross-resistance towards nifurtimox, benznidazole, megazol, CB1954 and LH17 was observed (Table 3). This phenotype was specific to this class of compound, as the RH1 selected cells were equally sensite to the non TbNTR-activated compounds, including ABQ22 and other ICL inducing agents, as wild type T. brucei.

Studies aimed at deciphering the RH1 resistance mechanism demonstrated that although the Tbntr copy number was similar and Tbntr gene sequences were identical in the compound selected and wild type lines, the $RH1^{RC}$ cells had a lower (50%) Tbntr mRNA expression level (Fig. 4). Intriguingly, when extended to genes expressed in the same polycistron as Tbntr, all the tested ORFs exhibited the same trait in relation to copy number and transcript levels. The observed reduc-tion in gene expression within the Tbntr-containing poly-cistron in the RH1 selected cells is specific to this region as additional ORFs present elsewhere in the T. brucei genome (for example Tb927.7.7490 and Tb927.7.6620, and the genes encoding for the DNA repair enzymes TbSNM1, TbMRE11, TbRAD51, TbXPG, TbEXO1, TbCSB and TbMSH3) are expressed at equivalent levels in $RH1^{RC}$ and control parasites.

Aziridinyl benzoquinones promote cell cycle arrest and DNA damage in trypanosomes

Aziridinyl benzoquinones mediate their toxicity against mammalian cells through formation of ICLs that promote cell cycle arrest and DNA damage (Kim et al., 2004; Dehn et al., 2005; Begleiter et al., 2007). To determine if this is the case in T. brucei, parasites at various stages in the cell cycle were identified in asynchronous cultures by staining their nuclear (N) and mitochondrial (known as the kinetoplast (K)) genomes with DAPI; a non-dividing trypanosome cell usually contains one mito-chondrion and hence one kinetoplast. The ratio of these two DNA-containing structures represents an excellent marker for the trypanosomal cell cycle, with T. brucei in the G1/S phase having a 1N1K arrangement, those in G2/M phase possessing a 1N2K ratio while cells dis-playing a 2N2K profile are in the post-M stage (Wood-ward and Gull, 1990; Siegel et al., 2008; Glover and Horn, 2012). For untreated T. brucei and cells exposed to phleomycin, most (approximately 80%) were in the G1/S stage of the cell cycle with a smaller percentage (12 to 20%) in G2/M (Fig. 5). In contrast, when trypano-somes were treated with RH1 or mechlorethamine (a well characterized ICL inducing agent), 58% and 45% of the cells displayed a configuration typical of the G2/M phase, respectively, with only 37% and 53% exhibiting a 1N1K DNA staining pattern, respectively. This indicates that treatment of T. brucei with RH1 (or mechloreth-amine) results in a G2/M cell cycle arrest phenotype, potentially as a result of damaged DNA and is consist-ent with observations made with mammalian cells (Kim et al., 2004; Dehn et al., 2005).

In most cells, ICLs are repaired through the concerted action of a number of complementary and overlapping pathways with enzymes belonging to the SNM1/PSO2 family playing a specific role. In T. brucei, the enzyme TbSNM1, a member of the SNM1/PSO2 nuclease fam-ily, has been shown to play a specific and key role in repairing such damage (Sullivan et al., 2015). To evalu-ate whether deletion of both copies of Tbsnm1 from the T. brucei genome altered the cells sensitivity to ABQs, the null mutant trypanosomes were grown in the pres-ence of selected trypanocidal quinones and the EC_{50} values for each compound determined (Table 4; Fig. 6). For all the ABQ prodrugs tested, cells lacking the nucle-ase were up to 6.6-fold more susceptible to these

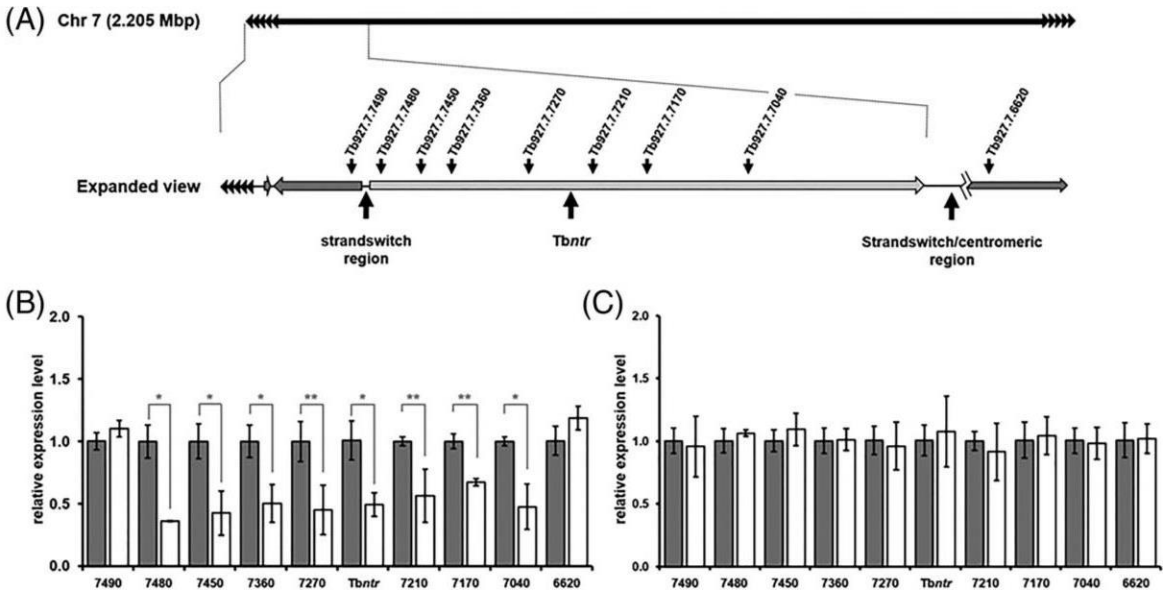

Fig. 4. Evaluating the mechanism underlying RH1 resistance in T. brucei.

A. Schematic of T. brucei chromosome 7 that contains Tbntr. This gene is part of a 200 kbp polycistronic region (see Expanded view) that encodes for 60 open reading frames (ORF) (light grey arrowed box) and is approx. 75 kbp downstream from a 'strandswitch' region, areas on the trypanosomal chromosome that are postulated to be regions where polycistronic transcription is initiated (Imboden et al., 1987; Muhich and Boothroyd, 1988). The position of selected ORFs from the Tbntr-containing polycistronic transcriptional unit plus the telomeric repeats (black arrow repeats) are shown. Other selected polycistrons on chromosome 7 are also highlighted (dark grey arrowed boxes).

B and C. The mRNA levels (panel B) and gene copy number (panel C) of selected ORFs located on chromosome 7 from wild type (grey bar) and $RH1^{RC1}$ (white bar) cells was evaluated by qPCR. This was compared against the expression level/gene copy number of a standardized control (Tbtert) and the average fold difference, as judged by $2–(DDC_T)$ from reactions performed in triplicate 6 standard deviation, plotted as a measure of the relative expression level. The asterisk and double asterisk indicates significant differences in relative mRNA expression levels (P <0.01 and <0.02, respectively) between the wild type and $RH1^{RC1}$, as assessed by Student's t test (GraphPad Software).

structures than control parasites. In contrast, assays using ABQ23 and ABQ24, the two ABQs that do not function as TbNTR- or TbCPR-activated prodrugs, and the trypanocidal agents nifurtimox and DFMO, revealed no significant difference in the EC_{50} exhibited by the engineered and control lines.

To conclusively demonstrate that the above altered susceptibility phenotype was solely due to lack of TbSNM1 activity, the sensitivity of null mutant cells expressing an ectopic copy of Tbsnm1 towards DZQ, RH1 and ABQ22 was evaluated (Fig. 6). In all three cases, the TbSNM1-complemented line generated dose response curves and EC_{50} values distinct from those observed when using TbSNM1 null mutant cells but sim-ilar to those obtained using wild type parasites.

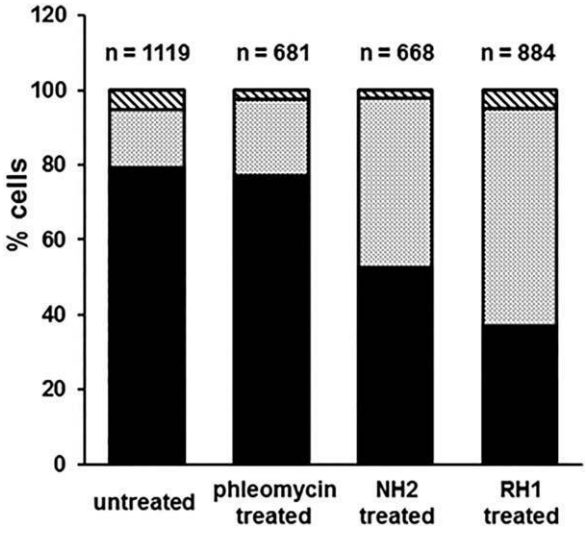

Fig. 5. RH1 promotes cell cycle arrest in T. brucei.

The effect of ICL inducing agents (mechlorethamine (HN2) or RH1) on the trypanosome cell cycle was analysed by determining the relative number of nuclear (N) and mitochondrial (K) genomes structures within a single parasite. T. brucei in the G1/S phase have a 1N1K arrangement (black bar), those in G2/M phase possess a 1N2K ratio (grey bar) while cells displaying a 2N2K profile are in the post-M stage (hatched bar) (Woodward and Gull, 1990; Siegel et al., 2008; Glover and Horn, 2012). The number of cells (n) analysed for each treatment (untreated, phleomycin treated, mechlorethamine (HN2) or RH1) is given.

Linking prodrug activation with DNA damage

To establish whether there is a link between activation of the trypanocidal ABQs and the TbSNM1-mediated DNA repair pathway, the susceptibility of Tbsnm1 null-mutants expressing ectopic copies of Tbntr or Tbcpr2 towards selected compounds was evaluated (Fig. 7). When these lines were treated with RH1 or TZQ, an

Table 4. Susceptibility of T. brucei Tbsnm1 null mutants to ABQ compounds.

Compound	EC_{50} (nM) Control	DTbsnm1	Ratio
Nifurtimox	2850 6 20	2250 6090	0.79
DFMO	27500 6 108	27100 6850	0.99
DZQ	157 6 23	43 62*	0.27
RH1	19 6 1	5 61*	0.26
TZQ	253 6 33	46 61*	0.18
ABQ22	138 6 25	21 65*	0.15
ABQ23	2300 6 60	2410 6160	1.01
ABQ24	1470 6 120	1130 6100	0.77

Data represent the EC_{50} values of selected ABQ compounds towards wild type T. brucei (control) and T. brucei Tbsnm1 null mutants (DTbsnm1). All values are means 6 standard deviation of four independent experiments. The ration of EC_{50} values between the two parasite lines are given. *Indicates significant differences in susceptibility ($P < 0.01$) between the wild type and DTbsnm1 lines, as assessed by Student's t test (GraphPad Software).

increased susceptibility was observed relative to wild type controls (Fig. 7A); Tbsnm1 null-mutants and T. bru-cei over expressing Tbntr were threefold and fivefold more susceptible to RH1, respectively, and 2.7- and 3.4-fold more susceptible to TZQ than wild type T. brucei. For Tbsnm1 null parasites expressing an ectopic copy of Tbntr, this increase in potency was magnified further, with these cells showing a 15-fold increase in suscepti-bility to both compounds as compared against wild type. Extending these studies to investigate the susceptibility of Tbsnm1 null-mutant parasites engineered to express an ectopic copy of Tbcpr2 towards ABQ22 yielded simi-lar results (Fig. 7B). When Tbsnm1 null mutants or wild type cells engineered to express an ectopic copy of Tbcpr2 were treated with ABQ22 a sevenfold increase in susceptibility was observed by both lines compared against controls. The growth inhibitory effect of this compound was further enhanced in trypanosomes that lack TbSNM1 activity while expressing elevated levels of TbCPR2 (Fig. 7B), with these cells being 12.5-fold more sensitive to ABQ22 than wild type. The above altera-tions in susceptibilities were specific to the ABQs as all lines tested exhibited equivalent sensitivities to the non-DNA damaging trypanocidal agent DFMO.

Discussion

ICLs represent a highly toxic form of DNA damage that blocks processes dependent on DNA strand separation, such as replication and transcription. As rapidly dividing cells are particularly susceptible to this type of lesion, agents that are able to promote ICLs are of interest in the treatment of cancer and infectious diseases (Chen and Hu, 2009; Deans and West, 2011; Wilkinson et al., 2011). Here, we report that several ABQs, ICL inducing chemicals originally developed as anti-cancer agents, can also function as highly potent anti-trypanosomatid prodrugs with different structures able to undergo activa-tion via different pathways. In these cases, activation promotes a type of DNA damage that is repaired by a pathway where SNM1, a nuclease that only functions in ICL repair, plays a key role.

Invariably, aziridine-containing compounds function as prodrugs with activation requiring protonation of the azir-idinyl nitrogen. The ease with which this reaction can occur is governed by the compound's chemical compo-sition and how this influences the pKa of the aziridine. For certain structures (e.g., triethylenemelamine, thio-TEPA and 'simple' ABQs including ABQ11) protonation can readily take place in aqueous solution due to the relatively high pKa of the aziridine within such back-bones (Akhtar et al., 1975). However, for other agents, the pKa of the heterocycle is comparatively low,

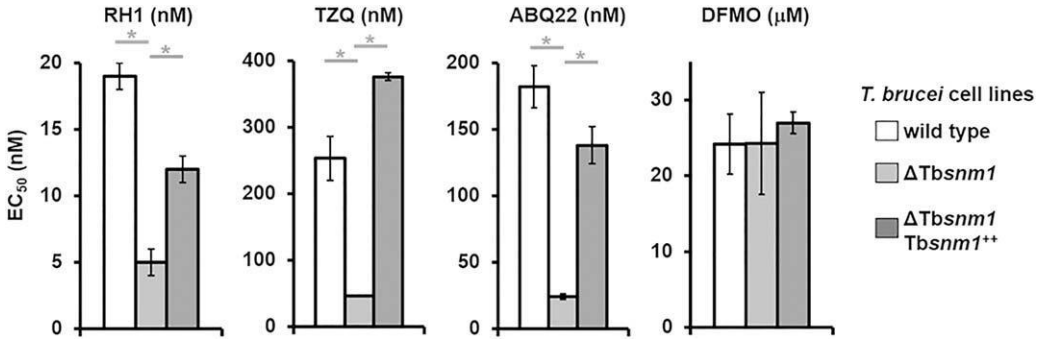

Fig. 6. Susceptibility of T. brucei lines expressing altered levels of TbSNM1 to selected azirindinyl benzoquinones. Growth inhibitory effects, as judged by EC_{50} values, of RH1, TZQ and ABQ22 (all in nM) in the T. brucei wild type, Tbsnm1 null mutant (DTbsnm1) and Tbsnm1 null mutants expressing an ectopic copy of Tbsnm1 (DTbsnm1 $Tbsnm1^{11}$) lines (Sullivan et al., 2015). DFMO (in mM) was used as a non-DNA damaging agent control. Data are mean values 6 standard deviations from experiments performed in quadruplicate. The asterisk indicates significant differences in susceptibility ($P < 0.001$) between wild type and DTbsnm1 or between DTbsnm1 and DTbsnm1 $Tbsnm1^{11}$ cells to RH1, as assessed by Student's t test (GraphPad Software).

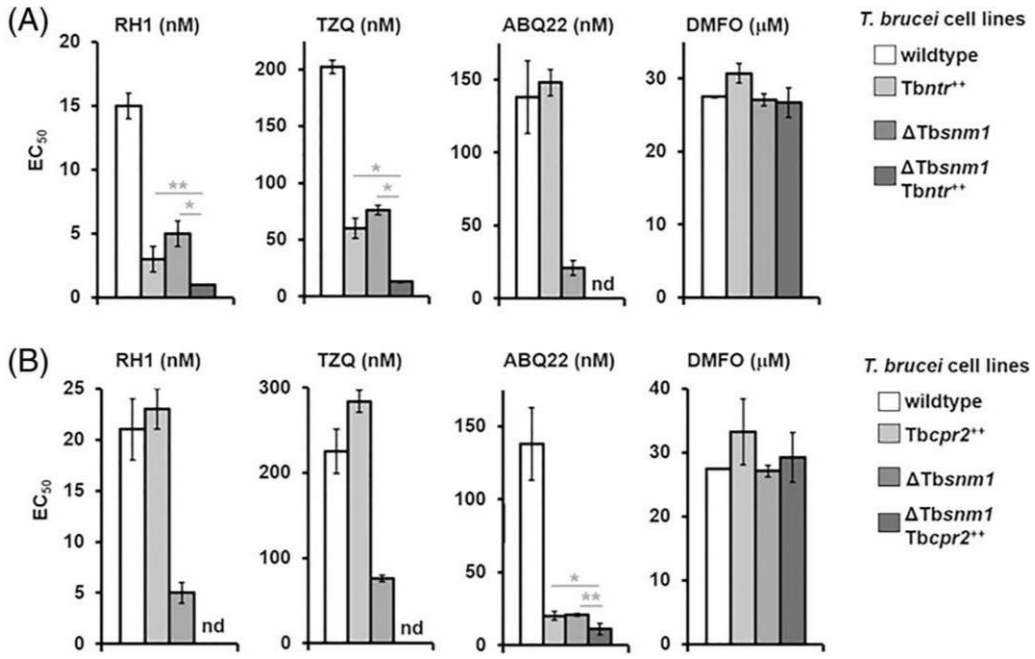

Fig. 7. Linking aziridinyl benzoquinone prodrug activation to DNA damage.
A. Growth inhibitory effects, as judged by EC_{50} values, of RH1, TZQ, ABQ22 (all in nM) and DFMO (in mM) in the T. brucei wild type, T. brucei expressing an ectopic copy of Tbntr (Tbntr^{11}), Tbsnm1 null mutant (DTbsnm1) and Tbsnm1 null mutants expressing elevated levels of Tbntr (DTbsnm1 Tbntr^{11}) lines. The asterisk and double asterisk indicates significant differences in susceptibility (P <0.001 and <0.03, respectively) between the DTbsnm1 Tbntr^{11} line relative to the Tbntr^{11} or DTbsnm1 parasites to RH1 and TZQ, as assessed by Student's t test (GraphPad Software).
B. Growth inhibitory effects, as judged by EC_{50} values, of RH1, TZQ and ABQ22 (all in nM) in the T. brucei wild type, T. brucei expressing an ectopic copy of Tbcpr2 (Tbcpr2^{11}), Tbsnm1 null mutant (DTbsnm1) and Tbsnm1 null mutants expressing elevated levels of Tbcpr2 (DTbsnm1 Tbcpr2^{11}) lines: the latter lines was validated as previous described (Hall et al., 2011; Sullivan et al., 2015). DMFO (in mM) was used as a non-DNA damaging agent control. The asterisk and double asterisk indicates significant differences in susceptibility (P 5 0.01 and P < 0.003, respectively) between the DTbsnm1 Tbcpr2^{11} line relative to the Tbcpr2^{11} or DTbsnm1 parasites to ABQ22, as assessed by Student's t test (GraphPad Software).
Data in panels A and B are mean values 6 standard deviations from experiments performed in quadruplicate.

therefore preventing the above activation event. To cir-cumnavigate this issue, the aziridine motif can be incor-porated into a chemical backbone that also contains a bioreductive moiety, such as a quinone or nitroaromatic. Here, enzymatic reduction of carbonyl oxygen or nitro groups triggers a redistribution of electrons around the associated cyclical structure that can raise the pKa of the aziridinyl ring, and thus facilitating nitrogen protona-tion (Fig. 8A) (Hargreaves et al., 2000).

Using a combination of a whole genome loss-of-function screen, selection of resistant lines and/or functional genomic approaches, we have shown that T. brucei expresses at least two ABQ bioreductive sys-tems. For the eight compounds evaluated as potential prodrugs, half (DZQ, MeDZQ, RH1 and TZQ) were shown to be NTR activated, one (ABQ22) was shown to be dependent on a CPR activity, while the remainder (ABQ23, 24 and 30) were not reduced by any of the systems tested. For those that appeared not to function as prodrugs, this may be due to their structures, as these compounds contain methyl substituted aziridines (Fig. 8B). These alkyl groups may block protonation and thus activation of the aziridinyl nitrogen by lowering this motif's pKa and/or hinder access of oxidoreductases to the carbonyl groups (Lusthof et al., 1989; Phillips et al., 1999). These possibilities may also account for why other compounds that contain methyl/dimethyl aziridine substitutions (e.g., ABQs 25–30 and 31–34) consistently displayed no or a lower activity against T. brucei than their non-substituted counterparts, mirroring observa-tions made in high throughput oncological screens (Kim et al., 2016).

For those compounds that do function as trypanocidal prodrugs, the nature of the side chains found at the 3,6 positions on the benzoquinone ring appears to influence which activation mechanism predominates (Fig. 8B). For structures possessing small substituents at one or both sites, reduction occurs via a type I NTR activity with this mechanism unaffected by the presence of equivalent (e.g., hydrogen for DZQ, methyl for MeDZQ) or diver-gent (e.g., hydroxymethyl and methyl in RH1, aziridine and hydrogen in TZQ) groupings at the 3,6 positions. Such small side chains may aid type I NTR/compound interaction or help the prodrug (or its activated products)

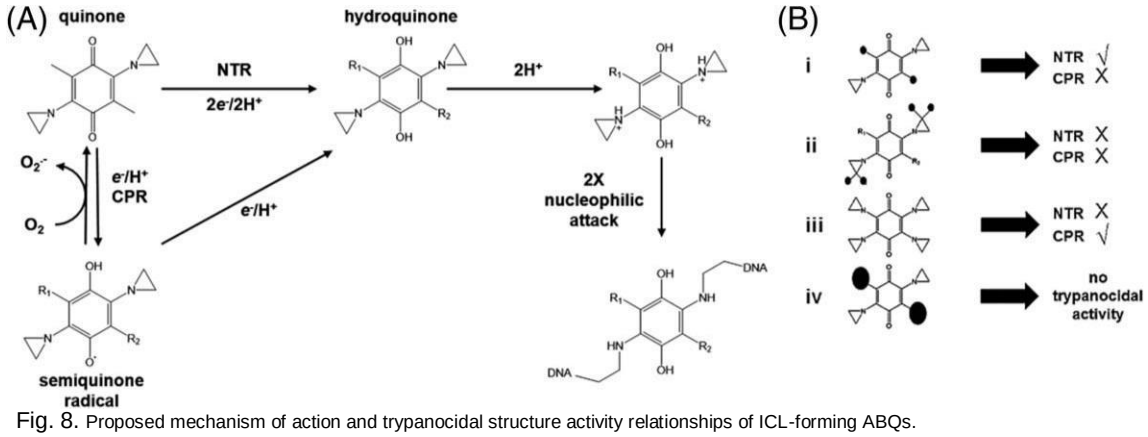

Fig. 8. Proposed mechanism of action and trypanocidal structure activity relationships of ICL-forming ABQs.

A. Quinones can be reduced to hydroquinones by two distinct pathways. In one pathway, enzymes such as cytochrome P450 reductase (CPR) mediate the $1e^{-}$ reduction of the quinone to a semiquinone radical. This then undergoes further reduction to the hydroquinone. In the presence of O_2, the semiquinone can undergo futile cycling to form $O^{\cdot}{}_2^{2}$ and the parental quinone. In the other system, reduction of the quinone to the hydroquinone occurs directly via a $2e^{-}$ reduction event as typified by a type I nitroreductase (NTR) activity. Formation of the hydroquinone then facilitates protonation of the nitrogen atoms in the aziridine rings with these electrophilic intermediates undergoing nucleophilic attack (e.g., by DNA), promoting opening of the aziridinyls, formation of aliphatic amine intermediates and alkylation of the target. As ABQs contain two (or more) aziridinyls they can covalently bind the two complementary DNA strands together resulting in an interstrand crosslink.

B. ABQs (e.g., DZQ, MeDZQ, RH1 and TZQ) possessing small (e.g., hydrogen, methyl, hydroxymethyl) substituent groups (small solid spheres) at the 3,6 positions on a benzoquinone core are more likely to be activated in T. brucei by the type I nitroreductase (NTR) but not by cytochrome P450 reductase (CPR) (i). ABQs that contain methyl substituted (small solid spheres) aziridines (e.g., ABQ23, 24 and 30) are not activated in T. brucei by NTR or CPR (ii). ABQ22, a compound that contains aziridinyl rings at the 3,6 positions on the benzoquinone core, is readily activated within the trypanosome by CPR but not by NTR (iii). ABQs (e.g., ABQ9–19) having bulky substituent groups (large solid spheres) at the 3,6 positions on the benzoquinone ring generally display no significant trypanocidal activity (iv).

gain access to the site(s) of action. In contrast, the presence of bulkier groups (e.g., aziridines for ABQ22) at both sites results in CPR activation. Why this mecha-nism operates to reduce this particular compound is open to speculation but it may reflect a steric hindrance effect such that the four aziridine groups found in ABQ22 preclude TbNTR from interacting with and reducing its quinone carbonyl groups while facilitating associations with TbCPR isoforms. Alternatively, this dif-ference could be due to subcellular localisation such that ABQ22 may be readily transported into the T. brucei endoplasmic reticulum, the organelle where the TbCPRs are believed to reside, but unable to gain access to the parasite's mitochondrion, the site where TbNTR is found (Wilkinson et al., 2008).

Following protonation of the aziridinyl nitrogen, the resultant electrophilic intermediate undergoes nucleophilic attack leading to opening of the heterocyclic ring, formation of an aliphatic amine then alkylation of the target (Fig. 8A) (Hargreaves et al., 2000). If the targeting compound contains multiple aziridinyl groups, as is the case for the ABQs tested here, and the nucleophile is DNA, then two nucleobases within the nucleic acid double helix become covalently crosslinked. In many eukaryotes the SNM1 (also known as PSO2) nuclease plays a key role in resolving such DNA damage, with cells lacking this activity being specifically and highly susceptible to ICL inducing agents (Cattell et al., 2010). By phenotypically screening a selected set of trypanocidal ABQs against a T. brucei snm1 null mutant line, we demonstrated that trypanosomes lacking this DNA repair enzyme were more susceptible to NTR and CPR activated prodrugs relative to wild type. Moreover, in parasites where TbSNM1 was absent but the activation mechanism (either TbNTR or TbCPR) is elevated, this susceptibility phenotype was exacerbated, providing a direct link between the two oxidoreductase activities and DNA damage. Extending these assays to investigate the trypanocidal action of ABQs that do not undergo NTR or CPR activation, revealed that these do not promote a form of DNA damage that can be repaired through an SNM1-dependent pathway. It is plausible that these agents may still function as monofunctional or bifunc-tional DNA alkylating agents, leading to formation of a single site adduct or intrastrand crosslink or could act as modifiers of other biological molecules via their aziridinyl or quinone ring structures.

The continuous in vitro culturing of bloodstream form T. brucei in the presence of RH1 generated a parasite line that displayed cross-resistance to a range of NTR-activated prodrugs. Analysis of clones revealed that these cells had reduced Tbntr expression. Additionally, lower mRNA levels were also noted for other open read-ing frames across the 200 kb Tbntr-containing

Table 5. Structure of aziridinyl 1,4-benzoquinones used in this study.

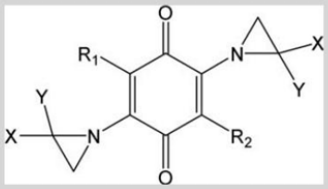

Compound	Structure	Compound	Structure
ABQ1 (DZQ)	$R_1$5$R_2$5X5Y5H	ABQ18	$R_1$5$R_2$5NHCO$(CH_2)_5CH_3$; X5Y5H
ABQ2 (MeDZQ)	$R_1$5$R_2$5CH_3; X5Y5H	ABQ19	$R_1$5$R_2$5NHCOPhenyl; X5Y5H
ABQ3	$R_1$5$R_2$5Br; X5Y5H	ABQ20 (AZQ)	$R_1$5$R_2$5NHC(O)OCH_2CH_3; X5Y5H
ABQ4	$R_1$5$R_2$5F; X5Y5H	ABQ21 (TZQ)	$R_1$5azirindyl; $R_2$5X5Y5H
ABQ5 (RH1)	$R_1$5CH_2OH; $R_2$5CH_3; X5Y5H	ABQ22	$R_1$5$R_2$5azirindyl; X5Y5H
ABQ6	$R_1$5$R_2$5OCH_3; X5Y5H	ABQ23	$R_1$5$R_2$5X5H;Y5CH_3 (r orientation)
ABQ7	$R_1$5$R_2$5OCH_2CH_3; X5Y5H	ABQ24	$R_1$5$R_2$5X5H;Y5CH_3 (s orientation)
ABQ8	$R_1$5$R_2$5O$(CH_2)_2CH_3$; X5Y5H	ABQ25	$R_1$5$R_2$5Br; X5H; Y5CH_3
ABQ9	$R_1$5$R_2$5NH_2; X5Y5H	ABQ26	$R_1$5$R_2$5Br; X5Y5CH_3
ABQ10	$R_1$5$R_2$5NHCH_3; X5Y5H	ABQ27	$R_1$5$R_2$5Cl; X5H;Y5CH_3
ABQ11	$R_1$5$R_2$5NHCH_2CH_3; X5Y5H	ABQ28	$R_1$5$R_2$5Cl; X5Y5CH_3
ABQ12	$R_1$5$R_2$5NH$(CH_2)_6CH_3$; X5Y5H	ABQ29	$R_1$5$R_2$5F; X5H;Y5CH_3
ABQ13	$R_1$5$R_2$5NH$(CH_3)CH_3$; X5Y5H	ABQ30	$R_1$5$R_2$5F; X5Y5CH_3
ABQ14	$R_1$5morpholinyl; $R_2$5F; X5Y5H	ABQ31	$R_1$5$R_2$5NHCOCH_3; X5H; Y5CH_3
ABQ15	$R_1$5$R_2$5NHCOCH_3; X5Y5H	ABQ32	$R_1$5$R_2$5NHCOCH_3; X5Y5CH_3
ABQ16	$R_1$5$R_2$5NHCOCH_2CH_3; X5Y5H	ABQ33	$R_1$5$R_2$5NHCOCH_2CH_3; X5H;Y5CH_3
ABQ17	$R_1$5$R_2$5NHCO$(CH_2)_2CH_3$; X5Y5H	ABQ34	$R_1$5$R_2$5NHCOOCH_2CH_3; X5Y5CH_3

All compounds tested satisfy Lipinski's Rule of 5 (http://pubchem.ncbi.nlm.nih.gov/) although all are predicted to have toxicity risks (http://www.organic-chemistry.org/prog/peo).

polycistron; however, this effect did not extend to the surrounding transcriptional units. In contrast to trypanosomes selected for resistance towards other NTR activated prodrugs such as nifurtimox or fexinidazole (Wilkinson et al., 2008; Wyllie et al., 2016), the copy number of all tested open reading frames in the Tbntr-containing transcriptional unit were equivalent to wild type, indicating that the observed reduction in gene expression was not due to a large (>10 kb) DNA dele-tion event; the 'strandswitch' region, areas on the trypa-nosomal chromosome postulated to be regions where polycistronic transcription is initiated (Imboden et al., 1987; Muhich and Boothroyd, 1988), between the Tbntr-containing and adjacent transcriptional units is 6 kb. Although the exact molecular basis that leads to RH1 resistance has yet to be deciphered, it is plausible that the transcription initiation site of one of the two Tbntr-containing polycistrons (T. brucei has a diploid nuclear genome) may have been compromised resulting in the reduction in mRNA levels.

We have demonstrated that ABQs display significant growth inhibitory activities against T. brucei, T. cruzi and L. major, with two compounds (RH1 and TZQ) exhibiting high potency (EC_{50} values < 100 nM) against all three pathogens. However, this is accompanied by toxicity against macrophage (-like) mammalian cells, a trait previ-ously noted in primary mouse splenocytes (Miliukiene et al., 2014). This unwanted activity may be because such immune cells have the ability to constitutively express or to upregulate quinone oxidoreductases includ-ing NQO1 and NQO1-independent activities that promote oxidative stress and/or DNA damage (Tudor et al., 2005; Potts-Kant et al., 2012; Miliukiene et al., 2014). Although these cytotoxicity issues may preclude the use of these ABQs as therapies for the treatment of systemic infec-tions, understanding how they mediate their trypanocidal activities can inform drug development. By exploiting the chemical features that facilitate NTR or CPR specific acti-vation such as those reported here, novel trypanocidal prodrugs could be generated. Following their activation, these compounds could be designed to release cytotoxic metabolites that affect a range of biological processes potentially targeting different biochemical pathways. Such agents would be best used in a polytherapy, as is the case with the anti-HAT nifurtimox-eflornithine combination therapy, in order to minimize potential resistance.

Experimental procedures

Compounds

The compounds used in this study were obtained from the following sources: The aziridinyl benzoquinones (DZQ, MeDZQ, AZQ, TZQ and ABQ3–4, 6–19, 22–34) (Table 5)

were supplied by the Drug Synthesis and Chemistry Branch, Developmental Therapeutics Program, Division of Cancer Treatment and Diagnosis, National Cancer Institute, United States, while RH1 was donated by Prof Frank Guziec Jr (Southwestern University, TX). The chemical, physical and potential toxicological properties of each compound can be accessed via the PubChem database (http://pubchem.ncbi.nlm.nih.gov/) or OSIRIS Property Explorer software (http://www.organic-chemistry.org/prog/). Nifurtimox was obtained from Prof Simon Croft (London School of Hygiene and Tropical Medicine, UK), DFMO from Prof Mike Barrett (University of Glasgow, UK), mechlorethamine HCl from Stratech Scientific, while puromycin, blasticidin, phleomycin, hygromycin b and tetracycline were purchased from Melford Laboratories.

Cell culturing

Bloodstream form T. brucei brucei (MITat 427 strain; clone 221a) cells were cultured in HMI-9 media (Life Technologies) supplemented with 36 mM sodium bicarbonate, 0.014% (v/v) b-mercaptoethanol and 10% (v/v) heat-inactivated foetal calf serum (GE Healthcare) as described (Hirumi and Hirumi, 1989). A cell line (2T1) engineered to constitutively express the tetracycline repressor protein was grown in the modified lg ml^{21} HMI-9 medium, supplemented with 1

lg ml^{21} phleomycin (Alsford et al., 2005). T. brucei Tbntr heterozygote lines were cultured in the presence of 10 blasticidin while transformed 2T1 parasites over

expressing Tbntr, Tbcpr2 or Tbcpr3 were maintained in the modified HIM-9 medium supplemented with 1 lg ml^{21} phleomycin, 2.5 lg ml^{21} hygromycin b and, where appropriate, 1 lg ml^{21} tetracycline to induce protein expression (Hall et al., 2011). T. brucei lines expressing altered levels of the DNA repair enzyme TbSNM1 were grown in the presence 1 lg ml^{21} phleomycin, 10 lg ml^{21} blasticidin and/ or 2 lg ml^{21} puromycin, as appropriate (Sullivan et al., 2015).

The epimastigote form of T. cruzi was cultured in RPMI-1640 medium (Lonza) supplemented with 5 g l^{21} trypticase, 5: g l^{21} HEPES pH 8.0, 20 mg l^{21} haemin, 0.34 g l^{21} sodium glutamate, 0.22 g l^{21} sodium pyruvate, 2500 U l^{21} penicillin, 0.25 g l^{21} streptomycin (all Sigma-Aldrich) and 10% (v/v) heat-inactivated foetal calf serum (GE Health-care) at 258C (Kendall et al., 1990).

The promastigote form of L. major MHOM/IL/80/Friedlin was cultured at 258C in modified M199 medium (Invitrogen) supplemented with 4 mM sodium bicarbonate, 40 mM HEPES pH 7.4, 0.1 mM adenine, 0.005% (w/v) haemin (all Sigma-Aldrich), 25000 U l^{21} penicillin, 25 mg l^{21} streptomycin (GE Healthcare) and 10% (v/v) heat-inactivated foetal bovine serum (GE Healthcare) (Kapler et al., 1990).

The human acute monocytic leukemia (THP-1) cell line was grown at 378C under a 5% (v/v) CO_2 atmosphere in RPMI-1640 medium (Lonza) supplemented with 2 mM pyruvate, 2 mM sodium glutamate, 2.5 U ml^{21} penicillin and 2.5 lg ml^{21} streptomycin, 20 mM HEPES pH 7.4 and 10% (v/ v) heat-inactivated foetal calf serum (GE Healthcare). Differentiation of THP-1 toward macrophage-like cells was carried out using 20 ng ml^{21} phorbol 12-myristate 13-acetate (Sigma-Aldrich) (Rovera et al., 1979).

Selective screening of the T. brucei RNAi library

Selection of the T. brucei RNAi library was performed as described (Glover et al., 2015). Parasites (5 3 10^6 cells) were treated for 24 hours with 1 lg ml^{21} tetracycline to induce RNAi prior to addition of 30 nM RH1. Periodically, the cell density of the culture was determined and when appropriate, diluted in growth medium containing fresh RH1 (30 nM) and tetracycline (1 mg ml^{21}). Once an outgrowth population had been selected, genomic DNA was prepared for RNAi target identification (Alsford et al., 2012).

Selection of laboratory generated RH1-resistant T. brucei

Wild type bloodstream form T. brucei seeded at 1 3 10^4 cells ml^{21}, were cultured in the presence of sub-lethal concentration of RH1 (5 nM). Over a 100 day period, the ABQ concentration in the culture media was increased in a stepwise manner reaching a final concentration of 40 nM. The resulting line (designated as RH1^R) was cloned by limiting dilution in the presence of RH1 and the phenotype of two clones (RH1^{RC1} and RH1^{RC2}) analysed.

Parasite growth inhibition assays

All growth inhibition assays were carried out in a 96-well plate format (ThermoScientific). Bloodstream form T. brucei, L. major promastigotes and T. cruzi epimastigotes parasites in the logarithmic phase of growth were seeded at 1 3 10^4, 5: 3 10^5 and 5 3 10^5 cells ml^{21} respectively in 200 ll growth medium containing different concentrations of the compound under study. After incubation at 378C for 3 days (T. brucei), 258C for 6 days (L. major) or 258C for 14 days (T. cruzi), resazurin (Sigma Aldrich) was added to each well at a final concentration of 12.5 mg ml^{21} (or 2.5 mg per well). The plates were further incubated at 378C for 8 hours (T. brucei), 258C for 24 hours (L. major) or 258C for 24–48 hours (T. cruzi) before measuring the fluorescence of each culture using a Gemini Fluorescent Plate reader (Molecular Devices) set at kEX 5 530 nm and kEM 5 585 nm with a fil-ter cut off at 550 nm. The change in fluorescence resulting from the reduction of resazurin is proportional to the num-ber of live cells. A compound's EC_{50} value was established using the non-linear regression tool on GraphPad Prism (GraphPad Software) and the statistical significance of any differences in parasite susceptibilities assessed using the Student's t test calculator (GraphPad Software).

Mammalian inhibition assays

Differentiated THP-1 cells seeded at 2.5 3 10^4 cells ml^{21} were incubated for 3 days at 378C in a 5% (v/v) CO_2 atmosphere in 200 ll modified RMPI-1640 growth medium containing various concentrations of the compound under

study. Resazurin (2.5 mg per well) was added to each cul-ture and the plates incubated for a further 8 hours before determining the fluorescence of each sample.

Experiments involving animals were approved by the Ani-mal Welfare and Ethics Review Board at LSHTM and con-ducted under license in accordance with the Animals (Scientific Procedures) Act 1986 (UK Home Office Project Licence PPL70/6997). Peritoneal macrophages were iso-lated from BALB/c mice by lavage 24 hours after intraperi-toneal injection of 2% (w/v) soluble starch (Sigma). Macrophages (40,000) in RPMI-1640 medium (Lonza) sup-plemented with 10% (v/v) heat-inactivated foetal calf serum (GE Healthcare) were adhered overnight at 378C in a 5% (v/v) CO_2 atmosphere onto a 16-well chamber slide. Cells were then treated with various concentrations of the com-pound under study and the cultures incubated at 378C up to 5 days under a 5% (v/v) CO_2 atmosphere. Untreated controls were analysed in parallel on each slide. Macro-phages were fixed in 100% (v/v) methanol, stained with 10% (w/v) Giemsa, visualized with Leica DMRA2 light microscope using a 3100 oil immersion objective and images captured using a Retiga EXi Fast 1394 digital cam-era. The number of cells per field of view was determined with a minimum of 10 fields examined for each drug treat-ment. The average number of cells per field of view was determined and expressed as a % relative to untreated controls. All treatments were performed in quadruplicate.

Quantitative PCR (qPCR)

The copy number and mRNA levels of various genes were analysed by qPCR. Genomic DNA or total RNA was pre-pared from wild type or RH1-resistant T. brucei using the DNeasy Blood and Tissue or RNeasy Extraction kits (Qia-gen), respectively. cDNA was synthesized from total RNA using the Superscript VILO cDNA synthesis kit (Invitrogen). All qPCRs were performed in triplicate with the PerfeCTa qPCR FastMix kit (Quanta Biosciences) on a CFX96 Touch Real-Time PCR Detection System (BioRad). Fluorescence data was collected using the CFX Manager Software (Bio-Rad), the products analysed by a melt curve after the final cycle and normalized against telomerase reverse transcrip-tase (Tbtert; Tb11.01.10190) using the comparative CT method (Schmittgen and Livak, 2008; Brenndorfer and Boshart, 2010).

Cell cycle arrest assay

Wild type T. brucei (5 3 10^5 ml^{21}) were cultured for 16 hours in the presence of mutagen (1 mg ml^{21} phelomycin; 35 mM mechlorethamine; 100 nM RH1). Cells were washed in phosphate buffered saline (PBS), fixed in 2% (w/v) para-formaldehyde in PBS and washed once more in PBS. Ali-quots of the cell suspension (10^5 cells) were air-dried onto microscope slides and the samples mounted in Vectashield containing 4, 6-diamidino-2-phenylindole (Vector Laboratories). Images were captured using Leica DMRA2 epi-fluorescent microscope fitted with a digital cam-era (Hamamatsu Photonics).

Acknowledgements

The Wellcome Trust provided funding to DH (Project grant 093010/B/10/Z, Investigator Award 100320/Z/12/Z) and SA (Institutional Strategic Support Fund fellowship). KS was sup-ported by a grant jointly funded by the Medical Research Council and the Department for International Development (grant MR/ J008702/1). ELM and AK were recipients of a BBSRC Doctorial Training Studentship and QMUL College studentship, respectively.

References

Akhtar, H.M., Begleiter, A., Johnson, D., Lown, J.W., McLaughlin, L., and Sim, S.K. (1975) Studies related to anti-tumour anti-biotics. Part VI. Correlation of covalent cross-linking of DNA by bifunctional aziridinoquinones with their antineoplastic activity. Can J Chem 53: 2891–2905.

Alsford, S., Kawahara, T., Glover, L., and Horn, D. (2005) Tagging a T. brucei RRNA locus improves stable trans-fection efficiency and circumvents inducible expression position effects. Mol Biochem Parasitol 144: 142–148.

Alsford, S., Eckert, S., Baker, N., Glover, L., Sanchez-Flores, A., Leung, K.F., et al. (2012) High-throughput decoding of antitrypanosomal drug efficacy and resist-ance. Nature 482: 232–236.

Alsford, S., Kelly, J.M., Baker, N., and Horn, D. (2013) Genetic dissection of drug resistance in trypanosomes. Parasitology 140: 1478–1491.

Baker, N., Alsford, S., and Horn, D. (2011) Genome-wide RNAi screens in African trypanosomes identify the nifurti-mox activator NTR and the eflornithine transporter AAT6. Mol Biochem Parasitol 176: 55–57.

Barrett, M.P. (2006) The rise and fall of sleeping sickness. Lancet 367: 1377–1378.

Barrett, M.P., and Croft, S.L. (2012) Management of trypa-nosomiasis and leishmaniasis. Br Med Bull 104: 175–196.

Beena, D.S., and Rawat, (2013) Antituberculosis drug research: a critical overview. Med Res Rev 33: 693–764.

Begleiter, A., Leith, M.K., Patel, D., and Hasinoff, B.B. (2007) Role of NADPH cytochrome P450 reductase in activation of RH1. Cancer Chemother Pharmacol 60: 713–723.

Brenndorfer, M., and Boshart, M. (2010) Selection of refer-ence genes for mRNA quantification in Trypanosoma bru-cei. Mol Biochem Parasitol 172: 52–55.

Cattell, E., Sengerova, B., and McHugh, P.J. (2010) The SNM1/Pso2 family of ICL repair nucleases: from yeast to man. Environmental Mol Mutagen 51: 635–645.

Chen, Y., and Hu, L. (2009) Design of anticancer prodrugs for reductive activation. Med Res Rev 29: 29–64.

Deans, A.J., and West, S.C. (2011) DNA interstrand cross-link repair and cancer. Nat Rev Cancer 11: 467–480.

Dehn, D.L., Winski, S.L., and Ross, D. (2004) Development of a new isogenic cell-xenograft system for evaluation of NAD(P)H:quinone oxidoreductase-directed antitumor qui-nones: evaluation of the activity of RH1. Clin Cancer Res 10: 3147–3155.

Dehn, D.L., Inayat-Hussain, S.H., and Ross, D. (2005) RH1 induces cellular damage in an NAD(P)H:quinone oxidoreductase 1-dependent manner: relationship between DNA cross-linking, cell cycle perturbations, and apoptosis. J Pharmacol Exp Ther 313: 771–779.

Ernster, L., Danielson, L., and Ljunggren, M. (1962) DT diaphorase. I. Purification from the soluble fraction of rat-liver cytoplasm, and properties. Biochim Biophys Acta 58: 171–188.

Garavaglia, P.A., Cannata, J.J., Ruiz, A.M., Maugeri, D., Duran, R., Galleano, M., and Garcia, G.A. (2010) Identification, cloning and characterization of an aldo-keto reductase from Trypanosoma cruzi with quinone oxidoreductase activity. Mol Biochem Parasitol 173: 132–141.

Glover, L., and Horn, D. (2012) Trypanosomal histone gammaH2A and the DNA damage response. Mol Biochem Parasitol 183: 78–83.

Glover, L., Alsford, S., Baker, N., Turner, D.J., Sanchez-Flores, A., Hutchinson, S., et al. (2015) Genome-scale RNAi screens for high-throughput phenotyping in bloodstream-form African trypanosomes. Nat Protoc 10: 106–133.

Grellier, P., Maroziene, A., Nivinskas, H., Sarlauskas, J., Aliverti, A., and Cenas, N. (2010) Antiplasmodial activity of quinones: roles of aziridinyl substituents and the inhibi-tion of Plasmodium falciparum glutathione reductase. Arch Biochem Biophys 494: 32–39.

Hall, B.S., and Wilkinson, S.R. (2012) Activation of benznidazole by trypanosomal type I nitroreductases results in glyoxal formation. Antimicrob Agents Chemother 56: 115–123.

Hall, B.S., Bot, C., and Wilkinson, S.R. (2011) Nifurtimox activation by trypanosomal type I nitroreductases gener-ates cytotoxic nitrile metabolites. J Biol Chem 286: 13088–13095.

Hall, B.S., Meredith, E.L., and Wilkinson, S.R. (2012) Targeting the substrate preference of a type I nitroreductase to develop antitrypanosomal quinone-based prodrugs. Antimicrob Agents Chemother 56: 5821–5830.

Hargreaves, R.H., Hartley, J.A., and Butler, J. (2000) Mechanisms of action of quinone-containing alkylating agents: DNA alkylation by aziridinylquinones. Front Biosci 5: E172–E180.

Henderson, G.B., Ulrich, P., Fairlamb, A.H., Rosenberg, I., Pereira, M., Sela, M., and Cerami, A. (1988) "Subversive" substrates for the enzyme trypanothione disulfide reduc-tase: alternative approach to chemotherapy of Chagas disease. Proc Natl Acad Sci USA 85: 5374–5378.

Hirumi, H., and Hirumi, K. (1989) Continuous cultivation of Trypanosoma brucei blood stream forms in a medium containing a low concentration of serum protein without feeder cell layers. J Parasitol 75: 985–989.

Hoet, S., Opperdoes, F., Brun, R., and Quetin-Leclercq, J. (2004) Natural products active against African trypanosomes: a step towards new drugs. Nat Prod Rep 21: 353–364.

Imboden, M.A., Laird, P.W., Affolter, M., and Seebeck, T. (1987) Transcription of the intergenic regions of the tubu-lin gene cluster of Trypanosoma brucei: evidence for a polycistronic transcription unit in a eukaryote. Nucleic Acids Res 15: 7357–7368.

Iyanagi, T., and Yamazaki, I. (1970) One-electron-transfer reactions in biochemical systems. V. Difference in the mechanism of quinone reduction by the NADH dehydrogenase and the NAD(P)H dehydrogenase (DT-diaphorase). Biochim Biophys Acta 216: 282–294.

Kapler, G.M., Coburn, C.M., and Beverley, S.M. (1990) Sta-ble transfection of the human parasite Leishmania major delineates a 30-kilobase region sufficient for extrachro-mosomal replication and expression. Mol Cell Biol 10: 1084–1094.

Kendall, G., Wilderspin, A.F., Ashall, F., Miles, M.A., and Kelly, J.M. (1990) Trypanosoma cruzi glycosomal glyceraldehyde-3-phosphate dehydrogenase does not conform to the 'hotspot' topogenic signal model. EMBO J 9: 2751–2758.

Kim, J.Y., Kim, C.H., Stratford, I.J., Patterson, A.V., and Hendry, J.H. (2004) The bioreductive agent RH1 and gamma-irradiation both cause G2/M cell cycle phase arrest and polyploidy in a p53-mutated human breast cancer cell line. Int J Radiat Oncol Biol Phys 58: 376–385.

Kim, S., Thiessen, P.A., Bolton, E.E., Chen, J., Fu, G., Gindulyte, A., et al. (2016) PubChem substance and compound databases. Nucleic Acids Res 44: D1202–D1213.

Kubata, B.K., Kabututu, Z., Nozaki, T., Munday, C.J., Fukuzumi, S., Ohkubo, K., et al. (2002) A key role for old yellow enzyme in the metabolism of drugs by Trypanosoma cruzi. J Exp Med 196: 1241–1251.

Lee, E.J., Van Echo, D.A., Egorin, M.J., Nayar, M.S., Shulman, P., and Schiffer, C.A. (1986) Diaziquone given as a continuous infusion is an active agent for relapsed adult acute nonlymphocytic leukemia. Blood 67: 182–187.

Lin, A.J., Cosby, L.A., Shansky, C.W., and Sartorelli, A.C. (1972) Potential bioreductive alkylating agents. 1. Benzoquinone derivatives. J Med Chem 15: 1247–1252.

Lusthof, K.J., De Mol, N.J., Janssen, L.H., Verboom, W., and Reinhoudt, D.N. (1989) DNA alkylation and formation of DNA interstrand cross-links by potential antitumour 2,5-bis(1-aziridinyl)-1,4-benzoquinones. Chem Biol Inter-act 70: 249–262.

McKeown, S.R., Cowen, R.L., and Williams, K.J. (2007) Bioreductive drugs: from concept to clinic. Clin Oncol 19: 427–442.

Miliukiene, V., Nivinskas, H., and Cenas, N. (2014) Cytotoxicity of anticancer aziridinyl-substituted benzoqui-nones in primary mice splenocytes. Acta Biochim Pol 61: 833–836.

Moore, J.O., Dodge, R.K., Amrein, P.C., Kolitz, J., Lee, E.J., Powell, B., et al. (1997) Granulocyte-colony stimulating factor (filgrastim) accelerates granulocyte recovery after intensive postremission chemotherapy for acute myeloid leukemia with aziridinyl benzoquinone and mitoxantrone: Cancer and Leukemia Group B study 9022. Blood 89: 780–788.

Muhich, M.L., and Boothroyd, J.C. (1988) Polycistronic tran-scripts in trypanosomes and their accumulation during heat shock: evidence for a precursor role in mRNA synthesis. Mol Cell Biol 8: 3837–3846.

O'Brien, P.J. (1991) Molecular mechanisms of quinone cytotoxicity. Chem Biol Interact 80: 1–41.

Patterson, S., and Wyllie, S. (2014) Nitro drugs for the treatment of trypanosomatid diseases: past, present, and future prospects. Trends Parasitol 30: 289–298.

Perry, M.R., Prajapati, V.K., Menten, J., Raab, A., Feldmann, J., Chakraborti, D., et al. (2015) Arsenic expo-sure and outcomes of antimonial treatment in visceral leishmaniasis patients in Bihar, India: a retrospective cohort study. PLoS Negl Trop Dis 9: e0003518.

Phillips, R.M., Naylor, M.A., Jaffar, M., Doughty, S.W., Everett, S.A., Breen, A.G., et al. (1999) Bioreductive activation of a series of indolequinones by human DT-diaphorase: structure-activity relationships. J Med Chem 42: 4071–4080.

Pinto, A.V., and de Castro, S.L. (2009) The trypanocidal activ-ity of naphthoquinones: a review. Molecules 14: 4570–4590.

Potts-Kant, E.N., Li, Z., Tighe, R.M., Lindsey, J.Y., Frush, B.W., Foster, W.M., and Hollingsworth, J.W. (2012) NAD(P)H:quinone oxidoreductase 1 protects lungs from oxidant-induced emphysema in mice. Free Radic Biol Med 52: 705–715.

Powis, G. (1989) Free radical formation by antitumor quinones. Free Radic Biol Med 6: 63–101.

Priotto, G., Kasparian, S., Mutombo, W., Ngouama, D., Ghorashian, S., Arnold, U., et al. (2009) Nifurtimox-eflornithine combination therapy for second-stage African Trypanosoma brucei gambiense trypanosomiasis: a multicentre, rando-mised, phase III, non-inferiority trial. Lancet 374: 56–64.

Ramos, E.I., Garza, K.M., Krauth-Siegel, R.L., Bader, J., Martinez, L.E., and Maldonado, R.A. (2009) 2,3-diphenyl-1,4-naphthoquinone: a potential chemotherapeutic agent against Trypanosoma cruzi. J Parasitol 95: 461–466.

Rovera, G., O'brien, T.G., and Diamond, L. (1979) Induction of differentiation in human promyelocytic leukemia cells by tumor promoters. Science 204: 868–870.

Schmittgen, T.D., and Livak, K.J. (2008) Analyzing real-time PCR data by the comparative C(T) method. Nat Protoc 3: 1101–1108.

Schofield, C.J., Jannin, J., and Salvatella, R. (2006) The future of Chagas disease control. Trends Parasitol 22: 583–588.

Siegel, T.N., Hekstra, D.R., and Cross, G.A. (2008) Analy-sis of the Trypanosoma brucei cell cycle by quantitative DAPI imaging. Mol Biochem Parasitol 160: 171–174.

Siegel, D., Kepa, J.K., and Ross, D. (2012) NAD(P)H:quinone oxidoreductase 1 (NQO1) localizes to the mitotic spindle in human cells. PLoS One 7: e44861.

Sullivan, J.A., Tong, J.L., Wong, M., Kumar, A., Sarkar, H., Ali, S., et al. (2015) Unravelling the role of SNM1 in the DNA repair system of Trypanosoma brucei. Mol Microbiol 96: 827–838.

Tan, C.T., Hancock, C.H., Mondora, A., and Hoffman, N.W. (1984) Phase I study of aziridinylbenzoquinone (AZQ, NSC 182986) in children with cancer. Cancer Res 44: 831–835.

Tudor, G., Alley, M., Nelson, C.M., Huang, R., Covell, D.G., Gutierrez, P., and Sausville, E.A. (2005) Cytotoxicity of RH1: NAD(P)H:quinone acceptor oxidoreductase (NQO1)-independent oxidative stress and apoptosis induction. Anticancer Drugs 16: 381–391.

Voak, A.A., Gobalakrishnapillai, V., Seifert, K., Balczo, E., Hu, L., Hall, B.S., and Wilkinson, S.R. (2013) An essen-tial type I nitroreductase from Leishmania major can be used to activate leishmanicidal prodrugs. J Biol Chem 288: 28466–28476.

WHO (2013) Control and surveillance of human African trypanosomiasis. World Health Organ Tech Rep Ser 984: 1–237. http://apps.who.int/iris/handle/10665/95732

WHO (2014) Human African Trypanosomiasis (sleeping sickness). Factsheet 259. http://www.who.int/mediacentre/factsheets/fs259/en/

Wilkinson, S.R., Taylor, M.C., Horn, D., Kelly, J.M., and Cheeseman, I. (2008) A mechanism for cross-resistance to nifurtimox and benznidazole in trypanosomes. Proc Natl Acad Sci USA 105: 5022–5027.

Wilkinson, S.R., and Kelly, J.M. (2009) Trypanocidal drugs: mechanisms, resistance and new targets. Expert Rev Mol Med 11: e31.

Wilkinson, S.R., Bot, C., Kelly, J.M., and Hall, B.S. (2011) Trypanocidal activity of nitroaromatic prodrugs: current treatments and future perspectives. Curr Top Med Chem 11: 2072–2084.

Woodward, R., and Gull, K. (1990) Timing of nuclear and kinetoplast DNA replication and early morphological events in the cell cycle of Trypanosoma brucei. J Cell Sci 95: 49–57.

Wyllie, S., Foth, B.J., Kelner, A., Sokolova, A.Y., Berriman, M., and Fairlamb, A.H. (2016) Nitroheterocyclic drug resistance mechanisms in Trypanosoma brucei. J Antimicrob Chemother 71: 625–634.

Yun, O., Priotto, G., Tong, J., Flevaud, L., and Chappuis, F. (2010) NECT is next: implementing the new drug combination therapy for Trypanosoma brucei gambiense sleeping sickness. PLoS Negl Trop Dis 4: e720.

Free Radical Biology and Medicine 112 (2017) 524–533

Contents lists available at ScienceDirect

Free Radical Biology and Medicine

journal homepage: www.elsevier.com/locate/freeradbiomed

Original article

Functional characterisation of the methionine sulfoxide reductase repertoire in Trypanosoma brucei

Sergio A. Guerrero[a], Diego G. Arias[a], Matias S. Cabeza[a], Michelle C.Y. Law[b], Maria D'Amico[b], Ambika Kumar[b], Shane R. Wilkinson[b,]

[2] Instituto de Agrobiotecnología del Litoral, CONICET-Universidad Nacional del Litoral, 3000 Santa Fe, Argentina
[2] School of Biological & Chemical Sciences, Queen Mary University of London, Mile End Road, London E1 4NS, UK

ARTICLE INFO

Keywords:
Trypanosoma brucei
Methionine
Tryparedoxin
Trypanothione
Recombinant protein expression
RNA interference GFP

ABSTRACT

To combat the deleterious effects that oxidation of the sulfur atom in methionine to sulfoxide may bring, aerobic cells express repair pathways involving methionine sulfoxide reductases (MSRs) to reverse the above reaction. Here, we show that Trypanosoma brucei, the causative agent of African trypanosomiasis, expresses two distinct trypanothione-dependent MSRs that can be distinguished from each other based on sequence, sub-cellular lo-calisation and substrate preference. One enzyme found in the parasite's cytosol, shows homology to the MSRA family of repair proteins and preferentially metabolises the S epimer of methionine sulfoxide. The second, which contains sequence motifs present in MSRBs, is restricted to the mitochondrion and can only catalyse reduction of the R form of peptide-bound methionine sulfoxide. The importance of these proteins to the parasite was de-monstrated using functional genomic-based approaches to produce cells with reduced or elevated expression levels of MSRA, which exhibited altered susceptibility to exogenous H_2O_2. These findings identify new reparative pathways that function to fix oxidatively damaged methionine within this medically important parasite.

1. Introduction

The Trypanosomatida represent an order of parasitic protozoa be-longing to the Class Kinetoplastidea [1]. They are responsible for sev-eral infections in humans with Trypanosoma brucei and Trypanosoma cruzi causing human African trypanosomiasis (HAT) and Chagas dis-ease, respectively. In addition, more than 20 Leishmania species can trigger a spectrum of pathologies collectively termed leishmaniasis. Spread by the hematophagous habits of insect vectors, these pathogens are endemic throughout tropical and sub-tropical regions of the world and cause more than 55,000 deaths per year (http://www.dndi.org/).

All organisms living in an aerobic environment are exposed to a range of reactive oxygen species (ROS) primarily generated as by-pro-ducts of respiration. These can readily react with various macro-molecules leading to formation of other toxic metabolites and/or da-mage to the target. One target that ROS have a considerable effect on are proteins, resulting in oxidation of certain residues such as cysteine, histidine, tyrosine, and methionine (Met), which can reducing equiva-lents into change and, in some cases, modification of protein function [2,3]. Oxidation of Met produces methionine sulfoxide (MetSO) that exists as a mixture of two epimers, methionine-(S)-sulfoxide (Met(S)O) and methionine-(R)-sulfoxide (Met(R)O). To combat the potentially deleterious effect of these diastereomers, cells express several unrelated enzymes, known as methionine sulfoxide reductases (MSRs), that cat-alyse reduction of MetSO back to Met [4,5]. These distinct activities can be distinguished based on sequence and substrate specificity. Metabo-lism of both free and protein-bound Met(S)SO is performed by me-thionine sulfoxide reductase A (MSRA) [6,7] while reduction of free or protein-bound Met(R)O is mediated by free methionine-(R)-sulfoxide reductase (fRMSR) or methionine sulfoxide reductase B (MSRB), re-spectively [8–10]. The activity of these enzymes is generally driven by a thioredoxin/thioredoxin reductase-dependent redox cascade that facil-itate transfer of reducing equivalents from NADPH to the MSR, al-though other molecules such as metallothionein or glutaredoxin, may also act as source of reductant [8,11–14]. The importance of these pathways has been demonstrated as organisms lacking MSR(s) are more susceptible to oxidative stress, often have a shortened life span and, in the case of bacterial pathogens, reduced virulence [7,15–19].

In contrast to their mammalian hosts, trypanosomatids lack a raft of enzymes including Cu/Zn- and Mn-superoxide dismutase (SOD), cata-lase, selenium-dependent glutathione peroxidase, glutathione reductase and thioredoxin reductase, activities that help maintain the redox bal-ance in many other eukaryotic cells. Instead, they express alternative mechanisms that fulfil the above activities, with many of these

Corresponding author.
E-mail address: s.r.wilkinson@qmul.ac.uk (S.R. Wilkinson).

http://dx.doi.org/10.1016/j.freeradbiomed.2017.08.023
Received 6 June 2017; Received in revised form 10 August 2017; Accepted 29 August 2017
Available online 01 September 2017

proposed as potential targets for chemotherapeutic intervention. For example, removal of superoxide anions by trypanosomes and leishma-nial parasites is exclusively catalysed by Fe-SOD, enzymes normally found in bacteria, lower eukaryotes and the chloroplasts of plants, while maintenance of the intracellular thiol redox homeostasis is centred upon the trypanosomatid-specific molecule trypanothione [20–22]. In a pathway analogous to the glutathione (GSH)/glutathione reductase system, trypanothione is maintained in its reduced, dihy-drotrypanothione ($T(SH)_2$) form by the activity of a NADPH-dependent flavoprotein trypanothione reductase (TR) [23,24]. $T(SH)_2$ then drives a series of two component cascades, facilitating flux of reducing equivalents into tryparedoxins (TXNs), GSH or ascorbate which in turn reduce various peroxidases, reductases, glyoxalases and transferases [25,26].

One recipient of the electron flux via the $T(SH)_2$/TXN cascade is MSRA, with analysis of the T. cruzi and Leishmania major homologues revealing its role as an anti-oxidant enzyme within the parasite [27,28]. Here, we report the dissection of two MetSO metabolising pathways expressed by T. brucei focusing on the biochemical properties, sub-cellular localisation, and functional importance of its MSRA and MSRB complement.

2. Materials and methods

2.1. Parasites

Bloodstream form (BSF) T. brucei SMB and 2T1 trypomastigotes that constitutively express the tetracycline repressor protein were grown at 37 °C under a 5% (v/v) CO_2 atmosphere in modified Iscove's medium containing 2.5 μg ml-1 G418 (SMB) or 1 μg ml^{-1} phleomycin (2T1) [29–31]. Transformed parasites were maintained in this growth medium supplemented with 2.5 μg ml^{-1} hygromycin. DNA and total RNA were extracted from parasites using the DNeasy® Tissue and RNeasy® mini kits (Qiagen), respectively. T. brucei genes that encode for TbmsrA and TbmsrB were identified from the TriTrypDB (http:// tritrypdb.org/tritrypdb/) database [32]: TriTrypDB Gene ID Tb927.8.550 and Tb927.11.11930.1 for TbmsrA and TbmsrB, respec-tively.

2.2. Protein purification

DNA fragments containing the full length coding sequence of TbmsrA and a version of TbmsrB lacking its 5' (1–130 bp) region were amplified from T. brucei genomic DNA using the primer combinations TbMSRA-1/TbMSRA-2 or TbMSRB-1/TbMSRB-2 (Table 1),

Table 1
Oligonucleotides used in this study. The sequences in lower case italics correspond to restriction sites incorporated into the primers to facilitate cloning.

Function	gene	Primer name	sequence (5' to 3')
Protein expres-sion	TbmsrA	TbMSRA-1	aaaggatccTGAACCCAAATGCTGTTGCTA
		TbMSRA-2	gggaagcttCCATTCACCAGTAGAGACGGT
	TbmsrB	TbMSRB-1	aaaagatctTGACACACTGCGCAAGTAAGA
		TbMSRB-2	aaaaagcttTTACTTCTCGGATTGAAAACG
RNAi	TbmsrA	TbMSRA-3	aaaggatccACTTTTGCTGCAGGTTGCTT
		TbMSRA-4	aaactcgagAATACCCATTGGGGTTTTCC
	TbmsrB	TbMSRB-3	aaaagatctGCCCTCTTATTTTTCCTGCC
		TbMSRB-4	aaactcgagCGTTCGTTAGGTGGTGGATT
Localisation	TbmsrA	TbMSRA-5	aaaaagcttATGAACCCAAATGCTGTTGCT
		TbMSRA-6	aaatctagaCCAGTAGAGACGGTGTGCACA
	TbmsrB	TbMSRB-5	aaaaagcttATGCGCAGCAGGAACCTGTCC
		TbMSRB-6	aaatctagaCTTCTCGGATTGAAAACGAAT
qPCR	TbmsrA	TbMSRA-7	TAGTAGTGCTAAGGTTGTAAC
	TbmsrB	TbMSRB-7	ACGGAAATTTTATGCAATGCG
	Tbtert	Tbtert-F	AGGAACTGTCACGGAGTTTGC
		Tbtert-R	GAGCGTGTGACTTCCGAAGG

respectively. The products were digested with BamHI/HindIII (TbmsrA) or BglII/HindIII (TbmsrB) and cloned into the BamHI/HindIII sites of the expression vector pTrcHis-C (Invitrogen).

Protein expression and purification were conducted as previously described [27]. Overnight cultures of E. coli BL21 (DE3) transformed with the expression plasmid were diluted 1/100 in Terrific Broth (12 g l^{-1} peptone, 24 g l^{-1} yeast extract, 4 ml l^{-1} glycerol, 2.3 g l^{-1} KH_2PO_4, 12.5 g l^{-1} K_2HPO_4, pH 7.0) supplemented with 100 μg ml^{-1} ampicillin and grown to exponential phase at 37 °C with aeration. Ex-pression of the HIS-tagged recombinant protein was induced with 0.5 mM IPTG, followed by incubation at 25 °C. After 4 h, cells were harvested and bacterial pellets stored at −20 °C. Purification of re-combinant protein was performed using a Ni^{2+}–HiTrap column (GE Healthcare). Briefly, the bacterial pellet was resuspended in binding buffer (20 mM Tris.HCl, pH 7.5, 10 mM imidazole and 400 mM NaCl) and disrupted by sonication. The lysate was centrifuged (10,000 g, 30 min) to remove cell debris. The resultant crude extract was loaded onto a Ni^{2+}–HiTrap column (1 ml) previously equilibrated with binding buffer. After washing with 15 bead volumes of binding buffer plus 30 mM imidazole, the recombinant protein was eluted with elution buffer (20 mM Tris.HCl, pH 7.5, 400 mM NaCl, 300 mM imidazole). Purified enzyme fractions were pooled, concentrated by ultrafiltration, and stored at −80 °C in 20 mM Tris.HCl pH 7.5; 100 mM NaCl and 10% (v/v) glycerol.

2.3. Enzyme activity

MSR activity was measured by monitoring NADPH oxidation at 340 nm by means of a coupled assay that guaranteed the regeneration of TXNI to its reduced form [27]. All enzyme assays were performed at 30 °C using a Multiskan Ascent one-channel vertical light-path filter photometer (Thermo Electron Co.). The reaction mixture (final volume of 50 μl) contained (unless otherwise specified) 100 mM Tris.HCl, pH 7.5, 2 mM EDTA, 300 μM NADPH, 2 U ml^{-1} TcTR, 100 μM $T(SH)_2$ (Bachem), 10 μM TcTXNI, and the respective MSR included in a specific range of concentrations (0.5–3.5 μM TbMSRA or TbMSRB). TcTXN1 was used in these assays as it was readily available in our laboratory and was assumed to function in an equivalent manner to its T. brucei counterpart (TcTXNI and TbTXN1 share 62% identity [33]). Reactions were started by the addition of 5 mM MetSO substrate (racemic N-acetyl MetSO (N-AcMetSO) (Bachem), racemic L-MetSO (Sigma-Al-drich), L-Met(S)SO, L-Met(R)SO or N-Acetyl Met(R)SO: The enantiomers were prepared as previously described [34]). Addition of EDTA into the reaction did not affect TbMSRB activity and as such was included in assays to minimise heavy metal mediated thiol oxidation.

For TbMSRB steady-state kinetic analysis, the assay was performed using 20–2500 μM N-AcMet(R)SO and 0.5–20 μM TcTXNI. Kinetic data were plotted as initial velocity (μM min^{-1}) versus substrate con-centration (μM). The kinetic constants were acquired by fitting the data with a nonlinear least-squares formula and the Michaelis–Menten equation using the program Origin 7.0. Kinetic constants were the means of at least three independent sets of data, and they were re-producible within ± 10%.

2.4. Yeast complementation

In vivo MSR activity of T. brucei enzymes was checked using the triple msr mutant GY202 (msrA msrB fRmsr) [18]. The Sacchar-omyces cerevisiae GY202 strain was transformed with parental plasmid p425GPD, p425GPD–TbmsrA or p425GPD–TbmsrB and selected for leucine prototrophy on Yeast Nitrogen Based (YNB)-agar medium supplemented with L-Met [35]. To perform the complement assay, each recombinant clone was cultivated on YNB-agar medium supplemented with L-Met, a L-MetSO racemic mix, L-Met(S)SO-or L-Met(R)SO (all 100 μM) at 30 °C until growth was visualized.

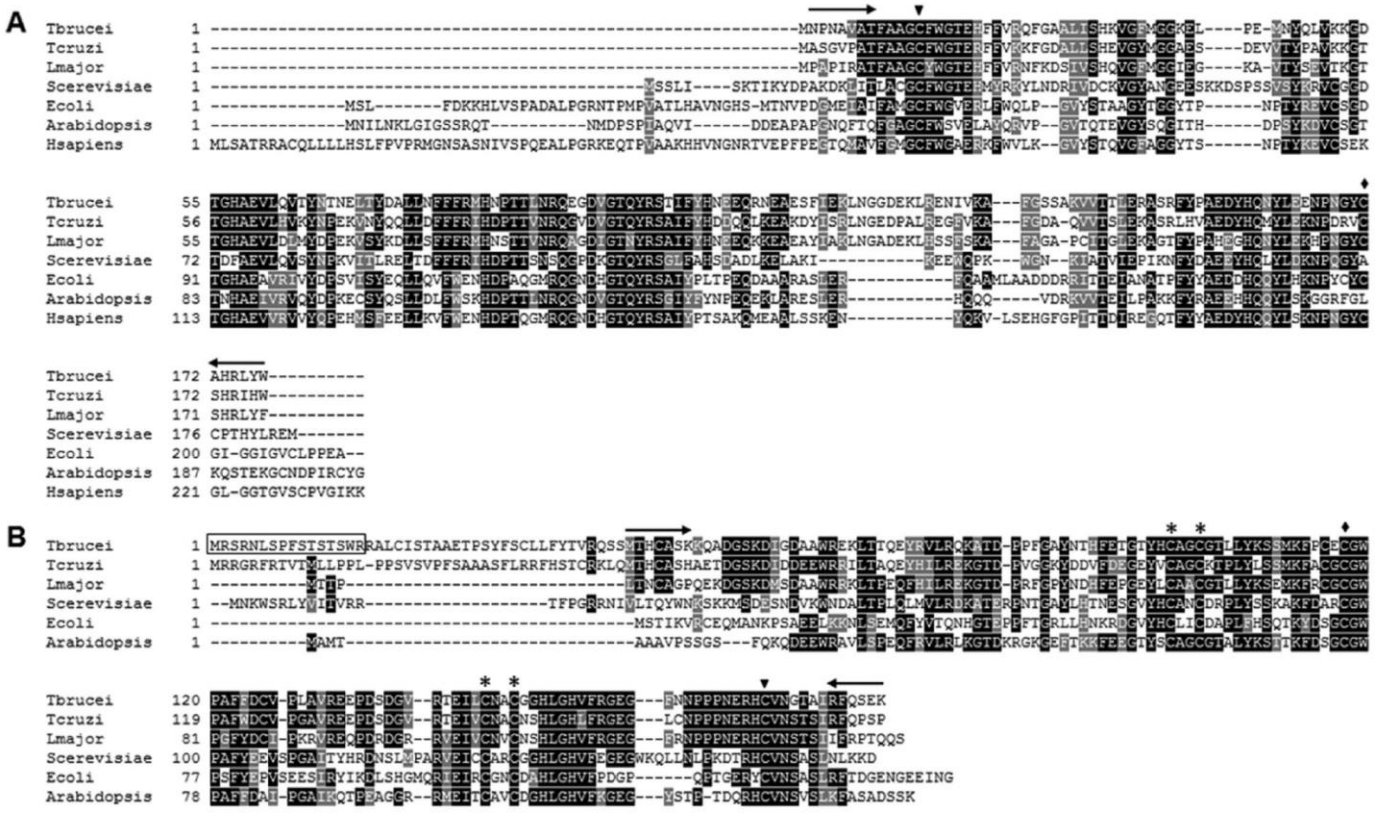

Fig. 1. Sequence analysis of T. brucei methionine sulfoxide reductases. (A). Alignment of MSRA sequences from T. brucei (AAZ12826), T. cruzi (EAN83377), Leishmania major (CAJ07082), Saccharomyces cerevisiae (NP_010960), Escherichia coli (WP_044721421), Arabidopsis thaliana (NP_56893) and Homo sapiens (NP_036463). Residues that are highly or moderately con-served are highlighted in black or grey, respectively. The catalytic (C13; triangle) and recycling (C171; diamond) cysteines are highlighted [5]. (B). Alignment of MSRB sequences from T. brucei (XP_829255), T. cruzi (XP_817746), Leishmania major (XP_001684552), Saccharomyces cerevisiae (NP_009897), Escherichia coli (AE016761_217) and Arabidopsis thaliana (NP_193915). Residues that are highly or moderately conserved are highlighted in black or grey, respectively. The putative amino terminal mitochondrial targeting sequence in the T. brucei MSRB sequence (boxed), the catalytic (C171; triangle), recycling (C117; diamond) and zinc binding (C99, C102, C145 and C148; asterisk) cysteines are all highlighted [5]. For both TbMSRA and B, the arrows corresponds to the primers used for expression of the recombinant protein (Experimental Procedures).

2.5. RNA interference

Fragments corresponding to internal sequences of TbmsrA (491 bp) and TbmsrB (426 bp) were amplified from T. brucei genomic DNA using the primers TbMSRA-3/TbMSRA-4 or TbMSRB-3/TbMSRB-4 (Table 1), respectively. The products were digested with BamHI/XhoI (TbmsrA) or BglII/XhoI (TbmsrB) and cloned into the BamHI/XhoI sites of the vector p2T7^{Ti} [36]. In this vector, the inserted DNA is flanked by two opposing T7 promoters with each promoter under the control of a tetracycline operator. Constructs were linearised with NotI, electroporated into T. brucei SMB parasites and transformants selected using hygromycin [37]. Induction of RNA interference (RNAi) was initiated by adding 1 μg ml^{-1} tetracycline to the culture. To demonstrate down regulation of the TbmsrA or TbmsrB transcript, cDNA generated using the Superscript® VILO™ cDNA synthesis kit (ThermoFisher Scientific) from total RNA extracted from cells induced to undergo RNAi for 48 h was subject to qPCR using the QuantiTect SYBR® Green PCR kit (Qiagen) and the primer combinations TbMSRA-7/TbMSRA-2 or TbMSRB-7/TbMSRB-2 (Table 1), respectively. All reactions were performed in triplicate on two independently generated cDNA samples. From the resultant sig-moidal curves, the cycle threshold (CT) value was determined and normalized against standardized control (Tbtert; primer combination TbTERT-R and TbTERT-F) amplified in parallel [38] using the com-parative CT method [39].

2.6. Trypanosomal epitope tagging vectors

The full length coding sequences of TbmsrA and TbmsrB were amplified from genomic DNA using the primer combinations TbMSRA-5/TbMSRA-6 or TbMSRB-5/TbMSRB-6 (Table 1), respectively. The products were digested with HindIII/XbaI and cloned into the corre-sponding sites of the vectors pRPa$^{C\text{-}GFP}$ or BSF-9e10 [31,40]. The cloning was carried out such that the sequences coding for the green fluorescence protein (GFP) or 9E10 epitope from the human c-myc protein were inserted in-frame at the 3' end of the Tbmsr-derived DNA fragment. The AscI digested constructs were introduced into T. brucei 2T1 and transformants selected using hygromycin. Expression of the recombinant protein in the parasite was initiated by adding 1 μg ml^{-1} tetracycline to the culture.

2.7. Localisation

BSF trypanosomes expressing TbMSRB-GFP were suspended at 5 × 10^6 cells ml^{-1} in medium containing 100 nM MitoTracker Red (Molecular Probes) and incubated at 37 °C for 5 min. Cells were washed twice in phosphate buffered saline (PBS), fixed in 2% (w/v) paraf-ormaldehyde/PBS then washed again in PBS. Aliquots of the cell sus-pension (10^5 cells) were then air dried onto microscope slides. Parasite DNA was stained with Vectashield containing 200 pM. 4, 6-diamidino-2-phenylindole (DAPI) (Vector Laboratories Ltd) and slides were viewed using a Leica SP5 confocal microscope. BSF trypanosomes ex-pressing TbMSRA-GFP were treated similarly except the MitoTracker Red step was omitted.

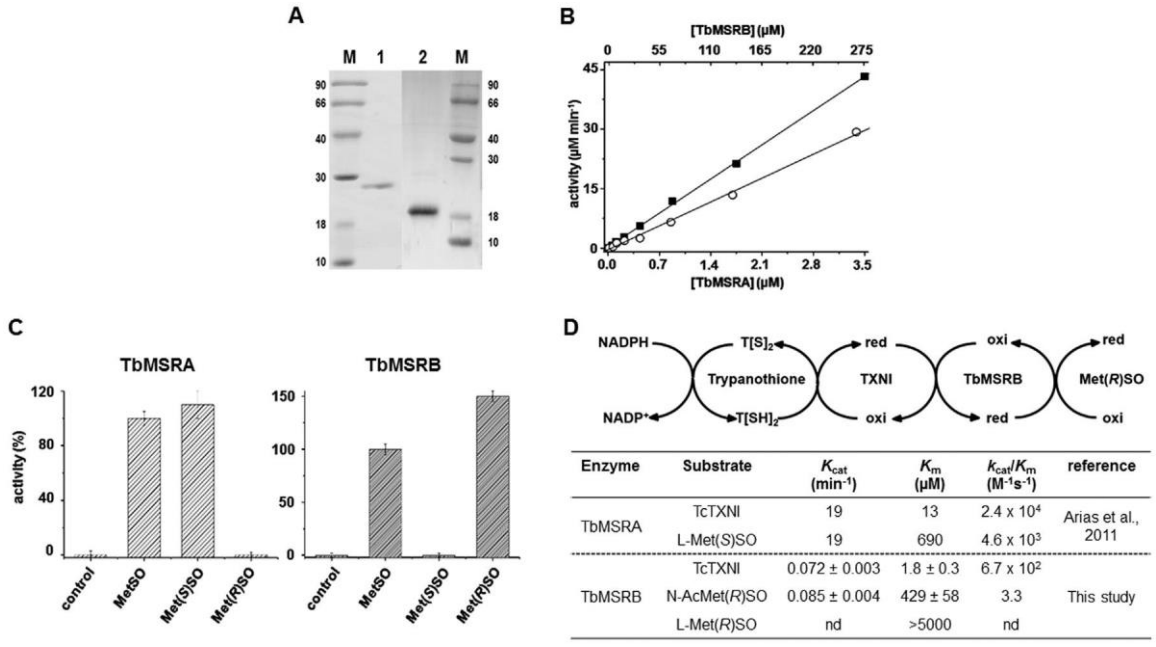

Enzyme	Substrate	K_{cat} (min^{-1})	K_m (μM)	k_{cat}/K_m ($M^{-1}s^{-1}$)	reference
TbMSRA	TcTXNI	19	13	2.4 x 10^4	Arias et al., 2011
	L-Met(*S*)SO	19	690	4.6 x 10^3	
TbMSRB	TcTXNI	0.072 ± 0.003	1.8 ± 0.3	6.7 x 10^2	This study
	N-AcMet(*R*)SO	0.085 ± 0.004	429 ± 58	3.3	
	L-Met(*R*)SO	nd	>5000	nd	

Fig. 2. T. brucei expresses functional methionine sulfoxide reductases. (A). Coomassie-stained SDS-PAGE gel (15%) containing size standards (in kDa; lane M) and purified, recombinant TbMSRA (lane 1) and TbMSRB (Lane 2). (B). MSR activity of TbMSRA or TbMSRB was followed by monitoring NADPH oxidation at 340 nm using a coupled assay that maintained tryparedoxin (10 μM) to its reduced form (see panel E). Reactions were carried out in 100 mM Tris–HCl pH 7.5, 2 mM EDTA buffer containing NADPH (300 μM), trypanothione reductase (2 U ml^{-1}) and $T(SH)_2$ (100 μM), to generate reduced tryparedoxin, and different concentrations of TbMSRA (0.05–3.5 μM) or TbMSRB (4–270 μM). Assays were initiated by addition of N-AcMetSO (5 mM) to reactions. (C). The MetSO isomer specificity of TbMSRA and TbMSRB (20 μM) was performed using L-Met(S)SO or N-AcMet(R)SO (both 5 mM) as substrate (see Section 2). The data are presented as mean % activity values (± standard deviations) derived from three independent experiments relative to assays performed using racemic L-MetSO (5 mM) as substrate. (D). Proposed scheme for the metabolism of Met(R)SO via a tryparedoxin-mediated TbMSRB pathway. Tryparedoxin (TXNI) acts as a redox shuttle between trypanothione and TbMSRB. Trypanothione disulfide (TS_2) is converted to dihydrotrypanothione ($T[SH]_2$) at the expense of NADPH by the activity of trypanothione reductase (TR) with "red" and "oxi" representing the reduced and oxidized form of proteins/substrates, respectively. The interactions of TbMSRB with TXNI (reaction I) and Met(R)SO (reaction II) are indicated. Kinetic parameters of recombinant TbMSRs is shown in the associated Table. To study Reaction I, the interaction between TXNI with TbMSRB, TbMSR activity was assayed as described in panel B using different concentrations of TXN1 (0.3–20 μM) and a fixed concentration of N-AcMet(R)SO (2.5 mM). For Reaction II, the interaction between TbMSRB with N-AcMet(R)SO, TbMSR activity was assayed as described in panel B using a fixed concentration of TXN1 (10 μM) and different concentrations of N-AcMet(R)SO (40–2500 μM). *Data relating to TbMSRA activity taken from Arias et al. [27].

2.8. Peroxide sensitivity experiments

T. brucei BSF parasites were seeded at 1×10^4 ml^{-1} in 200 μl growth medium containing different concentrations of H_2O_2 and tetracycline (1 μg ml^{-1}), where appropriate. After incubation at 37 °C for 3 days 2.5 μg resazurin (Sigma Aldrich) was added to each culture and the plates incubated for a further 8 h. Cell densities were determined by monitoring the fluorescence of each culture using a Gemini Fluorescent Plate Reader (Molecular Devices (UK) Ltd, Wokingham, UK) at an ex-citation λ = 530 nm, emission λ = 585 nm and a filter cut off at 550 nm, and EC_{50} values established using the non-linear regression tool on GraphPad Prism (GraphPad Software Inc.).

3. Results

3.1. Trypanosoma brucei express functional methionine sulfoxide reductases

Reduction of the MetSO stereoisomers to Met is mediated by distinct MSRs. Analysis of the T. brucei genome database [32] identified two hypothetical genes that encode for two such activities. One 543 bp open reading frame (Tb927.8.550; designated as TbmsrA) located on chro-mosome 8 has potential to be translated into a 20 kDa protein related to peptide MSRs, a family of enzymes that mediate metabolism of Met(S) SO [6,7]. The second 423 bp open reading frame (Tb927.11.11930.1; designated as TbmsrB) located on chromosome 11, has potential to encode for a 16 kDa protein that has homology to SelR enzymes which catalyse reduction of Met(R)SO [8]. The two T. brucei MSRs share no homology but do have approximately 60% identity to their trypanosomal and leishmanial orthologues (Fig. 1). When compared to other sequences, TbMSRA exhibits similar % identities (35–40%) to counterparts from plants, humans, fungi and bacteria while TbMSRB has higher identity to SelR proteins of plant (~48%) and fungal (~38%) origin relative to bacterial and human (both ~25%) enzymes. Based on sequence, TbMSRA is composed of a single peptide methionine sulf-oxide reductase (PF01625) domain that contains a characteristic G-CFWG motif [5]. In MSRAs from other organisms, cysteine (Cys13 in TbMSRA) at this site plays a key role to catalyse reduction of MetSO, with a second conserved cysteine (Cys171 in TbMSRA) found towards the carboxyl terminal helping maintain the catalytic cysteine in its re-duced, active form (Fig. 1A). Further searches using localisation pre-diction algorithms (e.g. PSORT II) indicates that TbMSRA lacks any classical sub-cellular localisation signals, suggesting that this enzyme is mostly likely found in the parasite's cytoplasm. Similarly, TbMSRB is composed of a single SelR (PF01641) domain containing several con-served cysteines [5]. MSRBs from other organisms also contains several conserved cysteine (or selenocysteine) residues. These are involved in oxidoreductase activity (Cys117 and Cys171 in TbMSRB), with the latter cysteine (or selenocysteine) catalysing substrate reduction and the former functioning to maintain the catalytic cysteine in its reduced, active form, or zinc co-factor binding (Cys99, Cys102, Cys145 and Cys148 in TbMSRB) (Fig. 1B). Here, localisation prediction algorithms (e.g. PSORT II, iPSORT and TargetP) suggest that the amino terminal of this enzyme, characterized by the presence of hydrophobic and basic amino acids and a lack of acidic residues, may function as a mi-tochondrial targeting signal.

To investigate whether the trypanosomal proteins can function as MSRs, the DNA sequences encoding for their catalytic domains were

cloned into pTrcHis-C (Invitrogen) and expressed in E. coli. In this system, the recombinant enzymes were tagged at their amino terminus with a histidine-rich sequence and an epitope detectable with the anti-Xpress monoclonal antibody (Invitrogen). For TbMSRA, expression of the full length gene generated soluble recombinant protein. In contrast, the only construct that gave functional TbMSRB was a deletion deri-vative in which the recombinant protein lacked the amino terminal, mitochondrial targeting extension (Fig. 1B). After induction with iso-propyl β-D-thiogalactoside, these constructs generated ~24 and ~21 kDa proteins corresponding to HIS-tagged TbMSRA and TbMSRB respectively, proteins that could be readily purified after one round of affinity chromatography on a nickel-HiTRAP column (Fig. 2A).

Previous studies on trypanosomal MSRA revealed that their activity is driven by a TXN-dependent cascade, with NADPH being the source of reducing equivalents [27]. Using a coupled assay that guaranteed re-generation of TXN, the activity of TbMSRA and TbMSRB was monitored by following NADPH oxidation at 340 nm (Fig. 2B). Under the condi-tions employed, both enzymes were able to reduce N-AcMetSO con-firming that they exhibited MSR activities, with the rate of substrate reduction being dependent upon TbMSR concentration (Fig. 2B). When any of the constituents (TR, $T(SH)_2$, TXN or TbMSRA/TbMSRB) of the pathway were missing, no activity was observed. TbMSRA was able to metabolise N-AcMetSO more readily than TbMSRB with TbMSRA ex-hibiting an apparent k_{cat} > 110-fold higher than that of TbMSRB for this substrate: TbMSRA and TbMSRB display apparent k_{cat} values of 12.3 and 0.11 min^{-1}, respectively, towards N-AcMetSO.

3.2. TbMSRs display different MetSO isomer specificity

To determine TbMSRA or TbMSRB specificity, their activity was followed using different MetSO stereoisomers as substrate and com-pared to reactions using a MetSO racemic mix (Fig. 2C). In agreement with MSRs from other organisms [5], TbMSRA could only metabolise L-Met(S)SO while TbMSRB was specific for towards L-Met(R)SO.

To investigate substrate specificity further and provide additional evidence that the two T. brucei enzymes do function as MSRs, the TbmsrA and TbmsrB DNA sequences in pTrcHis-C were transferred into the yeast expression vector p425-GPD. The resultant plasmids were transformed into a S. cerevisiae strain lacking three MSR enzymes and growth of the modified yeast on YNB agar plus dextrose agar supple-mented with Met or different MetSO monitored (Fig. 3). On medium containing L-Met, the growth of all fungal line was supported. In con-trast, only strains expressing TbMSRA or TbMSRB could grow on medium where L-MetSO racemate was the sole source of L-Met. When using L-Met(S)SO or L-Met(R)SO supplemented YNB, only S. cerevisiae transformed with the TbMSRA could grow on the former medium whereas only yeast expressing TbMSRB displayed strong growth on the latter.

Previous work revealed that TbMSRA activity could be readily sa-turated by TXN and L-Met(S)SO [27]. Here, we showed that free L-Met (R)SO was not efficiently metabolised by TbMSRB indicating that this was not the physiological substrate for this enzyme (Table 1). Instead TbMSRB displayed Michaelis-Menten type kinetics towards TXN and N-AcMet(R)SO although metabolism of this particular substrate via this pathway was extremely low (k_{cat} of 0.085 min^{-1}) (Fig. 2D). Comparison of K_m values suggests that the rate limiting step within this pathway

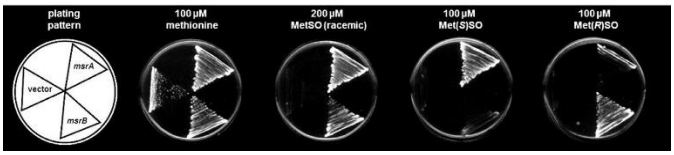

may be the interaction of TbMSRB with N-AcMet(R)SO (TbMSRB has a K_m of 1.8 ± 0.3 µM towards TXN and a K_m of 429 ± 58 µM towards N-AcMet(R)SO). These low kinetic values are typical for those reported for bacterial, plant and mammalian MSRBs [41–43] while the ability of the parasite enzyme to metabolise N-AcMet(R)SO indicates that it can ef-fectively reduce protein bound Met(R)SO: this form of MetSO is often used as substrate to test for peptide bound MSR activity [44].

3.3. TbMSRs are targeted to different cellular localisations

The subcellular location of the trypanosomal MSRs was examined by expressing GFP-tagged versions of each enzyme in BSF parasites. The DNA sequences encoding for TbMSRA and TbMSRB were amplified then cloned in-frame and upstream of the GFP gene in a trypanosomal vector that facilitated tetracycline inducible gene expression. The lo-calisation constructs were electroporated into T. brucei and re-combinant parasites selected.

To induce expression of the tagged protein, cells were incubated in the presence of tetracycline for 48 h. The parasites were then examined by western blotting using an antibody against GFP (Fig. 4A), with each extract containing a single band of the expected size (bands of ~48 and ~45 kDa were observed in TbMSRA-GFP or TbMSRB-GFP containing lanes), or were fixed and examined by confocal microscopy (Fig. 4C and D). For T. brucei induced to express tagged TbMSRA, a fluorescence signal was observed throughout the main body of the cell but absent from the nucleus indicating that this protein is found in the parasite's cytoplasm (Fig. 4C). In contrast, for parasites expressing TbMSRB-GFP, a lattice-like structure spread throughout the cell and reminiscent of the pattern reported for proteins that localise to the parasite's large, single mitochondrion, was observed (Fig. 4D). To confirm this, cells were co-stained with the mitochondrial dye, MitoTracker. When the images were superimposed, a pattern of co-localisation (yellow staining) was noted indicating that TbMSRB was located in the same compartment as MitoTracker. When cells expressing untagged GFP were analysed, fluorescence was detected throughout the whole cell (Fig. 4B). The above localisation patterns were observed by immunofluorescence studies using parasites expressing TbMSRA or B variants tagged at their carboxyl terminal with the 9E10 epitope from the human c-myc protein (see below).

3.4. Functional analysis of TbMSRs in T. brucei

To assess the importance of MSR activity to BSF T. brucei, an RNAi-based approach was employed. DNA fragments corresponding to the central regions of TbmsrA and TbmsrB were amplified and cloned into the vector $p2T7^{Ti}$. The RNAi constructs were transformed into T. brucei and recombinant parasites selected.

The effect of inducing RNAi was examined by following the cell density of tetracycline-treated cultures over a 4 day period and com-pared against untreated controls (Fig. 5A). In the absence of RNAi, all recombinant cell lines were found to grow at roughly the same rate as wild type control cells. For cells undergoing RNAi targeting the TbmsrA transcript, no significant difference in rate of growth was observed over the initial 24 h period (Fig. 5B). However, over the following 24 h, a dramatic and reproducible reduction in the cell density was observed in all replicates and clones tested, with this correlating to ~75% fall in the

Fig. 3. Yeast complementation assay demonstrates substrate preference of T. brucei MSRs. The growth of S. cerevisiae GY202 triple mutant (msrA msrB fRmsr) transformed with plasmids that facilitate expression of TbmsrA (msrA) or TbmsrB (msrB) on YNB agar the vectorplus dextrose agar supplemented with Met or different MetSOs was compared against control strains transformed with empty vector (p425 GPD).

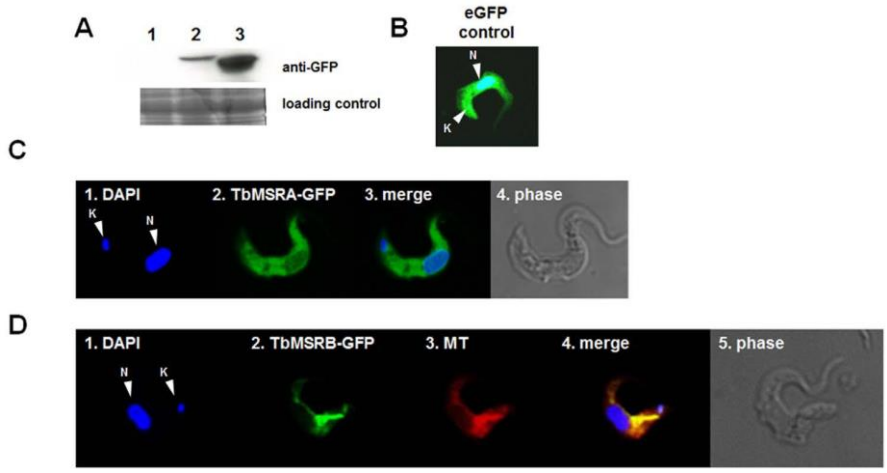

Fig. 4. Localisation of TbMSRs in bloodstream form T. brucei. (A). Expression of GFP tagged TbMSRs was examined by probing a blot containing cell lysates from T. brucei wild type (lane 1) and TbMSRA-GFP or TbMSRB-GFP expressing cells (lanes 2 and 3 re-spectively) using an anti-GFP antibody (upper panel). Protein from 1×10^7 cells was loaded in each track and equal loading verified by Coomassie staining (lower panel). (B). T. brucei expressing un-tagged GFP. The blue spots correspond to the nuclear (N) and mitochondrial (K) genomes of a trypano-some expressing GFP alone. (C). T. brucei cells ex-pressing TbMSRA-GFP (panel 2) were co-stained with DAPI (panel 1) with the merged signals (panel 3) and phase image (panel 4) shown. (D). T. brucei cells expressing TbMSRB-GFP (panel 2) were co-stained with DAPI (panel 1) and Mitotraker (TM; panel 3). The merged GFP/DAPI/Mitotraker signals (panel 4) and phase image (panel 5) are shown, with the yellow pattern in panel 4 revealing the co-loca-lisation on TbMSRB-GFP and Mitotraker. Scale bar in B, C and D = 5 μm (For interpretation of the refer-ences to color in this figure legend, the reader is referred to the web version of this article.).

TbmsrA transcript, as judged by qPCR. Further, the presence of cell debris was noted in these cultures, suggestive that a proportion of the parasite population had undergone lysis, while any remaining viable cells exhibited reduced movement. From 48 h onwards, an outgrowth of viable parasites were observed in all replicates, a type of reversion previously observed when targeting transcripts important to the growth of BSF T. brucei [36,45,46].

In contrast, cells undergoing RNAi targeting the TbmsrB transcript continued to grow throughout the entire period albeit with a reduced rate: over the first 24 h, the growth rate of tetracycline-treated cells was roughly half that of untreated cultures with this falling further to ap-proximately 20% in the next 24 h (Fig. 5B). Over the subsequent 48–72 h, an outgrowth of viable parasites were observed.

Alteration of MSR expression levels in other organisms has shown that they play an important role in protecting cells from exogenous oxidants [7,15,19,27,28]. Here, we investigated whether down-reg-ulation of the trypanosomal MSR transcripts altered parasite suscept-ibility to H_2O_2. Tetracycline induced and non-induced cells harbouring the TbmsrA or TbmsrB RNAi constructs were grown in the presence of oxidant and the effective compound concentration that inhibits parasite

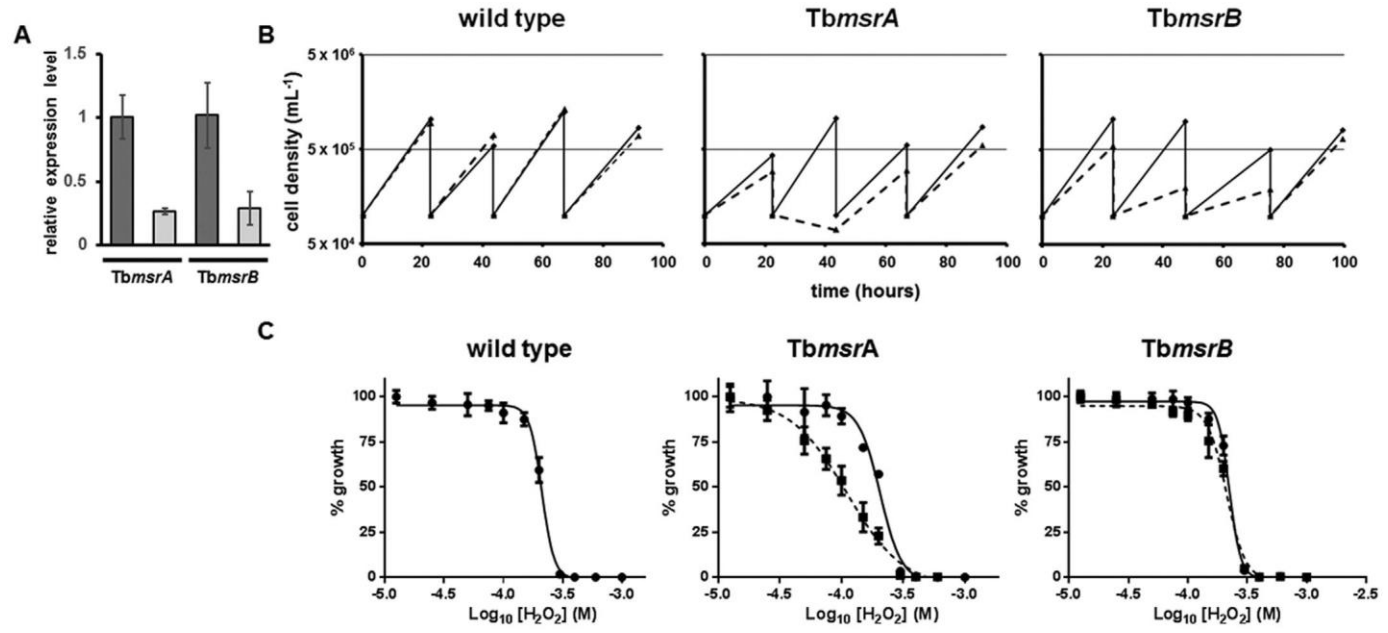

Fig. 5. Phenotypic analysis of RNAi cell lines. (A). The TbmsrA or TbmsrB transcript levels from non-induced cells (dark grey) and trypanosomes induced for 48 h to undergo RNAi (light grey) was assessed by qPCR and compared against the expression level of a standardized control (Tbtert). The relative fold difference, as judged by 2-(C_T) from reactions performed in triplicate ± standard deviation, was plotted as a measure of the relative expression level. The difference in relative expression levels between the non-induced and induced lines was judged to be statistically significant ($P < 0.01$), as assessed by the Student's t-test. The TbmsrA or TbmsrB mRNAs were both ~3.5-fold lower in the corresponding RNAi line relative to controls. (B). Growth of cells induced to undergo RNAi (dashed lines) targeting the TbmsrA or TbmsrB transcript was compared against non-induced cultures (solid line). The growth patterns shown relate to a single clone. Two other clones analysed in parallel exhibited the same profiles. (C). The BSF RNAi-TbmsrA and RNAi-TbmsrB lines were grown for 24 h in the presence of tetracycline (1 μg ml^{-1}) (square, dotted line), seeded at 1×10^4 ml^{-1} and then exposed to various concentrations of H_2O_2 (12.5–1000 μM): where applicable, RNAi induction was maintained in peroxide treated cultures by addition of fresh tetracycline to the growth medium. After 3 days at 37 °C, resazurin (2.5 μg) was added to each culture and used to determine cell density (Experimental Procedures). Untreated (circles, solid line) and wild type parasites were analysed in parallel. From the resultant dose response curves, the EC_{50} of each line towards H_2O_2 was calculated. All data points are means for experiments performed in quadruplicate ± standard deviation. The difference in susceptibility to H_2O_2 displayed by the tetracycline-treated and untreated RNAi-TbmsrA cells as judge by EC_{50} values was statistically significant ($P < 0.0001$), as assessed by Student's t-test.

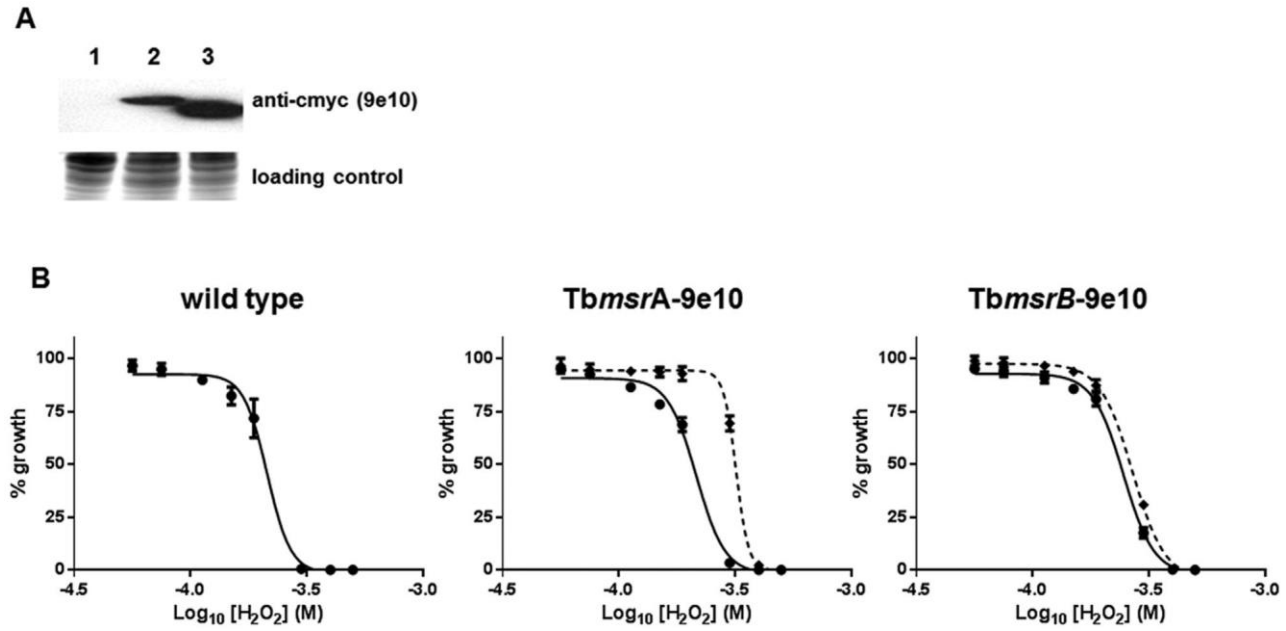

Fig. 6. Overexpression of TbMSRs in bloodstream form T. brucei. (A). Expression of -myc (9e10) tagged TbMSRs was examined by probing a blot containing cell lysates from T. brucei wild type (lane 1) and TbMSRA-9e10 or TbMSRB-9e10 expressing cells (lanes 2 and 3 respectively) using c-myc (9e10) anti-serum (upper panel). Protein from 1×10^7 cells was loaded in each track and equal loading verified by Coomassie staining (lower panel). (B). The T. brucei TbmsrA-9e10 and TbmsrB-9e10 lines were grown for 24 h in the presence of tetracycline (1 μg ml^{-1}) (diamond, dotted line), seeded at 1×10^4 ml^{-1} and then exposed to various concentrations of H_2O_2 (50–500 μM). After 3 days at 37°C, resazurin (2.5 μg) was added to each culture and used to determine cell density (Experimental Procedures). Untreated (circles, solid line) and wild type parasites were analysed in parallel. From the resultant dose response curves, the EC_{50} of each line towards H_2O_2 was calculated. All data points are means for experiments performed in quadruplicate ± standard deviation. The difference in susceptibility to H_2O_2 displayed by the tetracycline-treated and untreated TbmsrA-9e10 cells as judge by EC_{50} values was statistically significant ($P < 0.0001$), as assessed by Student's t-test.

growth by 50% (EC_{50}) determined (Fig. 5C). For cells expressing re-duced levels of TbMSRB, no significant difference in parasite sensitivity was observed: the EC_{50} values ranged from 210 to 225 μM. In contrast, recombinant T. brucei induced to undergo RNAi targeting the TbmsrA transcript were approximately 2-fold more susceptible to H_2O_2 than controls: the EC_{50} of non-induced RNAi parasites was 204.7 ± 9.4 μM in comparison to tetracycline treated cells that exhibited an EC_{50} of 111.4 ± 13.5 μM.

As parasites with reduced levels of TbmsrA are more susceptible to oxidative stress, we tested whether MSR overexpression leads to re-sistance. TbmsrA and TbmsrB, minus their STOP codon, were amplified then cloned in-frame and upstream of the DNA sequence encoding for the 9E10 epitope from the human c-myc protein in a trypanosomal vector that facilitated tetracycline inducible gene expression. The constructs were introduced into T. brucei and recombinant parasites selected. To verify expression of the tagged TbMSRs, cell extracts generated from parasites cultured in the presence of tetracycline for 48 h were examined by western blotting using an antibody against c-myc epitope (Fig. 6A). A single band was observed in lanes where TbMSRA-9e10 (~21 kDa) or TbMSRB-9e10 (~20 kDa) expression had been induced. Tetracycline treated and untreated T. brucei were then grown in the presence of H_2O_2 and EC_{50}s determined (Fig. 6B). For cells expressing TbMSRB-9e10, no significant difference in parasite sensi-tivity was observed. When these studies were extended to TbMSRA, parasites expressing the c-myc-tagged enzyme were 1.5-fold more re-sistant to H_2O_2 than controls: the EC_{50} of non-induced parasites was 212.9 ± 7.7 μM in comparison to tetracycline induced cells that ex-hibited an EC_{50} of 320.4 ± 2.9 μM.

4. Discussion

Throughout its life cycle, T. brucei is continually exposed to ROS. To combat their detrimental effects, this parasite expresses a series of novel protection strategies that collectively constituent this pathogen's oxi-dative defence system. As these mechanisms are distinct from those of its mammalian host [21,22,47–49], with several components being essential for growth of the medically relevant parasite stage, they are viewed as potential targets for development of new HAT che-motherapies [21,36,49,50]. Here, we report the characterisation of two additional components of the trypanosomal oxidative defence system, showing that T. brucei expresses two structurally unrelated MSRs (TbMSRA and TbMSRB) that can be distinguished on the basis of their sequence, substrate specificity and sub-cellular localisation.

Although functionally related, TbMSRA and TbMSRB share no sig-nificant sequence homology with this diversity conferring difference in substrate specificities. In the case of TbMSRA, the presence of a GCFWG motif in its sequence coupled with it being only able to metabolise the S epimer of MetSO establishes this as a member of the peptide methionine sulfoxide reductase, or MSRA, family of antioxidant proteins (Figs. 1A, 2 and 3). In contrast, TbMSRB contains a domain structure that places it in the SelR, or MRSB, group of methionine sulfoxide reductases, with enzymatic and phenotypic screening showing that this parasite oxi-doreductase can only mediate conversion of peptide-bound Met(R)SO to Met (Figs. 1B, 2 and 3).

Based on sequence and substrate specificity, the two parasite en-zymes are typical members of the MSRA or MRSB clades although they are different in relation to the pathways that facilitate their reduction. In many instances, the concerted action of thioredoxin reductase, thioredoxin and MSR act as intermediaries to shuttle reducing equiva-lents from NADPH to MetSO [11]. As trypanosomes lack thioredoxin reductase this pathway cannot operate in T. brucei. In the case of TbMSRA, its in vitro activity is dependent upon TR and trypanothione. Using NADPH as electron donor, these parasite specific factors fulfil the role of 'thioredoxin reductase', functioning to maintain TXN in its re-duced state [51], with reducing equivalents then transferred onto Met (S)SO to form Met via the trypanosomal MSR (Fig. 2D) [27]. Steady state kinetics indicate that the rate limiting step of this pathway appears to be the TbMSRA mediated reduction of free Met(S)SO to Met, a trait noted for MSRAs from other organisms [27,52–54]. As all components of this cascade are widely distributed throughout the parasite cytosol

(Fig. 4C) [47,55] and that TbMSRA exhibits reasonable kinetics towards both TXN and free Met(S)SO, it is hypothesized that the above pathway functions within T. brucei, acting to repair damaged Met, specifically free Met(S)SO, at this particular subcellular site. Intriguingly, our yeast complementation studies indicate that TbMSRA (and TbMSRB) can utilize non-trypanothione redox cascades as source of reducing equivalents suggesting that the activity of these enzymes within the trypanosome may be driven by an alternative system to that described above. This is analogous to the situation seen with other tryparedoxin-dependent enzymes, including the tryparedoxin peroxidases, which can exploit different thioredoxin/thioredoxin-like molecules as electron donor [48,56]. We postulate that the trypanosomal MSRs are able to interact with the yeast thioredoxin system and complement for the appropriate fungal mutation to produce the observed growth pheno-type.

In contrast, the pathway that operates to maintain TbMSRB in its reduced state is unclear. Biochemical studies on recombinant enzyme has shown that the TR/T[SH]$_2$/TXN system can support TbMSRB ac-tivity resulting in slow turnover of N-AcMet(R)SO (Fig. 2). The kinetic values exhibited by the parasite protein to both TXN and MetSO are on par with those noted for other MSRBs, with the rate of N-AcMet(R)SO reduction limited by the enzyme/substrate interaction [8,57]. Such observations, coupled with the MSRBs preference to bind and meta-bolise protein-bound Met(R)SO, has led to the idea that free MetSO may not be the major physiological substrate for these reductases [8] and may account for the fact that some organisms have evolved other free Met(R)SO metabolising activities (e.g. fRMSRs), with turnover of this particular substrate taking place at an appreciably faster rate than MSRBs [9,10]. Further, the components that support the trypanothione-dependent, TbMSRB reduction cascade are not present at the same cellular site: TR and TbMSRB are restricted to the cytosol and mi-tochondrion, respectively, while TXNI is apparently found across both sites (Fig. 4B) [47,55]. By implication, either TbMSRB activity is sup-ported by an unidentified pathway found entirely within the parasite mitochondrion or the TR/T[SH]$_2$/TXN redox cascade is split across different cellular compartments, with comparative analysis indicating that the thiol constituent being the transferable factor. In other eu-karyotic cells, GSH is maintained at high (mM) levels in the mi-tochondrial lumen even though this organelle lacks the biosynthetic machinery to make this tripeptide. Instead, cytosolic pools of GSH are transferred into mitochondria via several transporters which may in-clude dicarboxylate and 2-oxoglutarate carriers [58–60]. If an equiva-lent T[SH]$_2$ translocation mechanism(s) does function in trypanosomes then given the unique properties of the parasite specific thiol, any transport system would be mechanistically distinct from that which operates in the transfer of GSH and as such would be of particular in-terest as a target(s) for chemotherapy. Once in the mitochondrion, T[SH]$_2$ can then facilitate transfer of reducing equivalents via TXN and TbMSRB to Met(R)SO. Intriguingly, data released as part of the TrypTag project [61] indicates that trypanosomes express a classical thioredoxin (Tb927.9.3370 on TriTrypDB [32]) which can be readily reduced by T(SH)$_2$ [62,63], present throughout the parasite mitochondrion. If correct, this may also function as an intermediary in shuttling reducing equivalents from T[SH]$_2$ to TbMSRB.

Our data shows that TbMSRA and TbMSRB are located in the T. brucei cytoplasm and mitochondrion respectively, a distribution also observed with the S. cerevisiae counterparts (Fig. 4) [64]. Why trypa-nosomes and yeast target these two enzymes to only these sites is un-clear given that mammalian cells possess multiple isoforms of each enzyme type at different sub-cellular sites (mammalian cells express cytosolic, mitochondrial and nuclear versions of MSRA and MSRB while an isoform of the latter is also present in the endoplasmic reticulum [65–67]). Taking into consideration their substrate specificity, the specific localisation displayed by TbMSRA and TbMSRB raises a number of interesting questions such as how is free or protein bound Met(S)SO metabolised in parasite organelles and how is free or protein bound Met(R)SO detoxified at non-mitochondrial sites. Part of this may be attributed to uncharacterised activities (e.g. T. brucei appears to have potential to encode for a cytoplasmic fRMSR (Tb927.5.1250 on Tri-TrypDB)) or could reflect the importance of various MetSO forms in different compartments of the cell (e.g. it may be favourable to export free MetSO epimers out of the mitochondrion into the cytoplasm to facilitate conversion back to Met, rather than carrying out this repair within the organelle).

MSRs represent key components in an organism's oxidative defence armoury, functioning in processes such as bacterial and protozoal virulence [7,28,68–70] and ageing [16,17,71]. To evaluate the im-portance of trypanosomal enzymes to T. brucei, functional genomic approaches were used to generate parasite lines expressing altered le-vels of each reductase. Using RNAi, each enzyme was shown to be important but not essential for the growth of bloodstream form para-sites (Fig. 5). For trypanosomes engineered to express reduced levels of the TbmsrA transcript, the stalling of parasite growth was accompanied by an increased susceptibility to exogenous H_2O_2 with the reciprocal phenotype observed in cells engineered to over express this enzyme. In contrast, the reduction in cell growth observed when targeting the TbmsrB or the elevated expression of this reductase in T. brucei did not affect parasite sensitivity to H_2O_2. The observed susceptibility pheno-types suggest that the amount of exogenous oxidant added to cultures is sufficient to promote MetSO formation in targets found in the parasite's cytosol, damage that can be readily repaired by TbMSRA. However, these peroxide levels are not sufficient to cause significant Met oxida-tion in the trypanosomal mitochondrion, presumably because this oxi-dant is detoxified by the various tryparedoxin peroxidase systems ex-pressed by T. brucei [47,49].

In summary, we have demonstrated that T. brucei expresses cyto-solic and mitochondrial methionine sulfoxide reducing pathways which together constitute a new arm of this parasite's oxidative reparative defence system. As the redox cascades associated with these activities rely upon trypanosome-specific factors and that the activity of the terminal reductase is important for pathogen growth, these mechanisms may have potential as chemotherapeutic targets.

Conflict of interest

The authors declare that they have no conflicts of interest with the contents of this article.

Acknowledgments

We thank Guy Hanke (QMUL) for their critical review of this manuscript. We acknowledge the members of the T. brucei genome (http://tritrypdb.org/tritrypdb/) and TrypTag (http://tryptag.org) projects for sequence and localisation data, respectively. A component of this work was supported by grants from ANPCyT (PICT-2015-1149; PICT-2014-2103). SAG, and DGA are investigator career members from CONICET. AK was a recipient of a Queen Mary University of London PhD studentship

References

EEEEEEEEE. J.R. Stevens, H.A. Noyes, C.J. Schofield, W. Gibson, The molecular evolution of Trypanosomatidae, Adv. Parasitol. 48 (2001) 1–56.
FFFFFFFFF. E.R. Stadtman, Protein oxidation and aging, Science 257 (5074) (1992) 1220–1224.
GGGGGGGGG. B. Friguet, Oxidized protein degradation and repair in ageing and oxidative stress, FEBS Lett. 580 (12) (2006) 2910–2916.
HHHHHHHHH. C. Achilli, A. Ciana, G. Minetti, The discovery of methionine sulfoxide reductase enzymes: an historical account and future perspectives, Biofactors 41 (3) (2015) 135–152.
IIIIIIIII. S. Boschi-Muller, A. Olry, M. Antoine, G. Branlant, The enzymology and biochem-istry of methionine sulfoxide reductases, Biochim. Biophys. Acta 1703 (2) (2005) 231–238.
JJJJJJJJJ. S.I. Ejiri, H. Weissbach, N. Brot, Reduction of methionine sulfoxide to methionine by Escherichia coli, J. Bacteriol. 139 (1) (1979) 161–164.
KKKKKKKKK. T.M. Wizemann, J. Moskovitz, B.J. Pearce, D. Cundell, C.G. Arvidson, M. So,

H. Weissbach, N. Brot, H.R. Masure, Peptide methionine sulfoxide reductase con-tributes to the maintenance of adhesins in three major pathogens, Proc. Natl. Acad. Sci. USA 93 (15) (1996) 7985–7990.
8 R. Grimaud, B. Ezraty, J.K. Mitchell, D. Lafitte, C. Briand, P.J. Derrick, F. Barras, Repair of oxidized proteins. Identification of a new methionine sulfoxide reductase, Biol. Chem. 276 (52) (2001) 48915–48920.
8 F. Etienne, D. Spector, N. Brot, H. Weissbach, A methionine sulfoxide reductase in Escherichia coli that reduces the R enantiomer of methionine sulfoxide, Biochem. Biophys. Res. Commun. 300 (2) (2003) 378–382.
8 Z. Lin, L.C. Johnson, H. Weissbach, N. Brot, M.O. Lively, W.T. Lowther, Free methionine-(R)-sulfoxide reductase from Escherichia coli reveals a new GAF domain function, Proc. Natl. Acad. Sci. USA 104 (23) (2007) 9597–9602.
8 N. Brot, L. Weissbach, J. Werth, H. Weissbach, Enzymatic reduction of protein-bound methionine sulfoxide, Proc. Natl. Acad. Sci. USA 78 (4) (1981) 2155–2158.
8 J. Moskovitz, J.M. Poston, B.S. Berlett, N.J. Nosworthy, R. Szczepanowski, E.R. Stadtman, Identification and characterization of a putative active site for peptide methionine sulfoxide reductase (MsrA) and its substrate stereospecificity, J. Biol. Chem. 275 (19) (2000) 14167–14172.
8 D. Sagher, D. Brunell, J.F. Hejtmancik, M. Kantorow, N. Brot, H. Weissbach, Thionein can serve as a reducing agent for the methionine sulfoxide reductases, Proc. Natl. Acad. Sci. USA 103 (23) (2006) 8656–8661.
8 C. Vieira Dos Santos, E. Laugier, L. Tarrago, V. Massot, E. Issakidis-Bourguet, Rouhier, P. Rey, Specificity of thioredoxins and glutaredoxins as electron donors to two distinct classes of Arabidopsis plastidial methionine sulfoxide reductases B, FEBS Lett. 581 (23) (2007) 4371–4376.
219: J. Moskovitz, B.S. Berlett, J.M. Poston, E.R. Stadtman, The yeast peptide-methio-nine sulfoxide reductase functions as an antioxidant in vivo, Proc. Natl. Acad. Sci. USA 94 (18) (1997) 9585–9589.
220: J. Moskovitz, S. Bar-Noy, W.M. Williams, J. Requena, B.S. Berlett, E.R. Stadtman, Methionine sulfoxide reductase (MsrA) is a regulator of antioxidant defense and lifespan in mammals, Proc. Natl. Acad. Sci. USA 98 (23) (2001) 12920–12925.
221: H. Ruan, X.D. Tang, M.L. Chen, M.L. Joiner, G. Sun, N. Brot, H. Weissbach, S.H. Heinemann, L. Iverson, C.F. Wu, T. Hoshi, High-quality life extension by the enzyme peptide methionine sulfoxide reductase, Proc. Natl. Acad. Sci. USA 99 (5) (2002) 2748–2753.
222: D.T. Le, B.C. Lee, S.M. Marino, Y. Zhang, D.E. Fomenko, A. Kaya, E. Hacioglu, G.H. Kwak, A. Koc, H.Y. Kim, V.N. Gladyshev, Functional analysis of free methio-nine-R-sulfoxide reductase from Saccharomyces cerevisiae, J. Biol. Chem. 284 (7) (2009) 4354–4364.
223: C. Zhao, A. Hartke, M. La Sorda, B. Posteraro, J.M. Laplace, Y. Auffray, Sanguinetti, Role of methionine sulfoxide reductases A and B of Enterococcus faecalis in oxidative stress and virulence, Infect. Immun. 78 (9) (2010) 3889–3897.
224: A.H. Fairlamb, P. Blackburn, P. Ulrich, B.T. Chait, A. Cerami, Trypanothione: a novel bis(glutathionyl)spermidine cofactor for glutathione reductase in trypanoso-matids, Science 227 (4693) (1985) 1485–1487.
225: S.R. Wilkinson, S.R. Prathalingam, M.C. Taylor, A. Ahmed, D. Horn, J.M. Kelly, Functional characterisation of the iron superoxide dismutase gene repertoire in Trypanosoma brucei, Free Radic. Biol. Med. 40 (2) (2006) 198–209.
226: F. Dufernez, C. Yernaux, D. Gerbod, C. Noel, M. Chauvenet, R. Wintjens, V.P. Edgcomb, M. Capron, F.R. Opperdoes, E. Viscogliosi, The presence of four iron-containing superoxide dismutase isozymes in trypanosomatidae: characterization, subcellular localization, and phylogenetic origin in Trypanosoma brucei, Free Radic. Biol. Med. 40 (2) (2006) 210–225.
227: S.L. Shames, A.H. Fairlamb, A. Cerami, C.T. Walsh, Purification and characteriza-tion of trypanothione reductase from Crithidia fasciculata, a newly discovered member of the family of disulfide-containing flavoprotein reductases, Biochemistry 25 (12) (1986) 3519–3526.
228: R.L. Krauth-Siegel, B. Enders, G.B. Henderson, A.H. Fairlamb, R.H. Schirmer, Trypanothione reductase from Trypanosoma cruzi. Purification and characteriza-tion of the crystalline enzyme, Eur. J. Biochem. 164 (1) (1987) 123–128.
229: B. Manta, M. Comini, A. Medeiros, M. Hugo, M. Trujillo, R. Radi, Trypanothione: a unique bis-glutathionyl derivative in trypanosomatids, Biochim. Biophys. Acta 1830 (5) (2013) 3199–3216.
230: F. Irigoin, L. Cibils, M.A. Comini, S.R. Wilkinson, L. Flohe, R. Radi, Insights into the redox biology of Trypanosoma cruzi: trypanothione metabolism and oxidant de-toxification, Free Radic. Biol. Med. 45 (6) (2008) 733–742.
231: D.G. Arias, M.S. Cabeza, E.D. Erben, P.G. Carranza, H.D. Lujan, M.T. Tellez Inon, Iglesias, S.A. Guerrero, Functional characterization of methionine sulfoxide reductase A from Trypanosoma spp, Free Radic. Biol. Med. 50 (1) (2011) 37–46.
6: F.M. Sansom, L. Tang, J.E. Ralton, E.C. Saunders, T. Naderer, M.J. McConville, Leishmania major methionine sulfoxide reductase A is required for resistance to oxidative stress and efficient replication in macrophages, PLoS One 8 (2) (2013) e56064.
7: H. Hirumi, K. Hirumi, Continuous cultivation of Trypanosoma brucei blood stream forms in a medium containing a low concentration of serum protein without feeder cell layers, J. Parasitol. 75 (6) (1989) 985–989.
8: E. Wirtz, C. Clayton, Inducible gene expression in trypanosomes mediated by a prokaryotic repressor, Science 268 (5214) (1995) 1179–1183.
9: S. Alsford, T. Kawahara, L. Glover, D. Horn, Tagging a T. brucei RRNA locus im-proves stable transfection efficiency and circumvents inducible expression position effects, Mol. Biochem. Parasitol. 144 (2) (2005) 142–148.
10: M. Aslett, C. Aurrecoechea, M. Berriman, J. Brestelli, B.P. Brunk, M. Carrington, D.P. Depledge, S. Fischer, B. Gajria, X. Gao, M.J. Gardner, A. Gingle, G. Grant, O.S. Harb, M. Heiges, C. Hertz-Fowler, R. Houston, F. Innamorato, J. Iodice, J.C. Kissinger, E. Kraemer, W. Li, F.J. Logan, J.A. Miller, S. Mitra, P.J. Myler, Nayak, C. Pennington, I. Phan, D.F. Pinney, G. Ramasamy, M.B. Rogers, D.S. Roos, C. Ross, D. Sivam, D.F. Smith, G. Srinivasamoorthy, C.J. Stoeckert Jr., S. Subramanian, R. Thibodeau, A. Tivey, C. Treatman, G. Velarde, H. Wang, TriTrypDB: a functional genomic resource for the Trypanosomatidae, Nucleic Acids Res. 38 (Database issue) (2010) D457–D462.
221 S.R. Wilkinson, D.J. Meyer, M.C. Taylor, E.V. Bromley, M.A. Miles, J.M. Kelly, The Trypanosoma cruzi enzyme TcGPXI is a glycosomal peroxidase and can be linked to trypanothione reduction by glutathione or tryparedoxin, J. Biol. Chem. 277 (19) (2002) 17062–17071.
222 H.L. Holland, J.X. Gu, F. Orallo, M. Camina, P. Fabeiro, A.J. Willetts, Enantioselective synthesis and pharmacological evaluation of a new type of ver-apamil analog with hypotensive and calcium antagonist activities, Pharm. Res. 16 (1999) 281–287.
223 G.H. Kwak, K.Y. Hwang, H.Y. Kim, Analyses of methionine sulfoxide reductase activities towards free and peptidyl methionine sulfoxides, Arch. Biochem. Biophys. 527 (1) (2012) 1–5.
224 S.R. Wilkinson, D. Horn, S.R. Prathalingam, J.M. Kelly, RNA interference identifies two hydroperoxide metabolizing enzymes that are essential to the bloodstream form of the african trypanosome, J. Biol. Chem. 278 (34) (2003) 31640–31646.
225 A.K. Ingram, D. Horn, Histone deacetylases in Trypanosoma brucei: two are es-sential and another is required for normal cell cycle progression, Mol. Microbiol. 45 (2002) 89–97.
[38] M. Brenndorfer, M. Boshart, Selection of reference genes for mRNA quantification in Trypanosoma brucei, Mol. Biochem. Parasitol. 172 (1) (2010) 52–55.
[39] T.D. Schmittgen, K.J. Livak, Analyzing real-time PCR data by the comparative C(T) method, Nat. Protoc. 3 (6) (2008) 1101–1108.
[40] S.R. Wilkinson, M.C. Taylor, D. Horn, J.M. Kelly, I. Cheeseman, A mechanism for cross-resistance to nifurtimox and benznidazole in trypanosomes, Proc. Natl. Acad. Sci. USA 105 (13) (2008) 5022–5027.
[41] A. Olry, S. Boschi-Muller, G. Branlant, Kinetic characterization of the catalytic mechanism of methionine sulfoxide reductase B from Neisseria meningitidis, Biochemistry 43 (36) (2004) 11616–11622.
[42] C. Vieira Dos Santos, S. Cuine, N. Rouhier, P. Rey, The Arabidopsis plastidic me-thionine sulfoxide reductase B proteins. sequence and activity characteristics, comparison of the expression with plastidic methionine sulfoxide reductase A, and induction by photooxidative stress, Plant Physiol. 138 (2) (2005) 909–922.
[43] H.Y. Kim, V.N. Gladyshev, Different catalytic mechanisms in mammalian seleno-cysteine- and cysteine-containing methionine-R-sulfoxide reductases, PLoS Biol. 3 (12) (2005) e375.
[44] N. Brot, J. Werth, D. Koster, H. Weissbach, Reduction of N-acetyl methionine sulfoxide: a simple assay for peptide methionine sulfoxide reductase, Anal. Biochem. 122 (2) (1982) 291–294.
[45] M. Drozdz, S.S. Palazzo, R. Salavati, J. O'Rear, C. Clayton, K. Stuart, TbMP81 is required for RNA editing in Trypanosoma brucei, Embo J. 21 (7) (2002) 1791–1799.
[46] T. Furuya, P. Kessler, A. Jardim, A. Schnaufer, C. Crudder, M. Parsons, Glucose is toxic to glycosome-deficient trypanosomes, Proc. Natl. Acad. Sci. USA 99 (22) (2002) 14177–14182.
[47] E. Tetaud, C. Giroud, A.R. Prescott, D.W. Parkin, D. Baltz, N. Biteau, T. Baltz, A.H. Fairlamb, Molecular characterisation of mitochondrial and cytosolic trypa-nothione-dependent tryparedoxin peroxidases in Trypanosoma brucei, Mol. Biochem. Parasitol. 116 (2) (2001) 171–183.
[48] H. Hillebrand, A. Schmidt, R.L. Krauth-Siegel, A second class of peroxidases linked to the trypanothione metabolism, J. Biol. Chem. 278 (9) (2003) 6809–6815.
[49] T. Schlecker, A. Schmidt, N. Dirdjaja, F. Voncken, C. Clayton, R.L. Krauth-Siegel, Substrate specificity, localisation and essential role of the glutathione peroxidase-type tryparedoxin peroxidases in Trypanosoma brucei, J. Biol. Chem. (2005).
[50] S.R. Prathalingham, S.R. Wilkinson, D. Horn, J.M. Kelly, Deletion of the Trypanosoma brucei superoxide dismutase gene sodb1 increases sensitivity to ni-furtimox and benznidazole, Antimicrob. Agents Chemother. 51 (2) (2007) 755–758.
[51] H. Ludemann, M. Dormeyer, C. Sticherling, D. Stallmann, H. Follmann, R.L. Krauth-Siegel, Trypanosoma brucei tryparedoxin, a thioredoxin-like protein in African trypanosomes, FEBS Lett. 431 (3) (1998) 381–385.
[52] S. Boschi-Muller, S. Azza, G. Branlant, E. coli methionine sulfoxide reductase with a truncated N terminus or C terminus, or both, retains the ability to reduce methio-nine sulfoxide, Protein Sci. 10 (11) (2001) 2272–2279.
[53] B.C. Lee, Y.K. Lee, H.J. Lee, E.R. Stadtman, K.H. Lee, N. Chung, Cloning and characterization of antioxidant enzyme methionine sulfoxide-S-reductase from Caenorhabditis elegans, Arch. Biochem. Biophys. 434 (2) (2005) 275–281.
[54] N. Rouhier, B. Kauffmann, F. Tete-Favier, P. Palladino, P. Gans, G. Branlant, J.P. Jacquot, S. Boschi-Muller, Functional and structural aspects of poplar cytosolic and plastidial type a methionine sulfoxide reductases, J. Biol. Chem. 282 (5) (2007) 3367–3378.
[55] K. Smith, F.R. Opperdoes, A.H. Fairlamb, Subcellular distribution of trypanothione reductase in bloodstream and procyclic forms of Trypanosoma brucei, Mol. Biochem. Parasitol. 48 (1) (1991) 109–112.
[56] L. Flohe, T. Jaeger, S. Pilawa, H. Sztajer, Thiol-dependent peroxidases care little about homology-based assignments of function, Redox Rep. 8 (5) (2003) 256–264.
[57] A. Olry, S. Boschi-Muller, M. Marraud, S. Sanglier-Cianferani, A. Van Dorsselear, G. Branlant, Characterization of the methionine sulfoxide reductase activities of PILB, a probable virulence factor from Neisseria meningitidis, J. Biol. Chem. 277 (14) (2002) 12016–12022.
[58] J. Martensson, J.C. Lai, A. Meister, High-affinity transport of glutathione is part of a multicomponent system essential for mitochondrial function, Proc. Natl. Acad. Sci. USA 87 (18) (1990) 7185–7189.
[59] Z. Chen, L.H. Lash, Evidence for mitochondrial uptake of glutathione by di-carboxylate and 2-oxoglutarate carriers, J. Pharmacol. Exp. Ther. 285 (2) (1998)

608–618.
[60] Z. Chen, D.A. Putt, L.H. Lash, Enrichment and functional reconstitution of glu-tathione transport activity from rabbit kidney mitochondria: further evidence for the role of the dicarboxylate and 2-oxoglutarate carriers in mitochondrial glu-tathione transport, Arch. Biochem. Biophys. 373 (1) (2000) 193–202.
[61] S. Dean, J.D. Sunter, R.J. Wheeler, TrypTag.org: a trypanosome genome-wide protein localisation resource, Trends Parasitol. 33 (2) (2017) 80–82.
[62] N. Reckenfelderbaumer, H. Ludemann, H. Schmidt, D. Steverding, R.L. Krauth-Siegel, Identification and functional characterization of thioredoxin from Trypanosoma brucei brucei, J. Biol. Chem. 275 (11) (2000) 7547–7552.
[63] H. Schmidt, R.L. Krauth-Siegel, Functional and physicochemical characterization of the thioredoxin system in Trypanosoma brucei, J. Biol. Chem. 278 (47) (2003) 46329–46336.
[64] A. Kaya, A. Koc, B.C. Lee, D.E. Fomenko, M. Rederstorff, A. Krol, A. Lescure, V.N. Gladyshev, Compartmentalization and regulation of mitochondrial function by methionine sulfoxide reductases in yeast, Biochemistry 49 (39) (2010) 8618–8625.
[65] H.Y. Kim, V.N. Gladyshev, Methionine sulfoxide reduction in mammals: char-acterization of methionine-R-sulfoxide reductases, Mol. Biol. Cell 15 (3) (2004) 1055–1064.
[66] H.Y. Kim, V.N. Gladyshev, Alternative first exon splicing regulates subcellular distribution of methionine sulfoxide reductases, BMC Mol. Biol. 7 (2006) 11.
[67] K.U. Schallreuter, K. Rubsam, B. Chavan, C. Zothner, J.M. Gillbro, J.D. Spencer, J.M. Wood, Functioning methionine sulfoxide reductases A and B are present in human epidermal melanocytes in the cytosol and in the nucleus, Biochem. Biophys. Res. Commun. 342 (1) (2006) 145–152.
[68] M.E. Hassouni, J.P. Chambost, D. Expert, F. Van Gijsegem, F. Barras, The minimal gene set member msrA, encoding peptide methionine sulfoxide reductase, is a virulence determinant of the plant pathogen Erwinia chrysanthemi, Proc. Natl. Acad. Sci. USA 96 (3) (1999) 887–892.
[69] S. Dhandayuthapani, M.W. Blaylock, C.M. Bebear, W.G. Rasmussen, J.B. Baseman, Peptide methionine sulfoxide reductase (MsrA) is a virulence determinant in Mycoplasma genitalium, J. Bacteriol. 183 (19) (2001) 5645–5650.
[70] Y. Lei, Y. Zhang, B.D. Guenther, J. Kreth, M.C. Herzberg, Mechanism of adhesion maintenance by methionine sulphoxide reductase in Streptococcus gordonii, Mol. Microbiol. 80 (3) (2011) 726–738.
[71] A. Koc, A.P. Gasch, J.C. Rutherford, H.Y. Kim, V.N. Gladyshev, Methionine sulf-oxide reductase regulation of yeast lifespan reveals reactive oxygen species-de-pendent and -independent components of aging, Proc. Natl. Acad. Sci. USA 101 (21)

References

Abdullah, U. B. *et al.* (2017) 'RPA activates the XPF-ERCC1 endonuclease to initiate processing of DNA interstrand crosslinks', *The EMBO Journal*, 36(14), pp. 2047–2060. doi: 10.15252/embj.201796664.

Actis, M. L. *et al.* (2016) 'Identification of the first small-molecule inhibitor of the REV7 DNA repair protein interaction', *Bioorganic & Medicinal Chemistry*, 24(18), pp. 4339–4346. doi: 10.1016/j.bmc.2016.07.026.

Al-Minawi, A. Z. *et al.* (2009) 'The ERCC1/XPF endonuclease is required for completion of homologous recombination at DNA replication forks stalled by inter-strand cross-links', *Nucleic acids research*. doi: 10.1093/nar/gkp705.

Allerston, C. K. *et al.* (2015) 'The structures of the SNM1A and SNM1B/Apollo nuclease domains reveal a potential basis for their distinct DNA processing activities', *Nucleic Acids Research*, 43(22), pp. 11047–11060. doi: 10.1093/nar/gkv1256.

Alsford, S. *et al.* (2005) 'Tagging a T. brucei RRNA locus improves stable transfection efficiency and circumvents inducible expression position effects', *Molecular and Biochemical Parasitology*, 144(2), pp. 142–148. doi: 10.1016/j.molbiopara.2005.08.009.

Alsford, S. *et al.* (2012) 'High-throughput decoding of antitrypanosomal drug efficacy and resistance.', *Nature*. Nature Publishing Group, 482(7384), pp. 232–6. doi: 10.1038/nature10771.

Baker, N. *et al.* (2012) 'Aquaglyceroporin 2 controls susceptibility to melarsoprol and pentamidine in African trypanosomes', *Proceedings of the National Academy of Sciences*, 109(27), pp. 10996–11001. doi: 10.1073/pnas.1202885109.

Baker, N., Alsford, S. and Horn, D. (2011) 'Genome-wide RNAi screens in African trypanosomes identify the nifurtimox activator NTR and the eflornithine transporter AAT6.', *Molecular and biochemical parasitology*, 176(1), pp. 55–7. doi: 10.1016/j.molbiopara.2010.11.010.

Barber, L. J. *et al.* (2005) 'DNA Interstrand Cross-Link Repair in the Saccharomyces cerevisiae Cell Cycle : Overlapping Roles for PSO2 (SNM1) with MutS Factors and EXO1 during S Phase', *Molecular and Cellular Biology*. American Society for Microbiology, 25(6), pp. 2297–2309. Available at: http://www.ncbi.nlm.nih.gov/pubmed/15743825 (Accessed: 25 November 2017).

Barnes, R. L. and McCulloch, R. (2007) 'Trypanosoma brucei homologous recombination is dependent on substrate length and homology, though displays a differential dependence on mismatch repair as substrate length decreases.', *Nucleic acids research*. Oxford University Press, 35(10), pp. 3478–93. doi: 10.1093/nar/gkm249.

Barrett, M. P. *et al.* (2003) 'The trypanosomiases.', *Lancet*, 362(9394), pp. 1469–80. doi: 10.1016/S0140-6736(03)14694-6.

Batenburg, N. L. *et al.* (2015) 'Cockayne syndrome group B protein regulates DNA double-strand break repair and checkpoint activation', *The EMBO Journal*, 34(10), pp. 1399–1416. doi: 10.15252/embj.201490041.

Bauer, G. B. and Povirk, L. F. (1997) 'Specificity and kinetics of interstrand and intrastrand bifunctional alkylation by nitrogen mustards at a G-G-C sequence', *Nucleic Acids Research*, 25(6), pp. 1211–1218. Available at: https://www.ncbi.nlm.nih.gov/pmc/articles/PMC146567/pdf/251211.pdf (Accessed: 4 December 2017).

Bell, J. S. *et al.* (2004) 'Characterization of components of the mismatch repair machinery in Trypanosoma brucei.', *Molecular microbiology*, 51(1), pp. 159–73. Available at: http://www.ncbi.nlm.nih.gov/pubmed/14651619 (Accessed: 16 October 2017).

Beneke, T. *et al.* (2017) 'A CRISPR Cas9 high-throughput genome editing toolkit for kinetoplastids.', *Royal Society open science*. The Royal Society, 4(5), p. 170095. doi: 10.1098/rsos.170095.

Bernhard, S. C. *et al.* (2007) 'Melarsoprol- and pentamidine-resistant Trypanosoma brucei rhodesiense populations and their cross-resistance', *International Journal for Parasitology*, 37(13), pp. 1443–1448. doi: 10.1016/j.ijpara.2007.05.007.

Bessho, T. (2003) 'Induction of DNA replication-mediated double strand breaks by psoralen DNA interstrand cross-links.', *The Journal of biological chemistry*. American Society for Biochemistry and Molecular Biology, 278(7), pp. 5250–4. doi: 10.1074/jbc.M212323200.

Boiteux, S. and Jinks-Robertson, S. (2013) 'DNA repair mechanisms and the bypass of DNA damage in Saccharomyces cerevisiae.', *Genetics*. Genetics Society of America, 193(4), pp. 1025–64. doi: 10.1534/genetics.112.145219.

Bonatto, D. *et al.* (2005) 'The eukaryotic Pso2/Snm1/Artemis proteins and their function as genomic and cellular caretakers.', *Brazilian journal of medical and biological research*, 38(3), pp. 321–34.

Bot, C. *et al.* (2013) 'Evaluating 5-nitrofurans as trypanocidal agents.', *Antimicrobial agents and chemotherapy*, 57(4), pp. 1638–47. doi: 10.1128/AAC.02046-12.

Brenndörfer, M. and Boshart, M. (2010) 'Selection of reference genes for mRNA quantification in Trypanosoma brucei', *Molecular and Biochemical Parasitology*, 172(1), pp. 52–55. doi: 10.1016/j.molbiopara.2010.03.007.

Brosh, R. M. and Cantor, S. B. (2014) 'Molecular and cellular functions of the FANCJ DNA helicase defective in cancer and in Fanconi anemia', *Frontiers in Genetics*, p. 372. doi: 10.3389/fgene.2014.00372.

Brun, R. *et al.* (2010) 'Human African trypanosomiasis.', *Lancet*, 375(9709), pp. 148–59.

doi: 10.1016/S0140-6736(09)60829-1.

Burkard, G., Fragoso, C. M. and Roditi, I. (2007) 'Highly efficient stable transformation of bloodstream forms of Trypanosoma brucei', *Molecular and Biochemical Parasitology*, 153(2), pp. 220–223. doi: 10.1016/j.molbiopara.2007.02.008.

Calderano, S. G. *et al.* (2015) 'Single molecule analysis of Trypanosoma brucei DNA replication dynamics.', *Nucleic acids research*. Oxford University Press, 43(5), pp. 2655–65. doi: 10.1093/nar/gku1389.

Callebaut, I. *et al.* (2002) 'Metallo- b -lactamase fold within nucleic acids processing enzymes : the b -CASP family', 30(16), pp. 3592–3601.

Campos, M. C. *et al.* (2017) 'Genome-wide mutagenesis and multi-drug resistance in American trypanosomes induced by the front-line drug benznidazole', *Scientific Reports*. Nature Publishing Group, 7(1), p. 14407. doi: 10.1038/s41598-017-14986-6.

Carvalho, A. S. De *et al.* (2014) 'Megazol and its bioisostere 4H-1,2,4-triazole: comparing the trypanocidal, cytotoxic and genotoxic activities and their in vitro and in silico interactions with the Trypanosoma brucei nitroreductase enzyme', *Memórias do Instituto Oswaldo Cruz*, 2(ahead), pp. 1–9. doi: 10.1590/0074-0276140497.

Castresana, J. (2000) 'Selection of conserved blocks from multiple alignments for their use in phylogenetic analysis.', *Molecular biology and evolution*, 17(4), pp. 540–52. Available at: http://www.ncbi.nlm.nih.gov/pubmed/10742046 (Accessed: 22 November 2017).

CDC - Global Health - Neglected Tropical Diseases (2018). Available at: https://www.cdc.gov/globalhealth/ntd/index.html (Accessed: 5 January 2018).

Chaudhury, I., Stroik, D. R. and Sobeck, A. (2014) 'FANCD2-Controlled Chromatin Access of the Fanconi-Associated Nuclease FAN1 Is Crucial for the Recovery of Stalled Replication Forks', *Molecular and Cellular Biology*, 34(21), pp. 3939–3954. doi: 10.1128/MCB.00457-14.

Chaudhury, I., Stroik, D. R. and Sobeck, A. (2014) 'FANCD2-controlled chromatin access of the Fanconi-associated nuclease FAN1 is crucial for the recovery of stalled replication forks.', *Molecular and cellular biology*. American Society for Microbiology (ASM), 34(21), pp. 3939–54. doi: 10.1128/MCB.00457-14.

Chiurillo, M. A. *et al.* (2016) 'Subtelomeric I-SceI-Mediated Double-Strand Breaks Are Repaired by Homologous Recombination in Trypanosoma cruzi.', *Frontiers in microbiology*. Frontiers Media SA, 7, p. 2041. doi: 10.3389/fmicb.2016.02041.

Clauson, C., Schärer, O. D. and Niedernhofer, L. (2013) 'Advances in understanding the complex mechanisms of DNA interstrand cross-link repair.', *Cold Spring Harbor perspectives in biology*. Cold Spring Harbor Laboratory Press, 5(10), p. a012732. doi: 10.1101/cshperspect.a012732.

Cole, R. S. (1971) 'Inactivation of Escherichia coli, F' episomes at transfer, and

bacteriophage lambda by psoralen plus 360-nm light: significance of deoxyribonucleic acid cross-links.', *Journal of bacteriology*, 107(3), pp. 846–52. Available at: http://www.ncbi.nlm.nih.gov/pubmed/4937788 (Accessed: 29 November 2017).

Cybulski, K. E. and Howlett, N. G. (2011) 'FANCP/SLX4: A Swiss army knife of DNA interstrand crosslink repair', *Cell Cycle*, 10(11), pp. 1757–1763. doi: 10.4161/cc.10.11.15818.

Czichos, J., Nonnengaesser, C. and Overath, P. (1986) 'Trypanosoma brucei: cis-Aconitate and temperature reduction as triggers of synchronous transformation of bloodstream to procyclic trypomastigotes in vitro', *Experimental Parasitology*. Academic Press, 62(2), pp. 283–291. doi: 10.1016/0014-4894(86)90033-0.

D'Silva, C. (2007) 'Human African trypanosomiasis: Future prospects for chemotherapy', *Drugs of the Future*, 32(2), p. 149. doi: 10.1358/dof.2007.032.02.1072584.

Daee, D. L. and Myung, K. (2012) 'Fanconi-like crosslink repair in yeast', *Genome Integrity*. Genome Integrity, 3(1), p. 7. doi: 10.1186/2041-9414-3-7.

Deaconescu, A. M. (2013) 'RNA polymerase between lesion bypass and DNA repair', *Cellular and Molecular Life Sciences*, 70(23), pp. 4495–4509. doi: 10.1007/s00018-013-1384-3.

Dean, S., Sunter, J. D. and Wheeler, R. J. (2017) 'TrypTag.org: A Trypanosome Genome-wide Protein Localisation Resource', *Trends in Parasitology*. Elsevier Ltd, 33(2), pp. 80–82. doi: 10.1016/j.pt.2016.10.009.

Dereeper, A. *et al.* (2008) 'Phylogeny.fr: robust phylogenetic analysis for the non-specialist', *Nucleic Acids Research*, 36(Web Server), pp. W465–W469. doi: 10.1093/nar/gkn180.

Devlin, R. (2015) *An investigation into the initiation of VSG switching in Trypanosoma bruceiNo Title*.

Dobson, R. *et al.* (2011) 'Interactions among Trypanosoma brucei RAD51 paralogues in DNA repair and antigenic variation', *Molecular Microbiology*, 81(2), pp. 434–456. doi: 10.1111/j.1365-2958.2011.07703.x.

Dominski, Z. (2007) 'Nucleases of the metallo-beta-lactamase family and their role in DNA and RNA metabolism.', *Critical reviews in biochemistry and molecular biology*, 42(2), pp. 67–93. doi: 10.1080/10409230701279118.

Dong, H. *et al.* (2015) 'Update of the human and mouse Fanconi anemia genes', *Human Genomics*. BioMed Central, 9(1), p. 32. doi: 10.1186/s40246-015-0054-y.

Doyle JJ, Hirumi H, Hirumi K, Lupton EN, C. G. (1980) 'Antigenic variation in clones of animal-infective Trypanosoma brucei derived and maintained in vitro.', *Parasitology*, 80, pp. 359–369.

Dronkert, M. L. and Kanaar, R. (2001) 'Repair of DNA interstrand cross-links.', *Mutation research*, 486(4), pp. 217–47. Available at: http://www.ncbi.nlm.nih.gov/pubmed/11516927

(Accessed: 29 November 2017).

Dudás, A. *et al.* (2007) 'Further characterization of the role of Pso2 in the repair of DNA interstrand cross-link-associated double-strand breaks in Saccharomyces cerevisiae.', *Neoplasma*, 54(3), pp. 189–94. Available at: http://www.ncbi.nlm.nih.gov/pubmed/17447848 (Accessed: 13 January 2018).

Edelheit, O., Hanukoglu, A. and Hanukoglu, I. (2009) 'Simple and efficient site-directed mutagenesis using two single-primer reactions in parallel to generate mutants for protein structure-function studies', 8, pp. 1–8. doi: 10.1186/1472-6750-9-61.

Edgar, R. C. (2004) 'MUSCLE: multiple sequence alignment with high accuracy and high throughput.', *Nucleic acids research*, 32(5), pp. 1792–7. doi: 10.1093/nar/gkh340.

Enoiu, M., Jiricny, J. and Schärer, O. D. (2012) 'Repair of cisplatin-induced DNA interstrand crosslinks by a replication-independent pathway involving transcription-coupled repair and translesion synthesis', *Nucleic Acids Research*, 40(18), pp. 8953–8964. doi: 10.1093/nar/gks670.

Ensminger, M. *et al.* (2014) 'DNA breaks and chromosomal aberrations arise when replication meets base excision repair.', *The Journal of cell biology*. Rockefeller University Press, 206(1), pp. 29–43. doi: 10.1083/jcb.201312078.

Fernandez-Capetillo, O., Allis, C. D. and Nussenzweig, A. (2004) 'Phosphorylation of histone H2B at DNA double-strand breaks.', *The Journal of experimental medicine*. The Rockefeller University Press, 199(12), pp. 1671–7. doi: 10.1084/jem.20032247.

Fernández-Orgiler, A. *et al.* (2016) 'A putative Leishmania DNA polymerase theta protects the parasite against oxidative damage.', *Nucleic acids research*. Oxford University Press, 44(10), pp. 4855–70. doi: 10.1093/nar/gkw346.

Fontebasso, Y. *et al.* (2013) 'The conserved Fanconi anemia nuclease Fan1 and the SUMO E3 ligase Pli1 act in two novel Pso2-independent pathways of DNA interstrand crosslink repair in yeast', *DNA Repair*, 12(12), pp. 1011–1023. doi: 10.1016/j.dnarep.2013.10.003.

Franco, J. R. (2014) 'Epidemiology of human African trypanosomiasis', *Clinical Epidemiology*, 6, pp. 257–275.

Friedberg, E. C. (1995) 'Out of the shadows and into the light: the emergence of DNA repair.', *Trends in biochemical sciences*, 20(10), p. 381. Available at: http://www.ncbi.nlm.nih.gov/pubmed/8533146 (Accessed: 29 November 2017).

Genois, M.-M. *et al.* (2014) 'DNA repair pathways in trypanosomatids: from DNA repair to drug resistance.', *Microbiology and molecular biology reviews : MMBR*, 78(1), pp. 40–73. doi: 10.1128/MMBR.00045-13.

Glover, L. and Horn, D. (2012) 'Trypanosomal histone γh2A and the DNA damage response', *Molecular and Biochemical Parasitology*, 183(1), pp. 78–83. doi: 10.1016/j.molbiopara.2012.01.008.

Glover, L., McCulloch, R. and Horn, D. (2008) 'Sequence homology and microhomology dominate chromosomal double-strand break repair in African trypanosomes', *Nucleic Acids Research*, 36(8), pp. 2608–2618. doi: 10.1093/nar/gkn104.

Graf, F. E. *et al.* (2013) 'Aquaporin 2 mutations in Trypanosoma brucei gambiense field isolates correlate with decreased susceptibility to pentamidine and melarsoprol.', *PLoS neglected tropical diseases*. Edited by E. Matovu, 7(10), p. e2475. doi: 10.1371/journal.pntd.0002475.

Grossmann, K. F. *et al.* (2001) 'S. cerevisiae has three pathways for DNA interstrand crosslink repair', *Mutation Research - DNA Repair*, 487(3–4), pp. 73–83. doi: 10.1016/S0921-8777(01)00106-9.

Grossmann, K. F., Ward, A. M. and Moses, R. E. (2000) 'Saccharomyces cerevisiae lacking Snm1, Rev3 or Rad51 have a normal S-phase but arrest permanently in G2 after cisplatin treatment.', *Mutation research*, 461(1), pp. 1–13. Available at: http://www.ncbi.nlm.nih.gov/pubmed/10980408 (Accessed: 2 October 2017).

Guindon, S. *et al.* (2010) 'New algorithms and methods to estimate maximum-likelihood phylogenies: assessing the performance of PhyML 3.0.', *Systematic biology*, 59(3), pp. 307–21. doi: 10.1093/sysbio/syq010.

Hakem, R. (2008) 'DNA-damage repair; the good, the bad, and the ugly.', *The EMBO journal*. European Molecular Biology Organization, 27(4), pp. 589–605. doi: 10.1038/emboj.2008.15.

Hall, B. S. *et al.* (2010) 'Exploiting the drug-activating properties of a novel trypanosomal nitroreductase.', *Antimicrobial agents and chemotherapy*, 54(3), pp. 1193–9. doi: 10.1128/AAC.01213-09.

Hall, B. S., Bot, C. and Wilkinson, S. R. (2011) 'Nifurtimox activation by trypanosomal type I nitroreductases generates cytotoxic nitrile metabolites.', *The Journal of biological chemistry*, 286(15), pp. 13088–95. doi: 10.1074/jbc.M111.230847.

Hall, B. S., Meredith, E. L. and Wilkinson, S. R. (2012) 'Targeting the substrate preference of a type I nitroreductase to develop antitrypanosomal quinone-based prodrugs.', *Antimicrobial agents and chemotherapy*, 56(11), pp. 5821–30. doi: 10.1128/AAC.01227-12.

Hammond, S. M. (2005) 'Dicing and slicing: The core machinery of the RNA interference pathway', *FEBS Letters*. No longer published by Elsevier, 579(26), pp. 5822–5829. doi: 10.1016/J.FEBSLET.2005.08.079.

Hartley, C. L. and McCulloch, R. (2008) 'Trypanosoma brucei BRCA2 acts in antigenic variation and has undergone a recent expansion in BRC repeat number that is important during homologous recombination.', *Molecular microbiology*, 68(5), pp. 1237–51. doi: 10.1111/j.1365-2958.2008.06230.x.

Hashimoto, S., Anai, H. and Hanada, K. (2016) 'Mechanisms of interstrand DNA crosslink repair and human disorders', *Genes and Environment*. Genes and Environment, 38(1), p. 9.

doi: 10.1186/s41021-016-0037-9.

Hazrati, A. *et al.* (2008) 'Human SNM1A suppresses the DNA repair defects of yeast pso2 mutants.', *DNA repair*, 7(2), pp. 230–8.

Helfert, S. *et al.* (2001) 'Roles of triosephosphate isomerase and aerobic metabolism in Trypanosoma brucei.', *The Biochemical journal*, 357(Pt 1), pp. 117–25. Available at: http://www.ncbi.nlm.nih.gov/pubmed/11415442 (Accessed: 22 November 2017).

Hirumi H, H. K. (1989) 'Continuous cultivation of Trypanosoma brucei bloodstream forms in a medium containing a low concentration of serum protein without feeder cell layers.', *J Parasitol*, 75, p. 985.

Ho, T. V. *et al.* (2011) 'Structure-dependent bypass of DNA interstrand crosslinks by translesion synthesis polymerases', *Nucleic Acids Research*, 39(17), pp. 7455–7464. doi: 10.1093/nar/gkr448.

Horn, D. (2014) 'Antigenic variation in African trypanosomes', *Molecular and Biochemical Parasitology*, 195(2), pp. 123–129. doi: 10.1016/j.molbiopara.2014.05.001.

Horn, D. and McCulloch, R. (2010) 'Molecular mechanisms underlying the control of antigenic variation in African trypanosomes.', *Current opinion in microbiology*. Elsevier, 13(6), pp. 700–5. doi: 10.1016/j.mib.2010.08.009.

Houten, B. V. A. N. *et al.* (1986) 'Action mechanism of ABC excision nuclease on a DNA substrate containing a psoralen crosslink at a defined position', *Proceedings of the National Academy of Sciences of the United States of America*, 83(November), pp. 8077–8081. doi: 10.1073/pnas.83.21.8077.

Huang, Y. and Li, L. (2013) 'DNA crosslinking damage and cancer - a tale of friend and foe', *Translational Cancer Research*, 2(3), pp. 144–154. doi: 10.21037/1080.

Iyama, T. *et al.* (2015) 'CSB interacts with SNM1A and promotes DNA interstrand crosslink processing', *Nucleic Acids Research*, 43(1), pp. 247–258. doi: 10.1093/nar/gku1279.

Iyama, T., Wilson, D. M. and III (2016) 'Elements That Regulate the DNA Damage Response of Proteins Defective in Cockayne Syndrome.', *Journal of molecular biology*. NIH Public Access, 428(1), pp. 62–78. doi: 10.1016/j.jmb.2015.11.020.

Jackson, S. P. (2002) 'Sensing and repairing DNA double-strand breaks.', *Carcinogenesis*, 23(5), pp. 687–96. Available at: http://www.ncbi.nlm.nih.gov/pubmed/12016139 (Accessed: 21 January 2018).

Jin, H. and Cho, Y. (2017) 'Structural and functional relationships of FAN1.', *DNA repair*, 56, pp. 135–143. doi: 10.1016/j.dnarep.2017.06.016.

Johnson, R. A., Hellens, R. P. and Love, D. R. (2011) 'A transient assay for recombination demonstrates that Arabidopsis SNM1 and XRCC3 enhance non-homologous recombination.', *Genetics and molecular research : GMR*, 10(3), pp. 2104–32. doi: 10.4238/vol10-3gmr1347.

Jones, M. J. K. and Huang, T. T. (2012) ‘The Fanconi anemia pathway in replication stress and DNA crosslink repair.’, *Cellular and molecular life sciences : CMLS*, pp. 3963–3974. doi: 10.1007/s00018-012-1051-0.

Jones, R. ; and Petermann, E. (2012) ‘Replication fork dynamics and the DNA damage response’, *Biochemical Journal Biochem. J*, 443(443), pp. 13–2613. doi: 10.1042/BJ20112100.

Kato, N., Kawasoe, Y., Williams, H., Coates, E., Roy, U., Shi, Y., Beese, L. S., *et al.* (2017) ‘Sensing and Processing of DNA Interstrand Crosslinks by the Mismatch Repair Pathway’, *Cell Reports*, 21(5), pp. 1375–1385. doi: 10.1016/j.celrep.2017.10.032.

Keijzers, G., Bohr, V. A. and Rasmussen, L. J. (2015) ‘Human exonuclease 1 (EXO1) activity characterization and its function on flap structures.’, *Bioscience reports*. Portland Press Ltd, 35(3). doi: 10.1042/BSR20150058.

Kelley, L. A. *et al.* (2015) ‘The Phyre2 web portal for protein modeling, prediction and analysis’, *Nature Protocols*. Nature Publishing Group, 10(6), pp. 845–858. doi: 10.1038/nprot.2015.053.

Kennedy, P. G. (2013) ‘Clinical features, diagnosis, and treatment of human African trypanosomiasis (sleeping sickness).’, *Lancet neurology*. Elsevier Ltd, 12(2), pp. 186–94.

Kidwell, M. A., Chan, J. M. and Doudna, J. A. (2014) ‘Evolutionarily conserved roles of the dicer helicase domain in regulating RNA interference processing.’, *The Journal of biological chemistry*. American Society for Biochemistry and Molecular Biology, 289(41), pp. 28352–62. doi: 10.1074/jbc.M114.589051.

Kim, M. and Kim, J. M. (2016) ‘The role of USP1 autocleavage in DNA interstrand crosslink repair’, *FEBS Letters*. Edited by A. Nebreda, 590(3), pp. 340–348. doi: 10.1002/1873-3468.12060.

Kimura, S. *et al.* (2005) ‘The expression of the rice (Oryza sativa L.) homologue of Snm1 is induced by DNA damages’, *Biochemical and Biophysical Research Communications*, 329(2), pp. 668–672. doi: 10.1016/j.bbrc.2005.01.161.

Klein Douwel, D. *et al.* (2017) ‘Recruitment and positioning determine the specific role of the XPF-ERCC1 endonuclease in interstrand crosslink repair.’, *The EMBO journal*. EMBO Press, 36(14), pp. 2034–2046. doi: 10.15252/embj.201695223.

Kozmin, S. G. and Jinks-Robertson, S. (2013) ‘The mechanism of nucleotide excision repair-mediated UV-induced mutagenesis in nonproliferating cells’, *Genetics*, 193(3), pp. 803–817. doi: 10.1534/genetics.112.147421.

Kreuzer, K. N. (2013) ‘DNA damage responses in prokaryotes: regulating gene expression, modulating growth patterns, and manipulating replication forks.’, *Cold Spring Harbor perspectives in biology*. Cold Spring Harbor Laboratory Press, 5(11), p. a012674. doi: 10.1101/cshperspect.a012674.

Krishnan, V., Tay, L. S. and Ito, Y. (2015) ‘The Fanconi Anemia Pathway of DNA Repair and Human Cancer’, in *Advances in DNA Repair*. InTech. doi: 10.5772/59995.

Kumari, A. *et al.* (2008) ‘Replication bypass of interstrand cross-link intermediates by Escherichia coli DNA polymerase IV.’, *The Journal of biological chemistry*, 283(41), pp. 27433–7. doi: 10.1074/jbc.M801237200.

Lagerwerf, S. *et al.* (2011) ‘DNA damage response and transcription’, *DNA Repair*, 10(7), pp. 743–750. doi: 10.1016/j.dnarep.2011.04.024.

Lam, A. F., Krogh, B. O. and Symington, L. S. (2008) ‘Unique and overlapping functions of the Exo1, Mre11 and Pso2 nucleases in DNA repair.’, *DNA repair*, 7(4), pp. 655–62. doi: 10.1016/j.dnarep.2007.12.014.

Lambert, S. *et al.* (2003) ‘Schizosaccharomyces pombe checkpoint response to DNA interstrand cross-links.’, *Molecular and cellular biology*. American Society for Microbiology, 23(13), pp. 4728–37. doi: 10.1128/MCB.23.13.4728-4737.2003.

Lange, A. *et al.* (2007) ‘Classical nuclear localization signals: Definition, function, and interaction with importin ??’, *Journal of Biological Chemistry*, 282(8), pp. 5101–5105. doi: 10.1074/jbc.R600026200.

Lavin, M. F. (2008) ‘Ataxia-telangiectasia: from a rare disorder to a paradigm for cell signalling and cancer’, *Nature Reviews Molecular Cell Biology*. Nature Publishing Group, 9(10), pp. 759–769. doi: 10.1038/nrm2514.

Lee, S. Y. *et al.* (2016) ‘Cephalosporins inhibit human metallo β-lactamase fold DNA repair nucleases SNM1A and SNM1B/apollo’, *Chem. Commun.*, 52(40), pp. 6727–6730. doi: 10.1039/C6CC00529B.

Lehoczký, P., McHugh, P. J. and Chovanec, M. (2007) ‘DNA interstrand cross-link repair in *Saccharomyces cerevisiae*’, *FEMS Microbiology Reviews*, 31(2), pp. 109–133. doi: 10.1111/j.1574-6976.2006.00046.x.

Leung, K. F. *et al.* (2011) ‘Ubiquitylation and developmental regulation of invariant surface protein expression in trypanosomes.’, *Eukaryotic cell*, 10(7), pp. 916–31. doi: 10.1128/EC.05012-11.

Li, X., Hejna, J. and Moses, R. E. (2005) ‘The yeast Snm1 protein is a DNA 5’-exonuclease.’, *DNA repair*, 4(2), pp. 163–70. doi: 10.1016/j.dnarep.2004.08.012.

Li, X. and Moses, R. E. (2003) ‘The beta-lactamase motif in Snm1 is required for repair of DNA double-strand breaks caused by interstrand crosslinks in S. cerevisiae.’, *DNA repair*, 2(1), pp. 121–9. Available at: http://www.ncbi.nlm.nih.gov/pubmed/12509272 (Accessed: 13 September 2017).

Liang, C.-C. *et al.* (2015) ‘UHRF1 Is a Sensor for DNA Interstrand Crosslinks and Recruits FANCD2 to Initiate the Fanconi Anemia Pathway’, *Cell Reports*, 10(12), pp. 1947–1956. doi: 10.1016/j.celrep.2015.02.053.

Limoli, C. L. *et al.* (2002) 'UV-induced replication arrest in the xeroderma pigmentosum variant leads to DNA double-strand breaks, gamma -H2AX formation, and Mre11 relocalization.', *Proceedings of the National Academy of Sciences of the United States of America*. National Academy of Sciences, 99(1), pp. 233–8. doi: 10.1073/pnas.231611798.

Lopes, A. H. *et al.* (2010) 'Trypanosomatids: Odd Organisms, Devastating Diseases', *The Open Parasitology Journal*, 4, pp. 30–59. Available at: https://pdfs.semanticscholar.org/0076/3954077fd1fab53bc33130784ad176353ae9.pdf (Accessed: 18 December 2017).

Luo, Z. *et al.* (2001) 'Ultraviolet radiation alters the phosphorylation of RNA polymerase II large subunit and accelerates its proteasome-dependent degradation.', *Mutation research*, 486(4), pp. 259–74. Available at: http://www.ncbi.nlm.nih.gov/pubmed/11516929 (Accessed: 8 September 2017).

M. Mandel, A. H. (1970) 'Calcium-dependent bacteriophage DNA infection', *Journal of molecular biology*, 53(1), pp. 159–162.

Machado, C. R. *et al.* (2014) 'Nucleotide excision repair in Trypanosoma brucei: specialization of transcription-coupled repair due to multigenic transcription.', *Molecular microbiology*, 92(4), pp. 756–76. doi: 10.1111/mmi.12589.

Marchetti, M. A. *et al.* (2000) 'Import of proteins into the trypanosome nucleus and their distribution at karyokinesis.', *Journal of cell science*, 113 (Pt 5), pp. 899–906. Available at: http://www.ncbi.nlm.nih.gov/pubmed/10671379 (Accessed: 26 November 2017).

Mäser, P. *et al.* (1999) 'A nucleoside transporter from Trypanosoma brucei involved in drug resistance.', *Science (New York, N.Y.)*, 285(5425), pp. 242–4. Available at: http://www.ncbi.nlm.nih.gov/pubmed/10398598 (Accessed: 28 November 2017).

Matthews, K. R., Ellis, J. R. and Paterou, A. (2004) 'Molecular regulation of the life cycle of African trypanosomes', *Trends in Parasitology*, 20(1), pp. 40–47. doi: 10.1016/j.pt.2003.10.016.

McCulloch, R. and Barry, J. D. (1999) 'A role for RAD51 and homologous recombination in Trypanosoma brucei antigenic variation.', *Genes & development*. Cold Spring Harbor Laboratory Press, 13(21), pp. 2875–88. Available at: http://www.ncbi.nlm.nih.gov/pubmed/10557214 (Accessed: 19 December 2017).

McHugh, P. J., Spanswick, V. J. and Hartley, J. A. (2001) 'Repair of DNA interstrand crosslinks: molecular mechanisms and clinical relevance.', *The Lancet. Oncology*, 2(8), pp. 483–90. doi: 10.1016/S1470-2045(01)00454-5.

McHugh, P. J., Ward, T. A. and Chovanec, M. (2012) 'A prototypical Fanconi anemia pathway in lower eukaryotes?', *Cell Cycle*, 11(20), pp. 3739–3744. doi: 10.4161/cc.21727.

McVey, M. (2010) 'Strategies for DNA interstrand crosslink repair: insights from worms, flies, frogs, and slime molds.', *Environmental and molecular mutagenesis*, 51(6), pp. 646–58. doi: 10.1002/em.20551.

Meredith, E. L. *et al.* (2017) 'Distinct activation mechanisms trigger the trypanocidal activity of DNA damaging prodrugs', *Molecular Microbiology*, 106(2), pp. 207–222. doi: 10.1111/mmi.13767.

Mitchell, D. J. and Minchin, R. F. (2008) 'E. coli nitroreductase/CB1954 gene-directed enzyme prodrug therapy: role of arylamine N-acetlytransferase 2', *Cancer Gene Therapy*. Nature Publishing Group, 15(11), pp. 758–764. doi: 10.1038/cgt.2008.47.

Moldovan, G.-L. and D'Andrea, A. D. (2009) 'How the fanconi anemia pathway guards the genome.', *Annual review of genetics*, 43, pp. 223–49. doi: 10.1146/annurev-genet-102108-134222.

Molinier, J., Stamm, M.-E. and Hohn, B. (2004) 'SNM-dependent recombinational repair of oxidatively induced DNA damage in Arabidopsis thaliana', *EMBO reports*, 5(10), pp. 994–999. doi: 10.1038/sj.embor.7400256.

Morrison, L. J., McCulloch, R. and Hall, J. P. J. (2015) 'DNA Recombination Strategies During Antigenic Variation in the African Trypanosome', *Microbiology Spectrum*. asm Pub2Web, 3(2), pp. 409–435. doi: 10.1128/microbiolspec.MDNA3-0016-2014.

Munari, F. M. *et al.* (2013) 'New features on Pso2 protein family in DNA interstrand cross-link repair and in the maintenance of genomic integrity in Saccharomyces cerevisiae', *Fungal Genetics and Biology*. Elsevier Inc., 60, pp. 122–132. doi: 10.1016/j.fgb.2013.09.003.

Nair, N. *et al.* (2014) 'Identification and characterization of MUS81 point mutations that abolish interaction with the SLX4 scaffold protein', *DNA Repair*. Elsevier B.V., 24, pp. 131–137. doi: 10.1016/j.dnarep.2014.08.004.

Nicolini, M. (1988) *Platinum and Other Metal Coordination Compounds in Cancer Chemotherapy : Proceedings of the Fifth International Symposium on Platinum and Other Metal Coordination Compounds in Cancer Chemotherapy Abano, Padua, ITALY - June 29-July 2, 1987*. Springer US. Available at: https://books.google.co.uk/books?id=1GfdBwAAQBAJ&pg=PA25&lpg=PA25&dq=CB1954+intrastrand+crosslinks&source=bl&ots=TYB0Jbyjqy&sig=Est44Vxrt9dhGro-5I4c3nRpGWA&hl=en&sa=X&ved=0ahUKEwiI0aWX4t_XAhVC3KQKHfNWDxQQ6AEIWjAH#v=onepage&q=CB1954 intrastrand crosslinks&f=false (Accessed: 27 November 2017).

Noll, D. M., Mason, T. M. and Miller, P. S. (2006) 'Formation and repair of interstrand cross-links in DNA.', *Chemical reviews*. NIH Public Access, 106(2), pp. 277–301. doi: 10.1021/cr040478b.

O'Donnell, L. and Durocher, D. (2010) 'DNA repair has a new FAN1 club', *Molecular Cell*. Elsevier Inc., 39(2), pp. 167–169. doi: 10.1016/j.molcel.2010.07.010.

ORTIZ, D. *et al.* (2009) 'Two novel nucleobase/pentamidine transporters from Trypanosoma brucei', *Molecular and Biochemical Parasitology*, 163(2), pp. 67–76. doi: 10.1016/j.molbiopara.2008.09.011.

de Padua, R. A. P. *et al.* (2017) 'Characterisation of the fumarate hydratase repertoire in Trypanosoma cruzi', *International Journal of Biological Macromolecules*. Elsevier B.V., 102, pp. 42–51. doi: 10.1016/j.ijbiomac.2017.03.099.

Panier, S. and Durocher, D. (2013) 'Push back to respond better: regulatory inhibition of the DNA double-strand break response', *Nature Reviews Molecular Cell Biology*, 14(10), pp. 661–672. doi: 10.1038/nrm3659.

Park, J.-Y. *et al.* (2016) 'Complementation of hypersensitivity to DNA interstrand crosslinking agents demonstrates that XRCC2 is a Fanconi anaemia gene.', *Journal of medical genetics*, 53(10), pp. 672–680. doi: 10.1136/jmedgenet-2016-103847.

Passos-Silva, D. G. *et al.* (2010) 'Overview of DNA Repair in Trypanosoma cruzi, Trypanosoma brucei, and Leishmania major.', *Journal of nucleic acids*, 2010, p. 840768. doi: 10.4061/2010/840768.

Patrick, K. L. *et al.* (2009) 'Distinct and overlapping roles for two Dicer-like proteins in the RNA interference pathways of the ancient eukaryote Trypanosoma brucei', *Proceedings of the National Academy of Sciences*, 106(42), pp. 17933–17938. doi: 10.1073/pnas.0907766106.

Paull, T. T. and Gellert, M. (1998) 'The 3' to 5' exonuclease activity of Mre 11 facilitates repair of DNA double-strand breaks.', *Molecular cell*. Elsevier, 1(7), pp. 969–79. doi: 10.1016/S1097-2765(00)80097-0.

Peng, D. *et al.* (2014) 'CRISPR-Cas9-mediated single-gene and gene family disruption in Trypanosoma cruzi.', *mBio*. American Society for Microbiology, 6(1), pp. e02097-14. doi: 10.1128/mBio.02097-14.

Pichierri, P., Averbeck, D. and Rosselli, F. (2002) 'DNA cross-link-dependent RAD50/MRE11/NBS1 subnuclear assembly requires the Fanconi anemia C protein.', *Human molecular genetics*, 11(21), pp. 2531–46. Available at: http://www.ncbi.nlm.nih.gov/pubmed/12354779 (Accessed: 3 October 2017).

Pizzolato, J. *et al.* (2015) 'FANCD2-associated Nuclease 1, but Not Exonuclease 1 or Flap Endonuclease 1, Is Able to Unhook DNA Interstrand Cross-links *in Vitro*', *Journal of Biological Chemistry*, 290(37), pp. 22602–22611. doi: 10.1074/jbc.M115.663666.

Proudfoot, C. and McCulloch, R. (2005) 'Distinct roles for two RAD51-related genes in Trypanosoma brucei antigenic variation.', *Nucleic acids research*, 33(21), pp. 6906–19. doi: 10.1093/nar/gki996.

Qian, M.-B. and Zhou, X.-N. (2016) 'Global burden on neglected tropical diseases.', *The Lancet. Infectious diseases*. Elsevier, 16(10), pp. 1113–1114. doi: 10.1016/S1473-3099(16)30328-0.

Rajski, S. R. and Williams, R. M. (1998) 'DNA Cross-Linking Agents as Antitumor Drugs', *Chemical Reviews*, 98(8), pp. 2723–2796. doi: 10.1021/cr9800199.

Robinson, N. P., McCulloch, R., Conway, C., Browitt, A. and David Barry, J. (2002) 'Inactivation of Mre11 does not affect VSG gene duplication mediated by homologous recombination in Trypanosoma brucei', *Journal of Biological Chemistry*, 277(29), pp. 26185–26193. doi: 10.1074/jbc.M203205200.

Robinson, N. P., McCulloch, R., Conway, C., Browitt, A. and Barry, J. D. (2002) 'Inactivation of Mre11 Does Not Affect *VSG* Gene Duplication Mediated by Homologous Recombination in *Trypanosoma brucei*', *Journal of Biological Chemistry*, 277(29), pp. 26185–26193. doi: 10.1074/jbc.M203205200.

Rodríguez-Marí, A. and Postlethwait, J. H. (2011) 'The Role of Fanconi Anemia/BRCA Genes in Zebrafish Sex Determination', in *Methods in cell biology*, pp. 461–490. doi: 10.1016/B978-0-12-381320-6.00020-5.

Rudd, S. G. *et al.* (2013) 'PPL2 translesion polymerase is essential for the completion of chromosomal DNA replication in the African trypanosome.', *Molecular cell*. Elsevier, 52(4), pp. 554–65. doi: 10.1016/j.molcel.2013.10.034.

Ruiz-Postigo, J. A. *et al.* (2012) 'Human African trypanosomiasis in South Sudan: how can we prevent a new epidemic?', *PLoS neglected tropical diseases*. Public Library of Science, 6(5), p. e1541. doi: 10.1371/journal.pntd.0001541.

Sancar, A. *et al.* (2004) 'Molecular Mechanisms of Mammalian DNA Repair and the DNA Damage Checkpoints', *Annual Review of Biochemistry*, 73(1), pp. 39–85. doi: 10.1146/annurev.biochem.73.011303.073723.

Sarkar, S. *et al.* (2006) 'DNA interstrand crosslink repair during G1 involves nucleotide excision repair and DNA polymerase ζ', *The EMBO Journal*, 25(6), pp. 1285–1294. doi: 10.1038/sj.emboj.7600993.

Schmittgen TD, L. K. (2008) 'Analyzing real-time PCR data by the comparative C(T) method.', *Nat Protoc*, 6, pp. 1101–8.

Schoenfeld, A. R. *et al.* (2004) 'BRCA2 is ubiquitinated in vivo and interacts with USP11, a deubiquitinating enzyme that exhibits prosurvival function in the cellular response to DNA damage.', *Molecular and cellular biology*. American Society for Microbiology (ASM), 24(17), pp. 7444–55. doi: 10.1128/MCB.24.17.7444-7455.2004.

Schumann Burkard, G., Jutzi, P. and Roditi, I. (2011) 'Genome-wide RNAi screens in bloodstream form trypanosomes identify drug transporters.', *Molecular and biochemical parasitology*, 175(1), pp. 91–4. doi: 10.1016/j.molbiopara.2010.09.002.

Sczepanski, J. T. *et al.* (2009) 'Double-strand break formation during nucleotide excision repair of a DNA interstrand cross-link.', *Biochemistry*. NIH Public Access, 48(32), pp. 7565–7. doi: 10.1021/bi901006b.

Seed, J. R. and Wenck, M. A. (2003) 'Role of the long slender to short stumpy transition in the life cycle of the african trypanosomes.', *Kinetoplastid biology and disease*. BioMed Central, 2(1), p. 3. doi: 10.1186/1475-9292-2-3.

Sengerová, B. *et al.* (2012) ‘Characterization of the human SNM1A and SNM1B/Apollo DNA repair exonucleases.’, *The Journal of biological chemistry*. American Society for Biochemistry and Molecular Biology, 287(31), pp. 26254–67. doi: 10.1074/jbc.M112.367243.

Sharma, S. and Canman, C. E. (2012) ‘REV1 and DNA polymerase zeta in DNA interstrand crosslink repair’, *Environmental and Molecular Mutagenesis*, 53(9), pp. 725–740. doi: 10.1002/em.21736.

Shen, X. *et al.* (2006) ‘REV3 and REV1 play major roles in recombination-independent repair of DNA interstrand cross-links mediated by monoubiquitinated proliferating cell nuclear antigen (PCNA).’, *The Journal of biological chemistry*, 281(20), pp. 13869–72. doi: 10.1074/jbc.C600071200.

Shen, X. and Li, L. (2010) ‘Mutagenic repair of DNA interstrand crosslinks.’, *Environmental and molecular mutagenesis*. NIH Public Access, 51(6), pp. 493–9. doi: 10.1002/em.20558.

Siddiqui, M. Q. *et al.* (2017) ‘Studies of protein–protein interactions in Fanconi anemia pathway to unravel the DNA interstrand crosslink repair mechanism’, *International Journal of Biological Macromolecules*. Elsevier B.V., 104, pp. 1338–1344. doi: 10.1016/j.ijbiomac.2017.05.166.

Simarro, P. P. *et al.* (2011) ‘The human African trypanosomiasis control and surveillance programme of the World Health Organization 2000-2009: the way forward.’, *PLoS neglected tropical diseases*, 5(2), p. e1007.

Simhadri, S. *et al.* (2014) ‘Male Fertility Defect Associated with Disrupted BRCA1-PALB2 Interaction in Mice’, *Journal of Biological Chemistry*, 289(35), pp. 24617–24629. doi: 10.1074/jbc.M114.566141.

Singh, N. P. *et al.* (1988) ‘A simple technique for quantitation of low levels of DNA damage in individual cells.’, *Experimental cell research*, 175(1), pp. 184–91. Available at: http://www.ncbi.nlm.nih.gov/pubmed/3345800 (Accessed: 21 January 2018).

Stanojcic, S. *et al.* (2016) ‘Single-molecule analysis of DNA replication reveals novel features in the divergent eukaryotes Leishmania and Trypanosoma brucei versus mammalian cells’, *Scientific Reports*. Nature Publishing Group, 6(1), p. 23142. doi: 10.1038/srep23142.

Stevens, J. R. *et al.* (2001) ‘The molecular evolution of Trypanosomatidae.’, *Advances in parasitology*, 48, pp. 1–56. Available at: http://www.ncbi.nlm.nih.gov/pubmed/11013754 (Accessed: 6 October 2017).

Steverding, D. (2008) ‘The history of African trypanosomiasis.’, *Parasites & vectors*, 1(1), p. 3. doi: 10.1186/1756-3305-1-3.

Stevnsner, T. *et al.* (2008) ‘The role of Cockayne Syndrome group B (CSB) protein in base excision repair and aging.’, *Mechanisms of ageing and development*. NIH Public Access, 129(7–8), pp. 441–8. doi: 10.1016/j.mad.2008.04.009.

Stortz, J. A. *et al.* (2017) 'Genome-wide and protein kinase-focused RNAi screens reveal conserved and novel damage response pathways in Trypanosoma brucei.', *PLoS pathogens*. Public Library of Science, 13(7), p. e1006477. doi: 10.1371/journal.ppat.1006477.

Sullivan, J. a *et al.* (2015) 'Unravelling the role of SNM1 in the DNA repair system of Trypanosoma brucei.', *Molecular microbiology*, pp. 1–39. doi: 10.1111/mmi.12973.

Szankasi, P. and Smith, G. R. (1992) 'A DNA exonuclease induced during meiosis of Schizosaccharomyces pombe.', *The Journal of biological chemistry*, 267(5), pp. 3014–23. Available at: http://www.ncbi.nlm.nih.gov/pubmed/1737756 (Accessed: 8 September 2017).

T.N. Siegel, D.R. Hekstra, G. A. M. C. (2008) 'Analysis of the Trypanosoma brucei cell cycle by quantitative DAPI imaging', *Molecular & Biochemical Parasitology*, 160(2), p. 171.

Takahashi, D. *et al.* (2015) 'Human FAN1 promotes strand incision in 5???-flapped DNA complexed with RPA', *Journal of Biochemistry*, 158(3), pp. 263–270. doi: 10.1093/jb/mvv043.

Tan, K. S. W., Leal, S. T. G. and Cross, G. A. M. (2002) 'Trypanosoma brucei MRE11 is non-essential but influences growth, homologous recombination and DNA double-strand break repair.', *Molecular and biochemical parasitology*, 125(1–2), pp. 11–21. Available at: http://www.ncbi.nlm.nih.gov/pubmed/12467970 (Accessed: 8 September 2017).

Tan, W. and Deans, A. J. (2017) 'A defined role for multiple Fanconi anemia gene products in DNA-damage-associated ubiquitination.', *Experimental hematology*, 50, pp. 27–32. doi: 10.1016/j.exphem.2017.03.001.

Teixeira, D. E. *et al.* (2012) 'Interactive Multimedia to Teach the Life Cycle of Trypanosoma cruzi, the Causative Agent of Chagas Disease', *PLoS Neglected Tropical Diseases*. Edited by Y. M. Traub-Csekö. Public Library of Science, 6(8), p. e1749. doi: 10.1371/journal.pntd.0001749.

Tiefenbach, T. *et al.* (2007) 'Biochemical analysis of SNM1 nuclease activity suggests a link between several DNA repair pathways during ICL repair proteins', *submitted*, pp. 1–10.

Tijsterman, M. *et al.* (1997) 'Transitions in the coupling of transcription and nucleotide excision repair within RNA polymerase II-transcribed genes of Saccharomyces cerevisiae.', *Proceedings of the National Academy of Sciences of the United States of America*. National Academy of Sciences, 94(15), pp. 8027–32. Available at: http://www.ncbi.nlm.nih.gov/pubmed/9223308 (Accessed: 21 January 2018).

Trenz, K. *et al.* (2006) 'ATM and ATR promote Mre11 dependent restart of collapsed replication forks and prevent accumulation of DNA breaks', *The EMBO Journal*, 25(8), pp. 1764–1774. doi: 10.1038/sj.emboj.7601045.

Ullu, E., Tschudi, C. and Chakraborty, T. (2004) 'RNA interference in protozoan parasites', *Cellular Microbiology*, 6(6), pp. 509–519. doi: 10.1111/j.1462-5822.2004.00399.x.

de Villartay, J.-P. *et al.* (2009) 'A histidine in the beta-CASP domain of Artemis is critical for

its full in vitro and in vivo functions.', *DNA repair*, 8(2), pp. 202–8.

Wang, A. T. *et al.* (2015) 'A Dominant Mutation in Human RAD51 Reveals Its Function in DNA Interstrand Crosslink Repair Independent of Homologous Recombination', *Molecular Cell*, 59(3), pp. 478–490. doi: 10.1016/j.molcel.2015.07.009.

Wang, W. (2007) 'Emergence of a DNA-damage response network consisting of Fanconi anaemia and BRCA proteins', *Nature Reviews Genetics 2007 8:10*. Nature Publishing Group, 8(10), p. 735. doi: 10.1038/nrg2159.

Ward, T. a *et al.* (2012) 'Components of a Fanconi-like pathway control Pso2-independent DNA interstrand crosslink repair in yeast.', *PLoS genetics*, 8(8), p. e1002884. doi: 10.1371/journal.pgen.1002884.

Waters, L. S. *et al.* (2009) 'Eukaryotic translesion polymerases and their roles and regulation in DNA damage tolerance.', *Microbiology and molecular biology reviews : MMBR*, 73(1), pp. 134–54. doi: 10.1128/MMBR.00034-08.

'WHO | Trypanosomiasis, human African (sleeping sickness)' (2017) *WHO*. World Health Organization. Available at: http://www.who.int/mediacentre/factsheets/fs259/en/ (Accessed: 13 December 2017).

'WHO | World Health Organization' (2018) *WHO*. World Health Organization. Available at: http://www.who.int/en/ (Accessed: 5 January 2018).

Wilkinson, S. R. *et al.* (2006) 'Functional characterisation of the iron superoxide dismutase gene repertoire in Trypanosoma brucei', *Free Radical Biology and Medicine*, 40(2), pp. 198–209. doi: 10.1016/j.freeradbiomed.2005.06.022.

Wilkinson, S. R. *et al.* (2008) 'A mechanism for cross-resistance to nifurtimox and benznidazole in trypanosomes.', *Proceedings of the National Academy of Sciences of the United States of America*, 105(13), pp. 5022–7.

Wilkinson, S. R. and Kelly, J. M. (2009) 'Trypanocidal drugs: mechanisms, resistance and new targets.', *Expert reviews in molecular medicine*, 11(October), p. e31. doi: 10.1017/S1462399409001252.

Williams, S. A. *et al.* (2011) 'Functional and physical interaction between the mismatch repair and FA-BRCA pathways', *Human Molecular Genetics*, 20(22), pp. 4395–4410. doi: 10.1093/hmg/ddr366.

Wilson, D. M. *et al.* (2017) 'Systematic analysis of DNA crosslink repair pathways during development and aging in Caenorhabditis elegans', *Nucleic Acids Research*, 45(16), pp. 9467–9480. doi: 10.1093/nar/gkx660.

Wirtz, E. *et al.* (1999) 'A tightly regulated inducible expression system for dominant negative approaches in *Trypanosoma brucei*', *Molecular & Biochemical Parasitology*, 99(1), pp. 89–101. doi: 10.1016/S0166-6851(99)00002-X.

Wolter, R., Siede, W. and Brendel, M. (1996) 'Regulation of SNM1, an

inducibleSaccharomyces cerevisiae gene required for repair of DNA cross-links', *Molecular and General Genetics MGG*, 250(2), pp. 162–8. Available at: http://link.springer.com/article/10.1007/BF02174175 (Accessed: 3 April 2014).

Wood, R. D. (2011) 'Nucleotide excision repair proteins and interstrand crosslink', *Environmental and Molecular Mutagenesis*, 51(6), pp. 520–526. doi: 10.1002/em.20569.Nucleotide.

Woodward, R. and Gull, K. (1990) 'Timing of nuclear and kinetoplast DNA replication and early morphological events in the cell cycle of Trypanosoma brucei.', *Journal of cell science*, 95, pp. 49–57.

Wu, Y. and Brosh, R. M. (2009) 'FANCJ helicase operates in the Fanconi Anemia DNA repair pathway and the response to replicational stress.', *Current molecular medicine*, 9(4), pp. 470–82. Available at: http://www.ncbi.nlm.nih.gov/pubmed/19519404 (Accessed: 7 September 2017).

Zha, S., Boboila, C. and Alt, F. W. (2009) 'Mre11: roles in DNA repair beyond homologous recombination', *Nature Structural & Molecular Biology*, 16(8), pp. 798–800. doi: 10.1038/nsmb0809-798.

Zhang, J. and Walter, J. C. (2014) 'Mechanism and regulation of incisions during DNA interstrand cross-link repair.', *DNA repair*. Elsevier B.V., 19, pp. 135–42. doi: 10.1016/j.dnarep.2014.03.018.

Zhang, X.-Y. *et al.* (2009) 'Xpf and Not the Fanconi Anaemia Proteins or Rev3 Accounts for the Extreme Resistance to Cisplatin in Dictyostelium discoideum', *PLoS Genetics*. Edited by R. J. Monnat. Public Library of Science, 5(9), p. e1000645. doi: 10.1371/journal.pgen.1000645.

Zurita-Leal, A. (2016) 'Translesion DNA Polymerases and genome maintenance in Trypanosoma brucei', in *British Society of Parasitology Symposium*.